320
2-8-80

MASTER

DR. 675

CONF-791127

Proceedings of the DOE Chemical Energy Storage and Hydrogen Energy Systems Contracts Review

November 13 and 14, 1979

Sheraton International Conference Center
Reston, Virginia

Sponsored by
U.S. Department of Energy
Assistant Secretary for Conservation and Solar Energy
Division of Energy Storage Systems
Washington, D.C.

Published February 1980

DISCLAIMER

Available from:

National Technical Information Service (NTIS)
U.S. Department of Commerce
5285 Port Royal Road
Springfield, VA 22161

Price:
Printed Copy: ~~$10.75~~ 14.00
Microfiche: ~~$3.00~~ 3.50

CONF-791127
Dist. Category UC-94d

Proceedings of the DOE Chemical Energy Storage and Hydrogen Energy Systems Contracts Review

November 13 and 14, 1979

Sheraton International Conference Center
Reston, Virginia

Sponsored by
U.S. Department of Energy
Assistant Secretary for Conservation and Solar Energy
Division of Energy Storage Systems
Washington, D.C.

Under Contract to
Jet Propulsion Laboratory
Pasadena, California

Conference Coordination and Arrangements by
Courtesy Associates, Inc.
Washington, D.C.

FOREWORD

A Chemical Energy Storage and Hydrogen Energy Systems Contracts Review is held annually by the DOE Division of Energy Storage Systems (STOR). The review includes the presentation of results of contracted and in-house efforts, with questions and discussions, followed by an Executive Session in which invited reviewers from outside the program provide evaluations to STOR. The fourth annual review was held at the Sheraton International Conference Center at Reston, Virginia, on November 13 and 14, 1979, followed by an Executive Session on November 15th.

Brief summaries of the individual activities are included in this document, along with one page summary sheets. An overview is given by the Program Manager, Dr. Robert R. Reeves. This is followed by a summary of the Electrolysis-Based Hydrogen Storage Systems by Alessio Mezzina, Brookhaven National Laboratory, who manages that activity. Following the summaries of work under the Brookhaven Program is a Summary of the NASA Hydrogen Energy Storage Technology Project by James H. Kelley, Manager of Hydrogen Systems and Technology, Jet Propulsion Laboratory. The final pages of the document list the Reviewers and other participants in this review.

The Review this year was arranged by the Jet Propulsion Laboratory with Courtesy Associates, Inc., serving as Conference Coordinator. I would like to thank Congressman Charles E. Grassley, 3rd District, Iowa, for serving as our guest speaker. I would also like to thank our reviewers for their contributions during this three day review. I would like to express my appreciation to Mrs. Annmarie Pittman of Courtesy Associates and to her assistant, Miss Peggy Lyons for their outstanding job in organizing the review, handling the correspondence and documentation and for conducting the three days of the review as an efficient, smooth-running function. I would also like to thank Mrs. Wanda Nelson of JPL for reviewing facilities and selecting this site and for establishing and managing our contract with Courtesy Associates.

James H. Kelley, Manager
Hydrogen Systems and Technology
Jet Propulsion Laboratory
Pasadena, California

The Honorable Charles E. Grassley
U. S. House of Representatives
Guest Speaker

Banquet

"Show and Tell"

CONTENTS

I. OVERVIEW

DOE Chemical/Hydrogen Energy Storage Program 1
R. Reeves
U. S. Department of Energy

II. ELECTROLYSIS-BASED HYDROGEN STORAGE SYSTEMS

Overview and Rationale of the Brookhaven National Laboratory Managed Program 3
A. Mezzina
Brookhaven National Laboratory

III. HYDROGEN PRODUCTION

Development Status of Solid Polymer Electrolyte Water Electrolysis For Large Scale Hydrogen Generation 7
J. H. Russell
General Electric Company

Selection and Evaluation of Materials for Advanced Water Electrolyzers 11
S. Srinivasan, R. S. Yeo, G. Kissel, E. Gannon, F. Kulesa, J. Orehotsky and W. Visscher
Brookhaven National Laboratory

New Developments in Alkaline Water Electrolysis 14
M. R. Yaffe and J. N. Murray
Teledyne Energy Systems

Investigation of Nickel Whisker Electrodes 19
P. J. Moran, G. L. Kahen, Jr., and G. E. Stoner
University of Virginia

The Oxygen and Hydrogen Evolution Reaction on Oriented Single Crystals of Ruthenium Dioxide 22
L. I. Berger, F. H. Pollak, and Y. Canives
Brooklyn College of City University of New York
W. O'Grady
Brookhaven National Laboratory

IV. HYDROGEN STORAGE SYSTEMS

Hydride Beds: Engineering Tests 26
M. J. Rosso, Jr. and G. Strickland
Brookhaven National Laboratory

Modeling Solid Hydrogen Storage Beds 31
P. W. Fisher and J. S. Watson
Oak Ridge National Laboratory

Hydrogen Storage for Automobiles 34
G. Strickland
Brookhaven National Laboratory

Hydrogen Homestead Program Review and Continuation Plan 38
R. E. Billings, L. D. Hadden, G. L. Kimball, and R. L. Woolley
Billings Energy Corporation

Development Status of Microcavity Hydrogen Storage Systems For Automotive Applications 39
R. J. Teitel
Robert J. Teitel Associates

Underground Storage of Hydrogen 43
S. M. Foh, M. Novil, P. L. Randolph, and E. M. Rockar
Institute of Gas Technology

Design, Construction and Testing of a Thermally Activated Hydrogen Chemical Compressor 48
E. Snape
Ergenics
F. E. Lynch
Denver Research Institute

V. HYDROGEN STORAGE MATERIALS

Hydrogen Storage Materials Research and Development Work at Brookhaven National Laboratory 52
J. R. Johnson
Brookhaven National Laboratory

Development of New Hydrogen Storage Systems For Automotive Hydrogen Fuel Storage 56
F. G. Eisenberg, J. J. Sheridan, III, and David A. Zagnoli
Air Products and Chemicals, Inc.

Development of Hydrogen Storage Materials for Application to Energy Needs 61
C. E. Lundin, J. Liu, and C. B. Magee
Denver Research Institute

Surface Poisoning of Metal Hydrides 64
P. D. Goodell and G. D. Sandrock
INCO Research and Development Center

VI. END-USE APPLICATIONS AND SYSTEMS STUDIES

Overview: BNL End-Use Applications Projects 68
M. Bonner
Brookhaven National Laboratory

Hydrogen Production from Small Hydropower Sites 70
E. L. Wilkinson, B. N. Kriebel, and K. J. Ramundo
Air Products and Chemicals, Inc.

Hydropowered Electrolysis in New York State 74
P. D. Mathusa and R. A. Wiley
New York State Energy Research and Development Authority

VII. CHEMICAL HEAT PUMP/CHEMICAL ENERGY STORAGE SYSTEMS

Chemical Heat Pump/Chemical Energy Storage Systems 77
T. E. Botts
Brookhaven National Laboratory

A Chemical Heat Pump Based on the Reaction of Calcium Chloride and Methanol for Solar Heating, Cooling and Storage 80
P. O'D. Offenhartz, D. Schwartz, and R. E. Malsberger
EIC Corporation

Sulfuric Acid and Water Chemical Heat Pump/Chemical Energy Storage System 83
E. C. Clark and O. M. Morgan
Rocket Research Company

The Metal Hydride Chemical Heat Pump 84
J. M. Clinch, D. M. Gruen, P. A. Nelson, C. A. Blomquist, J. S. Horowitz, G. J. Lamich, and I. Sheft
Argonne National Laboratory

VIII. NASA HYDROGEN ENERGY STORAGE TECHNOLOGY PROJECT

NASA Hydrogen Energy Storage Technology Project 89
J. H. Kelley
Jet Propulsion Laboratory

IX. SYSTEMS STUDIES AND ASSESSMENT

Assessment of Solar/Hydrogen Systems 93
W. J. D. Escher and R. W. Foster
Escher:Foster Technology Associates, Inc.
J. A. Hanson
Jet Propulsion Laboratory

Solar Hydrogen Production Via the Sulfur/Iodine Thermochemical Water-Splitting Cycle 101
J. R. Schuster, G. E. Besenbruch, H. D. Chiger, and K. H. McCorkle
General Atomic Company

A Study of Industrial Hydrogen and Syngas Supply Systems 108
W. J. Amos and J. Solomon
Air Products and Chemicals, Inc.

Hydrogen From Coal - Cost Estimation Seminar 112
R. L. Woolley
Billings Energy Corporation

X. THERMOCHEMICAL HYDROGEN PRODUCTION CYCLES

Progress Report on the Development of the General Atomic Thermochemical Water-Splitting Cycle 113
G. E. Besenbruch, J. H. Norman, K. H. McCorkle, J. S. Rode, G. Caprioglio, and R. Sharp
General Atomic Company
M. Yoshimoto
Idemitsu Kosan Company, Ltd.

Update on the Sulfur Cycle Hydrogen Production Process 117
G. H. Parker
Westinghouse Advanced Energy Systems

Studies on Thermochemical Water-Splitting Cycles 121
R. J. Remick and S. E. Foh
Institute of Gas Technology

The LASL Thermochemical Hydrogen Program Status on September 30, 1979 125
K. E. Cox
Los Alamos Scientific Laboratory

Corrosion Testing of Materials in Hot Concentrated Sulfuric Acid . . . 129
O. H. Krikorian
Lawrence Livermore Laboratory

XI. ADVANCED PRODUCTION CONCEPTS

Photoelectrochemical Decomposition of Water 132
R. D. Rauh
EIC Corporation

Studies of Solar Energy Storage Reactions Involving Polynuclear Rhodium Isocyanide Complexes 135
H. B. Gray and V. M. Miskowski
A. A. Noyes Laboratory of Chemical Physics
A. Gupta
Jet Propulsion Laboratory

Preliminary Evaluation of Processes for Recovering Hydrogen From Hydrogen Sulfide 140
R. W. Bartlett, D. Cubicciotti, D. L. Hildenbrand, D. D. Macdonald, and K. Semrau
SRI International
M. E. D. Raymont
Scitech Enterprises, Ltd.

XII. TRANSMISSION AND DISTRIBUTION

Study of the Behavior of Gas Distribution Equipment in Hydrogen Service - Phase II 144
W. J. Jasionowski and H. D. Huang
Institute of Gas Technology

XIII. CONTAINMENT MATERIALS

The Hydrogen Compatibility of Structural Materials for Energy Storage and Transmission 150
W. R. Hoover, J. J. Iannucci, J. R. Spingarn, S. L. Robinson, and R. E. Stoltz
Sandia Laboratories

The Influence of Ferrous Microstructure on the Fatigue Crack Growth Rate in Air and in Hydrogen 155
H. F. Wachob
NASA Ames Research Center

Evaluation of Laser Welding Techniques for Hydrogen Transmission . . . 160
J. Mucci and J. A. Harris
Pratt & Whitney Aircraft Group

Influences of Stress State on Hydrogen Embrittlement 167
M. R. Louthan, Jr., R. P. McNitt, T. A. Adler, J. Murali and P. E. Smith
Virginia Polytechnic Institute and State University

Near-Threshold Fatigue Crack Propagation in Pipeline Steels in High Pressure Environments 172
M. R. Mitchell, N. E. Paton, and N. Q. Nguyen
Rockwell International Science Center
R. O. Ritchie
Massachusetts Institute of Technology

Hydrogen and Fatigue Properties of Steel 176
H. H. Johnson
Cornell University

XIV. PROJECT SUMMARIES

Hydrogen Energy Storage Technology (HEST) Project
Jet Propulsion Laboratory 178

Solar/Hydrogen System Assessment
Escher:Foster Technology Associates, Inc. 179

Sulfur/Iodine Thermochemical Cycle
General Atomic Company 180

A Study of Industrial Hydrogen and Syngas Supply Systems
Air Products and Chemicals, Inc. 181

Workshop on Cost of Hydrogen from Coal
Billings Energy Corporation 182

Sulfur Cycle Hydrogen Production Process
Westinghouse Electric Corporation 183

Copper Sulfate Thermochemical Cycle
Institute of Gas Technology 184

Thermochemical Process for Hydrogen Production
University of California, Los Alamos Scientific Laboratory 185

Materials Development for Thermochemical Cycles
Lawrence Laboratories, Livermore 186

Hydrogen Production by Photoelectrolytic Solar Energy Conversion
EIC Corporation 187

Hydrogen Produced by Solar Radiation Task
California Institute of Technology 188

Hydrogen Sulfide Decomposition
SRI International 189

Study of the Behavior of Gas Distribution Equipment in
Hydrogen Service; Phase II
Institute of Gas Technology 190

Hydrogen Compatibility of Structural Materials for
Energy Storage and Transmission
Sandia Laboratories - Livermore 191

Thermal Processing Task
NASA-Ames Research Center 192

Evaluation of Laser Beam Welding Techniques
Pratt & Whitney Aircraft Group 193

Effect of Stress State of Hydrogen Embrittlement
Virginia Polytechnic Institute 194

Near Threshold Fatigue Crack Propagation in Pipeline Steels in High-Pressure Environments
Rockwell International Science Center 195

Hydrogen and Fatigue Properties of Steel
Cornell University 196

An Assessment of Hydrogen Compressor Technology for Energy Storage and Transmission Systems
University of Miami 197

Direct Thermal Water Splitting
Battelle - Geneva Research Center 198

Assessment of Thermochemical Cycles
University of Kentucky 199

Solid Polymer Electrolyte Water Electrolyzer Technology Development
General Electric Company 200

Selection and Evaluation of Materials for Advanced Alkaline Water Electrolyzers
Brookhaven National Laboratory 201

Advanced Alkaline Water Electrolyzer Development
Teledyne Energy Systems 202

Selection and Evaluation of Materials for Advanced Alkaline Water Electrolyzers
University of Virginia 203

Optical and Electrocatalytic Investigations of Oxides of Ruthenium and Iridium
Brooklyn College, CUNY 204

Selection and Evaluation of Materials for Solid Polymer Electrolyte Water Electrolyzers
Brookhaven National Laboratory 205

Hydrogen/Halogen Energy Storage System
Brookhaven National Laboratory 206

Hydrogen-Technology Advanced Component Test System (HYTACTS)
Brookhaven National Laboratory 207

Hydride-Bed Heat-Transfer Modeling Study
Oak Ridge National Laboratory 208

Modification and Operation of the Hydrogen Homestead Hydride Vessel Energy Storage System
Billings Energy Corporation 209

Conversion of Hybrid MERADCOM Fork Lift Truck from Gaseous Hydrogen Fuel Storage to a Hydride Hydrogen Storage System
Billings Energy Corporation 210

Hydrogen Storage Using Glass Microspheres for Automotive Applications
Robert J. Teitel Associates 211

FeTi Storage System for Bulk Hydrogen Storage
Foster Wheeler Energy Corporation 212

Energy Storage Systems for Automobile Propulsion
Lawrence Livermore Laboratory
Brookhaven National Laboratory 213

The Development of Metal Hydride Systems for Hydrogen Compressor Applications
Ergenics--Denver Research Institute 214

Underground Storage of Hydrogen
Institute of Gas Technology 215

Hydrogen Storage Materials Development
Brookhaven National Laboratory 216

Advanced Hydrides Technical Support
Brookhaven National Laboratory 217

Development of New Hydrogen Storage Systems for Automotive Hydrogen Fuel Storage
Air Products and Chemicals, Inc. 218

Development of Hydrogen Storage Materials for Application to Energy Needs
Denver Research Institute 219

Metallurgical Studies of Hydrogen Storage Alloys
The International Nickel Company, Inc. 220

Hydrogen Production fron Small Hydropower Systems
Air Products & Chemicals, Inc. 221

Hydrogen Production from Small Hydropower Sites
New York State Energy Research and Development Authority 222

Methanol-Based Heat Pump for Storage of Solar Thermal Energy
EIC Corporation 223

Sulfuric Acid/Water Chemical Heat Pump
Rocket Research Company 224

HYCSOS: A Two Metal Hydride System for Energy Storage and Conversion
Argonne National Laboratory 225

DOE CHEMICAL/HYDROGEN ENERGY SYSTEMS PROGRAM

Robert R. Reeves

U. S. Department of Energy

Introductory Comments

This year marks a change in the management structure of the hydrogen program. In addition, Dr. Beverly Berger, program manager for the last two and one half years, has left for greener pastures in DOE's Biomass Program. The Storage Division's funding in the hydrogen program has also changed, with a significant drop from FY 1979.

The Program is now managed at the Department of Energy's Brookhaven Area Office (BHO) by Robert Friess. The Brookhaven National Laboratory supplies support by contracting and managing projects and provides input for program planning and direction under the leadership of Al Mezzina. The Jet Propulsion Laboratory continues to provide technical guidance for the thermochemical and advanced projects area. Both laboratories perform related R and D. The Aerospace Corporation is providing support to BHO with Larry Williams at the helm.

The Chemical Heat Pump (CHP) program elements are now incorporated into these activities. Previously CHP projects were part of the thermal program. Table I indicates the management structure, the key people, and the main program areas. All of the activities are under the supervision of Bob Friess.

At DOE Washington, we now redirect our activities somewhat with emphasis on long range planning, budget preparations, and inter-Divisional coordination. We expect these changes in responsibilities to fulfill the spirit of the decentralization philosophy, which includes the transfer of program management from Washington to a field location.

We appreciate BHO and Bob Friess for taking on this new role and look forward to a productive working relationship. At the same time, Al Mezzina, Brookhaven National Laboratory (BNL), has taken on management duties in the CHP area in addition to those in hydrogen, while the Jet Propulsion Laboratory (JPL) continues with Jim Kelley assisting in fulfilling commitments to the International Energy Agencies under Annex III of the hydrogen agreement concerned with market and costing projections.

A special thanks is due to the JPL staff who played an important role in the hydrogen program over recent years. The decentralization move required restructuring of management duties, but we are pleased that we will continue to have their assistance in the program.

The Chemical Heat Pump program was managed under C. J. Swet at DOE Washington by Bill Wilson and his group at Sandia Laboratories, Livermore (SLL). At the request of SLL, the management was transferred and BNL accepted the responsibility late in FY 79 and that transfer is just about complete. C. J. has left DOE to go into private business, and we will include C. J.'s and our own thanks to the SLL group for their many years of effort in establishing and structuring the CHP program for the Storage Division.

It may be noted here that the Division of Energy Storage Systems is now under The Assistant Secretary for Conservation and Solar Energy, rather than Energy Technology, which was recently dissolved in reorganization.

At the time of writing, the official budget numbers are not available, but it appears that the FY 80 budget for hydrogen will be $4.5 million, down from about $6.3 million in FY 79, while the Chemical Heat Pump program will be about $2.2 million in FY 80 compared to about $2 million in FY 79.

Perhaps it is appropriate to close here with just a few comments concerning programmatic emphasis. Hydrogen production is considered of paramount importance, and this is meant in the context of non-fossil fuel derived energy input. The SPE Electrolyzer development project at General Electric remains the largest single effort in the program. The electrolyzer has the potential for wide use with small hydroelectric, OTEC, photovoltaics as well as with off-peak electricity. The longer-term thermochemical cycles are being emphasized for solar energy systems as well as with other high temperature energy sources.

The Chemical Heat Pump program includes both heating and cooling applications. Technologies utilizing rapid cycling systems have advantages in terms of potential rapid pay back, since they are used more. Solar powered systems with COP of 0.6 in a cooling mode, have potential to increase the effective heat energy input by 60%, reducing the required solar collectors and providing some storage capabilities in addition.

The program has a large number of projects with excellent potential to contribute to the alleviation of the nation's energy problems. Driving these projects ahead is a large number of excellent scientists and engineers, who represent not only some of the best in the country, but also some of the most enthusiastic individuals in the entire energy field.

The chemical/hydrogen program brings with it excitement, and we look forward to the exciting results again and again over the coming years.

TABLE I .

CHEMICAL/HYDROGEN ENERGY STORAGE PROGRAM

Division of Energy Storage Systems, DOE

Robert Reeves

DOE Brookhaven Area Office - R. Friess

Jet Propulsion Laboratory

Chris England
D. D. Lawson

Aerospace Corporation

Larry Williams

Brookhaven National Laboratory

Al Mezzina

Main Program Areas

Brookhaven National Laboratory

Electrolysis Projects
Chemical Heat Pumps
Hydrogen Storage

Jet Propulsion Laboratory

Thermochemical Cycles
Advanced Projects

ELECTROLYSIS-BASED HYDROGEN STORAGE SYSTEMS
OVERVIEW AND RATIONALE OF THE BROOKHAVEN NATIONAL LABORATORY MANAGED PROGRAM*

A. Mezzina

Brookhaven National Laboratory
Upton, New York 11973

ABSTRACT

The Brookhaven National Laboratory program management, monitoring and in-house research and development activities in Chemical/Hydrogen Energy Storage Systems are summarized. The program objectives aim toward development of a technological base in chemical/hydrogen storage technology while identifying near-term opportunities for technology transfer. The emphasis is on conversion of our inexhaustible resources in a cost-effective manner. Budget allocations are summarized showing electrolytic hydrogen production as the highest priority area of R and D. A Budget/Activity Summary is presented. The program organization, in accordance with a work breakdown structure, includes a newly assumed responsibility transferred from Sandia Livermore Laboratories to BNL in Chemical Energy Storage/Chemical Heat Pump Systems Development.

INTRODUCTION

The BNL FY 79 program was highlighted by the broadening of focus of its technical and management activities to include Chemical Energy Storage/ Chemical Heat Pump technology development. In the last quarter of FY 79, program management responsibility for CES/CHP work was shifted by DOE/STOR from Sandia Livermore Laboratories to Brookhaven National Laboratory. Thus, system investigations will be directed toward a more comprehensive evaluation of energy storage and use alternatives. The approach will be based upon objective and function and not necessarily constrained by ties to hydrogen as an energy carrier or working fluid.

Programmatic actions begun in FY 78 and continued through FY 79 have shifted emphasis toward near-term payoff of technology application. The primary aim is the more effective use of our renewable or abundant resources. It is recognized that universal solutions and major impacts on our energy situation are highly desirable. Yet, there is the awareness that improvements in all energy consumption sectors can be made equally effective in incremental steps through the introduction of modest, unique or special purpose energy saving technologies.

FY 79 OVERVIEW

The thrust of the FY 79 program has been directed evaluation of accomplishments as well as barriers to meeting the stated objectives. Each of the major areas of investigation has been examined with regard to the prospects of a given innovation or development to penetrate our energy infrastructure. Promises are weighed against reality.

*Research performed under the auspices of the U.S. Department of Energy.

Hydrogen Production

Engineering development of solid polymer electrolyte water electrolysis maintains the highest programmatic priority. Base technology advances have been applied to the designs and fabrication of test modules and systems. It remains for the projected systems cost and performance benefits to be verified and for markets to be identified in order to justify further development such as scale-up to larger multi-megawatt systems. Modest efforts in advanced alkaline systems have been pursued whereby advanced components have been identified and have been tested under conditions suited to attaining operating efficiency improvements. These improvements will be equated to cost and used as baseline comparison for other advanced systems.

Storage Systems and Materials

Metal hydrides have been identified as safe and effective storage materials for hydrogen. Evaluation of current state-of-the-art materials development, looking to near-term applications, steers away from bulk hydride hydrogen storage due to cost and economic considerations as applied from the U.S. perspective. Metal hydrides appear in a much more favorable light when viewed as short-term storage media operated in a rapid cycling mode. Mobile storage systems, compressors and chemical heat pumps surface as potentially economically attractive systems.

Chemical Energy Storage/Chemical Heat Pump actions taken by BNL in the last quarter of FY 79 have been directed toward maintaining the momentum of previous Sandia Livermore Laboratories' programmatic efforts. The systems under investigation include sulfuric acid-water, methanol-calcium chloride and metal hydrides. The current development status of these systems points toward: (1) cost/performance verification testing of scaled-up "design-to-cost" H_2SO_4/H_2O systems; (2) engineering development testing of pilot-scale $CH_3OH/CaCl_2$ systems; and (3) engineering design and evaluation of the "proof-of-concept" HYCSOS systems.

A new material in terms of its use in hydrogen storage systems but commercially available owing to its application as a plastic filler promises to take on the role of hydrogen bulk storage and transport media. The material comprises hollow glass microspheres (approx. 40 micron) that can be filled to pressures in excess of 6000 psi. The diffusion characteristics are such that release of hydrogen is finite but negligible at ambient temperatures with rapid release effected in the higher regimes. Preliminary characterization of these materials verifies their application potential.

Efforts in determining the viability of underground storage of hydrogen are underway and indicate positive results from a technical and engineering standpoint with some cost consideration constraints due in large part to the cost of hydrogen, per se.

End-Use Applications and Systems Studies

Procurement actions have been taken and completed regarding the demonstration of hydrogen production from small hydropower sites. All indications are that specific sites are identifiable in reasonable proximity to merchant hydrogen markets and the cost of producing hydrogen using advanced water electrolysis technology is consistent with current market requirements.

This effort has been implemented in cooperation with the Division of Hydroelectric Resource Development and hopefully sets the stage for other inter-divisional, intra-divisional and even inter-agency efforts. Hydrogen can have logical ties with technology development in solar, transportation and synfuels technology.

A modest example of inter-agency cooperation derives from a cooperative arrangement between DOE/BNL and MERADCOM, Ft. Belvoir. A metal hydride storage bed will be designed and fabricated to provide hydrogen fuel for a fuel cell/battery hybrid powered fork-lift truck under test at Ft. Belvoir. Evaluations of the subsystems' interface and performance may permit future programmatic direction consistent with the mutual objectives of the participants.

FY 80 Programmatic Guide Lines

As in FY 79, scoping activities for FY 80 will focus on the accrual of near-to-midterm benefits via early technology transfer and actions to enhance technology commercialization. Yet, BNL strongly recommends that exploratory and fundamental investigations be continued since major breakthroughs come about primarily from these high-risk longer-term activities. Project activities for FY 80 are summarized as follows:

- Hydrogen production will retain programmatic priority but key decisions regarding future direction and budget outlays will be made based upon hard cost/performance evaluations and market projections.

- Resource conversion, especially renewable resources, will be assigned a lead priority with efforts extending from small hydropower to other targets-of-opportunity such as OTEC. Hydrogen production's relationship to synfuels from coal resources should be explored in greater depth.

- Storage systems and materials development will aggressively pursue the near-to-midterm applications with cost effectiveness being a major criteria in selecting options and establishing project priorities.

- Systems studies will complete technology development specifically in the areas of safety, environmental and economic benefits. Value from an energy conservation standpoint, will be equated to costs and where negative disparities are identified programmatic or technical redirection will be recommended.

BNL PROGRAM MANAGEMENT

The budgetary breakdown for the Electrolysis-Based Hydrogen Energy Storage Program is shown in Table 1. Funding allocations to each of the areas of technology and contractor funding for specific projects are illustrated along with BNL in-house R and D and technical monitoring support.

Additional funds (527K BA, 60K BO) have been provided for in-house and contract actions in support of the Chemical Energy Storage/Chemical Heat Pump Program. In this regard, BNL has implemented procurement actions for engineering development efforts for the methanol/calcium chloride and sulfuric acid/water CES/ CHP systems at EIC and Rocket Research Corporation, respectively. Project formulation actions dealing with analytical and design efforts in connection with HYCSOS have been taken to permit Argonne National Laboratory to continue its investigation into metal hydride chemical heat pump technology.

The Budget/Activity Summary for FY 79 is provided in Table 2 summarizing management actions taken at BNL in the Chemical/Hydrogen Energy Storage Program.

The Program Organization Chart (Figure 1) identifies the work breakdown structure and project principals associated with each of the areas of technology.

FIGURE 1

PROGRAM ORGANIZATION CHART

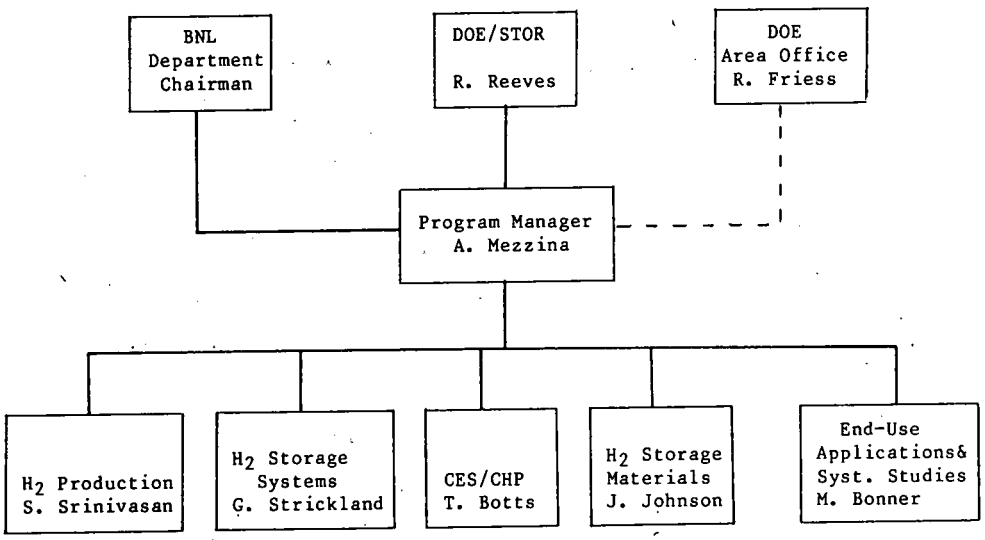

In-House

. Catalysis	. Storage Beds	.	. Ltwt Hydrides	. Tech.Assess
. Materials	. Heat Transfer	.	. Poisoning	. Econ.Assess
. Adv. Electrol.	. HYTACTS	.	. Separation	. Application

Contracts

. GE	. Billings	. RRC	. APCI	. NYSERDA
. TES	. ORNL	. EIC	. INCO	. APCI
. U. of Va.	. Foster Wheeler	. ANL	. DRI	
. Bklyn. Coll.	. IGT			
	. R.J. Teitel			

TABLE 1

CHEMICAL/HYDROGEN STORAGE SYSTEMS PROJECT
BUDGETARY BREAKDOWN

FY 79			FY 80 (Planning)		
Budget $3800K		$K	Budget $5200K		$K
H_2 Production 1900	GE	1590	H_2 Production 1600	GE	1200
	Teleyne	100		Teledyne	100
	Univ. of Va.	20*		Univ. of Va.	20
	Brooklyn Coll.	15*		Brooklyn Coll.	40
	BNL	215		BNL	230
H_2 Storage Sys. 370	Foster Wheeler	20	H_2 Storage Sys. 280	Foster Wheeler	0
	ORNL	40		ORNL	20*
	IGT	100*		IGT	-
	EDRI	40		EDRI	100
	Billings	60		Billings	30*
	BNL	245		BNL	0
				R.J. Teitel	150
H_2 Storage Mat. 330	DRI	100*	H_2 Storage Mat. 250	DRI	-
	INCO	30		INCO	100
	Air Products	50		Air Products	-
	R.J. Teitel	90		R.J. Teitel	100
	BNL	160		BNL	0
				FMI	50
End-Use Appl. 850	NYSERDA	655	End-Use Appl. 685	NYSERDA	655*
	Air Products	170		Air Products	55*
	BNL	30		BNL (FRG)	60
Chem. Heat Pumps 527	RRC	-	Chem. Heat Pumps 2000	RRC	385
	EIC	170		EIC	120*
				BNL	200
Project Mgmt.	BNL	410	Project Mgmt.	BNL	400

*Carryover/SRSA commitments

TABLE 2

BUDGET/ACTIVITY SUMMARY

Total Budget	$3,800,000
Contracts	2,200,000
Carry-over from FY 78	600,000
BNL Technical/Management Support	1,000,000
BNL	
In-house R&D	480,000
Technical Monitoring	170,000
Program Management	350,000

Activities
- Managed 18 R&D contracts (including CES/CHP)
- Evaluated 14 proposals
- Issued one major competitive procurement

Documents
- Summary Program Plan/Annual Operating Plan
- Monthly Progress Reports
- Annual Report
- Formal Program Reviews

Other
- Conducted FY 78 Contractors' Review Meeting
- Supported DOE/STOR in IEA activities
- Interaction with public and private sector

DEVELOPMENT STATUS OF SOLID POLYMER ELECTROLYTE WATER ELECTROLYSIS FOR LARGE SCALE HYDROGEN GENERATION

J. H. Russell

General Electric Company
Wilmington, Mass.

ABSTRACT

During 1979, progress continued on the joint Department of Energy, Electric and Gas Utility and General Electric Company sponsored development of the solid polymer water electrolysis technology for large scale hydrogen generation.

This program, which is aimed at achieving significant improvements in both capital cost and conversion efficiency, has progressed to the point where systems with capabilities of 500 and 2000 SCFH hydrogen are operational and are being used to evaluate multi-cell modules of 2.5 ft^2 active area cells. The systems are described and test results to date presented. Technology development in support of the scale up activities have resulted in several component design modifications to enhance sealing and improve performance. These design modifications are currently being incorporated into full sized hardware. Design of a 10 ft^2 active area cell - the next step in hardware scale up is in process. Manufacturing development of the 10 ft^2 is anticipated to begin in 1980 after demonstration of 2.5 ft^2 cells in a full 2000 SCFH module.

Background

The solid polymer electrolyte water electrolysis technology development for large scale hydrogen generation began in 1975 with a design study for Brookhaven National Laboratory (BNL) and has progressed since then under the sponsorship of the Department of Energy (DOE), the New York State Energy Research and Development Authority (NYSERDA), the Niagara Mohawk Power Corporation (NMPC), the Empire State Electric Energy Research Corporation (ESEERCO), the Gas Research Institute (GRI) and the General Electric Company.

The general goals of the program, established on the basis of the 1975 BNL study of a 58 MW system, are:

- Overall system efficiency 85-90%
- System capital cost (battery limits) - <$150/KW equivalent (1980 dollars)
- Life - Cells 40,000 Hrs
- System Life 20 Years
- Scale Up 2.5 ft^2, 10 ft^2
- Program Goal 5 MW Demonstration System

The overall milestone chart for the program is shown in Figure 1, the heavy lines indicating the present status.

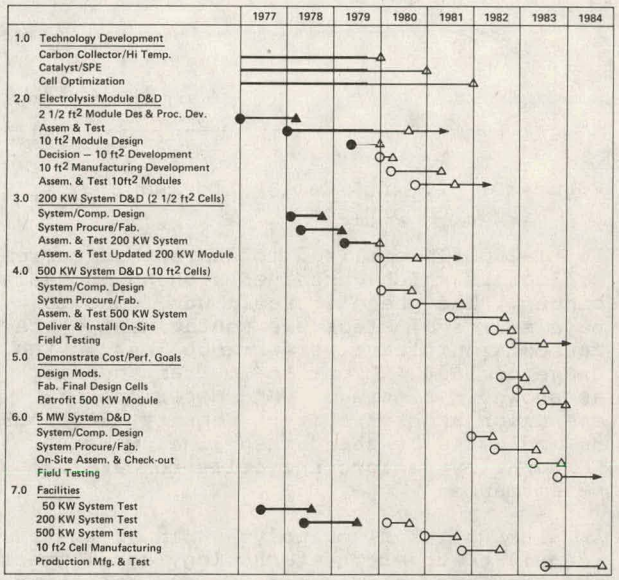

Figure 1. Major Milestones - Bulk Hydrogen Generation Program

2.5 ft^2 Cell Evaluation

Operational evaluation of full sized 2.5 ft^2 cells in a 50 KW test bed system which had begun late in GFY 78, continued throughout GFY 79. A total of 17 modules, containing from 1 to 12 cells, were tested with more than 2500 operational hours logged during GFY 79. Figure 2 shows a 2.5 ft^2 module on test in the 50 KW test system. As a result of this testing, design modifications aimed at improved performance, improved water flow and improved sealing were identified and are being incorporated into the 2.5 ft^2 hardware.

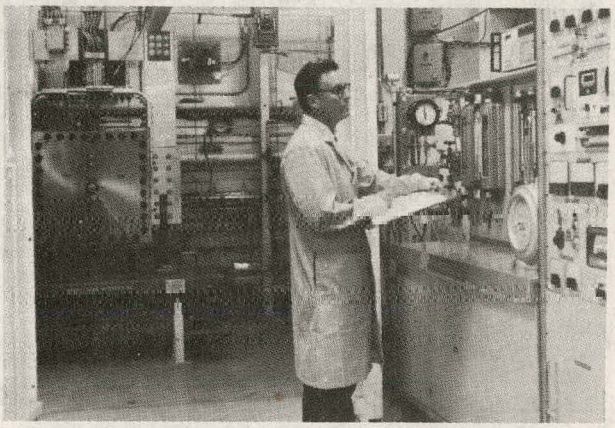

Figure 2. 2.5 ft^2 Module on Test in 50 KW Test Bed System

Performance

Figure 3 summarizes the performance demonstrated by full sized 2.5 ft^2 cells at 180°F during GFY 79.

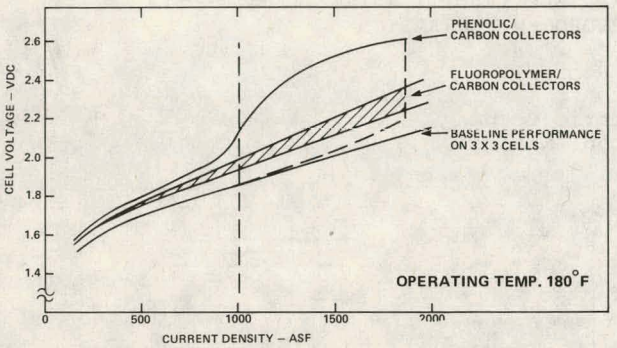

Figure 3. 2.5 ft^2 Cell Performance Comparison

Initial cells utilized molded carbon current collectors which contained a phenolic resin binder. The phenolic resin was found to be a source of electrode contaminant which caused significant performance loss in the range of 1000 AMP per ft^2 current density as shown in Figure 3. Short periods of operation at high current density (2000 ASF), as indicated by the dashed line, would temporarily restore the cells to baseline performance.

An alternative fluoropolymer binder was identified under the technology development program which eliminated the contamination and offered a significantly shorter molding cycle and thus reduced cost.

Full sized 2.5 ft^2 collectors utilizing the fluoropolymer/carbon mixture were successfully molded and demonstrated stable and improved performance in the range of 1000 ASF as can be seen in Figure 3. However, the resistance of the initial fluoropolymer collectors was relatively high with the protective foil to carbon/fluorocarbon interface being a major contributor. This interface is currently being optimized.

Water Flow

In the 2.5 ft^2 size modules, it was found that the 1 mil thick perforated titanium foil anode support allowed sufficient deflection into the oxygen/water flow field to cause increased pressure drop and reduced water flow which restricted operation at the higher current densities.

Under the technology development program, techniques to fabricate an alternative porous titanium plate anode support were developed. This type of support provides significantly improved anode support and, as shown in Figure 4, greatly reduced oxygen side pressure drop and improved water flow.

Cell Sealing

With the initial collector configuration, practical flatness tolerances in the molded collector led to marginal sealing even with extensive application of heat and compression pressure. The use of force amplifiers (sealing ridges) around the internal manifold ports and around the periphery of the collector were shown to improve sealing. The collector molds have been modified to produce molded-in force amplifiers, shown in Figure 5. Evaluation of collectors molded with force amplifiers will take place in the near future.

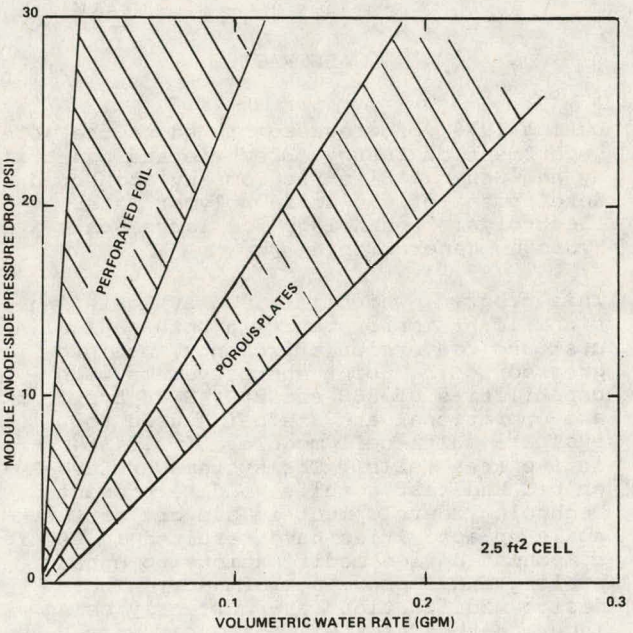

Figure 4. Effect of Various Anode Supports on Feed Water Flow

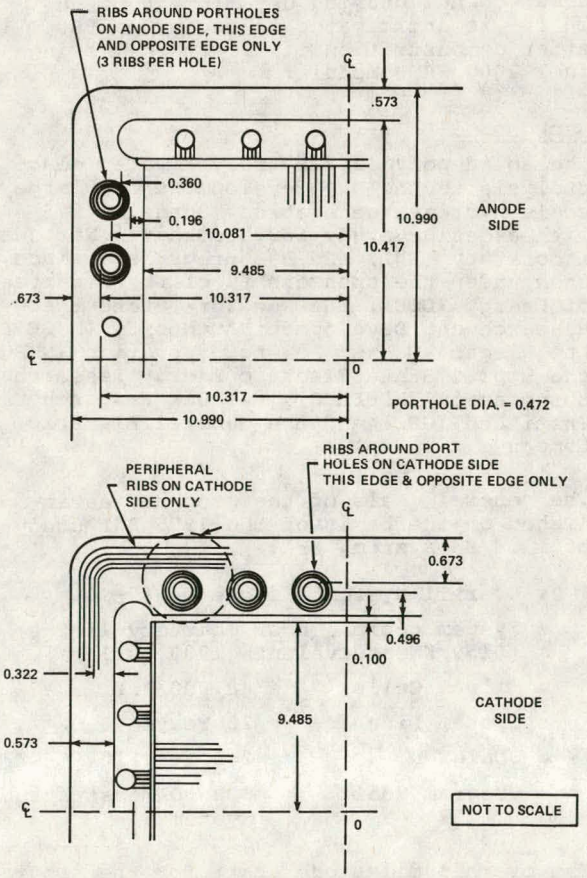

Figure 5. Collector Dimensions and Rib Locations

200 KW System

During GFY 1979, assembly and checkout of a 200 KW (2000 SCFH) system was completed.

The system schematic is shown in Figure 6. The system is modularly constructed and arranged as shown in Figure 7. Photographs of the main fluid control console and the electrical control console are shown in Figure 8 and 9 respectively. The system is fully monitored and configured with automatic shutdown provisions for safe, unattended operation.

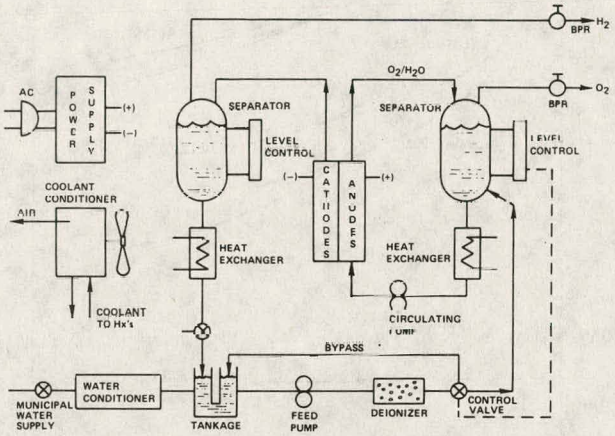

Figure 6. 200 KW System Schematic

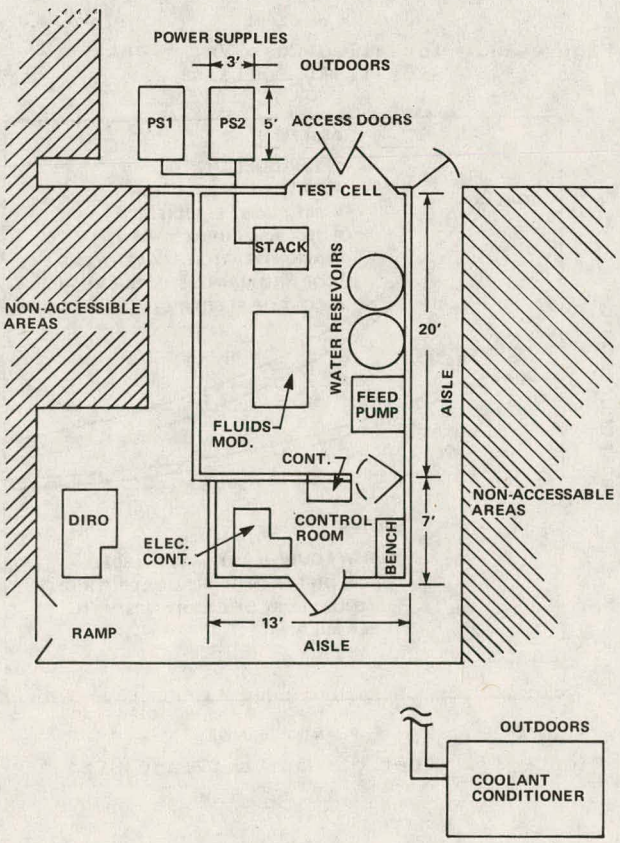

Figure 7. 200 KW System Layout Scale Drawing

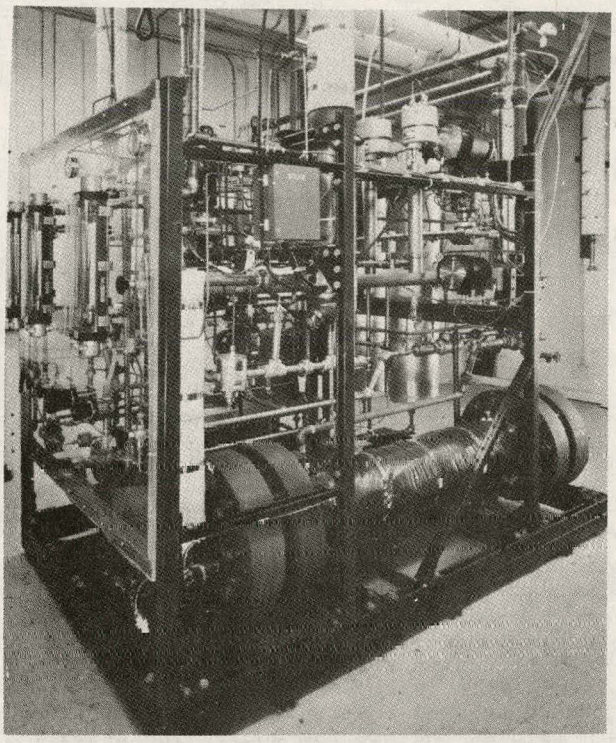

Figure 8. Fluid Component Sub Assembly

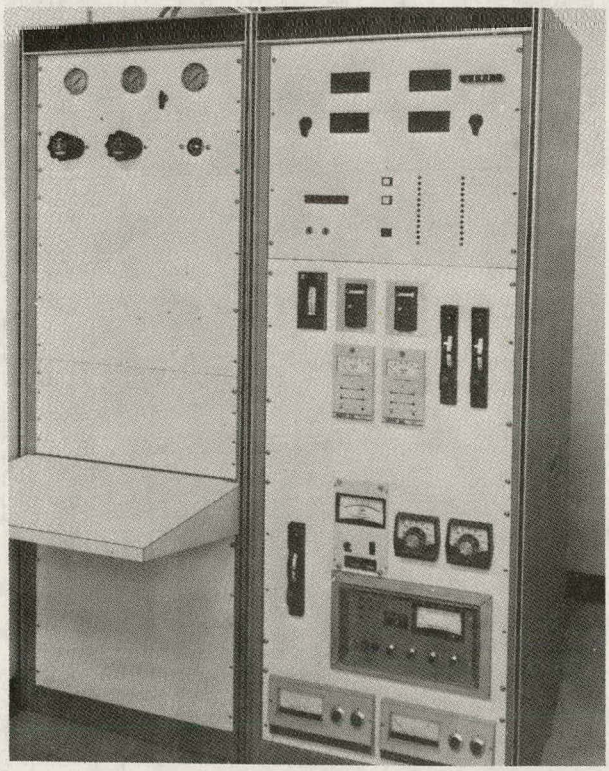

Figure 9. Electrical Control Console

The system has been operated using 6 cell (25 KW) modules for over 500 hours to date with no major difficulty. The majority of this time has been unattended operation.

It is planned to test a full 200 KW module in this system early in 1980.

10 ft^2 Cell Design

The next step in scale up - or cell with 10 ft^2 active area - is well underway. The collector design has been completed and design of the end plates, fluid plates and the remaining compression hardware is in progress. The cell is rectangular with overall dimension of approximately 75" x 24". The rectangular shape was selected based on anode side pressure drop, manufacturing process and material availability considerations.

Projected Production Cost

The results of the technology development program to date is shown in Figure 10. The present technology represents a 79% cost reduction relative to the 1975 base line. This is approximately 85% of the way toward the 93% cost reduction established in 1975 as the program goal. The primary cost reductions have been in the areas of current collectors and catalytic electrodes. To date, no suitable lower cost electrolyte material has been identified.

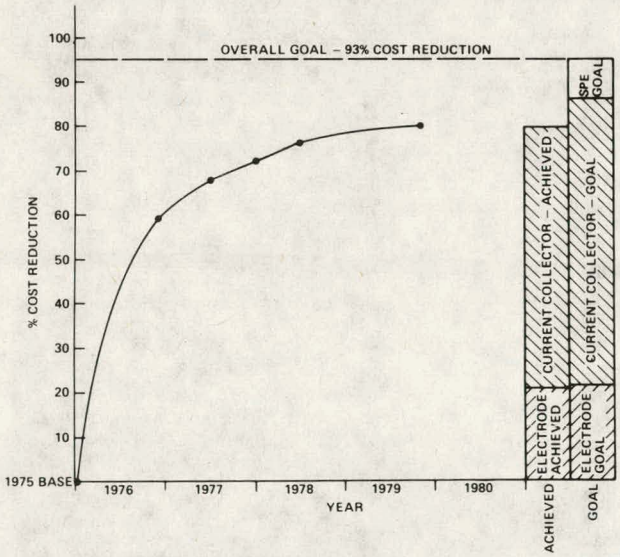

Figure 10. Electrolyzer Module Cost Reduction Resulting from Technology Development Program

The impact of the present technology versus goal electrolyzer cost on installed plant cost and cost of generated hydrogen (in 1980 dollars) is shown in Figures 11 and 12 respectively.

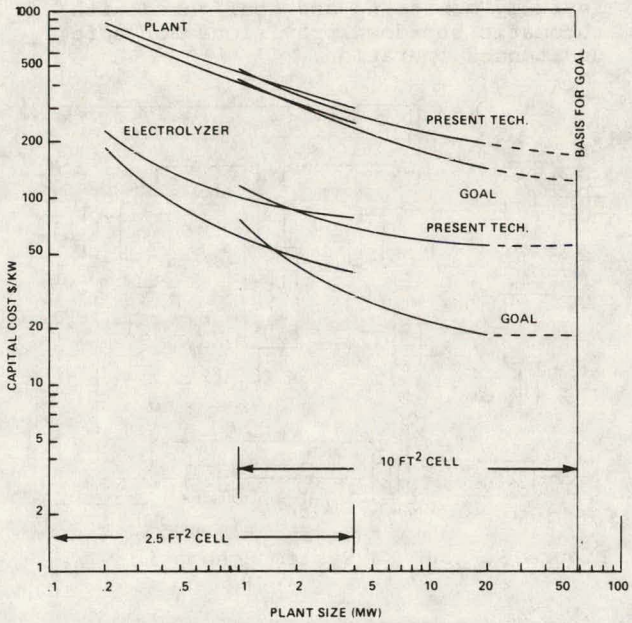

Figure 11. Installed Cost Vs. Plant Size (1980 Dollars)

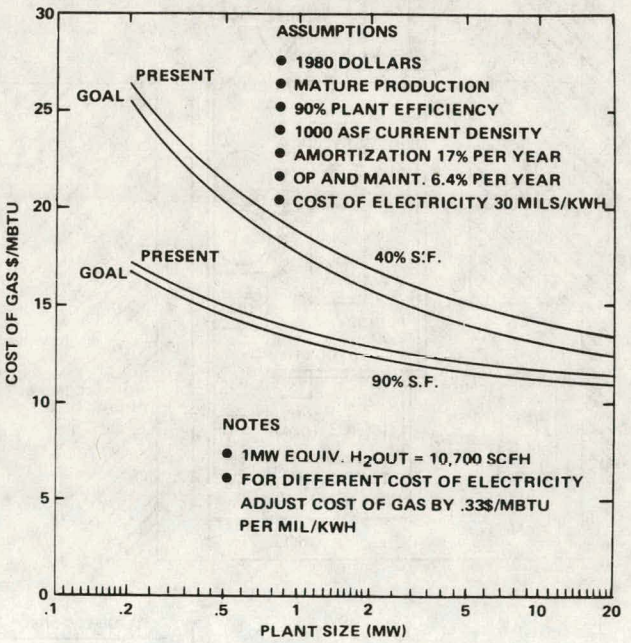

Figure 12. Cost of Gas Vs. Plant Size

SELECTION AND EVALUATION OF MATERIALS FOR ADVANCED WATER ELECTROLYZERS

S. Srinivasan, R.S. Yeo, G. Kissel, E. Gannon,
F. Kulesa, J. Orehotsky and W. Visscher

Department of Energy and Environment
Brookhaven National Laboratory
Upton, New York 11973

Abstract

Efforts are being made to find better and more stable (i) anode electrocatalysts for solid polymer electrolyte water electrolyzers and (ii) cell components (e.g., electrodes, separators) for advanced alkaline water electrolyzers. Of several mixed oxides of ruthenium examined as anode electrocatalysts in 1 N H_2SO_4, the ternary system (Ru-Ir-Ta) shows most promise. Most of these mixed oxides, prepared by the thermal decomposition method, exhibit low Tafel slopes for oxygen evolution. As with Pt and Ir, multicycling of a Ru-Ir electrode in H_2SO_4 produces a thick oxide layer, as ascertained ellipsometrically, with enhanced electrocatalytic activity for oxygen evolution. High surface area nickel or mild steel and nickel whisker electrodes reduce cell potentials for water electrolysis in alkaline electrolyte by about 100 mV. Composite barrier structures show prospects of improving chemical and mechanical stabilities of separators in alkaline electrolyte. The FY 1980 projects will consist of (i) assembly of LEED-Auger-ESCA system and development of methods to correlate electrocatalytic activity and surface properties; (ii) examination of promising ruthenium based mixed oxide electrocatalysts in single cells; (iii) electrochemical-ellipsometric investigation of Ru-Ir and Ru-Ir-Ta alloys; (iv) elucidation of role of hydrogen permeation in metals on time variation of hydrogen overpotential; (v) improvement of electrode configuration to lower overpotential losses; and (vi) examination of composite barrier materials.

1. Introduction

The activities at BNL during the year were concentrated in two areas: (i) finding better and more stable anode electrocatalysts for the General Electric Solid Polymer Electrolyte (SPE) Water Electrolyzer and (ii) evaluation of some materials as electrocatalysts or separators for advanced alkaline water electrolyzers. The Hewlett-Packard Data Acquisition System was programmed to collect and plot the results of current-potential measurements in four cells simultaneously. This included half and single cell measurements. The slowness of the oxygen electrode reaction is the major cause of efficiency losses in water electrolyzers(1). The overpotential for this reaction is at least 300 mV during acid or alkaline water electrolysis at desired current densities. A second problem, needing solution, is the increase of cell potential for water electrolysis with time. In acid electrolytes, this phenomenon is due to increase of oxygen overpotential with time while in alkaline electrolyte it is predominantly due to an increase of hydrogen overpotential(2). Efforts are in progress to elucidate the mechanism of time variation of overpotential and develop methods for its inhibition at BNL and the University of Virginia (UVA).

2. Anode Electrocatalysts for Solid Polymer Electrolyte Water Electrolyzers

2.1 Ruthenium Based Mixed Oxides

With the aim of stabilizing ruthenium based electrocatalysts for SPE water electrolyzers(3), mixed oxides of ruthenium with Ta, Zr, Hf, Ir, W, La, Mn, Pb and Sr were prepared by the thermal decomposition method on a titanium substrate and were examined as oxygen evolution electrocatalysts in 1.0 N H_2SO_4 at 25°C. With some of these oxides, the current-potential plots, obtained using the slow potential sweep technique, exhibit hysteresis, as shown in Figure 1 for $WRuO_x$. This behavior is characteristic of electrodes at which there is a time variation of overpotential. The mixed oxide $LaRuO_x$ behaved in a similar manner while the hysteresis was not observed with the other mixed oxides. The current-potential relations for oxygen evolution on RuO_x, IrO_x, $IrRuO_x$, $TaRuO_x$, $Ta_{0.5}Ir_{0.5}RuO_x$ and $TaIr_{0.5}Ru_{0.5}O_x$ were obtained using steady state techniques and the Tafel lines are shown in Figures 2 and 3. The time variation of overpotential at a constant current density of 50 mA cm^{-2} is considerably less on the binary and ternary oxides than on RuO_2. Elucidation of the mechanism responsible for improving and stabilizing the electrocatalytic activity of ruthenium by alloying with tantalum and iridium oxide awaits a detailed study of both the surface states and phase diagram of the TaIrRu oxide system.

2.2 Electrochemical and Ellipsometric Studies on Ru-Ir Alloy

A combined electrochemical-ellipsometric method was used with the aim of (i) drawing correlations between electrocatalytic and optical properties of oxide films formed on surfaces and (ii) elucidating the mechanism of the time variation of overpotential. Investigations were made on a Ru-Ir alloy (50-50 atomic percent) in 1.0 M H_2SO_4. Preliminary results showed that oxygen evolution kinetics can be improved by multicycling of the electrode between 0.1 to 1.5 volts vs DHE. Similar effects were observed with multicycling of Pt and Ir electrodes(4,5). A Tafel slope of 60 mV/decade was obtained, as shown in Figure 4. The performance improvement is attributed to the growth of oxide layer with thickness of about 30 Å. This layer is enriched in $Ir(OH)_3 \cdot XH_2O$ due to preferential dissolution of Ru. The oxide layer dissolved when oxidized at higher anodic potentials (say 2.1 volts vs DHE) and the resulting oxide layer is a poorer electrocatalyst. A Tafel slope of 80-85 mV/decade was observed on this oxide layer. In contrast to the oxide formed on Ir metal, this oxide layer on the Ru-Ir alloy cannot be reduced completely even at high cathodic potential which indicates the presence of ruthenium oxide. However, the composition of Ru in the oxide layer is lower than that in the bulk material.

3. Materials for Advanced Alkaline Water Electrolyzers

3.1 Anode and Cathode Electrocatalysts

During the reporting period, beryllium copper nickel alloy (0.44 Be, 30.25 Ni, 69.31 Cu), obtained from Kawecki Berylac Industries (KBI), high surface area nickel deposited on mild steel (from International Nickel Company-INCO) and nickel whisker electrodes with a high surface area deposited on mild steel from UVA were evaluated as electrocatalysts. The beryllium copper nickel alloys exhibited higher anodic and cathodic overpotentials than nickel. The high surface area nickel electrodes from INCO and from UVA were tested only as anodes. The deposited electrodes should be on nickel screens to be evaluated as cathodes. These high surface area nickel electrocatalysts showed a lowering of activation overpotential and merit further investigations at BNL in small cells and at Teledyne Energy Systems (TES) in the 5-cell test rig. The whisker electrodes showed a peculiar behavior in that there was a lowering of hydrogen overpotential, which further decreased with time. This was attributed to the observation that black deposits of nickel were found on the cathode. This process could have occurred only by disintegration or dissolution of the nickel particles from the high surface area whisker anodes and subsequent deposition of the nickel ions or particles in the electrolyte on the cathode.

3.2 Separators

There was a modest effort to develop sandwich barrier materials of asbestos coated on both sides with Teflon bonded potassium titanate. This type of approach may serve a two-fold purpose - mechanically stabilize Teflon bonded potassium titanate and chemically stabilize asbestos - in advanced alkaline water electrolyzers operating at temperatures above 100°C. A Mallory suggestion of asbestos sandwiched between Permion 300 showed a high electric resistance. Tin hydrosol treated asbestos from UVA increased the cathode overpotential. Polybenzimidazole (PBI), although acceptable as far as electrolyte resistance is concerned, showed poor physical stability.

4. Proposed Studies for FY 1980

The major tasks in FY 1980 will be (i) the assembly of the LEED-Auger-ESCA system and (ii) the development of methods using this instrument for identifying the chemical nature of metallic and non-metallic electrocatalysts before and after electrolysis and for elucidation of effects of crystallite size, orientation and alloying on electrocatalytic activities. A detailed electrochemical-ellipsometric investigation on Ru, Ru-Ir and Ru-Ir-Ta will be made to draw correlations between the electrocatalytic activities for oxygen evolution and optical properties of the oxide films formed on these substrates in the potential region for oxygen evolution in acid electrolytes. The promising ruthenium based mixed oxide anode electrocatalysts will be tested in acid electrolyte single cells at BNL. Recommendations will be made to the General Electric Company for further evaluation of these materials in SPE water electrolyzers. Investigations will be initiated to screen and evaluate low cost membranes as substitutes for the expensive Nafion in SPE water electrolyzers. Efforts will be made to elucidate the role of hydrogen permeation in metals (e.g., nickel) on the mechanism of time variation of hydrogen overpotential in alkaline electrolyte. The prospects for reduction in overpotential losses in alkaline water electrolyzers by changes in electrode configuration will be examined. Composite barrier materials will be further developed and tested in this electrolyte medium.

ACKNOWLEDGEMENTS

This work was carried out under the auspices of the U.S. Department of Energy. Dr. W. Visscher from the Technical University, Eindhoven, Netherlands and Dr. J. Orehotsky from Wilkes College, Wilkes-Barre, PA. were Visiting Scientists at BNL in the summer of 1979. The authors are grateful to Dr. S. Gottesfeld from Tel-Aviv University, Israel, a consultant on our program, and to Drs. J. McBreen and W.E. O'Grady for helpful discussions and suggestions.

REFERENCES

1. P.W.T. Lu and S. Srinivasan, "Advances in Water Electrolysis Technology," J. Appl. Electrochem. 9:269(1979).

2. G.E. Stoner and P.J. Moran, "Energy Losses Occurring in Alkaline Electrolyzers," Proc. of the Symposium on Industrial Water Electrolysis, S. Srinivasan, F.J. Salzano and A.R. Landgrebe (eds.), The Electrochemical Society, Princeton, N.J. 78-4:169(1978).

3. S. Srinivasan, "Selection and Evaluation of Materials for Advanced Water Electrolyzers," Proc. of the DOE Chemical/Hydrogen Energy Systems Contractor Review, Conf-781142, 27(1979).

4. S. Gottesfeld, M. Yaniv, D. Laser and S. Srinivasan, "Optical and Electrocatalytic Properties of Oxide Layers," J. de Physique. Colloque C5:145(1977).

5. S. Gottesfeld and S. Srinivasan, "Electrochemical and Optical Studies of Thick Oxide Layers on Iridium and their Electrocatalytic Activities for the Oxygen Evolution Reaction," J. of Electroanal. Chem. 86:89(1978).

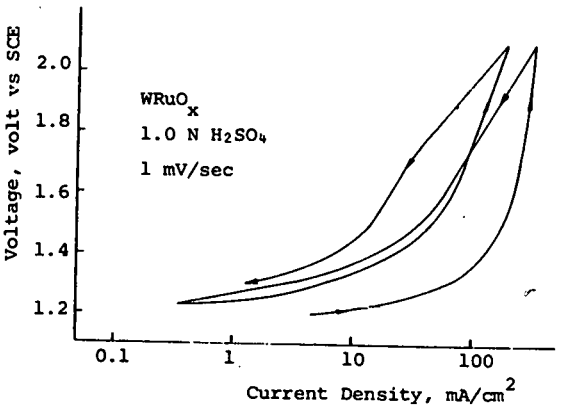

Figure 1. Voltage-current relationship for oxygen evolution reaction for $WRuO_x$ in 1.0 N H_2SO_4 at 25°C. Sweep rate: 1 mV/sec.

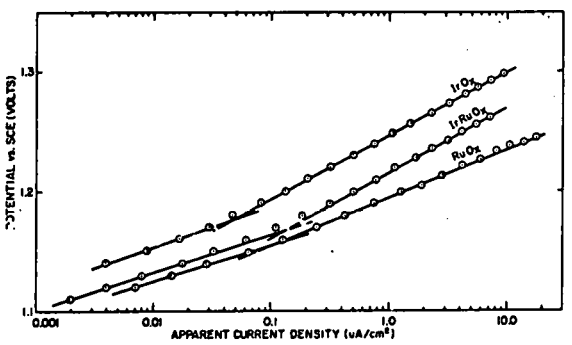

Figure 2. Tafel plots for oxygen evolution on IrO_x, $IrRuO_x$ and RuO_x in 1 N H_2SO_4 at 25°C.

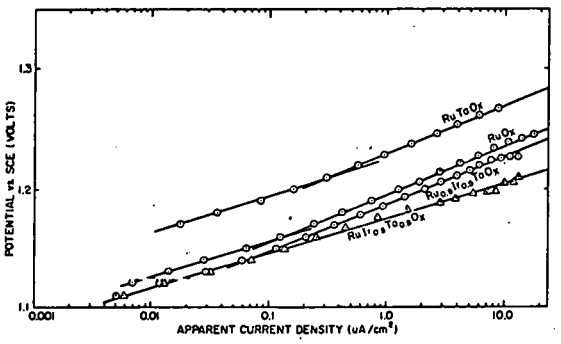

Figure 3. Tafel plots for oxygen evolution on RuO_x, $RuTaO_x$, $Ru_{0.5}Ir_{0.5}TaO_x$ and $RuIr_{0.5}Ta_{0.5}O_x$ in 1 N H_2SO_4 at 25°C.

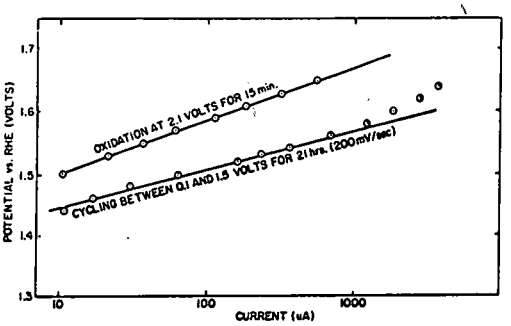

Figure 4. Tafel plots for oxygen evolution on oxides formed on Ru-Ir alloy in 1 M H_2SO_4 at 25°C.

NEW DEVELOPMENTS IN ALKALINE WATER ELECTROLYSIS

M. R. Yaffe and J. N. Murray
Teledyne Energy Systems
110 West Timonium Road
Timonium, Maryland 21093

Abstract

Work toward the advancement of alkaline water electrolysis technology has proceeded at Teledyne Energy Systems (TES) under contracts BNL 380750-S and BNL 480421-S during Government Fiscal Year (GFY) 1979. Operation of asbestos electrode separator cells for over 1000 hours at 100 C was demonstrated which included several short term periods at 125 C. Using the TES-C-110 cathode technology, cell voltages of 1.83 V at 450 ma/cm^2 and 100 C with negligible performance degradation was recorded for periods of over 1000 hours. Ten alternative advanced cathodes and anodes were tested during the year. The best performance observed was from cells containing the recently available, inexpensive TES-C-AN cathodes and nickel screen anodes (1.73 V at 100 C, 450 ma/cm^2). This value represents a 17% voltage improvement and allowed H_2 production at 86.5% thermal efficiency. Testing of polybenzimidazole (PBI) separators in the 5-cell, 300 cm^2 test module was also initiated. Summaries of the electrolysis cell component testing is presented in this report as well as preliminary plans for work in GFY 1980.

I. Introduction

Teledyne Energy Systems (TES) is a major manufacturer of water electrolysis systems for the production of high purity hydrogen. The current generation of TES technology utilizes a low temperature (60 C), medium pressure (100 psig), alkaline solution (25 w/o KOH), bipolar plate style electrolysis modules. For the last three years, TES has been involved in an alkaline water electrolysis technology development and testing effort in conjunction with the Brookhaven National Laboratory (BNL)/Department of Energy (DOE) hydrogen energy program. This report presents a review of work done on this effort during the Government Fiscal Year (GFY) 1979, and outlines the anticipated effort for GFY 1980.

The major thrust of the advanced alkaline electrolysis program has been to increase process efficiency along two lines, first by electrolyzing at higher temperatures, and second by demonstrating higher efficiency electrocatalysts, electrode structures, and separators.[1] Concomitant with this is the need to demonstrate better overall process economics as measured by the cost of the product, hydrogen gas.

The commercial baseline technology described above utilizes relatively low surface area nickel screen electrodes and relatively thick (0.075 cm) chrysotile asbestos as the interelectrode separator. The nominal current density for this design in TES commercial single irriguous (single flowing electrolyte) hardware is 373 ma/cm^2, corresponding to a cell voltage of greater than 2.2 volts or a voltage efficiency of less than 67%.[2] In early BNL contracted experiments, a baseline cell voltage of 2.07 V at 100 C and 450 ma/cm^2 was established using the "ARIES" (Applied Research Industrial Electrolysis System) in which both sides of the cell are supplied with electrolyte.[3] This value corresponds to a 71% voltage efficiency at a temperature of 100 C based on a 100% thermal efficiency equivalent to 1.48 volts.

The program in GFY 1979, briefly summarized in this report, was undertaken in two separate contracts, BNL 380750-S which was concluded on 30 April 1979 and BNL 480421-S which was started on 17 April 1979 and continues to date. The work itself can be separated for discussion purposes into three areas: (a) advanced electrode and separator screening tests, (b) extended advanced component testing, and (c) the hydrogen economics study. The results and detailed analysis from the evaluation of the first five electrode screening modules were recently summarized.[1, 4] This report will restate the major findings from that task and include the results from the most recent screening module (Module #11). One additional module was constructed (Module #12), however, evaluation was not started at the time of submittal of this report.

II. Advanced Component Screening Tests

As the increase in operating temperature of the electrolysis process itself resulted in an increase of (thermal) voltage efficiency to only 71% at 100 C using conventional technology, the attention was shifted to improvements via electrodes and electrocatalysts. A series of six advanced electrode screening modules were assembled and tested. These tests were conducted the ARIES system. For each screening test, two distinct pairs of advanced electrode cells and one baseline cell were assembled into a five-cell module. Each module was subsequently put on test in the ARIES system for periods of up to three weeks. Of the six electrode screening modules, three were dedicated to anode, and three to cathode evaluation. The normal operating procedure for these tests was to conduct specific module and individual cell characterizations such as cell voltage vs imposed current, voltage (at constant current) vs operating temperature, and voltage (at constant current) vs operating pressure. The electrolysis module was kept operating between these experiments and the normal system conditions were 50 psig gas generation pressure, flowing electrolyte of 25 w/o KOH at 100 C and module current of 135 amp (450 ma/cm^2). Table 1 summarizes the basic components of each screening module tested to date.

To compare the results of the various tests, the current-voltage data were broken down into linear and logarithmic portions using a least square regression about an equation of the form,

$$V = E + S \cdot \log (I) + I \cdot R \qquad (1)$$

where I and V are current and voltage, and E, S, R are best fit parameters roughly corresponding to electrode potential terms (E + S · log I) and a resistive term (I · R). The results of the analysis of the current-voltage curves at 100 C are summarized in Table 2. The table quotes values of total voltage at 135 amp (450 ma/cm^2) cell potential at 135 amp, and total cell pseudo-Tafel slope and resistivity independently. The values are averaged from many experiments; all data are from time stabilized modules with values taken after 10 hours operating time.

Anode Results and Discussion

Five different "advanced" anodes were tested in three screening modules along with cells containing the baseline nickel screen anode. Three different electrode structures were tried, these being (a) catalyst applied to the baseline nickel screen, (b) thermally sintered nickel powder (battery plaque), and (c) Teflon-bonded powder structures. Perhaps the most significant, although not encouraging, result from these cells was the lack of significant change in the potential or "I-R free" cell voltage term in the current-voltage curves among all the anodes. The best cell among the anodes tested was a Teflon-bonded cobalt nickel oxide spinel (Co_2NiO_4 - 40 mg/cm^2) purchased from Dr. A. C. C. Tseung of the City University, London. The improvement, ~80 to 90 mV, however, seemingly resulted from a low cell internal resistance rather than a truly catalytic effect suggested by the supplier.[5] More will be said about the cause of this effect later. It should be noted that the mathematically derived "R" term is a true resistance only insofar as Eq. (1) is a valid cell model and therefore some electrode effects may show up in the linear term. One certainly does not expect a Teflon-bonded semiconductor like Co_2NiO_4 to be more conductive than a pure metal screen. What was more telling is the analysis of results from the A-010-00 and A-010-10 anodes. These TES electrodes were similar Teflon-bonded powder structures, the first having only a 100 mg/cm^2 nickel powder loading as active material while the second had 90 mg/cm^2 Ni powder mixed with 10 mg/cm^2 Co_2NiO_4 catalyst also prepared at City University. The net voltage difference between the two formulations was only 5 to 10 mV, which in a cell configuration like the ARIES module is well within the measurement uncertainties caused by other factors. Therefore, little significant electrochemical benefits can be attributed to the freeze-dry prepared Co_2NiO_4. To summarize the results of the anode testing to date, no significant anode improvement has been demonstrated--or stated another way, the TES baseline screen anode is reasonably effective and superior in price relative to the other structures tested.

Cathode Results and Discussion

Definitely more encouraging than the anode testing, the advanced cathode work showed several relatively low cost cathodes significantly better than the baseline technology. All of the cathodes tested were based on catalysis and/or surface roughening processes applied to baseline nickel screen. The nickel boride technology (Ni_2B) is a proprietary process supplied by Deutsche Automobilgesellshaft (DAUG). The C-110-0, C-110, and C-110-A processes are all TES proprietary technologies similar in concept to each other, the latter two containing an additional light noble metal catalyst loading (<1 mg/cm^2 PT). The C-AN structure also involves a proprietary process and was supplied to TES.

According to results seen in cathode screening module testing, the best total cell voltage obtained was with the C-AN structures and the observations were as low as 1.71 volts (η_v = 87%) at 100 C and 450 ma/cm^2. This compares to a baseline cell voltage of 2.07 V (η= 71%) at the same current density and temperature. The module (#11) showing this performance contained plain wire screen anodes, asbestos separators and included the TES-C-110-A cathodes for comparison.

The internal resistance question mentioned in the anode discussion occurs in the cathode results also. From in-house studies done recently at TES, the separator compression has been indicated as a major source of this variability. In view of this, the cell components for module #11 were carefully chosen to yield an asbestos thickness of 0.038 ± 0.008 cm as opposed to past compression thicknesses of 0.046 ± 0.010 cm. The baseline cell of this module showed ~125 mV improvement at standard operating conditions over the average of previous baseline results and had a resistance of 1 mΩ compared to a value of 1.6 mΩ found with previous baseline cells. This compressive effect could also serve to explain the slightly favorable results from the Teflon-bonded Co_2NiO_4 anode cells as that electrode, being thicker than the baseline screen, would also increase the asbestos compression.

The temperature effect on voltage measured on the screening tests was also significant in that all cells, the baseline included, show similar $\Delta V/\Delta T$ values. The value obtained at 450 ma/cm^2 was -4.5 mV/C ± 0.5 mV/C. This slope was fairly constant over the 75 C to 125 C range with no sign of flattening out as the temperature approaches 125 C. This implies that a potential voltage reduction in the 100 to 125 mV/cell range is possible by operating at 125 C.

Separator Studies

At the time of writing, construction of the first high temperature separator screening module, module #12, was completed. The experimental separator material to be tested is polybenzimidazole (PBI) paper. This paper is 0.025 cm thick and prepared by Kimberly-Clark, Schweitzer Division, from a PBI fibrid developed and produced by Celanese Corporation. The PBI paper was tested by TES in a 50 cm^2 cell earlier this year in order to demonstrate viability with respect to the following questions: (a) Can the 0.025 cm thick material be used in multiple layers (since the asbestos is 0.076 cm thick? (b) Can the edges of the separator be adequately sealed? (c) Is the resistivity much greater than asbestos of a similar porosity? (d) Is the plastic stress creep phenomenon of manageable proportions? (e) Does the material rapidly decompose or begin to cross leak at low differential pressures? and (f) Can PBI be handled, i.e., is the physical integrity of the material adequate?. The results from limited testing have shown that none of these concerns have been manifest with the PBI separator and therefore the preliminary results were extremely encouraging. The thermal stability of wet PBI in KOH/O_2 and H_2 environments has been demonstrated in earlier studies and was reported last year.[6, 7]

The module was designed for PBI compression of 3 layers, 0.025 cm thick each, compressed to a final thickness of 0.038 cm. Electrodes will be three TES-C-110 cathodes, two nickel wire screen baseline cathodes, and conventional wire screen anodes. The testing will emphasize evaluation of the cell resistance relative to the asbestos separator cells and the test results will be discussed during the oral presentation.

III. Extended Testing - Modules #9 and #10

The major portion of Task 1, Contract 480421-S, consisted of an extended test of the best advanced electrodes seen to date. The cathodes chosen were TES-C-110 cathodes while the anodes were TES-A-010 type. These anodes were chosen not so much because they were "good" electrochemically but because they represent a well characterized and controlled test of the PTFE Teflon-bonded powder technology. There has been concern that the PTFE-bonded powder electrodes will not withstand the rigors of a hot KOH, O_2 evolution environment. The cathode was chosen as the best

available at the time since this choice was made before cathode screening module #11 was tested. The inter-electrode separators were asbestos.

The first module, module #9, was assembled incorrectly which resulted in deformed endplates. Proper endplates were then used for construction of module #10, and the result was much more reasonable with respect to voltage, the first three cells being very low (1.8 V at 450 ma/cm^2, 100 C) and the last two being somewhat worse than anticipated (1.89 and 1.93 V, at 450 ma/cm^2, 100 C). Although it has not been definitely proven, it is believed that these last cells again suffered from inadequate compression which subsequently resulted in the higher calculated cell resistance.

This module was tested in ARIES for over 1000 hours at temperatures up to 125 C and current densities up to 1000 ma/cm^2 with a few data points at current densities of 2 A/cm^2. Figure 1 shows an average (of all cells) performance over the test life of module #10. It is important to note that no significant degradation of module performance, especially in the first three cells, was seen during the course of the test. Figure 2 gives a representative set of volt-amp curves (average of first three cells) at various temperatures, again the test results confirmed the expectations from the screening tests. The module itself has not been disassembled for inspection as yet, pending a decision to subject it to further testing.

IV. Engineering Design and Economic Study

Task 2 of Contract 480421-S has just recently started. The goal of this task is the development of an alkaline water electrolysis system economic and design model. The need for this computational tool is apparent since the ultimate goal of the program is the reduction of the price of hydrogen product gas, and not the development of high efficiency systems, per se. It may be the case in many applications that a low efficiency, low capital cost system yields the lowest gas price (e.g., small systems, low electric rates, high interest rates), whereas in other applications, energy efficiency may be the overriding factor. The choice in most cases will not be obvious.

The Fortran-coded computer program will be used to optimize electrolytic hydrogen system design and to predict the cost of product gas given a set of input factors described in Table 3. This model will then be applied to several cases of interest describing advanced and baseline technology in various sized systems and in various applications. The study is scheduled to be completed by 31 December 1979.

At this time, the program (Model for Alkaline Water Electrolysis Systems) consists of the input considerations, a generic system breakdown and a rough algorithm. Specific coding has recently been started.

V. Summary and Future Requirements

In summary, during GFY 1979, this program has made significant strides in the identification of inexpensive advanced cathodes and in the operation of an alkaline electrolysis system at 100 C and above. The best cell voltage demonstrated in short term tests was in the 1.70 to 1.71 volt range at 100 C and 450 ma/cm^2. There are several possible electrode morphological improvements on the horizon which could conceivably lower the voltage another 100 mV to the 1.6 V region (92% η_V). Increasing the temperature another 25 C and a reduction in separator thickness could yield an additional 50 to 100 mV savings. The possibility of a stable improved anode electrocatalyst would then place the voltage very near to the isothermal operating point, i.e., 1.48 volts.

This, however, is conjectural, though based on reports from other groups.[8, 9, 10] The continuation of screening tests and long-term stability verification of these advances is scheduled to continue through GFY 1980 pending contract extension. Also scheduled is a literature search for materials corrosion data in the proposed 100 to 150 C temperature range for alkaline water electrolysis. In addition to this DOE/BNL supported work, TES has an active in-house development effort mainly concerned with system and cell characterization which has yielded important results such as the compression effect discussed previously and many design analysis procedures that can be employed in advanced technology modeling. These subroutines include such items as heat and mass balance, electrolysis module design with respect to strength, and shunt current loss modeling. Other applicable in-house work deals with cell modeling (i.e., total cell performance) and component reliability studies.

Together with the in-house work, the contract effort assures the continued development and improvement in the conversion of water and electric power to hydrogen, a major component of the hydrogen economy.

VI. References

1. Murray, J. N., Yaffe, M. R., Proc. of the 14th Intersociety Energy Conversion Engineering Conf., 1979, 747-751.
2. Murray, J. N., Laskin, J. B., Kincaide, W. C., Proc. of Symp. on Industrial Water Electrolysis, 1978, 39-53 (Proc. Vol. 78-4, The Electrochemical Society, Princeton, NJ).
3. Murray, J. N., Teledyne Energy Systems, March, 1979, TES-BNL-39.
4. Yaffe, M. R., Teledyne Energy Systems, August, 1979, TES-BNL-45.
5. Tseung, A. C. C., Jasem, S., Mahmood, M. N., Proc. of Symp. on Ind'l Water Electrolysis, 1978, 161-168.
6. Yaffe, M. R., Murray, J. N., Proc. of DOE Chem./Hyd. Energy Systems Contractor Review, 1979, 37-42, CONF-781142.
7. Chenevey, E. C., Celanese Research Co., June, 1979, NASA CR-159644.
8. Appleby, A. J., Crepy, G., Proc. of Symp. on Ind'l Water Electrolysis, 1978, 150-160 (Proc. Vol. 78-4, The Electrochemical Society, Princeton, NJ).
9. Moran, P. J., Cahen, G. L., Stoner, G. E., "Extended Abstracts," Spring, 1979, National Mtg. of the Electrochemical Society, Boston, Mass. (The Electrochemical Soc., Vol. 79-1, Princeton, NJ).
10. D. Hall, INCO Research and Devel. Center, Private Communications, August-September, 1979.

Table 1. Screening Modules

Module	Cathode(s)	Anode(s)	Period	Total Hrs.
4	NiB/C-110	Baseline	11/29/78 → 1/2/79	233
5	Baseline	Co_2NiO_4/A-111	1/8/79 → 1/29/79	443
6	Baseline	A-010-00/A-010-10	2/14/79 → 3/12/79	315
7	C-110/C-110-0	Baseline	3/15/79 → 4/6/79	373
8	Baseline	A-010-00/Plaque	4/16/79 → 5/3/79	350
11	C-AN/C-110-A	Baseline	8/24/79 → 9/24/79	526

Table 2. Results of Advanced Electrode Screening Tests
(25 w/o KOH, 50 psig, 100 C, 450 ma/cm^2)

Electrode	Module	η_V (%)	Total Voltage (V)	Cell Potential (V - I · R)	S (mV/decade)	R (mΩ)
Anodes						
1. Co_2NiO_4	5	74	1.985	1.850	235	1.0
2. A-010-10	6	72	2.055	1.850	220	1.5
3. A-010-00	6,8	72	2.050	1.860	235	1.4
4. A-111	5	70	2.120	1.885	255	1.7
5. Plaque	8	69	2.140	1.855	235	2.1
Cathodes						
1. C-AN	11*	86	1.730	1.575	100	1.1
2. C-110-A	11*	84	1.770	1.608	90	1.2
3. C-110	4,7	81	1.835	1.610	115	1.7
4. Ni_2B	4	79	1.880	1.700	160	1.3
5. C-110-0	7	76	1.960	1.630	120	2.4
Baseline						
1. Ni Screen	4,5,6,8	71	2.075	1.860	205	1.6
2. Ni Screen	11*	76	1.945	1.810	210	1.0

* Complete data analysis still in progress.

Table 3. Factors to be Considered in Optimizing the Economics and Design of Alkaline Water Electrolysis Systems

1. Size Factors
   a. Extended peak kilowatts
   b. Maximum safe current density
   c. Maximum pressure
   d. Maximum obtainable cell area
2. Operating Factors
   a. Power availability and duty cycle
   b. Gas demand and utilization profile
   c. Air temperature range
   d. Cooling water temperature range
   e. Electrolyte temperature range
3. Lifetime
   a. Total plant lifetime
   b. Electrolysis module lifetime
   c. Other component lifetimes
   d. Maintenance schedule
4. Specific Costs
   a. Fixed capital
   b. Working capital
   c. Power cost profile
   d. Other direct operating costs
   e. Maintenance and replacement costs
5. Efficiency Factors
   a. Power conditioning
   b. Current efficiency (Faradaic)
   c. Voltage efficiency (thermodynamic)
   d. Gas purification efficiency
6. Capitalization and Economic Factors
   a. Method of financing
   b. Write-off period
   c. Interest rates
   d. General inflation
   e. Incentives

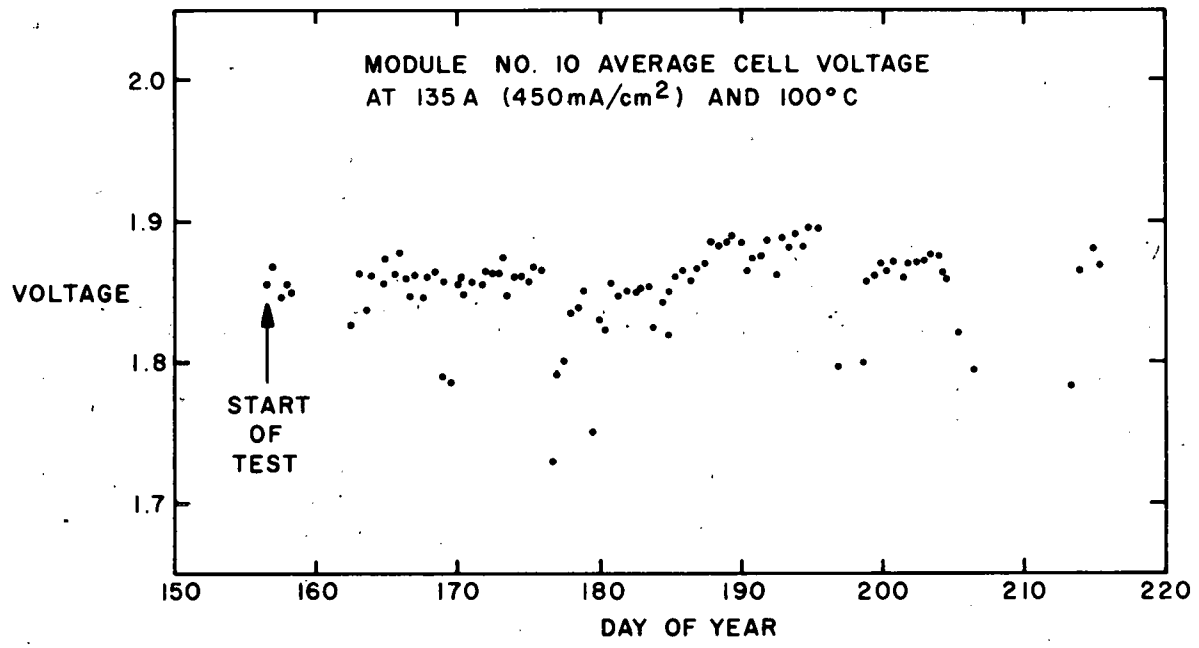

Figure 1. Module 10 Performance

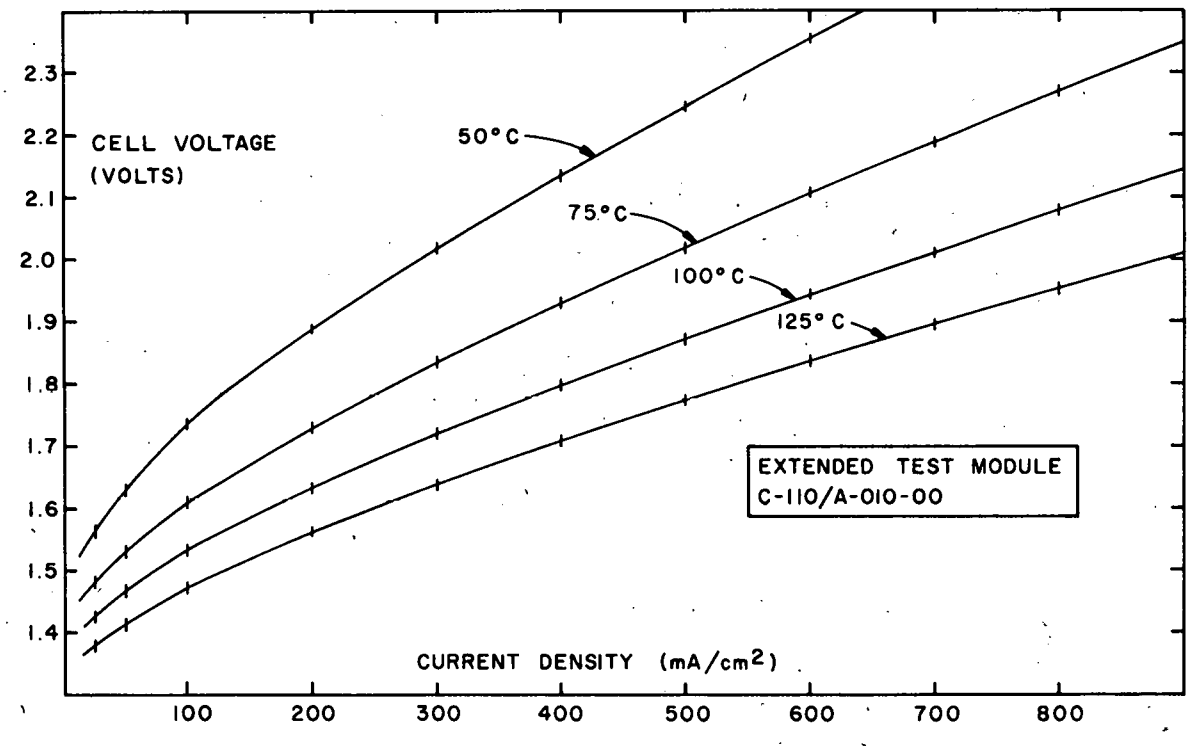

Figure 2. Module 10 Volt-Amp Curves

INVESTIGATION OF NICKEL WHISKER ELECTRODES

Patrick J. Moran,* George L. Cahen, Jr., and Glenn E. Stoner

Applied Electrochemistry Laboratory
Department of Materials Science
University of Virginia
Charlottesville, Virginia 22901

Abstract

Improvement in the operating efficiency of alkaline water electrolyzers can be achieved by lowering the overpotentials for the hydrogen and oxygen evolution reactions. A relatively new technique for the preparation of high surface area nickel electrodes is the use of polycrystalline nickel whisker electrodes. These electrodes are characterized by high porosity and relatively high surface area. Research efforts have indicated that whisker electrodes represent approximately a 10% efficiency improvement over conventional Ni-200 screen electrodes on an apparent current density basis. Additional improvements can conceivably be obtained by optimization of whisker morphology, the addition of catalysts, and maximization of electrochemically active surface area.

Introduction

Electrode overpotentials for the hydrogen and oxygen evolution reactions can be represented as

$$\eta = a + b \log i$$

where a and b are the Tafel constants for the reaction in consideration and i is the current density. The amount of gas product is proportional to the overall current while the overpotentials are lower for lower current densities. Therefore at any electrolysis current, efficiency can be improved by increasing the active electrode surface area and/or by the addition of catalysts to improve the Tafel constants. Various techniques exist for the preparation of high surface area electrodes. A relatively new technique was developed in Munich, Germany by Mr. Hermann Schladitz, now Research Professor of the School of Engineering and Applied Science at the University of Virginia. A review of the fabrication and general properties of these electrodes and electrochemical characterization of them are the topics of this paper.

Fabrication

Polycrystalline nickel whiskers are produced by chemical vapor deposition of nickel tetracarbonyl gas ($Ni(CO)_4$) in an electromagnetic field. The gas is pumped into a chamber which is heated to 300-350°C to accomplish gas phase decomposition. The chamber is surrounded by an electromagnet which creates magnetic field lines in the chamber parallel to the chamber's vertical axis. The liberated nickel particles align themselved along the field lines. Further deposition occurs on these aligned "substrates". Resulting whiskers have typical grain sizes of 200-400 Å. They are very strong, approaching 10^6 psi, and relatively defect free. Diameters and lengths range from 0.1 μ to 50 μ and from 1 mm to several cm respectively.

These whiskers can be fabricated into a whisker electrode (network) by sintering at 800 to 1000°C under pressure in a reducing atmosphere for approximately half an hour. A fine nickel screen is used as the substrate in the sintering process. The resultant electrode structure is random, fibrous, and highly porous. These whisker electrodes are 85 to 90% porous by volume. Their true specific surface area is 5×10^3 cm^2/gm. The roughness factors based on the cross-sectional area of the electrode have been estimated to be 2×10^3 to 5×10^3. The roughness factor of the individual whiskers has been estimated to be approximately ten. This estimate was obtained by scanning electron microscopic investigation and mathematical modeling.

Additionally several techniques for fixing individual whiskers to new or existing electrode substrates have been demonstrated. These include: sintering whiskers onto a substrate, "gluing" the whiskers onto a substrate by chemically vapor depositing nickel, and finally and most intriguing by growing whiskers directly onto an electrode substrate. This last method has the advantages of involving only one process step and control of whisker orientation with respect to the substrate. It is anticipated that these "hybrid whisker electrodes" will be tested for mechanical stability and electrochemical performance in the next year.

Electrochemical Characterization

Nickel whisker electrodes have been driven both anodically (oxygen evolution) and cathodically (hydrogen evolution) in 30 w/o KOH electrolytes at apparent current densities as high as 1000 mA/cm² for two days with no detectable loss in mechanical

*Present address: Department of Civil Engineering/Materials Science and Engineering, Johns Hopkins University, Baltimore, Md.

integrity. Scanning electron microscopic investigation indicated no detectable change in the whisker electrode morphology. This result is believed to be significant because mechanical integrity of sintered components and high surface area electrodes is of considerable importance.

Optical microscopic examinations of gas evolution at 80x magnification indicated that at equal apparent current densities the whisker electrode evolves smaller product gas bubbles than conventional nickel 200 screens. This result is presumably due to the lower current density and is important because smaller bubbles contribute less to ohmic overpotential thereby increasing efficiency.

The nickel whisker electrodes tested were cylindrical, measuring 3 cm in diameter and 1 mm in length. Each electrode's mass was approximately 2.3 g. For electrochemical comparison 5 layers of 200 mesh nickel 200 were spot welded together and a 3 cm diameter electrode was cut out of this with a resulting length of nearly 1 mm. The mass and bulk geometry of both electrodes was therefore approximately equal.

The whisker electrode and the nickel 200 screen electrode were tested for the hydrogen and oxygen evolution reactions in 30 w/o KOH electrolyte. The performance on an apparent current density basis is illustrated in the following figure:

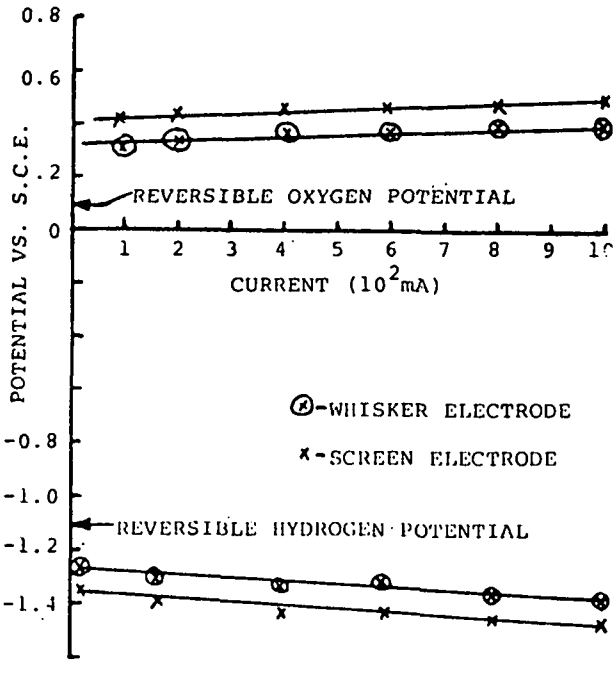

The whisker electrode exhibited an overpotential improvement of 60 to 100 mV for each reaction. The effect was presumably due to the higher surface area of the whisker electrode. The improvement represents about a 10% improvement in operating efficiency.

It was of interest to determine if the improvement obtained with whisker electrodes was due only to increased surface area or if, because of their different microstructure, whiskers were better catalysts for the gas evolution reactions. To evaluate this it was necessary to determine the true active surface area for both whisker and screen electrodes. Several surface area measuring techniques were employed; BET adsorption isotherm, cyclic voltammetry in a non-faradaic current region, geometric surface area considering the wires of the screens and the individual whiskers to be smooth cylinders, and capacitance measurement upon current interruption. The last technique is admittedly difficult with porous electrodes but allowed estimation of the active area in gas evolution conditons. The results of these measurements are shown in the following table

	NI-200 SCREEN ELECTRODE	NICKEL WHISKER ELECTRODE
Cross-Sectional Surface Area	7 cm^2	7 cm^2
Geometric Surface Area	$10^2 cm^2$	$10^3 cm^2$
Surface Area Via Cyclic Voltammetry	300 cm^2	$10^4 cm^2$
Surface Area Via BET Isotherm	--	$10^4 cm^2$
Surface Area Via Current Interruption	300 cm^2	$3 \times 10^3 cm^2$

Employing this data, predominantly that in the last row, a comparison of whisker electrode and screen electrode performance was obtained for the hydrogen evolution reaction. It was not done for the oxygen evolution reaction to avoid the complications of surface oxide states. The result of the comparison for hydrogen evolution was that the improvement obtained with the whisker electrode was due primarily, if not totally, to the increased surface area. In other words the Tafel constants for both electrodes were found to be nearly identical.

Discussion and Conclusions

Three important conclusions can be drawn from the previously described work:

1. The increase in efficiency obtained by using whisker electrodes is primarily due to increased surface area rather than improved catalytic performance. The nearly equal catalytic evaluation on a true surface area basis supports this conclusion. However, due to the nature of the techniques employed, which are generally accurate as an order of magnitude estimation, it should not be concluded that there is no difference in the catalytic ability of whiskers vs. drawn wires. More precise work with smaller, non-porous electrodes would be required to make an accurate statement concerning catalytic performance.

2. Although the highly porous whisker electrodes posess a rather large surface area, only about 1/3 of this area is active in the tested configuration. Thus, for commercial testing and/or application, the whiskers should be utilized in a manner to maximize the active surface area. Instead of using whisker electrodes, the hybrid type electrodes discussed earlier should be employed.

3. A final conclusion is that the 10% increase in efficiency obtained with whisker electrodes is potentially useful. Additional improvements can be achieved in several ways; the active surface area can be maximized with hybrid electrodes, whisker morphology can be controlled during growth to yield higher roughness factors, and catalysts, such as platinum, can be incorporated into the whisker-electrode systems. Work along the forementioned lines is being proposed for the upcoming year.

Acknowledgement

The support of the Department of Energy and the tehnical guidance of Brookhaven National Laboratories is gratefully acknowledged. The expertise of Mr. Hermann Schladitz is greatly appreciated. Finally, the assistance of our excellent electronics engineer, Mr. Louis L. Scribner, Jr. is acknowledged.

THE OXYGEN AND HYDROGEN EVOLUTION REACTION ON ORIENTED SINGLE CRYSTALS OF RUTHENIUM DIOXIDE*

L.I. Berger, Fred H. Pollak and Y. Canivez[a)]
Department of Physics
Brooklyn College of CUNY
Brooklyn, N.Y. 11210

and

W. O'Grady
Department of Energy and Enrironment
Brookhaven National Laboratory
Upton, N. Y. 11973

Abstract

A novel design for water electrolysis using a solid polymer electrolyte is being developed by General Electric. Ruthenium is one of the best electrocatalysts for the oxygen evolution reaction. There are problems connected with the significant loss in electrocatalytic activity with time. This performance degradation is presumably due to the gradual formation of an RuO_2 film.

We have performed electrochemical measurements on [100] , [110] and [111] oriented single crystals of RuO_2 in order to elucidate the mechanism of the electrocatalytic process. Large single crystals were grown by the vapor transport method. Our investigation has revealed several interesting differences for the various orientations. This study indicates that RuO_3 may be an important intermediate species prior to oxygen evolution and that the formation of the RuO_3 is the rate limiting process. Similar results were previously obtained for IrO_2.

I. Introduction

At the present time there is considerable interest in developing high efficiency and low cost water electrolyzers to meet the demands of hydrogen required by the chemical industry and as a fuel in fuel cells and gas turbines. The development of advanced technology for water electrolysis is essential to minimize the cost of hydrogen. The efficiency of water electrolysis systems depends critically on the behavior of the oxygen electrode. For oxygen evolution reaction (OER) on metals or alloys at constant potentials, the continuous decrease of current densities with time is one of the more difficult problems in water electrolysis. The time variation of current density has been pointed out by Schultze[1] in the anodic evolution of oxygen on platinum. More recently, similar behavior has been observed on iridium[2] and on nickel[3] anodes. It has been suggested that the current decay with time is connected with the continuous growth of a poorly conducting oxide film, which retards the electron transfer or inhibits the radical on the film surfaces[2,3,4]. Based on electrochemical and ellipsometric methods Srinivasan et al have concluded that the performance degradation for oxygen evolution on RuO_x catalyst is presumably due to the gradual accumulation of a RuO_2 film on the surface of the RuO_x particles by a dissolution/precipitation process.[4]

The OER always takes place on electrodes which are covered with an oxide layer. Little is understood about the properties of the oxide phase and, especially, about the properties of the oxide-electrolyte interface which are required to achieve improved performance in the OER. Evaluation of a number of metals and alloys as electrocatalysts for the oxygen evolution reaction, leads to nickel as a preferred anode material for the OER in alkaline solutions and to noble metals and their alloys as electrocatalysts for the OER in acid solutions. Among the noble metals, the performance of Ru, Ir and their alloys was found to be much superior to that of a pure Pt anode. Thus, the potential at which a steady state oxygen evolution current density of 1 mA cm^{-2} (real) is obtained on Pt at room temperature is about 1.8 V vs. RHE, while at a Ru or an Ir anode this potential is only about 1.4V (Ru) or 1.5V (Ir).[5,6] It is obvious, therefore, that analysis of the surface layer formed on Ru or Ir prior and during the evolution of oxygen, revealing the relationship between properties of this layer and the performance of the Ru (Ir)/ aqueous solution interface in the OER, may be an important key to the role of oxide layers in electrocatalysis. In addition the work of Srinivasan et al[4] has shown the significance of our understanding the properties of RuO_2 and IrO_2.

A novel design for water electrolysis is being developed by the General Electric Company using solid polymer electrolytes.[7] In this type of water electrolysis cell a solid sheet of perfluorinated polymer (Nafion) serves as the electrolyte. The electrocatalysts are platinum on the cathode side and iridium, ruthenium or binary and ternary alloys of these metals with transition metals on the anode side. Hence there is considerable interest from a practical point of view in gaining a better understanding of nature of electrocatalyst/electrolyte interface for these particular materials.

II. Experimental Results

We have performed cyclic voltammetry and steady state measurements on oriented single crystals of RuO_2. For comparison we have also studied unoriented single crystals of this material and as well as Ru metal. In the single crystal case [100] [110] and [111] crystallographic faces were investigated. This work on oriented single crystal material offers the advantage of a more clearly defined electronic mechanism compared to prior studies on multicrystalline material.[8,9] Fine grained material has many grain boundaries and in some cases inclusions containing impurities. It is also an important continuation of the work on single crystal IrO_2 reported at last year's meeting.[10]

*Work supported by Brookhaven National Laboratory Contract #EC77-C-023590 and by NATO.
a) Permanent address: Faculte des Sciences, University of Mons, Mons, Belgium.

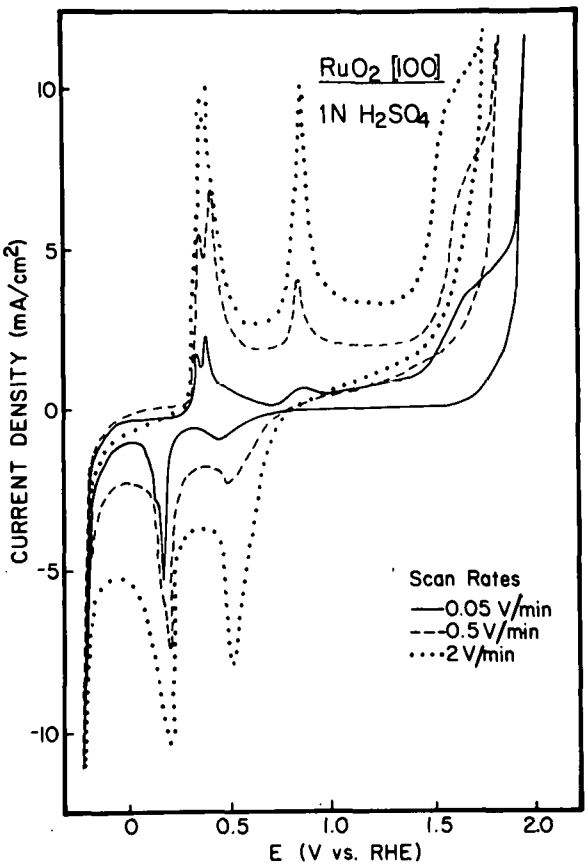

Figure 1. Cyclic voltammetry of single crystal RuO_2 with a [100] surface in a N_2 saturated solution of 1 N H_2SO_4 for several different scan rates.

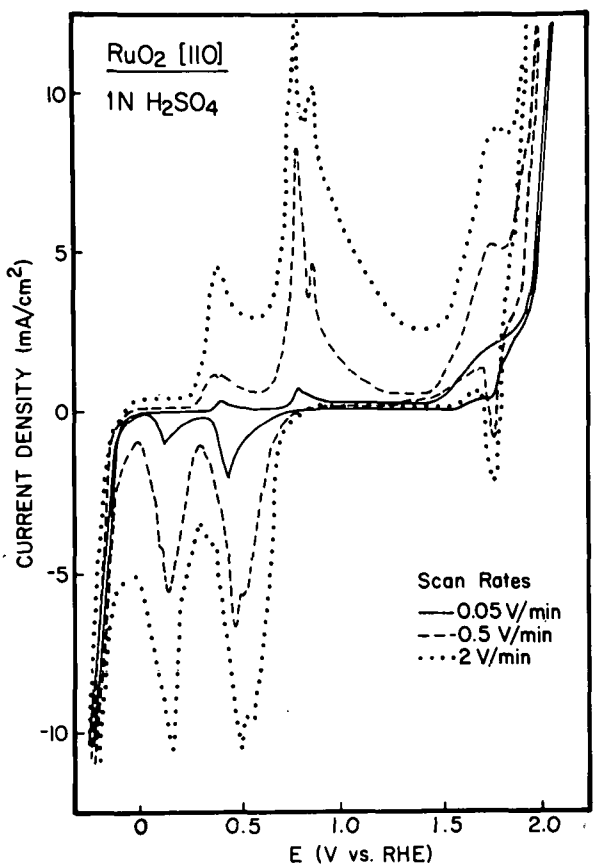

Figure 2. Cyclic voltammetry of single crystal RuO_2 with a [110] surface in a N_2 saturated solution of 1 N H_2SO_4 for several different scan rates.

Single crystals of RuO_2 were grown in our laboratory by the method of chemical transport reactions in a flowing system. This technique is similar to that used by Reames[11] to produce the large single crystals of IrO_2 that were used in our investigation reported at last year's meeting.[10] In the presence of oxygen at 800-1500°C gaseous oxides (RuO_3, IrO_3) exist. The reaction takes place by the following mechanism:

$$M(s) + \frac{3}{2}O_2 \rightarrow MO_3(g)$$

where M = Ru or Ir. The volatile MO_3 gas dissociates to MO_2 in the cooler region. In our procedure several grams of Ru metal powder were contained in an alumina source boat. This boat was placed inside a Mullite tube at the center of furnace which was raised to a temperature of 1400°C. Oxygen at atmospheric pressure was passed through the Mullite tube at a flow rate of about 15 cm^3/min. A second boat, which acted as a substrate, was placed 210 cm from the source boat in a cooler portion of the furnace. After several days crystals of dimensions up to 6mm x 4mm x 2mm had formed in the substrate boat. Recently Shafer et al have also reported the growth of comparable sized single crystals of RuO_2.[12]

A number of crystals were examined by X-ray Laue backscattering which indicated that they were of relatively good quality. Using the X-ray orientation technique natural [100], [110] and [111] faces were found for the electrochemical investigation.

Shown in Figures 1, 2 and 3 are cyclic voltammograms for [100], [110] and [111] surfaces of RuO_2, respectively, in a 1 N solution of H_2SO_4 saturated with N_2 at different scan rates. Figure 4 shows the results of a similar investigation on an unoriented single crystal. Measurements were actually prtformed at scan rates of 0.05, 0.1, 0.2, 0.5, 1.0 and 2.0 V/min. but for convenience only three rates (0.05, 0.5 and 2.0 V/min.) are displayed. Below about 1.5 V vs RHE the four curves are qualitatively similar with major features at 0.4 and 0.7 V vs RHE on the anodic portion and at about 0.5 and 0.2 V vs RHE in the cathodic region. The potentials of these features are independent of sweep rate.

For the [100] case (see Figure 1) the first anodic peak (0.4 V vs RHE) consists of a well-defined doublet and there is some structure on the cathodic peak at 0.2 V vs RHE. For the [110] crystallographic face (see Figure 2) the second anodic peak (0.75 V vs RHE) is a doublet and there is structure on both cathodic peaks. The [111] face (see Figure 3) shows no structure on either the anodic or cathodic peaks at voltages below ~ 1.5 V vs RHE. Is is of interest to note that the two anodic peaks are at the same voltage for the three orientations while there are small differences (~ 0.1 V vs RHE)

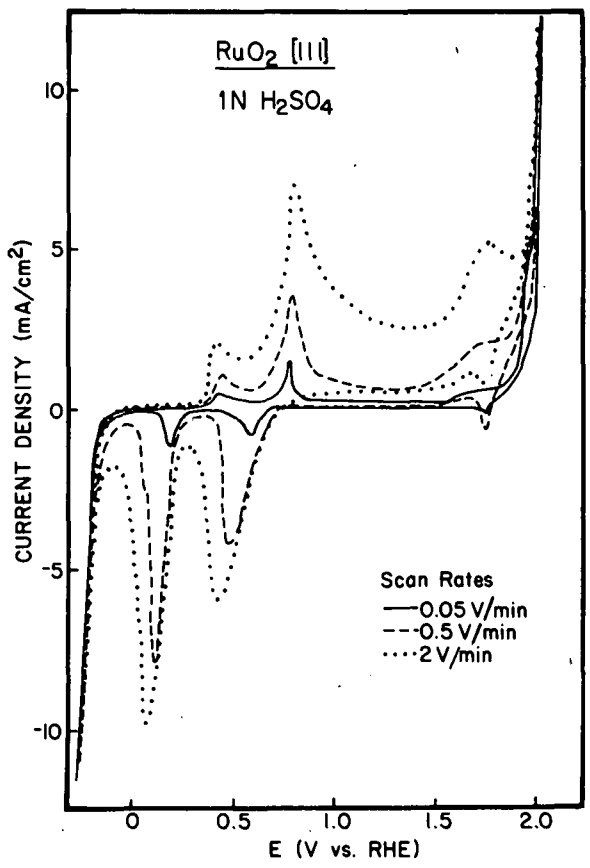

Figure 3. Cyclic voltammetry of single crystal RuO_2 with a [111] surface in a N_2 saturated solution of 1 N H_2SO_4 for several different scan rates.

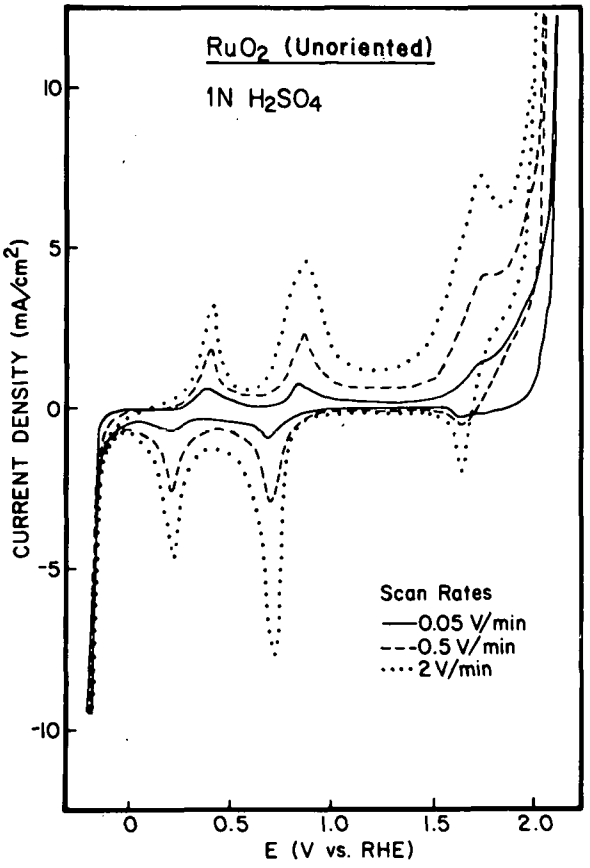

Figure 4. Cyclic voltammetry of an unoriented single crystal of RuO_2 in a N_2 saturated solution of 1 N H_2SO_4 for several different scan rates.

for the cathodic features (averaging out the structure in each case). For the unoriented sample (Figure 4) no structure is seen on either the anodic or cathodic peaks. In addition, the voltage difference between corresponding anodic and cathodic peaks is less than for the oriented samples. We attribute the observed structure in the cyclic voltammograms below 1.5 V vs RHE to the Ru_2O_3/Ru (lowest voltage anodic-cathodic pair) and the Ru_2O_3/RuO_2 couple.

Recently several investigators[8,9] have studied the electrochemical properties of RuO_2 including some work on oriented single crystals by Shafer et al.[13] They also report structure in the same general voltage range where we have seen features (although there are some differences in values) and also attribute them to the above mentioned couples. However, our cyclic voltammetry peaks are much sharper and reveal more structure than those observed by other workers.

Shafer et al report that no obvious differences were seen between the six different crystal faces that they studied.[13] Also their cyclic voltammetry curves taken or individual faces were similar to those on thermally oxidized Ru-metal. In contrast we have seen some interesting differences for the different crystallographic orientations (Figs. 1, 2 and 3).

At voltages above 1.5 V vs RHE there are also some interesting relations between the four situations we have studied. For all cases, including the unoriented sample, there is a well-defined anodic structure (~1.7 V vs RHE) preceeding the onset of the OER. There is a corresponding cathodic peak for the [110], [111] and unoriented cases but none is observed for the [100] face. These anodic features occur at the same voltage for the four samples but for the cathodic peak there is a small difference for the unoriented sample.

A similar anodic process has been observed in the case of single crystal IrO_2 (labelled A in Figure 2 of Ref. 10) and has been associated with the oxidation of IrO_2 to the higher state IrO_3. Therefore, we attribute the feature at about 1.7 V vs RHE in our case to the oxidation of RuO_2 to RuO_3.

In terms of the OER potential the [111] face shows no dependence on sweep rate (see Fig. 3) while for the other cases there are shifts to higher voltages with decreasing scan speed. We have also investigated cyclic voltammetry for Ru metal in a 1 N H_2SO_4 solution saturated with N_2 for the same scan speeds used in the RuO_2 cases. In the case of the Ru metal the OER potential does not depend on scan rate, similar to our observations for the [111] face. Although we do not completely understand these differences it is interesting to

note that for the [111] orientation of rutile (the crystal structure of RuO_2) it is possible to have a crystal face free of oxygens, i.e. only metal atoms. Thus the [111] case may be closer to the metallic situation.

In addition to the cyclic voltammetry we have also studied the steady-state electrochemical behavior of the various oriented RuO_2 samples. The log current density vs potential curves, obtained by the steady state measurements in the anodic region, were linear between 1.55 and 1.8 V vs RHE. All samples showed a slight decrease in slope at about 1.8 V vs RHE. It is interesting to note that this is the voltage of the feature that we have attributed to the oxidation of RuO_2 to RuO_3. Our measured Tafel slopes were $\sim$ 100 mV/dec with small differences between the orientations. It appears that the [100] Tafel slope is somewhat larger than those for the other two orientations although this is not conclusive. Shafer et al have also evaluated Tafel slopes for various orientations.[13] Although their general values are in agreement with ours they appear to find more of a difference for the various faces.

III. Summary of Results

We have grown large single crystals of RuO_2 by the vapor transport method. Electrochemical investigations have been carried out on various oriented surfaces of the single crystal material as well as on a sample of unoriented single crystal material. A number of significant similarities and differences have been observed between the various faces that have been studied. Our results have revealed considerably more structure in the cyclic voltammetry curves than reported by other investigators. Thus our work on oriented single crystal RuO_2 contains important information concerning the electrocatalytic process.

IV. Future Work

We plan to grow single crystals of IrO_2 in order to further develop the work reported at last year's meeting.

Additional electrochemical studies will be performed on oriented single crystals of IrO_2 and RuO_2. This includes measurements using the rotating disc electrode method to be done in collaboration with Brookhaven National Laboratory.

Preliminary optical investigations (reflectivity and photoemission) have already been performed on single crystal IrO_2. We propose a much more detailed study of this area on both IrO_2 and RuO_2 in order to gain information concerning their fundamental electronic structure.[14] The photoemission work is being done in collaboration with the University of Mons, Mons, Belgium.

Our ultimate goal is to relate the observed electrochemical behavior of single crystal IrO_2 and RuO_2 with the fundamental electronic structure.

References

1. J. W. Schultze, Z. Phys. Chem. 73, 29 (1970).
2. D. N. Buckley and L. D. Burke, Faraday Transactions I, 72, Part I, 2431 (1977).
3. E. Deltcombe, N. de Zoubov and M. Pourbaix, "Atlas of Electrochemical Equilibrium in Aqueous Solutions." (Pergamon Press, London, 1966) p. 343.
4. S. Srinivasan, P. W. T. Lu, G. Kissel, F. Kulesa and J. Orehotsky, Proceedings of the DOE Chemical/Hydrogen Energy Systems Contractors Review, Washington, 1978. (NTIS, Springfield, Va., 1979) p. 27.
5. J. P. Hoare, "The Electrochemistry of Oxygen" (Interscience, N.Y. 1968).
6. S. Srinivasan, P. W. T. Lu, G. Kissel, F. Kulesa, C. R. Davidson, H. Huang, S. Gottesfeld and J. Orehotsky, Proceedings of the DOE Energy Storage and Hydrogen Energy Systems Contract Review, Hunt Valley, Md., 1977 (JPL Publication 78-1) p. 39.
7. J. H. Russell and L. J. Nuttall, Proceedings of the DOE Chemical/Hydrogen Energy Systems Contractors Review, Washington, 1978 (NTIS, Springfield, Va., 1979) p. 13.
8. J. Horkans and M. W. Shafer, J. Electrochem. Soc. 124, 1202 (1977).
9. D. Galizzioli, F. Tantardini and S. Trasatti, J. Appl. Electrochem. 4, 57 (1974).
10. S. H. Shin, F. H. Pollak and F. M. Reames, Proceedings of the DOE Chemical/Hydrogen Energy Systems Contractors Review, Washington, 1978 (NTIS, Springfield, Va., 1979) p. 31.
11. F. M. Reames, Mat. Res. Bull. 11, 1019 (1976).
12. M. W. Shafer, R. A. Figat, B. Olsen, S. J. La Placa and J. Angilello, J. Electrochem. Soc. 126, 1625 (1979).
13. M. W. Shafer, R. A. Figat, R. Johnson and R.A. Pollak, to be published.
14. L. F. Mattheiss, Phys. Rev. B13, 2433 (1976).

HYDRIDE BEDS: ENGINEERING TESTS*

M. J. Rosso, Jr. and G. Strickland

Brookhaven National Laboratory
Upton, New York 11973

ABSTRACT

The BNL Hydrogen Storage Program engineering effort is directed toward finding solutions to the engineering problems associated with metal hydrides--principally $FeTiH_x$. Measurements of thermal conductivity in non-enhanced, copper mesh-enhanced and aluminum foam-enhanced hydride beds have been made and indicate that the form of the enhancement material is the critical factor. The completion of the HYTACTS and its initial shakedown runs suggest the many applications for this new facility in the area of advanced hydrogen component testing. The performance testing of the Variable Parameter Test Unit-2 (VPTU-2) will begin following the BNL Safety Committee approval. A description of this vessel is included. The purpose, description and status of the Variable Parameter Test Unit -1 (VPTU-1) is reported as well as the results of the first set of tests performed in this vessel.

INTRODUCTION

The idea that hydrogen will be used on a large scale as an energy carrier in this country within fifty years is becoming fairly well accepted by at least the scientific community. The use of hydrogen presupposes the need for storage in a form that is safe, economically viable, and both environmentally and esthetically acceptable. Hydrogen, as well as most other gases, has traditionally been stored and transported as a compressed gas at pressures approaching 3000 psi in very heavy-walled steel cylinders. Hydrogen in liquid form, although orders of magnitude lighter in weight, is probably not a viable option because of safety and economic considerations.[1] Metal hydride storage is a proven technology which may have, because of their inherently high heats of reaction, greater application in the areas of chemical compressors and heat pumps, than in the hydrogen storage area.[2-4] Other occluder type materials such as molecular sieves have been considered in the past but were generally discounted due to their fairly low hydrogen storage density. Recently a small effort has been directed toward evaluating the viability of a new concept which involves the use of hollow glass microspheres for storing hydrogen.[5] Comparative energy storage densities can be found in Table I.

Although BNL has taken an active role in the evaluation of many hydrogen storage options, the "in-house" effort has been generally directed toward the development of the metal hydride storage concept. In the engineering area, where our efforts have focused primarily on iron-titanium hydride, solutions are being sought to the engineering problems presented by the characteristics inherent to this system. The fact that metal hydrides become extremely fragile, due to cracking upon hydrogen activation, causes the material to crumble into fine particles whenever the bed is disturbed. In larger systems (where the bed depth is greater than a "not-yet-determined" critical value) the forces generated by the expanding alloy as it absorbs the hydrogen are not only sufficient to greatly aggravate the attrition problem, but it has been reported that enough force can be generated to distort the walls of the pressure vessel.[6] As the hydrogen is made to flow through the hydride bed, fairly high pressure drops can also be experienced as the particles get very small after an extended number of charge/discharge cycles.[7] This will be an important consideration in fast-fluid flow-rate systems such as for automotive applications and for the chemical compressor application where even higher flow rates are anticipated. The poor thermal conductivity of the bed as a result of the many contact resistances is one of the problems on which BNL has applied its energies.

*Research performed under the auspices of the U.S. Department of Energy

ENGINEERING TEST PROGRAM

Heat Transfer Enhancement

The addition of small amounts of high conductivity material to the hydride bed in an attempt to enhance the heat transfer was investigated. It was decided to use an approach that would involve the transient thermal transfer mode since the results would be more representative of actual operating conditions. The experimental apparatus included a thin-walled (2.45" I.D. x .095" wall) cylindrical copper vessel 11 1/4 inches long, rated at 200 psia, and flanged at both ends. Two temperature-controlled baths (30° and 80°C) were used to provide the constant temperature environment at the outside wall of the test vessel. Three shielded thermocouples were positioned at the vessel center line with longitudinal displacements of 2.3 inches between the hot junctions. The two extreme thermocouples were provided only to insure that end effects were minimal and heat flow was axial. All the data presented in this report were measured by the center thermocouple. For each set of experiments the test vessel was assembled, filled with hydride (2365 grams) and machine packed by raising and dropping the vessel with its holder (total weight 25 lb) a distance of 0.75 inches at the rate of 1 1/2 taps per second for 30 minutes ($\sim$2700 taps). This procedure was adopted to eliminate variances in the bed's void fraction which was computed using bed height measurements taken through holes in the top flange. Each heating run was started by causing all three thermocouples in the test apparatus to approach the bath temperature (30°C)to within 0.2°C.

The test vessel was then removed and immediately immersed in the high temperature (80°C) bath and the data measurement started. The rate at which the data were recorded was chosen so as to provide a minimum of fifty data points for each run. Generally each run was repeated three times and the results were extremely reproducible. Three configurations were used: 1) no enhancement, 2365 g packed bed of -30+80 mesh deactivated FeTi hydride; 2) the same bed with 5 wt % of the hydride removed and replaced with an equal weight of copper in the form of a knitted mesh;[8] 3) the same bed with 5.6% of aluminum in the form of a reticulated foam.[9] Each of these configurations was tested with 150 μm, 1.0 psia and 200 psia hydrogen pressure in the test vessel. The data were treated as given by Churchill, R.V., in his "Operational Mathematics."[10]

For the above geometry the solution of the temperature profile is given by:

$$\theta(\eta,\tau) = 1 - 2\sum_{n-1}^{\infty} \frac{J_0(\lambda_n \eta)}{\lambda_n J_1(\lambda_n)} e^{-\lambda_n^2 \tau} \qquad (1)$$

where

θ = Dimensionless temperature at η and τ = $(T_W - T_0)/(T_t - T_0)$

η = Dimensionless radial distance from center = r/R

τ = Dimensionless time = $\alpha t/R^2$

α = Thermal diffusivity = $k/(\rho C_p)$ in ft^2/hr

k = Effective thermal conductivity of bed in $Btu/hr\text{-}ft^2\text{-}^oF\text{-}ft$

ρ = Bulk density of bed = $\varepsilon\rho_g + (1-\varepsilon)\delta\rho_E + (1-\varepsilon)(1-\delta)\rho_H$

where g refers to gas, E refers to enhancement material and H to hydride.

C_p = Average specific heat of the bed = $\left[\varepsilon(\rho_g C_{pg}) + (1-\varepsilon)\delta(\rho_E C_{pE}) + (1-\varepsilon)(1-\delta)(\rho_H C_{pH})\right]/\rho$

ε = Bed void fraction

δ = Fraction of hydride replaced by enhancement material

λ_n = Bessel function value = 2.40483 for n=1

$J_n(\lambda_n)$ = Bessel function value = 0.51915 for n=1

T_W = Test vessel inside wall temperature (assumed to be the same as bath temperature)

T_0 = Bed center line temperature at t = 0

T_t = Bed center line temperature at time t

For sufficiently long times at the center line of the bed Eq. (1) indicates that

$$\ell n\left[\frac{1}{1-\theta(0,\tau)}\right] = \lambda_1^2\tau - \ell n\,\frac{2}{\lambda_1 J_1(\lambda_1)} \qquad (2)$$

Substituting $\alpha t/R^2$ for τ and the numerical equivalent for λ_1 and $J_1(\lambda_1)$ (2.40483 and 0.51915, respectively) into Eq. (2) and solving for α we get:

$$\alpha = \frac{\left[\ell n\left[\frac{1}{1-\theta(0,\tau)}\right] + \ell n\left[\frac{2}{\lambda_1 J_1(\lambda_1)}\right]\right]R^2}{\lambda_1^2 t} \qquad (3)$$

Solving Eq. (3) at the half time when $T_t = 55^oC$ we get:

$$\alpha = \frac{(.69315 + .47123)R^2}{5.7832\ t_{55}} = \frac{.002098}{t_{55}} = \frac{k}{\rho C_p}$$

The effective thermal conductivity can then be determined by measuring only the half time and calculating the bulk density and specific heat for each system tested.

$$k = \frac{.002098\rho C_p}{t_{55}}$$

The results are listed in Table II.

Four very definite conclusions may be drawn from these results:

- The greatest contribution to the thermal transport of the system is made by the hydrogen gas.
- The form of the enhancement material is a more important consideration than the conductivity of the material.
- The addition of 5.6% aluminum foam enhances the effective thermal conductivity of a hydride bed at 200 psi hydrogen by a factor of 2.6.
- This technique is a very convenient and quick method of screening new heat transfer enhancement concepts.

The thermal conductivity values for the no-enhancement runs compared favorably with measurements reported by Reilly[11] and Yu[12] being slightly higher than Reilly's but lower than Yu's. Both of their results were made using essentially the same bed material but an entirely different experimental technique.

Hydrogen Technology Advanced Component Test System HYTACTS

Since hydrogen technology is viewed as a long term but highly probable option, the establishment of a hydrogen test system where advanced component designs may be tested makes sense. Such a system has been completed at BNL and is undergoing the initial shakedown operation using nitrogen.

early Safety Committee approval, the HYTACTS will have completed testing on the Variable Parameter Test Unit-2 (VPTU-2) bulk hydrogen storage vessel by the end of the 1979 calendar year.

The HYTACTS is mainly a moderate pressure (600 psia) system that is constructed entirely of TIG welded, 316 stainless steel 1" schedule 10 pipe for the process gas, and 2" schedule 10 stainless steel pipe for the thermal transport system. Both the thermal transport fluid flow rate and the hydrogen flow rate are accurately controlled and measured by digital flow control valves (FCV). The FCV's are capable of maintaining constant fluid flow rates with changing upstream and downstream pressures and temperatures because of their built-in computer processor. The flow-rate range for the hydrogen valves (3) are from 20 SCFM to 6000 SCFM providing a wide operating range for a wide class of experimental apparatuses. The thermal transport system is closed and uses a 50/50 mixture of ethylene glycol and distilled water for heating and cooling. A 7.5 ton chiller and a 125 kW heater provide the cooling and heating at a fluid flow rate of 130 gpm for the assemblies under test. All test points are monitored by a Doric Digitrend 240 Data Scanner at the rate of 10 per second and each point may be dedicated to read one of five different functions and respond to any one of the four alarms on each. The data may be stored on either magnetic tape or floppy disc for analysis within the Tektronix 4051 Graphics computer. A compressor-purifier-dryer system not yet completed has the capability of upgrading tube trailer purity hydrogen (99.95%) to ultra pure hydrogen (99.999%) at the rate of 20 SCFM. With the puification system operational, off gas from test vessels can be purified, recompressed and stored in the 120,000 SCF volume storage tubes. The HYTACTS has been tested and is awaiting operating approval. All alarms and automatic shutdowns have been activated by simulated pressure or temperature excursions and the hygrometer and O_2 analyzer values are within acceptable limits. The first operation to be performed using the HYTACTS will be the initial activation of the alloy (3825 lb $TiFe_{.85}Mn_{.15}$) of the bulk storage vessel. This process will begin at the completion and acceptance by the BNL Safety Committee of the HYTACTS Safety Analysis Report.[13]

Variable Parameter Test Unit-2 (VPTU-2)

The VPTU-2 was built for the purpose of evaluating the fluidization concept of loosening a deep hydride bed and measuring the performance characteristics of a large vessel at various rates of constant hydrogen charge/discharge operation. The vessel was built by the Foster Wheeler Corporation under contract to BNL; and a detailed description and design considerations are included in their final report.[14]

Basically the vessel is a shell and tube heat exchanger that is flanged at one end for easy removal of the tube bundle. The vessel is constructed of A-106 Grade B pipeline steel, is rated for 500 psia working pressure and was proof-tested to 750 psia. The shell is 26" in diameter and has a torispherical head at each end. A number of 4" and 2" pipe nozzles provide access to the internals for gas, vacuum and water lines as well as feedthroughs for instrument lines. The vessel is 10 ft long overall with a 7-ft long hydride bed area. It contains 33 - 1" diameter stainless steel thermal transport "U" tubes, six fluidizing tubes at the bottom of the vessel and four filter vent tubes at the top. A spring-loaded hollow-center body 2" wide x 25" high runs the full length of the bed and acts as a crushable member to relieve the vessel wall of the expansion induced stresses.

A number of hydrogen charging/discharging cycles to the maximum storage capacity at times ranging from 5 hrs to 10 hrs will be completed. All pertinent bed temperature and pressure data will be recorded and the bulk storage vessel operating performance will be evaluated. A number of attempts will be made to confirm the viability of the fluidizing concept as a bed loosening technique. The rapid changes in pressure above and below the bed at incipient fluidization will provide the only data on which to base the assessment. The VPTU-2 is expected to perform according to the Foster Wheeler projections which are based on an empirical correlation of performance rate data from the 6"-ESEERCO/BNL vessel and the 12"-PSE&G/BNL vessel. The bulk storage vessel VPTU-2 will also be used to test the HYTACTS control systems and data acquisition.

Variable Parameter Test Unit-1 (VPTU-1)

This smaller vessel (24" O.D. x 3 ft long x 1/2" wall) was designed and fabricated at BNL for the purpose of screening new advanced concepts at a larger than bench scale but smaller than engineering scale. The shell, flange and end caps are all made of A-106-Grade B pipe line steel and it is rated and has been proof tested for a working pressure of 500 psia. Enough nozzles were provided for almost any internal configuration imaginable. A viewing port at the top enables viewing of the intervals with the aid of a fiberoptic boroscope. This feature was extremely valuable when attempting to evaluate the bed fluidization option. An 11" deep hydride bed was fluidized using nitrogen and helium and the results extrapolated to hydrogen to set the mass flow rate for the first fluidization attempt in the VPTU-2. The measured values were considerably higher than the handbook values using Leva's equation for minimum fluidization[15] probably because the bed was already well beyond the minimum fluidization point before we could visually detect motion. The VPTU-1 will next be used to determine the feasibility of using heat transfer panels, on which the thermal transport fluid channels are embossed, as the container for the hydride. The scheme, in actual practice, is to have the pressure vessel in the vertical orientation with conical heat transfer trays stacked in such a way that the top of one tray provides the heat transfer surface for the bottom of the tray above it. By limiting the tray depth, and consequently the bed depth, to less than some critical value ($\sim$4-6"), the hydride should be free to rise to the surface thus alleviating problems induced by the expanding hydride during the absorption of the hydrogen. A tray simulating a segment of a cone has been fabricated and installed in the VPTU-1 test vessel. The tray can be tilted by means of an external screw-jack mechanism in order to allow the hydride to slump toward one end of the tray thereby contacting the top heat transfer surface. Twelve thermocouples have been located in the bed to measure the temperature profile as a function of hydrogen flow rate and also as a function of tilt angle.

The system is ready for testing; but a re-emphasis of priorities has caused a hold in operation of test. No problems are anticipated but some doubt exists as to the adequacy of the heat transfer surface provided.

REFERENCES

1. Mathis, D.A., Hydrogen Technology for Energy, Noyes Data Corp., Park Ridge, New Jersey, (1976).

2. Powell, J.R., Salzano, F.J., Yu, W-S., and Milau, J.S. High Efficiency Power Cycles Using Metal Hydride Compressors, January 1975, BNL 50447.

3. Auh, P.C., Powell, J.R., Salzano, F.J., Beaufrere, A., and Fogelson, S.A. Design of Metal Hydride Compressor for 1000 MW(e) Central Power Plant, Final Report, October 1976, BNL 24076.

4. Lundin, C.E., Lynch, F.E., and Snape, E. The Development of Metal Hydride Systems for Hydrogen Compressor Applications, prepared for Jet Propulsion Laboratories under Consultant Agreement 686084, August 1978.

5. Teitel, R.J., Henderson, T.M., Luderer, J.E. and Powers, J. Microcavity Systems for Automotive Applications, Final Progress Report, prepared for Brookhaven National Laboratory under Contract 43615-S, November 1978.

6. Strickland, G., Milau, J., and Rosso, M. Some Observations on the Effects of the Volumetric Expansion of Iron-Titanium Hydride on Vessels Built at BNL, August 1977, BNL 23130.

7. Rosso, M.J., Strickland, G., and Milau, J.S. Pressure-Drop-Fluid-Flow Correlation For Fixed Beds of Small, Irregularly Shaped Particles, November 1976, BNL 50589.

8. Knitted copper mesh complimentary samples were provided by P.P. Usher, Metex Corp., Edison, N.J. The mesh was knitted of 0.0075" diameter wire triple crimped, Metex #R-76-5 1/2.

9. Aluminum foam manufactured by Energy Research and Generation, Inc., Oakland, California. 140 Grams of 10 pore per inch material with a measured density of 5.8% and 6.1% was added to the bed for a total aluminum density of 5.6%.

10. Private Communication from G.P. Delancy, Stevens Institute of Technology, Hoboken, New Jersey, and P.J. Fischer, Oak Ridge National Laboratory.

11. Reilly, J.J. and Wiswall, R.H., Jr., Hydrogen Storage and Production System II, August 1972 - June 1974, BNL 19436.

12. Yu, W-S., Suuberg, E., and Waide, C. Modeling studies of fixed-bed metal hydride storage systems, Proc. of THEME Conference, Miami, Florida, 1974.

13. Salzano, F., Strickland, G., Rosso, M., Bonner, M., and Schoener, G., Safety Analysis Report on the Hydrogen Technology Advanced Component Test System (HYTACTS) and Variable Parameter Test Unit-2, October 1979 (in press).

14. Franklin, H.N., Anelli, J., Kane, R., and Rabe, G., Use of Metal-Hydride Hydrogen Storage for Bulk Storage Applications, Final Report, prepared for Brookhaven National Laboratory, by Foster Wheeler Energy Corp., Livingston, N.J., July 1979.

15. Leva, M., Fluidization, p 63, McGraw Hill, New York, 1959.

ACKNOWLEDGMENTS

The construction and operation of the thermal conductivity enhancement apparatus as well as the data tabulation and plotting was performed by Win Lewis whose expertise and cooperation were invaluable.

The construction of the HYTACTS was under the supervision of Rod Richter who assumed the responsibility for this large complex system and brought it to completion in an extremely workmanlike manner. To him we extend our thanks.

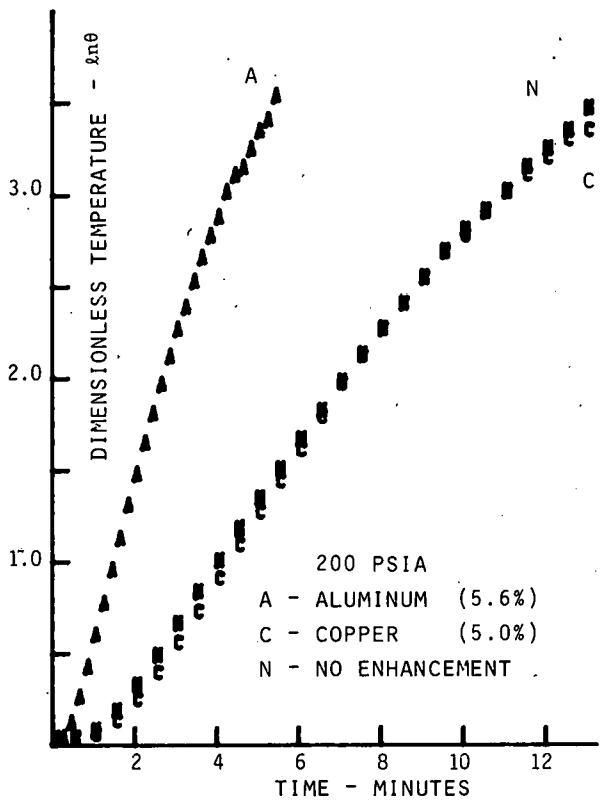

FIG. 1 RELATIVE MERIT OF THERMAL TRANSPORT ENHANCEMENT SCHEMES.

TABLE I

HYDROGEN STORAGE SYSTEMS PERFORMANCE/COST COMPARISON

	Compressed Hydrogen 2400 psi	MgH_x 10% Ni Hydride	FeTi Hydride	Micro-sphere	Liquid
*Gravimetric Energy Density Btu/lb	502 (1)	839 (1.7)	514 (1.4)	2390 (4.8)	7300 (14.5)
*Volumetric Density $Btu/ft^3 \times 10^3$	32.4 (1)	61.1 (1.9)	59.8 (1.9)	50.6 (1.6)	113 (3.5)
Cost Dollars/MBtu	1.67	2.00	2.50	0.77	3.88

*Numbers in parentheses are normalized to compressed gas

TABLE II

HEAT TRANSFER ENHANCEMENT OF BEDS OF $FeTiH_x$

Run No.	Hydrogen Pressure	ε Void Fraction	Enhancement	α Thermal Diffusivity	k Effective Thermal Conductivity Btu/hr-ft^2-^{o}F	t_{55} Half Time Minutes
3A	150 µm	0.490	None	0.000754	0.0189	167
1A-CE		0.497	5% Cu	0.00235	0.058	53.5
1G-AE		0.545	5.6% Al	0.00494	0.109	25.5
5A	1 psia	0.490	None	0.0148	0.371	8.5
2A-CE		0.497	5% Cu	0.159	0.394	7.9
2A-AE		0.545	5.6% Al	0.0829	1.834	1.52
8A	200 psia	0.513	None	0.0396	0.954	3.2
3A-CE		0.497	5% Cu	0.0362	0.902	3.5
3A-AE		0.545	5.6% Al	0.1122	2.497	1.12

MODELING SOLID HYDROGEN STORAGE BEDS*

P. W. Fisher and J. S. Watson

Chemical Technology Division
Oak Ridge National Laboratory
Oak Ridge, Tennessee 37830

Abstract

Computer programs are being developed to predict the performance of hydrogen storage beds from the physical and chemical properties of the hydrogen storage material, the geometry of the bed, and the desired operational characteristics of the bed. The data base for these programs contains the properties of iron-titanium (FeTi) alloy, but the base could be extended to include properties of any material. Predictions have been made for two different shell-and-tube geometries in which the storage material is either in the shell or in the tubes. The programs predict bed pressure and temperature profiles as a function of flow rate, or flow rate as a function of pressure. Bed dimensions, temperature of the heat transfer fluid, and heat transfer coefficient are parameters.

The mathematical models that are being developed for these programs are evaluated by comparing predicted results with experimental data supplied by Brookhaven National Laboratory. A model that assumes rapid kinetics (equilibrium) and contains no empirical parameters produces bed pressures and temperatures which are in good qualitative agreement with experimental data; however, events such as maximum (or minimum) pressure and center-line temperature are predicted to occur at times different from those observed. An example of these results is presented here.

Introduction

Development of the best design of a solid hydrogen storage bed for any particular application is a very complex and difficult problem for several reasons:

1. A vast number of possible hydrogen storage materials, each having different characteristics, must be considered.
2. The geometry of the bed, the heat transfer surface area, and the heat transfer configuration must be specified.
3. The extent to which heat transfer enhancement can be used effectively must be evaluated.
4. All factors must be optimized within the constraints of the application (e.g., total bed weight, operating pressure, required maximum flow rate, heat transfer fluid temperatures, etc.).

Obviously, evaluation of all these parameters by constructing and operating test beds is not practical. Therefore, the objective of this program has been to use mathematical analysis, computer simulations, and experimental measurements to develop techniques and procedures for interpreting experimental data and for designing storage beds which meet requirements of specific applications using properties of the storage material.

*Research sponsored by the Division of Energy Storage Systems, U.S. Department of Energy under contract W-7405-eng-26 with the Union Carbide Corporation.

The Model

The model equations are a set of mass and energy balances in cylindrical geometry. Energy balances include heat accumulation, heat produced by reaction, and heat transferred by conduction. The bed is subdivided into annular shells, and the material in each shell is considered to be uniform and homogeneous. Boundary conditions for the equations include either the bed pressure or the hydrogen flow rate. Equations for a bed geometry in which the hydrogen storage material is inside tubes (with heat transfer fluid on the outside) have been presented previously;[1] an analogous set of equations is available for the case in which the bed is in a tank (or shelf) penetrated by several cooled heat transfer tubes.[2] Solution of the model equations requires an iterative procedure which is outlined in reference 3.

Physical Property Data

Heat transport and thermodynamic properties are represented in the data base as functions of temperature, pressure, and composition whenever the necessary experimental data are available. Figure 1 shows a comparison between experimental data[4] and predictions from the data base for the FeTi alloy--hydrogen desorption isotherm. The predicted curves are composed of equations for six different curve segments, each covering a different range of compositions. All equations were derived at 40°C; isotherms at other temperatures (dashed curves in

Fig. 1) are produced by applying the van't Hoff relationship at each composition. Equilibrium adsorption isotherms are generated in a similar manner. Heat of reaction and thermal conductivity are represented in the data base as functions of composition and hydrogen pressure respectively. Other properties, such as heat capacity and heat transfer coefficient, are taken as constants because they have not been well characterized experimentally.

The sensitivity of the model predictions to any one of these parameters has been examined. Thermal conductivity and the shape of the equilibrium sorption isotherm appear to be the most sensitive parameters; even a 20% change in the heat capacity, the heat transfer coefficient, or the heat of reaction produces less than 1% change in predicted loading times and bed pressure.

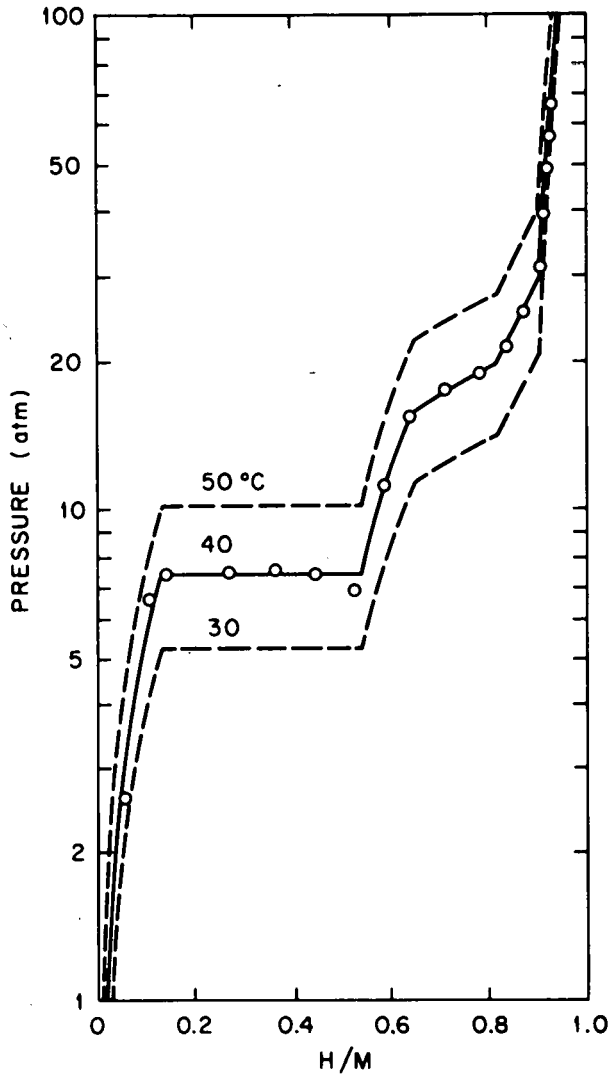

Fig. 1. Desorption isotherms of NL-2A-M FeTi alloy: points are experimental data,[4] and lines are predictions from the data base.

Results

Figure 2 shows predicted bed pressure, composition, and temperature as a function of time for a run reported by Strickland and Yu.[5] In this run, they used an externally cooled, 6.4-in.-ID cylindrical bed that contained 84 lb of FeTi alloy and had a hydrogen withdraw rate of 10 std liters/min. Comparison of these curves with the experimental results in Fig. 3 shows that the model (which contains no adjustable parameters) correctly predicts the shape and the magnitude of the experimental curves, but predicted events such as minimum pressure and temperature occur at times later than those observed experimentally. This discrepancy in time scale is believed to result from a combination of the effects of chemical kinetics and hysteresis (which occur when switching from adsorption to desorption). These effects are not taken into account in the model. The equilibrium isotherms contained in the data base were recorded in the range from 1 to 65 atm; however, the experiments cover only the range from 1 to 34 atm. Because there is a large gap (hysteresis) between the present adsorption and desorption isotherms (on the order of 10 atm at H/M = 0.84), there is a discontinuity in the model at this point. Interpolation procedures presently under development will bring the isotherms together at the composition of the bed when operation is switched from unloading to loading.

Programs have also been prepared to predict the behavior of beds with the same length and containing the same amount of alloy as the previous bed, but with internal cooling tubes (rather than external cooling). Runs with several different sizes and numbers of cooling tubes have shown that the bed pressure (rather than the maximum temperature or loading time) is the most difficult parameter to match between external and internal cooling configurations. The calculated results show that a bed with cooling tubes designed on the basis of these criteria to meet or exceed performance of the externally cooled 6.4-in.-ID bed would require six 0.25-in.-OD tubes, four 0.5-in.-OD tubes, or three 1-in.-OD tubes. Note that, as the diameter of the tube decreases, the number of tubes increases but the total heat transfer surface area actually decreases.

This analysis of hydride bed performance has proved to be extremely useful in understanding existing experimental data on bed performance, in identifying the critical parameters in bed design, and in pinpointing areas where more accurate experimental data are needed. It will also be useful in preparing designs of new experimental and demonstration units.

References

1. P. W. Fisher, S. E. Mitchell, and J. S. Watson, "Modeling Solid Hydrogen Storage Beds," Proceedings of the DOE Chemical/Hydrogen Energy Systems Contractor Review, Washington, D.C., Nov. 27-30, 1978, CONF-781142 (1979).

2. P. W. Fisher and J. S. Watson, "Modeling Solid Hydrogen Storage Beds, July 1979 Progress Report," submitted to M. J. Rosso, Jr., Brookhaven National Laboratory, Aug. 13, 1979.

3. J. S. Watson and S. D. Clinton (compilers), Advanced Technology Section Semiannual Progress Report for the Period Oct. 1, 1978, to Mar. 31, 1979. Volume 2: Engineering Science Programs, ORNL/TM-6891/V2 (in preparation).

4. M. J. Rosso, Jr., Brookhaven National Laboratory, private communication, Dec. 7, 1978.

5. G. Strickland and W. S. Yu, Some Rate and Modeling Studies on the Use of Iron-Titanium Hydride as an Energy Storage Medium for Electric Utility Companies, BNL-50667 (Apr. 26, 1977).

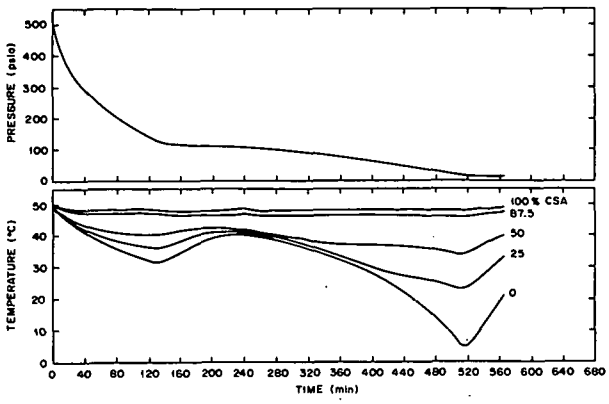

Fig. 3. Experimental unloading response of the bed with a hydrogen withdraw rate of 10 std liters/min (Ref. 5, Run E-08D1).

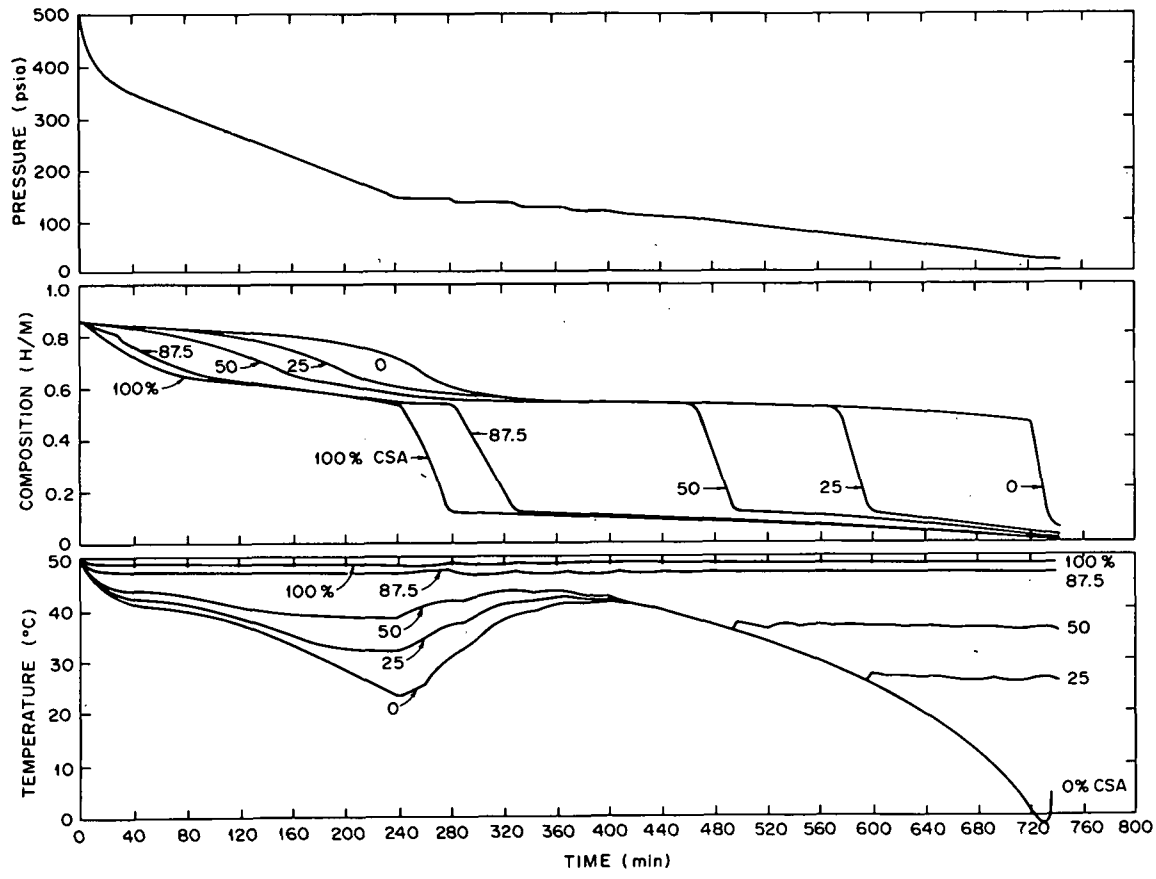

Fig. 2. Predicted unloading response of the bed with a hydrogen withdraw rate of 10 std liters/min.

Dup

HYDROGEN STORAGE FOR AUTOMOBILES*

Gerald Strickland

Brookhaven National Laboratory
Upton, New York 11973

ABSTRACT

Results of an analysis of hydrogen-fueled automobiles are presented as a part of a continuing study conducted by Lawrence Livermore Laboratory (LLL) on Energy Storage Systems for Automobile Propulsion. The hydrogen is stored either as a metal hydride at moderate pressure in $TiFe_{0.9}Mn_{0.1}H_x$ and at low pressure in MgH_x catalyzed with 10 wt % Ni, or it is stored in hollow glass microspheres at pressures up to about 400 atm. Improved projections are given for the two hydrides, which are used in combination to take advantage of their complementary properties. In the dual-hydride case and in the microsphere case where Ti-based hydride is used for initial operation, hydrogen is consumed in an internal-combustion engine; whereas in the third case, hydrogen from Ti-based hydride is used with air in an alkaline fuel cell/Ni-Zn battery combination which powers an electric vehicle. Each system is briefly described; and the results of the vehicle analysis are compared with those for the conventional automobile, with electric vehicles powered by Pb-acid or Ni-Zn batteries and with previous results for a liquid-hydrogen-powered vehicle. Comparisons are made on the basis of automobile weight, initial user cost and life-cycle cost. In this report, the results are limited to those for the 5-passenger vehicle in the period 1985-1990, and are provided as "probable" and "optimistic" values.

INTRODUCTION

Various energy storage devices are being examined as alternates to carbon-based liquid fuels. These devices consist of flywheels, batteries, fuel cells, and containers of hydrogen in various forms. Hydrogen is used in a modified internal combustion engine (ICE), or with air in a fuel cell, to power an electric vehicle. Environmentally, hydrogen is a desirable fuel because water is the main product of its combustion. Like many other fuels, hydrogen naturally occurs in the form of compounds, and thus requires energy to produce it in elemental form. Water is preferable to coal as the hydrogen source, and it is desirable to use a renewable source of energy such as various forms of solar-derived power, or geothermal or nuclear power, to produce the hydrogen. For widespread use, transmission and distribution systems would have to be constructed. The realization of these developments is several decades away; however, there could be a near-term specialized use of hydrogen-fueled vehicles where the higher cost is offset by the environmental advantages. These vehicles would be used in controlled areas such as warehouses, mines, and in some city sections. Furthermore, use of the hydrogen-air fuel cell would double the overall efficiency. The storage device design would be similar to that for automobiles. These fleet vehicles could have their hydrogen supply generated locally. Developments emerging from these experiences would be helpful in consideration of expanding the vehicular use of hydrogen.

The information presented here in brief form is taken from LLL's FY-79 annual report which is preceded by two others.[1-3] This continuing study is being conducted for the purpose of identifying the systems which appear to be best suited for automotive use in the remaining years of this century. Other national laboratories, industrial firms, and consultants are assisting; and funding is provided by the U.S. Department of Energy through the Division of Energy Storage Systems.

The study team is comprised of three panels reporting on energy storage technology and one analyzing vehicle performance and cost factors; namely the Electrochemical, Mechanical, and Chemical Energy Storage Panels, and the Automotive End-Use Panel. Members of the Chemical Panel are G. Strickland (Chairman), J. R. Johnson, J. McBreen, and M. J. Rosso of BNL, and consultants W. J. D. Escher and R. W. Foster of Escher:Foster Technology Associates, Inc.

In FY 79 the Chemical Energy Panel provided updated information on Hydride-Hydrogen Storage, introduced the Microcavity System (MCS) for Hydrogen Storage, and added the Alkaline Fuel-Cell/Battery System. There were no significant changes projected for the Liquid-Hydrogen System; so the projections listed are those from the FY-78 report.[2]

In defining vehicles for analysis, the End-Use Panel established four levels of performance, in terms of range and acceleration, and four vehicle sizes. The characteristics of ICE-powered automobiles so defined served as the basis for comparison. Evaluation of the alternate systems was done by replacing the ICE-power system with the alternate system sized to supply the required performance. The calculated vehicle weight, size, energy use and cost then serve as a measure of comparison. Details are provided in the full report.[1] In this brief report, projections are limited to those for a 5-passenger vehicle in the intermediate time period, 1985-1990, and are listed as probable and optimistic to indicate the expected range of values.

*Research performed under the auspices of the U.S. Department of Energy.

II. METAL HYDRIDE STORAGE

Substantial increases were made for the projections on available hydrogen content of the BNL Fast-Charge Reservoir, mainly on the basis of vehicular results that Daimler-Benz AG of West Germany obtained for their tube-type reservoir. A sketch of the BNL design, which also has the hydride packaged in tubes, is provided in the FY 78 report.[2] Briefly, arrays of 1-in.-diam. tubes are connected to opposite sides of a rectangular plenum and the assembly has a sheet-metal cover; a hydrogen connection is made at the plenum, and the cover has inlet and outlet connections for engine coolant. Aluminum alloy is used for the Ti-based hydride and stainless steel is used for the Mg-based hydride. For the Ti-based reservoir, the probable and optimistic values for hydrogen content (1985-1990) were increased 23%, and 9%, respectively. A similar adjustment for Mg-based hydride, coupled with a 13% reduction in wall thickness increased the probable and optimistic values by 23% and 17%, respectively. Use of a thinner wall was possible by reducing the charging pressure from 500 to 300 psia for the Mg-based hydride.

III. MICROCAVITY SYSTEM

The concept of storing high-pressure hydrogen in small, hollow glass spheres (microspheres) has been named the Microcavity System (MCS) for Hydrogen Storage by its proponent, R. J. Teitel.[4,5] It is based on hydrogen's high and selective permeability through glass at temperatures near 200°C, and on low permeability (leakage) at ambient temperature. To serve as storage media the microspheres are heated, pressurized with hydrogen via a compressor (200-400 atm), and then cooled. They can be transported or stored for use in a low-pressure container. Hydrogen is released by simple heating of the microsphere bed. A hydrogen content of up to 10 wt % is projected for microspheres of optimum size and composition.

For automotive use the MCS requires a complementary source of hydrogen until the bed is sufficiently heated by exhaust gas via a heat exchanger in the bed. This need is met by the use of a Ti-based hydride reservoir, which in addition to providing the initial hydrogen, also absorbs the hydrogen released from the microspheres during cooldown, through the use of a small compressor. About 80% of the hydrogen on board is stored in microspheres. An analysis conducted during the first year of work showed that in comparison with the dual-hydride system, the MCS was projected to weigh about 40% less, cost about half as much, and occupy about twice the volume.[6] In a recent laboratory-scale demonstration it was shown that glass microspheres can be loaded to a pressure of 200-400 atm, that the leakage is low at ambient temperature, and that the hydrogen can be released at a rate exceeding the engine demand by heating to 200°C.[7] Work on the MCS is still in an early stage of development and is being funded by the U.S. Department of Energy, Division of Energy Storage Systems, via BNL's Hydrogen Program. Further information on the MCS is provided in the article by R. J. Teitel in this Proceedings.

IV. FUEL CELL/BATTERY SYSTEM

Background

The hydrogen-air fuel cell is an attractive alternate to the heat engine for automobile propulsion because it has a substantially higher thermal efficiency and much lower emission and noise levels. Characteristically, fuel cell efficiency does not decrease significantly at loads down to 25% of rated output, nor does it decrease as rapidly compared with heat engines for smaller plant sizes (10-100 kW). The NO_x emissions are greatly reduced and there are no significant particulate emissions. Noise would be mainly limited to that from electric motors.

Although there is little apparent industrial development of fuel cells for land-based vehicles, a collaborative program entitled "Development of Fuel-Cell Technology for Vehicular Applications," was initiated in FY 78, the participants being Los Alamos Scientific Laboratories (LASL), U.S. Army Mobility Equipment Research and Development Command (MERADCOM), and BNL.[8] This effort evolved from a workshop on fuel-cell-powered vehicles at LASL in 1977, where representatives from the fuel-cell industry, automotive industry, national laboratories, and universities met to consider the applications of fuel cells to vehicular transportation.[9] The report evolving from the workshop contains a detailed technical and economic evaluation of the potential applications for fuel cells in transportation. City and highway buses, a delivery van, and the automobile were evaluated. The propulsion system considered was a fuel cell coupled with a battery driving an electric motor. This combination can provide performance close to that of current automobiles at nearly double the efficiency of internal combustion and diesel engines. Thus the fuel cell/battery combination is worthy of a detailed evaluation and development. Work thus far has been primarily directed to space applications, where cost is not a major factor, and toward utility applications, where weight and volume are less important. Therefore, revised designs are required for transportation applications, especially for the automobile where costs are more critical.

In the LASL workshop, three types of fuel cells were mentioned as contenders for vehicular applications: alkaline, phosphoric acid, and solid polymer electrolyte (SPE). The former was selected for the first analysis of this study. Phosphoric acid cells are now made for utility applications and integrated energy systems; and MERADCOM has reported on use of a phosphoric-acid fuel cell/Pb-acid battery used for a fork-lift truck.[10] SPE fuel cells have been used extensively in the space program, and have been assessed for mobile applications.[11] The hydrogen fuel can be stored in liquid form, as a compressed gas, or as a metal hydride. Alternatively, it can be obtained from methanol by use of an on-board reformer. All of these options require further evaluation.

Alkaline-Electrolyte Fuel Cell

This type of fuel cell was selected for the initial analysis of a fuel-cell/battery-powered vehicle because of several favorable factors; namely construction without noble-metal catalysts is possible; metal components can be used to resist shock and vibration; and the large-scale development of air electrodes for air-depolarized, chlorine electrolysis cells could result in lowering fuel-cell costs.

The usual practice for a fuel-cell/battery vehicle is to specify the fuel cell for range and the battery for initial operation and power surges. Thus the battery is used for cold starting and for about five minutes of operation until the fuel cell reaches its operating temperature (80°C), and also for acceleration. During cruise and deceleration the battery can be charged. For this analysis, the Ni-Zn battery was selected because it will apparently be the successor to the lead-acid battery when higher power density is advantageous. A Ni-Zn battery designed for peak power use was selected; its rating at 80% discharge is 310 W/kg.

Nearly a decade ago, Kordesch demonstrated the use of an alkaline fuel cell/Pb-acid battery system in a 4-passenger car weighing 909 kg (2000 lb).[12] A 6-kW fuel cell connected in parallel with a 4-kWh battery supplied power to a 7-kW (20-kW peak) DC motor. The hydrogen supply of 1.69 kg (660 ft^3), which was stored as a compressed gas in six lightweight steel cylinders, provided a range of about 322 km (200 miles). The operation of this automobile showed that the fuel cell/battery combination is viable, and that the car behaved essentially like a gasoline-fueled car, except that its top speed was limited to 88 km/hr (55 mph).

The components required for an alkaline-electrolyte fuel cell are the cell stack, a circulation system for the electrolyte (50% KOH), an electrolyte reservoir, a hydrogen feed and circulation sytem, an air circulation system with a CO_2 scrubber, a water-vapor condenser, a nitrogen supply for blanketing the cells during overnight standby, and associated instrumentation and controls. In the present case, hydrogen is supplied by a Ti-based hydride ($TiFe_{0.9}Mn_{0.1}H_x$). Hot electrolyte (80°C) flowing through the heat exchanger of the hydride reservoir releases the hydrogen. About half of the water produced in the hydrogen-air reaction is removed in the air-cooled condenser. A soda-lime scrubber removes CO_2 in the inlet air. Details on the component materials, and on projected weights, volumes and efficiencies for 10-20 kW fuel cells are given in the FY-79 report.[1] The projections are based on recent experimental results obtained at BNL.

Future Work

It is recognized that fuel-cell technology is still in an early stage of development; whereas the internal combustion engine has evolved over more than 50 years. In view of this advantage, systematic and carefully planned programs are essential in pursuing the development of a practical fuel-cell/battery automobile. Such a vehicle could logically follow the battery-powered electric vehicle as an alternative offering performance close to that of current automobiles. The fuel cell/battery is also a candidate for other traction vehicles (trucks, buses and trains) which can carry large amounts of fuel to attain the desired range; whereas batteries are unsuited for this service.

Continued efforts over a wide front are required in developing this new technology. These deal with improving cell performance, reducing costs, obtaining practical experience with vehicles, analyzing the system technically and economically, and planning for fuel production. Those attending the LASL workshop in 1977 expressed a mood of cautious optimism, and believe that the results of their analysis indicate that a fuel-cell/battery vehicle can be a reality in the 1990's.

Comparison of Vehicles

Some weight and cost projections (tentative) resulting from the vehicle analysis are presented in Table 1. The data are limited to 5-passenger vehicles for the 1985-1990 period, and are stated as probable and optimistic values. Actual weights and costs are listed for the baseline ICE vehicle (fueled by gasoline), and factors related to these values are used for comparison of the other vehicle types.

A review of the projected weight data shows that only the ICE vehicle fueled with liquid hydrogen is comparable to the baseline-ICE vehicle. The vehicle with hydrogen stored in microspheres is the closest competitor to liquid hydrogen. The fuel cell/battery vehicle has a higher performance level than either battery vehicle and also weighs significantly less. The dual-hydride vehicle qualifies for equivalent performance, at an appreciable weight penalty, but offers little advantage over the Ti-based-hydride vehicle at the lowest levels.

In terms of initial user cost, the liquid-hydrogen vehicle is projected to be comparable to the baseline vehicle, and the microsphere vehicle is a close second, except at equivalent performance. The fuel cell/battery vehicle is lower in cost than either of the battery vehicles, but costs more than either of the hydride vehicles.

Similarly for life-cycle costs, the ranking is generally the same. The liquid-hydrogen vehicle has lost some of its advantage, and the microsphere vehicle is close to it, except for the equivalentperformance case.

According to these projections, the vehicle powered by liquid hydrogen is the closest competitor to the baseline ICE vehicle. Safety issues in handling liquid hydrogen remain to be resolved. The microsphere-powered vehicle is a contender if a H_2 content of 10 wt % can be achieved. Hydride vehicles are more competitive in the limited and minimum performance levels, where the simplicity of the Ti-based hydride vehicle is preferable. The fuel cell/battery vehicle is superior to the battery vehicles at the two higher performance levels; whereas the latter have lower costs at the minimum performance level. It appears that the fuel cell/battery vehicle is a candidate for larger and heavier traction vehicles where its much higher efficiency can substantially reduce fuel consumption. For such use liquid hydrogen or methanol (reformed to hydrogen) appear to be the preferable form of fuel.

REFERENCES

1. Forsberg, H. C., et al, Energy Storage Systems For Automobile Propulsion: 1979 Study, Vol. 2. Detailed Report, UCRL-52841, Draft Report (in press).

2. Behrin, E., et al, Energy Storage Systems for Automobile Propulsion: 1978 Study, Vol. 1 Overview and Findings, Vol. 2. Detailed Report, UCRL 52553, December 1978.

3. Behrin, E., et al, Energy Storage Systems for Automobile Propulsion: 1978 Study, Vol. 1 Overview and Findings, Vol. 2. Detailed Report, UCRL 52303, December 1977.

4. Teitel, R. J., "Processing and Apparatus for Achieving Hydrogen Storage and Dispensing," Offenlegungsschrift 2527910, Bundersrepublik Deutschland Deutches Patentant, Aug. 1, 1976.

5. Teitel, R. J., and Solomon, D. E., "Nuclear Fuel Pellets and Methods of Making Them," Great Britain Patent No. 1,492,572.

6. Teitel, R. J., Henderson, T. M., Luderer, J. E., Powers, J., Microcavity Systems for Automotive Applications, Final Progress Report, RJTA Report No. 780001006U-R1, prepared for Brookhaven National Laboratory, Contract No. 436153-S, November 1978.

7. Private Communication from R. J. Teitel, and demonstration conducted at Brookhaven National Laboratory, Upton, N.Y., on June 11, 1979.

8. McBreen, J., Taylor, E. J., Kordesch, K. V., Kissel, G., Kulesa, F., and Srinivasan, S., Development of Fuel Cell Technology for Vehicular Applications, Annual Report, October 1, 1977 - September 30, 1978, November 1978. BNL 51047.

9. McCormick, B., Huff, J., Srinivasan, S., and Bobbett, R., Application Scenario for Fuel Cells in Transportation, LA-7634-MS, Informal Report, February 1979.

10. Dowgiallo, E. J., A fuel cell-battery power source for electric vehicles, Proc. of the Fifth International Electric Vehicle Symposium, Philadelphia, Pennsylvania, October 2-5, 1978.

11. McElroy, J. R., An assessment of the solid polymer electrolyte fuel cell for mobile power plants, Proc. of the 28th Power Sources Symposium, Atlantic City, New Jersey, June 12, 1978.

12. Kordesch, K. V., Research Memorandum, CRM-244, Hydrogen-Air/Lead Battery Hybrid System for Vehicle Propulsion, Union Carbide Corp., Consumer Products Division, Research Laboratory, Parma, Ohio, August 1970.

TABLE 1

5-PASSENGER VEHICLE WEIGHTS, COSTS, AND FACTORS FOR 1985-1990

PERFORMANCE:	EQUIVALENT		INTERMEDIATE		LIMITED		MINIMUM	
Part A: Curb Mass (kg) and Factors Relative to ICE Values								
Projection	Prob.	Opt.	Prob.	Opt.	Prob.	Opt.	Prob.	Opt.
Baseline ICE	1130	1090	985	945	930	890	870	830
Pb-Acid Batt.	-	-	-	2.43	2.17	1.72	1.63	1.42
Ni-Zn Batt.	-	-	-	1.85	1.75	1.44	1.42	1.26
Fuel Cell/Batt.	-	1.86	1.78	1.40	1.39	1.18	1.24	1.14
Dual Hydride	1.74	1.41	1.25	1.14	1.05	1.05	1.00	1.01
$TiFe_{0.9}Mn_{0.1}H_x$	-	-	1.61	1.44	1.17	1.14	1.08	1.07
Microspheres	-	1.50	-	1.20	-	1.07	-	0.99
Liquid Hydrogen	1.02	0.95	0.97	0.95	0.95	0.95	0.93	0.95
Part B: Initial User Costs (1977 $) and Factors Relative to ICE Values								
Projection	Prob.	Opt.	Prob.	Opt.	Prob.	Opt.	Prob.	Opt.
Baseline ICE	3550	3540	3400	3390	3350	3340	3260	3260
Pb-Acid Batt.	-	-	-	2.37	1.88	1.52	1.30	1.19
Ni-Zn Batt.	-	-	-	2.41	2.03	1.56	1.40	1.21
Fuel Cell/Batt.	-	2.72	2.42	1.74	1.77	1.36	1.49	1.24
Dual Hydride	2.49	1.85	1.44	1.21	1.10	1.07	1.05	1.03
$TiFe_{0.9}Mn_{0.1}H_x$	-	-	1.75	1.49	1.14	1.11	1.08	1.06
Microspheres	-	1.34	-	1.09	-	1.04	-	1.01
Liquid Hydrogen	1.10	1.08	1.05	1.04	1.02	1.02	1.02	1.02
Part C: Life-Cycle Costs (1977¢/km) and Factors Relative to ICE Values								
Projection	Prob.	Opt.	Prob.	Opt.	Prob.	Opt.	Prob.	Opt.
Baseline ICE	8.64	8.58	8.21	8.15	8.08	8.02	7.90	7.84
Pb-Acid Batt.	-	-	-	1.71	1.53	1.20	1.14	1.01
Ni-Zn Batt.	-	-	-	1.58	1.67	1.16	1.25	0.98
Fuel Cell/Batt.	-	2.11	2.10	1.56	1.70	1.35	1.52	1.35
Dual Hydride	2.19	1.72	1.53	1.35	1.30	1.26	1.26	1.23
$TiFe_{0.9}Mn_{0.1}H_x$	-	-	1.73	1.53	1.34	1.28	1.28	1.24
Microspheres	-	1.42	-	1.18	-	1.12	-	1.02
Liquid Hydrogen	1.24	1.20	1.14	1.12	1.12	1.12	1.11	1.11

HYDROGEN HOMESTEAD

PROGRAM REVIEW AND CONTINUATION PLAN

R.E. Billings, L.D.Hadden, G.L.Kimball, R.L.Woolley

Billings Energy Corporation
Provo, Utah 84601

Abstract

A hydrogen storage vessel containing approximately 4000 pounds of metal hydride was tested by Billings Energy Corporation during 1978 as part of the Homestead Project. The final report related to this testing is reviewed. Recommendations from the First Year Final Report and from Brookhaven National Laboratory form the basis for the described study.

This study will yield information related to:

1. The length of time the Homestead Hydride Vessel can sustain flow rates from 12 lb H_2/day to 2 lb H_2/day.

2. The suitability of the storage vessel to meet user demands at one or more homesteads.

3. The requirements for safe functioning of the Homestead complex.

An improved electrolyzer to produce hydrogen for the hydride vessel and a 12-bit A-D computer board are being installed. The hydride vessel is charged with hydrogen in preparation for the present study.

DEVELOPMENT STATUS OF MICROCAVITY HYDROGEN STORAGE SYSTEMS FOR AUTOMOTIVE APPLICATIONS

Robert J. Teitel

Robert J. Teitel Associates
San Diego, California

Abstract

Robert J. Teitel Associates under sponsorship of the U.S. Department of Energy is developing a new concept (microcavity storage) for hydrogen storage. The microcavity hydrogen storage concept proposes to use hollow glass microspheres for the storage of high pressure gas. Last year, the concept was detailed sufficiently to perform an engineering economic evaluation of the system and compare it to an equivalent metal hydride system. The microcavity storage system was lighter and more economical. However, the volume was larger. The study provided goals and a reference system for further engineering and experimental studies.

An experimental program to evaluate two candidate commercially available microspheres for storage beds was initiated this year. Fillite grade 300/7 and 3M grade 32D/4500 were selected for the study. The Fillite grade proved to require an higher temperature source than available in automotive applications. The commercial grade 32D/4500 has more suitable properties. The only property that did not meet the target microsphere bed characteristic set by last year's study was the hydrogen storage medium weight density ($\sim$ 0.055 gmH_2/gm of bed).

Two engineering studies were conducted this year. One was an engineering economic study of alternate concepts of a microsphere filling plant. The other was an engineering comparison of a hydrogen distribution system for the microcavity storage system to that for a metal hydride system.

Background

The microcavity hydrogen storage concept was introduced last year.[1] Basically, the concept proposes to store hydrogen in small pores or cavities. Many cellular arrangements are possible. Hollow glass microspheres are being considered at present. Typically, these microspheres are 5-200 μm in diameter and have wall thicknesses of 0.25 to 5 μm .

An engineering evaluation of the concept was completed last year.[1] One of the conclusions of the study was that, with the assumptions made concerning the performance of microspheres, a microcavity system is lighter and more economical than an equivalent advanced metal hydride system. However, the microcavity system required more space. This disadvantage is inherent in the storage of high pressure hydrogen gas. A set of properties for microsphere beds was developed during that study which have been used as an objective in the current experimental studies. During the study last year, a hydrogen filling plant was designed and evaluated. This plant served as a reference design for further improvement evaluations studies.

This year, RJTA has initiated an experimental program to seek commercial grades of microsphere beds to meet automotive storage requirements. The investigations were approached from a bed performance characterization rather than an individual microsphere performance. The program also included two engineering studies. One looked at alternative microsphere filling plants, and, the other took a preliminary look at hydrogen distribution systems for both the microcavity and metal hydride storage systems and compared them with regard to their relative safety and economics.

Experimental Studies

A study on hydrogen filling, retention and dispensing properties of two commercial microsphere beds is being conducted. The techniques for evaluating the candidate microsphere beds were selected to closely simulate the performance of a hydrogen storage system.

The first step in the program was to select two commercially available microsphere grades. This selection was primarily based on available information from the literature and supplier technical publications. The 3M grade D32/4500 was selected because of its higher strength and the Fillite grade 300/7 was selected for its potential economics.

A key analytical technique used in the study was the "sink-float" test. It consisted of mixing a microsphere sample into a fluid (water, methanol or isopropl alcohol). After the mixture was allowed to settle, the solids either float or sink to the bottom. The floaters were whole microspheres and the sinkers were debri or segments of broken spheres. Both the sinkers and floaters were dried and weighed. This test provided quantitative

data on breakage. It was used on a larger scale to recover strong microspheres after pressure treatments.

In crush tests, the microspheres were subjected to high pressure gas. The residuals were recovered and submitted to sink-float tests. Crush tests were conducted on a number of microsphere grades at pressures up to 6000 psi of nitrogen gas. The strongest grade of microspheres was the 3M grade D32/4500 with 96% survival at 3500 psi, 66% survival at 4500 psi, 55% survival at 5500 psi and 50% survival at 6000 psi. Recently, 3M grade B38/4000 was added to the program. Its crush strength properties paralled that of the 3M-D32/4500 grade showing 92%, 46% and 37% survivals at 3000, 4500 and 6000 psi pressures, respectively. Repeated pressurization of survivors to the crush pressure did not lead to continued breakage. Specimens of "as received" 3M grade D32/4500 were subjected to 10 and 20 repeated pressurizations at 6000 psi. Survivals of 49 and 50%, respectively, were essentially the same as exposure in the first pressure cycle. Unlike the other microsphere grades, the crush test survival count for the Fillite grades did not decrease with crush pressures between 3000 and 6000 psi. These grades were considered suitable for hydrogen storage.

Fill-Dispense Studies

Fill and dispense tests were basic to the whole study. They demonstrated, on a miniature scale, the operation of a microsphere hydrogen storage bed exclusive of thermal dynamics. Samples, 5-10cc in volume, were filled in high pressure, (up to 12,000 psi) hydrogen at temperatures up to 400°C. Filled microspheres were stored for tests on dispensing, storage life and demonstrations.

Samples of filled microspheres (.1 to 5cc) were placed in a glass tube and heated for dispension studies. The tube was attached to a gas buret through a linear mass flow meter. Data was taken on the bed temperature, H_2 flow rate, and accumulated volume of gas at one minute intervals. The temperature was increased step wise. At each temperature level the flow rate was monitored till it fell below a practical flow rate. Then, the temperature was raised 20°C and the operation repeated until the bed was depleted. Signs of breakage during the test was monitored by listening for popping sounds and watching for irratic fluctuations in hydrogen flow. It is very likely that breakage of one microsphere caused others near to it to break also. Thereby, causing a large group of microspheres to break at one instant. Data obtained from the dispension experiments were used to obtain pertinent data on flow rates, permeation rates, microsphere strength and storage life.

During the filling and dispensing tests it was possible to establish a threshold strength for the 3M grade D32/4500 microspheres. It was noticed that pressures above 5000 psi, external or internal to microsphere, initiated breakage. Using the familar hoop stress relationships and the ratio of microsphere diameter to wall thickness, the threshold stress in the microsphere wall was about 50,000 psi. Once this was established, our experimental procedures were evaluated and redesigned to keep the pressure gradient across the walls below 5000 psi. Eventually, we were able to fill microspheres with very little breakage.

Properties of the 3M grade D32/4500 are given in Table 1. About 55 percent of the stored hydrogen was recovered at practical rates at temperatures below 200°C. This was lower than desired. The option of changing the chemical composition of the microspheres was not available. Therefore, a smaller size was explored. "As received" 3M D32/4500 grade was modified by sieving the material to recover a <325 mesh (<45 μm) size fraction. About 50 weight percent of the "as received" 3M microsphere were below the 325 mesh size. The modified 3M grade exhibited higher dispension rates and the available hydrogen increased to ∿70-75 percent. In the study last year, an availability of 85 percent was assumed. If the maximum temperature is increased to 250°C, the availability increased to ∿80%.

Another design feature that the modified 3M grade failed to meet was the storage pressure. In last year's study, an assumed storage pressure was 491 atm or a hydrogen weight storage density of 0.11 g H_2 per g of bed. Weight densities obtained in our expermental studies were .055-.060 g H_2 per g of bed. This is about half of the target value.

Specimens of "as received" 3M grade were submitted to repeated fill and dispense cycles. These tests were done early in the test program and probably the procedure caused wall pressure gradients to exceed strength limitations. Breakage was encountered on each cycle. As discussed above, pressure cycles to the same pressure levels did not result in further breakage. Some work was done on the properties of another 3M grade, B38/4000. It appears that this grade required higher temperatures. The characterization of Fillite grade microsphere beds was curtailed because the bed failed dispense hydrogen within the automotive heat source temperature range.

Handling the filled microspheres in the laboratory did not result in excessive breakage. Therefore it was concluded that, as long as the wall strength limitation of 5000 psi is not exceeded, the microspheres are mechanically sound. Some

empty 3M grade microspheres were tumbled for an extended period without any detectable breakage.

Storage life was investigated by taking samples of filled microspheres from storage periodically. The residual hydrogen was determined by dispensing the hydrogen content and comparing that quantity with an earlier sample of the same batch. The measured half life (the time to lose half of the content) varied over a range from 30 to 120 days. The 3M grade D32/4500 unmodified had a demonstrated storage half life over 120 days. The shorter storage half lives were attributed to poor storage conditions (repeated exposure to air, high temperature and humidity). Storage conditions could be improved. For example, if the microspheres were refrigerated to 0°C in storage, the storage half life could be extended 5 to 6 fold according to extrapolations using permeability data. In the study performed last year, the assumed storage half life was about forty nine days.

Microsphere Costs

The Fillite Corporation and 3M Corporation were requested to project costs for Fillite grade 300/7 and 3M grade D32/4500 at a production level of 3.5×10^5 tons/yr for a single plant or an overall annual production of 7.2×10^7 tons/yr. Fillite estimated a cost equivalent to $.23/lb to $.38/lb (based on a 1975$) for their product and 3M estimated $.77/lb. to $1.15/lb., on the same basis, for their product. Our study last year assumed a breakage of 5 per cent and this was a significant cost factor at $.10/lb. Our studies show that, if the strength limits are not exceeded it may be possible to maintain a very low breakage and to counteract the higher prices of microspheres should they develop. There are also other engineering trade-offs to be considered that await further developments.

Engineering Studies

This activity was divided into two parts. The first was an engineering economic evaluation of alternate microsphere filling plant processes. The other was an engineering comparison of hydrogen distribution systems for a microcavity storage system and a metal hydride storage system.

Two steady-state, continuous-flow filling processes were compared to the batch process evaluated last year. Process variables used in the study included: three hydrogen pressure feeds, 500, 1000 and 3000 psi; two filling temperatures, 300 and 350°C. The allowable pressure gradient across the microsphere walls was raised to 3000 psi; and, an encapsulation pressure of 400 atm was assumed.

One process design (Fluidized Bed Process) assumed that the hydrogen and microspheres were perfectly mixed. Under these conditions the contained hydrogen pressure in microspheres of the same size within a process vessel was uniform. The second process design (Plug Flow Process) assumed that the gas and suspended microspheres move together (co-currently) through the process vessels. Ideally, the contained hydrogen pressure within each size range is uniform at any particular plane perpendicular to flow and increases in the direction of flow.

In both of the above concepts, the microspheres were transported from one vessel to the next by passing microspheres through pressure locks. The microspheres were subjected to step-wise increases in pressure as they passed from vessel to vessel. Block flow diagrams were developed for both processes and used in the economic evaluations.

The modified processes evaluated show potential for reducing the filling plant costs derived through our study last year, $2.76 down to $1.05/million Btu. However, the cost of hydrogen feed still dominated the total cost.

The study performed this year confirms the conclusion of the study performed last year. Both indicated that the microcavity hydrogen storage system promises to be less expensive than a comparable advanced metal hydride hydrogen storage system.

In the second part of the engineering study, a hydrogen distribution system for both the microcavity system and the metal hydride system was designed sufficiently to perform a non-quantitative evaluation for safety and cost.

For the microcavity system, it was assumed that the hydrogen was encapsulated at the hydrogen production plant and transmitted, in microspheres, from the production plant to the vehicle. For the metal hydride system, pipe-line transmission of gas from the production plant to the service station was assumed. The operations of loading the hydrogen into the fuel tank at the service station were also considered.

It was apparent from the engineering study that the microcavity storage system because of its cellular storage, is safer and more economical. However, the transmission costs for the microspheres would have to be less than half of the gas pipe line transmission to cover costs for the return of empty microspheres to the filling plant.

Status

The status of the microcavity storage systems is summarized in Table I. The 3M grade D32/4500 has been studied in detail. The properties measured for this grade indicate that it will come close to meeting all the specifications except for storage density. The microspheres held pressures up to 250 atm. at room temperature without incurring breakage during the fill and dispense cycle.

Future Directions

The program thus far has shown that the microcavity hydrogen storage concept has great promise. The hoop stress limitation was disappointingly low (50,000 psi). Strengths up to 1,000,000 psi have been reported for glass fibers. Therefore, a development of improved microspheres is warrented.

Future activities should be directed into the following problem areas:

1. Safety and transporation studies
2. Continued exploration of microsphere sources.
3. Scale-up bed performance tests
4. Engineering of storage vessels
5. Large scale testing of Microsphere Beds.
6. An engineering re-evaluation of the system taking into account the experimental information gained through the program this year.

References

1. R.J. Teitel, T.M. Henderson, J.E. Luderer and J. Powers, "Microcavity Systems for Automotive Applications", Final Progress Report submitted to the Brookhaven National Laboratory November, 1978.

Acknowledgements

The fill process design studies were performed by Professor J. Powers, University of Michigan, Ann Arbor, Mich. and the laboratory assistance by J.W. Niemeyer of Robert J. Teitel Associates. The author acknowledges the sponsorship and cooperation of the Brookhaven National Laboratory and, in particular, M. Rosso, Technical Monitor.

Table 1
Properties of 3M D32/4500 Hydrogen Storage Bed

Thermal

Softening Temperature(°C)	715
Max. Operating Temp.(°C)	~550

Glass Composition

SiO_2 (mole %)*	80.9
B_2O_3	2.3
CaO	8.6
Na_2O	8.2

* Normalized to metal oxide content (about 5.7 wt% unidentified)

Strength

Max. External Press. (psi)	~5000
Max. Internal Pressure	~5000
Threshold Hoop Stress in Microsphere Wall (psi)	50,000

Crush Survivors (%)

3500 (psi)	96
4500	66
6000	50

Hydrogen Permeability

Temperature (°K)	cc (STP) mm / cm^2 sec.(cm of Hg)
300	9.6×10^{-15}
413	1.5×10^{-13}
473	6.6×10^{-13}
573	2.3×10^{-12}
623	3.9×10^{-12}
673	5.8×10^{-12}

Storage Bed Characteristics

Bulk Density (g/cc)	0.2
Av. Microsphere Size (μm)	27.7
Microsphere Size Range (μm)	5-60
Surface Area (m^2/g)	0.77
Glass Density (g/cc)	2.15
Density of Stored Hydrogen Gas (g/cc)	0.017
Bed Weight Density (gH_2/g bed)	0.053
Bed Volume Density (gH_2/cc bed)	0.012
Packing Fraction	0.63
Filling Conditions	
Temperature (°C)	>300
Time (hr.)	<1
Fill Pressure (psi)	3500
Operating Bed Temp. (°C)	140-200
Dispension Rates at Temperatures below 200°C (ccm/cc of bed)	0.71
Available Hydrogen at 200°C (%)	55
Available Hydrogen at 250°C (%)	70
Storage Half Life (da.)	~110

Cost Factors*

Current ($/lb.)	
Lot Size (lbs.)	
100-300	15.33
400-2,300	14.18
>2400	13.68
Projected ($/lb.)	0.77-1.15

*Data obtained from 3M Corporation

UNDERGROUND STORAGE OF HYDROGEN

Stephen M. Foh, Martin Novil, Philip L. Randolph and Evelyn M. Rockar

Institute of Gas Technology
Chicago, Illinois

Abstract

This paper briefly summarizes an extensive study of the technical and economic feasibility of storing hydrogen gas in underground reservoirs. A depleted field, an aquifer, a salt cavern, and an excavated rock cavern were studied. The only major technical limitation is that of hydrogen embrittlement, which at the present time restricts reservoir pressures to 1200 psi or less. An economic methodology was developed to predict the cost of service for hydrogen storage. This methodology was verified and tested on natural gas storage. Costs of service ranged from 26% to 150% of the cost of the gas stored.

Background

The first successful underground storage of natural gas was accomplished in Ontario, Canada, in 1915 in a partially depleted gas field. As of 1977 there were 385 natural gas storage reservoirs in the United States with a total storage capacity of 7.2 trillion cubic feet. Of these 385 reservoirs, about 52 are aquifers, about 15 are salt caverns, 1 is an excavated mine, and the remainder are depleted gas or oil fields. Each of these field types has a different geological distribution throughout the United States. Aquifers exist mostly in the Midwest, salt caverns exist in the Great Lakes region and along the Gulf Coast, and depleted fields are scattered among 26 states.

In addition to natural gas, other fluids have been successfully stored in underground reservoirs. Liquified gases have been stored in excavated and solution-mined caverns since 1951. Hydrogen gas has been successfully stored in solution-mined salt caverns in England by Imperial Chemical Industries at Teeside. This storage utilizes three brine-compensated caverns to store hydrogen at 750 psi at a depth of 1200 feet. In a reservoir near Beynes, France, Gaz de France operated a storage aquifer for hydrogen-rich (50% to 60%), low-Btu manufactured gas from 1956 to 1972. The field was successfully converted to natural gas storage in 1973. Helium has been stored by the U.S.G.S. in Bush Dome near Amarillo, Texas, since 1960.

Modes of Storage

Facilities for the underground storage of gases fall into two categories: 1) porous media storage, in which the gas occupies the naturally occurring pore space between mineral grains or crystals in sandstones or porous carbonates, and 2) cavern storage, in which the gas is contained in excavated or solution-mined cavities in dense rock. Porous media storage, either in partially depleted oil or gas fields or in aquifers, accounts for the large majority of all underground storage facilities for natural gas. Natural gas is stored in solution-mined salt caverns and in one excavated cavern. While no excavated cavern has as yet been developed specifically for the storage of natural gas, they are widely used for the storage of propane and other hydrocarbons in liquified form. Since a supernatant vapor phase is invariably present overlying the hydrocarbon liquids in such facilities, consideration of the facilities is appropriate for the underground storage of any gas in the vapor phase.

Although each mode of underground storage has its own set of critical characteristics, there are several basic considerations common to all forms of underground storage. Both categories of storage must possess sufficient capacity and containment for the gas in order to be successful. These two requirements are satisfied by different mechanisms with each mode of storage. In porous media, these requirements are met by a porous reservoir rock and an overlying confining enclosure; whereas, in cavern storage, capacity is achieved from the chamber volume with containment provided by the impermeable host rock surrounding the cavern. Several factors greatly influence the magnitude of capacity and containment for a given storage mode; chief among these is pressure. Since most rock lithologies cannot be considered to be absolutely impermeable, the limiting pressure for almost all forms of underground storage is related to the hydrostatic pressure gradient or, for purposes of approximation, 0.433 psi per foot of depth below the water table.

The overburden pressure, 1.0 psi/ft of depth, is the load of the rock column and when approached may result in hydraulic fracturing, or lifting, of the overburden. To remain safely below this limit, storage facilities that operate above the hydraulic pressure do not often exceed a gradient of 0.7 psi/ft of depth, which allows for a margin of safety.

Most existing underground facilities for natural gas have maximum operating pressures in the range of 1000 to 2000 psi, although there are facilities operating at both extremes, from a low pressure of 160 psi to a maximum of over 3500 psi. As the storage pressure increases, less void volume is required for a given quantity of stored gas.

Mechanisms Controlling — Containment or Loss

The same mechanisms that serve to contain gas in porous media storage apply also to cavern storage; however, the emphasis is different. In porous media storage, a major concern is the intrinsic characteristics of the lithologic confining elements, particularly their permeability and threshold pressure. In cavern storage, the site is normally selected specifically because the host rock is dense with very low intrinsic permeability and very high intrinsic threshold pressure. Purely hydrological confining mechanisms such as the transport of gas in solution in water are even less pertinent since the density and impermeability

of the host rock minimize both the mobility of the water phase and the extent of gas contact with it.

The term gas "loss" requires definition, particularly as distinguished from "leakage". It is probable that there is some finite gas loss from virtually all storage reservoirs: loss through cap rock, loss through solution in water, loss through solution defects in the wells themselves. Not only are many of these losses very minor in quantity, but they are also a predictable consequence of the environment of gas storage and the technology for its development. They do not necessarily have an impact upon life or property in the surface or near-surface environment.

In terms of frequency of occurrence but not necessarily in terms of volumes of gas lost, the greatest single factor affecting the containment of gas within a storage reservoir is the wells themselves. Gas losses from this source are normally comparatively easy to detect and remedy and commonly originate from corrosion of casing or failure of the cement bond between casing and host rock. A large body of well-developed technology is available to detect and remedy such defects.

Consequences of seismic activity upon the integrity of underground storage reservoirs appear to be minimal. No report of gas loss directly attributable to seismicity, even among the several depleted field storages in seismically active portions of California, is known to exist. In general, subsurface installations in competent rock should be much less susceptible to damage arising from earthquakes than would associated surface facilities such as pipelines, aboveground storage, and compressor stations.

The sucessful history of storing natural gas in underground reservoirs leads us to conclude that there are no overriding constraints that would prohibit the similar storage of hydrogen gas. There are properties of hydrogen gas, though, that must be considered in an underground storage operation. Those properties that imply limits to the successful storage of hydrogen are discussed in the following section.

Technical Evaluation of Hydrogen Properties

Safety

Gas storage is regulated by the Code of Federal Regulation, Title 49, Part 192, "Transportation of Natural and Other Gas by Pipeline: Minimum Federal Safety Standards." This code applies to hydrogen as well as to natural gas. It will require only one significant change to be made when a natural gas facility is converted to hydrogen: It specifies conformation to the National Electrical Code, an otherwise nonmandantory but industrially accepted standard, which will make it necessary for most electrical equipment in the facility to be replaced. A few other very minor changes may be necessary, but there appear to be no other codes or regulations that would require a hydrogen storage facility to be treated any differently from a natural gas facility. Although surface monitoring and delivery instrumentation will have to be changed to that for hydrogen service, safety requirements for the design of the surface buildings, roads, and relative location of pipelines should be no different for hydrogen than for natural gas.

Environmental Effects

The preparation of an environmental impact statement for an underground hydrogen storage facility would follow the format of impact statements presently being required for the testing, construction, and operation of underground natural gas storage facilities.

The underground storage of hydrogen gas does not appear to pose any significant adverse impacts to the terrestrial or aquatic ecosystems in the vicinity of storage facilities. There are two ways that hydrogen could escape from the storage horizon and possibly reach the surface. First, gradual seepage from a storage reservoir could occur through overlying rock layers due to geological mechanisms; secondly, rapid leakage at damaged well heads can occur due to mechanical leaks that usually are short-term and promptly corrected.

Free hydrogen (H_2) exists in the atmosphere in very minute amounts. It is the lightest of elements and, consequently, very buoyant, which would lead to its rapid dispersal upon entering the atmosphere. Free hydrogen is not known to be toxic to living organisms, consequently, the likelihood of significant adverse impacts arising from the release of hydrogen into the surface environments is very small.

Theoretically, imperceptible seepage by molecules of a gas from a storage reservoir over a prolonged period of time is possible through the confining rock layers as well as fractures in joints. Such gradual diffusion could reach the surface in undetectable volumes of gas at atmospheric pressure. Significant leakage of large volumes of gas due to geological mechamisms is rare. In one reported case, the leakage of detectable quantities of methane (CH_4) from underground storage facilities caused localized minor crop and vegetation damage. The nontoxicity of hydrogen precludes such damage in the rare event that large volumes would gradually escape through geological mechanisms.

Hydrogen could rapidly escape from the storage area as a result of a damaged wellheads; however, damage to well heads can be repaired and avoided. A rapid release of hydrogen from an injection/withdrawal well could create a noise problem that can be minimized by locating wellheads away from residences. If the damage to the wellheads were also to ignite the hydrogen, it would produce an intense upwardly dispersed clean-burning flame. The only anticipated product from an accident of this type would be water vapors (H_2O). Such an accident of this type could ignite surrounding vegetation and cause injury to anyone involved in the accident; however, the potential for such an adverse impact is considered remote. If the escaping hydrogen is not ignited, it would rapidly disperse in the atmosphere causing no impact to the surface environment.

Hydrogen Embrittlement

The purpose of our investigation of hydrogen embrittlement is to determine whether equipment used in natural gas storage facilities is suitable for hydrogen service, and, if it is not suitable, what must be changed. There is considerable industrial experience in this country in the

handling of high-pressure hydrogen. Petrochemical industries, hydrogenation operations, and retailers of commodity gases all have considerable experience with hydrogen service. In addition, there is a limited base of experience in the design of pipelines for hydrogen service. Because of a lack of understanding of the basic mechanisms involved in hydrogen embrittlement, we found that present designs are based on a variety of empirically determined formulas, with no generally accepted method prevailing. Industrial experience is specific to particular applications and not directly applicable to the determination of the ability of equipment designed for methane service to handle hydrogen in storage applications.

We conclude that, if the pressure at storage facilities is limited to values of approximately 1000-1200 psi, equipment presently in service at natural gas storage facilities will stand up to hydrogen service with respect to hydrogen embrittlement, with several constraints. Before the actual conversion of any given facility from natural gas to hydrogen service (regardless of the pressure level) in-place equipment must be surveyed to determine the number of flaws, hard spots, and plastic deformation. A detailed inspection of this nature may not be cost-effective at existing storage facilities. In that case, we would recommend a replacement of all welded sections subjected to pressures above several hundred psig.

Reactions of Hydrogen With Chemical Species Found in Underground Reservoirs

Sandstone, depleted fields, and mined cavern reservoirs are composed primarily of stable, nonreactive silicate minerals consisting of quartz, feldspars, and lesser amounts of garnets, spinels, and micas. However, minor sulfide, sulfate, carbonate, and oxide minerals often occur either as cementing materials or as small crystals coating the surfaces of larger grains. Because of the large amount of exposed surface area of these minerals in sandstone-type reservoirs, in excess of the quartz itself, and the large quantity of these minerals in limestone and salt reservoirs, possible reactions with hydrogen could proceed to the complete consumption of the reacting mineral. This might involve measurable quantities of hydrogen and the generation of toxic gases. We examined the possible chemical reactions, with hydrogen, of about 15 minerals common to underground reservoirs assuming a reservoir temperature of 298 K (77°F) and a pressure of 2000 psi. Only oxygen, Fe_2O_3, and sulfur could possibly react with hydrogen. An increase in temperature of as much as 50°F would not change reaction directions, nor would reaction directions be changed by a decrease in pressure. However, these three reactions require either temperatures above those in the reservoirs or catalysis.

Similar to inorganic reactions, most hydrogenation and cracking reactions require temperatures in excess of normal reservoirs. Some anaerobic bacteria are capable during fermentation processes of reducing hydrogen and sulfates to hydrogen sulfide and water, but this activity is rare in reservoirs.

Although the reactions and the case studied cannot be considered to represent the full range of possible reactions that could occur in a reservoir, with the lack of theoretical prediction and the absence of hydrogen reactions in the Gaz de France fields, there is little evidence for serious problems with underground storage for long periods of time.

Economic Analysis of Hydrogen Storage Methodology Development

For this project, we developed a computerized discounted cash flow analysis using constant dollars. The methodology has been modified from the standard textbook approach to reflect financing specific to utilities. This includes consideration of the "Allowance for Funds Used During Construction (AFUDC) in the utility rate base."

In this analysis, it was assumed that base gas was financed along with facility construction. That is, base gas was purchased and financed during the construction period for delivery after construction completion. This technique of financing base gas was considered important for a study of hydrogen storage facilities because base gas costs could be a large percentage of the facility cost and not supplied by the parent company to the storage facility.

Using information on specific fields supplied to us by operators of those fields, we determined the levelized cost of service for the storage of natural gas. The cost of service was then verified for a "typical" field operation by these operators. Satisfying ourselves that the methodology gave good values for cost of service, we varied the input parameters to see their effect on the cost of service. This analysis was carried out for an aquifer, a depleted field, a salt cavern, and a hypothetical excavated cavern. The parameters varied were base gas cost, physical plant cost, plant construction cost, operating cost, cost of debt, cost of equity, and the fraction of debt financed. Figure 1 illustrates the effect varying each of these parameters has on the base case for a depleted field type of operation. For the four types of fields analyzed for natural gas storage, the most sensitive parameters (steepest slope) were plant cost and cost of equity; the least sensitive were always construction time and operating costs. Dashed segments are extrapolations.

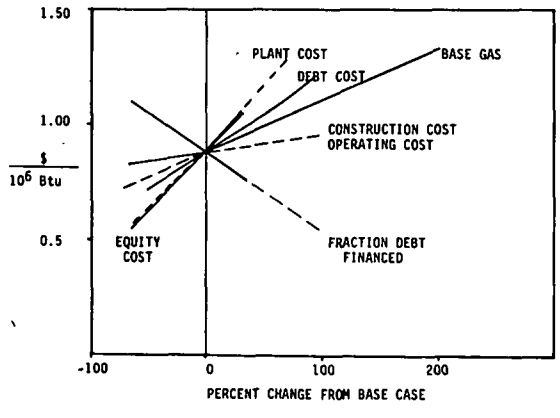

Fig. 1 Depleted field — natural gas case.

Table 1 Hydrogen economic evaluation – base case

	Salt Cavern	Excavated Cavern	Aquifer	Depleted Field
Erected Plant Cost, 10^3	16,400	50,000	31,900	6600
Throughput/yr, 10^{12}	1.44	2.03	1.7	0.976
Cost of Base Gas/10^6 Btu	6.00	6.00	6.00	6.00
Operating Cost/yr, 10^3	350	425	1025	230
Construction Time, years	3	3	3	3
Cost of Debt, %	10	10	10	10
Cost of Equity, %	15	15	15	15
Fraction Debt Financed	0.6	0.6	0.6	0.6
Lifetime for Economics, years	27	27	27	27
Cost of Service/10^6 Btu	3.03	5.27	6.59	4.47
Variation in Cost of Service/10^6 Btu	(2.44-4.27)	(3.23-7.51)	(4.18-10.03)	(2.76-8.89)

Hydrogen Storage

The hydrogen storage economic analysis was carried out using the methodology developed for natural gas storage. Each type of field was analyzed again with base case values that reflect reasonable assumptions for hydrogen storage. These base case values were then parametrically varied as they were for natural gas storage.

From an economic viewpoint, it appears that there will be little difference between the conversion of an existing natural gas storage/facility and the development of a new field specifically for hydrogen service. The major capital cost items (wells, gas compression systems, and pipefields) will likely need to be replaced in a conversion of an existing natural gas facility to hydrogen service. From a technical viewpoint, the same general type of system and many of the minor parts of the system will be applicable to both natural gas and hydrogen service. There appear to be no major gaps in either technology or operational procedure for underground hydrogen storage (except, perhaps, for unspecified material for very high pressure storage fields).

The economic effect of ownership and value a field might have when actually converted will be discussed in detail in the final report of this project. Table 1 summarizes the base cases and cost of service for the storage of hydrogen. An annual load cycle was assumed.

Salt Cavern

The base case plant costs and operating costs for hydrogen storage were assumed to be the same as the costs for natural gas storage. The salt cavern assumed to be operating from 1000 to 3500 psi per annual cycle. With this assumption, the amount of throughput of the field is 1.44 X 10^{12} Btu. Choosing $6.00/$10^6$ Btu for the cost of the base gas and the same financial parameters as for natural gas, the base cost of service is $3.03/$10^6$ Btu (1978 dollars). The cost of service is relatively insensitive to the cost of the base gas.

Excavated Cavern

The excavated cavern was studied for depths of 2500, 3500, and 4500 feet. The 3500-foot depth was considered as the base case giving a base gas volume of 1.903 X 10^6 SCF at a temperature of 77°F. The large cost of service derives from the large development cost of the field. Using $6.00/$10^6$ Btu gas as base gas, the cost of service becomes $5.27/$10^6$ Btu. The cost of service is relatively insensitive to the cost of the base gas.

Aquifer

Some changes in the physical plant costs primarily due to lower compressor costs for a smaller throughput per annual cycle make the analysis for hydrogen storage similar to natural gas storage. The cost of service is 6.59/10^6 Btu. The base case cost of service is higher for hydrogen than for natural gas due to the smaller throughput per year. Unlike the cavern storage, the cost of service is sensitive to the cost of base gas for an aquifer.

Depleted Field

The results of the economic analysis for a depleted field for hydrogen storage are illustrated in Figure 2. The case illustrated considers 0.976 X 10^{12} Btu/yr for throughput and gives a value of $4.46/$10^6$ Btu cost of service. Two other values for throughput were also examined to see the effect of additional compressor and well costs to produce additional throughput by reducing the amount of base gas. For a throughput of 1.7 X 10^{12} Btu/yr, the cost of service drops to $2.21/$10^6$ Btu, and for a throughput of 2.4 X 10^{12} Btu/yr, the cost of service further drops to $1.51/$10^6$ Btu. So the investment in increased compression is more than compensated for by the decrease in cost of service. All of the above were determined for developing the field as a new operation. For the case of conversion, a retrofit case was considered. Basically, some of the plant costs and line costs were eliminated. For the case illustrated in Figure 2, a plant cost reduction to $1850 X 10^3 gives a levelized cost of service of $3.34/$10^6$ Btu.

Conclusion

The costs of service for hydrogen storage determined in this study varied from 26% to 150% of the cost of the gas stored. This compares with a range of 23% to 193% for natural gas. Although each type of field must be considered separately and examined with respect to the cost of the gas being stored, we could generalize to say that it is as economic to store hydrogen as it is to store natural gas. With the exception of the limitation of 1200 psi reservoir pressure set by hydrogen

embrittlement, there are no technical constraints on storing hydrogen underground.

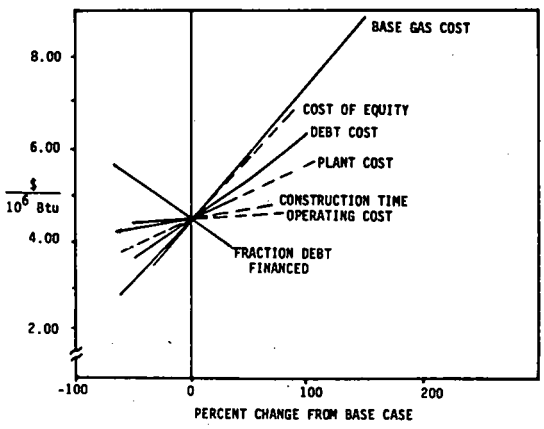

Fig. 2. Depleted field — hydrogen case.

Acknowledgment

Information and critical review of the data in this study was generously provided by the Northern Illinois Gas Company, Texas Gas Transmission Company, and Transco Corporation. Additional support was provided by Dames and Moore. The many hours of effort by all of these companies is sincerely appreciated.

DESIGN, CONSTRUCTION AND TESTING OF A THERMALLY ACTIVATED HYDROGEN CHEMICAL COMPRESSOR

E. Snape, Ergenics
and
F.E. Lynch, Denver Research Institute

Abstract

With support from the US Department of energy and its subcontractor, Denver Research Institute, Ergenics is developing a metal hydride compressor which is expected to improve the overall economics of hydrogen production and handling. Several critical modelling experiments have been performed and a compressor design selected. Construction of the compressor is in progress and testing and evaluation are expected to be completed within six months. Progress to date and work plans for completion of Phase I of this project are summarized.

I. Introduction

The projected increasing requirements for hydrogen necessitate large-scale handling. This generally requires the use of a compressor. Mechanical compressors are already universally used in both "captive" and "merchant" hydrogen applications. Unfortunately, their capital cost is high and they are costly to operate due to high energy consumption and maintenance problems. This project concerns a novel approach to hydrogen compression - a thermally activated chemical compressor which utilizes metal hydrides. The design offers the following significant advantages over the current mechanical compressors:

1. lower initial capital cost
2. operation on waste or solar heat
3. reduced maintenance
4. no moving parts-hence less vibration
5. longer life
6. more compact
7. higher-purity hydrogen output

This report describes the design and construction of a prototype thermal-chemical compressor.

II. Principle of Hydride Compressor Operation

The use of metal hydrides for hydrogen compression depends upon the exponential increase of hydrogen equilibrium pressure with temperature. Figure 1 shows this behavior for the well known hydride of the intermetallic compound $LaNi_5$.

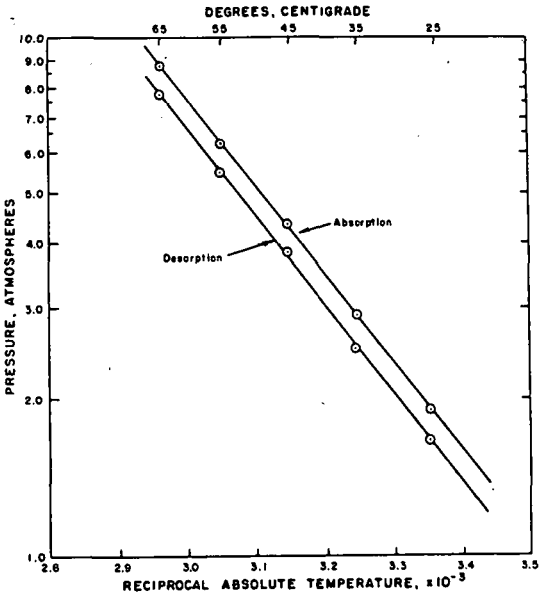

FIGURE 1 VAN'T HOFF RELATIONSHIPS FOR ISOTHERMALLY DETERMINED ABSORPTION AND DESORPTION EQUILIBRIA AT 0.5 H/M IN THE $LaNi_5$-H SYSTEM.

It is evident that from this typical Van't Hoff plot that only modest temperature increases are required to achieve substantial compression ratios. The principle is very simple and is shown in Figure 2.

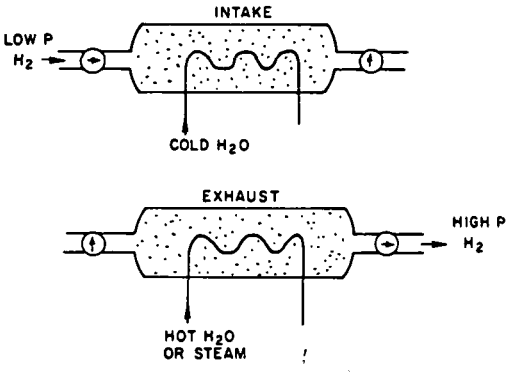

FIGURE 2 - THERMAL COMPRESSION OF HYDROGEN USING HYDRIDES.

The hydride compressor operates by a two-step procedure. The "intake" step involves absorption of hydrogen into the bed at low temperature and pressure and the "exhaust" step involves the desorption of hydrogen at a higher bed temperature and hence higher pressure.

The major forms of energy consumption in hydride compressors are:

1. $Cp\Delta T$
2. Hydride ΔH

For $LaNi_5$, the Cp is 0.18 cal/gm - °c. The weight of hydride needed to compress one gm. mole of hydrogen is about 150gm. Thus, for a temperature rise of 1°c, the heat required to compress one gm. mole of hydrogen is 27 calories. Assuming an ideal compression from 2 to 151 atmospheres, the minimum energy requirement would be 11,000 calories, including the enthalpy for decomposition. Since the work accomplished during the compression is $RT \ln \frac{151 \text{ atm}}{2 \text{atm}}$ or 2560 calories. The maximum efficiency for an ideal compressor is therefore 22%. The extent to which this efficiency is attained depends largely on the $Cp\Delta T$ of the container and the degree to which the pressure-temperature-composition relationships approach ideality.

Clearly, the use of high-grade energy such as electricity is not desirable in the long term because of the relatively low efficiency of hydride compressors. A more attractive approach would be to use multiple stage hydride beds, different hydrides and low grade or waste heat. While this is the approach which will be adopted in the commercialization stage, it was felt that electrical resistance heating was most convenient for the prototype demonstration.

III. Prototype Compressor Design and Construction

Selection of the prototype design and performance specifications was based on input from low pressure electrolyzer manufacturers since it was felt that electrolyzer manufacturers could be amongst the first commercial users. The specifications sought are shown below:

Input Pressure	1 Atm. Abs. (0 PSIG)
Output Pressure	120 Atm. Abs. (1750 PSIG)
Capacity	0.8 Std. Liter/sec (100 SCFH)
Peak*Power Requirement	20 Amps @208 VAC 1 PH
Hydride Content	30 kg $LaNi_{4.5}Al_{0.5}$ (annealed)
Peak Temperature	300°C

*Peak power demand occurs when the system is cool and decreases as the temperature rises. Average power will be determined by experiment for efficiency calculations.

It is recognized that an output pressure of 120 atm. may not be achievable in a single stage and some compromise may be necessary in this specification. Actually the compressor is able to operate over a considerable range of pressure and flow. Cooling air temperature and input pressure determine charging time while the output pressure requirement fixes the discharge time. During Phase I of the proposed work the performance of the unit will be mapped. The effects of these variables can then be compared with theoretical performance to help identify and improve points of inefficiency in the design. Figure 3 shows the operational block diagram for the compressor.

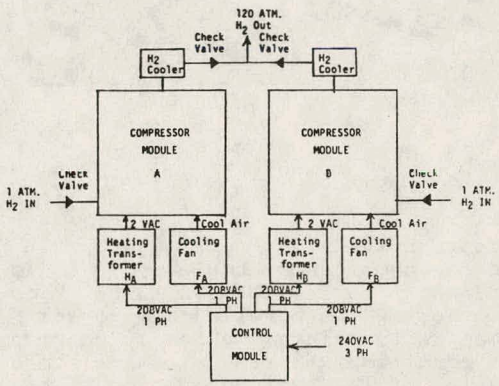

Figure 3. Compressor Operation. Prime Marks Denote "off" condition

Operation #	State	Function
1	H_A F_A' H_B' F_B	A Discharges, B Charges
2	H_A' F_A H_B' F_B	A Cools, B Charges
3	H_A' F_A H_B F_B'	A Charges, B Discharges
4	H_A' F_A H_B' F_B	A Charges, B Cools

The control module (Figure 4) which sequences the operations has variable timers so that "on" and "off" periods can be independently adjusted to match the compressor with a continuous input from any hydrogen source whose pressure and flow are within the range of the compressor's performance.

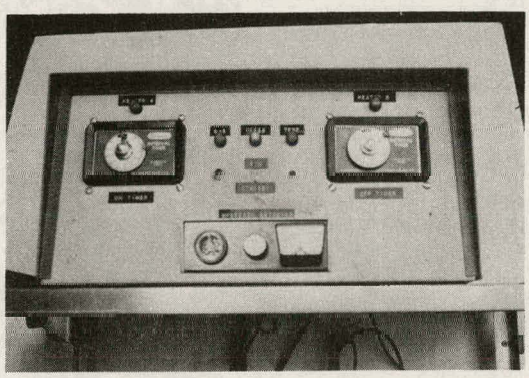

Figure 4

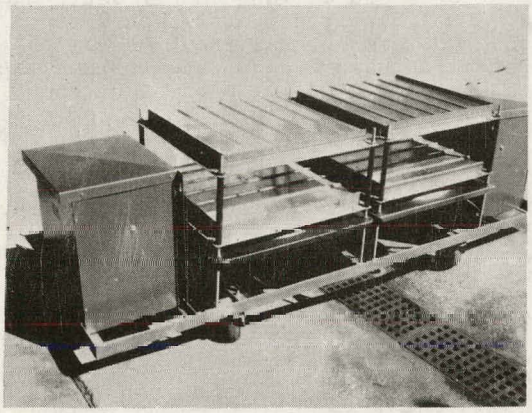

Figure 5

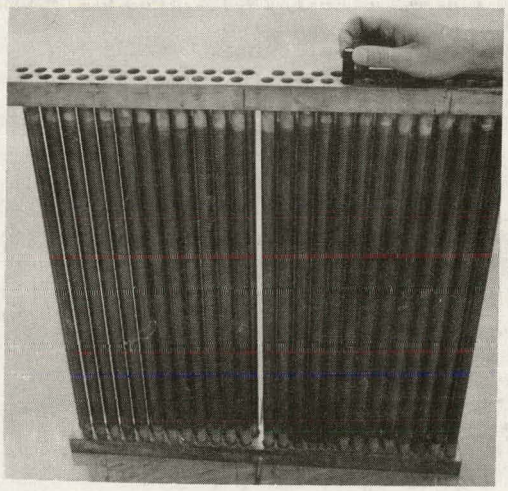

Figure 6

Figure 5 shows the cooling trays in which the compressor modules will be located, and the transformers. The objective of using two parallel compressor modules is to maintain a nearly constant input condition, thereby allowing steady operation of the hydrogen source. Considering the cost of electrolysis equipment, idle time should be minimized. An alternative method consists of using one compressor module and one storage or damping module to hold the output of the electrolyzer while the compressor is heating, discharging and cooling. This method requires more metal hydride and a larger temperature rise than the parallel system.

In addition to sequencing the operations of the compressor modules, the control module contains the necessary safety contols. These include overheat switches, an overpressure switch and a hydrogen detector. If one or more of these hazard conditions occurs, the control module turns on both cooling fans and signals the failure mode by means of signal lights until the unit is manually reset.

The compressor module consists of 316 stainless steel tubes brazed into copper headers. The stainless steel tubes serve both as electrical conductors and manifolding in this design. The heating is accomplished by passing current through the stainless tubes.

Figure 6 shows the construction of the compressor module.

The critical heat transfer aspect of this system is the cooling and recharge period. Air is passed over the 5/8" OD tubes by a blower at about 20 ft/sec (higher flows give little improvement). A typical modeling experiment is shown in Figure 7. Activated $CaNi_5$ contained in a 5/8" OD copper tube at about 2 gms/cc loading density was placed in a 20 ft/sec air flow at 25°C. Hydrogen at 30 psia was maintained by a regulator while the consumption of gas was noted by the decrease in pressure in a gas cylinder.

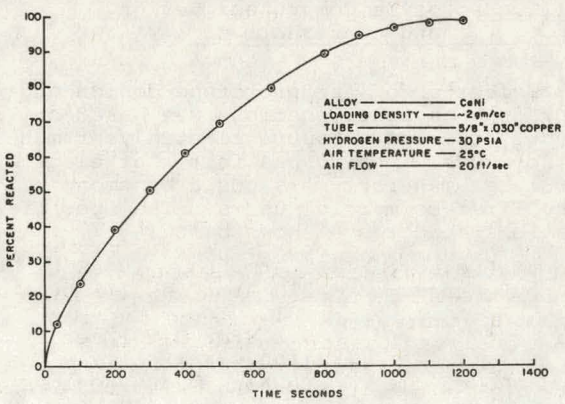

FIGURE 7 TYPICAL RECHARGE MODELING EXPERIMENT

IV. Design Problems

Several problems had to be overcome to ensure successful operation of the prototype.

Early modeling experiments were fraught with difficulties including packing of the hydride powders into dense masses which impeded gas flow and caused bulges and fractures in the tubes. These problems have been overcome through the use of capsules of the type shown in Figure 8.

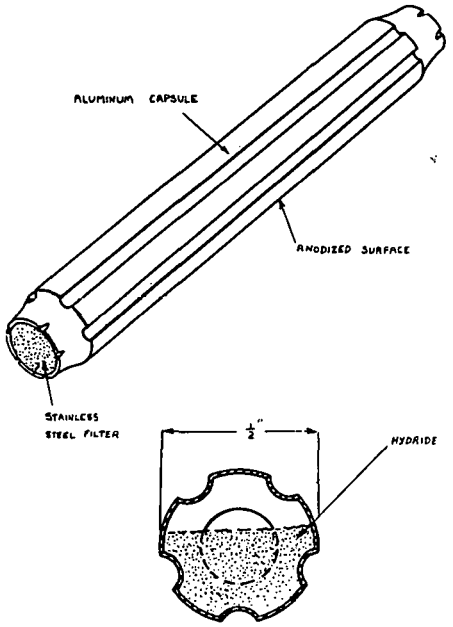

FIGURE 8

These aluminum capsules have flutes along the sides and filters in the ends to facilitate gas flow. The length-to-diameter ratio is small enough to prevent gross migration of the alloy which may occur if the alloy were simply loaded into the stainless tube without the use of capsules.

The use of a copper header to serve both as a gas manifold and electrical current carrier posed a difficult joining problem. The type 316 stainless steel tubes which comprise both the hydrogen/hydride containers and resistance elements must be joined to the copper header in such a way as to produce a leak free seal capable of undergoing many temperature/pressure cycles. Also, the capsules containing the hydride must be insulated from the surrounding stainless steel tubes (resistance elements) to avoid local hot spots.

Brazing trials confirmed the need to copper plate the stainless steel tubes and braze in vacuum to ensure an adequate joint.

Insulation of the hydride capsules from the stainless steel tubes is achieved by anodizing the surface of the capsules. Tests have confirmed that this anodized layer should provide adequate insulation. Every capsule was checked for possible insulation failure before loading in the compressor modules.

V. SYSTEM EVALUATION

Before evaluating the performance of the prototype and conducting cyclic trials, the compressor modules are being pressure tested. The entire system will then be tested to establish hydrogen flow rate and output pressure. The prototype will be subjected to at least 100 cycles to assess performance stability.

VI. SUMMARY

A prototype hydride compressor has been designed. Construction and final assembly is nearing completion and testing should be in progress by the time of this meeting. A complete assessment of the potential of hydride compressors to harness waste or low grade heat and thereby reduce the overall capital and operating cost should be completed within six months.

Dup

HYDROGEN STORAGE MATERIALS RESEARCH AND DEVELOPMENT WORK AT BROOKHAVEN NATIONAL LABORATORY*

John R. Johnson

Department of Energy and Environment
Brookhaven National Laboratory
Upton, New York 11973

Abstract

The intermetallic compound $TiCr_2$ exists as two temperature dependent allotropes. Both forms of this material will react with hydrogen or deuterium reversibly to yield two hydride (deuteride) phases. The higher hydride/deuteride phases can store an appreciable weight percent of gas. The hydride and deuteride phases formed by the two intermetallics are generally very unstable thermodynamically with the deuterium systems more stable than the corresponding hydrides of the same intermetallic. This paper is in the nature of a brief progress report encompassing research done from October 1, 1978 to September 30, 1979 at Brookhaven National Laboratory dealing with properties of importance in the utilization of $TiCr_2$ intermetallics (parent compounds or substituted systems) as energy storage media or for nonmechanical compression/liquefaction applications. Additionally, preliminary research into the feasibility of hydrogen separation from mixed gas streams, using intermetallic compounds, will be briefly reported.

I. Introduction

In the past year, research at Brookhaven National Laboratory in the hydrogen storage materials development program has been concerned with several areas of work. The areas of investigation and emphasis include the following: [1] a definition of the low-temperature $TiCr_2$-D system; [2] completion of studies on the high-temperature $TiCr_2$-H system; [3] continuation of studies on the hydriding properties of manganese substituted stoichiometric $TiCr_2$ compounds of the general formula $TiCr_{2-x}Mn_x$ and defect compounds represented as $TiCr_{2-x}Mn_{x-y}$; [4] hydrogen separation from methane (simulating natural gas)-hydrogen gas mixtures using metal hydrides; and [5] management responsibilities for several DOE contracts in this area. Work in areas 1 through 4 will be discussed below briefly. The research performed under items 1 to 3 above was primarily concerned with elucidating properties of the parent $TiCr_2$-H/D and manganese substituted hydride systems (both high-temperature and low-temperature intermetallics) of importance for energy storage utilization, as isotopic separation media and also possibly for use in nonmechanical compression or liquefaction applications. Research in area 4, dealing with the separation of hydrogen from mixed gas streams containing potential hydride poisons, represents a new field of investigation at BNL and as such only some preliminary results will be presented below.

II. Nonsubstituted Chrome-Titanium Alloy Hydrides/Deuterides

The binary titanium-chromium phase diagram[1], as shown in Figure 1, exhibits only one intermetallic compound, $TiCr_2$, of which there are two temperature dependent forms. Both compounds are Laves phases, intermetallics having only tetrahedral interstitial positions, with the low-temperature phase having the face centered cubic $MgCu_2$ (C15) structure while the high-temperature (C14) form has the hexagonal $MgZn_2$ structure. Both allotropes react with hydrogen or deuterium to form distinct hydride or deuteride phases with an appreciable gas storage capacity. The maximum achievable hydrogen content for both starting intermetallics is nearly 2.5 weight percent with deuterium approximately double this value. Additionally, the deuterides formed by the parent systems are considerably more stable than the corresponding hydrides which is opposite to typical behavior for such systems.[2]

The Low-Temperature (C15) $TiCr_2$-D System

In previous publications[3-5], properties of the low-temperature $TiCr_2$-hydrogen system have been presented. To date, no information has been reported on the low-temperature $TiCr_2$-deuterium system. This system is of considerable importance since it shows a reverse isotope effect. That is the deuterides formed from the parent (C15) cubic intermetallic are more stable than the corresponding hydrides and the equilibrium isotopic separation factor α_{H-D} is reasonably large. Also, the rates of reaction of hydrogen and deuterium with cubic $TiCr_2$ are vastly different suggesting that the separation of H_2 and D_2 might be performed effectively on a kinetic basis.

The cubic $TiCr_2$-D system has been studied by measurement of pressure-composition-temperature (p-c-T) isotherms and by structural X-ray diffraction investigations. The pressure-composition isotherms for this system are shown in Figure 2. Basically, this figure shows that two distinct deuteride phases are formed at -78°C with compositions corresponding to $TiCr_{1.8}D_{2.4}$ and $TiCr_{1.8}D_{3.5}$. The reactions taking place at this temperature can be written as follows:

$$1.67TiCr_{1.8}D_{1.2} + D_2 \rightleftarrows 1.67TiCr_{1.8}D_{2.4} \quad (1)$$

$$1.82TiCr_{1.8}D_{2.4} + D_2 \rightleftarrows 1.82TiCr_{1.8}D_{3.5} \quad (2)$$

Reaction number (1) represents the formation of the first deuteride phase from the deuterium saturated solid solution whereas reaction (2) indicates the formation of the second deuteride phase of maximum deuterium content beginning with the first deuteride phase of lowest deuterium content. These reactions are virtually identical to those for the low-temperature $TiCr_2$-hydrogen system at the same temperature however the stabilities of the deuteride phases are higher. This is apparent when the plateau equilibrium dissociation pressures are compared at -78°C. Those for the deuterides are $\sim$ 0.4 and 12 atm whereas the hydride values are $\sim$ 2.2 and 50 atm. A comparison of the relative partial molal enthalpies and free energies of the hydrides and deuterides, calculated from the isotherms, also verifies this stability relationship. It should also be noted from these isotherms that the first

*Work performed under the auspices of U.S. Dept. of Energy.

plateau region (2 phase region) appears to be non-existent at room temperature. That this is, in fact, the case was confirmed by X-ray diffraction studies of deuterides with varying D/M ratios. X-ray diffraction work on deuterides taken to a D/M ratio exceeding 1.2 indicate that the original cubic (C15) $MgCu_2$ structure of the starting compound is maintained. There is therefore no structural change on going from the starting intermetallic to the compound of highest deuterium content; merely an isotropic expansion of the cubic unit cell. This result is similar to findings reported by other researchers who have investigated Laves phase hydrogen or deuterium systems.[6-8] It is, however, different than the behavior of the low-temperature hydrogen system which has a two phase region at room temperature.[5] The critical temperature for this first two phase region may therefore be placed between 10 and 25°C.

The High-Temperature (C14) $TiCr_2$-H System

The limits of homogeneity of the hexagonal (C14) $TiCr_2$ phase are both temperature and composition dependent as can be seen from Figure 1. The intermetallic exists, however, in the composition range from $TiCr_{1.75}$ to $TiCr_{1.95}$. All such compositions are metastable below the temperature interval from 850 to 1150°C. The high-temperature intermetallics may, however, be prepared and their reaction properties with hydrogen or deuterium studied since the rate of transformation to the low-temperature intermetallic, the stable compound at temperatures below those given above, is negligibly small for our experimental conditions.

Previously, we reported some preliminary results on the high-temperature (C14) $TiCr_2$-hydrogen system.[4] These results were deduced from a limited number of equilibrium desorption isotherms. Complete characterization of this system has now been carried out by measuring additional absorption-desorption (p-c-T) isotherms and by investigating this system by X-ray diffraction techniques.

Pressure-composition desorption isotherms at a series of temperatures ranging from -100 to +30°C for this system are shown in Figure 3. It is evident from this figure that hydrogen reacts with the high-temperature intermetallic sequentially at -78°C to form two distinct hydride phases. The hydride phases formed in this system are somewhat more stable than those for the low-temperature intermetallic. This can be seen by comparing the dissociation pressures (plateau) of the low-temperature and high-temperature hydrides which are ∿ 2.2 and 50 atm versus ∿ 0.2 and 30 atm at -78°C. This is also shown to be the case if thermodynamic calculations are performed for both systems by utlizing the p-c-T data. The reactions which take place in this system at -78°C starting with the hydrogen saturated solid can be written as follows:

$$2.5TiCr_{1.9}H_{1.6} + H_2 \overset{\leftarrow}{\rightarrow} 2.5TiCr_{1.9}H_{2.4} \quad (3)$$

$$1.67TiCr_{1.9}H_{2.4} + H_2 \quad 1.67TiCr_{1.9}H_{3.6} \quad (4)$$

Phase boundaries in the high-temperature intermetallic-hydrogen system are, however, quite temperature dependent as can also be ascertained from the preceding figure. Additionally, it appears, from the p-c-T desorption isotherms, that there is no hydride phase present at room temperature. The starting intermetallic lattice simply absorbs hydrogen at this temperature to its maximum content while retaining the original hexagonal (C14) intermetallic structure and undergoing an increase in the unit cell volume. This conclusion has been confirmed by measurement of X-ray diffraction patterns for a number of such high-temperature systems with varying hydrogen contents. Behavior such as this has been observed for the low-temperature $TiCr_2$-D system as mentioned above. By combining the p-c-T and room temperature X-ray diffraction data, a partial phase diagram for the high-temperature (C14) $TiCr_2$-hydrogen system can be constructed. Such a diagram is illustrated in Figure 4.

Hysteresis measurements have also been carried out for this system. Results of these measurements are shown in Figure 5. This system, as for the low-temperature intermetallic, exhibits no hysteresis. That is, the absorption and desorption equilibrium pressures, at a given temperature, are the same indicating true reversibility of reaction with hydrogen. Such behavior is similar to that for the low-temperature cubic $TiCr_2$-hydrogen system[5] but different from other unstable alloy-hydrogen systems.[9-10]

III. Manganese Substituted $TiCr_2$ Hydrides

The "Rule of Reversed Stability"[11] predicts the formation of stable hydrides for the high-temperature and low-temperature intermetallics. As has been seen hydrides for these systems are very unstable[4-5] even to the point of limited utility for most practical applications. It should, however, be possible to modify the hydriding properties of the parent $TiCr_2$ systems by substitution of a third transition metal for part of the chromium as is the case in substituted ferro-titanium alloys.[4,12] To this end, investigations were initiated in FY 78 to study the hydriding properties of compounds represented by the general formulas $Ti_xCr_{2-x}Mn$, $Ti_{1+x}Cr_{1-2x}Mn_{1+x}$ and $TiCr_{2-x}Mn_x$. Nearly all previous work reported[4] has been concerned with the first two types of systems. Neither of these appeared very promising because of a significant decrease in hydrogen storage capacity with increasing titanium content. The third general system, $TiCr_{2-x}Mn_x$, appeared more attractive based on only a few preliminary hydriding experiments. Work has continued in FY 79 on the $TiCr_{2-x}Mn_x$-hydrogen ($x \geq 1$) systems. The principal findings as a result of this research were: [1] alloys of exact stoichiometric composition $TiCr_{2-x}Mn_x$ ($x \geq 1$) will not absorb hydrogen under any reasonable experimental conditions; and [2] alloys off stoichiometry which may be represented by the general formula $TiCr_{2-x}Mn_{x-y}$ ($x \geq 1$, $y \geq 0.3$)will absorb large quantities of hydrogen (greater than 2 weight percent) and as the manganese content increases the stability of the hydrides formed increases. The plateau dissociation pressures which can be spanned by a variation in the manganese content encompasses several orders of magnitude. These results are consistent with the fact that the stoichiometric compound $TiMn_2$ absorbs no hydrogen while removal of manganese to form the defect compound $TiMn_{1.7}$ results in a large hydrogen absorption.[13]

IV. Hydrogen Separation From Mixed Gas Streams

Hydrogen has been identified as an efficient energy carrier and the development of technology for its production has suggested options for converting our more abundant coal and renewable resources to this flexible fuel form. Complementary investigations are aimed toward storage, transmission and distribution of hydrogen such that it be

compatible with the U.S. energy infrastructure. One possibility is the direct injection of hydrogen into the available natural gas transmission and distribution networks where hydrogen would be considered as a fuel supplement.

For many applications such as use in refinery operations, ammonia production, fuel cells and automotive systems, hydrogen demand is expected to increase significantly in the near future. Logistics and site-specific considerations will dictate the most effective manner for hydrogen supply to these systems. The development of low cost separation systems will maximize the options available to the potential user thus further enhancing the market penetration of alternatives to conventional energy conversion systems.

Reversible metal hydride absorption-desorption cycles appear to offer characteristics that may permit the selective absorption of hydrogen from certain types of gas mixtures. The attractiveness of these separation systems will be based upon cost comparisons with alternative hydrogen production (separation) schemes such as steam reforming of natural gas and partial oxidation of hydrocarbons. The key to cost effective application of metal hydrides is contamination resistance and extensive recycling of the hydride compounds.

The development of selectively absorbing metal hydrides may also have application beyond removal of hydrogen from natural gas mixtures. Such other separation uses might be in the following areas: [1] direct recovery of hydrogen from coal gasification and/or shift reaction mixtures; and [2] recovery of hydrogen from refinery gas streams. Of course, such recoveries, undoubtedly, would be more difficult than removal of hydrogen from natural gas since these gas streams will contain a larger amount of potential hydride poisons.

Hydrogen separation experiments were therefore initiated in FY 79 at BNL. The alloys initially chosen for investigation were $LaNi_5$, $LaCuNi_4$ and $TiFe_{0.85}Mn_{0.15}$. This selection was based on a rather thorough literature search and previous research done at Brookhaven[14] which indicated that these compounds were more poison resistant than other intermetallic hydride forming materials. The only gas mixture studied, to date, consisted of 10 volume percent hydrogen - 90 volume percent methane. This is a typical composition for a natural gas-hydrogen mixture which could be transported now in most existing natural gas lines without serious problems. Each of the above intermetallics (activated) were temperature cycled in this gas mixture. The cycling consisted of allowing the alloys to absorb and desorb hydrogen from this gas mixture at set temperatures. New gas was used for each absorption-desorption cycle and the absorption time was set at a constant value. No loss of activity was noted for any of these intermetallics after 20 cycles. The methane, therefore, did not seem to cause any interference with the hydrogen absorption-desorption reactions.

References

1. P.A. Farrar and H. Margolin, "A Reinvestigation of the Chromium-Rich Region of the Titanium-Chromium System," Trans. Met. Soc. AIME 227, 1342(1963).

2. G.G. Libowitz, The Solid State Chemistry of Binary Metal Hydrides, W.A. Benjamin, Inc., New York 57(1965).

3. J.R. Johnson and J.J. Reilly, "The Metal Hydride Development Program at Brookhaven National Laboratory," Proc. of the DOE Chemical Energy Storage and Hydrogen Energy Systems Contracts Review, JPL 78-1, Hunt Valley, Maryland, November 1977.

4. J.R. Johnson and J.J. Reilly, "The Metal Hydride Research and Development Program at Brookhaven National Laboratory," Proc. of the DOE Chemical/Hydrogen Energy Systems Contractor Review, Washington, D.C., November 1978.

5. J.R. Johnson and J.J. Reilly, "The Reaction of Hydrogen with the Low Temperature Form (C15) of $TiCr_2$," Inorg. Chem. 17, 3103(1978).

6. A. Pebler and E.A. Gulbransen, "Thermochemical and Structural Aspects of the Reaction of Hydrogen with Alloys and Intermetallic Compounds of Zirconium," J. Electrochem. Tech. 4, Nos. 5-6, 211(1966).

7. A. Pebler and E.A. Gulbransen, "Equilibrium Studies on the Systems $ZrCr_2$-H_2, ZrV_2-H_2, and $ZrMo_2$-H_2 between 0° and 900°C," Trans. Met. Soc. AIME 239, 1593(1967).

8. D. Shaltiel, I. Jacob and D. Davidov, "Hydrogen Absorption and Desorption Properties of AB_2 Laves-Phase Pseudobinary Compounds," J. Less-Common Metals 53, 117(1977).

9. J.J. Reilly and R.H. Wiswall, Jr., "Formation and Properties of Iron Titanium Hydride," Inorg. Chem. 13, 218(1974).

10. F.A. Kuijpers and H.H. van Mal, "Sorption Hysteresis in the $LaNi_5$-H and $SmCo_5$-H Systems," J. Less-Common Metals 23, 395(1971).

11. H.H. van Mal, K.H.J. Buschow and A.R. Miedema, "Hydrogen Absorption in $LaNi_5$ and Related Compounds: Experimental Observations and Their Explanation," J. Less-Common Metals 35, 65 (1974).

12. J.J. Reilly and J.R. Johnson, "Titanium Alloy Hydrides, Their Properties and Applications," Proc. 1st World Hydrogen Energy Conference, Miami Beach, Florida, March 1966.

13. T. Yamashita, T. Gamo, Y. Moriwaki and M. Fukuda, "Hydride Formation of Ti-Mn Binary Alloys," J. of the Japan Institute of Metals 41, #2, 148(1977).

14. J.J. Reilly and R.H. Wiswall, Jr., "Hydrogen Storage and Purification Systems I," Brookhaven National Laboratory Report No. 17136, August 1972.

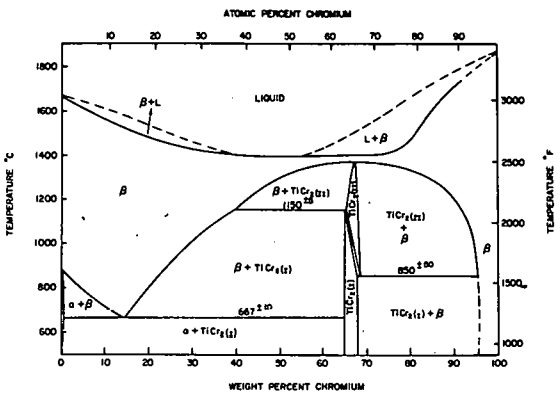

Figure 1. Phase Diagram of the Binary Ti-Cr System.

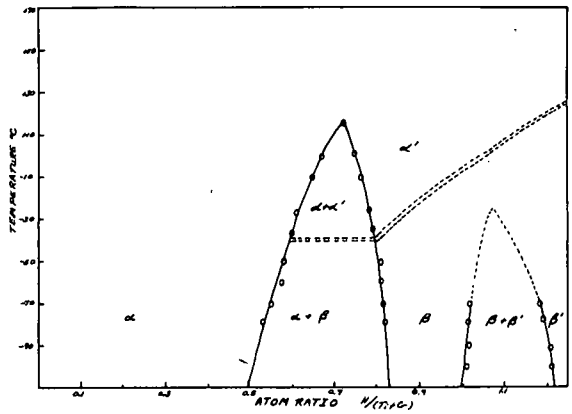

Figure 4. Partial Phase Diagram of the High-Temperature (C14) $TiCr_{1.9}$-H System.

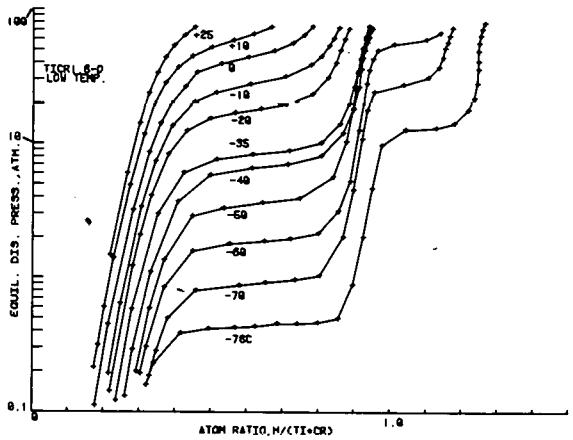

Figure 2. Pressure-Composition Desorption Isotherms for the Low-Temperature (C15) $TiCr_{1.8}$-D System at Various Temperatures.

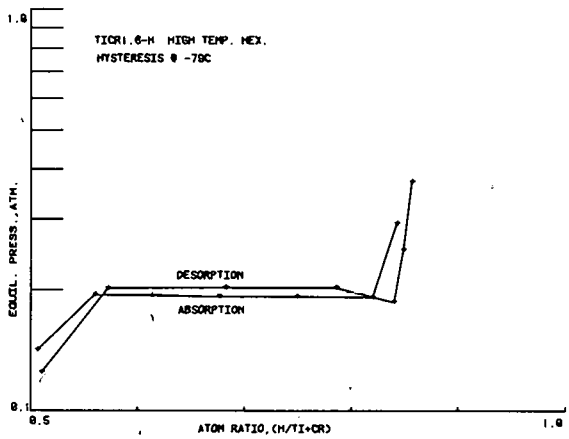

Figure 5. Hysteresis in the High-Temperature (C14) $TiCr_{1.8}$-H System at -79°C.

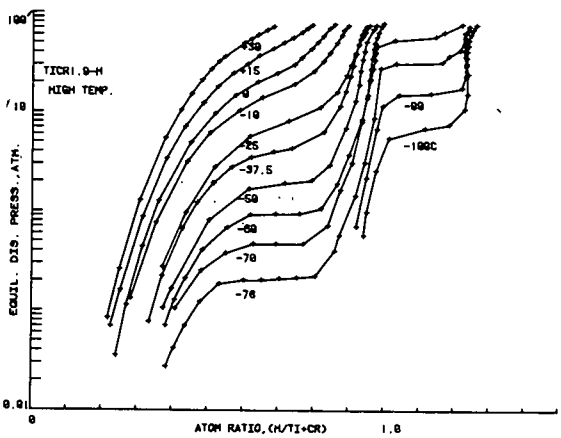

Figure 3. Pressure-Composition Desorption Isotherms for the High-Temperature (C14) $TiCr_{1.9}$-H System at Various Temperatures.

DEVELOPMENT OF NEW HYDROGEN STORAGE SYSTEMS FOR AUTOMOTIVE HYDROGEN FUEL STORAGE

Fred G. Eisenberg
John J. Sheridan, III
David A. Zagnoli

Air Products and Chemicals, Inc.
Allentown, Pennsylvania

Abstract

Mg_5Al_8 has been identified on the basis of thermodynamic considerations as a good candidate for automotive hydrogen fuel storage. The kinetics of the alloy/hydrogen reaction are poor, however, and the objectives of this study were to define the products of reaction and study the effect Ni has upon the rate of reaction.

To accomplish the first objective, reacted and unreacted alloy samples were characterized by x-ray diffraction. Results indicated that the reacted alloy had rearranged to form pockets of MgH_2 and Al rather than the ternary hydride. The second objective, Ni catalysis of the alloy, was studied by incorporating Ni as a powder, plating, and alloy with fine particle size Mg_5Al_8. The Ni is ineffectual in increasing the rate of absorption, but enhances the rate of desorption. Furthermore, there is evidence that surface morphology and particle size, as well as method of Ni incorporation, are important to the kinetics. It is concluded that further work is necessary to clarify the individual effect each of these factors has on the kinetics.

Introduction

Work was initiated in February 1978 to develop new Mg-based intermetallics to achieve the following target properties, identified to be necessary, for the development of a practical hydride system for automotive applications:

- a hydrogen storage capacity of at least 3% by weight;
- a one atmosphere decomposition temperature less than 250 °C and approaching 175 °C.

Our approach was based on the hypothesis that the chemistry of hydrides, rather than the metallurgy and physical aspects (i.e., crystal structure), control the important hydride properties.

In terms of the target properties, the best system found was Mg_5Al_8 (often referred to as Mg_2Al_3), which exhibits a one atmosphere decomposition temperature of 233 °C and an ultimate hydrogen capacity of 3.2% by weight.

During the study, two important observations were noted:

1. The ultimate hydrogen capacity of the Mg-alloys could be assigned based on the formation of MgH_2 within the alloy, and suggested a disproportionation reaction for the hydriding step:

$$MgX + H_2 \longrightarrow MgH_2 + X$$

The data suggests that the second metal (X) simply acts as "dead weight", and does not not contribute to the hydride capacity. This reaction has been proposed by J. Reilly of BNL, and others, for several Mg alloys (e.g. Mg_2Cu).

2. The rates of hydrogen absorption and desorption are prohibitively slow over the temperature range, 200-275 °C. Therefore, use of these alloys as automotive hydrogen storage media would be untenable even with favorable thermodynamics.

Based on these observations, work was initiated in June 1979 to study in detail the disproportionation reaction, the kinetics of hydride formation, and the potential of catalysts for improving the reaction rates.

Previous work with catalysts and metal hydrides has shown that small additions of Cu or Ni accelerate the kinetics of hydrogen absorption. For example, trace additions of Ni have been found necessary to form MgH_2 directly from Mg and hydrogen. The authors believe that in addition to the presence of a catalyst (such as Ni) the form, distribution, and concentration of the particular catalyst may be important. In addition, the surface area and morphology of the alloy need be considered. For example, the authors have succeeded in forming magnesium hydride without a catalyst through the exposure of Mg filings (25μ x 75μ x 200μ) at 343 °C to 800 psig hydrogen, with reasonable H_2 absorption rates. The authors attribute this result to the high surface area of the magnesium.

At the onset of the program the authors posed the following questions:

1. What are the functions and roles of "hydride catalysts" in the Mg-alloy/hydrogen system?
2. How does one optimize the use of catalysts for Mg-based alloys? Can the judicious employment of "optimized" catalyst systems and/or catalytic techniques significantly improve the kinetic properties associated with the hydrides of Mg-based alloys?

While each represent interesting areas of investigation, together they help focus the work towards a meaningful conclusion—the development of practical, workable metal hydride systems.

The results of the study are highlighted below and suggest that catalysts will be important to the development of practical metal hydrides for automotive applications. While the findings are encouraging, it is clear to the authors that we have just exposed "the tip of the iceberg". Considerable work in this area lies ahead of the field.

Sample Preparation, Characterization and Experimental Procedure (Disproportionation and Kinetics Study)

Mg_5Al_8 was prepared by a single melt (33.35 gms Mg and 54.11 gms Al) in an induction furnace at Air Products' Metal Hydride laboratory. The ingot (number 3424-16) was ground with a mortar and pestle, and screened to form two lots:

- -200 mesh (Fine)
- -120+140 mesh (Coarse)

Charges were taken from these two lots for the disproportionation and catalyst studies. Table I identifies the charges used in these two types of experiments.

TABLE I

IDENTIFICATION OF SAMPLES FOR DISPROPORTIONATION AND CATALYSIS STUDIES - INGOT #3424-16, Mg_5Al_8

Charge	Wt. (gms)	Particle Size	Experiment Disproportion.	Catalysis
A	7	Fine	X	
B	7	Fine	X	
C	3	Fine		X
D	3	Fine		X
E	3	Fine		X
F	3	Coarse		X
G***	3	Fine		X

***Mg_5Al_8 alloyed with 1% Ni (#3424-17)

Characterizations of the ingots (numbers 3424-16 and 3424-17) were obtained at Lehigh University, under the supervision of Professor Michael Notis, using x-ray microprobe. The samples proved to be primarily the desired β phase (Mg_5Al_8) with a small amount of a second, Al rich phase. Ingot 3424-17 was primarily $Mg_5Al_8Ni_{.058}$. The five charges used for the kinetic study are described in Table II.

In the disproportionation study two samples were simultaneously hydrided and dehydrided for 8 cycles at 343 °C. One sample was then removed in the dehydrided state and placed in dry ice. The second sample was hydrided again, and then removed and placed in dry ice. These samples were then analyzed by x-ray diffraction at Lehigh University.

The five samples for the catalyst/kinetics study were evaluated on a side-by-side basis. The five samples at 343 °C were simultaneously exposed to 800 psig hydrogen. After achieving equilibrium, the five samples were simultaneously desorbed. This cycling was repeated nine times. On the tenth cycle, rate data were recorded (i.e., the reactor pressure vs. time was monitored).

Results and Discussion

Results of the x-ray diffraction study confirm the disproportionation mechanism for Mg_5Al_8. The pattern for the fully hydrided sample shows clear and distinct peaks for MgH_2 and Al. Since regions of ~100Å or more are required to give a good diffraction pattern, the clarity of the sample patterns leads us to conclude that the original Mg_5Al_8 sample rearranges into "micropockets" of MgH_2 and Al of at least 100Å diameter. The authors believe the reaction mechanism to be:

$$Mg_5Al_8 + 5H_2 \xrightarrow{343\ ^oC} 5Mg + 8Al + 5H_2 \rightarrow 5MgH_2 + 8Al \quad (1)$$

Through this mechanism, the Mg is viewed to dissociate from the aluminum, diffuse to a nucleation (reacting) site, and react with hydrogen. The x-ray pattern for the fully desorbed sample, which was allowed to remain at 343 °C for four days after desorption prior to cooling and removal from the reactor, was identical to one for a virgin sample of Mg_5Al_8, indicating that the alloy had rearranged back to its original crystal structure.

The five samples for the kinetic study were evacuated, heated to 343 °C, and then exposed to 800 psia hydrogen. Activation times for the five samples are shown in Table II. This is the time lapse before each sample's initial uptake of hydrogen gas.

Figure 1 shows typical absorption curves for the five samples. Any differences in rate occur during the first 30 seconds of absorption. The control, Ni powder, and Ni alloy samples have approximately the same rate; the fine and coarse Ni plated samples have approximately 2/3 this rate. After 30 seconds, the rates are all equivalent.

This suggests that the Ni does not increase the absorption rate in high surface area Mg_5Al_8, and in fact, could interfere with the absorption as in the case of the Ni plated samples. One possibility is that the Ni plating reduces the surface area of the particles.

Figure 2 shows typical desorption rate data. Inspection of the curves shows that each sample exhibits its maximum desorption rate at a time corresponding to 20% hydrogen desorption. At this time the fine mesh, Ni plated sample desorbs about 7 times faster than the Ni alloy and 9.5 times faster than the control. Ni is a well known hydrogenation catalyst and possibly aids in hydrogen recombination ($2H \cdot \rightleftharpoons H_2$) in the Ni-catalyzed samples. The observation that these samples desorb faster than the control suggests that hydrogen recombination is one rate limiting step. The fact that the fine mesh, Ni plated sample, #3, desorbs faster than the alloyed sample suggests that the Ni distribution, or incorporation, is also important to the kinetics. Furthermore, the fact that the fine mesh, Ni plated sample desorbs about 7 times faster than the coarse mesh, Ni plated sample suggests that the particle size is also a factor in the kinetics. Further work is required to elucidate the roles of Ni (or other catalysts), catalyst incorporation, surface morphology, and particle size in metal hydride chemistry.

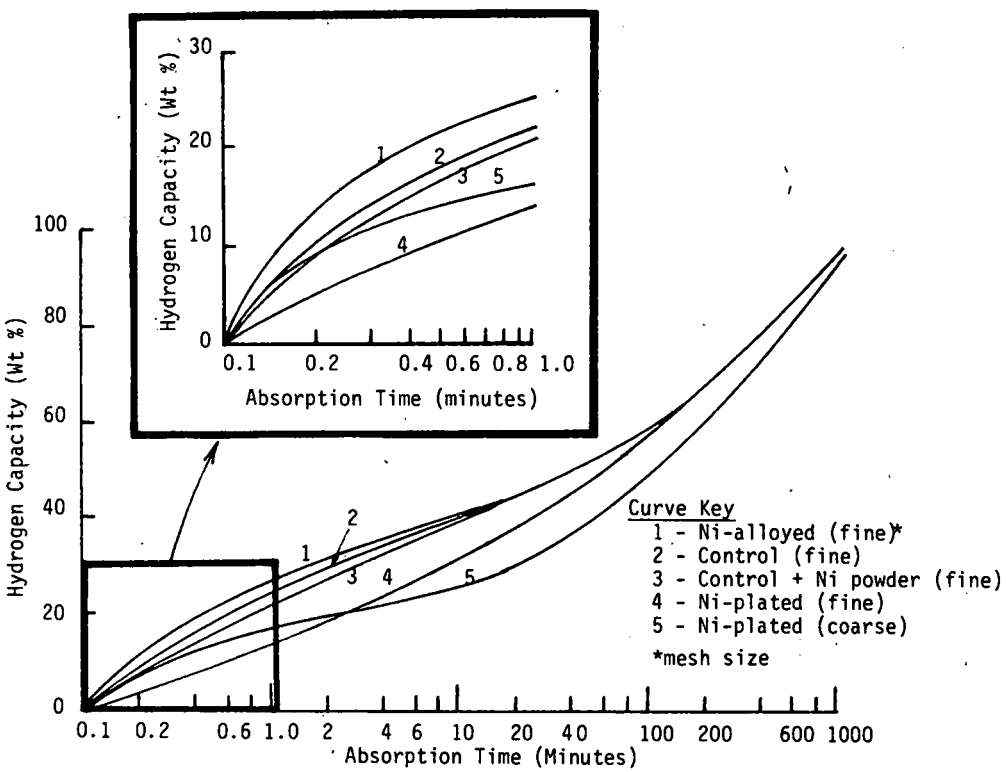

Figure 1. H_2 Absorption Rates for Mg_5Al_3 and Ni/Mg_5Al_8 Systems at 343 °C

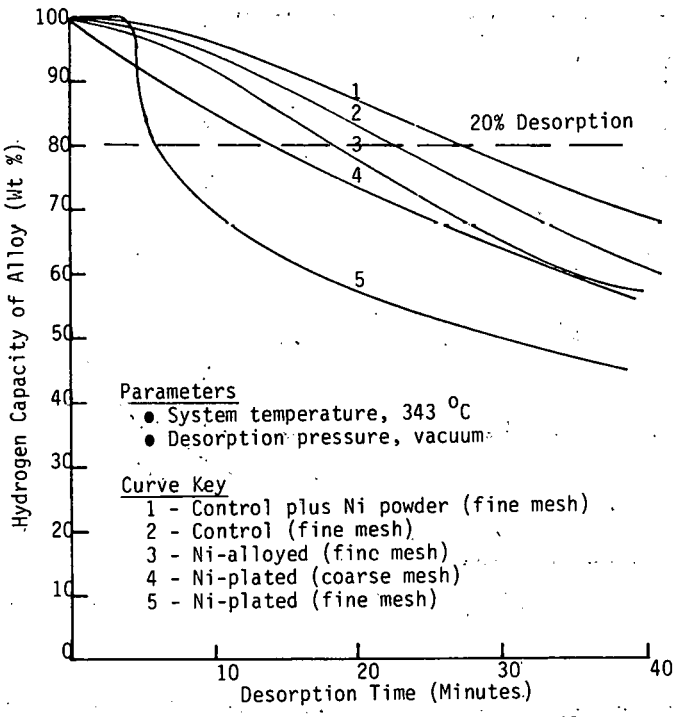

Figure 2. Hydrogen Capacities of Mg_5Al_8 and Ni/Mg_5Al_8 Systems Versus Desorption Time

TABLE II

SAMPLES USED IN KINETIC STUDY

Sample	Particle Size	Ni Incorporated As	Wt % Ni	Activation Time
1 (3424-16-1)	-200 mesh	-	0	48 hrs
2 (3424-16-2)	-200 mesh	Powder (-80 mesh)	1%	72 hrs
3 (3424-16-3)	-200 mesh	Electroless Plated	>1%*	Immediate
4 (3424-16-4)	-120+140 mesh	Electroless Plated	>1%*	6 hrs
5 (3424-17-1)	-200 mesh	Alloyed**	1%	2-3 hrs

* Analysis not yet complete.
**Prepared in separate melt.

Rapid desorption is believed to yield an unstable form for Mg_5Al_8; namely, "micropockets" of Mg and Al ($5MgH_2 + 8Al \xrightarrow{343\ ^oC} 5Mg + 8Al$). Given sufficient time and temperature, the unstable Mg and Al will rearrange to their more stable form, Mg_5Al_8 ($5Mg + 8Al \rightarrow Mg_5Al_8$). The authors hypothesize that alloy disproportionation is one rate controlling step; therefore, compared with Mg_5Al_8, disproportionated Mg + Al should exhibit an enhanced hydrogen absorption rate.

To test this hypothesis, a sample of $Mg_5Al_8H_{10}$ was rapidly desorbed (1½ hr) into vacuum at 343 °C in an attempt to prepare disproportionated Mg and Al. At this time, analytical data on the extent of disproportionation within the alloy are not available. In addition, we have yet to determine how rapidly one must desorb the alloy to preserve the disproportionated form. After forming the disproportionated Mg + Al sample, hydrogen at 800 psia was introduced into the system. The hydrogen uptake was measured, the results of which are shown on Figure 3. Figure 3 compares the rate of hydrogen absorption for Mg_5Al_8 and "disproportionated" Mg + Al. The data show that the initial rate of hydrogen absorption for the "disproportionated sample" is twice the rate for Mg_5Al_8. This suggests that disproportionation is a rate controlling step for absorption. Further experiments are required in this area.

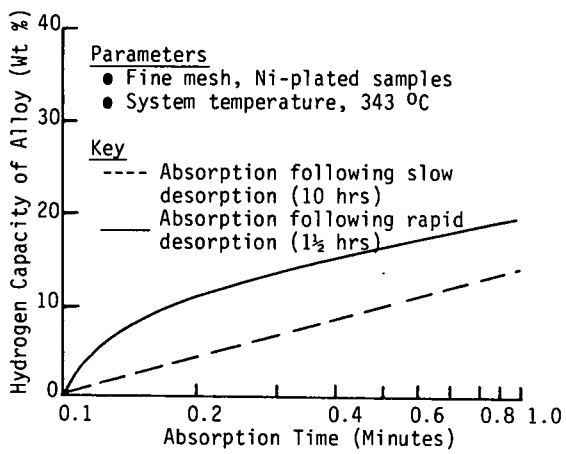

Figure 3. Hydrogen Absorption Rates for Mg_5Al_8 and "Disproportionated" Mg + Al

Summary

1. Mg_5Al_8 disproportionates to MgH_2 and Al in the absorption reaction. The MgH_2 and Al may form micropockets of at least 100Å diameter.

2. Disassociation of H_2 to H· is not rate controlling for absorption.

3. Desorption is enhanced by Ni catalyst.

4. The rate controlling step in H_2 absorption appears to be the diffusion of Mg to the hydride nucleation sites.

Acknowledgements

We would like to thank Professor Michael Notis of Lehigh University for his assistance in analyzing the x-ray diffraction patterns. Thanks are also due to Inco, who electroless plated our Mg_5Al_8 samples for the catalysis study. And finally, we are grateful to BNL and DOE for their support under Contract No. 485875-S.

DEVELOPMENT OF HYDROGEN STORAGE MATERIALS FOR APPLICATION TO ENERGY NEEDS

C. E. Lundin, J. Liu, C. B. Magee
Denver Research Institute
University of Denver
Denver, Colorado 80208

Abstract

The hydriding characteristics of many selected alloy combinations have been systematically investigated. Accurate pressure-temperature-composition relationships of the selected alloy systems were determined. The objectives of this program were to extend the number of hydrides useful for hydrogen storage, and to increase their storage capacities. The goal to develop a hydride with a capacity of at least three weight percent hydrogen has been arbitrarily established. Several alloy compositions in the Ti-V-Mn system are able to hydride to a capacity of over three weight percent hydrogen. Other alloys with the structure types: $CrB(B_4)$, $SnNi_3(DO_{19})$, $TiAl_3(DO_{22})$, $AuCu_3(L1_2)$, $BaAl_4$ $(D1_3)$, $ThB_4(D1_e)$, $CaCu_5(D2_d)$, $AlB_2(C32)$ and $MgCu_2(C15)$, as well as the Ti-V-Mn system and Ti-V-Cr system were screened. Since there are no ternary phase diagrams available for the Ti-V-Mn and the Ti-V-Cr systems, in order to design alloys with possible single phases in those systems, phase equilibrium had to be predicted from projections of the related binary systems.

Geometric investigations of the CrB(Bf) type structure were made. The intermetallic compound LaNi was chosen for analysis. The sizes and relative positions of tetrahedral holes in this type of intermetallic compound were considered in detail. There are different types of holes in this structure than were found in the more symmetric structures studied previously. Individual holes and clusters of holes favorable for hydrogen occupancy were identified, and maximum hydrogen concentration, in solid solution, in this type of compound was predicted. These predictions compare favorably with the very limited amount of experimental data available for the hydriding behavior of these compounds.

I. Introduction

Those metallic alloys or compounds which can form a hydride with a standard heat of formation of approximately -6 Kcal/mole H_2 or less in general fall into a category of so called "less stable hydrides". The absorption and desorption of hydrogen for these metallic systems is accomplished isothermally and reversibly at room temperature under moderate hydrogen pressures by extracting an appropriate amount of heat during the absorption process. This unique property of these types of hydrides offer a convenient and safe method for hydrogen storage for energy needs. Therefore, the investigation of some potentially useful systems and the evaluation of appropriate properties of these metallic hydride systems were the overall objectives of this program. The principle goal was to develop a hydride material with a hydrogen capacity of at least three weight percent or more. The general approach of selection of materials was not arbitrary, but was based on predictive criteria formulated at DRI[1] or taken from the literature. The selection process relied heavily on two criteria: 1) At least one of the elements of an alloy combination had to be a hydride former; and 2) The empirical correlation that the free energy of formation (per mole H_2) of intermetallic compound hydrides decreases (i.e., the stability increases) as the tetrahedral hole sizes in the parent intermetallic compound increases.

Concurrent with the materials properties studies there has been an effort to obtain a better understanding of the hydrogen occlusion phenomena from a more fundamental approach. A number of families of intermetallic compounds have been analyzed in terms of the numbers, sizes, and relative positions of tetrahedral holes in the compounds, as well as the clustering of holes that would be favorable for hydrogen occupancy. In the case of the CrB(Bf) type intermetallic compounds, holes and hole clusters have been identified which would appear to be the most likely sites for occlusion of hydrogen. As in the cases of other intermetallic compound-hydrogen systems, these sites have been related to maximum absorptivities.

II. Discussion

Alloy Development Studies

1. Ti-V-Mn System

It has been shown that Ti-V alloys of composition $TiV_{1.4}$ absorb hydrogen to a composition $TiV_{1.4}H_{4.6}(H/M=1.92)$ [2]. This composition corresponds to a weight percent of 3.7. This hydride system is, however, too stable for practical hydrogen storage utilization. Therefore, ternary additions to this binary alloy have been studied in an attempt to retain the high hydrogen content, while at the same time reducing the temperature required for desorption. Manganese additions were first investigated by one of us[3] in a restricted composition range, and from these results the entire Ti-V-Mn systems appeared promising for further study. Complete phase diagrams for this ternary system have not been determined. It was necessary, therefore, to predict ternary behavior based on the three binary systems Ti-V, Ti-Mn, and V-Mn. Single phase compositions were projected from the binary

systems, and metallography examination showed that this method was, in the majority of cases, successful.

Over the past year 36 different alloy compositions were investigated as to their hydriding behavior. A few of these contained quarternary additions of Fe, Co, Ni, or Cr. A typical isotherm is shown for the $Ti_{0.15}V_{0.75}Mn_{0.1}$ alloy in Figure 1. As can be seen in the Figure, the alloy absorbs about 1.85 atoms of hydrogen per metal atom at room temperature when the applied pressure is about 40 atm. This corresponds to a weight percent of 3.5. When hydrogen is removed from the hydride the pressure abruptly decreases to about 0.2 atm. at an H/M ratio of about 1.7. Obviously there is no evidence of a plateau pressure(indicative of two condensed phases in equilibrium) in this composition range at room temperature. This is typical of the room temperature behavior of all the Ti-V-Mn alloys (and those with quarternary additions) investigated.

When the sample of Figure 1 is heated to about 200°C the pressure increases and the H/M ratio decreases as would be expected. More significantly the desorption isotherm at this temperature shows more curvature than that at room temperature. For other alloys at somewhat higher temperatures the change in slope is more pronounced than that shown in Figure 1. In fact the isotherms tend to flatten out (although no definite plateaus have been observed) indicating an eventual miscibility-gap in these alloy-hydrogen systems.

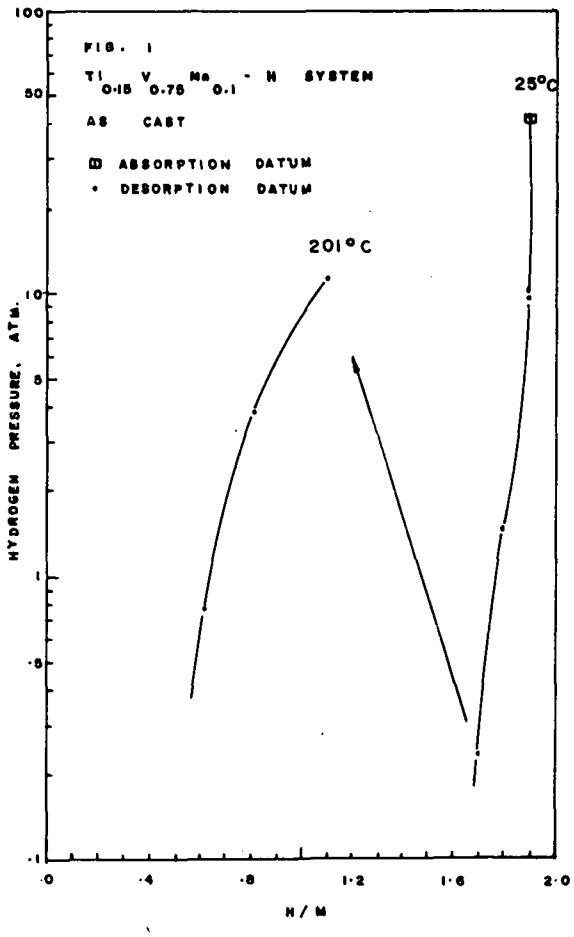

2. Ti-V-Cr System

No intermetallic compounds have been identified in the Ti-V and Cr-V binary systems. The intermetallic compound $TiCr_2$ exists in the Ti-Cr system. Metallographic analysis showed that all 5 alloys selected from this ternary system were multiphased. The isotherms obtained were similar to those shown in Figure 1, but in general the saturated H/M values were less than those obtained for the Ti-V-Mn system.

3. B_f Structure Type Alloys

From the limited experimental results that we obtained, the conclusion is that alloys of this structure type absorb hydrogen to a H/M value between one and two at room temperature and under hydrogen pressures of up to 100 atmospheres. Desorption isotherms showed that metal to hydrogen bonds are rather strong.

4. AB_3 and AB_4 Types of Combination Alloys

All 13 alloys in this type of combination that we selected for study (examples were $TiNi_3$ and $LaAl_4$) were very poor hydride formers at room temperature and under a hydrogen pressure of up to 160 atmospheres.

5. Borides

None of the 11 binary borides selected for study are good hydride formers by direct formation with gaseous hydrogen. Some elements such as H, B, C, and N with relatively small atomic radii (B: ~0.9 A°, H: 0.46 A°) alloying with transition metals tend to form so called "interstitial compounds", and their actual composition depends upon the degree of filling of the interstitial sites. Both B and H fall into this category. In case of TiB, when the amount of titanium was progressively substituted by vanadium, the H/M values increased from 0.29 for an alloy of composition $(Ti_{0.8}V_{0.2})B$ to 1.07 with an alloy of composition $(Ti_{0.2}V_{0.8})_{0.8}B_{0.2}$. Without crystallographic evidence and based only on hydriding experimental data, it is tentatively proposed that in these systems boron atoms occupy some of the interstitial hole sites that otherwise would be positions for hydrogen atom occupation.

6. AB_5 System

The intention of modification to the $MMNi_5$ system was to lower the cost of the alloy by replacing Ni with less expensive elements, such as Fe, Cu, V, and Mn. The results of temperature-pressure-composition diagrams showed those modified systems studied are of no commercial interest.

7. Ca-base Alloys

The $Ca_{0.32}La_{0.68}$ alloy showed a good saturation, yet it is very stable. $CaNi_5$ forms a fairly stable hydride with a plateau pressure of about 0.5 atm at room temperature. $Cr_{0.2}La_{0.8}Ni_5$ formed a hydride with a comparable H/M value to that of $LaNi_5$. Also it shows similar desorption characteristics i.e., a plateau pressure of about 1.5 atm. at room temperature. Because Ca is more abundant than La, the substituted compound would be favorable from the point of view of cost.

Figure 2 shows the 25°C desorption isotherm of this alloy.

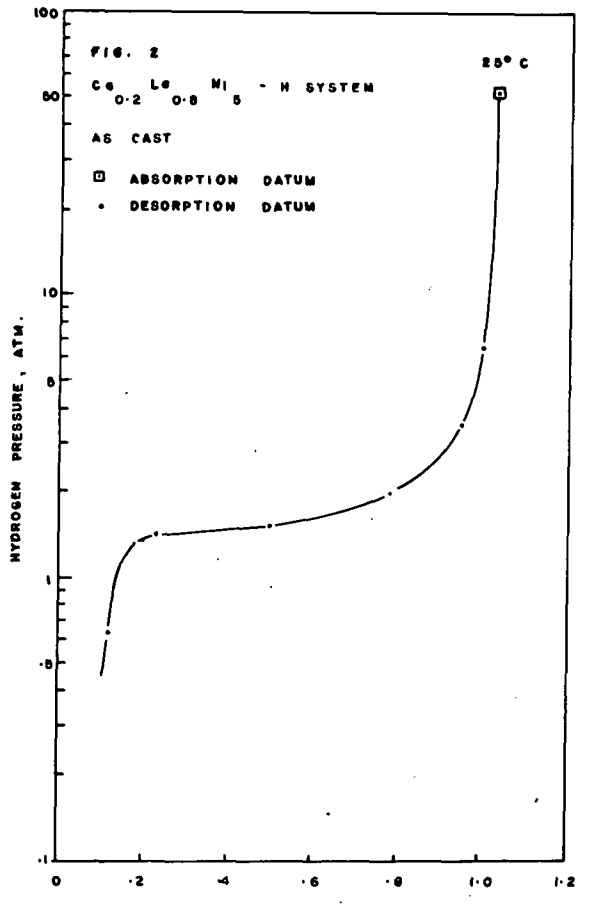

Relationships Between Intermetallic Compound Structures and Hydride Formations

The $CrB(B_f)$ type compounds that have been studied absorb hydrogen to a hydrogen/metal ratio between 1 and 2 at room temperature and pressures up to 100 atm. No phase changes have been observed. The A_4 and A_2B_2-4C holes are of sufficient size to accommodate hydrogen to a H/M=1 with little distortion. When hydrogen is absorbed to a H/M value of between 1 to 2, the most likely sites for hydrogen occupancy are binary clusters of A_3B and A_2B_2-8f holes. There remains a question for these hydrides, however, as to whether or not a true solid solution or hydride phase exists. Decomposition to binary hydrides is a possibility and must be investigated.

References

1. Denver Research Institute, Development of Hydrogen Storage Materials for Application to Energy Needs, Interim Progress Report 1, 2, 3, and 4 (1978), Denver, Colo. 80208.

2. C. E. Lundin, F. E. Lynch, and C. B. Magee, J. Less Common Metals, 56 (1977) p. 19-37.

3. T. R. P. Gibb, Jr., Primary Solid Hydrides in Progress in Inorganic Chemistry, 3 (1962), p. 494.

4. J. Liu, U. S. Patent No. 4,111,689.

Acknowledgments

The authors are grateful for the support of U.S. Department of Energy through the Brookhaven National Laboratory under contract EI-78-S-02-5104, for the period October 1978 to October 1979. The help and cooperation of Dr. John R. Johnson of BNL is particularly acknowledged.

SURFACE POISONING OF METAL HYDRIDES

P. D. Goodell and G. D. Sandrock
Inco Research and Development Center
Suffern, New York

Abstract

This report is a brief summary of an extensive experimental program designed to understand the surface poisoning of metal hydrides by impurities in the hydrogen used. Alloys investigated were $LaNi_5$, FeTi, and $Fe_{0.85}Mn_{0.15}Ti$. Gaseous impurities studied were O_2, H_2O, and CO. The nature of the surface structures formed, and consequently the degree of poisoning varies markedly from alloy to alloy and from impurity to impurity. Examples of complex compound film formation, chemisorption, and possibly physisorption can be seen. Results show the hope of developing surface structures with significant resistance to impurity gases and especially the possibility of designing practical regeneration cycles.

Introduction

There is growing worldwide interest in the practical application of rechargeable metal hydrides in the areas of energy storage and conservation, as well as in the existing industrial hydrogen sector. One of the fundamental problems that must be addressed is the phenomenon of "surface poisoning". By surface poisoning we mean a loss of hydrogen absorption (or desorption) kinetics and/or capacity that occurs when impure hydrogen is used. As the term implies, it is generally assumed that the impurity gas forms some sort of surface film or structure that "poisons" the surface catalytic properties of the storage alloy particles necessary for the hydriding (or dehydriding) process.

At present there is very little information available on the fundamental mechanisms of hydride surface poisoning. Even less practical engineering data on the effects of various gaseous impurities is available. In this contract, just being completed, we have attempted a major systematic study designed primarily to understand mechanisms of surface poisoning, and secondly to provide some practical data on a few common storage alloys and gaseous impurities. This report will concentrate on some of the practical data obtained and briefly summarize some of the mechanisms being deduced from this and other data. Because of space limitations only a small fraction of the results can be presented. A complete set of results and discussion are given in the Final Report for the contract[1].

Experimental Procedures

The overall experimental philosophy was outlined at the last Contractor's Review Meeting[2] and needs only brief review and updating here.

Alloys and Gaseous Impurities

Three model alloys were used: (1) $LaNi_5$, the classic AB_5 compound; (2) FeTi, the classic AB compound; and (3) $Fe_{0.85}Mn_{0.15}Ti$, a modified FeTi-type alloy chosen to test for ternary substitution effects. Three impurity gases were studied: (1) O_2, a likely candidate for surface compound (oxide) film formation; (2) H_2O, a possible candidate for surface physisorption; and (3) CO a candidate for possible surface chemisorption.

Cyclic Poisoning Tests

Cyclic tests were run on our Continuous Cycling Absorption Desorption (CCAD) apparatus, described last year[2], using a special high-conductivity specimen holder. Before cycling the samples in mixed H_2-X gases, they were activated and cycled in hydrogen of super high purity (SHP-H_2) obtained from a specially constructed hydride/dehydride purifier. This allowed the generation of atomically clean active surfaces and the establishment of baseline (unpoisoned) kinetic and capacity data. Cycling was then continued with H_2 contaminated with various levels of O_2, CO, or H_2O, with the decrease in kinetics and effective capacity measured as a function of the number of cycles. Those curves that will be shown here represent effective hydrogen transfer capacity for a 30 minute cycle (15 minutes absorption-15 minutes desorption) with the charging pressure set so that, in the unpoisoned state, half of the charging occurs in the first minute. In the case of FeTi and $Fe_{0.85}Mn_{0.15}Ti$ only the lower plateau was used.

In addition to the basic poisoning tests, ease of reactivation was determined for almost all samples, a most important practical property. A number of thermal and pressure dependence H_2 absorption studies were done on poisoned samples to help understand the mechanism by which the impurity surface film impedes absorption.

Absorption Tests

The reaction of each pure contaminant, X, with the activated surface of each alloy was determined with a series of low pressure (10 Torr) adsorption tests. The quantity of impurity X and the temperature excursion was monitored which allowed estimates of surface film thickness and heats of adsorption.

Results

Cyclic Poisoning Tests

The effects of cycling (at room temperature) with H_2 containing 300 ppm O_2, H_2O, or CO are shown for each alloy in Figure 1. A wide variety of behaviors are observable, depending on the alloy-impurity gas combination. In particular the following things should be noted:

1. O_2 and H_2O produce very similar effects.

2. FeTi and $Fe_{0.85}Mn_{0.15}Ti$ show continuous poisoning in the presence of O_2 and H_2O, but $LaNi_5$ does not. After an initial partial loss of capacity in O_2-or H_2O-containing H_2, $LaNi_5$ almost completely recovers and then exhibits substantial

immunity.

3. CO is far more detrimental than O_2 or H_2O to all three alloys.

4. $Fe_{0.85}Mn_{0.15}Ti$ shows at least some resistance to CO in comparison to Mn-free FeTi. After some loss of capacity, $Fe_{0.85}Mn_{0.15}Ti$ reaches a level where little further damage occurs, whereas FeTi soon loses all hydrogen capacity. $LaNi_5$ behaves like FeTi in the presence of CO.

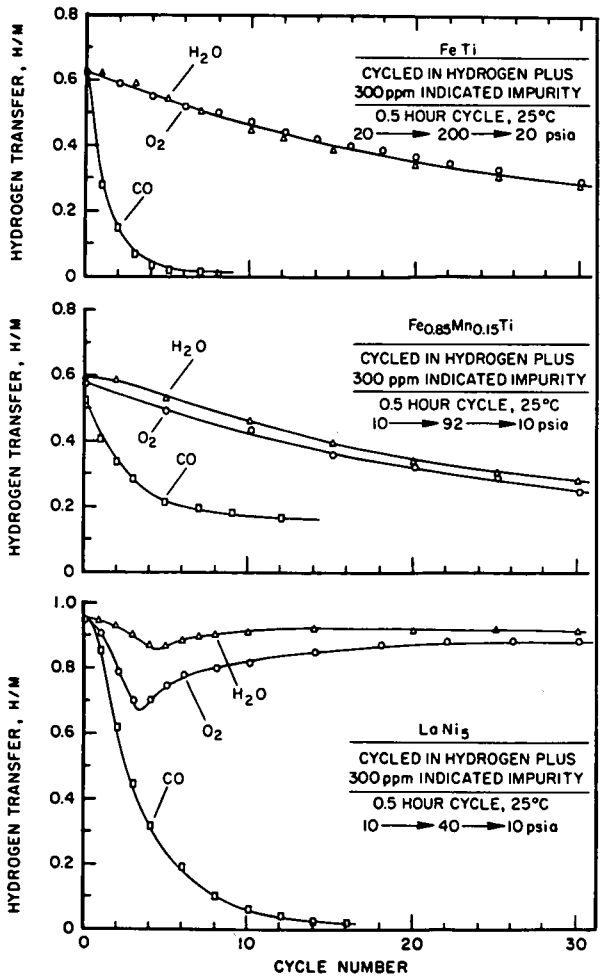

Fig. 1 Cycling response of the three test alloys in hydrogen containing 300 ppm H_2O, O_2, or CO impurity.

By using suitable reactivation procedures a substantial fraction of kinetics and capacity could be recovered in all cases. In some cases recovery would occur simply by continuing the cycling procedure in SHP-H_2. For example, the recoveries of the three alloys during room temperature SHP-H_2 cycling after poisoning in H_2-100 ppm CO are shown in Figure 2. Here, again, dramatic differences from alloy to alloy can be seen. $Fe_{0.85}Mn_{0.15}Ti$ was extremely easy to reactivate, whereas FeTi was very difficult to reactivate. $LaNi_5$ was intermediate. Modest heating (say to 45°C) greatly helped the reactivation of CO poisoned FeTi.

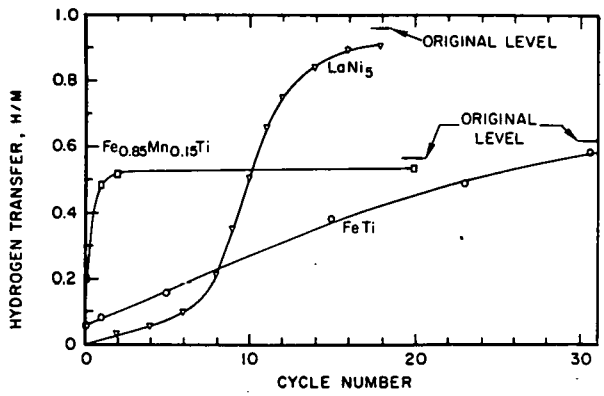

Fig. 2 Recovery of hydrogen transfer capability during cycling in SHP-H_2 after poisoning in H_2 containing 100 ppm CO.

The reactivation of O-poisoned FeTi and $Fe_{0.85}Mn_{0.15}Ti$ was more difficult than CO-poisoned samples. By heating to 80°C and cycling with SHP-H_2, however, a substantial degree of reactivation could be achieved. $Fe_{0.85}Mn_{0.15}Ti$ was easier than FeTi to reactivate after O-poisoning.

Adsorption Tests

As an example of the data generated during the adsorption tests, Figure 3 shows the surface adsorptions of oxygen as a function of time and the temperature excursions associated with each adsorption experiment. The adsorption data is normalized to the effective surface area generated during the activation process (0.5 m^2/g for FeTi and $Fe_{0.85}Mn_{0.15}Ti$ and 0.2 m^2/g for $LaNi_5$). This has also been converted, on the right scale, to an approximate film thickness in monolayers. These tests were run on samples activated with H_2 but thoroughly dehydrided before exposure to the 10 Torr O_2.

The curves show that substantial quantities of oxygen are adsorbed (tens of monolayers) exothermically. The reactions were largely complete within the first minute. The adsorption of H_2O was qualitatively similar but the time scale was over several hours rather than one minute. The absorption of CO was, on the other hand, radically different from O_2 or H_2O in that only about one monolayer was quickly adsorbed with no further reaction occurring.

From the temperature excursions and quantities of gas adsorbed, approximate heats of reaction were calculated. These are shown in Table I. These results, along with the reference heats of reaction from the literature, are very useful in establishing the nature of the adsorbed film and will be discussed in the next section.

Reactivation studies were done on the samples after the adsorption tests. In general, they are comparable and complementary to the reactivation results obtained with samples poisoned on the cyclic apparatus. In particular, the development of practical immunity to O_2 by $LaNi_5$ was strikingly confirmed.

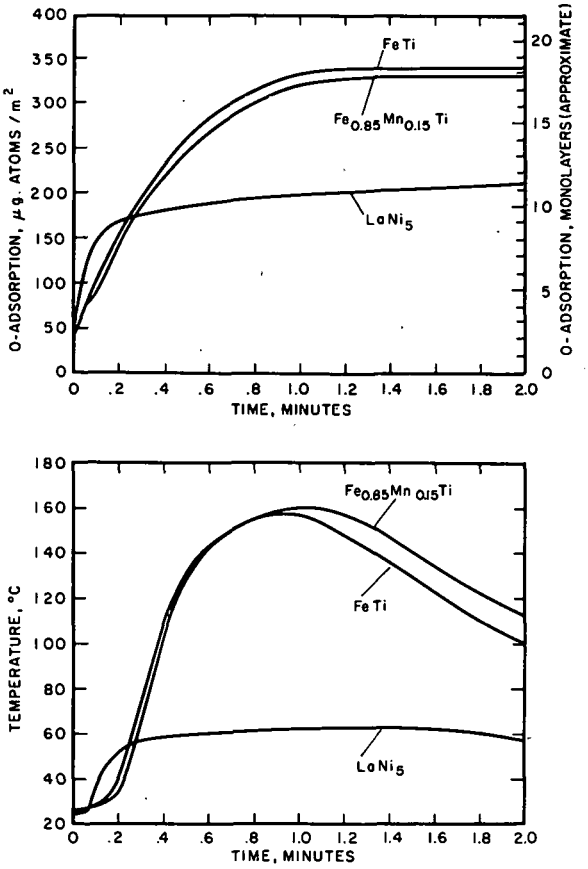

Fig. 3 Oxygen adsorption and corresponding thermal excursion curves. Oxygen pressure = 10 Torr.

Table I Estimated Heats of Adsorption

Alloy	ΔH_{AD}, kcal/mol gas		
	O_2	CO	H_2O
$LaNi_5$	-187	- 42	-41
FeTi	-186	- 86	-78
$Fe_{0.85}Mn_{0.15}Ti$	-198	-134	-69

Some Reference Values From the Literature

ΔH_f° (La_2O_3) = - 305 kcal/mol O_2

ΔH_f° (NiO) = - 117 kcal/mol O_2

ΔH_f° (TiO_2) = - 218 kcal/mol O_2

ΔH_f° (FeO) = - 127 kcal/mol O_2

ΔH_f° ($Ni(CO)_4$) = - 37 kcal/mol CO

ΔH_f° ($Fe(CO)_5$) = - 46 kcal/mol CO

ΔH_f° ($Mn_2(CO)_{10}$) = - 40 kcal/mol CO

ΔH_c (H_2O) = - 9.65 kcal/mol H_2O

Significance of the Results

Surface poisoning appears to result from the formation of a surface "structure" that inhibits rapid catalytic $H_2 \rightarrow 2H$ dissociation and/or hydrogen penetration, both of which are necessary for practical use of a rechargeable hydride. The experimental results of this contract suggest that a wide variety of surface structures can result, depending on the alloy and impurity gas. Consequently, there is wide variation in the degree of poisoning resistance and ease of reactivation.

O_2-Contamination

The adsorption data suggest a fairly thick oxide film forms for all three alloys. The heats of adsorption (Table I) suggest that there is some selective oxidation of La or Ti but also that some of the Ni or Fe must be oxidizing. In effect, we believe that initially complex oxides (i.e., $La_xNi_yO_z$ and $Ti_xFe_yO_z$) form. From magnetic and other surface studies[3,4] it is evident that these films must disproportionate providing metallic Ni, Fe and stable oxides in the films. In the case of $LaNi_5$, this process (which takes a few hours) clearly results in catalytically active Ni thus restoring the $LaNi_5$ surface much along the lines of Schlapbach's model[3]. Even though a similar structure apparently develops for FeTi the end results are opposite that of $LaNi_5$, i.e., there is no "self restoration" of FeTi activity. This strongly suggests that either (1) metallic Fe is not the $H_2 \rightarrow 2H$ catalytic species or (2) the TiO_x film, unlike La_2O_3, is impermeable to hydrogen penetration.

CO-Contamination

In the case of $LaNi_5$, CO appears to form a simple chemisorbed monolayer with heats of adsorption comparable to Ni-Carbonyl formation (Table I). This renders inactive the Ni-atom sites at which catalytic dissociation of hydrogen occurs. In the case of FeTi, and especially $Fe_{0.85}Mn_{0.15}Ti$, the heats of adsorption suggest that the CO is at least partially split to oxidize and/or carburize the surface, again blocking hydrogen dissociation sites. The Mn atoms seem to have significant catalytic activity even in this state so that site blockage is less severe in $Fe_{0.85}Mn_{0.15}Ti$.

H_2O-Contamination

H_2O is very similar to O_2. Apparently the H_2O molecule is split on the surface, resulting effectively in surface oxidation (or hydrolysis). The rate of oxidation reaction is moderated somewhat, perhaps by the presence of some physisorbed H_2O.

Practical Significance

From a practical applications point of view, there are a number of obvious conclusions that can be directly drawn from this work.

1. If significant amounts of O_2 or H_2O are expected in the H_2, use $LaNi_5$ (or possibly some other AB_5 compound).

2. If CO is expected, use (Fe,Mn)Ti.

3. Binary FeTi will be a problem for any gaseous impurities.

4. All alloys can be reactivated after poisoning with procedures that are conceptually simple. Some (e.g., FeTi) are harder to reactivate than others (e.g., $LaNi_5$ or (Fe,Mn)Ti).

From a long range development point of view, we venture two conclusions:

1. There are marked alloy to alloy variations giving hope for some day developing the understanding necessary to design specific poison resistance into an alloy.

2. If complete resistance to all poisoning is impossible (as it probably is), there should be ways to design reactivation cycles into the particular process or device involved.

Future Work

A one year continuation of this work has been proposed. It will be directed mainly toward the generation of more practical data of direct use in applications. A small amount of fundamental work will be continued where appropriate. The work will concentrate on the following areas:

1. New gaseous impurities, e.g., H_2S.

2. Combined impurities and interaction effects.

3. Reactivation procedures, including practical reactivation schemes.

4. Improved operating procedures to increase hydride life before the need to reactivate.

Acknowledgement

This work was performed under Contract BNL 451117-S, funded by the U.S. DOE and Inco.

References

1. P. D. Goodell and G. D. Sandrock: "Metallurgical Studies of Hydrogen Storage Alloys", Final Report for Contract BNL 451117-S. Inco Research and Development Center, Suffern, New York 10901, October, 1979.

2. G. D. Sandrock and P. D. Goodell: "Mechanisms of Surface Poisoning of Metal Hydrides", Proceedings of the DOE Chemical/Hydrogen Energy Systems Contractor Review, DOE CONF-781142 (May, 1979), p.245-250.

3. L. Schlapbach, A. Seiler, H. C. Siegmann, T. V. Waldkirch, P. Zürcher, and C. R. Brundle "Self Restoring of the Active Surface in $LaNi_5$" 2nd World Hydrogen Energy Conference, Zurich, 1978.

4. G. Busch, L. Schlapbach, F. Stucki, P. Fischer, and A. F. Andresen, "Hydrogen Storage in FeTi: Surface Segregation and Its Catalytic Effect on the Hydrogenation and Structural Studies by Means of Neutron Diffraction", 2nd World Hydrogen Energy Conference, Zurich, 1978.

Dup

OVERVIEW: BNL END-USE APPLICATIONS PROJECTS*

M. Bonner

Brookhaven National Laboratory
Upton, New York 11973

ABSTRACT

An overview is given of the end-use applications area of the BNL Hydrogen Program. At present, it consists of only two contract efforts for development of small-scale hydropower for hydrogen production. Background information on the project is provided.

The end-use applications area of the BNL Hydrogen Program consists of those projects which demostrate hydrogen use in new or modified equipment or complete system demonstrations involving hydrogen production, storage, distribution and use. The major project in this area is the latter type and involves two contracts aimed at demonstrating hydrogen production from small hydropower sources. The hydrogen would subsequently be distributed and sold in commercial/industrial markets. The contracts are currently in the study phase but sites have been selected and it is expected that at least one site will be developed and producing hydrogen within the next three years.

Each of these contract efforts will be described in more detail in the papers that follow but some background on the scope and objectives of the project will be given here. The concept of hydrogen production from small hydropower sites was proposed initially by the Institute of Gas Technology (IGT). A feasibility assessment was funded by DOE STOR through Brookhaven, completed by IGT in 1978, and presented at last year's Contractors' Review Meeting.[1] The study concluded that:

A. Though the total resource is small (<1 Quad), about 20,000 sites exist in the Northeast in the 250 kW - 5 MW_e range suitable for hydrogen production. (Fig. 1).

B. The hydrogen could be produced at competitive costs and would have markets as a chemical commodity. (Fig. 2)

With this study as a baseline, DOE STOR sponsored an RFP solicitation for undertaking a proof-of-concept demonstration project. The complete project would include site selection and acquisition, dam renovation and construction, H_2 equipment installation and the marketing/distribution and sale of the product hydrogen. After a comprehensive evaluation process, two contracts were awarded in mid-1979. The contractors selected were Air Products & Chemicals and a team led by New York State ERDA. Two awards were made because the contractors presented essentially different approaches to the problem.

Air Products is employing the "over the fence" approach in which they are starting with a well defined market area (large user) and plan to develop a site nearby such that the hydrogen could be piped "over the fence" to the customer.

The New York State ERDA approach involves an established site (Potsdam, New York) and tying in with a program producing electric power from small hydro for local use, with the excess power used to produce hydrogen. The hydrogen would then be sold commercially to small users within a 50-mile radius.

As far as status, the Air Products contract has been signed and they have been working since June. The New York State ERDA contract is near sign-off after resolving some legal problems with subcontractors. The study phases of both contracts are expected to be completed in mid-1980 at which time a decision will be made regarding the follow-on construction.

REFERENCES

1. Johnson, Dale G., Escher, William J. D., Palumbo, J. P., Ostrowski, W. M. Hydrogen From Small Existing Falling-Water Sites: An Initial Feasibility Assessment, prepared for Brookhaven National Laboratory under contract No. 423391-S, for the U.S. Department of Energy, June 1978.

*Research performed under the auspices of the U.S. Department of Energy.

FIGURE 1*

Survey Area (Source of Information)	Number of Sites	Total Gross Power, 10^6 kW	Total Gross Annual Energy, 10^9 kWhr	Annual Hydrogen Production Energy 10^{15} Btu
Northeastern U.S.-- IGT/PG&W**	10,490	0.71	3.76	0.009
Northeastern U.S.-- New York Polytechnic	20,917	3.80	19.95	0.049
Northeastern U.S.-- Corps of Engineers	20,000	9.18	30.89	0.077
Total U.S.-- Corps of Engineers	60,000	30.47	97.02	0.241

*From IGT Report
**Known to be incomplete--see text.

FIGURE 2*

Facility Size, kW	Cost of Hydrogen (Estimate) High	Low
	---------$/$10^6$ Btu---------	
250	25.00	13.25
1000	14.70	8.80
5000	7.60	5.20

*From IGT Report

HYDROGEN PRODUCTION FROM SMALL HYDROPOWER SITES

E. L. Wilkinson, B. N. Kriebel, and K. J. Ramundo

Air Products and Chemicals, Inc.
Allentown, Pennsylvania

Abstract

In a U. S. Department of Energy sponsored program, Air Products and Chemicals, Inc. (APCI) recently began studying the commercial feasibility of producing hydrogen with electrolytic cells powered by electricity generated from a small hydroelectric site. The conversion of hydro-power directly into hydrogen is being evaluated as a more promising mode of developing this energy resource than simply generating and transmitting electricity into the grid. The costs of connection, and the incongruency of the demand for and supply of the power to the grid frequently prohibits development in this manner. Since hydrogen can be stored to an extent, the conversion of hydro-power into hydrogen can mitigate these obstacles to small dam development. Whether utilized as a fuel in blending with natural gas or as a chemical feedstock (primarily produced by steam reformation of natural gas), hydrogen produced from small dams has the potential of reducing natural gas demand in the near and mid-term. The program also seeks to demonstrate the suitability of small dam (low-head) hydroelectric power for on-site industrial applications.

The study will consist of three phases. The Systems Analysis phase will primarily involve an engineering and economic analysis of a "typical" 1.5 MW hydroelectric electrolytic hydrogen facility, including a sensitivity analysis of the major cost components of the delivered price of hydrogen as a chemical feedstock to establish site selection criteria. The purpose of the Site Selection phase is to select an actual site which will minimize the mix of fixed and variable costs of production and distribution. In the third phase, Site Engineering and Economics, a budget cost estimate for an actual facility complete with preliminary drawings will be prepared. Definitive estimates of power, hydrogen production, and distribution costs will be prepared. If the facility appears commercially viable, final engineering, construction, and operational phases would follow.

Introduction

The objective of the program is the design, engineering, and construction of a small (<15MW) hydroelectric electrolytic hydrogen facility using advanced state-of-the-art (Electrolyzer Unipolar cells) and developmental (General Electric Solid Polymer Electrolyte cells) systems. The portion of the program currently being undertaken involves site evaluation, preliminary engineering, and cost estimating activities. The results of this work, scheduled for conclusion in March, 1980, will serve as a basis for deciding whether or not the proposed facility is commercially viable and should be built.

A program approach has been developed to enhance the prospects for commercial success. It will focus on the marketing of hydrogen not as a fuel but as chemical feedstock where the requirement is non-substitutable and its value ranges from $6.00/MM BTU to almost $30.00/MM BTU. Under the alternative, hydrogen would be directly competing with natural gas which sells for $2.00/MM BTU to $4.00/MM BTU.

The anticipated location for the facility is the industrialized New York/New England region where natural gas prices are high, shortages have been experienced, and where there are many potential sites. Most of these sites had been previously developed to provide hydro-mechanical power during the 1800's. A large number were later renovated for hydroelectric generation. In either case, such a site could be rehabilitated for less than the cost of an undeveloped site, thus reducing the effective cost of electric service. As will be presented subsequently, the single most important factor in the cost competitiveness of electrolytic hydrogen is electric power costs.

Only sites having nominal capacities of 1.5 MW or less will be investigated. The licensing and environmental problems associated with smaller sites are manageable at a cost which does not preclude industrial development. A 1.5 MW facility would produce a maximum of 7 MM scf of hydrogen monthly. Attempts will be made to locate a site near a large volume hydrogen user. In this case, a short pipeline could be used to supply the gas, adding only a small incremental cost in arriving at the delivered hydrogen cost. The alternative, serving a regional market, would involve the relative expensive distribution of the gas by tube trailer in smaller quantities over longer distances.

Program participants include Essex Development Associates, Inc., an experienced hydro-power development firm, General Electric and Electrolyzer Inc. Ltd., respective suppliers of SPE and Stuart electrolytic cells, and Allis Chalmers, a manufacturer of hydro-turbine/generator systems. A civil engineering firm will complete the project team.

The program is in the early stages of execution; consequently, final results or conclusions are unavailable. This paper will discuss small dam development issues and the comparative economics of hydrogen production methods including the commercial prospects for electrolytic hydrogen.

Small Hydrosite Development Issues

The issues affecting the proposed development of small hydro-sites can be divided into three categories:

- o Hydrologic considerations related to producing hydroelectric energy to power an electrolytic hydrogen facility;
- o Licensing and related environmental issues; and
- o Hydro-site economics.

Hydrologic Problems

As an energy source, low-head hydro-power suffers from its inability to provide a constant supply of power. Figure 1 is representative of the wide variation in flow which is typical throughout river systems in the Northeast, where the proposed facility would be built. Reservoirs which are used in large scale hydroelectric development to stabilize the flow rate, are generally not available at low-head sites. Although turbine equipment selection can be made to attain maximum utilization of the flow through the use of differently sized turbines or variable blade and vane options, the problem of variable power generation at a facility which must satisfy a relatively constant hydrogen demand persists. There are several alternatives for mitigating this problem.

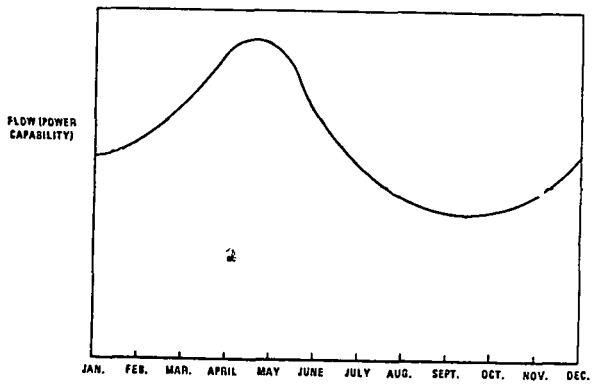

FIGURE 1. Typical Variation in Water Flow for Small Hydroelectric Sites

A flow duration curve is used to illustrate the problem in Figure 2. The hydroelectric equipment is sized to provide the maximum power required to match hydrogen production and demand which is relatively constant throughout the year. The power generation potential and hydrogen production are seasonal due to flow variation. During low flow periods, liquid hydrogen, which would be stored on-site, could be used to supplement hydrogen production. The decoupling of hydrogen production and demand would be achieved at the expense of providing a liquid storage system and the vehicle capacity to transport liquid hydrogen for periods during the year.

Another alternative would be to connect the hydro facility to the power grid, selling power not needed to produce hydrogen, and buying power to supplement the hydro-power to produce needed hydrogen during low flow periods. The purchase of off-peak power for hydrogen production, the costs of connecting to the grid, and the selling price of the generated power are considerations relevant to this alternative. An on-site diesel generator could also be used to provide supplemental power to maintain hydrogen production. The ease of shutting down and starting up an electrolytic facility introduces additional flexibility in synchronizing production and demand. A final possibility would be to select a site with flow characteristics which would be adequate to supply constantly the required amount of energy to satisfy hydrogen facility power requirements.

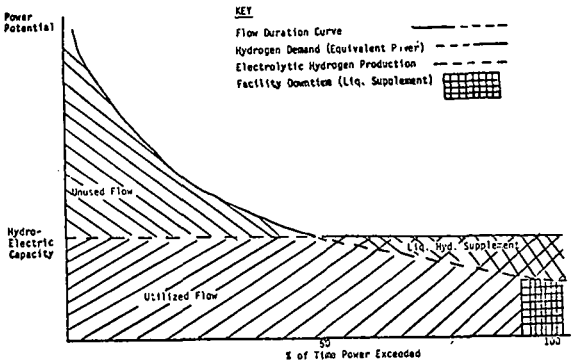

FIGURE 2. Flow Utilization and Hydrogen Production/Demand

Licensing/Environmental Problem

A significant fixed cost in any hydro-site development is satisfying licensing and environmental requirements. For sites with capacities of 1.5 or more megawatts, the license and environmental requirements are prohibitive. Sites smaller than 1.5 MW involve more expedient compliance. The environmental problems for a minor license (less than 1.5 MW) are usually restricted to providing fish passageways, if required, and historic preservation, and involve only two agencies, the State Historical Commission and the U. S. Fish and Wildlife Service.

Probable Economics

Essex Development Associates, Inc. has evaluated the economics of specific sites classified according to the opportunity present for restoration of existing facilities. In a facility requiring entirely new civil works, powerhouse, turbine, generator, and related equipment, the cost range under conventional financing is between 31-39 mills in 1978 dollars. Installations requiring retro-fitting or rehabilitation of existing equipment can produce power costing between 20-30 mills. In some installations which have remained in operation, power is provided at 8-15 mills. However, these facilities are probably providing power under long term supply contracts and would not be available for the proposed project.

The point illustrated above is that the cost of electric generation at a small damsite is extremely capital intensive. The opportunity to minimize site specific capital costs through

rehabilitation will be an important consideration in site selection.

Equipment

Hydroelectric Equipment

It is anticipated that Allis Chalmer's Tube^{R} turbines will be utilized in the program. These turbines are available in standard design and capacities and have been developed primarily for low-head hydro applications. Standardized production techniques have reduced production costs and a low profile design minimizes associated civil work. The combined effect has been to reduce the installed costs of low-head hydro turbine equipment.

Electrolytic Cells

Existing Technology There are two classes of existing operational cells, the bipolar (filter press) and the unipolar cells. The stated efficiencies of these cells range from 60 to 73%. Of these commercially available electrolyzers, the cell of the Electrolyser Corporation Ltd. (Canada) represents the best state-of-the-art for use in a commercial electrolytic hydrogen facility. The Electrolyser cell is estimated to have the lowest installed cost along with the highest efficiency. In addition, this cell has an excellent service life lasting 10 years before requiring overhaul. This dependable, high performance cell has been selected to provide the base load requirement of 1.0 MW for the proposed plant.

Developing Technology An advanced hydrogen electrolyzer cell which is under development and scheduled to be ready for field testing in 1981 is the G.E. SPE cell. This cell is projected to have a relatively low installed capital cost and achieve an efficiency of 93% for cells rated at 5 MW of capacity. Air Products and G.E. have agreed to incorporate two 200-kw cells in the proposed electrolytic hydrogen plant, allowing an early field demonstration of this new equipment.

A schematic of the proposed facility is included as Figure 3.

Hydrogen Production Methods Comparative Economics

Steam Reforming

Almost all commercial hydrogen is produced by steam reforming of natural gas, followed by catalytic shift and purification stages; chemically represented as:

$$CH_4 + 2H_2O \longrightarrow CO_2 + 4H_2.$$

The process is energy intensive, requiring approximately 500 scf of natural gas to produce 1000 scf of hydrogen. As indicated in Figure 4, steam reforming is also capital intensive. At production rates greater than one million scf/day, the cost of hydrogen becomes fairly constant and directly reflects the price of natural gas. Below this volume, the cost of steam reformed hydrogen is quite sensitive to fixed costs which constitute a larger percentage of production cost at lower volumes. In addition, steam reformers are usually operated continually, even if in a turned down mode, since start-up and shut-down consumes substantial time and energy. Operation in a turned down mode consumes natural gas and reduces the average onstream time to about 75%, thus increasing the effective capital and operating costs.

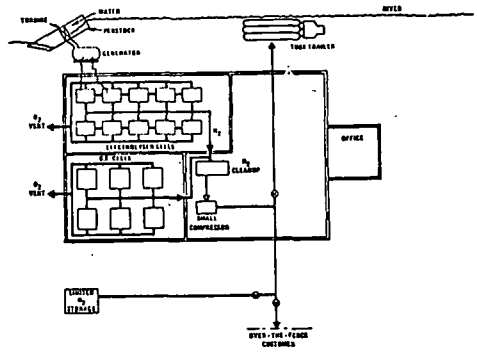

Figure 3. Possible layout for Electrolytic Hydrogen Plant

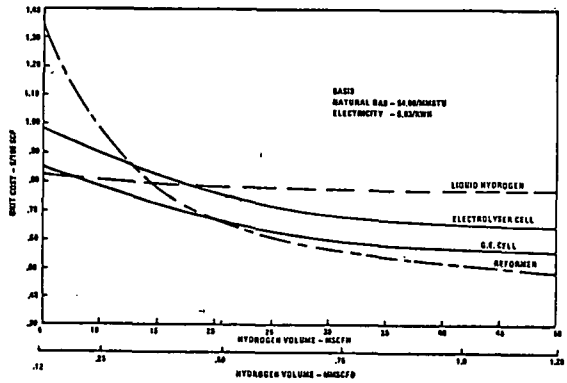

FIGURE 4. Hydrogen Production Costs as a function of Production Volume

Electrolysis

As a means of hydrogen production, electrolysis has not been widely used in the United States due to the high costs of electrical power, compounded by low cell efficiency, and historically low costs of natural gas used in the competing steam reforming process. Returning to Figure 4, the production cost of electrolytic hydrogen is less sensitive to volume than with reforming. The reason is that variable power costs are relatively more significant than fixed costs to the total production cost of electrolytic hydrogen. For example, with energy at $.025/Kwh and cells at 73% efficiency (Electrolyzer cell rating), the power cost component to produce 100 scf of hydrogen would equal $.32, approximately thirty to forty-five percent of the total production cost depending on the size of the electrolytic hydrogen facility. Higher cell efficiencies will reduce production costs significantly, however, at the smaller production levels considered for this program, reduction in the installed capital cost will have the greater effect. The General Electric SPE cell is being developed with the twin objectives of capital cost reduction and maximum cell efficiency (estimated at 93%).

Merchant Supply

As an alternative to the "on-site" sources mentioned above, a hydrogen user can also buy liquid hydrogen which is supplied by industrial gas producers by truck, stored at the customer's location, and vaporized as needed. Liquefying the hydrogen is cost effective for large scale production and the only economical means of distributing large volumes considerable distances. Hydrogen is also supplied in gaseous form to low volume users (<25,000 scf/day) but the distribution economics become prohibitive beyond 125 miles of the source.

Cost Comparison

Comparison of the cost/volume curves for the major sources of hydrogen presented in Figure 4, indicates that SPE electrolyte hydrogen could be competitive as an on-site source for an individual user with requirements of between 220,000 and 500,000 scf per day. In a certain range immediately below the lower limit, liquid hydrogen supply from a vendor would be more economical while on-site steam reformation would be preferred for requirements above the upper limit. The exact point of equivalency between liquid/electrolytic sourcing is dependent upon many factors including electrical power costs for electrolytic production, distribution costs of the liquid hydrogen, and the general competitive environment.

It must be kept in mind that the curves shown reflect the delivered cost of hydrogen for large volume users. The costs of steam reforming and electrolysis assume on-site production and hence very low delivery costs, while the liquid hydrogen cost includes delivery charges.

If an on-site customer could not be found, electrolytic hydrogen would have to be competitive on a delivered cost basis with other sources of gaseous hydrogen which is used by customers too small to warrant liquid supply. The proposed facility will be more proximate to the regional market, with corresponding distribution savings which should offset the product cost advantage currently enjoyed at existing gaseous hydrogen facilities. The latter is produced by vaporizing liquid hydrogen, at regional facilities, and by purifying residual hydrogen product from certain industrial processes.

Figures 5 and 6 introduce graphically the effect of energy costs on steam reforming and electrolytic hydrogen production processes. With respect to steam reforming, the sensitivity of hydrogen cost to the change in natural gas cost shows a large relative effect at high production levels (over one million scf/day) while hydrogen production levels below that level are more sensitive to the capital intensive nature of steam reformers.

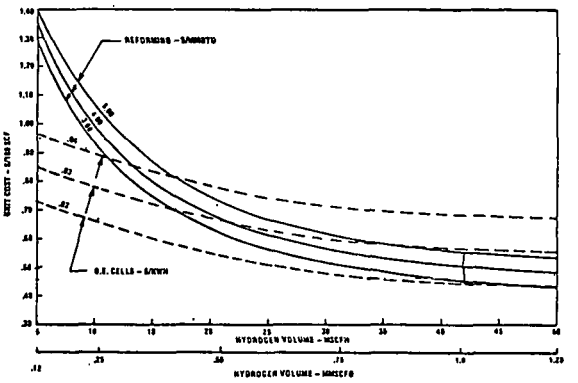

FIGURE 5. Sensitivity of Hydrogen Production Costs to Energy Costs Reforming vs. GE Cells.

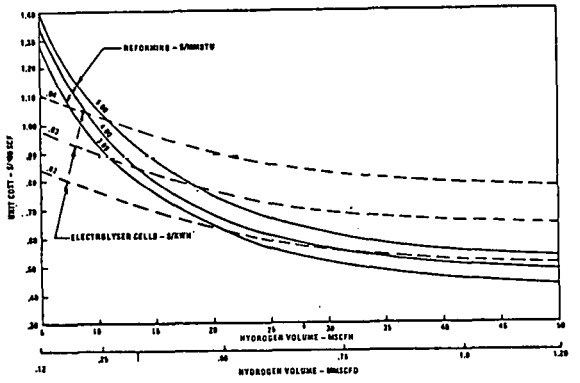

FIGURE 6. Sensitivity of Hydrogen Production Costs to Energy Costs Reforming vs. Electrolyser Cells.

The sensitivity of electrolytic hydrogen production costs to the cost of electrical power for both the G.E. SPE cells and the Electrolyser Corp. cells is also shown. The cost of electrical power is the single most important component on which to focus in reducing the cost of electrolytic hydrogen; hence the interest in low-head hydroelectric power.

Although the determination of the cost of electricity from small dams and the cost of hydrogen generated from this power source must await the conclusion of the program, the competitiveness of the proposed facility will surely improve with time, because the cost of low-head power is largely escalation proof while the costs of alternative sources, which rely on fossil fuels, is expected to continually rise.

HYDROPOWERED ELECTROLYSIS IN NEW YORK STATE

Parker D. Mathusa and Rudolf A. Wiley, Ph.D.
New York State Energy Research and Development Authority
Albany, New York

Abstract

An inventory of New York State's hydropower potential conducted by the New York State Energy Research and Development Authority has located more than 1,000 sites with dams in the state which could be refurbished to produce power. It is estimated that these facilities can be made to generate 3.8-billion kilowatt hours of (firm) electrical power per annum. The present low rates which the utilities are willing to pay for excess dumped energy have motivated hydropower developers to find more lucrative means of utilizing excess power. Specifically, the Village of Potsdam has found that the use of excess power to operate an advanced technology solid polymer electrolyzer can produce research grade hydrogen whose kilowatt-hour equivalent value is more than 10 times greater than that of dumped electrical energy. To achieve this goal, the Village's hydropower facility will be equipped with two, 350-kilowatt tube turbines and a 200-kilowatt electrolyzer. The latter will produce approximately 18-million standard cubic feet of hydrogen annually which will be sold for $.50 per hundred cubic feet.

I. Introduction

A considerable amount of the state's hydro potential remains unutilized for power production. An inventory of the state's hydro potential conducted by the New York State Energy Research and Development Authority has located approximately 1,700 sites in the state which could generate power. Seven hundered fifty-four (754) of these sites have been categorized by size and presence or absence of dams as shown in the table below:

Tabulation of Undeveloped Capacity 50 Kw Minimum

Capacity Range Mw	Undeveloped Capacity in Kw			
	# of Sites	With Dams	# of Sites	Without Dams
100-50	4	284,000	4	343,000
50-30	2	78,000	6	203,000
30-15	17	324,000	18	381,000
15-10	14	168,000	15	176,000
10-5	38	270,000	26	190,000
5-1	114	286,000	77	178,000
1-.5	44	37,000	38	26,000
.5-.25	80	38,000	40	14,000
.25-.10	101	16,000	37	6,000
.10-.05	54	6,000	25	2,000
Total	468	1,507,000	286	1,519,000

Analysis of the hydropower statistics for New York State indicates that while 3,000 megawatts of hydropower potential may be harnessed, only about one-third of this power is estimated to be economically attractive at this time.

Some of the hydropower sites that could undergo feasibility examination for expansion of hydroelectric production are now operated by industries that can create more jobs if increased power at a reasonably stable cost is made available.

II. Alternative Hydropower Concepts

The alternate use of hydropower is one of several strategies being studied by the Authority in its efforts to broaden its hydropower program and accelerate the redevelopment of other facilities.

The development of the hydropower site at the Village of Potsdam is one of several examples. In this instance, the power at the site will be used to operate an electrolyzer, which will create hydrogen and oxygen from water via dissociation. In this respect, the water will serve a dual purpose, namely that of the driving force used to power the electrolyzer, and the fuel which will be used to generate hydrogen gas. Hydrogen is conventionally produced from fossil fuels.

The Village of Potsdam's power house was built in 1926 as an addition to the existing Village water treatment plant. It contained two flumes, each designed for 9.5-feet of head and 268-cubic feet per second of flow. A 42-inch, 238-HP, Type B James Leffel and Company turbine was installed in one of the flumes and the other left for future turbine installation. A second turbine was never installed, however, and the plant operated until 1971 with only one machine which at that time, was decommissioned.

The Village expressed an interest in redeveloping the old site in 1978 thus initiating a feasibility study to assess what opportunities existed at the site. The Village of Potsdam suggested in the first instance that four of its existing facilities: the water treatment plant; the police station; the sewage treatment plant; and the ice skating arena would be candidate recipients of the electrical energy generated by the hydroelectric facility. During 1976-77, the average annual electrical energy consumption for these four facilities totalled 2,000,000 kilowatt hours, with a peak demand of 550 kilowatts. With a proposed expansion of the existing water treatment plant, and the conversions of the heating system in the police station to electrical resistance heating, it was anticipated that the maximum demand would rise to 690 KWs and that the annual energy consumption would consequently rise to 2,250,000 Kw hours.

Because of the time variations in supply and demand it became clear that a significant amount of excess electrical energy produced by the facility would have to be dumped into the utility's grid. The five-mil per kwh rate which the utility (in this case the Niagara Mohawk Power Corporation) would pay for dumped energy motivated the Village to

explore other and more lucrative means of utilizing this excess power. Solid polymer electrolysis, a high-efficiency electrolytic process being developed by the General Electric Company proved to be an economically viable option tailored to meet the Village's needs. At an 85 percent conversion efficiency it may be shown that one kwh of electrical energy may be used to produce 8.8 scf of research grade hydrogen whose present market value ranges from $.75 to $1.25 per hcf. This price represents an equivalent value ranging from 132 to 220 mils per kwh (electrical).* On this basis, the Village decided to couple the hydroelectric facility to a 200-kw electrolysis module and convert excess electrical energy to hydrogen (and oxygen) gas.

Excess power produced over that needed to operate the four village facilities and the hydrogen production system will be sold to the Niagara Mohawk Power Corporation as dump power of the plant's 700-KW total; approximately 500 KW and 200 KW will be dedicated to electrical and hydrogen production, respectively. For the case of hydrogen production, the power needed to run the electrolyzer will be deducted from the excess available and the rest sold as dump power. Two of the five facilities are not located in the immediate vicinity of the power plant, and must have power transmitted (or "wheeled") to these facilities over Niagara Mohawk power lines.

III. Project Development

The total construction cost for the 700-KW plant with the hydrogen production system is approximately $2,480,000, of which $299,000 and $1,900,000 include the cost of the hydrogen production system and the redevelopment cost of the hydroelectric plant, respectively. The balance will be used to rehabilitate the dam. The reactiviation of the hydroelectric plant will cost $2,714/KW. Over the useful life of the facility, total costs amount to slightly less than $12,000,000 while benefits amount to just over $31,000,000, resulting in a net benefit of approximately $19,000,000. Nearly all the benefits are a result of displacing power that would have to be purchased from Niagara Mohawk for the four village facilities. A present worth analysis is performed by using a rate of return of eight percent. The present worth of the costs is computed to be slightly greater than $3,400,000, while the present worth of the benefits is nearly $5,700,000, indicating a rate of return exceeding eight percent. The project's total cost is $2,929,100.

Construction costs include rehabilitation of the dam, modifications to the powerhouse, purchase and installation of turbine/generator units, and engineering. The costs of dam rehabilitation and the building renovation are estimated on the basis of similar projects, while turbine/generator costs are obtained from equipment manufacturers. Engineering costs are derived by taking a percentage of the total construction cost. Construction costs include the electrolyzer and gas storage facilities as well. These costs were obtained from data supplied by General Electric (the electrolyzer manufacturer). It is further assumed that the village will pay for the construction through a bond issue to be repaid over a 25-year period at six percent interest.

Operation and maintenance costs for the hydroelectric plant are assumed to require one man-year annually. An operator's wage is estimated and multiplied by a factor to account for parts and contractual repair work. Operating costs for the electrolyzer are taken as the loss in revenues for the dump power used by the unit. Maintenance costs are derived from data supplied by the manufacturer.

IV. Project Economics

A 40-year period is used for the analysis of the proposed project as this is the expected useful life for similar facilities. The Potsdam plant is expected to begin operation in 1981. The prices for purchased power and "wheeling" and dump power are, therefore, adjusted to reflect expected costs at that time. Construction costs include a contingency factor for the same purpose.

A decreasing factor of inflation is used to account for future price changes except for the sales of hydrogen gas which have a constant inflation factor over the entire period. Also, the revenues for dump power sales are held constant over five-year periods in accordance with Niagara Mohawk's policy of negotiating five-year contracts for dump-power purchases.

V. Assumptions

1. The hydropower plant has a capacity of 700 kilowatts and an average annual output of 5,600,000 kilowatt-hours. 2,250,000 kilowatt-hours will be used by the Village at its various buildings; 2,016,000 kilowatt-hours will be used by the electrolyzer; and 1,334,000 kilowatt-hours will be sold as dump power. 1,550,000 kilowatt-hours used by the Village has to be transmitted, or "wheeled" from the plant to other locations by way of lines owned by the area electric utility company.

2. The Village will bond $938,600 at six percent interest for 25 years.

3. Hydrogen gas production will average 180,000 HCF per year. The gas will sell for $0.50/HCF and will increase four percent per year.

4. Operation and Maintenance for the power plant will start at $12,000 per year. Operation and Maintenance for the electrolyzer (which will include an annual cost for the cell replacement costs, cost of annual maintenance for the cells, and costs of power to run the plant at dump power rates) starts at $21,000.

*The Village did not choose to exclusively produce hydrogen because such a project would have proven to be extremely capital intensive. The prototype price of the electrolyzer is estimated at several thousand dollars per installed kw.

5. Operation and Maintenance costs, "wheeling" costs, and the cost of the displaced power increase annually at the following rates:

1981 to 1985	12 percent
1986 to 1990	10 percent
1991 to 1995	8 percent
1996 to 2000	6 percent
2001 to 2020	4 percent

6. Dump power rates are re-negotiated every five years and are assumed to increase as if they had increased annually according to No. 5 given above.

7. Costs in 1981 dollars are:

Operation and Maintenance	$ 33,000
Purchased Power	$100,125
Dump Power Sales	$ 7,951
"Wheeling"	$ 2,325
Hydrogen Gas Sales	$ 90,000

VI. Summary of Benefit - Cost Analysis

TOTAL COSTS

Debt Service	$ 4,550,600
Operation and Maintenance	$ 6,914,891
"Wheeling"	487,129
TOTAL	$11,952,620

TOTAL BENEFITS

Hydrogen Gas Sales	$ 8,552,292
Dump Power Sales	$ 1,608,175
Value of Power Used if Purchased	$20,980,500
TOTAL	$31,140,967

POTENTIAL SAVINGS

Total Benefits	$31,140,967
Total Costs.	11,952,620
TOTAL	$19,188,347

VII. Summary of Present Worth Analysis

BENEFITS

Hydrogen Gas Sales	$ 1,752,758
Dump Power Sales	$ 250,382
Value of Power Used if Purchased	$ 3,684,008
TOTAL	$ 5,687,148

COSTS

Debt Service	$ 2,106,875
Operation and Maintenance	1,214,197
"Wheeling"	85,540
TOTAL	$ 3,406,612

VIII. SUMMARY

It is expected that the 18-million standard cubic feet of hydrogen that will be produced at the site annually will sell at prices under current market quotations. Furthermore, the oxygen will produce ozone which will be used to purify the local water supply at the Village of Potsdam's water treatment plant adjacent to the hydropower facility

Rehabilitation of the site will produce both hydrogen and an increased amount of electricity for local use. Current production of about 150 kilowatts will increase to more than 700 kilowatts.

Of the new total, about 500 kilowatts will be used by the town of Potsdam and about 200 kilowatts will be used for the hydrogen production process.

The oxygen gas will be used in the purification process at the adjacent water treatment plant. The village expects to manufacture ozone, which will be used in water treatment, more economically from oxygen that it currently does from air.

Results of the Potsdam experiment are expected to be equally applicable at some 50 other sites in the state. The installation of similar equipment at the other sites would dedicate a total of 47 additional firm megawatts of electrical power at a 90 percent capacity factor. This power potential is equivalent to a state-wide hydrogen production of 3.2 billion cubic feet of hydrogen per annum. This in turn translates into a 30 million dollar per year business for New York State.

This demonstration, in addition to producing hydrogen, is also part of the overall plan to increase production of hydroelectric power across the state as outlined above.

CHEMICAL HEAT PUMP/CHEMICAL ENERGY STORAGE SYSTEMS†

Thomas E. Botts

Department of Nuclear Energy
Brookhaven National Laboratory
Upton, N. Y. 11973

Abstract

Chemical Heat Pump/Chemical Energy Storage (CHP/CES) systems offer the potential for very high density energy storage with negligible losses, heating coefficients of performances (COP's) greater than one, and both space heating and cooling. Using solar collector panels as the source of thermal energy the opportunity exists to increase the solar fraction for a given collector array area with CHP/CES. In implementing CHP/CES a range of configurations of the system appear to be possible and attractive. A more fruitful program may follow if some consideration is given to the way such a system is to be laid out (e.g. does one drive the heat pump electricically when auxiliary power is required?) in its commercial form. Institutional concerns become prominent at this time. Cost-benefit analysis and an improved definition of loads can lead to a better understanding of market needs. Such an understanding can enhance the desirability of CHP/CES.

Introduction

Chemical Heat Pump/Chemical Energy Storage (CHP/CES) systems are being developed as a possible means to improve solar collector efficiency and provide high density energy storage. As a heat pump these systems operate using a thermodynamic cycle similar to that of an absorbtion chiller. Thermal energy from a solar collector panel or other source drives a dissociation reaction in which one of the products remains in a condensed state while the other product is transported by a difference in vapor pressure to another container where it condenses. The two products are then recombined by altering the temperature of the two species in order that the relative difference in the vapor pressure of the mobile species will now drive the chemical reaction in the opposite direction. Excellent descriptions of such cycles are provided in the literature.[1-3] Of prime import to a CHP/CES system is the reversibility of the chemical reaction. Extensive investigations have been carried out which have identified a wide range of such chemical systems.[1-3] At the present time systems based upon metal hydrides, ammoniated salts, methanolated salts, hydrated salts, sulfuric acid-water, and some liquid or slurry systems are being investigated presently.

Space heating is accompiished via recombination of the two product species, excess heat from the heat source, and the heat of condensation of the vapor phase. Such a system can operate with a heating COP > 1 as the heat of vaporization is supplied via air at ambient temperature. Vapor transport is again driven by differing vapor pressures. The capacity to operate with a heating COP between 1.2 and 1.7 has been demonstrated in single stage experimental units.[1,2] If an application requiring a greater COP is identified multistaging of CHP's is considered to be quite feasible. Cooling, with a COP<1 is accomplished by extracting thermal energy to drive the evaporator.

The third function of a CHP/CES system is energy storage. Very high energy densities, characteristically 300-1100 MJ/m^3, are also a feature of these systems. Due to the nature of chemical energy storage there is no loss of stored energy content with time, as occurs with phase change and sensible heat systems. However, to provide both heat pumping and energy storage in one cycle the chemical costs must be low enough to provide energy storage at a cost competitive with other forms of storage. In doing such a comparison, however, one should be mindful to include the added benefit with CES of extended storage periods.

Cycle time, the characteristic time required for a charge/discharge of the system, is another differentiating characteristic. Rapid cycle times are favored when the chemical costs dominate for a longer cycle time. Longer cycle times are favored when sensible heat removal is sluggish, large amounts of thermal storage are deemed attractive, or slow reaction rates limit cycle time. By rapid cycle time a range of minutes to tens of minutes is envisaged while longer cycle times are characteristically diurnal. As various CHP/CES units approach the level of engineering test unit the economies governing cycle time will be more clearly understood. Future conclusions may be that diurnal cycles are most suited to solar space heating while more rapid cycle times may be more appropriate for industrial waste heat management. At the present it appears as if sensible heat removal considerations tend to favor longer cycle times for solid based systems (e.g. $CaCl_2$-CH_3OH, $CaCl_2$-NH_3, $MgCl_2$-H_2O). Liquid and liquid-like systems (e.g. H_2SO_4-H_2O) appear to be capable of of operation over a wide range of cycle times. Metal-hydride systems appear to require short cycle times in order to limit inventories of relatively expensive hydridable metals.

When solar collector panels are used to provide thermal energy to a CHP/CES system the interplay between collector cost and

†This work was performed under the auspices of the U. S. Department of Energy

and efficiency as a function of temperature and CHP/CES cost and efficiency as a function of temperature must be considered. One of the prime motivations for CHP/CES in solar space heating applications is to reduce the cost of the collector array. Higher generator temperatures may increase COP while necessitating more advanced collectors (vacuum tube or concentrating collectors). Furthermore, higher collector exit temperatures imply lower collector efficiencies. This effect must be borne in mind when designing an entire system.

CHP/CES appears to at the present time have a lower ambient temperature operating limit of -10 to -20°C. This is a practical limit for space heating based upon COP considerations. Upper temperature limits exits for cooling as well. When this temperature range isexceeded in either direction auxiliary power is needed. Auxiliary power demands can easily dominate the system requirement for energy from nonrenewable sources due to the small electrical power demands of CHP/CES. Indeed, excessive parasitic power requirements can greatly reduce its appeal. Therefore, thorough consideration will be given to choosing chemical reactions well suited to their anticipated operating temperature range. Secondary reactions, which may occur very slowly, can lead to the production of corrosive and noncondensible species. Such considerations must be addressed as well as they influence the long term performance. It may well be that no one chemical system is optimal for all ranges of input and output temperatures which will be encountered.

One further consideration is that of vapor transport. A range of pressures will occur dependant upon ambient, load, and heat source temperatures as well as the degree of charge of the system, in some cases. A broader range of pressures ($\sim 10^{-4}$--1.0 MPa) exists over the range of chemical systems presently under investigation. As the pressure of the transported vapor is lowered noncondensible foreign material becomes a more serious impediment to mass transfer. Noncondensibles may be limited either with a very clean, vacuum-tight system, or some active means of vapor purification. Furthermore, very low or high operating pressures may influence overall cost due to the need for larger i.d. or thicker walled piping, respectively.

CHP/CES System Considerations

One very basic issue which must be faced squarely when CHP/CES cost-benefits are addressed. This question is: Conservation at what price? For the case of a solar driven space heating application the solar fraction offers a very good representation of the fractional energy savings of such a system, neglecting energy investments in production, installation, and maintainance. This is due to the small electrical energy requirements of CHP/CES. However, experience and computer simulations tend to show that as the solar fraction approaches 1.0 energy storage becomes quite large to account for periods of unusually length of hot or cold weather.[2,5] Lifetime costs of an entire unit provides a means of comparing systems based on differing chemical reactions and different amounts of thermal storage capacity. Maintainance costs, as well as parasitic and auxiliary power costs, including an appropriate energy cost escallation factor, must be discounted back to the time of installation and included along with first costs.

By deriving costs for various CHP/CES sysyems installed in various parts of the country it would appear as if a decision can be made regarding which systems to persue for differing climatologies. An effort to derive some of these costs for various parts of the country has already been undertaken.[1,2,3,6,7] Another way to address this issue is to model CHP/CES performance using a computer simulation code (e.g. TRNSYS[4]) in order to set bounds upon as many parameters as possible which could be used to define a cost effective unit for different locales. For either method costs in dollars and benefits in dollars or megajoules converted to dollars of nonrenewable energy resources not consumed would then be calculable.

Further refinements to such an analysis would be to attempt to account for CHP/CES and collector performance losses with time, estimate repair costs, and a more realistic model for space heating loads than is presently being utilized. Building heating and cooling loads vary both with site and age. If the retrofit market is to be addressed building age may well need to be considered.

One possible method for taking both locale and building age into account is to extract data for space heating and cooling from the Regional Reference Energy Systems[8]. Age can be obtained by comparing demand for cities with varying rates of new building. One important conclusion to be drawn may be to define markets where CHP/CES could real benefits with the shortest possible lead time, and therefore provide more impetus for commercialization. Another benefit to be accrued would be to gain a more complete understanding of the range of operational modes open to CHP/CES. One mode could be to provide some space heating, cooling, or charging of the thermal storage unit with off-peak electric. Careful analysis could provide a decision making scheme for controlling the use of off-peak electric, or other sources. One future source could be waste heat driven district heating.

Conclusions

Scientific evaluation and engineering test units are now being operated to gain engineering experience and to gather data on the long term behaviour of some of the reversible chemical reactions which are

the basis of CHP/CES. In order to make the rather large step to engineering test units and prototypes analysis and design must be carried forth together in a thoughtfulmanner. Realizing the greatest benefits of CHP/CES is essential to assure its acceptance on engineering, economic, and institutional grounds. Further benefits may be realized through a well thought out initial point of market penetration.

References

1. Offenhartz,P. O'D., "Methanol-Based Heat Pumps for Storage of Thermal Energy", SAND 79-8188, 1/79.
2. Clark, E. C., et. al.,"Final Report-Phase II-a Sulfuric Acid and Water Chemical Heat Pump/Chemical Energy Storage Program", to be released.
3. Sheft, I., Gruen, D., and Lamich, G., "HYCSOS: A Chemical Heat Pump and Energy Conversion System Based on Metal Hydrides", ANL-79-8, 4/79.
4. Klein, S. A., "TRNSYS: A Transient Simulation Program", Solar Energy Laboratory, University of Wisconsin-Madison, Engineering Experiment Station Report 38-10, 6/79.
5. Thomas, W. R. L. and Navon, U., "A Computer Simulation of a Solar-Driven Chemical Heat Pump System", EXXON/GRU.1BED.78, 12/78.
6. Leonard Greiner, Chemical Energy Specialists, private communication.
7. "Economic Assessment of Thermal Energy Storage Technologies", draft final report to Argonne National Laboratory, Arthur D. Little, Inc., 4/78.
8. Hermelee, A. L., "Regional Reference Energy Systems", EPRI-EA-462, 6/77.

A CHEMICAL HEAT PUMP BASED ON THE REACTION OF CALCIUM CHLORIDE AND METHANOL FOR SOLAR HEATING, COOLING AND STORAGE

P. O'D. Offenhartz, D. Schwartz and R. E. Malsberger

EIC Corporation
55 Chapel Street
Newton, Massachusetts 02158

Abstract

A thermally activated heat pump system based on the reaction of $CaCl_2$ and CH_3OH to form solid-phase $CaCl_2 \cdot 2CH_3OH$ has been developed. Preliminary experiments have been carried out on a bench-scale unit with approximately 1000 BTU storage capacity. This unit incorporates a novel "finned-tube-in-container" heat exchanger, which can provide low-cost salt containment, tight hermetic sealing, good mass transport of vapor to the salt, and complete isolation of the vapor and salt from the heat transfer fluid. The experiments show that an absorption rate around 10% of capacity per hour can be maintained while pumping heat up a 45°C gradient, e.g., from an evaporator at -5°C to salt bed heat transfer fluid at 40°C. Anhydrous salt can be regenerated in less than 6 hours with solar collector temperatures below 140°C (CH_3OH condenser at 40°C). Projected coefficients of performance are 1.6 for heating and 0.6 for cooling, and the energy storage density is ca. 4×10^5 kJ m^{-3}. Based on these results, an engineering development test unit with 100,000 BTU storage capacity -- approximately 25% of the design capacity of a residential scale unit -- has been designed and constructed. Current plans call for this unit to be evaluated over the course of the next year. Tests will include standard and off-design cycling in both heating and air-conditioning modes, simulated process upsets, long-term cycling, and experimental validation of the coefficients of performance.

Background

The basis for a chemical heat pump thermal storage system is a reaction that proceeds in one direction at high temperature and in the opposite direction at low temperature. A gas-solid reaction is particularly suitable because it provides constant vapor pressure at a given temperature, and can hence give constant heat pumping performance over the full extent of chemical reaction. Furthermore, separation of the reactants upon heating is inherent. Methanol is especially suitable as the vaporizable liquid due to its low freezing point, high entropy of vaporization, high vapor pressure (compared to water), and relative freedom from hazards. Calcium chloride was selected as the vapor-absorbing solid after an extensive experimental investigation of salt candidates[1]. The reaction scheme is

$$CaCl_2 \cdot 2CH_3OH(solid) \xrightarrow{T_2} CaCl_2(solid) + 2CH_3OH(vapor)$$

$$CH_3OH(vapor) \xrightarrow{T_1} CH_3OH(liquid)$$

In the storage mode, T_2 is the solar collector temperature (120-140°C) and T_1 is a temperature suitable for heat exchange to the space to be heated or for heat rejection to outdoor ambient air during the cooling season (45°C). In the heat pump mode, the reactions proceed in reverse, and T_2 is about 40-45°C while T_1 is in the range -5 to +5°C. Thus, the reaction can be used for both heating and air conditioning as well as for thermal storage.

Measurements of the heat of reaction of CH_3OH vapor with $CaCl_2$ have been carried out at Sandia Livermore[2]. Experimental results for the dependence of vapor pressure on temperature and composition are shown in Figure 1. The reaction proceeds in a single step to form $CaCl_2 \cdot 2CH_3OH$, and the

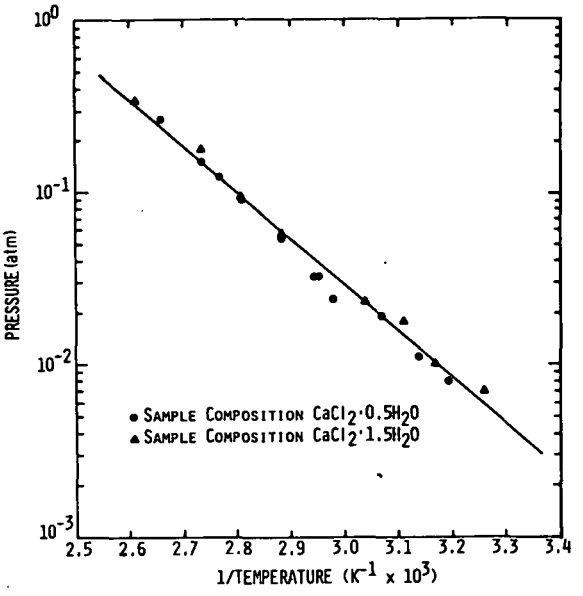

Fig. 1. Dependence of vapor pressure of the $CaCl_2$-CH_3OH system on temperature and composition.

second law enthalpy and entropy are 51.7 kJ (mole $CH_3OH)^{-1}$ and 126 J deg^{-1}(mole $CH_3OH)^{-1}$, respectively. Taking into account the enthalpy and entropy of vaporization and the heat capacities of all chemicals and container materials, the projected coefficients of performance are 1.6 for heating, and 0.6 for cooling.

Small-scale cycling and corrosion tests have indicated the complete absence of side reactions. No corrosion of Al or Cu has been observed. During the initial reaction of $CaCl_2$ with CH_3OH, the salt

expands to accommodate the vapor. When this expansion is carried out in a confined space, the salt forms a porous cake, which does not substantially expand or contract on subsequent cycling. The cake has sufficient porosity to allow vapor flow in and out without a serious pressure drop.

Experiments on the Bench-Scale Prototype

The bench-scale prototype previously described[1] was used to evaluate the effectiveness of our "finned-tube-in-container" heat exchanger. In the present design of the salt bed, the prime surface (copper tubing) is 7.0 cm^2 per unit bed length, while the area of the aluminum fins is 67.6 cm^2 (for 0.5 cm fin spacing). The overall heat transfer coefficient (for typical rates of fluid flow within the tube) is about 40 $J\text{-}sec^{-1}m^{-2}K^{-1}$ (7 BTU $hr^{-1}ft^{-2}{}^{\circ}F^{-1}$). The temperature drop between the warmest part of the salt bed (halfway between the fins) and the heat transfer fluid during methanolation (formation of $CaCl_2 \cdot 2CH_3OH$) is about 3°C.

The results of a typical methanolation experiment are shown in Figure 2. The near-constancy of the reaction rate may at first seem surprising, since the reaction interface moves away from the heat transfer fins as the reaction proceeds. However, as we have noted earlier[1], methanolation of $CaCl_2$ increases the conductivity of the salt bed, and this largely compensates for the increase in heat transfer distance.

The results in Figure 2 indicate that a heat pumping temperature gradient of 42-48°C can be maintained at a reaction rate around 10% of capacity per hour, i.e., at 0.2 moles CH_3OH per mole $CaCl_2$ per hour. Thus, to provide a given heat rate (say 50,000 BTU/hr) over an 8 hour period, the storage capacity must be 8 times the heat rate (i.e., 400,000 BTU). The heat absorbed in vaporizing CH_3OH is roughly 0.7 times the heat of reaction, so the same storage capacity could provide 35,000 BTU/hr (3 tons) of cooling over an 8 hour period.

Typical demethanolation results are shown in Figure 3. From thermodynamic considerations alone, it can be shown that the solar collector fluid temperature must be at least 70°C above the condenser temperature for demethanolation to occur. In practice, with the condenser at 40°C, rapid

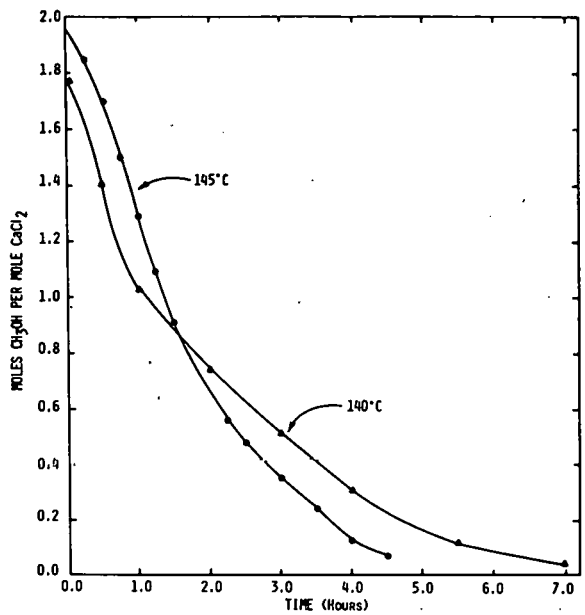

Fig. 3. Demethanolation of $CaCl_2 \cdot 2CH_3OH$ in the small-scale prototype with condenser at 40°C and salt-bed heat transfer fluid at 140-145°C.

demethanolation begins when the heat transfer fluid in the bed reaches 120°C, only 10°C above the minimum (equilibrium) value. However, because the thermal conductivity of the bed decreases rapidly upon demethanolation, the rate of reaction diminishes rather quickly when the heat transfer fluid is maintained at 120°C. To achieve complete de-

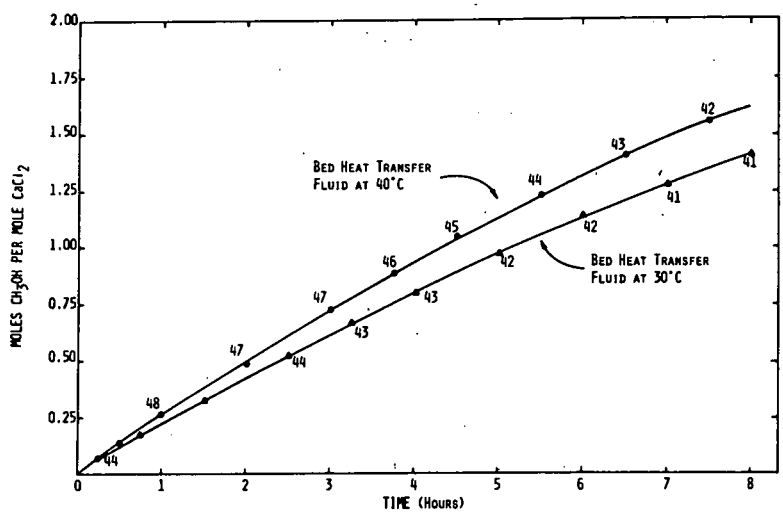

Fig. 2. Moles of CH_3OH absorbed vs. time for the small-scale prototype. Numbers show temperature difference between salt-bed heat transfer fluid and CH_3OH evaporator.

methanolation, the temperature must be gradually increased to 140°C, as shown in Figure 3. Thus, the required solar collector temperature is in the range 120-140°C, which is well within the capability of evacuated tube collectors.

Engineering Development Test Unit

A larger scale test unit, with 100,000 BTU of storage capacity, has been designed and constructed. This scale is large enough for a detailed energy balance to be carried out experimentally, and the size of the individual salt beds is comparable to that planned for use in a residential unit. During the coming year, this prototype unit will be evaluated in detail, with a focus on long-term cycling performance, salt-bed stability, behavior under normal and process upset conditions, and characterization of heat exchanger performance. While the prototype is not suitable for field use -- it lacks required fluid-to-air heat exchangers, and contains only a single bed, so that simultaneous solar collection and heat pumping cannot be carried out -- it should provide most of the information needed for confident scaling up to a system suitable for field testing.

At the time of writing this report, preliminary evaluation of the engineering development prototype was just beginning. Available data will hence be presented orally.

Acknowledgements

This work has been supported by the Energy Storage Division of the U.S. Department of Energy, and has been technically monitored by Sandia Laboratories, Livermore, California. After August 1, 1979, responsibility for technical monitoring has been transferred to Brookhaven National Laboratory.

References

1. P. O'D. Offenhartz, "Methanol-Based Heat Pumps for Storage of Solar Thermal Energy," Third Annual Proc. of Thermal Energy Storage Contractors' Information Exchange Meeting (CONF-781231), Springfield, VA, December 5-6, 1978, p. 425.

2. P. O'D. Offenhartz, F. C. Brown, R. W. Mar, and R. W. Carling, "A Heat Pump and Thermal Storage System for Solar Heating and Cooling Based on the Reaction of Calcium Chloride and Methanol," Sandia Laboratory Report SAND79-8512, August, 1979. (Submitted to J. Solar Engineering.)

SULFURIC ACID AND WATER CHEMICAL HEAT PUMP/CHEMICAL ENERGY STORAGE SYSTEM

E. Charles Clark
Project Manager
Rocket Research Company
Redmond, Washington

Olwen M. Morgan
Development Engineer
Rocket Research Company
Redmond, Washington

ABSTRACT

A chemical heat pump/chemical energy storage system (CHP/CES) has been designed, fabricated, and successfully tested under U.S. Department of Energy (DOE)/Sandia Corp. funding. This first operational chemical heat pump is a key milestone in DOE's long-term thermal energy storage goals.

The sulfuric acid/water chemical heat pump is suitable for both heating and cooling with an inherent energy storage density in excess of 600 Btu/lb of diluted H_2SO_4. During Phase II, an engineering model was constructed which demonstrated an energy storage density of up to 569 Btu/lb.

During Phase II-A, now complete, the engineering model was used to test high temperature closed loop cycling, reduction of evaporator/condenser coils, absorption column size, and elimination of one acid tank. Preliminary investigations of commercial-type plumbing were made. Future problems for commercialization were investigated and a survey made of applicable building codes to determine any additional system requirements which would be imposed by these regulations. A preliminary economic study based on weather tapes from Albequerque, New Mexico determined that a CHP/CES system using solar energy input could provide heating and cooling at equivalent energy rates of $0.040/kw-hr including the cost of solar collectors.

Phase III, funded by Brookhaven National Laboratories, is now under way. A commercial-type verification test unit (VTU) is to be designed, built and tested.

This paper covers the work conducted to date since the previous contractors meeting in December 1978,[1] plus anticipated activities for the future.

INTRODUCTION

Phase I of the H_2SO_4 program was a 9-month conceptual design and laboratory demonstration of the primary components.[2] Feasibility of the thermal storage concept and separation and direct liquid recombination of the chemicals were demonstrated. During the Phase II program the chemical heat pump concept was identified, and an engineering model was designed, constructed and demonstrated.[3]

The Phase II-A program extended the system analysis to study economics and an asessment was made of the institutional barriers to commercialization of the solar/CHP/CES.[4] Also completed during Phase II-A was component optimization testing with the Phase II engineering system.

The simplest form of sulfuric acid/water chemical heat pump consists of an evacuated acid tank and a water tank in vapor communication. The system is charged (acid concentration) by distilling the dilute acid under constant pressure. Water vapor released from the acid is condensed in the water tank. The condensing temperature controls the system pressure and the heat of condensation is either used directly for heating or rejected. Heat pumping occurs in the discharge (acid dilution) mode. Cooling the concentrated acid lowers its vapor pressure and forces water vapor to flow from the water tank. The water is kept from freezing by abstracting low temperature energy from the surroundings. Discharging the system reclaims both the heat of vaporization of water plus the heat of dilution of the acid.

Expanding the basic concept described above into a system capable of providing both heating and cooling requires additional components. Figure 1 presents a simplified schematic of such a CHP/CES system and shows all the major components except the heat source. The system is similar to an absorption cycle refrigeration unit with the addition of storage tanks for the acid and water.

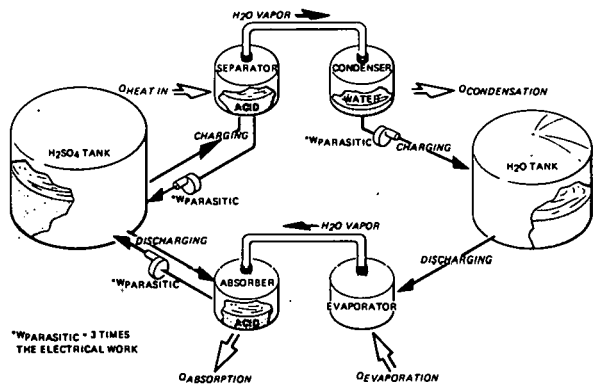

Figure 1. Solar/CHP/CES System Schematic

A further advantage is possible with this system. If the heat removed from the water condenser during the charge cycle is used to meet the heating load, a coefficient of performance (COP) greater than unity is possible. Referencing Figure 1, the definition of COP for the heating mode is:

$$COP = \frac{Q_{absorption} + Q_{condensation}}{Q_{heat\ in} + Q_{parasitic}}$$

The CHP/CES system additionally can provide cooling capability by abstracting heat from the building via the evaporator.

The primary objective of the Phase III program, now starting up, is to design, construct and test a sulfuric acid CHP/CES verification test unit (VTU) which incorporates as many commercial, mass producible design features as possible to demonstrate system economics as well as technical feasibility in several operational modes. Potential applications, and their related economics, other then solar heating and cooling will be reviewed. The VTU will

incorporate low cost chemical storage tanks and be capable of operation in the COP>1 mode described above, as well as providing space cooling with simultaneous charge and discharge capability (absorption cycle refrigeration mode.) The nominal storage design capacity will be about 10^6 Btu with a nominal delivered heat rate of approximately 150,000 Btu/hr.

ENGINEERING MODEL TEST SYSTEM

The principle components of the engineering model test system consist of two glass acid tanks each loaded with 150 lb of 93% H_2SO_4, a 316 stainless steel water tank and two glass shell and tube heat exchangers. All components are supported by a steel tube framework. A control panel is mounted on the structure containing system rotometers and pertinent valve controls. Inputs from twenty-two thermocouples, two flowmeters, and three pressure transducers are recorded on a computerized digital data logger and strip chart recorders. A more complete description of the system and its operation is given in reference 1.

Since its original construction, the engineering model CHP/CES unit has been modified to use commercial grade plumbing, valves and pumps. Figure 2 is a close-up of the system showing the Duriron acid pump and improved teflon-lined steel piping.

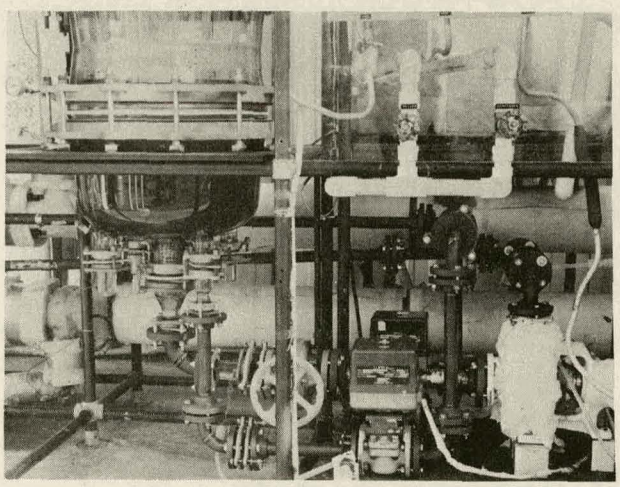

Figure 2. CHP/CES Engineering Model Test System

TEST RESULTS

To date, the engineering model test system has been in operation 475 hours, accumulating 74 closed-loop charge/discharge cycles of which 29 cycles had peak simulated collector temperatures of 400°F and peak acid concentrations of 96 to 98 per cent. An approximate total of 15 million Btu's were charged and discharged.

After 41 cycles, the engineering model was modified to operate with a single acid tank to verify performance with smaller components. Baseline tests at 200 and 400°F maximum system temperatures showed that system performance was not significantly changed. The average charge rate for the single tank system was 32,700 Btu/hr versus 38,000 Btu/hr for the dual tanks and the average discharge rate was 30,100 Btu/hr versus 32,000 Btu/hr. The reduction in transfer rates was caused by higher fluid system pressure drops in the single acid tank version.

The last 17 cycles were operated in a single tank configuration with half the normal Raschig ring absorption column. At the same time, the all-Teflon acid lines were replaced with Teflon-lined steel pipe and improved design vacuum-sealing valves were tested in the acid system (reference Figure 2).

Table 1 summarizes results from dual acid tank testing, single acid tank testing, half column testing and component examination and testing. The engineering system worked well and will be used in Phase III to verify system performance using atmospheric pressure storage tanks and an air-driven low temperature sink.

Table 1. Engineering Model Closed Loop Test Results Summary

Task/Item	Results
• Baseline tests	• Repeatable system charge/discharge performance established at 200° and 400°F maximum temperatures.
• Boiler and condenser optimization tests	• Showed that reduction in boiler or condenser surface areas in water tank reduced stored energy and energy transfer rates as expected. Verified computer model sizing analysis.
• Throttled acid flow test	• Reduced acid flow, increased heat exchanger ΔT, and slightly reduced system energy transfer rates as expected.
• Acid-doped water tests	• No decrease in system performance with up to 5% acid in the water tank. Reduced water freezing point to 29°F.
• New acid tests	• Showed that new H_2SO_4 gave same system performance as old cycled acid.
• Single acid tank baselines	• System performed well with only slight reduction in heat transfer rates.
• Single acid tank, acid carryover tests – full column	• No significant acid carryover up to 400°F system operating temperature.
• Single acid tank with 50% absorption column, acid carryover tests	• Acid carryover starts show 300°F system temperature. However, maximum carryover of 0.04% by weight per cycle will allow 20 years of operation without replacing acid or water.
• Acid pump	• Reliable model manufactured by Duriron Company demonstrated. High silicon cast iron material shown compatible with hot H_2SO_4. Good vacuum sealing. Kal-rez high temperature shaft seal required.
• Acid valves	• Teflon plug style valves (mfg. by Duriron Co.) reliable. Small vacuum leaks.
• Heat exchanger	• All-glass shell and tube, Dow Corning glass (pyrex) exchanger showed no deterioration. No leakage or structural failures.
• Absorption column	• Ceramic Raschig rings worked well. Fifty percent column size reduction possible for discharging without lowering mass transfer rates.
• Glass acid tanks	• Adequate only for pilot model. Girth flange leakage.
• Acid lines	• Teflon-lined steel pipe manufactured by Dow or Resistoflex works well. No leaks.
• Water tank	• 316 CRES works well. Copper coils inside tank for boiler and condenser showed slight discoloration. Galvanic corr/plating will be studied after further testing.
• Kynar-coated steel	• Satisfactory operation at the top of the acid tank (low temperature region).
• Water tank circulation pump	• Improves water tank heat transfer. Magnetic coupling provides good vacuum seal.

ECONOMIC ANALYSIS

A preliminary system economic analysis was conducted to determine the most cost-effective approach for an integrated chemical heat pump and solar collector system. The costs/size of solar systems are greatly affected by the geographical placement and solar insolation, thus a computer model was generated to provide a tool for this and future economic studies. Storage requirements for the CHP/CES system were determined as a function of solar collector field size, assuming that 100% of the building thermal loads were met by the solar/CHP/CES system. An Albequerque, New Mexico, annual weather tape was used for the program input data with heating and

cooling loads analyzed in hourly time increments. Figure 3 presents the results of the sizing analysis for the operational modes where COP = 1 and COP = 1.45 with both heating and cooling provided. The peak in the graph represents the minimum collector field size required to provide 100 percent of the energy demand. Systems with smaller collector fields will require alternate energy systems to meet the annual building loads. As additional solar collectors are supplied (above the minimum), the system energy storage capacity can be reduced while still maintaining a 100 percent solar/CHP/CES. The results in Figure 3 indicate that if the minimum collector field size is doubled, the energy storage required is reduced roughly by a factor of four. The curves beyond the storage size peak represent the optimized storage capacity that can be used to satisfy the 100 percent solar requirement for the Albequerque area.

The benefits of operating in the COP higher than 1 are also apparent in Figure 3. For example, for a given solar collector aperture areas of 0.2, the storage capacity needed for the COP = 1.45 mode is 2.5 times smaller than when operating with a COP = 1.0; conversely, for a given storage size, for example 4,000 Btu/ft^2 of floor area, the solar collector field can be reduced by a factor of 30 percent.

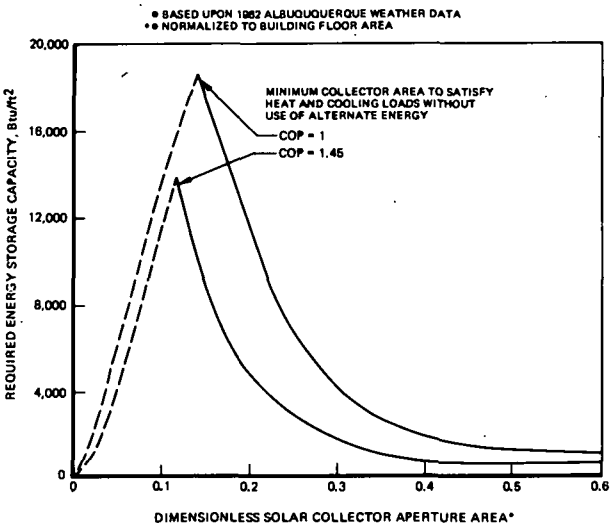

Figure 3. Required Thermal Energy Storage Capacity Versus Solar Collector Aperture Area

The results of the sizing analysis indicate the trade-off between the solar collector costs and CHP/CES system costs which determines the most cost-effective approach. Also when operating with a COP greater than unity, substantial reductions in system size can be achieved.

Comparing the CHP/CES and solar collector costs indicates that the most cost-effective system will require approximately 0.2 square feet of collector area per square foot of building floor area. The minimum normalized capital cost is \$4/ft^2 (referencing floor area). Amortized over a 20-year life cycle, the solar/CHP/CES will provide building heating and cooling at equivalent energy rates of 0.040 \$/Kw-hr when including capital cost, installation, loan interest at 10%, maintenance and operating costs. The minimum cost system has additional reject heat since it operates with oversized solar collectors. If this reject heat is fully utilized (for example hot water heating or industrial process heat), the amortized energy rate is lowered by nearly a factor of 2.

It was concluded that the sulfuric acid solar/CHP/CES has potential for producing economical building space conditioning without fossil fuel-driven backup systems. In the future the economic analysis will be expanded to include two additional geographic areas from DOE's standardized heat pump locations.

ASSESSMENT FOR COMMERCIALIZATION

An investigation into the potential problems for commercialization of the solar/CHP/CES system was conducted. The study comprised three areas: a survey of existing and future applicable codes and regulations, an evaluation of industry acceptance, and a brief examination of public acceptance.

The results indicate that there are no major codes and regulations that apply directly to the solar/CHP/CES. However, building permits and environmental impact statements constitute two important potential institutional constraints. The severity of future codes and regulations adopted to ensure public safety will likely be influenced by public opinion. It is believed that public and industry acceptance will be positive when system economics and safety can be demonstrated.

References

1. Clark, E.C., "Sulfuric Acid and Water Chemical Heat Pump/Thermal Energy Storage," Energy Technology: Third Annual Proceedings of Thermal Energy Storage Contractors' Information Exchange Meeting, December 5-6, 1978, pg. 415.

2. Rocket Research Company, "Phase I Final Report, Sulfuric Acid-Water Chemical Energy Storage System, ERDA Contract No. E(04-3)-1185," Rocket Report No. RRC-76-R-530, August, 1976.

3. Clark, E. C., "Final Report-Phase II Sulfuric Acid-Water Chemical Heat Pump and Storage System, DOE Contract No. EY-76-C-03-1185," Rocket Report No. RRC-78-R-595, December, 1978.

4. Clark, E.C., "Final Report-Phase II-A, Sulfuric Acid and Water Chemical Heat Pump/Chemical Energy Storage Program, Sandia Contract No. 18-4958," Rocket Report No. RRC-79-R-627, September, 1979.

THE METAL HYDRIDE CHEMICAL HEAT PUMP

J.M. Clinch, D.M. Gruen, P.A. Nelson
C.A. Blomquist, J.S. Horowitz, G.J. Lamich, I. Sheft

Argonne National Laboratory
Argonne, Illinois 60439

Abstract

The Argonne National Laboratory (ANL) HYCSOS Metal Hydride Chemical Heat Pump Program activities for FY 1979 are described in this paper. HYCSOS is a chemical heat pump which utilizes the heat of adsorption/desorption of hydrogen in a metal alloy for the storage and recovery of thermal energy for heating and cooling. The acronym HYCSOS refers to a hydride conversion and storage system. The HYCSOS heat pump is attractive because its design can be tailored to provide heating and/or cooling over a wide range of temperatures. The HYCSOS system can be used with a variety of heat sources such as industrial waste heat, solar energy, or even a fossil fuel. The HYCSOS heat pump system can be designed for both residential and industrial users and also for a community energy systems.

With regard to accomplishments, the proof of the HYCSOS concept has been demonstrated and the viability of a residential-size unit established. In addition, an engineering development phase is now underway. The objective of the program is to develop a residential-size HYCSOS chemical heat pump for space heating and cooling. Solar energy or waste heat can be used to operate the pump and thus eliminate or reduce fossil fuel requirements. To meet this objective ANL has performed experimental and analytical studies of the HYCSOS system. The results of these studies are discussed in the body of the paper.

Also to be discussed is the proposed program plan for FY 80 and beyond.

INTRODUCTION

Metal Hydrides

About a decade ago, it was discovered that intermetallics of the form AB_5 (A is a lanthanide and B is a transition metal) possessed the ability to easily absorb and reversibly desorb large amounts of hydrogen. At constant temperature, the hydriding process consists of two distinct phases, α and β, with a mixed phase between them. The α phase corresponds to low hydrogen/metal (H/M) ratios and, in this region, increasing amounts of hydrogen are dissolved in the metal alloy with an increase in pressure. The β phase occurs at high H/M ratios where the metal alloy becomes saturated with hydrogen. Between these distinct phases, there is a pressure plateau where the pressure is relatively constant. In addition the H/M range of the plateau region is shortened somewhat with increasing temperature. The absorption and desorption curves for metal alloy hydrides may not be identical but exhibit a hysteresis as shown for $LaNi_5$ in Fig. 1. Although attributed to internal stresses on hydride formation, hysteresis effects are poorly understood, can vary with preparation conditions, and are generally undesirable.

By varying the materials A and B and the ratio B/A, pressure-temperature relationships over wide ranges are obtainable. Ternary alloys of $LaNi_{5-x}Al_x$ ($0 < x < 1.5$), recently developed by ANL, are

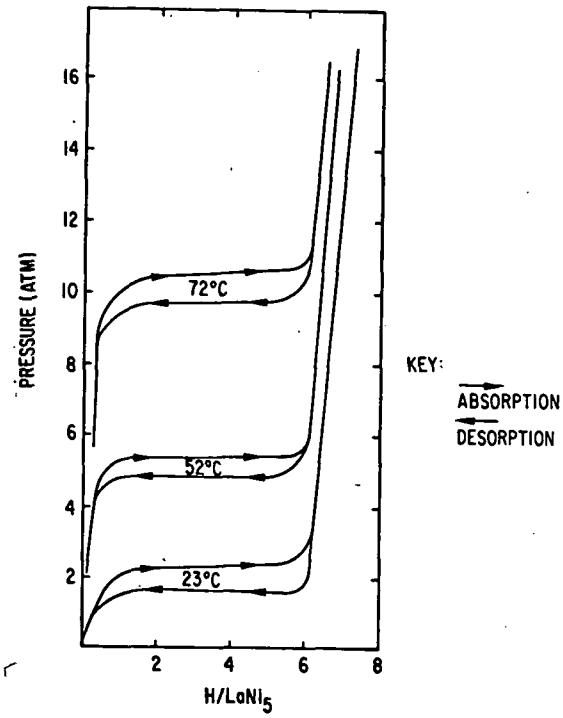

Fig. 1 Absorption-Desorption Diagram for $LaNi_5 + H_2$

effective in lowering hydrogen decomposition pressures by about three orders of magnitude in going from $LaNi_5$ to $LaNi_4Al$. Furthermore, the properties of the ternary alloys are in general improved over the original alloy, $LaNi_5$. Because of their desirable properties, metal alloy hydrides have been proposed for thermal energy storage applications and for thermal energy conversion cycles.

The HYCSOS system is capable of thermal energy storage, space conditioning, and electrical power generation. As a thermal storage medium, metal hydrides provide a high-energy density but the economics of such a system are currently unattractive. As a chemical heat pump, a metal hydride system offers the promise of using solar energy, waste heat, and other energy sources to provide space heating and cooling. The incorporation of an electrical power generation cycle is also possible.

Heat Pump Operation

In its simple form, a hydride heat pump consists of two different hydride beds that are interconnected to allow hydrogen gas transfer between them. The heat pumping action of the system involves a four-step process:

1. High temperature (solar) heat is applied to the first bed causing it to desorb hydrogen at a pressure higher than the second bed. Therefore, hydrogen flows to the second bed where it is absorbed with a release of heat at an intermediate temperature. This heat is rejected to the building (heating mode) or to the outside atmosphere (cooling mode).

2. The two beds are cooled, the first to an intermediate temperature and the second to a low temperature. This step insures that the correct pressure differential between beds exists for reverse hydrogen flow during the next step.

3. Heat from the building (cooling mode) or from the outside atmosphere (heating mode) is added to the second bed to desorb hydrogen at a pressure higher than the first bed. Hydrogen now flows to the first bed where it absorbed and releases heat at the intermediate temperature. This heat is rejected to the building (heating mode) or to the outside atmosphere (cooling mode).

4. During this step both beds are heated, the first to a high temperature, and the second to an intermediate temperature, in preparation for the start of the next four-step cycle. It should be noted that the coefficient of performance (COP) of this theoretical cycle is 1.0 for cooling and 2.0 for heating if the net energy to heat and cool the beds (steps 2 and 4) is zero. These COP values can be improved by cascading units.

Near-continuous heat pumping action provided by even multiple pairs of hydride beds. The hydrides of $CaNi_5$ and $LaNi_5$ have been used and exhibit extremely rapid kinetics. The recent development of ternary alloys of $LaNi_{5-x}Al$ ($0 < x < 1.5$) by ANL allows operation over a wide range of preselected temperatures and permits optimization of the chemical heat pump system.

Purpose

The purpose of this program is to develop a residential-size chemical heat pump based on metal hydrides for space heating and cooling. Solar energy or waste heat will be used to operate the pump and thus eliminate or reduce fossil fuel requirements.

Past Work

Argonne National Laboratory has constructed a laboratory-scale test facility to evaluate experimentally the HYCSOS chemical heat pump and energy conversion concept. The hydrides of $LaNi_5$ and $CaNi_5$ are used in a four-bed system. The heat exchangers were fabricated from 4-inch, Sch. 10 stainless steel pipe and contain four internal concentric bare-tube coils and two external coils. Water is the heat transfer fluid and is heated electrically to simulate a solar heat source. Tap water is used as the heat sink. Pressures, temperatures, and flowrates are measured remotely, monitored, and recorded[1].

Under contract to ANL, TRW carried out a conceptual design study to determine the approximate performance and cost for a 100-ton solar-powered HYCSOS air conditioning unit[2]. The study demonstrated that the concept was technically feasible, and design calculations showed that such a unit would have a cost slightly less than current $LiBr-H_2O$ absorption unit selling prices and a competitive coefficient of performance (COP). Since a large fraction of the cost of the HYCSOS system is in the hydride material, and since $LiBr-H_2O$ absorption units exhibit large economics of scale, small-scale residential HYCSOS units should show particular promise.

Based upon the above considerations, a second subcontract was awarded TRW to assess the residential applications of HYCSOS for space heating, space cooling, and electrical generating using R-114 as a heat transfer fluid[3]. A computer program was developed to calculate hydride bed heat transfer rates, pressure, and temperature flows, COP, cost, and power generation for HYCSOS. Efforts were directed toward optimizing the HYCSOS design for residential applications with solar energy input.

An economic evaluation based on total annualized cost was prepared for two cities -- Boston and Albuquerque. The results showed that compared with conventional systems, the HYCSOS system had a higher annual cost, due to the high capital cost, but it used considerably less energy. Also when comparisons were made with solar heating and cooling systems, the HYCSOS system had lower costs for both Albuquerque and Boston.

Fiscal 1979 Program

During fiscal 1979, the Chemistry and Energy and Environmental Systems (EES) Divisions performed HYCSOS development work. The areas in which work was done was divided as follows:

Chemistry Division

- Heat exchanger performance measurements
- Simulated cooling cycle
- Hydride studies

EES Division

- Systems design studies
- Heat transfer analysis
- Heat transfer experiments
- Conceptual design studies
- System integration into solar/storage systems

A discussion of each area, as well as the accomplishments, is presented in the following sections.

CHEMISTRY DIVISION

Heat Exchanger Performance

To explore the performance of advanced hydride heat exchangers, ANL contracted with Energy Research and Generation, Inc., of Oakland, California to design and fabricate a high performance heat exchanger. In this design, $LaNi_5$ powder is poured into open-cell aluminum foam to provide enhanced heat transfer between the hydride powder and the heat transfer fluid. The foam is 93% void with approximately 20 pores to the inch. Also the half thickness of the hydride bed was reduced from 0.12 inches in the current design to 0.02 inches to improve the heat transfer rate. A preliminary adiabatic hydrogen absorption on $LaNi_5$ in a test module showed that the equilibrium pressure was reached in approximately 30 seconds compared to 3 minutes for the current units.

In addition to this advanced design, more conventional designs are also being investigated. A commercially available compact plate-fin heat exchanger was ordered from Hughes-Treitler Corporation. The alloy containing side of the heat exchanger has 20 fins per inch, and a heat transfer surface of 55 square feet. The heat transfer fluid side, with 15 fins/inch, has 20 square feet of heat transfer surface. Two units will be filled with about 10 moles of $LaNi_5$, and two with a similar amount of $LaNi_{4.7}Al_{0.3}$.

Simulated Cooling Cycle

In an effort to simulate a complete cooling cycle, hydrogen was transferred from $CaNi_5$ hydride at 110°C to $LaNi_5$ at 33°C while at the same time hydrogen was desorbed from $LaNi_5$ hydride in the cooling loop at 9°C and absorbed on $CaNi_5$ at 33°C for cooling cycle II. For this simulation, the hydrogen valves were open and the heat transfer fluid loops were manually switched at cycle times of about 7-10 minutes with data taken at 1 minute intervals. Five complete cycles were run starting with a thermally equilibrated system. Corrected for the lower hydrogen transfer in the cooling loop for Cycle 1, the coefficient of performance (COP) for this cycle was approximately 1.1 compared to a theoretical COP of 2.1 calculated for the temperatures used. A similar measurement for other cycles would be less meaningful because lack of regeneration heat exchange coupled with the large heat capacity of the loop external to the heat exchanger would require a substantial amount of heat to arrive at the starting temperatures. The temperatures used were not optimum and should be selected to prevent hydrogen buildup in the heat exchanger.

Hydride Studies

Since the rates of reaction between hydrogen and the metal surface is limited by heat transfer, the thermal conductivity is an important characteristic determining heat transfer of powder beds. Lehrfeld and Boser[4] have measured an effective thermal conductivity of activated $LaNi_5$ and found that the filling factor, the ratio of powder packing density to the bulk material density, affects thermal conductivity more strongly than either temperature or hydrogen pressure. This result is consistent with the generally accepted model that conduction in a powder bed is limited by the point contact between adjacent particles, and the greater the compression the higher is the thermal conduction.

Using the transfer of hydrogen from one alloy bed to another to provide the temperature difference between the bed and the heat transfer fluid in the coiled tubing heat exchangers currently used in the HYCSOS system, a fairly constant, 1.0 ± 0.1 BTU/(°F·Ft·Hr), was determined for both $CaNi_5$ hydride and $LaNi_5$ hydride over a filling factor range of 0.4-0.6. This compares with a Lehrfeld and Boser[4] value of 0.27 BTU/(°F·Ft·Hr) at 0.4 filling factor and 0.41 BTU/(°F·Ft·Hr) at 0.6. Although the thermal conductivity measurements are, at best, approximate, the relative constancy of the determinations would indicate the importance of factors other than composition or filling factor, e.g., bed disruption during hydrogen mass transport, on the effective conductivity of powder beds in these heat exchangers.

One scheme[5] to improve heat transfer characteristics of metal hydrides is to make compactions with a metal powder, i.e., Cu, Ni or Al, having a much larger thermal conductivity than the hydride. Metal hydride electrodes for electrochemical storage, and hydrogen storage beds for automotive applications have been reported using this method[6, 7].

Work at Argonne is progressing on the preparation of compactions with rapid hydride reaction kinetics which will maintain physical integrity during repeated cycles.

Long term thermodynamic stability of AB_5 hydrides has yet to be determined. Substantial degradation of $CaNi_5$ was found in the laboratory scale facility. Much of the plateau deterioration occurred while the hydrided alloy was at room temperature. The plateau determined at 97°C between dissociation pressures of 5 atm and 6 atm had a composition range between $CaNi_5H_{2.3}$ and $CaNi_5H_{3.3}$. A A similar plateau for a small sample (~ 10 gm) of the alloy when received was between $CaHi_5H_{1.5}$ and $CaNi_5H_{4.0}$. Similar but less extensive degradation has been reported in some $LaNi_5$ systems. Additions of aluminum appears to stabilize the hydride system.

The HYCSOS System Instrumentation and Control

The HYCSOS instrumentation was designed to, 1) provide real-time indication of important system characteristics, 2) provide for logging of data generated during system operation, 3) provide a means of processing raw data, and 4) provide a way to automatically control system operation. Data is input through a data logger containing thirty voltage and thirty thermocouple channels, to a Tektronix Graphics System. Interface and control circuitry for automatic control of HYCSOS operations have been constructed and installed. Any system characterisitc, e.g. temperature, gas or liquid flow, or thermal change can be used to monitor and control HYCSOS operation.

EES DIVISION

System Design Studies

In order to determine the sensitivity of the HYCSOS system to various design parameters, a computer study was performed. The computer program developed by TRW[3] was modified, and used for this purpose. A report describing the results of this study is given in Ref. 8. Briefly, the results obtained were:

1. The cost and coefficient of performance (COP) are very sensitive to cycle time, but only slightly sensitive to regeneration time.

2. The cost and COP are strong functions of the heat flux, but this dependence is lessened at higher heat fluxes.

3. Hydride composition does not have a definite effect on cost or COP for the baseline case. In general, both the cost and COP of $LaNi_{5-x}Al_x$ hydride is lower than for $LaNi_5$ hydride.

4. The unit cost of the system decreases rather strongly with the system rating.

5. The COP decreases linearly as the inert mass/hydride mass ratio increases.

6. Large changes in bed conductance or working fluid temperature resulted in very small system effects.

7. The addition of fins to the aluminum foam hydride heat exchanger was of marginal value.

8. The program was modified to use a single phase coolant-air or ethylene glycol. However, satisfactory results have not been obtained.

Heat Transfer Analysis

To gain insight into the performance of hydride heat exchangers, an analytical study was performed. The model used in this work was a one-dimensional slab of hydride. One face of the slab was subject to a step change of surface temperature while the other face was insulated. The heat of reaction of the absorption/desorbtion of hydrogen was included in this analysis. The results of this analysis were put into dimensionless form, and the relationships among these dimensionless numbers were determined. A discussion of these results is beyond the scope of this paper. Details of the analysis and a discussion of the results are given in Ref. 9.

Heat Transfer Experiments

An experimental heat transfer program was initiated in FY79 to obtain information on heat transfer to hydride beds. An experimental loop was constructed to conduct basic heat transfer experiments. Test sections of various sizes with different heat transfer geometries (e.g., fins can be accommodated).

During the past year, the loop was constructed and shakedown tests conducted. Preliminary results on a plain tube heat exchanger were obtained, Fig. 2. A description of the results of the experiments to date is presented in Ref. 10.

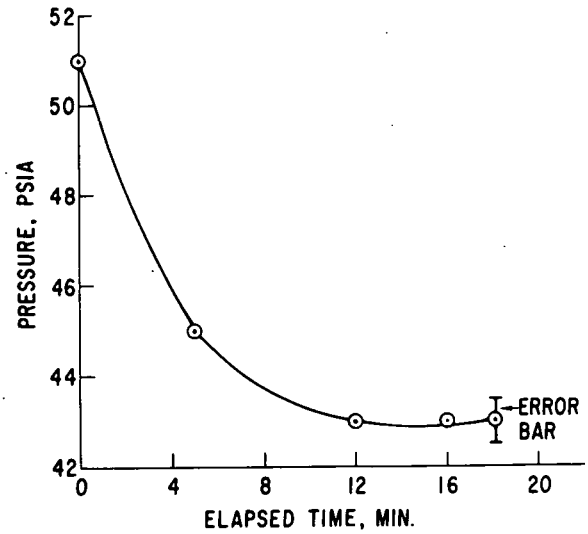

Fig. 2 Sample Plain Tube Heat Transfer Data

Conceptual System Design

Much of the work to date, has been directed towards what might be called an "external" system in which the hydrogen flows between heat exchangers through a plumbing system. ANL is presently developing an "internal" system in which the hydrogen is individually encapsulated in a large number of heat exchanger elements (Fig. 3). This system has a number of advantages including: no hydrogen valves, simplified integration into heating and cooling systems, and high reliability due to a large number of independent heat exchanger elements.

This design has been investigated through a series of scoping calculations. A system has been sized, and rough estimates of the system performance made. The results of these studies are shown in Table 1.

System Integration into Solar/Storage System

An engineering study has been subcontracted to provide a first cut analysis of how a HYCSOS heat

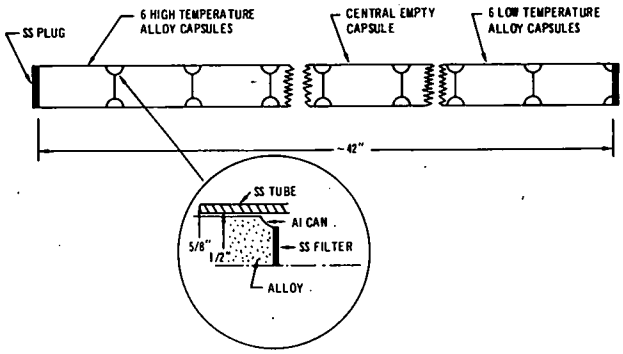

Fig. 3 Tubular Heat Exchange Design

Table 1. Summary of Tubular System Design

Physical	
Number of element bundles	24
Number of tubular elements per bundle	10
Total pounds of hydride	110 lb
Cycle time	4 min
Performance	
Design Rating	50,000 Btu/hr
Coefficient of Performance (Heating)	1.55
Coefficient of Performance (Cooling)	.55
Cost $/1000 Btu (Heating)	$110/1000 Btu/hr

pump would be integrated into a solar system to provide residential heating and cooling. Systems were designed for three areas of the country as represented by Albuquerque, Boston, and Chicago. The results of this study, Ref. 11, contain an engineering description of the three systems. Included in this study were:

- flow diagrams
- component sizing and description
- calculation of heating and cooling loads
- cost estimate of balance of system (excluding the heat pump)

Program Planning

A three year program plan was developed, and submitted as a part of Ref. 12. This plan outlines the development of the HYCSOS system through the production of a prototype. Figure 4 presents a milestone chart of the proposed program elements.

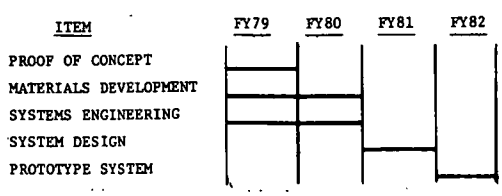

Fig. 4 Hydride Heat Pump (HYCSOS) Milestone Chart

REFERENCES

1. I. Sheft, D.M. Gruen, and G. Lamich, *HYCSOS: A Chemical Heat Pump and Energy Conversion Based on Metal Hydrides - 1979 Status Report,* ANL-79-8, April, 1979.
2. R. Gorman, *Performance and Cost Analysis of a Hydride Air Conditioning System,* prepared by TRW Energy Systems Group for Argonne, ANL/EES-TM-65, April, 1977.
3. R. Gorman and P. Moritz, *Hydride Heat Pump. Vol. I: Users Manual for HYCSOS System Design Program* and *Vol. II: Cost, Performance, and Cost Effectiveness,* prepared by TRW Energy Systems Group for Argonne, ANL/EES-TM-66, Vol. I and Vol. II, May, 1978.
4. D. Lehrfeld, and O. Boser, *Absorption-Desorption Compressor for Spaceborne/Airborne Cryogenic Refrigerators,* Philips Laboratories Technical Report AFFDL-TR-74-21, p. 46, March, 1974.
5. M. Ron, Proc. 11th IECEC, State Line, Nevada, p. 954, 1976.
6. M.H.J. van Rijswich, *Metal Hydrides for Electrochemical Energy Storage,* Geilo, Norway, Pergammon Press, New York, p. 261, 1977.
7. O. Bernauer, Workshop discussion, Hydride Storage Reservoir Symposium, Brookhaven National Laboratory, Upton, New York, June 20-21, 1978.
8. J. Horowitz, *HYCSOS: Hydrogen Conversion and Storage System,* ANL/EES-TM-63, September, 1979.
9. J. Horowitz, *Analytical Modeling of a Hydride Heat Exchanger,* ANL/EES-TM-61, September, 1979.
10. H.P. Egbert, J.S. Horowitz, G.M. Warapius, *Single Tube Hydride Heat Exchanger Test Exchanger,* ANL/EES-TM-64, October, 1979.
11. H. Nicenski, Chicago, Illinois, unpublished information prepared for Argonne (1979).
12. C. A. Blomquist, *HYCSOS: Chemical Heat Pump and Energy Conversion Systems Based on Metal Hydride - Mid-year Program Report,* ANL/EES-TM-50, June 1979.

NASA HYDROGEN ENERGY STORAGE TECHNOLOGY PROJECT

James H. Kelley

Jet Propulsion Laboratory
California Institute of Technology
Pasadena, California

Abstract

A portion of the DOE/STOR Hydrogen Energy Storage Program has been conducted by NASA for DOE under an interagency agreement. That portion consists of research and development in the areas of advanced (solar) production concepts, thermochemical cycles, transmission and distribution, containment materials and associated system studies as well as the attendant project management. With the program budget decreasing 60% in FY80 this project is being phased out. The reported work is primarily from FY79, so the project is described for FY79.

Introduction

The Department of Energy (DOE), Division of Energy Storage Systems (STOR), in implementing a Hydrogen Energy Storage Program, established an agreement with the National Aeronautics and Space Administration (NASA) for NASA to assume project responsibility for a portion of the program beginning in FY78. This project assignment encompasses system studies and assessments, thermochemical and other advanced hydrogen-production techniques, and containment and transportation technologies. Through Interagency Agreements (IA) EC-77-A-31-1035 and ET-78-I-01-3112, NASA provided assistance to DOE in the execution of these program elements in FY77 and FY78. The responsibility for implementing this project, hereinafter titled the Hydrogen Energy Storage Technology (HEST) project, has been assigned to the Jet Propulsion Laboratory (JPL) with the Ames Research Center (ARC) having responsibility for containment materials technology.

The planned DOE/STOR budget for Hydrogen Energy Storage in FY80 is about 60% below the FY79 budget. As a result this project at JPL will be terminated. Cognizance for chemical production of hydrogen is expected to continue at a lower funding level. A phase-out proposal for the project has been submitted by JPL. The project description which follows refers to the FY79 activities.

Objectives of the HEST Project

The DOE Hydrogen Energy Storage Program Five Year Plan described in DOE/ET-0046 dated April 1978 is comprised of seven program components:

Hydrogen Energy System Components	1. Production
	2. Storage
	3. Transport
	4. Use
Support Components	5. Supporting Research and Technology
	6. Systems Studies and Assessments
	7. Program Management

Two field centers, JPL and BNL, provide major support to DOE/STOR in this program. Brookhaven National Laboratory carries out responsibilities for electrolytic hydrogen production, underground and occluder materials hydrogen storage, and a number of related systems developments and supporting research and technology. NASA/JPL carries out the responsibilities shown in Figure 1: this figure compares in pattern with Figure 3-1 in DOE/ET-0046 to illuminate the relationship between the HEST Project and the overall DOE Program.

The broad objectives of the HEST project can be stated as follows:

To explore and develop thermochemical hydrogen production cycles to the point that (1) technically and economically feasible thermochemical cycles are developed, or (2) it is determined that none such are likely in the foreseeable future.

To stimulate, monitor and manage the proposal, evaluation and development of advanced hydrogen production and storage concepts which, in production versions, could exceed the net energy efficiencies and cost effectiveness of water electrolysis and thermochemical cycles.

To develop and maintain coherent and valid projections of hydrogen market penetration in the near, mid- and long-range future.

To develop hydrogen production-to-use systems concepts which will support the earliest possible implementation of non-petroleum or natural gas-based hydrogen production/energy storage technologies.

To develop a scientific and engineering foundation of knowledge and practice which will allow the use of low-cost, plentiful containment materials in hydrogen production, storage, transport and use.

To monitor and maintain the pace of technological developments in gaseous pure hydrogen and hydrogen blends transmission, distribution and storage to the end that these technologies maintain a level of maturity consistent with the development of hydrogen production and end-use technologies.

Within the management structure of the HEST project, these six broad objectives are grouped into five project elements -- markets analyses and the development of production-to-use systems

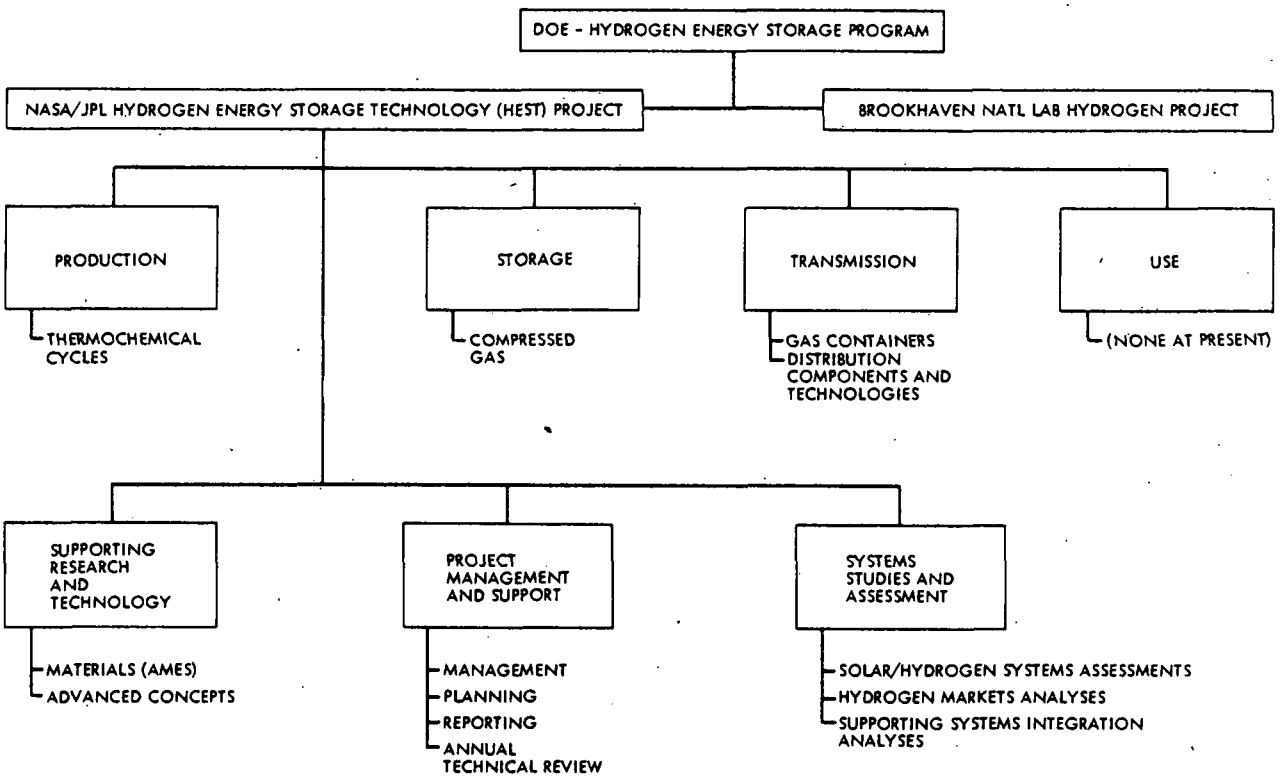

Figure 1. HEST Project Elements Expressed in the Pattern of the DOE/STOR Hydrogen Energy Storage Program Elements. (See Also Figure 3-1 in DOE/ET-0046)

concepts being grouped within the Systems Studies and Assessments Element and the remaining broad objectives, each expressed as a project element in and of itself. Figure 2 shows these elements in the HEST project organization along with a project Management and Support Element.

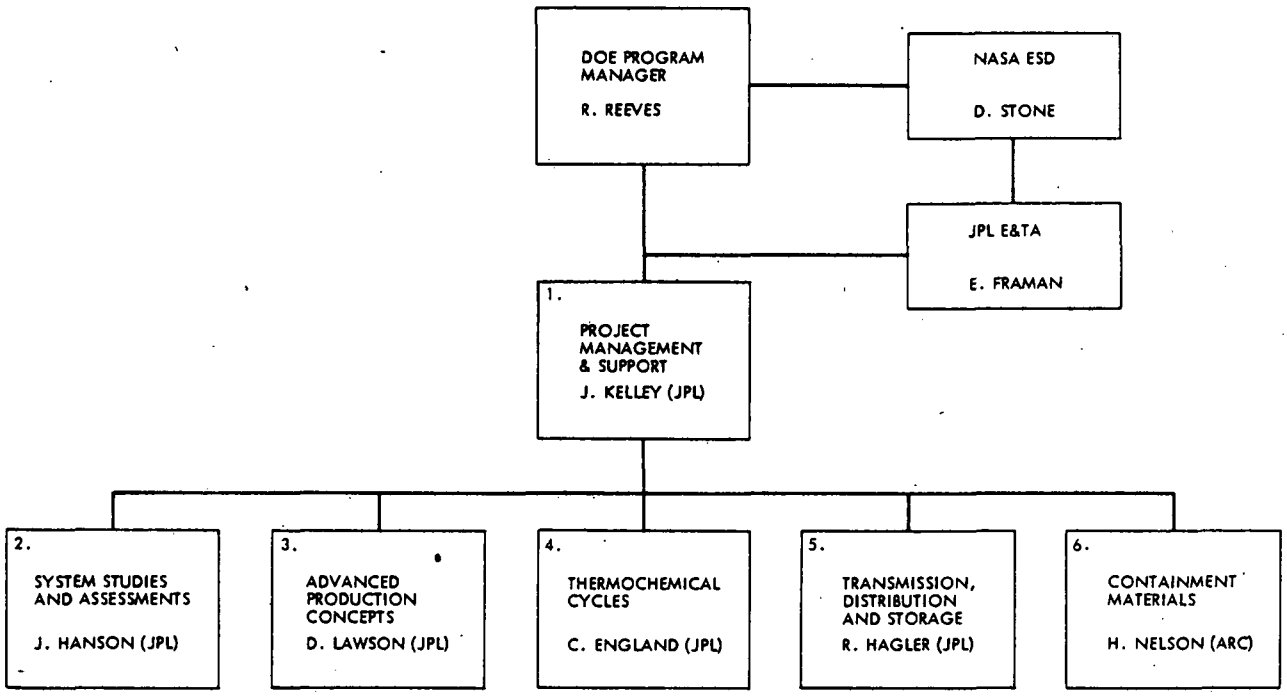

Figure 2. Project Organization

HEST Project FY79 Work Breakdown Structure

The six HEST project elements are each made up of several tasks and, where appropriate, tasks may be broken down further into subtasks. Most of the identified tasks and subtasks are performed by contractors: as a matter of policy, JPL manages contracts and performs enough technical work in-house to assure maintenance of its competence at the forefront of the technologies involved and to validate some technical results. Contracts may be let and managed by JPL or ARC or, when it is more expedient, may be let directly by DOE and then technically managed by JPL or ARC. Table I lists contracts and task orders in order of the tasks and subtasks. Figure 3 summarizes the hierarchical relationships among HEST project elements, tasks and contracts.

Table I. HEST Project Contracts and Task Orders

TASK	CONTRACTOR	SUBJECT
1.3	Courtesy Associates	Annual Contracts Review
2.1.1	Escher: Foster	Solar/Hydrogen Systems Assessment
2.1.2	General Atomic	Hydrogen Production from Solar Energy/ Water
2.2.1	Air Products	Hydrogen Markets/ Supply Options
2.2.4	Billings	Workshop on Cost of Hydrogen from Coal
3.1.1	EIC	Hydrogen Photo-electric Conversion
3.1.2	Caltech/JPL	Photocatalytic Decom-position of Water
3.1.3	Battelle	Direct Thermal Water Splitting
3.2.1	Univ. of Georgia	Photochemical Energy Storage
3.3.1	SRI International	Hydrogen Sulfide
4.1.1	General Atomic	Sulfur-Iodine Cycle Development
4.1.2	Westinghouse	Sulfur-Electrochemical Development
4.2.1	IGT	Hybrid Cycles/Solar Heat Sources
4.2.2	LASL	Thermochemical Pro-cesses
4.2.4	LLL	Materials Development
4.2.5	Univ. of KY	Open Thermochemical Cycles
4.3.1	Univ. of KY	Evaluation of Thermo-chemical Processes
5.1	IGT	Natural Gas Equip. in Hydrogen Service
6.1	SLL	Compatibility of Exist-ing Pipelines
6.2.1	ARC	Microstructural Influences
6.2.2	P&W	Laser Welding
6.3.1	VPI	State of Stress
6.3.2	Rockwell	Threshold Fatigue
6.3.4	Cornell	Influence on Fatigue

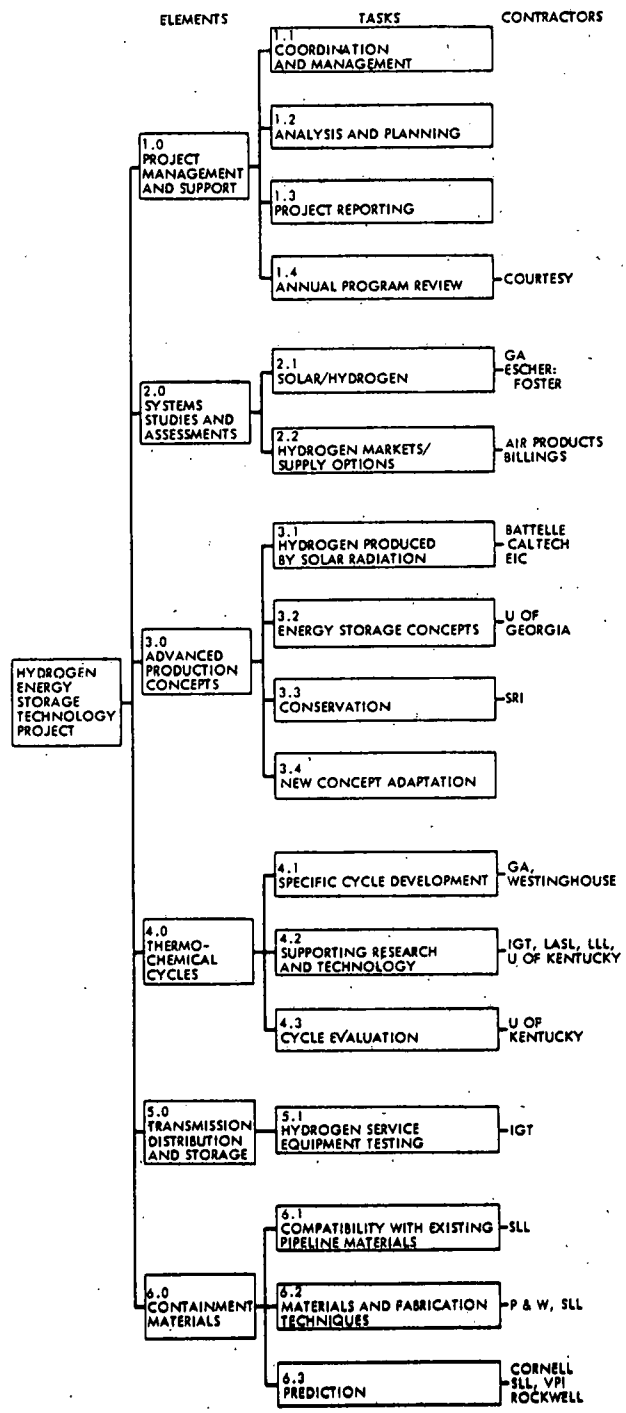

Figure 3. Element and Task Relationship Within the HEST Project (FY79)

HEST Project Funding

In addition to DOE funding through NASA for contracts and in-house work, some efforts under this project are funded directly by DOE. These include funding of DOE laboratories and continuation of some contracts initiated by DOE prior to the formation of the HEST project.

Table II lists the project elements with FY79 direct DOE funding, FY78 DOE-funded and NASA/JPL-funded contracts which require FY79 management, and FY79 New Obligation Authority (NOA) for the baseline budget. The managed funds total about $3 million.

Table II. HEST Project Funding ($K)

NO.	ELEMENT	DIRECT DOE FUNDING		FUNDING THROUGH NASA	
		FY79	FY78*	FY78 CARRYOVER	FY79 NON OBL AUTHORITY
1	Management and Support			46	190
2	Systems Studies			248	173
3	Advanced Concepts		40	300	113
4	Thermochemical Cycles	705	60	125	429
5	Trans. Dist. and Storage		30	11	130
6	Containment Materials	236	45	177	65
	TOTALS	941	175	907	1100

ASSESSMENT OF SOLAR/HYDROGEN SYSTEMS

by

William J.D. Escher
Richard W. Foster

Escher:Foster Technology Associates, Inc.
P.O. Box 189
St. Johns, Michigan 48879

and

Joe A. Hanson

California Institute of Technology
Jet Propulsion Laboratory
Pasadana, California 91103

Abstract

Solar energy represents a very large renewable energy resource which can, theoretically, be utilized in numerous ways to produce hydrogen from water. An initial assessment of solar/hydrogen systems is currently being completed. A large number of identified candidate production means have been characterized, from a technology standpoint, for both the direct and indirect solar energy conversion modes.

Based on the status of the relevant technologies, and on the feasibility of production systems encompassing these technologies, a screening of the candidates capable of commercialization by the year 2000 is being carried out. One clear indication is that water electrolysis will play a key and unique role in such nearer-term applications.

This paper reviews the context and coverage of the study and comments on the technologies assessed. (Details of the screening were not available for this paper.)

Introduction and Background

Rationale for Solar/Hydrogen Systems

The future of the world's energy system appears quite uncertain. Logic and prudence dictate that our available energy systems options provide alternatives to the present fossil-fuel-based systems. Further, it would be advantageous that such systems be compatible with present primary energy resources, and the energy resources that are hoped to be brought into being in future decades would aid the transition to new alternative energy systems. Further, if the basic energy media could be progressively intermixed and the resources in diminishing supply phased out without major disruptions of the world's energy system, this would also represent a desirable alternative.

Recent events have cast great uncertainty on the future of the nuclear "burner" and "breeder" reactor industry. The future of fusion energy systems is a subject for much debate. Even if both families of systems achieve great market success, traditionally, their output is associated with electricity generation. Electricity cannot be stored, it cannot, economically, be transmitted long distances, nor is it compatible with certain applications, e.g., air transportation. Fluid fuels are required along with electricity, and the nuclear production of fuel forms is technically feasible. But, in the interest of developing a range of future alternatives, other-than-nuclear-based fuel possibilities appear to be limited to geothermal and solar energy. Without commenting on the former, which appears to have its own unique advantages and limitations, the sun appears to be the major primary energy source of opportunity. Thus, the solar-production of fuels should be an option brought clearly into focus for energy planners and decision-makers. Solar/production of hydrogen, being the fundamental step in solar-fuels production, is a specific topic of interest and the subject of the study reported on here.

As an informed commentary, this sizing-up of the solar/hydrogen prospect by Dr. Wolf Haefeli of the International Institute of Applied Systems Analysis is appropriate here:[1]

> "Solar power is obviously a big option. The total input at the outer boundary of the atmosphere is 178,000 TW* and this is practically forever. So the resources are not the problem, nor the power, in principle. The problem is how to get hold of it.
>
> A salient point in all that is energy storage. Both the daily and the seasonal cycle must be bridged...for deep-seated reasons of physics, thermal, or mechanical storage would not do it, instead the energy must be stored on the negentropic level of the molecules, that is in terms of chemistry.
>
> And here the most elegant solution is again hydrogen. In the foreseeable future hydrogen would be produced through electrolysis or through thermochemical means, while in the long run a biotechnological approach might turn out to be a better solution."

* Present world total energy use is about 8 TW, projected to grow to 25-40 TW in 2030.

Background of the Study

In early 1978, the Caltech Jet Propulsion Laboratory (JPL) initiated an in-house task entitled "Assessment of Solar/Hydrogen Systems." Using the inputs of both JPL researchers and outside consultants, state-of-the-art documentation for a broad range of direct and indirect solar energy conversion and related hydrogen production processes was developed. By late-1978, a study "core group" had developed a basic study plan-of-progression aimed at the identification of the more attractive solar/hydrogen system approaches. The recommended assessment work-flow was developed.

Subsequently, with the initial tasks underway, JPL elected to contract the continuation and completion of the study to Escher:Foster Technology Associates, Inc. (E:F). The contract was initiated in mid-June 1979 and is scheduled for completion at the end of November 1979.

This paper is a brief summary of the assessment activity status as of the beginning of October 1979. Two earlier references covering initial phases of the assessment have been published.[2,3]

Assessment Definitions, Guidelines and Documentation

There are four basic considerations implicit in an energy system. These are 1) the primary energy resource, 2) the energy form produced from the primary energy resource, 3) the delivery of that energy form, and 4) the use of that energy form. Here the primary energy resource is the sun, and the hydrogen production step is the area of inquiry specifically treated here. The technologies associated with the delivery of the energy form, although within the scope of this assessment, are of a secondary level-of-interest (documented for completeness): Hydrogen use is not directly covered but is tied in to the study by means of thorough referencing.

The first level of differentiation can be helpfully separated into two basic sub-steps (within the total solar/hydrogen production step):

1. Solar Energy Conversion, through which the electromagnetic solar radiation is converted to some intermediate energy form, and
2. Hydrogen Production, through which the converted energy form is used, generally in a water-splitting process, to produce the product: hydrogen (and usually oxygen).

Emphasizing the technological facets, a more complete definition of these two steps is implied in these sub-step titles: 1) Solar Energy Conversion Technologies (SECTS), and 2) Hydrogen Energy Production Technologies (HEPTS), respectively.

Further, inspection of the nature of the energy conversion technologies suggests further that solar/hydrogen technologies fall into two classes (Figures 1 and 2):

1. Direct Conversion Technologies, where the principal conversion step is operated directly by solar radiation.
2. Indirect Conversion Technologies, where an intermediate medium is utilized to operate the conversion process and where, often, large time constants are encountered.

Figure 1 graphically presents the taxonomy of solar/hydrogen production processes as determined in the study. The direct and indirect SECTS are noted on the left-hand side of the diagram; the HEPTS are called out in the middle of the diagram as the ellipses, leading to the hydrogen product at the right. Of special interest is the interlinking of SECTS and HEPTS via heat and work processes.

Figure 2 illustrates an entire solar/hydrogen energy system showing the SECTS (Item 1.1) and HEPTS (Item 1.2) as these combine to form the entire production system. Delivery and use are conventional.

To provide focus and to establish a line-of-direction within the assessment, in context with the solar/hydrogen technologies and systems represented in Figures 1 and 2, a general guideline was adopted, whose essence is given in five points:

- Solar technologies that can become commercially viable within the next 20 years are to be emphasized.
- Solar technologies that are capable of evolving with, and supporting, a gradually expanding hydrogen market are to be preferred.
- The eventual use of solar energy as the primary energy source for hydrogen production should be viewed as a future energy option worthy of preservation.
- Lead time requirements associated with development and deployment of new technologies, as process which must be completed before significant impact is made on any energy sector, suggest that the hydrogen fuel issue is one of immediate concern.
- A United States purview, rather than international coverage, is to be maintained.

The first point, introduces a pragmatic forcing-function which serves as a strong sorting-out means, to narrow down those technologies and systems to be assessed from a general standpoint of detailed technoeconomic characterization and implementation.

The assessment is being documented in two report volumes:

- Volume I, "Systems Assessment," emphasizes the technoeconomic description of those candidate technologies and systems which are viewed as the most promising for commercialization by the year 2000.
- Volume II, Technology Review," comprehensively documents a review of all solar/ hydrogen technologies which have been considered in the assessment. Emphasis is on the production step, with an appropriate summary review of the hydrogen delivery step as well.

In brief, Volume I presents more detailed information on prospective nearer-term solar/hydrogen

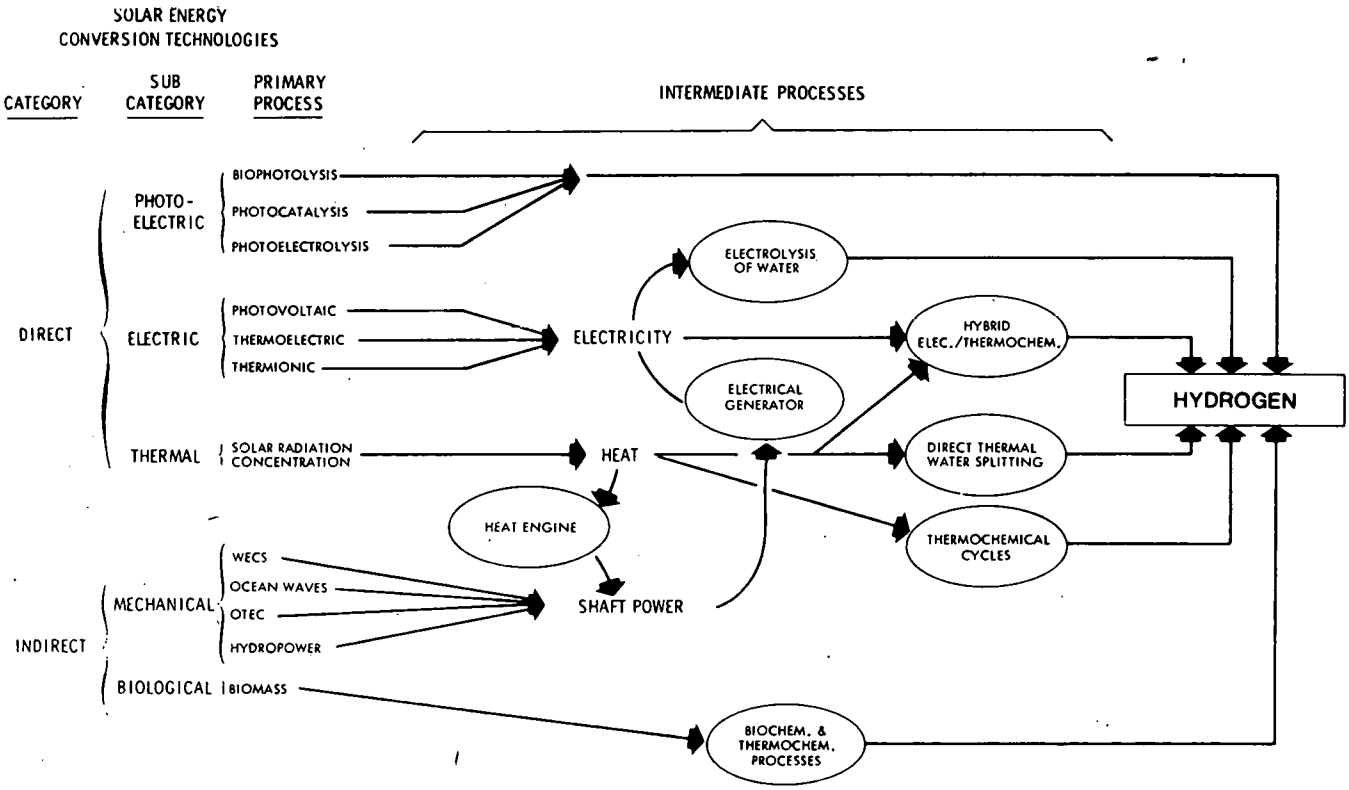

Figure 1. TAXONOMY OF SOLAR/HYDROGEN PRODUCTION PROCESSES

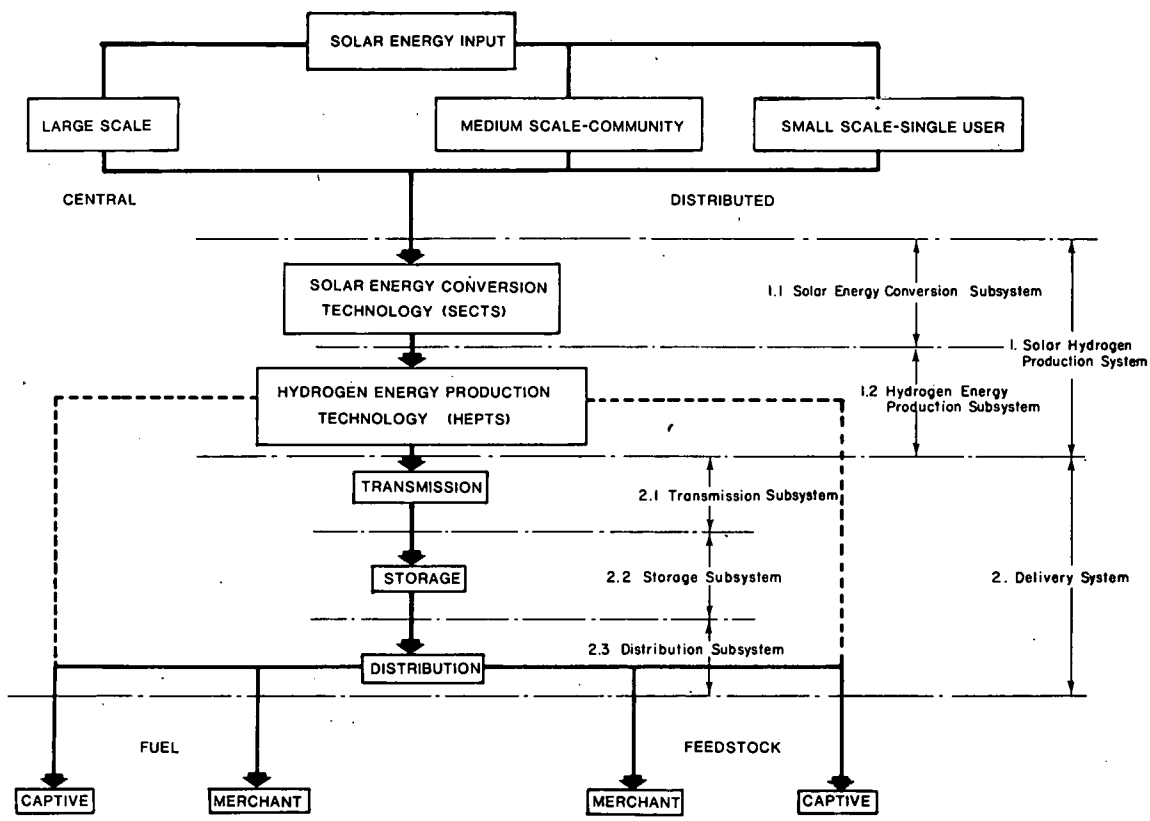

Figure 2. FUNCTIONAL PRESENTATION OF THE SOLAR/HYDROGEN SYSTEM

systems and technologies characterized more generally, but comprehensively, in Volume II.

Review of Solar/ Hydrogen Technologies

Direct Solar Energy Conversion Processes

This category of processes consists of three subcategories (photic, electric, and thermal) and a number of specific conversion processes, as shown in Figure 2.

1. Photic Processes. This subcategory includes three specific solar energy conversion processes — biophotolysis, photocatalysis, and photo-electrolysis. The commonalities shared by these processes are : 1) in each process, photons initiate electrochemical reactions which result in water splitting, and 2) each process is in its developmental infancy, with respect to forseeable large-scale hydrogen production.

The direct photo production of hydrogen by biological systems uses water as an electron source (biophotolysis) and includes the use of living algae (in vivo) and the construction of artificial systems from biological components (in vitro). Both in vivo (living systems) and in vitro (artificial systems containing subcellular components) are under investigation. However, this technological pathway must, for now, be assessed as one which at best is far from commercial-scale realization. Even if sustained reactions having acceptable efficiencies are achieved, the resultant hydrogen and oxygen emerge mixed from the surface of the aqueous medium, and safe and cost-effective means for separating the two under the necessary conditions are not now obvious.

Nevertheless, considerable interest has developed in constructing hydrogen producing systems with isolated biological components (in vitro). This approach promises higher conversion efficiency than in vivo systems but requires the solution of a number of difficult technical problems, including: 1) stabilization of biological components, 2) physical separation of oxygen and hydrogen producing activities, 3) simplification of the photo-synthetic system, and 4) developing systems for utilizing the entire incident solar spectrum. These activities are highly research-oriented and practical in vitro systems are not likely to be forthcoming in the immediate future.

b. Photocatalysis. The objective of photocatalytic systems is to produce an effect similar to boiphotolysis without the involvement of biological media. Current approaches involve near simultaneous photo-catalytic oxidation and reduction reactions that yield oxygen and hydrogen followed by a dark reaction in which the reagents recombine to their original form. The challenge implicit in photocatalytic processes is to add recyclable material to water that will absorb solar light spectra and deliver the absorbed energy to a hydrogen and oxygen producing reaction. Reactions currently under study require the use of relatively rare and expensive materials, primarily rhodium complexes; cycles based on far more abundant catalysts must be developed before this technology can be considered as a potential source of hydrogen for either centralized or distributed systems in either the near-term or far-term future.

c. Photoelectrolysis (or Photoelectro-catalysis). Photoelectrolysis, or photoelectric-catalysis is a fluid analog of a photovoltaic cell combined with an electrolytic cell. Theoretical conversion efficiencies of 45% have been calculated. The best experimental conversion efficiencies of 10% to 11% have been achieved with monochromatic light. The best total solar spectral efficiency attained thus far is on the order of 2% to 3%. Aside from these low practical efficiencies, the major problem with these systems is that no electrode materials have been found that are thermodynamically stable when the cell is operating. Corrosion of electrodes and the resulting drop in conversion efficiency presents the major problem. This field, like others in this subcategory, is relatively unexplored and breakthroughs are possible. Nevertheless, it cannot now be included among the near-term contenders for commercial hydrogen production.

2. Electric Processes. The term "electric processes" is employed here to encompass photovoltaic and concentrating hybrid photovoltaic concepts, thermionic technologies, and solar thermo-electric phenomena — the latter being distinct from the solar thermal-to-heat engine-to-electric generation concept in that electricity is produced directly.

a. Photovoltaic Systems.

(1) Terrestrial Photovoltaic Technology. Photovoltaic cells are a form of solid state diode and can be made from various semiconductor materials. While there are a variety of possible materials, the preponderance of U.S. experience is with silicon cells. They have been in use since 1955, when Bell Telephone Laboratories successfully powered telephone amplifiers in field tests and their technology and reliability are well known.

Presently, cost reduction is the prime objective of such efforts as DOE's Low-Cost Solar Array (LSA) Program. This program is funding technology developments and volume solar cell procurements as a push-pull means of cost reduction.

Silicon photovoltaic cell production processes are well understood although some process validation is still necessary before sequence automation can be undertaken. Currently, there are some process sequences that result theoretically in costs equal to the LAS Project goals of $2.00 per watt by 1982 and $0.50 per watt in 1986 (1975 dollars), and some advanced technology cell processes show promise of further cost reductions.

(2) Solar Power Satellite Concept. While terrestrial applications of the photovoltiac concept may range from the miniscule to quite large, the Solar Power Satellite (SPS) concept is intrinsically a "macro system." As presently seen, SPS involve large photovoltaic arrays located in a geostationary orbit 36,000 kilometers above the Earth's equator. Each SPS would be in sunlight more than 99% of the time and in continuous line-of-sight contact with its unique ground receiving station. Electrical power produced on the satellite by photovoltaic conversion of sunlight would then be converted to radio frequency energy at high efficiency, formed into a

focused beam and precisely directed to the SPS ground stations. The ground station receiving antenna system would reconvert the energy into electricity for distribution. Conceptually, electrolytic hydrogen could be produced as an alternative to electricity.

The SPS concept is presently being critically assessed by a special DOE/NASA task force, in which a whole range of impacts and ramifications are being looked at. An assessment report is due in mid-1980. At the earliest, deployment of the SPS system is planned in the post-2000 period.

b. Concentrating Hybrid Photovoltaic Processes. The present high cost per unit of photovoltaic cells might theoretically be circumvented by the use of optical concentrating methods which could increase the rate of energy delivery per unit area (solar flux) applied to photovoltaic cells. In addition to the direct mechanism of reducing the cell area required, the resulting heat rejected to a cooling medium (if any) can be conceivably used as an energy source for a bottoming cycle heat-engine system.

Concentrating hybrid photovoltaic systems are presently being investigated in the United States. The applicability of this technology to the commercial-scale production of hydrogen from solar energy is highly dependent upon the actual extent to which cost reductions, vis-a-vis straight photovoltaic systems, csn be achieved. However, to date, design and analysis work has not yet proceeded far enough to support detailed assessments of the potential of this technology.

c. Thermoelectric Systems. The generation of a voltage between the junctions of dissimilar metals where a temperature difference exists between the two (the Seebeck effect) is the basis of operation of thermocouple/thermopile systems. This effect has found practical application, with low energy conversion efficiency, in spacecraft power supply systems using radioisotopes as heat sources. While significant advances have been made in this technology, low conversion efficiency remains the major barrier to its application to solar energy conversion devices. Moreover, solar thermoelectric technology is not being developed in the United States.

d. Thermionic Processes. The unique features and characteristics of solar thermionic power include relatively high theoretical efficiencies, on the order of 20%, and the potential for operating these systems at high temperature. High temperature operation of solar thermionic systems, like concentrating hybrid systems, offers the opportunity to use the discharge thermal energy to drive shaft-power devices (Rankine, Stirling, or Brayton cycle) in bottoming cycles.

With presently known materials, the optimum hot-to-cold junction temperature ratio is about 2. Today's best materials can produce this ratio but the temperature of the total system at which this ratio is produces is too low to permit the cost effective operation of inexpensive shaft power devices to support a bottoming cycle.

Presently, the major limitation is that, with higher temperatures, the cold electrode becomes an electron emitter and acts to reduce the potential available from the junction. New breakthroughs in materials are required. Work on this particular problem is being supported in the Soviet Union to a greater extent than in the United States. Thermionic technology is not considered to be an attractive candidate for commercialization in the United States within the next two decades.

3. Thermal Processes. Solar thermal energy, derived from optical concentration of solar radiation, may result in the production of hydrogen from water by taking any of three paths: 1) heat engine through electrical generation to electrolysis, 2) as the heat source for thermochemical or hybrid electrolytic-thermochemical cycles, and 3) if sufficiently high temperatures can be achieved and maintained, direct thermal water-splitting.

a. Solar Thermal Engine Processes. Solar thermal engine system research and development in the United States is developing along several paths. The JPL is pursuing the development of small distributed systems in which the focal point and heat engine are integral with the parabolic reflector. Sandia Livermore Laboratory is pursuing the "power tower" concept in which multiple reflectors are concentrated on a single thermal cavity supported by a central tower. Sandia Laboratories at Albuquerque, New Mexico, are investigating arrays of line-focusing parabolic cylindrical reflecting concentrators. These are at the demonstration stage, e.g., irrigation water pumping. Rankine-, Brayton-, and Stirling-cycle engine applications are all under investigation.

The solar thermal engine approach shares with the photovoltaic approach the status of a relatively mature developmental technology in which the remaining objectives are to lower capital costs while deriving low maintenance designs with high long-term reliability; therefore, it is included in the list of potential candidates for commercial-scale solar hydrogen production by the year 2000.

b. Direct Thermal Water Splitting. At temperatures of 3000 K and one atmosphere pressure, approximately 14% of water vapor is dissociated. This fraction, as would be expected, increases as the pressure is decreased and the temperature increased. This concept has received earlier theoretical attention.

At present, Battelle Geneva is conducting an initial empirical investigation of the potential technical feasibility of this approach via a small contract with JPL. The Battelle process is held as proprietary until the point results are available. No definitive results have been obtained. Moreover, even if the laboratory method indicates basic technical feasibility, ultimate commercial attractiveness may still lie far in the future. Materials will pose challenges as will methods for obtaining acceptable system net energy efficiencies, considering the very high temperatures that must be maintained. Additionally, this approach shares with biophotolysis the problem of separating the product hydrogen and oxygen. Therefore, direct thermal water-splitting must be considered to be no more than a theoretical long-range possibility for commercial hydrogen production.

c. Solar Thermochemical and Hybrid Electrolytic-Thermochemical Production of

Hydrogen. As a consequence of worldwide efforts in thermochemical water-splitting, there are a great number of sets of closed-cycle reactions that provide for the dissociation of water into hydrogen and oxygen, while preserving the intermediate reagents for recycling. A key requirement for the realization of commercial thermochemical hydrogen production is a continuous high temperature (1550° to 2200°FO heat source is available. However, pending major advances in high temperature thermal energy storage, solar energy could be harnessed to provide attractive continuous thermal energy sources. However, the commercial potential of the solar thermochemical and hybrid electrolytic-thermochemical approaches to hydrogen production appears remote at this time. It would appear that this approach merits no further consideration until such time as: 1) commercially attractive reactions are practically demonstrated, and 2) a commercially viable, high-temperature, thermal energy storage technology which is able to compensate for the intermittency of the primary solar energy resource is demonstrated.

Indirect Solar Energy Conversion Processes

Indirect solar energy processes fall into three classes: 1) thermal, as manifested in the ocean thermal gradient, 2) kinetic, as manifested in winds, waves, and hydraulic reservoirs,* and 3) biological, as manifested in the production of biomass. However, the related primary conversion technologies fall into only two subcategories in the categorization system employed here; (1) mechanical, and (2) biological.

1. Mechanical Solar Conversion Technologies. Examined briefly under this subcategory are wind energy conversion systems, ocean thermal energy conversion, ocean wave power, and hydropower.

a. Wind Energy Conversion Systems. Wind systems are presently being developed by the U.S. Department of Energy in its Wind Energy Conversion Systems (WECS) Program. The present emphasis is on relatively large wind turbine generators (0.1 to 1.0 megawatts) and on horizontal axis machines. There does exist, however, a smaller effort directed toward small-scale wind energy conversion systems with the intent of applying such systems to distributed or decentralized system designs. There is no doubt that wind energy conversion systems represent a potentially large and near-term energy contribution.

One of the well known technical problems is the fluctuation of output power due to wind velocity variations (power output is proportional to the cube of the wind velocity). Wind velocity may vary significantly in minutes, in a wide range daily, and from zero to some maximum on a weekly or monthly basis. Moreover, zero-output situations may persist for days or weeks in some locations. Thus, without tie-ins to a power grid, storage systems are of great significance to practical wind systems. This is where hydrogen may offer a very attractive potential.

Because the technology is reasonably mature in general, and because new design approaches are producing meaningful results, the WECS technology must be considered a near-term candidate for hydrogen production via water electrolysis.

b. Ocean Thermal Energy Conversion (OTEC). In the tropical oceans, the temperature gradient between the warm surface water and the cold intermediate water 500 to 600 meters below is approximately 40°F. This ΔT gives a theoretical Carnot efficiency of approximately 7%. The oceanic temperature gradient represents a huge resource if it can be tapped. At present, the closed Rankine Cycle employing ammonia as the working fluid is the technology of choice although open cycles such as the one tested unsuccessfully by Claude in the 1920's as well as several exotic approaches to vaporization and hydraulic head production are being examined by some investigators. With all proposed approaches, the requirements for pumping huge volumes of water, pressure drops within the system and other parasitic losses result in the most optimistic estimates of practical system efficiencies for electricity production being no more than 1% or 2%, and some observers doubt seriously that OTEC can produce net energy at all.

In spite of OTEC's low net energy prospects, the U.S. DOE supported OTEC component and subsystem developments at a funding level of about $40 million in Fiscal Year 1979. The first subsystem tests of heat exchangers and cold water pumping are scheduled in 1980 aboard a converted ship hull, called "OTEC-1" since the sizing of the components will reflect a theoretical one megawatt electrical production capacity. OTEC-5 (5 megawatts) is scheduled for test operations by the mid-1980's and is expected to include a Rankine engine and electrical generation capability. Should OTEC-1 and OTEC-5 be successful, it seems probable that OTEC developments will be accelerated and that the first pilot scale tests (approxiamtely 25 megawatts) will occur in the early 1990's.

Because most tropical oceanic locations offering the necessary depths are not close to major urban industrial complexes, a perplexing problem arises should OTEC become otherwise commercially attractive. Either the complexes will be obliged to move to the OTEC sites (the island of Hawaii might thereby become a major industrial complex) or the energy must be transmitted over considerable distances in some form. Analyses have been performed that indicate that OTEC can be particularly useful for manufacturing chemical fuels, such as hydrogen or ammonia in liquid forms. However, delivered costs of the product still would be about three times present gasoline prices (in 1975 dollars). OTEC is viewed as a special, but still tenuous, candidate for commercial-scale solar/hydrogen production by the close of this century.

c. Hydropower. Hydropower systems employ very mature technology. However, most available and suitably located large hydropower resources in the continental United States already have been exploited.

The use of existing non-hydroelectric dams for the production of hydrogen and oxygen from water is being investigated by the U.S. DOE. Two development and demonstration projects are being supported on modest scales. The total U.S. resource of such

* Even though they are renewable energy sources, ocean currents and tides are not included in this discussion since they are not purely solar energy forms.

sites is large in number but relatively small in total energy content — representing less than 0.3 quads at most. Thus, small hydropower hydrogen production systems represent at least limited opportunities to establish near-term solar/hydrogen energy systems. It is likely that these would affect merchant gas markets on a local basis only. However, this contribution is not to be overlooked.

d. Ocean Wave Power. Ocean wave power as a renewable energy resource is being pursued at a modest level in the United States. A cooperative program involving the United Kingdom and Japan is being participated in at this time. Should this approach be viewed favorably, it seems clear that electrolytic hydrogen, vs. electricity, could offer significant potential.

2. Biological Conversion Technologies. Concepts for producing hydrocarbon energy forms from biomass are many and varied. Primary biomass resources span the spectrum from urban and animal wastes as feedstocks through a variety of forestry and agricultural wastes, to a variety of specific plant grow-out options ranging from unicellular algaes, to grasses, to silviculture, to massive at-sea farms of the giant brown kelp, Macrocystus pyrifera. Authoritative estimates of the potential of biomass to supply U.S. energy needs range from a few percent to many hundreds of percent, depending upon the assumptions employed. Also, depending on the assumptions employed and the type of feedstock, both biochemical and thermochemical means of converting feedstocks to liquid and gaseous hydrocarbon fuels are possible, e.g., fermentation and gasification.

This solar/hydrogen assessment does not consider biomass sources to be leading candidates for large-scale hydrogen production within the foreseeable future. Although it certainly is technically feasible to derive hydrogen from cellulosic feedstocks through thermochemical processes, we offer the following several arguments against doing so on commercial scales:

1. the net energy efficiency of the process chain which stretches from biomass production to hydrogen delivery is well less than 1%.
2. processes with very low net energy efficiencies invariably will result in very expensive final products unless they display some strong remedial characteristics.
3. compared to common hydrocarbon fuels, hydrogen is difficult and expensive to store and transport.
4. Common hydrocarbon fuels can be derived from biomass feedstocks with higher net energy efficiencies and lower costs, in general, than can hydrogen; finally, when hydrocarbon fuels are continually derived from biomass, atmospheric CO_2 released upon their combustion is not a problem since the CO_2 is taken up again as the next generation of the biomass feedstock is grown.

Therefore, we see few if any logical technical or economic arguments for large-scale commercial production of hydrogen from biomass feedstocks even though we recognize that certain unusual, and probably localized, economic and institutional conditions could constitute exceptions to this generality.

Screening, Selecting, and Documentation of Promising Near-Term Systems

(Note: This taskwork was in progress at the time this paper was prepared, hence, specific results could not be included here.)

Context for the Screening and Selection Process

The task areas presently underway which will lead to the screening of the candidate technologies and systems listed above include:

- Alternative Futures — to provide a general context within which future solar/hydrogen systems can be appropriately assessed, a set of alternative futures has been assembled and their general economic, environmental, socio-political and institutional facets characterized.
- Total Costs — all candidates are being evaluated on the basis of total costs, defined as yhe combination of conventional economic costs, plus those significant non-direct costs, such as those associated with environmental damage and public health, safety considerations, and the basic issues of resource depletion and self-sufficiency.
- Institutional Variables — those controlling institutional variables which significantly influence the energy system selection process such as enacted Federal laws and regulations, tax treatment options, and the less tangible aspects of the decision-making environment, are under consideration as variables affecting decision-making, as part of the screening and selection process.

Selected System Concept Specifications

Once the screening and selection process is completed, one or more solar/hydrogen system (or class of systems) which are judged best able to meet the primary criterion of showing promise of achieving economic viability by 2000, will be characterized and documented. A brief engineering description in text-plus-graphical format will be developed for each candidate system based on the most recent technical information available.

In this documentation, it is planned to give due heed to potential implementation investment requirements foreseen both generally and for each of the selected systems.

Forthcoming Recommendations

Finally, recommendations with supporting rationale will be developed and documented to cover not only the selected "near term" candidates, but all of the technologies and systems related in the previous section. These will include treatment of:

a. Technologies and systems which are recommended to be considered for immediate RD&D
b. Incentives expected to maximize industrial participation in RD&D and commercialization of these systems.
c. Longer-term basic and applied research to be considered for the farther-term and/or less-developed but still promising solar/hydrogen technologies.

The assessment final documantation is scheduled to be available by year-end 1979.

References Cited

1. Hanson, J.A., "Concepts for Solar Production of Hydrogen," paper presented at the Institute of Gas Technology Symposium "Hydrogen for Energy Distribution, 24-28 July 1978, Chicago, (Proceedings).

2. Hanson, J.A., Escher, W.J.D., and Foster, R.W., "Futre Production of Hydrogen From Solar Energy and Water: A Review and Assessment of U.S. Developments," paper presented at the International Symposium "Hydrogen in Air Transportation, 11-14 September 1979, Stuttgart (Proceedings).

SOLAR HYDROGEN PRODUCTION VIA THE SULFUR/IODINE THERMOCHEMICAL WATER-SPLITTING CYCLE

J. R. Schuster, G. E. Besenbruch,
H. D. Chiger, and K. H. McCorkle
General Atomic Company
San Diego, California

Abstract

A study is being conducted to examine the requirements for producing hydrogen by driving the sulfur/iodine thermochemical water-splitting cycle using solar energy. The process configuration involves conducting the high temperature portion of the cycle (sulfuric acid decomposition) during daylight and storing sufficient SO_2 and O_2 to provide enough recycle materials to run the other portions of the cycle continuously. Various types of solar collectors have been evaluated for supplying heat for sulfuric acid decomposition. Cavity-type and fluidized bed-type tower central receivers are preferred. A comparison of molten salt sensible heat storage and additional SO_2/O_2 storage is in progress to determine the preferred energy storage method for driving the lower temperature portions of the process at night. Early indications are that the molten salt storage will be the preferred approach.

Introduction

As a means for producing hydrogen from non-fossil sources, the General Atomic Company (GA) sulfur/iodine thermochemical water-splitting cycle has been undergoing development for several years under the joint auspices of DOE, the Gas Research Institute (GRI), and GA. The cycle is characterized by the following three reactions:

$$xI_2 + SO_2 + H_2O \rightarrow H_2SO_4 + 2HI_x \quad 370K\ (206°F) \quad (1)$$

$$2HI_x \rightarrow H_2 + xI_2 \quad 393K\ (247°F) \quad (2)$$

$$H_2SO_4 \rightarrow H_2O + SO_2 + 1/2\ O_2 \quad 1144K\ (1600°F) \quad (3)$$

Bench-scale testing of the cycle is currently being conducted and a flowsheet has been prepared for a process design that accomplishes the cycle using heat and power produced by a Very High Temperature Gas Cooled Nuclear Reactor (VHTR).

Solar Energy is receiving wide-spread attention as a means of reducing our demand for conventional fuel sources. Most activity has centered on the use of solar energy to provide heat and electricity; however, if solar energy could be utilized in the production of fuels and chemicals, the potential for solar to displace conventional sources of energy would greatly expand.

The purpose of the current system study is to evaluate coupling the sulfur/iodine cycle to solar energy sources. The particular objectives include: 1) an evaluation of various types of solar energy collectors to determine those most suitable for supplying heat for the water-splitting cycle; 2) design of a conceptual flowsheet that utilizes solar energy to drive the cycle, paying particular attention to coupling the diurnal solar source to the continuous process energy demand; and 3) make recommendations for future development work.

This report describes progress to date on the study, including completion of the solar collector evaluation and interim results on a comparison of thermal energy storage and chemical energy storage.

Process Configuration

The basic problem in coupling a solar heat source to water splitting is that of devising systems that can use the time-varying solar heat input to permit a uniform level of hydrogen production over a 24-hr day. A thermochemical approach may readily lend itself to solar heating because many intermediate compounds are storable. Figure 1 illustrates a possible system arrangement for the sulfur/iodine cycle. The mirror field is divided into high-and intermediate temperature portions. The low temperature solution reaction is conducted 24 hours a day, producing H_2SO_4 and HI. The H_2SO_4 is stored and during daylight is pumped from storage, preheated, and is then decomposed in the heat receiver of the high-temperature mirror field. The acid decomposition products are then heat exchanged with the incoming acid, the oxygen and water are removed, and the SO_2 is stored for use in the low temperature solution reaction.

The intermediate temperature mirror field heats a heat transport fluid, such as a eutectic salt. During daylight the salt charges a heat-storage reservoir, generates steam to drive compressors and pumps, and provides heat for concentration and cracking of the HI to yield the hydrogen product and iodine for recycle to the main reaction. At night the heat transport fluid continues to perform these functions, but bypasses the heat receiver and is heated by the heat-storage reservoir.

An alternative to the use of a eutectic salt is to store sufficient additional SO_2 and O_2 during daylight to drive the lower temperature portions of the process at night utilizing the heat from the exothermal recombination of SO_2 and O_2 to give SO_3.

A plant heat requirement of 400 MW(t) has been selected because it corresponds approximately to commercial-sized solar plants being studied for electric power application, and it would result in a hydrogen plant of acceptable capacity with an estimated hydrogen output in the range of 4.44×10^5 m^3/day (1.57×10^7 ft^3/day).* This energy would be absorbed during daylight hours and used as necessary with the balance being stored for use at night. Of this energy, 100 MW(t) would be needed during the day for high temperature cracking of sulfuric acid. Because a 100 MW(t) high temperature solar receiver would be the single most technologically advanced component in the process, it was singled out for this study.

*Based on 45 percent process efficiency, the higher heating value of hydrogen, standard conditions, and a nominal eight-hour heat collection period.

Solar Collector Evaluation

Initial Considerations

The operating constraints imposed on the high-temperature receiver are quite severe. Within ±50%, the heat flux incident on it is 1 MW/m^2 (320,000 Btu/hr-ft^2), or that equal to about 1000 suns. It must run continuously for about 8 hours each day, be shutdown at night, and have an acceptable design lifetime.

Gaseous sulfuric acid enters the receiver at 90 kg/s, 517 kPa, and 798K (200 lb/sec, 75 psia, and 980°F). It flows through a packed catalytic bed, which aids in the endothermic cracking of the gas into water vapor, sulfur dioxide, and oxygen. This mixture leaves the receiver at about 1144K (1600°F). Hot ambient air outside the receiver blows at a design basis velocity of up to 3.58 m/s (8 miles/hour). These design basis operating conditions for the solar receiver are summarized in Table 1.

The conceptual design options available for the solar receiver concern the heat exchanger media and the receiver geometry. The function of the receiver is to collect the incident sunlight and transfer this heat to the cracking sulfuric acid. The heat transfer medium to accomplish this may be the sulfuric acid itself, directly receiving the incident light. It may also be a different fluid which absorbs the heat and then transfers it to the acid either within or outside the solar receiver. The receiver itself may be a single 100 MW central receiver which acts as the focal point for a field of heliostats, or it may be a system of smaller receivers upon which are incident portions of the total energy input. These possibilities are shown in Table 2. Discussions of them plus the structural problems generic to solar receivers follow.

Heat Exchanger Media

Gaseous sulfuric acid may be cracked using solar energy in any of three different systems.

1. The gas can be circulating as the only fluid inside the receiver, the receiver being the only high-temperature heat exchanger in the system.

2. The solar flux may be directed to a second fluid in the receiver. This fluid heats up and transfers the energy to the acid which is also circulating within the receiver.

3. The solar energy can be used to heat a second fluid in the receiver. This heats up and transfers this energy to the acid in a separate heat exchanger located outside the receiver.

The first two systems have the advantage that they require only one high temperature heat exchanger. Moreover, heating the acid directly in the receiver reduces the plumbing complexity, piping losses and unnecessary system entropy increases. Although direct heating of the acid in the receiver exposes it to the potentially non-uniform heating conditions common in solar receivers which makes the chemical reaction more difficult to control, and limits the flexibilities in choosing heat transfer fluids, it was decided that the advantages for this application lie with the system in which the acid is circulating within the receiver. As such, this study concentrated on systems that facilitated this method of heat transfer.

Receiver Types

There are several types of generic solar receivers, each characterized by a particular geometry, solar concentration ratio, and temperature range of operation. Figures 2 and 3 show typical receiver configurations and their operating ranges, respectively. Flat plate and evacuated chamber collectors are at the low end of the solar receiver spectrum, rarely achieving temperatures above 533K (500°F). Single-axis tracking trough collectors, with concentration ratios approaching 100, typically operate with temperatures in the range of 333 to 700 K (200 to 800°F) with a maximum of approximately 811K (1000°F). Of the concepts reviewed, only central receivers located atop a tower in a heliostat field and double-axis tracking paraboloidal dish receivers were capable of the very high concentration ratios necessary for the 1144K (1600°F) working temperature required for this application. The double-axis tracking dish receivers, commonly air heaters, envisioned for use in high temperature Stirling cycles, are typically low-power per module units. This imposes enormous design constraints (or a second operating fluid) on the high-power, uniform heating requirements of the thermochemical sulfuric acid cracking process. Therefore, although the paraboloidal dishes and cylindrical and parabolic trough systems even now on the market could be used for some of the other processes in the water-splitting operation (e.g., charging high temperature salt storage beds or cracking hydrogen iodide), only central receivers were evaluated in detail for this study.

External Central Receiver. The external central receiver considered has a single row of tubes in a cylindrical array whose external boundary is directly exposed to the concentrated light flux of the heliostat field. Ring headers at the top and bottom distribute and collect the heated fluid.

The thermal performance of external receivers suffers greatly because they are completely exposed to their surroundings. Assuming a light absorbing surface of high quality (α = 0.95), 5% of the incident light is reflected from the tube surface and immediately lost. At the high temperatures considered in this study, another 6% of the incoming energy is lost by reradiation; another 1% of the total energy is lost through the combined mechanisms of free and forced convection to the ambient air. Thus, a net receiver efficiency of 88% could be obtained for this unit.

The steady-state structural problems associated with this type of receiver can be attributed to the large tube wall gradients resulting from (1) high heat fluxes (hence large thermal wall gradients), (2) diametral tube temperature differences (temperatures on opposite faces of the tube) caused by insolation hitting only one-half of the total tube surface, and (3) tube-to-tube temperature differences caused by the asymmetric nature of the flux field. In addition, this system possesses little thermal inertia and is very susceptible to rapid temperature fluctuations should the heat flux vary (cloud cover).

Although conceptually simple, this receiver is by no means easy to design and analyze. Many critical pieces of information, both generic to solar receivers and specific to this geometry, need to be experimentally ascertained before design confidence can be obtained. The thermal behavior of the external receiver coatings on highly insolated surfaces for long durations at high temperatures is unknown and must be explored. The protective internal coating, which acts as a buffer between the sulfuric acid and the tube wall, must be completely reliable under these operating conditions. The coatings must not crack off (especially in view of the cyclic loading on the tube walls), and their performance must not degrade.

Little is known about the high Grashof number free convection regime which is the basis for the external boundary condition of the receiver. Even less is known about the combined mechanisms of natural and forced convection and aeroelastic loadings resulting from winds buffeting the receiver atop its high tower. Basic material properties, and thermal, structural, and manufacturing capabilities must be determined, and potentially long-term expensive testing performed, before final design decisions are made.

Cavity Central Receivers. Cavity central receivers are more complex than external central receivers. The cavity receiver tube bundle is similar to the external receiver but has a shell surrounding the cylindrical tube array with the insolation directed toward the interior, rather than the exterior, surface of the cylinder. The shell may be used simply as a protective barrier for inhibiting the energy loss mechanisms of reflection, reradiation, and convection, with the incident light primarily aimed at the interior tube absorbing walls; or it may be used as the first incident light surface, allowing the somewhat asymmetrical incident energy to be evenly distributed by the multiple cavity reflections. The former technique offers much greater thermal efficiency and was used in this study.

As in the external receiver, light entering the cavity and impinging on the tube walls is absorbed with about 5% reflected. For this receiver, however, the reflected light is not lost to the environment; rather, most of the light is internally reflected and absorbed. Only about 1% to 1-1/2% of the incoming energy is lost, depending upon geometry (total size, size of entry port, etc.). Approximately another 1% of the available energy is reradiated from the hot tubes, through the port, and out. Very little can be predicted about the complex natural convection flows into and out of the cavity, particularly without specifying the geometry of design. Scale model tests would be necessary to determine convective losses and a value of 1/2% was assumed to be typical.

In addition to the increased thermal efficiency of the cavity receiver over the external receiver (97% versus 88%), a slightly increased flux uniformity, due to internal reflections and reradiation may be anticipated. However, spillage, the amount of light reflected towards the receiver from the heliostat field but not hitting it, is larger in a cavity than an external receiver because the apparent target, the aperture, is much smaller.

Fluidized Bed Central Receivers. A fluidized bed heat exchanger consists of an array of tubes immersed in a bed of fine (10 to 1000μ) particles. A flowing gas percolates throughout the bed, causing fluid behavior of these particles. Such beds can exhibit great thermal mixing (uniform temperature), high heat transfer rates, and the ability to dissipate large heat fluxes. It is of particular interest that the heat exchanger tubes themselves typically occupy only 10% of the bed volume; hence, the total volumetric heat capacity of a fluidized bed can be orders of magnitude greater than that of the tubes alone.

In contrast to the previously described solar receivers, in a fluidized bed the tubes containing the sulfuric acid working fluid are exposed to a very uniform heat flux (which is beneficial both chemically and structurally) between tubes and around a single tube. This type of receiver also exhibits a more favorable response during transient operations.

Because the efficiency of the fluidized bed receiver is about equal to that of the external receiver, it is worthwhile to compare the transient response of the tube walls of the two receivers during rapid shutdown, i.e., cloud cover (Fig. 4). The slow transient of the high capacitance bed (compared with immediate response of the external receiver) coupled with the temperature uniformity discussed earlier gives the fluidized bed distinct design advantages for long-term use.

Direct Absorption Receivers. The direct absorption receiver consists of tubes immersed in a liquid bath. Its heat is picked up by a curtain of liquid cascading down the exposed walls (or past the open windows) of the receiver and directly absorbing the incident light. This system has the appearance of an external receiver and the thermal capacitance of a bed. Its potential advantage is that it decreases reradiation losses because there is no temperature drop through the receiver walls to the working fluid. Hence, the temperature of reradiation is as low as possible. This is particularly desirable when the hot working fluid can be the primary heat transfer medium (i.e., molten salt). However, in the case studied, the sulfuric acid cannot be directly exposed in this manner, and an even hotter, secondary fluid curtain temperature must be obtained to drive the immersed bed heat exchanger. For the working temperatures necessary, reradiation losses could not be reduced to less than 25%; therefore, this concept does not appear attractive.

Structural Considerations

In light of expected operating temperatures of up to about 1144 K (1600°F), structural considerations for the unit are critical. At such temperatures, allowable material stresses for extended operating times and frequent temperature changes (due to insolation variations) are small. Consequently, the pressure and dynamic loadings require that the components be relatively thick. However, this could lead to conflicting design requirements, because thermal stress generally increases as thickness increases. In extreme cases, simultaneous satisfaction of both the pressure and thermal stress criteria is impossible, and no design would exist for the material, geometry, and operating condition constraints under consideration. Therefore, an envelope of acceptable designs with boundaries defined by the various competing and limiting structural considerations is needed. Thus, it is

important to review candidate geometries early in the program, after initial receiver screening, and evaluate them with respect to both performance/sizing and structural capabilities. A by-product of this analysis is a description of concept operating envelopes. Structural design equations suitable for conceptual design must be developed for each selected heat exchanger concept in order to do these evaluations.

The major considerations are typically pressure containment and thermal stresses, such as those due to the temperature difference through the tube wall, across the tube diameter and between tubes. Other tube thermal stresses may also develop due to temperature differences between the tubes and their support structure, particularly those arising during transient heating conditions (e.g., startup, shutdown and insolation variations). Such temperature differences are a strong function of component response time which is directly proportional to component thermal capacitance. Designs with slow response times (large thermal capacitance) would limit such temperature differences and would be preferred. At present, the only measure of tube/structure thermal stresses is the comparative thermal capacitance since the complete structural concepts are not yet defined. These and other stresses are limited by material strength characteristics, which are a function of maximum material temperature. Thermal stresses are cyclic in nature and, therefore, have an allowable stress range which is a function of operating conditions. Expected operating conditions depend on the time-dependent characteristics of the solar heating. Hence, for elevated temperature designs in which operating thermal stresses are comparable to allowable cyclic stresses, there are severe restrictions on geometry, operating conditions, and material. Thus, it is necessary to select the best material by comparing the strongest of the wrought superalloys (e.g., Alloy 800H, Haynes 188, Inconel 617, or Hastelloy X) with the best ceramics (such as alpha-sintered silicon carbide or silicon nitride). It is possible that in the temperature ranges of interest and because of the cyclic thermal stresses, superalloys may only be acceptable for a limited design lifetime compared with ceramic materials.

Allowable cyclic stresses must be specified for the candidate materials before the structural concepts can be evaluated. Therefore, the expected operating cycles must be defined and the associated material behavior determined. Two types of operating cycles are generally expected to be critical: (1) a strain cycle with a single hold time and (2) a strain cycle with two hold times. For steady operations during the day, with shutdown to low temperature conditions at night, the governing material stress-strain cycle is characterized by a repeating hysteretic cycle with a sustained strain application (hold time) during the day. During the daily sustained strain application, creep relaxation occurs, and associated material creep damage must be within acceptable limits. When temperature changes associated with insolation fluctuations occur during the day (e.g., because of cloud cover), the governing cycle can be characterized by a strain cycle with two hold times, one at maximum heating rates and the other at a lower heat input. Elevated temperatures persist during the entire cycle so that there is creep relaxation at both cycle extremes. Operations with two hold times have more severe consequences for materials than the single hold time cycle and generally have lower allowable cyclic stress ranges. The creep data currently available for certain candidate materials may be insufficient for detailed life calculations. However, approximate allowable stress curves for the conceptual and preliminary design can be estimated from limited creep rupture data, which are generally available.

The structural supporting effort should basically consist of two different design phases: (1) initial concept definition (structural equations) and selection and (2) detailed design of a test component. It should be emphasized that, for the severe conditions anticipated in all candidate designs, structural efforts must be integrated with performance and sizing analyses and cannot be delayed until later design stages.

Heat Receiver Comparison. A comparison of the central receivers considered in this study, summarized in Table 3, shows that the cavity design is the preferred concept from the standpoint of thermal efficiency. However, structural requirements indicate a preference for designs with relatively small temperature gradients and large thermal capacitance. Hence, the fluidized bed concept may be competitive when both performance and structural upsets are considered. As such, these two different concepts should be studied further in a second conceptual design phase to define specific receiver geometries. This would allow determination of the structural integrity of the concept and the economic tradeoffs between the cavity and fluidized bed receivers.

Energy Storage Evaluation

Molten salt and the $SO_2 \rightleftarrows SO_3$ chemical conversion system have been chosen as the two energy storage candidates for providing the means to drive the lower temperature portions of the water-splitting cycle at night. Technical and cost comparisons of these two energy storage approaches will be made.

Molten Salt Storage

Sensible heat storage, rather than latent heat of fusion storage, has been selected as a result of DOE-funded studies of energy storage in solar power plants. It presents fewer technical uncertainties, it has acceptable cost, it provides heat over a range of temperature to match process heat demand, and there is some industrial experience with this technology. Draw salt (a 50% molar mixture of sodium nitrate and potassium nitrate) is the selected storage medium. It has low vapor pressure and, therefore, can be stored in unpressurized tanks, and with the proper cover gas and containment materials, it has good stability up to temperatures of 867K (1100°F).

A two-tank (hot and warm) approach, as opposed to a thermocline tank, was selected along with external thermal insulation to limit heat loss. The heat loss from the tanks is only a few percent.

Chemical Energy Storage

Figure 5 shows the process flowsheet for the SO_2-O_2 recombustion system for supplying the heat and work to the sulfur/iodine water-splitting cycle when there is no effective insolation. Material and energy balances have been prepared. The matching of this system to the energy demand is

needed before comparing its thermodynamic performance to that of the load matched draw salt energy storage system. The portion of the system flowsheeted thus far loses about 6% of the availability* [potential ideal work for a reject heat temperature of 300K (80°F)] for the material input/output conditions which have been specified. However, the input materials must be made by a similar but reversed reaction in the main water-splitting process. The availability loss with respect to captured solar heat, at the temperature at which it is exchanged into the main process SO_3 decomposer, will be nearly the same as the loss in the SO_2-O_2 combustor. The overall heat capture-and-recovery thermodynamic performance will, therefore, be at least 12% less than the initially captured availability and can be expected to have a similar effect on the overall energy efficiency of those storage-driven portions of the water-splitting process.

Tentative early indications are that it will be more economical to store SO_2-O_2 as gas at one atmosphere in telescoping gasholders than to compress the mixture and store it as a liquid SO_2-gaseous O_2 mixture.

Acknowledgment

This work was performed under JPL Contract No. 955263. Dr. Chris England is the Program Manager at JPL.

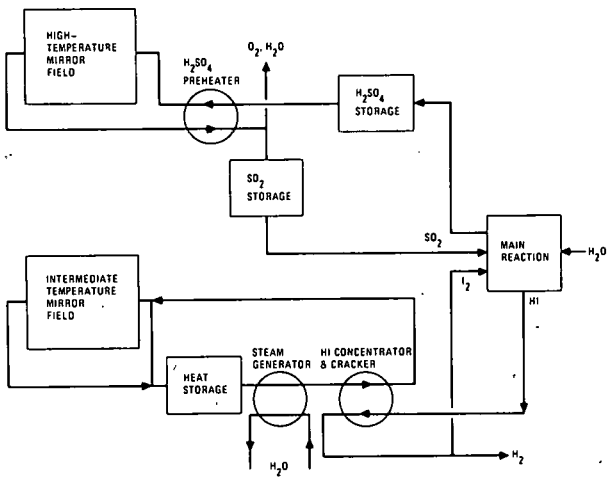

Fig. 1. Possible solar/thermochemical water-splitting configuration

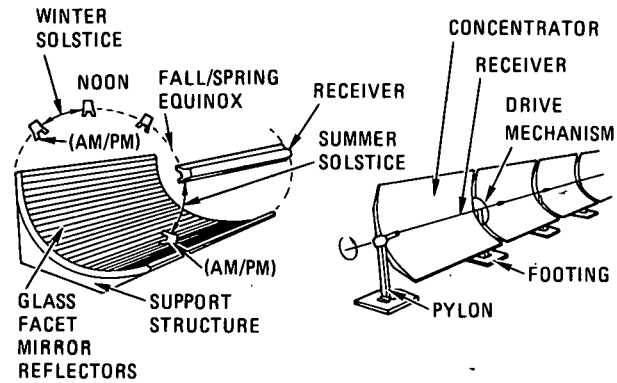

SINGLE AXIS TRACKING TROUGH COLLECTORS

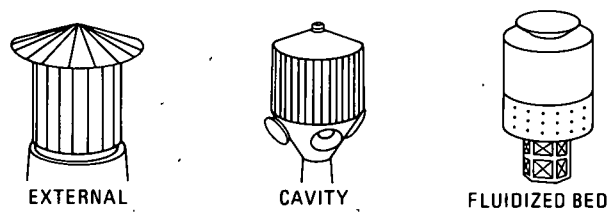

CENTRAL RECEIVERS

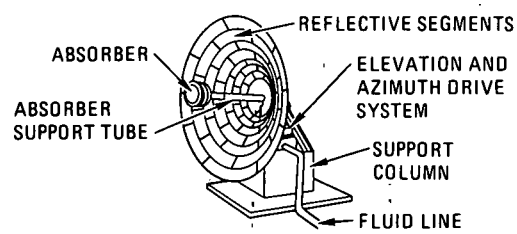

TWO AXIS TRACKING PARABOLOIDAL DISH COLLECTOR

Fig. 2. Typical receiver configurations

*The overall reaction has an availability (maximum work potential) of 136.5 kJ/0.993 g-mole H_2 product for an enthalpy of reaction of 186.6 kJ/0.993 g-mole H_2 product.

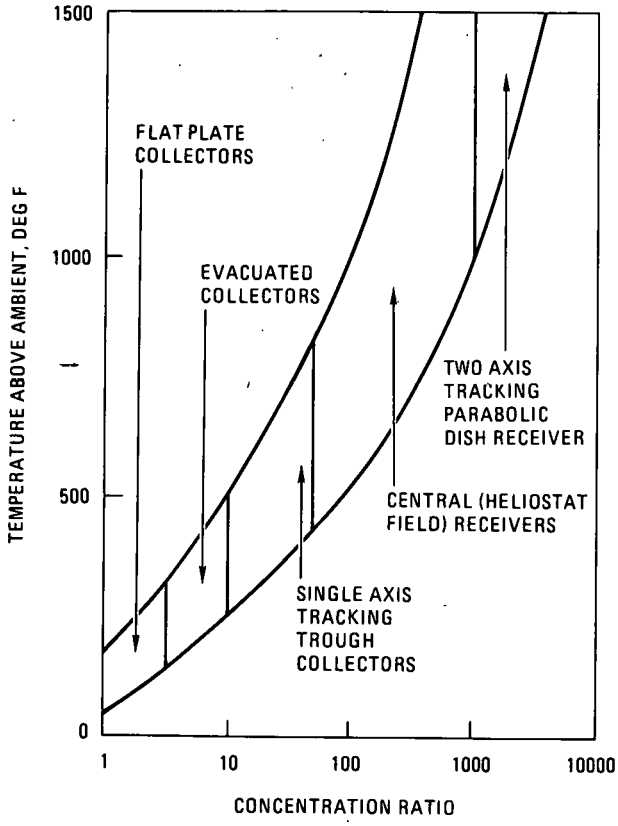

Fig. 3. Receiver Typical Operating Temperature Ranges

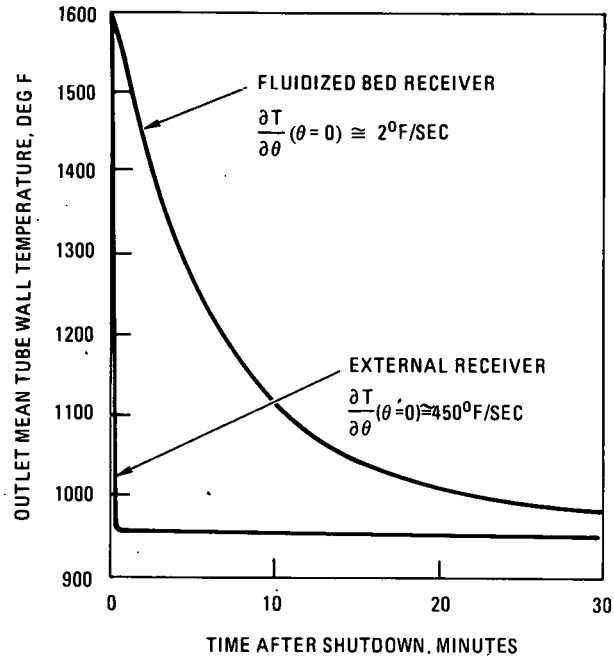

Fig. 4. Receiver Response Times to Shutdown Conditions (Chemical Equilibrium Effects Neglected)

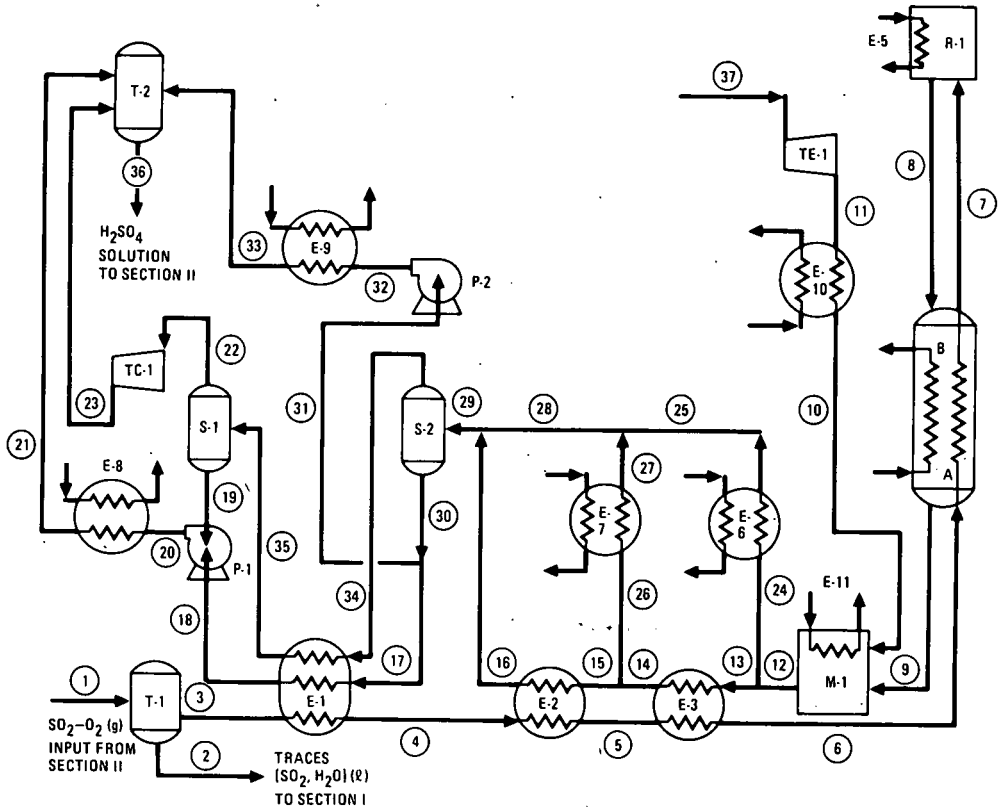

Fig. 5. SO_2–O_2 Combustion System

Table 1

SYSTEM CONSTRAINTS FOR HIGH-TEMPERATURE SULFURIC ACID SOLAR RECEIVER

Operating Conditions

Tubeside

Pressure	517 kPa (75 psia)
Temperature	800K (980°F) inlet; 1144K (1600°F) outlet
Fluid	90 kg/sec (200 lb/s) gaseous H_2SO_4 flowing over catalytic bed

Shell Side

Pressure	103 kPa (15 psia)
Temperature	311K (100°F)
Fluid	Air flowing at 3.58 m/s (8 miles/hr)

System Design Basis

100 MW(t) heat load required at high temperature

1 MW/m^2 (1000 suns) average heat flux

±50% insolation maldistribution around receiver

8-hr continuous daily operation; night shutdown

Reasonable life (10+ years)

All materials coated to minimize corrosion

Table 2

HIGH TEMPERATURE RECEIVER DESIGN OPTIONS

I. Fluid Medium

A. Direct insolation of H_2SO_4 within receiver.

B. Direct insolation of another fluid within a receiver containing that fluid and the H_2SO_4.

C. Direct insolation of another fluid within the receiver with the H_2SO_4 heated in a separate heat exchanger.

II. Design Geometry

A. Distributed point and line focus receiver systems

1. Single axis tracking trough
2. Double axis tracking parabolic dish

B. Central Receivers

1. External
2. Cavity
3. Fluidized bed
4. Direct absorption

Table 3

RESULTS FOR CENTRAL RECEIVER DESIGNS

	Efficiencies (%)				Temperatures[a] Differences °F			Thermal Capacitance ρVC_p (Btu/°F)	(b) Overall Receiver size-ft.	Tube size[c] (in.)
	Overall Efficiency	Reflective Loss	Reradiation Loss	Convective Loss	Tube Wall	Tube Diametral	Tube to Tube			
External	88	5	6	1	20	50	20	250	13D x 26H	0.5d x 0.01t
Cavity	97	1.5	1	0.5	20	50	18	250	10D x 18H	0.5d x 0.01t
Fluidized Bed	88	9	1	2	10	0	5	50000	23D x 30H	0.5d x 0.05t
Direct Absorption	68	5	25	2	10	0	5	50000	23D x 36H	0.5d x 0.05t

(a) Estimates based on mean expected heat flux levels at tube outlet

(b) D = Receiver diameter; H = Receiver height

(c) d = tube diameter; t = tube wall thickness

A Study of Industrial Hydrogen And Syngas Supply Systems

Wm. J. Amos, J. Solomon

Air Products & Chemicals, Inc.
Allentown, Pennsylvania

This summary outlines the work performed and conclusions reached under JPL Contract No. 955421.

This study evaluates the potential and incentives required for supplying hydrogen and syngas ($2H_2/1CO$) feedstocks to the U.S. chemical industry from coal gasification systems. Future hydrogen and syngas demand for chemical manufacture is estimated by geographic area. Projected economics for hydrogen and syngas manufacture are estimated with geographic area of manufacture and plant size as parameters. These estimates are made for natural gas, oil and coal feedstocks. The economic estimates for coal technology involve different coal type, lignite and bituminous, and also atmospheric and elevated pressure gasification.

Several problem areas presently affecting the commercial feasibility of coal gasification are considered in this study. The impact of potential process improvements are considered via the impact of hypothetical capital and operating cost improvements on hydrogen and syngas economics. Unique factors involved in financing coal gasification plants are discussed. Regulatory barriers are evaluated as they affect coal gasification. Coal mining/transportation, air quality regulations, and competitive feedstock pricing barriers are evaluated in summary fashion.

Finally, the study discusses the potential for making coal gasification the least costly H_2 and syngas supply option. Options to stimulate coal gasification system development are discussed.

Task 1. Evaluation of Chemical Industry Capacity Requirements and Projected Economics

Projected Chemical Industry Capacity Requirements

Chemical industry hydrogen (H_2), carbon monoxide (CO) and syngas (H_2/CO) capacity addition requirements during the 1978-1982 period are expected to amount to about 800 MM SCFD. The total will be dominated by chemical plant capacity additions in ammonia and methanol. About 80% of the expected 1978-1982 new H_2/CO syngas requirements are expected to be used for ammonia and methanol. This figure is somewhat misleading since the hydrogen requirements for ammonia, over 50% of the 1978-1982 total, resulted from plants planned in the mid-1970's when ammonia prices peaked.

The other major H_2/CO/syngas market categories will be about equally important during the 1978-1982 period. These general market categories are oxo alcohols, polyurethanes, fibers, and other chemicals. Requirements over the five year period will be in the range of 20 MM SCFD to 40 MM SCFD for each category. Polyurethanes are expected to be the largest market of the four, with the largest single factor in polyurethanes use being hydrogen for aniline.

The other chemicals category uses of hydrogen and carbon monoxide will be dominated by use of carbon monoxide for acetic acid production. Oxo alcohols, primarily solvent alcohols, will require about 20 MM SCFD syngas during the '78-'82 period.

Projected H_2/CO/syngas net additional markets will amount to about 450 MM SCFD during the 1983-'87 period. This is only about 60% of the projection for the previous five year period. No ammonia capacity additions are expected. Projected syngas requirements for methanol amount to about 75% of the total H_2/CO/syngas requirements for '83-'87. The oxo alcohols market is also projected to be strong during that period amounting to about 60 MM SCFD of syngas. Polyurethanes H_2 and CO requirements will decline to about 30 MM SCFD. New technology for chemical manufacture using H_2/CO/syngas is not expected to be an important factor in terms of new capacity brought on line between now and 1987.

Comparison of H_2 and Syngas Costs From Alternate Feedstocks

The costs of H_2 and syngas product via gasification of coal was compared with partial oxidation of residual oil and steam reforming of natural gas. All product cost calculations are in terms of 1978 dollars, with only energy costs assumed to escalate over a 15 year project life.

These comparisons were based initially on the draft JPL Energy Scenario developed in the Fall of 1978. The world petroleum market underwent severe upward price disruptions during the early months of 1979. This stiuation required a revision of the Energy Scenario projections used in economic comparisons.

The economic comparisons of alternate H_2 and syngas production costs which were used in this study are based on a combination of two criteria - return on equity invested in the project and discounted cash flow return. Both criteria were used assuming the equity owner of the project was an independent single project company. In the case of return on equity, a value was selected which resulted in both an acceptable initial year return and approximately level after tax book returns over the project life. This assumption follows from the usual preference among lenders for a level or increasing income stream from individual projects. Discounted cash flow return calculations assumed only income streams and tax payments from the project itself with regard to the utilization of investment tax credits and capital depreciation. This approach was used in order to put the basic feedstock/technology comparisons on the basis of the project itself, and therefore independent of the effects on the economic comparisons of income streams and tax payments associated with the other businesses in which the equity principal might be involved. In the case of a project specific situation, the evaluation of various feedstocks would of course include such effects consistent with the ability of the owner to utilize the available tax credits in early years of the project and consistent with the owner's actual investment analysis philosophy. Detailed methodology is further de-

scribed in the study; however, the approach employed results in a "year one" price and projected escalation curve for each feedstock/technology case considered, incorporating (1) the two above mentioned financial criteria, (2) the revised energy scenario, and (3) the relevant capital and operating costs. Hence, the competing feedstock/technology comparisons in this summary are described in terms of the "year one" component and the escalation curve component of the overall economic comparison.

The economic comparison of H_2 and syngas costs on coal, oil and natural gas feedstocks were computed for several parameters: (1) year of plant start-up, (2) geographic location of plant, (3) plant size and, (4) coal type. Conclusions based on the revised energy scenario and the above study bases for plants starting up in years 1982, 1987 and 2000 were as follows:

1. With one exception, coal-based H_2 and syngas were not estimated to be price competitive in year 1 of plant operation for any of the plant start-up years, plant size/slate and geographic regions studied. The only exception was the production of 150 MM SCFD hydrogen in the Ohio Valley with start-up in year 2000.
2. Conclusions on hydrogen and syngas product cost escalation for 1982 and 1987 plant start-up were as follows:
   a. In the Ohio Valley and Mid-Atlantic regions, oil feedstock was projected to result in average product price escalations at least twice as high as escalations for coal. Natural gas feedstock was projected to result in price escalations about five times greater than coal.
   b. In the Gulf Coast region, oil was projected to result in product escalations about 50% higher than coal. Product price escalations based on natural gas were projected to be at least twice as high as escalations for coal.
3. The competitive position of coal was projected to improve sharply for start-up years 1982 and 1987 in the major market identified, syngas. The average 1982 price premium for syngas from coal was about 50% at 40 MM SCFD and about 35% at 150 MM SCFD. By 1987 the premiums dropped to approximately 30% and 15%, respectively.
4. For the major chemical feedstock market identified in this study, syngas, natural gas was evaluated to have the lowest cost in initial year of plant operation for plants starting up in 1982. Oil was evaluated to have the lowest cost in initial year of plant operation for plants starting up in 1987 and 2000.
5. For the hydrogen product slate, natural gas was evaluated to have the lowest cost in initial year of plant operation for all plant start-up years evaluated, 1982, 1987 and 2000.
6. For both syngas and hydrogen and for plant start-up years 1982, 1987 and 2000, the Gulf Coast region had the lowest evaluated product cost followed by the Ohio Valley region. The Mid-Atlantic region was evaluated to be the highest product cost region.
7. Lignite and bituminous coal types were compared for both product slates and plant sizes in the Gulf Coast region. Lignite resulted in about a 10% premium in product price compared with bituminous. The higher capital and lower efficiency of lignite gasification more than offset the lower cost of lignite feedstock.

Task 2. Analysis of Problem Areas and Options To Stimulate Coal Gasification System Development

Analysis of Gasification Improvement Incentives

The effect of potential research and development impact on coal gasification economics was estimated by calculating product prices for capital cost improvements of 10%, 20% and 30%, and operating cost improvements of 10% and 20%.

Based on the above, capital cost and operating cost improvements resulted in no R&D cost reduction result which would make coal gasification competitive in the year of plant start-up with reforming, the most economic syngas option at 150 MM SCFD in 1982. A 30% capital improvement made coal competitive with oil at 150 MM SCFD syngas in 1987 when oil is the most economic alternative.

Cost comparisons of pressurized vs. atmospheric coal gasification were made for a Gulf Coast location producing syngas. Results at both 40 MM SCFD and 150 MM SCFD indicated an economic advantage of approximately 14% for pressurized gasification for design conditions of 350 psig product gas. While pressurized gasification economics were thus projected as more favorable than atmospheric pressure gasification, the difference was not large in relation to the accuracy of the estimates.

An economic evaluation was also made of co-producing fuel gas and syngas. The comparison assumed incremental medium Btu fuel gas production on a previsouly justified 150 MM SCFD syngas plant. The incremental fuel gas production was assumed to be 150 MM SCFD of medium Btu gas. Based on the revised Energy Scenario, incremental fuel gas was not competitive for 1982 or 1987 plant start up with either natural gas of fuel oil. Incremental medium Btu fuel gas is projected to be more than twice as expensive as natural gas in 1982 and 25% more expensive in 1987. The premium above fuel oil as calculated to about 20% in 1982 and 10% in 1987.

Analysis of Non-Technical Problem Areas and Options to Stimulate Coal Gasification System Development

Non-Technical factors present major barriers to construction of coal gasification plants. Two of the most important non-technical factors which can significantly affect coal gasification system development are discussed below.

While financing approaches can significantly affect projected product price, alternative project financing methods generally reflect the allocation of business exposure factors between the product buyer and product seller. The allocation process has been analyzed in this study according to two key effects of financing approach: the effect of capital structure in initial price and

the effect of debt leverage on the project return on total investment. Variation of debt/equity ratio from 0/100 to 75/25 affects initial year product price in the range of 10-15%. Increasing the debt interest rate from 8% to 10% increases initial year product price less than 5% for debt/equity and DCF return on equity criteria. The effect of debt leverage on project return on investment was calculated. Alternate debt/equity ratios and debt interest rates were considered for specific discounted cash flow returns on seller's equity and, as expected, the effect of leverage was significant. For example, a change from 0/100 debt/equity to 75/25 debt/equity had the impact of decreasing required return on total investment from 15% to 11.5% assuming the DCF return on equity is 15%. With a 20% DCF return on total investment, the ability to leverage the project from 0% debt to 75% debt results in an even greater decline in project return, from 20% to about 13%. Other financing approaches with potentially even lower apparent capital costs can be considered, such as leveraged leases; however, these and any highly leveraged approaches cannot be considered in the abstract, as is often done. The business arrangement between buyer and seller must first be defined before any financing approach or cost of capital can be meaningfully considered.

Among the various regulatory barriers affecting coal gasification, oil and natural gas pricing uncertainty are the most significant. Given the nature of the political process which determines U.S. oil and natural gas prices, the indirect regulatory barriers to coal gasification which result from historical price controls present a very difficult commercialization problem. Over the 1982-1987 period, this study projects that rapidly escalating oil and gas prices will reduce the "year one" premium of coal-based syngas to about 15%. However, the actual gap could be significantly different depending on the extent to which, directly and indirectly, the government affects the prices of oil and natural gas. Fortunately a reduction of government influence in the pricing of conventional energy appears to be underway. As this trend continues, government efforts to stimulate coal gasification system development will have a higher probability of success, as the current "subsidy gap" between the cost of gasified coal and the cost of H_2 and syngas from conventional feedstocks decreases through the effects of market forces.

Recommended Options to Stimulate Coal Gasification System Development

The economic analyses completed in this study indicate a requirement for significant additional financial incentives in order to place coal gasification in a competitive position for hydrogen and syngas production. The financial incentives which are most likely to succeed are those of a "front end" type which provide direct or indirect cash flow impact definable prior to start-up of a plant. Cash grant, cost share, and legislatively implemented investment tax credit and rapid write off are possible front end options.

There are three distinct areas considered in this study for the stimulation of coal gasification system development. Those areas are: (1) Government R&D expenditures that would significantly reduce coal gasification product costs, (2) significant reduction of government participation in pricing of oil and natural gas and (3) government encouragement of pioneer coal gasification plants through appropriate financial incentives. These areas are discussed in the following paragraphs.

For syngas, the major chemical feedstock market identified in this study, a coal gasification R&D effort resulting in a 30% capital cost reduction and a 20% operating cost reduction was evaluated. Syngas from a 1982 commercialization of these R&D results was projected to cost more than syngas from natural gas. By 1987, when oil was projected to be the least cost syngas option, a 30% reduction in coal gasification plant capital cost would be required to produce product competitively priced in the year of start-up. These R&D results would be difficult goals and do not appear to justify a massive Government R&D program.

The most important variable in coal gasification system development is expected to be competitive feedstock costs. Government involvement in U.S. energy pricing has clouded potential coal gasification plant investor's views of future competitive economics. For example, the premium in initial year of operation for syngas from coal was projected to be about 15% in the mid-1980's over the projected least cost feedstock, oil. An initial 15% premium might be acceptable to some plant investors today if other institutional barriers could be successfully dealt with and if the continuing potential of reimposed price controls on domestic oil and gas could be eliminated.

Under the financial analysis assumptions developed for this study, conventional ITC and accelerated depreciation are not sufficient incentives to make coal gasification competitive in the year of plant start-up, until 2000. Accelerated depreciation directly affects only the timing of cash flows and not the amounts. ITC affects both, providing taxes would otherwise be payable. As previously noted, the syngas producer on which this study is based, is assumed to be a separate company and thus, the amount of ITC and depreciation which benefits the company is constrained by pre-tax profit. This assumption was made in order to address the broadest range of business situations, including those which are constrained in the use of ITC and depreciation. In those specific situations where such constraints do not exist, accelerated depreciation and increased ITC can of course be effective incentives.

In summary, the most effective methods for stimulating coal gasification system development appear to be cash grant and cost share approaches as supplements to ITC and acclerated depreciation. These approaches can be implemented most effectively when a return on investment criterion for private capital is set and implemented as the project develops. In this way the tendency toward often unattainable goals such as initial firm determination of government cash grant or cost share amounts can be avoided. While such goals may be attractive in theory to the Government from a budgetary point of view, as a practical matter they can result in (1) discouraging all but very large companies or consortia from participa-

tion due to the magnitude of the projects, particularly in light of the many other project risks which have not been discussed in this summary - government design/construction/operation approvals, environmental law changes, etc. - which must be evaluated and provided for, and in light of the above, (2) requests for Government grants or cost share which may appear unrealistically high in order to provide for those business risks which are inherently very difficult to quantify.

These same basic shortcomings of "fixed amount" incentives also apply to production credits or subsidies unless specifically eliminated by the enabling legislation which would implement this type of incentive.

HYDROGEN FROM COAL - COST ESTIMATION SEMINAR

R. L. Woolley

Billings Energy Corporation
Provo, Utah

Abstract

A cost estimation seminar, sponsored by the U. S. Department of Energy, administered by Jet Propulsion Laboratories and hosted by Billings Energy Corporation was held at Snowbird, Utah on June 11-15, 1979. Presentations were made by several industrial organizations having potential involvement in coal operations, coal transportation, gasification, purification, and delivery of hydrogen.

Data was provided on equipment selection and component cost for a Koppers Totzek process by Koppers Engineering and Construction Company and for a Winkler process by Davy PowerGas. Both plans were developed in terms of a large facility to be sited in Southern Utah.

The cost of hydrogen from these plants was evaluated on a common basis using a computerized model patterned after the EPRI Technical Assessment Guide.

The Koppers plant was more costly than the Winkler, primarily because it was a grassroots design. Citing the following Koppers data as conservative, the following conclusions resulted. A plant with a capital cost of 1.66 billion dollars will produce 396 billion BTU/day (HHV) of hydrogen (4835MW). The product gas is 97.36% hydrogen by volume with the balance as follows: 1.96% methane, .17% argon, .51% nitrogen, less than 5 ppmv CO, 3 ppmv CO_2, 1 ppmv H_2S, and 2 ppmv H_2O.

Using agreed upon financial assumptions applied to the cost model, 13.48% of the 1.66 billion dollar capital cost must be returned each year. Annual costs are as follows:

Capital	223.8 million dollars/year
Labor (435 employees)	12.1
Variable operation & maintenance cost	31.4
Coal (12 million tons/yr at 22 $/ton	263.7
	531 million dollars/yr

These annual costs imply a hydrogen cost on a first year basis of 4.07 $/million BTU or 25 cents per pound of hydrogen.

Pipeline distribution adds 6 tenths cent per pound per 100 miles of pipeline according to data presented at the seminar.

To compare these costs to gasoline use the experimental result that 2.0 pounds of hydrogen provide the same driving range as one gallon of gasoline. This assumes that a hydrogen vehicle is 12.5% more efficient than its gasoline counterpart and is backed by data on a Postal Service Jeep which was 15% more efficient. Other costs that are added to compare to the pump price of gasoline are 10% retailing markup, 4 cents per gallon federal tax and 9 cents per gallon state tax. This results in a comparative cost of hydrogen of 81 cents per gallon.

By way of comparison, the amount of capital used to purchase two and one-half years of imported crude oil at 20 $/bbl would pay for the construction of enough coal to hydrogen plants (89 at a cost of 1.66 billion dollars each) to eliminate imported crude oil. The amount of hydrogen produced would equal the consumption of the four major fuels made from petroleum (motor gasoline, diesel oil, home heating oil, and jet fuel). Fifty hydrogen plans would provide fuel energy equal to the gasoline production from imported crude oil.

PROGRESS REPORT ON THE DEVELOPMENT OF THE GENERAL ATOMIC THERMOCHEMICAL WATER-SPLITTING CYCLE

G. E. Besenbruch, J. H. Norman, K. H. McCorkle
J. S. Rode, G. Caprioglio, R. Sharp
General Atomic Company
San Diego, California

and

M. Yoshimoto
Idemitsu Kosan, Co., Ltd.
Tokyo, Japan

Abstract

The major accomplishments on the DOE funded part of the total GA thermochemical water-splitting program are reported. They include:

1) Incorporation of significant process improvements into the process.
2) Development, review, and revision of an engineering flowsheet.
3) Screening, identification, and testing of potential materials-of-construction for the corrosive process fluids.
4) Increase of the process efficiency to ~47%.
5) Small-scale demonstration of the cycle in a closed loop under recycle conditions.
6) Installation of the next phase of scale-up equipment (bench-scale) and demonstration of parts of the process in this equipment.

The results of the work carried out during the last year have demonstrated that thermochemical water splitting by the sulfur-iodine cycle is a feasible process and have provided some confidence that thermal efficiencies as large as 50% are achievable.

Introduction

A program to investigate thermochemical water splitting has been underway at General Atomic since 1972. The sulfur-iodine cycle was selected after an extensive computer search of thermodynamically possible systems.

The cycle can be described by the following three chemical equations:

$$xI_2 + SO_2 + H_2O \rightarrow H_2SO_4 + 2HI_x \qquad 370\ K \qquad (1)$$

$$2HI_x \rightarrow H_2 + xI_2 \qquad 393\ K \qquad (2)$$

$$H_2SO_4 \rightarrow H_2O + SO_2 + 1/2\ O_2 \qquad 1144\ K \qquad (3)$$

In these equations, HI_x represents the average of several HI_n compounds formed in the initial solution reaction. Separation of the H_2SO_4 and HI_x takes place under gravity, since the two acids are nearly immiscible. The upper phase contains most of the H_2SO_4, and the lower phase contains most of the HI_x.

The main attributes of the cycle are that its thermal efficiency is expected to be high (about 50%) and that it can be conducted as an all-liquid and gas-phase process, a characteristic that should give it considerable engineering advantage over any cycle requiring solids handling. Also, during 1978, operation of the process in a closed loop under recycle conditions was demonstrated.

The process development is proceeding in four major areas:

1) Basic chemical investigations.
2) Materials investigations.
3) Process engineering studies
4) Bench-scale testing.

Chemical and materials investigations are under the joint sponsorship of the Gas Research Institute and GA; the engineering studies, the closed-loop cycle demonstration, and the bench-scale testing are sponsored by the U.S. Department of Energy (DOE), Hydrogen Storage Systems.

Process Engineering Studies

The process engineering design effort for the water-splitting cycle at GA was based on the following objectives and constraints:

1) Energy is supplied by a process heat high temperature gas-cooled reactor (HTR) having a helium inlet temperature of 772 K and an outlet temperature of 1265 K.
2) Process power is supplied from the helium loop and from a low-temperature, process-bottoming cycle.
3) The temperature match-up of the helium heat delivery line and the process heat demand line must be good to maintain efficiency.
4) Heat must be reused within the process until it is at such low quality that it must be rejected.
5) Reasonable estimates are used for unavailable thermochemical data.

Figure 1 illustrates the sulfur-iodine cycle process model, which consists of four distinct sections:

1) Section I produces the acids H_2SO_4 and HI from H_2O, SO_2, and I_2. The SO_2 that is fed to this section contains all the O_2 generated by the decomposition of the H_2SO_4. The O_2 product is removed from this section.
2) Section II concentrates and decomposes H_2SO_4 received from Section I.
3) Section III removes the unreacted SO_2 from lower phase product [HI_x (sol)] and then separates it into HI, I_2, and H_2O using H_3PO_4.
4) Section IV decomposes HI into H_2 and I_2 and separates products. The H_2 product is taken from this section.

5) Section V, not shown in the figure, is the intermediate helium loop that combines the helium-related parts for the delivery of nuclear heat and the generation of process power.

The second iteration of the flowsheet has been completed. This second iteration incorporates several new process improvements into the flowsheet, resulting in an increased theoretical efficiency to approximately 47%. These improvements include:

1) Elimination of the cryogenic SO_2/O_2 separation. The gas mixture is fed into the main reaction vessel where SO_2 is extracted. The remaining oxygen is water-washed and discharged.
2) Increase of the sulfuric acid concentration to ∿57% (wt.) through a boost reaction. The upper phase (H_2SO_4 - 50%) is reacted with liquid iodine and SO_2 to bring the concentration to ∿57%.
3) Utilization of a lower concentration phosphoric acid extraction system. In this process the lower phase ($HI/I_2/H_2O$) is treated with phosphoric acid and hydrogen iodide and water are extracted from the system.
4) Decomposition of hydrogen iodide in the liquid phase. The HI is liquefied with pressure and the decomposition is carried out using catalysts being developed at GA.

Figure 2 is a simplified diagram of Section I. The main solution reaction is initiated above the melting point of I_2 (386.5 K) using recycled I_2, SO_2, H_2O, and feed H_2O. The H_2SO_4 - HI_x liquid phases leave the bottom of the main solution reaction column at 368K, and the immiscible solutions are then separated by gravity. The upper phase (H_2SO_4) is treated with liquid I_2 and SO_2. This increases the H_2SO_4 concentration from 50% to 57 wt%. The evaporation step for the HI-I_2 heavy phase is to thoroughly remove the residual SO_2 under conditions sufficiently mild that the SO_2 and HI do not react. The heat output from the main solution reaction column is used to drive the low temperature bottoming cycle.

Figure 3 illustrates Section II, in which aqueous H_2SO_4 (∿57 wt%) is concentrated and decomposed into H_2O, SO_2, and O_2. The H_2SO_4 feed received from Section I is concentrated to 98 wt% in a series of flash evaporation stages at a pressure level of 200 kPa. The concentrated acid is then vaporized at 686 K and decomposed throughout its heatup to 1144 K, the maximum process temperature in the cycle. The last part of this heatup, from 800 K, is done in the presence of a catalyst to facilitate the decomposition of SO_3 into SO_2 and O_2. The reactant mixture is then disengaged from the catalyst and cooled down. Eventually, undecomposed SO_3 forms aqueous H_2SO_4, which at a concentration of 72 wt% is separated from wet SO_2/O_2 mixture and recycled to the third concentration stage. The wet SO_2/O_2 product is sent back to Section I.

Figure 4 illustrates Section III, in which I_2 is separated from HI and H_2O by liquid-liquid extraction using 95 wt% H_3PO_4 solvent. The extracted HI is then concentrated and dehydrated by extractive distillation from the H_3PO_4 solvent. The overhead from the extractive distillation containing 75% HI, 25% I_2, and traces of H_2O, S, and H_2S is then separated, giving an overhead stream of dry HI. The overhead stream is compressed and sent to Section IV for cracking, while the I_2 bottomstream is recycled to Section I. The wet H_3PO_4 is dried by a multistage vapor recompression evaporation system and recycled to the extraction stage.

Figure 5 illustrates Section IV, in which anhydrous HI from Section III is decomposed into H_2 and I_2. The feed is decomposed in the liquid phase essentially to equilibrium conditions. The effluent from the decomposer is cooled to condense out the I_2 and a large fraction of the HI. The HI-I_2 liquid is distilled to separate the HI and I_2. The H_2-HI gas phase is cooled further to condense out the HI. A water-wash step is used to remove a small amount of HI from the H_2. With the minor exception of the water-wash tower, this entire section has been modeled with DESIGN/2000. It is now possible to quickly recalculate this section, for example, for a different temperature in the HI decomposer reactor, such that a better heat match-up in the overall process can be obtained.

Figure 6 shows a simplified block diagram for Section V, where the heat and power needed in the processing sections are generated. The basic assumption has been that a high temperature gas-cooled nuclear reactor, similar to the one designed by General Atomic would be available.

Helium from the primary loop transfers its heat to three secondary helium loops through heat exchangers which operate at high, intermediate, and low temperatures. The high temperature loop provides the heat for the sulfuric acid decomposition reaction of flowsheet Section II. Recovered heat from Section II is utilized to provide heat for the HI distillation and phosphoric acid concentration of flowsheet Section III. The intermediate temperature loop provides the heat for flowsheet Section IV, the HI decomposition. Power for flowsheet Section III is generated through a helium turbine and a steam cycle. The low temperature loop provides low value heat to flowsheet Sections II and IV, sulfuric acid concentration and HI distillation. Additional power for flowsheet Section III is generated through a helium turbine and a second, low temperature steam cycle.

An obvious effort of the engineering flowsheet design is to achieve a high thermal efficiency. High thermal efficiency is attainable if the heat transfer temperature differences are reasonably small and if waste heat is rejected to the environment at temperatures not much above ambient. Flowsheet reconciliation work will continue to improve heat match-up. Also, Section III, which consumes 80% of the process power requirement, could benefit from an alternate processing approach.

Bench-Scale Testing

In 1977, GA started the design and construction of a bench-scale unit aimed at carrying out the reactions of the sulfur-iodine cycle in a continuous mode. The main objective of the bench-scale unit is the study of the cycle under continuous flow conditions by modeling the main solution reaction, product separation, and concentration and decomposition of H_2SO_4 and HI. The unit is divided into three subunits, and for the process model given in Figure 1, Subunit 1 corresponds to Section I (main solution reaction), Subunit 2 corresponds to Section II (H_2SO_4 concentration and decomposition), and Subunit 3 corresponds to Sections III and IV

combined (HI concentration and decomposition). The unit has been designed for an H_2 production rate of $\sim 6.6 \times 10^{-5}$ m^3/s ($\sim$4 liters per min.).

Subunit 1

In this subunit, the main solution reaction is carried out. The H_2O, I_2, and SO_2 are injected in a contact reactor where the two acid phases are formed. The products are then passed into a gas separator, where the excess SO_2 is removed for recycle, and eventually into a liquid-liquid separator, where the two phases are separated and collected.

Subunit 2

The H_2SO_4 phase from Subunit 1 is purified, concentrated, and pyrolized at temperatures up to 1144 K. Uncracked H_2SO_4 is recycled to the concentration column, and wet SO_2-O_2 product may then either be passed to a caustic scrub prior to metering and discharging or recycled to Subunit 1 without removal of O_2.

Subunit 3

This subunit separates HI from the lower phase product of the main solution reaction (containing HI, I_2, and H_2O) by a treatment with concentrated H_3PO_4. The HI is then catalytically decomposed at moderate temperature.

Status

A new enclosure has been constructed to house all three subunits. Subunit 1 and 2 have been installed and operated separately. Subunit 3 has been designed and the purchase orders written. Installation of Subunit 3 is scheduled for completion in March 1980. Operation of the integrated bench-scale unit is scheduled for 1981.

Closed Loop Cycle Demonstrator (CLCD)

As part of the bench-scale testing, DOE requested construction and operation of a separate, smaller unit, aimed at an earlier, simple demonstration of the cycle in a closed loop using recycled materials. The unit was designed and installed in four months. Production of hydrogen was demonstrated on January 4, 1979, and recycle of all reaction products was achieved. During one demonstration, the system was operated on total recycle for a time period equivalent to five turnovers of the original iodine inventory.

A schematic diagram of the CLCD is shown in Figure 7. The H_2O, I_2, and SO_2 are fed into a main reaction vessel, and the products are separated in the liquid phase separator. The H_2SO_4 is purified by boiling and decomposed in the H_2SO_4 cracker. The product is scrubbed and vented. The HI-containing lower phase is partially decomposed in the HI cracker without prior separation, and H_2O, I_2, and the remaining HI are recycled to the main reaction vessel.

Conclusions

Work carried out at GA on the sulfur-iodine thermochemical water-splitting process during the last year has resulted in significant accomplishments. Total recycle capability was demonstrated for the cycle, and major process improvements have resulted in an efficiency increase to 47%. It appears that 50% efficiency is well within reach. We believe that we have made great progress in the last year, and in the future we expect to show that thermochemical water-splitting utilizing the sulfur-iodine cycle is a viable, economic alternative for hydrogen production.

Acknowledgment

The work described was conducted under the sponsorship of the U.S. Department of Energy (Contract No. DE-AT03-76SF90351), the Gas Research Institute (Contract No. 5014-323-0122), and General Atomic Company.

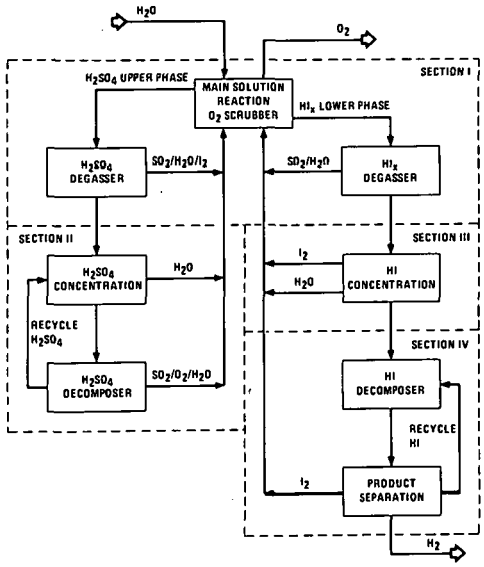

Fig. 1. Sulfur-iodine cycle process model

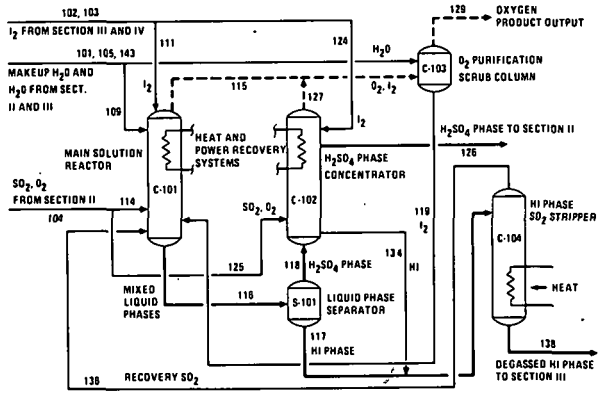

Fig. 2. Section I, Main Solution Reaction (H_2SO_4-HI production and separation and O_2 removal).

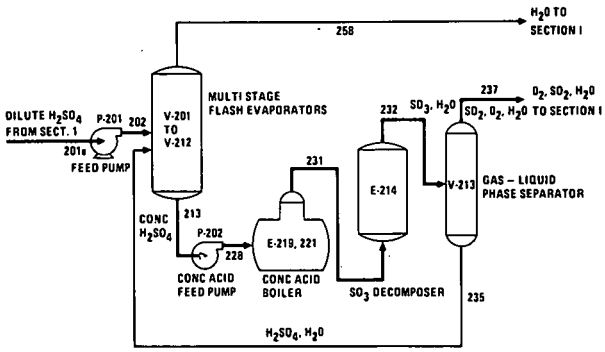

Fig. 3. Section II, H_2SO_4 Concentration and Decomposition

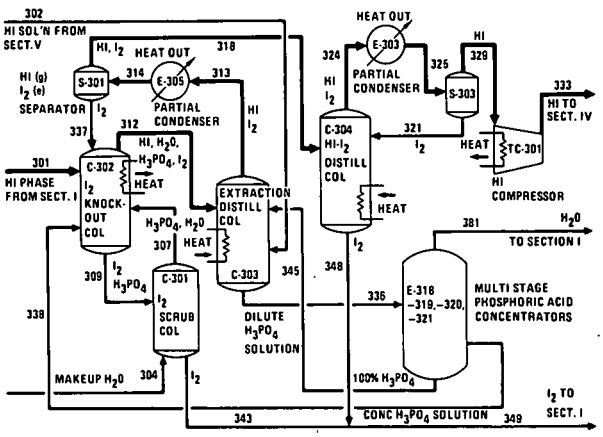

Fig. 4. Section III, HI Concentration

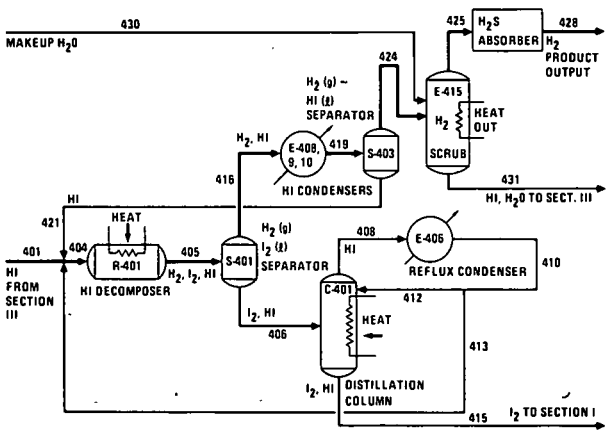

Fig. 5. Section IV, HI Decomposition

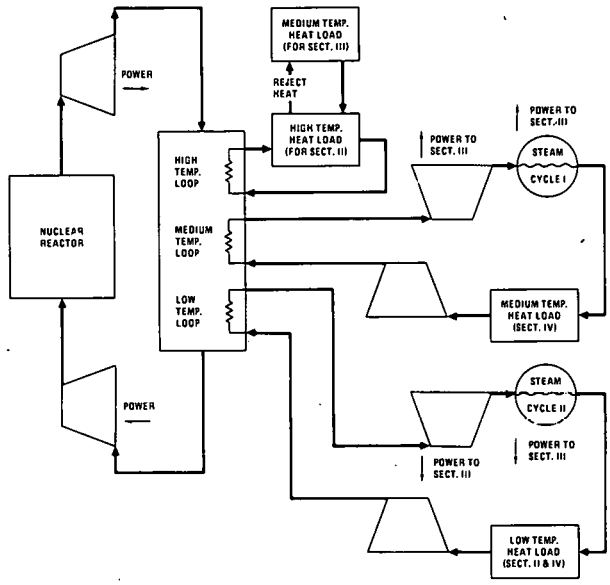

Fig. 6. Simplified Block Diagram for Section V

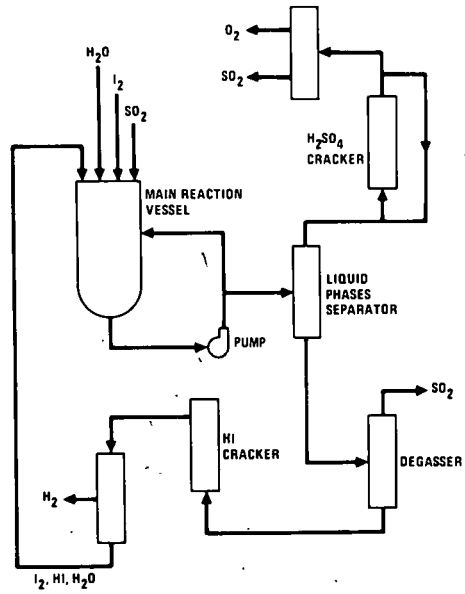

Fig. 7. Closed Loop Cycle Demonstrator

UPDATE ON THE SULFUR CYCLE HYDROGEN PRODUCTION PROCESS

G. H. Parker
Westinghouse Advanced Energy Systems
Pittsburgh, Pennsylvania 15236

Abstract

At last year's Contractor Review meeting, we highlighted progress through October, 1978 on the development of the Sulfur Cycle. At that time, we had designed and were constructing a closed cycle working Laboratory Model.

During November and December, 1978, assembly of the Model was completed, and initial testing occurred. This year, we have continued to use the Model as a valuable development tool for the high temperature and electrolytic steps of the process. This report provides a brief update on the Model and several other aspects of the Sulfur Cycle: sulfur dioxide electrolyzer development, high temperature materials evaluation, and catalyst testing for sulfur trioxide reduction.

Introduction

The program for the development of the Sulfur Cycle has been underway since 1973, with Westinghouse funding, and has been supported by the Department of Energy since 1976. The multiyear development program should lead to an integrated process development unit (PDU) by 1983, followed by pilot scale and large demonstration units.

The process is shown schematically in Figure 1. Hydrogen is generated at the cathode of an electrolysis cell which also oxidizes sulfurous acid to sulfuric acid at the anode. The sulfuric acid formed in the electrolyzer is vaporized, using heat from a high-temperature source. The vaporized sulfuric acid (sulfur trioxide-steam mixture) flows to a heated reduction reactor where the sulfur trioxide is cracked. Wet sulfur dioxide and oxygen flow to the separation system, where oxygen is extracted and the sulfur dioxide is recycled to the electrolyzer.

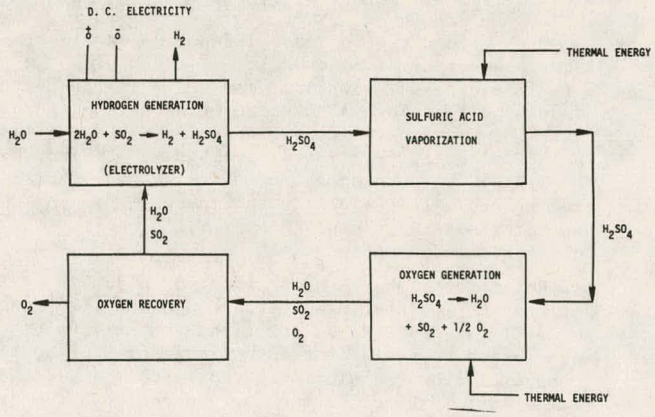

Figure 1. Hydrogen Generation Schematic Design

Process parameters for a commercial system will evolve as the technology matures. Conceptual design studies and experimental analyses have, however, led to the selection of a range of major process parameters that should result in a technically sound and economically competitive system. Table 1 summarizes these objectives.

Table 1: Major Process Parameters for a Commercial System

Parameters	Range	Objective
Electrolyzers		
Pressure, Atmospheres	3.5 - 30	20
Temperature, °C	50 - 125	100
Current Density, mA/cm^2	100 - 300	200
Electrolyte Sulfuric Acid Concentration, wt Percent	50 - 70	55
Cell Voltage, mV	450 - 1000	600
Sulfuric Acid Vaporization		
Pressure, Atmospheres	3.5 - 30	20
Temperature, °C	360 - 470	450
Oxygen Generation		
Pressure, Atmospheres	3.5 - 30	20
Maximum Temperature, °C	760 - 925	870

Laboratory Model

The Laboratory Model was designed, constructed and initially operated during 1978. The objectives of the Model were as follows:

- To provide an early demonstration of the cyclic operation of the process.
- To act as a test bed for subsequent long term testing of the electrolyzer and thermal decomposition reactor.
- To have capability for assessing interactions between various process steps.
- To serve as an operating facility to support the technical feasibility of hydrogen production via the Sulfur Cycle.

During December, 1978, the Laboratory Model was checked out and operated successfully; its operation represents a major milestone since the Model is the first of its kind in the United States.

During its initial operations in the closed cycle mode, the model vaporized and decomposed sulfuric acid, separated the resulting sulfur dioxide and oxygen streams and produced hydrogen and sulfuric acid in a five cell electrolyzer. The thermochemical portions of this model operated at design temperatures and pressures and were fully consistent in performance with expectations. While the pre-prototype electrolyzer did not meet all of its performance objectives, it did produce substantial quantities of hydrogen and permitted true closed cycle operation.

The design of the Laboratory Model was based on the following major criteria:

- Production of approximately two liters of hydrogen per minute.

- The oxygen production step ($SO_3 \rightarrow SO_2 + 1/2\ O_2$) to achieve at least 70% of the equilibrium reduction of sulfur trioxide for the selected operating pressure and temperature.
- The hydrogen production step should occur with an electrolyzer cell voltage of 600 mV and a current density of 200 mA/cm^2.
- Sulfuric acid concentration shall be 50 w/o.
- The Model shall be designed to operate at atmospheric pressure.

Figure 2 shows a schematic arrangement of the model. The composition of fluid streams and thermal loads at various locations were sized to meet the criteria listed above.

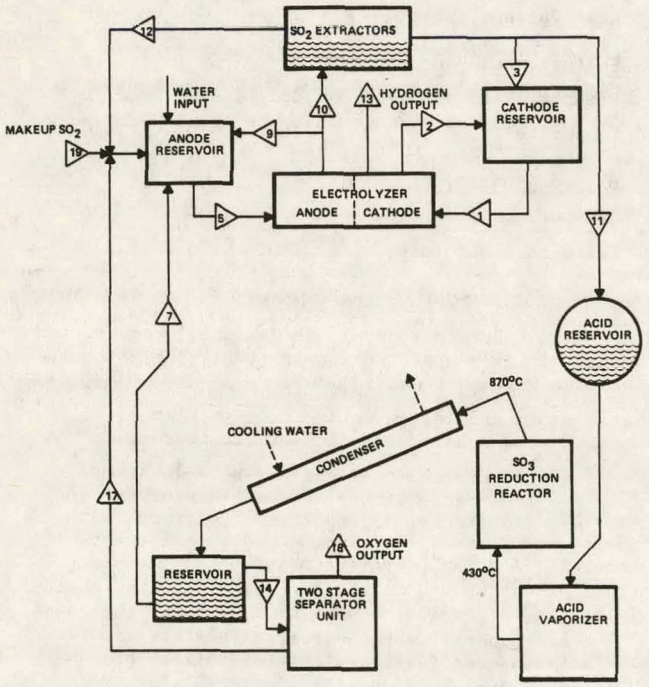

Figure 2. Laboratory Model Schematic

A layout drawing showing the equipment dimensions, locations, and supports for the Laboratory Model was prepared and used to determine the size of the ventilation hood coverage and the location of supports, utilities, controls, alarm systems and other safety equipment. A process and instrumentation diagram was prepared to indicate the number and location of all instrumentation for the Model. Photos of the Model and its control room are shown in Figures 3 and 4. The Model uses many glass components and the high temperature items, such as the acid vaporizer and reduction reactor, are custom designed and fabricated from quartz.

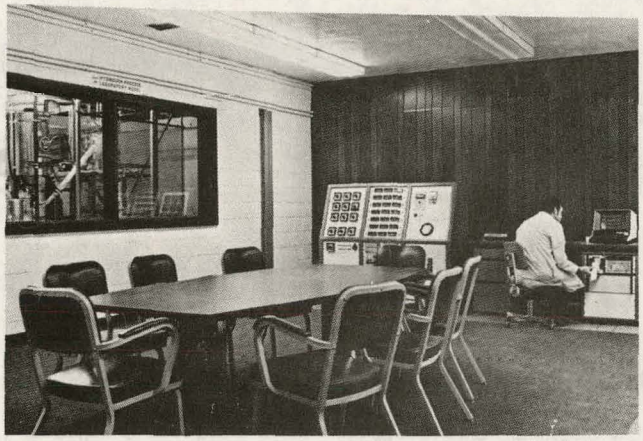

Figure 3. Laboratory Model Control Room

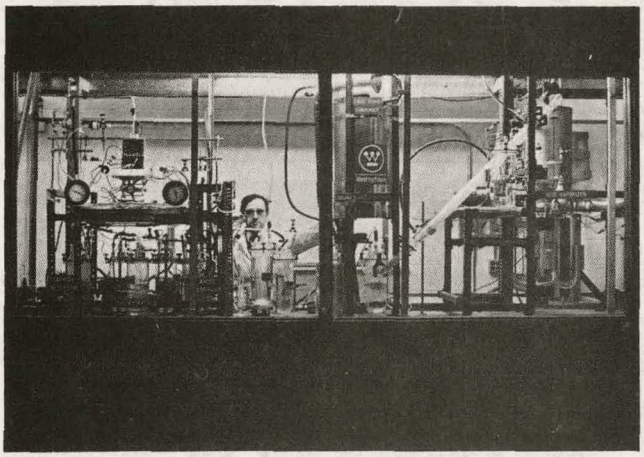

Figure 4. Laboratory Model

Sulfur Dioxide Electrolyzer Development

The cell voltage of an SO_2-depolarized electrolyzer plays a significant role in determining the overall energy efficiency of the sulfur cycle hydrogen production process. Recent efforts to achieve further improvements in cell performance have focused in the following areas: (a) evaluation of electrocatalysts; (b) development of the electrode fabrication process; (c) selection and investigation of separator materials; and (d) optimization of cell configuration.

Heretofore, most kinetic studies on the SO_2 oxidation reaction have been conducted on Pt (1-6) and Au (3,7) in dilute H_2SO_4 solutions. Quantitative information regarding the anodic oxidation of SO_2 in concentrated H_2SO_4 solutions or on metals other than Pt and Au is sparse. For these reasons, electrocatalytic activities of various candidate materials for SO_2 oxidation were studied in 50 w/o H_2SO_4 solution using a steady-state potentiostatic method. The observed Tafel slopes of these electrodes are very close to RT/F, where R is the gas constant, T the absolute temperature and F the Faraday constant. Referring to a proposed reaction scheme (1), a Tafel slope of RT/F strongly supports the hypothesis that the discharge step occurring on an active

site (i.e., $M + H_2O \rightarrow MO_{ads} + 2\ H^+ + 2\ e^-$) is rate determining. Moreover, most test electrodes have exhibited electrocatalytic activities similar to or pooror than Pt. However, the limiting current density for SO_2 oxidation on the catalyst WAE-3 is higher than Pt by a factor of ∿30.

Effects of temperature and acid concentration on electrode kinetic parameters for SO_2 oxidation were studied on WAE-3 electrodes. The polarization potential decreased distinctly with increasing temperature. An improvement of ∿100 mV in the overpotential was achieved by increasing the temperature from 25 to 90°C. The observed Tafel slopes were approximately constant at the temperatures of study (25 - 90°C), indicating that the reaction mechanism is independent of temperature. For solutions ranging from 40 to 70 w/o, the increase of acid concentration resulted in a significant decrease in the limiting current density and distinct enhancement in the polarization potential. The influence of acid concentration on the electrode kinetics was hardly detectable in less concentrated solutions (in the range of 20 - 40 w/o).

Attempts were also made to find out alternate catalysts of low cost and promising activities. Simple oxides and mixed oxides, prepared by a thermal decomposition technique on porous carbon and titanium substrates, respectively, were evaluated electrochemically for SO_2 oxidation in 50 w/o H_2SO_4 solution at room temperature. One oxide catalyst exhibited a high catalytic activity for SO_2 oxidation compared to the Pt-black/C electrode and one mixed oxide catalyst (MOA-2/Ti) was competitive to the Pt-black/Ti electrode.

A number of membranes, dveloped by DuPont and RAI Research Corporation, were evaluated as gas separators in an electrolyzer. Several membranes exhibited promising chemical and mechanical stabilities under the operating conditions (50 w/o H_2SO_4 at 50°C and 1 atm). Unfortunately, none of these membranes was impervious to SO_2, The migration of SO_2 molecules through the separators resulted in the formation of inclusions inside the membranes as evidenced in scanning electron micrographs. ESCA studies on the tested membranes revealed that the inclusions are essentially composed of sulfide, presumably formed through the reduction of penetrating SO_2 molecules by H_2.

On the basis of the filter-press design concept, a new electrolyzer was constructed for the evaluation of cell components. This single cell was made of lucite using O-ring seals. A pressure pad was placed on the back of the current collector to reduce the electric resistance in the electrode/collector interface and to minimize the inter-electrode spacing. The performance stability of the lucite cell in which a briquetted carbon cathode (containing 10 w/o Pt) and a Pt-impregnated carbon anode (loading: 10 mg-Pt/cm^2) were incorporated, has been tested at 50°C and atmospheric pressure using 50 w/o H_2SO_4 solution. Operating at a constant current density of 100 mA/cm^2, this cell has exhibited a voltage of ∿0.75 V (including the ohmic loss). Further improvements in the cell performance are expected from the use of the oxide catalyst OA2/C as an anode and the enhancement of SO_2-solubility by increasing the operating pressure.

Acid Vaporizer Materials Evaluation

The acid vaporizer has been identified as a critical component with respect to structural materials since both the liquid and vapor phases of sulfuric acid are present in the vaporizer at elevated temperatures and pressures, with process parameters in the range of 360°C to 450°C and 4 to 20 atmospheres.

The testing of materials in the presence of high temperature boiling sulfuric acid requires that a test vessel, inert to the acid environment, be utilized to contain the materials samples and the boiling acid. The initial test vessels were made of stainless steel with a removable internal gold liner. In the initial tests, Duriron and CVD SiC had the best corrosion resistance. Because welds in the gold liner developed leaks in the presence of sulfuric acid vapor, a vessel made of Duriron components has been used recently as the test vessel.

Tests have been run at 360°C for 250 hour increments using 98 w/o sulfuric acid and samples have been tested for total test times of 1000 hours or until the samples were so severely attacked that one or more samples of each material could not be placed back in test.

From corrosion tests on 34 materials, those which have the best corrosion resistance are polycrystal silicon, silicon carbide, CVD SiC, and silicon nitride. The matallic materials which are most corrosion resistant are Duriron and Durichlor 51.

Reduction Reactor Materials Evaluation

The objective of this materials evaluation is to screen potential materials for compatibility with reduction reactor conditions in the temperature range of 480°C to 870°C. The inlet gases of the reduction reactor consist of SO_3 and steam, while the outlet gases contain SO_3, SO_2, O_2 and steam.

The materials test beds utilize quartz structural materials for operations at or near atmospheric pressures. A quartz sample holder capable of holding six specimens fits inside a quartz combustion tube and is heated to the exposure temperature. The process stream for the inlet conditions is a once-through type and permits either anhydrous SO_3 or SO_3 with superheated steam to be introduced past the material samples. A second materials test bed, simulating reaction outlet conditions is similar to the reactor inlet conditions test apparatus except for the addition of SO_2 and O_2 gas lines to simulate the outlet gas streams. Although the inlet conditions tests utilize Ar as a carrier gas, no carrier gas is used in the outlet conditions tests.

Various sets of materialshave been exposed to the reactor inlet and outlet conditions for periods up to 1000 hours, and to date silicon, silicon carbide, and silicon nitride have the best corrosion resistance for both inlet and outlet conditions. At nominal 100-hour intervals, the samples were removed for visual inspection, photographing, weighing and thickness measurements.

Sulfur Trioxide Catalyst Evaluation

While cracking sulfur trioxide to sulfur dioxide and oxygen can be accomplished thermally, it proceeds at a slow rate. Therefore, it is of interest to identify a catalyst that can accelerate the conversion rate. To be compatible with the process requirements, a conversion rate of 70% at 870°C is desired with stable performance over an extended period of testing.

To provide a basis of comparison between the catalysts, equilibrium conversions for various feedstocks have been calculated throughout the temperature range of interest (650 - 900°C). By

normalizing the experimental results with the calculated equilibrium conversions, a conversion efficiency is determined for each test. A valid comparison between catalysts is then possible.

While the Sulfur Cycle reduces sulfur trioxide in the presence of steam (as vaporized sulfuric acid), catalyst tests are being conducted in wet and anhydrous environments. In both cases, argon is employed as a carrier gas.

Table 2 itemizes the catalysts and their test parameters evaluated in the past year. Of these catalysts, ENG-1, ALFA-2, ALFA-4, and CE-1 displayed relatively low conversion efficiencies while catalysts MB-2 and MB-3 provided acceptable conversion efficiencies.

Table 2: Catalysts Evaluated from August, 1978 to September, 1979

Catalyst	Composition and Geometry	Space Velocity (hr^{-1}) and Env. Wet	Dry
ENG-1	0.5% (by weight) Pt on alumina, 3.2 mm right circular cylinders	10,000	10,000
MB-2	1% (by weight) Pt on alumina 3.2 mm diameter spheres	1,000 5,000 10,000	1,000 -- 10,000
MB-3	1% (by weight) Pt on alumina 3.2 mm diameter spheres. Higher surface area than MB-2	1,000 5,000 -- -- 30,000 40,000 50,000	1,000 5,000 -- -- 30,000 40,000 50,000
ALFA-2	0.5% (by weight) Pd on alumina, 3.2 mm right circular cylinders	1,000 5,000	1,000 5,000
ALFA-4	20% (by weight) Fe_2O_3 on alumina, 3 2 mm right circular cylinders	1,000 5,000 10,000 20,000 25,000	1,000 5,000 10,000 20,000 25,000
CE-1	Fe_2O_3 Powder, >10, <20 mesh	1,000 5,000	1,000 5,000

NOTE: All catalysts evaluated over a temperature range of 650° to 900°C.

Catalyst MB-2 displayed a maximum conversion of ∿81.4% at a temperature of 900°C. The space velocity for this particular test was 5000 hr^{-1} using a simulated 80 w/o H_2SO_4 feed. When normalized with an equilibrium conversion of 90.5%, the result is a catalyst conversion efficiency of ∿90%.

Catalyst MB-3 achieved a maximum conversion rate of 79.8% at 900°C and of 5000 hr^{-1}. Additionally, a conversion rate of 78.6% was reached at a space velocity of 50,000 hr^{-1} and 900°C using 80 w/o H_2SO_4 feed. These conversion rates represent catalytic conversion efficiencies of ∿88% and ∿87%, respectively.

Catalyst MB-3 also was evaluated over a 1000 hour test. Test conditions were a space velocity of 10,000 hr^{-1}, 870°C, and as simulated 80 w/o H_2SO_4 feed. There was no decline in catalytic activity; a conversion rate of 74% was maintained throughout the endurance test. At 870°C using an 80 w/o H_2SO_4 feed, the equilibrium conversion is 87%. The experimental conversion rate of 74% translates into a conversion efficiency of 85%.

In addition, the Laboratory Model recently has been adapted for use as a catalyst evaluation facility. The Model has several advantages over the screening test facility. Among them are: the elimination of a carrier gas, a high tube diameter to particle diameter ratio, and the evaporation of sulfuric acid rather than a simulated feed of steam and sulfur trioxide.

Catalyst ALFA-4 has been evaluated in the Laboratory Model and produced encouraging results; at 890°C, a conversion rate of ∿84.0% was obtained. When compared to an equilibrium conversion of 89.5%, this represents a catalyst conversion efficiency of ∿94%. This increase in the efficiency, when compared to the screening tests, may be a direct result of the advantages mentioned above. To insure the accuracy of the test results with the Laboratory Model, the measurements techniques and method of analysis are being modified so that a complete mass balance on all species can be performed.

References

1. K. I. Rozental and V. I. Veselovskii, Zh. Fiz. Khim, 27, 1163 (1953).
2. G. A. Bogdanoskii and A. I. Shlygin, Ibid. 32, 418 (1958).
3. E. T. Seo and D. T. Sawyer, Electrochim. Acta, 10, 239 (1965).
4. M. Comtat and J. Mahenc, Bull. Soc. Chim., Fr., 3862 (1969).
5. A. J. Appleby and B. Pichon, J. Electroanal. Chem., 95, 59 (1979).
6. K. Wiesener, Electrochim. Acta, 18, 185 (1973).
7. Z. Samec and J. Weber, Electrochim. Acta, 20, pp. 403-412 and pp. 413-419 (1975).

Acknowledgement

This report is based on selected tasks of work performed by Westinghouse and funded by DOE/STOR under JPL Contract 955380 and by DOE/Solar under Contract ET-78-C-02-4705. Major contributors are R. L. Ammon, B. R. Krasicki, H. I. Irwin, W. T. P. Lu, J. F. Pierre, and G. O. Yatsko.

Dup

STUDIES ON THERMOCHEMICAL WATER-SPLITTING CYCLES

Robert J. Remick

Stephen E. Foh

Institute of Gas Technology
3424 South State Street
Chicago, Illinois 60616

Abstract

Thermochemical water-splitting cycles that use solid metal sulfates instead of sulfuric acid appear to offer the advantage of allowing the electrolytic oxidation of sulfurous acid to take place in relatively dilute solutions where anodic overpotential is expected to be minimized. The Institute of Gas Technology is investigating such systems in order to define preferred operating conditions and performance for the electrolytic step.

The current-voltage characteristics of smooth platinum for the oxidation of sulfur dioxide (SO_2) to sulfuric acid and the reduction of hydronium ions to hydrogen were determined at acid concentrations between 1 and 50 weight percent and over the temperature range from 1° to 75°C. At a constant applied overpotential, the current density for hydrogen generation increases with increasing acid concentration. With a given applied anodic overpotential, the rate of SO_2 electrochemical oxidation decreased somewhat with increasing acid concentration. In general, current densities at a given overpotential increased with temperature at both electrodes. However, at high temperature and anodic overpotential, the rate for SO_2 oxidation decreased over that expected, presumably a consequence of the temperature dependence of the SO_2 concentration.

The electrochemical performance of smooth platinum was observed to degrade at anodic potentials above 0.80 volts vs. RHE. This degradation could be the result of either oxide formation or preferential adsorption of sulfate ions on the catalytic platinum surface.

Introduction

Thermochemical water-splitting is a laboratory-proved concept and is currently undergoing intensive research. Thermochemical or hybrid, thermoelectrochemical hydrogen produced by efficient cyclical processes using nuclear reactors or solar concentrators as high-temperature heat sources offers an attractive, flexible, gaseous fuel supply. As a future fuel, hydrogen produced by decomposing water with a series of chemical steps could provide a larger and more cost-effective supply of hydrogen than power generation/electrolysis-based processes.

The bulk of the most developed water-splitting cycles to date involve the production, and subsequent decomposition, of sulfuric acid. The production of sulfuric acid via the electrolytic oxidation of sulfurous acid is a step common to the sulfuric acid cycle being developed at Westinghouse Corp.'s Advanced Energy Systems Division in this country and at the EURATOM (Ispra, Italy) and KFA (Juelich, West Germany) laboratories abroad. In this cycle (Reactions 1 to 3), the electrolytic oxidation of sulfurous acid (Reaction 1) must produce relatively concentrated sulfuric acid (>50 weight percent) to avoid large thermal energy requirements for subsequent acid concentration (Reaction 2). Reaction 1,

$$SO_2(g) + (2 + n)H_2O(\ell) \rightarrow H_2SO_4(aq) + H_2(g) \quad (1)$$

$$H_2SO_4(aq) \rightarrow H_2SO_4(\ell) + nH_2O(g) \quad (2)$$

$$H_2SO_4(\ell,g) \rightarrow H_2O(g) + SO_2(g) + \tfrac{1}{2}O_2(g) \quad (3)$$

however, would require less energy input if run at lower sulfuric acid concentrations (<50 weight percent) in order to minimize anodic overpotential.

The use of a metal oxide-metal sulfate pair to concentrate sulfuric acid appears to offer advantages over the sulfuric acid cycle. The use of a metal oxide to "concentrate" electrolytically produced sulfuric acid (by forming a metal sulfate) should allow the use of less concentrated acid (and, therefore, lower anodic losses) in the electrolytic step.

In 1978, the Institute of Gas Technology (IGT) demonstrated a hybrid copper oxide-copper sulfate cycle. This cycle (Reactions 4 to 6), denoted Cycle H-5 by IGT, is an example of the use of metal oxide-metal sulfate chemistry, where cycle closure is attained by decomposing a solid metal sulfate instead of concentrated sulfuric acid.

$$CuO(s) + SO_2(g) + (x + 1)H_2O(\ell) \rightarrow CuSO_4 \cdot xH_2O(s) + H_2(g) \quad (4)$$

$$CuSO_4 \cdot xH_2O(s) \rightarrow CuSO_4(s) + xH_2O(g) \quad (5)$$

$$CuSO_4(s) \rightarrow CuO(s) + SO_2(g) + \tfrac{1}{2}O_2(g) \quad (6)$$

The hydrogen-producing step, Reaction 4, may be accomplished as written in a single electrochemical cell or as consecutive electrochemical (Reaction 4a) and thermochemical (Reaction 4b) steps.

$$SO_2(g) + (x + 2)H_2O(\ell) \rightarrow H_2SO_4(aq) + H_2(g) \quad (4a)$$

$$H_2SO_4(aq) + CuO(s) \rightarrow CuSO_4 \cdot xH_2O(s,aq) + H_2O(\ell) \quad (4b)$$

$$CuO(s) + SO_2(g) + (x + 1)H_2O(\ell) \rightarrow CuSO_4 \cdot xH_2O(s,aq) + H_2(g) \quad (4)$$

In either case, concentrated sulfuric acid need not be produced electrochemically.

There are a number of literature references[1,2] and several ongoing research efforts that have defined the electrolytic oxidation of sulfurous acid in concentrated (>50 weight percent) sulfuric acid. In a program funded by the Jet Propulsion Laboratory under a Department of Energy subcontract, IGT is examining the electrolytic oxidation of sulfurous acid in dilute sulfuric acid solutions which are appropriate for metal oxide-metal sulfate cycles. The purpose of this program is to determine preferred cell operating conditions and to quantify expected performance improvements relative to concentrated acid systems. The IGT program will examine cell performance as a function of sulfuric acid concentration (0 to 50 weight percent), temperature (0° to 90°C), and electrode material to test for electrocatalytic activity. The cell will be operated with

and without copper oxide (or other metal oxide) present to test Reactions 4 and 4a. Thus far, we have only operated the cell without a metal oxide to provide baseline data on Reaction 4a.

Task IA

The purpose of Task IA is to determine the current-voltage characteristics of platinum electrodes for SO_2 oxidation and hydronium ion reduction to hydrogen as a function of acid concentration and temperature.

Acid Concentration

The relationship between current density and overpotential was investigated as a function of acid concentration using solutions of 1, 16, 33, and 50 weight percent sulfuric acid. An H-cell fitted with a "nafion" cell separator and polished platinum electrodes was used for this study. We used mercury/mercurous sulfate reference electrodes containing sulfuric acid of the same concentration as that under investigation in the cell. The platinum electrodes were anodized in sulfuric acid for 30 minutes prior to use. However, 10 minutes before the start of the experiment, the anode potential was adjusted to zero versus the Hg/Hg_2SO_4 reference electrode (0.612 volts vs. RHE) to provide a clean, oxide-free platinum surface.

The relationship between equilibrium current density and overpotential for the cathodic reaction at each of the four acid concentrations is illustrated in Figure 1. Each data point was determined by holding the potential constant for 5 minutes before determining current density.

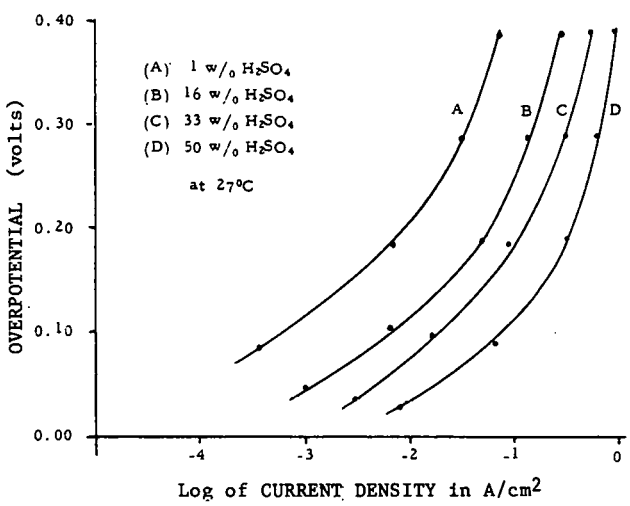

Fig. 1 Current density versus overpotential for hydronium ion reduction on a smooth platinum cathode as a function of acid concentration at 27°C.

In a similar manner the anodic polarization was determined as a function of current density using solutions saturated with SO_2. Because we were unable to obtain a constant and reproducible open circuit potential in the presence of SO_2, the polarization data presented in Figure 2 are plotted versus a reversible hydrogen electrode voltage rather than as overpotential.

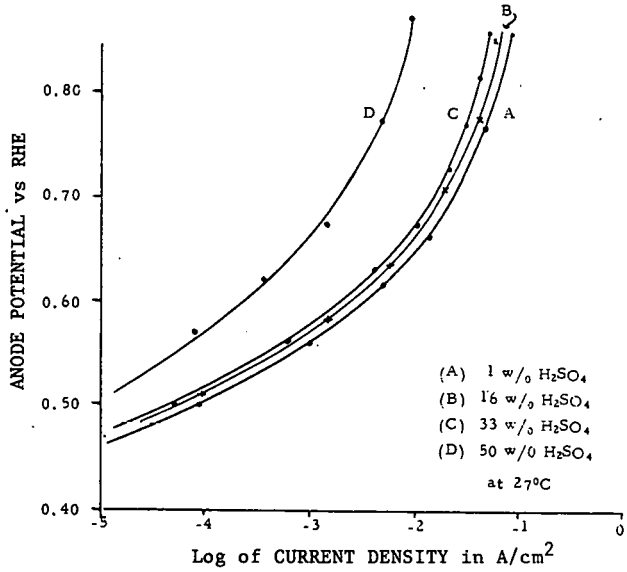

Fig. 2 Current density versus anode potential as a function of acid concentration for SO_2 oxidation on smooth platinum at 27°C. (SO_2 saturated)

As can be seen from Figures 1 and 2, the cathodic reaction exhibits a rather strong dependence on acid concentration as would be expected for the reduction of hydronium ion. The anodic reaction rate, on the other hand, decreases somewhat as acid concentration is increased. Because the anode experiments were conducted in acid solution saturated with SO_2 and the solubility of SO_2 in acid is inversely related to acid concentration in the range of 1 to 50 weight percent, the dependency of the anode reaction on acid concentration may be the result of differences in SO_2 concentration and water activity.

Temperature

The relationship between current density and overpotential as a function of temperature was investigated using 33 weight percent sulfuric acid and smooth platinum electrodes. Experiments were conducted in a constant temperature bath at 1°, 27°, 50°, and 75°C as measured in the anode chamber of the H-cell. The reference electrode was mercury/mercurous sulfate maintained at 27°C by a water jacket and fitted with a long Luggin capillary over which the thermal gradient was distributed.

Current-voltage characteristics of the cathode in pure acid and of the anode in SO_2-saturated acid are summarized in Figures 3 and 4, respectively. Both the anode and the cathode rates increase with temperature at low overpotentials. However, the experiments conducted at 27°, 50°, and 75°C indicate that the temperature dependence of the anode reaction inverts at higher potentials. Because the solubility of SO_2 in aqueous solution changes markedly with temperature, it may be that the inversion at high anodic potentials is the result of the concentration dependence of the SO_2 reaction.

Degradation of Electrode Performance

Figure 5 represents a plot of the equilibrium current density, measured after maintaining a constant voltage for 5 minutes, versus anode potential extended to potentials as high as 2.0 volts

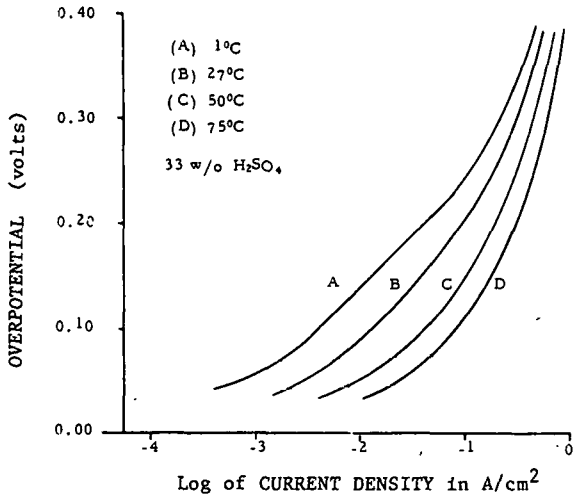

Fig. 3 Current density versus overpotential as a function of temperature for hydronium ion reduction on a smooth platinum cathode in 33 wt % sulfuric acid.
(Data points deleted for purposes of clarity.)

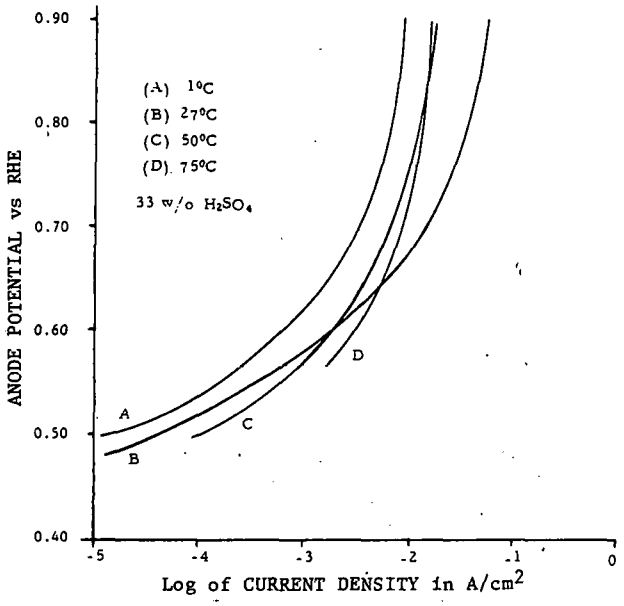

Fig. 4 Current density versus anode potential as a function of temperature for SO_2 oxidation on a smooth platinum electrode in SO_2 saturated 33 wt % sulfuric acid.
(Data points deleted for purposes of clarity.)

vs. RHE. Rather than reaching a limiting current density, the electrode performance actually degrades at potentials above 0.80 volts. This degradation is most severe in high acid concentrations. Furthermore, a hysteresis develops between the plot of increasing potential and that of decreasing potential only when the potential exceeds 0.8 volts. This behavior suggests that oxides may form on the platinum surface, reducing the electrocatalytic properties. However, an alternative explanation is suggested by the marked increase in degradation with acid concentration. The preferential adsorption of sulfate or hydrogen sulfate species at high anodic potentials could also account for this reduction in electrocatalytic activity.

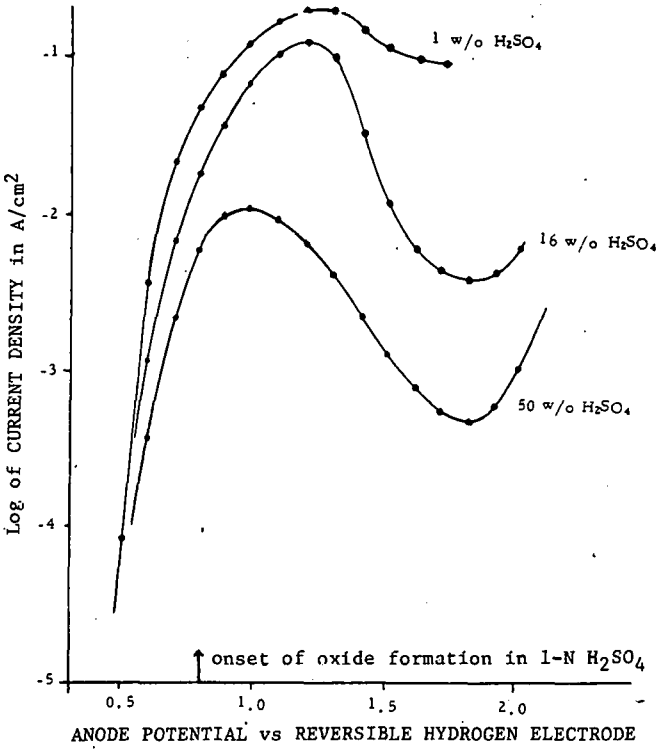

Fig. 5 Anode polarization as a function of acid concentration at 27°C on smooth platinum electrodes. Each data point was determined by maintaining a constant anode potential for five minutes before measuring current density.

Task IB

The purpose of Task IB is to evaluate the catalytic behavior of a variety of electrode materials using smooth platinum as a basis for comparison. To date, only platinum black and ruthenized titanium have been evaluated in 33 weight percent sulfuric acid at 27°C. Platinum black electrodes exhibit current densities an order of magnitude higher than those observed for smooth platinum under the same conditions. Ruthenized titanium, on the other hand, exhibited current densities two orders of magnitude lower than those recorded for smooth platinum.

Summary

Future program efforts will include the investigation of additional electrode materials (including palladium II oxide and porous graphite) and operation of the cell with metal oxide species (copper oxide and at least two others) present at the anode. It has been shown that the use of lower sulfuric acid concentrations lowers the open circuit voltage for the electrochemical oxidation of sulfurous acid.[1] Our studies show that lower acid concentrations lead to higher anode kinetics (current densities), which supports the original hypothesis that better cell performance can be attained in sulfuric acid concentrations below 50 weight percent. At the conclusion of this program in March of 1980, we will define preferred cell operating conditions.

References Cited

1. Appleby, A.J. and Pichon, B., "Electrochemical Aspects of the H_2SO_4-SO_2 Thermoelectrochemical

Cycle," in Proceedings of the Second World Hydrogen Energy Conference, Vol. 2, Zurich, Switzerland, August 21-24, 1978.

2. Appleby, A.J. and Pichon, B., "The Mechanism of the Electrochemical Oxidation of Sulfur Dioxide in Sulfuric Acid Solutions," J. Electroanal. Chem. 95, 59 (1979).

Dup

THE LASL THERMOCHEMICAL HYDROGEN PROGRAM STATUS ON SEPTEMBER 30, 1979*

Kenneth E. Cox

University of California
Los Alamos Scientific Laboratory
Los Alamos, New Mexico 87545

Abstract

The work described in this report was accomplished during the period October 1, 1978 - September 30, 1979. Most of the effort was applied to a study of the Los Alamos Scientific Laboratory (LASL) hybrid bismuth sulfate cycle. The work included a conceptual design of the cycly and experimental work to verify the design conditions. Key findings were:

- A 50.8% efficiency was obtained when an improved cycle design was coupled to a fusion energy source at 1500 K.
- Experimental results showed an endothermic heat requirement of + 172 kJ/mol for the decomposition of $Bi_2O_3.2SO_3$ to $Bi_2O_3.SO_3$ and SO_3.
- Reaction times for bismuth sulfate decomposition were determined as a function of temperature. At 1240 K, < 1.5 min were required for the first two stages of decomposition from $Bi_2O_3.3SO_3$ to Bi_2O_3.
- Tests made to determine the feasibility of decomposing $Bi_2O_3.2SO_3$ in a 1 inch diameter rotary kiln showed that $Bi_2O_3.2SO_3$ could be decomposed continuously.

In related work, support was given to the DOE Thermochemical Cycle Evaluation Panel (Funk).

The Second Annual International Energy Agency (IEA) Workshop on Thermochemical Hydrogen Production from Water met on September 24-27, 1979 at Los Alamos.

Fusion Synfuel (Hydrogen) Design Study

Introduction

Thermochemical cycles for hydrogen production have been investigated at the Los Alamos Scientific Laboratory (LASL) since the early 1970s. Process development is sponsored by DOE's Division of Energy Storage Systems (STOR). In recent months, our efforts were concentrated on the development of a thermochemical cycle compatible with a 1500 K heat source derived from a conceptual fusion driver. The major task of this study is to define nonelectrical fusion energy applications. Chief among these applications is the production of synfuel (hydrogen) from fusion power. The study is a joint effort involving thermochemical process development (under STOR) and design and engineering systems for extracting fusion heat (under the Office of Magnetic Fusion Energy).

The LASL Bismuth Sulfate Cycle

The LASL bismuth sulfate cycle has the following steps.

$$2H_2O(\ell) + SO_2(g) = H_2SO_4(aq) + H_2(g) \quad \text{Elec.350K} \quad (1)$$

$$Bi_2O_3.SO_3 + H_2SO_4(aq) = Bi_2O_3.2SO_3(s) + H_2O(\ell) \quad \text{Elec.350K} \quad (2)$$

$$Bi_2O_3.2SO_3(s) = Bi_2O_3.SO_3(s) + SO_3(g) \quad \text{1100-1250K} \quad (3)$$

$$SO_3(g) = SO_2(g) + (1/2)O_2(g) \quad \text{1100-1500K} \quad (4)$$

This cycle was originally devised as an alternative to those cycles employing H_2SO_4.

The LASL cycle, shown schematically in Fig. 1, has several advantages.

- The average endothermic heat requirement for the solid decomposition step is 172 kJ per mol of SO_2 removed.
- $Bi_2O_3.2SO_3$ is the stable solid phase in contact with H_2SO_4 over a 3~52.7 wt% range. In principle, the electrochemical oxidation of SO_2, step (1), could be carried out at a lower voltage. Operation at 10-20 wt% H_2SO_4 would be feasible.
- Sulfuric acid is not handled at high concentrations and temperatures or evaporated.
- Both sulfates present in step (3) remain as solids throughout the reaction.
- Maximum temperatures required for solids decomposition can be lower than in other cycles.

* Work performed under the auspices of the U.S. Department of Energy, Division of Energy Storage Systems.

In contrast to the other cycles, the LASL bismuth sulfate cycle involves solid-materials handling. Traditionally, liquids and gases are preferable to solids because of the problems of handling solids. The trade-off must be made between solids-handling and the difficulties (and expense) of handling highly corrosive, boiling H_2SO_4.

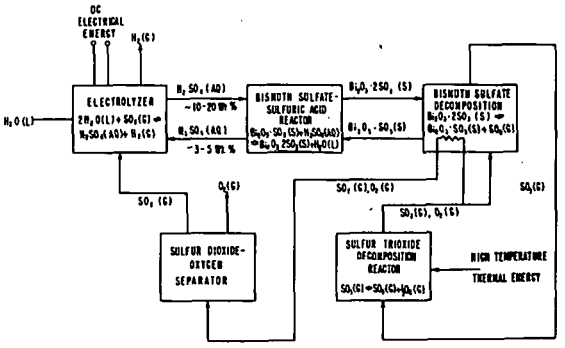

Fig. 1. Schematic of the LASL bismuth sulfate hybrid cycle.

Experimental Verification of Cycle

The experimental bases for the foregoing observations are shown in Figs. 2 and 3. Thermodynamic data on the endothermic heat of reaction for

$$Bi_2O_3.3SO_3(s) = Bi_2O_3.2S_3O(s) + SO_3(g) \quad (5)$$

and reaction (3) were obtained from isothermal batch experiments. The SO_3 pressure is shown as a function of temperature in Fig. 2. Straight-line plots of log Pso_3 vs 1/T give a value of 161 kJ/mol (38.4 kcal/mol) for the $Bi_2O_3.3SO_3$ decomposition and 172 kJ/mol (41.2 kcal/mol) for the $Bi_2O_3.2SO_3$ decomposition.

Kinetic data for the decomposition of $Bi_2O_3.3SO_3$ starting material are shown in Fig. 3. The data show the rate of SO_3 removal as a function of time at temperatures of 1050, 1150, and 1240 K. At 1240 K, ~ 1.5 min are required for the decomposition of $Bi_2O_3.3SO_3$ to $Bi_2O_3.SO_3$. Less time (roughly half) would be required for the intermediate step, $Bi_2O_3.2SO_3$ to $Bi_2O_3.SO_3$.

Process Design of Cycle

A thermochemical process design has been developed for the LASL bismuth sulfate cycle. The design aims were to produce an engineering flow sheet, compute mass and energy balances, and obtain a value for the thermal efficiency of the cycle.

A fusion reactor deposits neutrons in a high-temperature boiling lithium blanket at 1500 K. Thermal energy from the isothermal "lithium boiler" is transferred directly to a $SO_3/SO_2/O_2$ process stream for the high-temperature portion of the cycle. One heat exchanger thus provides all the primary thermal energy for the cycle. Heat from a low-temperature (800 K) portion of the fusion

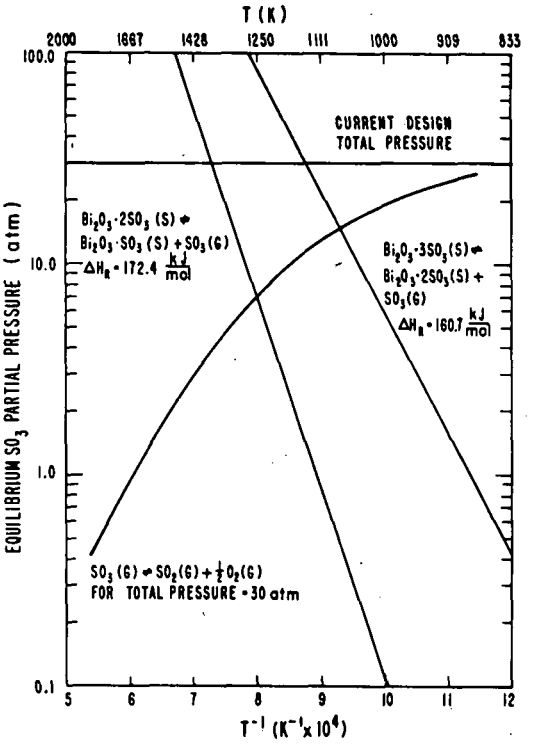

Fig. 2. Equilibrium data for bismuth sulfate and bismuth oxysulfate decomposition.

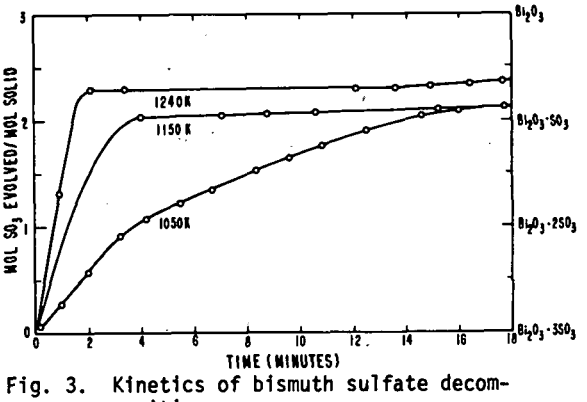

Fig. 3. Kinetics of bismuth sulfate decomposition.

blanket provides the electric power generation energy for the electrolysis section located in the low-temperature portion of the cycle.

For a representative energy balance and efficiency calculation, we chose the followng process conditions: maximum temperature, 1475 K; pressure, 30 atm; mols SO_2 removed, 1.0; mols H_2O entering, 5.0. The overall energy balance for the cycly is shown schematically in Fig. 4 for these conditions. Details of the design are given below.

The high-temperature portion of the cycle consists of three batteries: Battery A--Solids dewatering, Battery B--Solids decomposition, and Battery C--SO_3 decomposition.

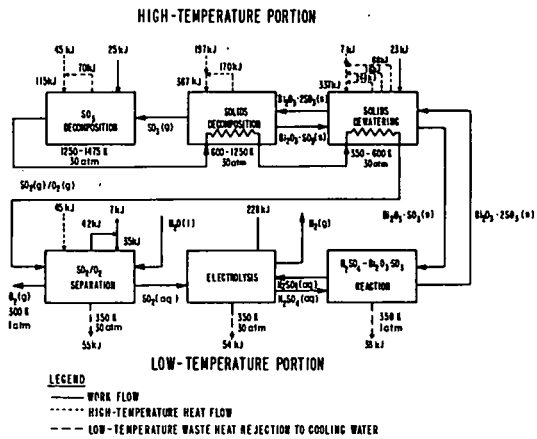

Fig. 4. Cycle energy balance.

A thermal energy balance was performed for each battery to identify the input and output of energy.

Battery A--Solids Dewatering. The function of Battery A is to dry the incoming $Bi_2O_3.2SO_3$ solids and to perform that task by recovering as much heat as possible from hot streams and exothermic reactions.

Battery B--Solids Decomposition. Battery B uses a large amount of heat for decomposing the entering solids to $Bi_2O_3.SO_3$ and SO_3.

Battery C--SO_3 Decomposition. Battery C operates at the highest temperature of the cycle (1475 K). A 25 K difference was arbitrarily chosen for heat transfer.

The low-temperature portion of the cycle operates at 350 K and consists of three batteries: Battery D--SO_2/O_2 separation, Battery E--Electrolyzer, and Battery F--Solids/acid reactor.

Battery D--SO_2/O_2 Separation. The main function of Battery D is to absorb SO_2 from the SO_2/O_2 gas mixture. Heating the purified oxygen stream to 1475 K for generating work in a turbine expander gives a net work gain.

Battery E--Electrolyzer. We assume a working voltage of 0.45 V, at an acid concentration of 15 wt% and a current density of 2000 A/m^2. The electrolyzer is designed for operation at 350 K and 30 atm.

Battery F--Solids/Acid Reactor. $Bi_2O_3.SO_3$ reacting with H_2SO_4 releases heat at 350 K to cooling water.

Overall Efficiency of Cycle

The cycle's efficiency is computed from the values given in Fig. 4. The net heat requirement is 294 kJ and the work requirement is 269 kJ--a total of 563 kJ. The efficiency is $\eta = 286/563 = 0.508$ (50.8%).

A parametric analysis was made to evaluate the effect of three major system variables on the cycle's efficiency. The variables chosen for this analysis were the electrolyzer cell voltage, the endothermic heat requirement in the high-tempera ture portion, and the maximum stream temperature in the cycle.

Of the three variables investigated, the cycle's efficiency was most affected by the electrolyzer voltage and the endothermic heat requirement. The efficiency is extremely sensitive to variation in electrolyzer voltage. The effect of maximum stream temperature variation is important primarily because it varies the equilibrium yield in the $SO_3 = SO_2 + (1/2)O_2$ reaction, hence changes the composition of the gas mixture leaving the high-temperature portion of the cycle. It also affects the rate of solids circulation.

Conclusions of Study

The LASL bismuth sulfate cycle is a promising approach to producing hydrogen from a high-temperature process heat source (1500 K) such as that from a fusion or solar reactor. It avoids the problem of evaporating H_2SO_4 solutions and has an estimated 50% efficiency, based on a flow-sheet analysis. Crucial issues still to be resolved are the demonstration of low-voltage electrolysis under production conditions, the recovery of latent heat of vaporization from drying solid $Bi_2O_3.2SO_3$, and the handling of large amounts of solids in a high-temperature decomposer vessel.

Bismuth Sulfate Decomposition Facility

A facility for studying continuous $Bi_2O_3.2SO_3$ decomposition is being built at LASL. Initially, we planned to carry out the decomposition reactions in a fluidized-bed reactor. Experiments with $Bi_2O_3.2SO_3$ showed "pilling" to take place on fluidization. Since then, we have constructed a 1-inch diameter laboratory-scale quartz rotary kiln. The atmosphere above the decomposing solids can also be controlled. We intend to study the effect of residence time, and temperature on the decomposition rate and yield of $Bi_2O_3.2SO_3$. Preliminary experiments have just begun and indicate complete conversion of the feed to $Bi_2O_3.0.7SO_3$ at temperatures in the range 1000-1100 K.

DOE Thermochemical Cycle Evaluation Panel

LASL support in being provided to the panel chaired by Professor J. E. Funk (Kentucky). At this time, two cycles are undergoing evaluation. They are the G.A. Sulfuric Acid-Iodine process and the LLL Zinc-Selenide process.

IEA Meeting, September 24-27, 1979, Los Alamos

A thermochemical cycle workshop was held at LASL under IEA auspices during the latter part of September. Over 40 persons attended the conference with international delegates from the European Common Market (EEC) Ispra laboratory, West Germany, and Japan. Leading emphasis was placed on sulfuric acid based cycles - sulfuric acid decomposition and materials problems.

In other discussion, the following topics were included:

- Electrochemical SO_2 reactions
- Hydrogen halide decomposition
- New cycles and heat sources
- Complete circuits (bench-scale)
- Techno-economic assessments.

Much technical progress was noted since the First Annual Workshop was held at Ispra, Italy in August 1978. The value of programs to identify new and alternative cycles was recognized and emphasized by the Workshop. Plans for future technical cooperation in these and other areas will be submitted to the IEA Executive Committee for consideration and approval.

CORROSION TESTING OF MATERIALS IN HOT CONCENTRATED SULFURIC ACID*

Oscar H. Krikorian

Lawrence Livermore Laboratory
Livermore, CA 94550

Abstract

We are testing and evaluating materials for a sulfuric acid boiler for use in thermochemical hydrogen cycles that require decomposition of H_2SO_4. Operating conditions call for boiling of 97 wt% H_2SO_4 at ~673K and 1 MPa pressure. We have determined that high silicon content materials can generally tolerate the corrosive conditions that prevail. Materials that appear most suitable at present, especially as heat exchanger materials, are Durichlor-51 and SiC. Preliminary tests on $CrSi_2$-coated Incaloy 800 also show good promise.

Background

We have had a study underway at the Lawrence Livermore Laboratory for the past two years to test and evaluate materials suitable for a sulfuric acid vaporizer for use in thermochemical hydrogen cycles being developed at the General Atomic and Westinghouse laboratories. Both the I_2-H_2SO_4 cycle under development at General Atomic and the SO_2-H_2SO_4 cycle at Westinghouse require concentrating of sulfuric acid solutions by boiling off water to form an azeotropic composition at ~97 wt% H_2SO_4, which is then boiled at ~673K (with an energy input of 26 kcal/mole) to produce sulfuric acid vapor at a pressure of ~1 MPa (10 atm). The vapor is then heated to temperatures of 1000-1150K where it is decomposed to produce SO_2, O_2 and H_2O. Boiling of the azeotropic H_2SO_4 composition imposes the most severe materials problem in this process sequence. All known ductile metals that are suitable for heat exchangers (except for gold and for the platinum group metals, which are too expensive for consideration) are rapidly attacked and dissolved by liquid H_2SO_4 under the azeotropic boiling condition. However, once vaporized, sulfuric acid is far less corrosive than the liquid.

In past work at the Lawrence Livermore Laboratory, we have established that silicon-rich materials generally have good corrosion resistance under operating conditions. Corrosion tests were conducted on specimens in sealed silica vials containing 97 wt% H_2SO_4 at 673K for times of 500-1100 h. Materials tested were the commercial high silicon cast irons (Duriron and Durichlor-51), single crystal Si, SiC, Si_3N_4, and $CrSi_2$. Of these the only materials that showed significant corrosion were Duriron and Durichlor-51. Of the two, Durichlor-51 performed the better, giving a protective scale that showed a uniform corrosion behavior over the entire surface. With Duriron, the surface scale varied considerably in thickness and showed significant amounts of spalling, fracturing, and corrosion pits. The scale on the Durichlor-51 after 520 h was 5 μm thick. Using a linear corrosion rate gives an extrapolated lifetime of about 6 y to attain a scale thickness of 0.5 mm. Assuming a parabolic corrosion rate would extend the lifetime even more. This is an encouraging observation, but long term proof tests are needed to substantiate the actual behavior.

The high silicon cast irons, Duriron and Durichlor-51 both contain 14.5% Si, 0.85% C, and 0.65% Mn. In addition, Durichlor-51 also contains 4.5% Cr. In reality, the term cast iron is misleading, since these materials are basically intermetallic compounds of the approximate composition Fe_3Si. As such, they have low tensile strength, poor ductility, poor impact resistance, and are difficult to fabricate. Quality control will be an important problem in the manufacture of these materials if they are to be used in this application. Internal porosities introduced during casting are of particular concern. Special machining and milling operations will need to be developed, since material surfaces are readily damaged by normal machining operations and produce surface fractures that promote subsequent corrosion. With proper quality control in manufacture, and with development of suitable machining and other fabrication techniques, we believe that Durichlor-51 type materials can be used for H_2SO_4 boilers.

Materials such as SiC and Si_3N_4 are considered to be ceramics, and substantial progress has been made in recent years in fabricating intricate shapes with them using ceramic fabrication techniques such as hot pressing or extrusion and sintering. The motivation for these developments has been mainly the need for high temperature ceramic turbines, but these materials may also have application in coal conversion process equipment. It is currently possible to obtain U-shaped SiC tubing for use in heat exchangers from commercial suppliers (e.g., Carborundum Co. and Norton Co.). We believe that the design and fabrication of an efficient heat exchanger system for an H_2SO_4 boiler based on SiC still remains a difficult and challenging problem. Si_3N_4 is also a potential future candidate material.

The excellent corrosion resistance shown by $CrSi_2$ presents us with another alternative for a heat exchanger design, i.e., by using $CrSi_2$ coatings to provide corrosion protection of more conventional heat exchanger alloy materials. Some work along these lines will be discussed in this report.

*This study was sponsored by the U. S. Department of Energy - Division of Energy Storage Systems and performed by the Lawrence Livermore Laboratory under contract No. W-7405-Eng-48.

Current Studies

Materials corrosion studies during the past year at the Lawrence Livermore Laboratory continued with the goal of testing and evaluating materials suitable for a sulfuric acid vaporizer. Tasks that were completed were (1) construction and operation of a boiling-circulating sulfuric acid corrosion test loop, and (2) testing of $CrSi_2$ coated specimens of 304 stainless steel, Inconel 600 and Incaloy 800.

The corrosion test loop was constructed of silica glass. It had a boiler chamber 1.5 cm i.d. x 14 cm high, a matching condensation chamber of the same size with silica glass piping joining the upper and bottom parts of the two chambers (see Figures 1 and 2). The assembled loop was mounted inside of an autoclave and placed in the furnace of the H_2SO_4 Corrosion Test Facility (see Figure 3). The test loop was heated primarily by heat from the autoclave, but a Nichrome heating element wound around the boiler was used to provide supplemental heat. An argon overpressure of 1.2 MPa (12 atm) was maintained inside of the autoclave to compensate for the boiling pressure of H_2SO_4 (~10 atm maximum) and maintain the silica under compression. The condenser was enveloped in a silica cooling jacket which was cooled by a high pressure flowing air stream. The cooling jacket was insulated on the outside with a fibrous ZrO_2 blanket to minimize heat exchange with the autoclave enclosure, and the inlet and outlet air temperatures and the air flow rates were measured to calorimetrically determine the amount of heat recovery from the condenser section. With the H_2SO_4 boiler operating at 400°C, an air flow rate (at 25°C) of 15 ℓ/min. and a temperature rise of 200°C were found to be optimum for loop operation. Using 26 kcal/mol for the heat of vaporization of H_2SO_4, this gives a boiling (condensation) rate of 200 g H_2SO_4/h.

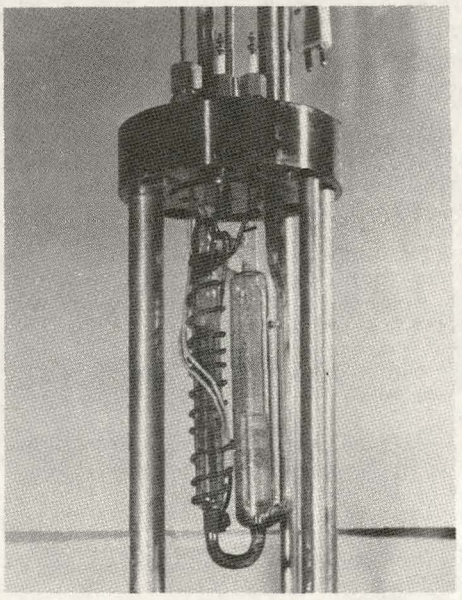

Figure 1. The H_2SO_4 circulating loop mounted on the autoclave flange. The boiler section is on the left and condenser on the right.

A corrosion test was run on a rod specimen of Durichlor-51, 0.58 cm x 0.58 cm x 11.4 cm, placed in the boiler section of the fused silica loop. Approximately 40 g of 97 wt% H_2SO_4 was used in the loop and the liquid covered about two thirds of the specimen. The test was carried out at 400°C at a boiling rate of 200 g H_2SO_4/h for a total of 170 h. Visual examination showed evidence of moderate corrosion (discoloration, pitting, and crystallites on the surface) for ~2 cm in the vicinity of the meniscus region. Above this region there was no evidence of attack, and below this region, the attack was minimal. The corrosion behavior appears to be identical to that observed in our earlier experiments which used static H_2SO_4 in contact with the samples in sealed silica bulbs.

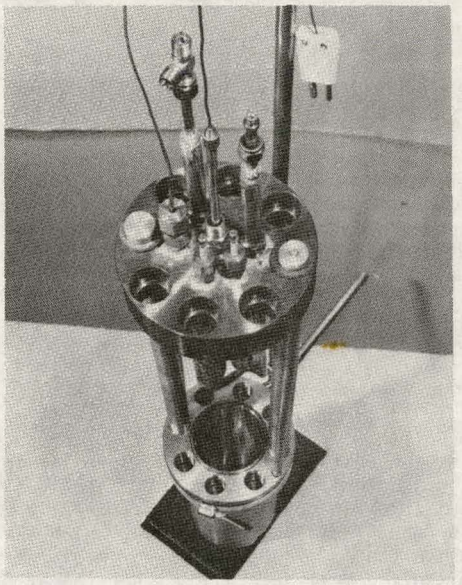

Figure 2. Top view of the H_2SO_4 circulating loop assembly. The support rods would be removed to lower the loop into the autoclave below.

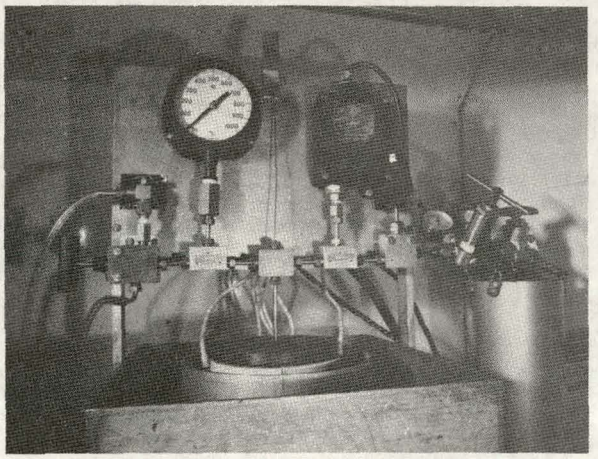

Figure 3. A view of the High Pressure H_2SO_4 Corrosion Test Facility showing the top of the furnace and the high pressure line.

A corrosion test on the $CrSi_2$ coated specimens was run in 97% H_2SO_4 at 400°C for 240 h using duplicate samples of 304 stainless steel, Inconel 600 and Incaloy 800 as substrates. The test was stopped at 240 h due to a pressure rise in the autoclave, and it was discovered that one of the capsules had failed between 175 and 240 hours (over the weekend). The specimens were rod-shaped with dimensions of about 1.5 mm x 4.5 mm x 5 cm. Coatings (~0.4 mm thick) were applied to the specimens by Dr. Charles M. Packer of Lockheed Missiles and Space Company of Palo Alto, California, using a slurry coat and rapid melt technique. The samples after test are shown in Figure 4. Samples 1 and 2 are Inconel 600, samples 3 and 4 Incaloy 800, and samples 5 and 6 304 stainless steel. The capsule that failed contained one of the coated 304 stainless steel samples. The failed sample showed large damaged areas in the $CrSi_2$ coating and massive attack of the substrate. It had a weight loss of 0.5 g for a 3.4 g sample. The other stainless steel sample also showed damaged areas in the coating accompanied by spalling, but apparently the spalling occurred after cooldown since no significant attack was visually apparent beneath the exposed areas, and the total weight loss was only 0.03 g for a 3.4 g sample. The coatings were all intact for the Inconel 600 and Incaloy 800 specimens, and showed little visible corrosion, although a yellow precipitate was present (as was also for the 304 stainless steel specimens) in the bottom of the bulb. Weight losses for the Inconel 600 specimens were 0.034 g and 0.056 g for sample weights of 3.6 g; and for the Incaloy 800 specimens weight losses were 0.002 g and 0.003 g for ~3 g samples. The $CrSi_2$ coated Incaloy 800 looks very promising for further development.

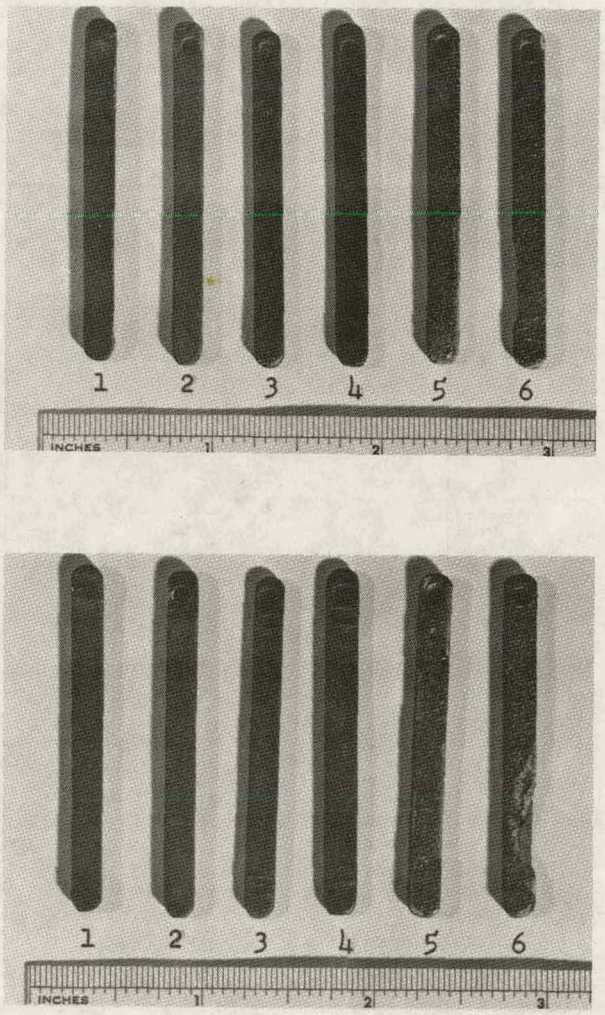

Figure 4. The upper part shows the front view, and the lower part, the rear view of $CrSi_2$ coated specimens of Inconel 600 (1 and 2), Incaloy 800 (3 and 4) and 304 stainless steel (5 and 6). These specimens were subjected to corrosion by 97% H_2SO_4 at 400°C for 240 h in silica vials.

PHOTOELECTROCHEMICAL DECOMPOSITION OF WATER

R. D. Rauh

EIC Corporation
55 Chapel Street
Newton, Massachusetts 02158

Abstract

The goal of this program is to achieve efficient photoelectrochemical decomposition of H_2O with visible light. Research has entailed 1) the synthesis and photoelectrochemical evaluation of ∿150 n-doped semiconducting transition metal oxides; 2) assessment of the stability and photoelectrochemical properties of several p-type photocathodes; 3) evaluation of several highly economical photoelectrochemical converters.

Introduction

The production of "solar fuels" by the direct conversion of photon energy to chemical energy is an attractive concept, providing us with a general route to renewable resources. In this program, we have concentrated on the use of photoelectrolysis at semiconducting electrodes to produce hydrogen from water. The principal challenge of this research is to achieve such a reaction with visible light, the major component of sunlight.

As outlined previously[1], the stability and energetic requirements for photoelectrodes are quite restrictive. Photoanodes (n-type semiconductors) must be stable under conditions of O_2 evolution, and must probably be oxides themselves. Photocathodes must be H_2 electrodes, stable under reducing conditions. For a photoelectrode to act alone in decomposing H_2O, a minimum thermodynamic requirement is the straddling of the energy levels for H_2 and O_2 evolution by the conduction and valence bands of the semiconductor. We refer to these as Class I materials. Photoelectrodes which require an additional bias of less than 1.23 eV to decompose H_2O are called Class II materials. Class II materials can still yield significant energy storage, either acting alone with an external power supply, or in conjunction with a suitably matched photoelectrode of opposite doping.

Summary of Results

During the last 18 months, our primary efforts on this program have been directed toward photoanode development. A practical Class I photoanode must have a band gap below 2.5 eV, for significant solar absorbtion, and a low electron affinity, to bring the conduction band above the H_2 evolution energy. These properties are often mutually exclusive in semiconducting oxides. The following conclusions are possible based on our accumulated results:

- Based on our experimental evaluation of over 150 oxide semiconductors, the best Class I photoanode yet discovered is $SrTiO_3$ (ΔE_g = 3.1 eV). No Class I oxide with ΔE_g <3 eV has yet been found.
- The best Class II photoanodes are Fe_2O_3 (ΔE_g = 2.1 eV) and $Fe_{2-x}Rh_xO_3$ (ΔE_g = 1.5-2 eV). These materials require an external bias of ∿0.5V to effect complete photoelectrochemical H_2O decomposition. As shown in Figure 1, the presence of Rh appears to enhance the photoresponse via sensitization to lower energy light. The flat band potential is not adversely affected. The external bias could be supplied by a suitably matched p-type semiconductor (e.g., p-CdTe).

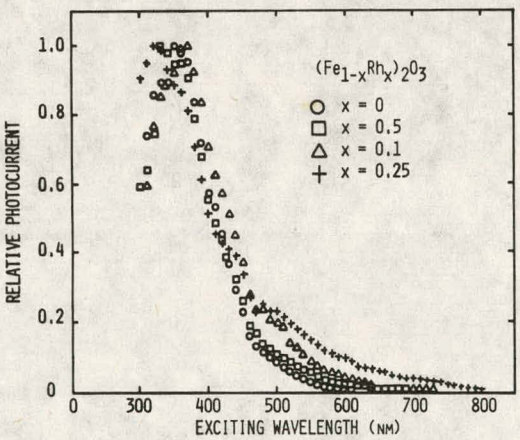

Fig. 1. Action spectra of Fe_2O_3 and Rh_2O_3 doped Fe_2O_3 thin film electrodes on sintered polycrystalline Fe_2O_3·0.02 TiO_2 substrates.

- The d-band oxide PdO is potentially a superior Class II photoanode, with V_{fb} ∿0.3-0.4V vs. NHE and ΔE_g ∿1.5 eV[2,3]. Films of PdO formed by thermal oxidation of the parent metal tend to be p-type, although some n-type specimens were obtained and tested. Since the PdO valence band is of d-electron origin, it does not lie as deeply in energy as a valence band derived mostly from the oxygen (2p) bonding orbital.
- Only limited success has been achieved so far with d^n/d^o mixed metal oxides (other than $Fe_{2-x}Rh_xO_3$). For example, results for TiO_2 substituted with Ru, Rh, Pd, Pt or Ir are presented in Table 1. Some of these metals do yield sensitization of the TiO_2 photoresponse to the visible spectrum, but with a decreased total photoresponse compared to the parent

Table 1. Photoelectrochemical properties of mixed platinum metal oxide-titanium dioxide photoelectrodes.

Electrode Material[a]	ΔE_g (eV)	V_{fb}[b]	Photocurrent[c] (mA/cm^2)
TiO_2	3.05	-0.730	1.83
$10TiO_2 \cdot 2.5RuO_2$	d	-0.3	0.1
$10TiO_2 \cdot 1RuO_2$	d	-0.5	0.15
$10TiO_2 \cdot 0.5RuO_5$	d	-0.3	0.28
$20TiO_2 \cdot 2.5Rh_2O_3$	d	-0.4	0.093
$20TiO_2 \cdot 1.0Rh_2O_3$	d	-0.45	0.1
$20TiO_2 \cdot 0.5Rh_2O_3$	2.7 (1.3)	-0.6	0.32
$20TiO_2 \cdot 0.25Rh_2O_3$	2.98(2.0)	-0.6	0.24
$20TiO_2 \cdot 0.1Rh_2O_3$	2.94(1.7)	-0.8	0.23
$20TiO_2 \cdot 0.25Rh_2O_3 \cdot 0.25Al_2O_3$	2.95(1.6)	-0.8	0.13
$10TiO_2 \cdot 2.5PdO$	2.90(2.0)	-0.6	0.12
$10TiO_2 \cdot 1PdO$	3.05	-0.8	0.77
$10TiO_2 \cdot 0.5PdO$	3.13	-0.7	1.4
$10TiO_2 \cdot 2.5PtO_2$	d	-0.3	0.43
$10TiO_2 \cdot 1PtO_2$	d	-0.35	0.19
$10TiO_2 \cdot 0.5PtO_2$	d	-0.75	0.007
$10TiO_2 \cdot 2.5IrO_2$	3.17	-0.76	0.48
$10TiO_2 \cdot 1IrO_2$	3.0	-0.77	0.53
$10TiO_2 \cdot 0.5IrO_2$	3.1	-0.8	1.6

[a] Thin films on a platinum substrate.
[b] Flat and potential versus SCE, pH = 10, 0.25M Na_2SO_4, 0.1M borate buffer.
[c] At +1V bias vs. SCE.
[d] Difficult to measure due to poor photoresponse, large dark currents, and/or unstable electrode.

compound. The flat band potentials (V_{fb}) are either unaffected or shifted more positive by the substitution. A Class I photoanode must have V_{fb} negative of the H_2 evolution of potential.

In these materials, it appears that the d^n cation sublattice only exhibits partial band formation. These cations often act as traps for holes and electrons, diminishing the overall photoresponse. However, excitation from these traps into the conduction band can also result in the weak photocurrents observed with visible light.

- The kinetics of electron transfer for water oxidation appear to be enhanced by the mediation of CO_3^{2-} oxidation, in the cases of Fe_2O_3 and Rh-substituted Fe_2O_3 (Figure 2). Similar effects have been observed by Gerstner et al.[4] with SO_4^{2-} at TiO_2 electrodes. Our measurements indicate that the O_2 evolution current efficiency is nearly 100% in these systems. Thus, it is possible that the efficiency of sunlight utilization in the water oxidation reaction can be increased by varying the composition of the solution.

- More limited research has been carried out in our laboratory on p-type photocathodes as Class I or Class II materials. In many respects, the stability of a photoelectrode under reducing conditions may be easier to obtain than under conditions of O_2 evolution. We have measured the coulometric efficiency of photoelectrochemical H_2 production of n-GaAs at several pHs and bias potentials. Efficiencies very close to 100% are observed, although ~0.1% AsH_3 production was detected in some samples. Similar stabilities are noted for p-CdTe and p-WSe_2. Photocurrent onsets are considerably negative of the flat band potentials of these electrodes, a possible result of surface states.

Recently, we have begun conducting research on photoelectrolysis schemes which exploit some of the unique practical advantages over the electrolysis of water using the output of photovoltaic devices. For example, it was first pointed out by Nozik[5] that particles of certain semiconductors can act as "photoelectrochemical diodes." We have studied photodecomposition of water on partially platinized particles of $SrTiO_3$ suspended in aqueous solution. A spontaneous liberation of a 2:1 H_2/O_2 mixture is noted under irradiation. We also observe a fatiguing process, which may involve deplatinization of the particles. Clearly, more research is required on the preparation and characterization of these catalytic diode structures.

Since the semiconductor-electrolyte junction is so intimate and readily formed, high photocurrent quantum yields have been observed for a wide variety of inexpensive fabricated polycrystalline electrodes.

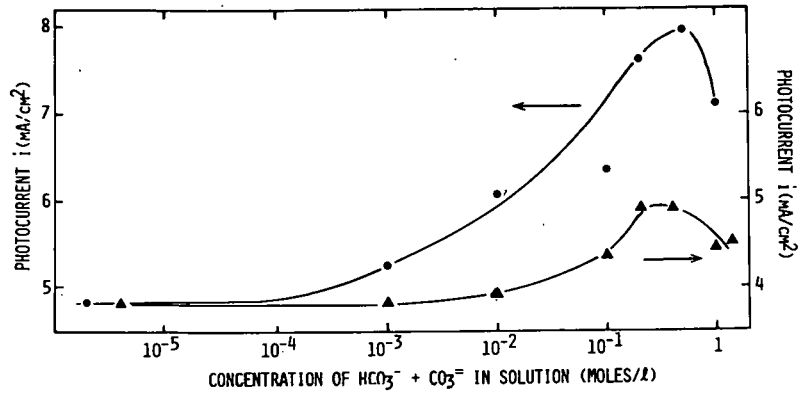

Fig. 2. Effect of biocarbonate/carbonate ions on the photoresponse of the Fe_2O_3 (1% TiO_2) photoelectrodes. ● and ▲ represent two different photoelectrodes. All solutions contained 0.25M Na_2SO_4 and 0.1M borate buffer and are adjusted to final pH = 10. First points on the left of the curve are photoresponses at $[HCO_3^- + CO_3^=] = 0$.

These include sintered ceramics and films prepared by evaporation, various forms of pyrolysis, and electrodeposition. Indeed, the optimization of such economical electrode structures may be the single most important aspect of the development of a practical photoelectrolysis plant.

Economics of Photoelectrolysis

Nozik[6] has presented a simple framework for considering the economics of photoelectrolysis of water. He assumes a total absorbed solar power of 2000 kWh/m^2-yr, typical of a nontracking collector in the Southwestern U.S. If this sunlight were used at 100% efficiency, it would produce H_2 equivalent to 6.86M BTU/m^2-yr. If CC is the capital cost per m^2 of the collector, and mortgage and upkeep of the collector amounts to 20% of CC/yr, then the cost of the H_2 product is

$$\text{Cost(\$1M BTU)} = \frac{CC(0.2)(100)}{6.8\ \alpha} \qquad (1)$$

where α is the solar conversion efficiency. In Figure 3, costs of H_2 are plotted vs. efficiency for collectors of different capital cost. Figure 3 shows that with an optimized system of 30% conversion efficiency and collector costs of \$10-\$50/m^2, H_2 costing \$1-\$5/M BTU could be obtained.*

What are the prospects regarding actual collector costs in such photochemical systems? Since there is no need for insulation for photon processes, only a shallow tray is necessary to contain the water and active elements. Additionally, H_2 must be given off in a restricted area to allow its collection, so a transparent cover may be required. If a particulate semiconductor system is used, an H_2/O_2 mixture would be evolved off of each grain. This would be the least costly configuration, e.g., a 0.1 mm x 1 m^2 layer of TiO_2 costs \$5/m^2 based on today's prices. Hence, \$10/m^2 is a realistic estimate for a simple photoelectrochemical collector as installed. A collector with photoelectrodes, where H_2 could be easily separated from O_2 would cost somewhat more depending on the configuration and materials.

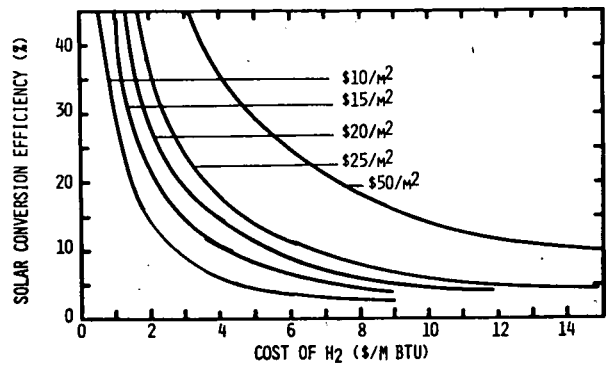

Fig. 3. Cost of H_2 produced by solar photoelectrolysis of water, as a function of solar conversion efficiency and collector cost (after Nozik, ref. (6)).

*A 1M^2 panel of solar cells giving an overall conversion efficiency of solar energy of H_2 of 10% (i.e., 100 peak W output) would cost at least \$500-\$1000 by today's costs, discounting the electrolyzer.

References

1. R. D. Rauh, J. M. Buzby, T. F. Reise and S. A. Alkaitis, J. Phys. Chem., 83, 2221 (1979).

2. H. Okamoto and T. Aso, Japan. J. Appl. Phys., 6, 779 (1967).

3. D. Rogers, R. Shannon and J. Gillson, J. Sol. State Chem., 3, 314 (1971).

4. M. E. Gerstner, J. Electrochem. Soc., 126, 944 (1979).

5. A. J. Nozik, Appl. Phys. Lett., 30, 567 (1977).

6. A. J. Nozik, Proc. 11th IECEC, Lake Tahoe, Nevada (1976).

STUDIES OF SOLAR ENERGY STORAGE REACTIONS INVOLVING POLYNUCLEAR RHODIUM ISOCYANIDE COMPLEXES

Harry B. Gray and Vincent M. Miskowski
A. A. Noyes Laboratory of Chemical Physics
California Institute of Technology
Pasadena, California 91125

Amitava Gupta
Energy and Materials Research Section
Jet Propulsion Laboratory
California Institute of Technology
Pasadena, California 91103

Abstract

The mechanism of photochemical evolution of hydrogen on long wavelength irradiation of solutions of rhodium isocyanide complexes in hydrohalic acids has been studied by measurement of quantum yields of products and by flash spectroscopy. The redox chemistry of these complexes has also been investigated in order to characterize the intermediate oligomeric species which are formed when $Rh_2(br)_4^{2+}$ is dissolved in hydrohalic acids and which initiate the primary photoprocess leading to hydrogen evolution.

Introduction

For the past three years we have been investigating the effect of long wavelength irradiation on rhodium isocyanide complexes in combination with various reagents. We initially[1] found that solutions prepared by dissolving the binuclear Rh(I) complex $[Rh_2(bridge)_4]^{2+}$ (bridge ≡ 1,3-diisocyanopropane) in aqueous hydrohalic acid generated H_2 upon 546 nm irradiation. We now report upon our progress in determining the composition of the species present under various conditions and the mechanisms of their photoreactions.

Description of the Chemical System

The redox chemistry of rhodium isocyanide complexes has proven to be extremely rich. The "parent" Rh(I)-bridge dinuclear complex possesses no formal metal-metal bond, whereas 2-electron oxidation yields a Rh(II) dinuclear complex with a full d^7-d^7 single metal-metal bond. Crystal structures show that the metal-metal distance actually decreases by 0.4Å upon 2-electron oxidation. A variety of polynuclear species in net oxidation states also exist intermediate to these extremes. There is a close analogy to the mixed-valence platinum chain compounds,[2] in solid state; however, the species described here are characterized in solution.

By means of redox titrations with various oxidants and reductants, e.g., H_2, Eu^{2+}, Cu^{2+}, Ce^{2+}, we have characterized several species of the form $[Rh_2(bridge)_4]_n^{(2n+2)+}$ in aqueous acid solution. Typical spectrophotometric titrations are shown in Figures 1 and 2. All of these species are two electrons short of the Rh(I) state, and thus, formally, possess one metal-metal bond per molecule. All also show a very intens electronic absorption transition attributable to a $\sigma \rightarrow \sigma^*$ metal-metal bonding-to-antibonding transition,[3] the wavelength of which is strongly dependent upon chain length. Values in 10M H_2SO_4(aq) are summarized in Table I.

Table I: $\sigma \rightarrow \sigma^*$ transitions for Rhodium-bridge chains

Oligomer	λmax(um)	εmax/Rh_2 unit($m^{-1}cm^{-1}$)
$[Rh_2(bridge)_4]^{4+}$	311	33,600
$[Rh_2(bridge)_4]_2^{6+}$	572	37,000
$[Rh_2(bridge)_4]_3^{8+}$	780	48,000
$[Rh_2(bridge)_4]_4^{10+}$	960	55,000

The red-shift with increasing chain length is attributed to delocalization, and is well reproduced by simple Huckel theory calculations. Even lower energy absorptions (1100 nm, 1350 nm, etc.) have been observed, and are presumably attributable to complexes with higher n values, and/or oligomers of the already characterized species. Under highly reducing conditions (100-fold excess of Cr^{2+}), the Rh(I) complex $[Rh_2(bridge)_4]^{2+}$ can be observed for the stable solutions in aprotic solvents. These results are confirmed by studies of $[Rh_2(TMB)_4]^{2+}$, TMB = 2,5-dimethyl-2,5-diisocyanohexane, which is stable in degassed INH_2SO_4(aq) in the absence of added reductants, and which does not itself oligomerize, presumably because of steric hindrance. Titration of $[Rh_2(bridge)_4]_2^{6+}$ with one or two equivalents of $[Rh_2(TMB)_4]^{2+}$ yields species with spectral properties nearly identical to $[Rh_2(bridge)_4]_3^{8+}$ and $[Rh_2(bridge)_4]_4^{10+}$, respectively.

We are now beginning to investigate reduction of the rhodium complexes below the Rh(I)-d^8 level. Again, there are analogous reduced platinum chain compounds.[2] Electrochemical reduction of solutions of $[Rh_2(bridge)_4]^{2+}$ in CH_3CN and related nonaqueous solvents occurs near 1.46 volts and is largely irreversible even at very high CV scan rates. Coulometric experiments show that a net 1-electron reduction occurs. The nature of the very air-sensitive reduction product is unknown as yet; its electronic spectrum is quite different from that of a reduced transient observed in flash photolysis experiments to be described below.

Hydrogen Stoichiometry

We now know that the reaction of $[Rh_2(bridge)_4]^{2+}$ with aqueous acid occurs in two net steps as set out below:

$$[2Rh_2(bridge)_4]^{2+} + 2H^+ \xrightarrow{\Delta} [Rh_2(bridge)_4]_2^{6+} \quad (1)$$

$$[Rh_2(bridge)_4]_2^{6+} + 2H^+ \xrightarrow{h\nu(546\ nm)} [2Rh_2(bridge)_4]^{4+} + H_2 \quad (2)$$

Neither (1) nor (2) has been observed in the absence of halide ions, and, in particular, the quantum yield of (2) is strongly sensitive both to the type of halide anion present and to its concentration.[3] Thus, ϕ varies from 2.8×10^{-4} to 7.9×10^{-3} as (HCl) increases from 9.1 M to 12.8 M, and is 4.4×10^{-2} and small in 9 M HBr(aq) and 10 M H_2SO_4(aq) respectively. Not surprisingly, stronger oxidants such as O_2 and Fe^{3+} are more effective than the proton in both thermal and photochemical oxidations, and careful degassing is required for limiting H_2 yields.

It is noteworthy that H_2 is an effective reductant for $[Rh_2(bridge)_4]^{4+}$, and in our photolysis experiments a photochemical steady-state is commonly achieved. Thus, an intermediate Toeppler pumping cycle, followed by additional irradiation and further pumping, was required in order to push reaction (2) to completion in hydrochloric acid solution. Evidently (2) is close to, or actually, uphill. Indeed, H_2 can effectively reduce $[Rh_2(bridge)_4]_2^{6+}$ to lower oxidation states. Like (1) and (2), this reaction is strongly halide sensitive. In 18 N H_2SO_4(aq), 30 mm of H_2 is sufficient for quantitative reduction to $[Rh_2(bridge)_4]_3^{8+}$.

Encouraged by some aspects of the thermal reduction chemistry, we have initiated attempts to catalyze (2) with species such as Fe^{2+}. Flash photolytic experiments set out below show that photochemical reduction of $[Rh_2(bridge)_4]_2^{6+}$ does occur in such systems. However, H_2 has not yet been reproducibly observed as a major product in the absence of halide ion.

Photochemical Mechanisms

We have performed extensive flash photolytic experiments with the aim of elucidating photochemical reaction mechanisms. Our original work[4] was restricted to the Rh(I) dimers exemplified by $[Rh_2(bridge)_4]^{2+}$. We found this molecule to display singlet emission at 650 nm with a lifetime and quantum yield of 1.3 ns and 0.056 respectively in aprotic solution. A long-lived transient, τ = 9μs, was also observed, and assigned to a triplet. This assignment has subsequently been confirmed by direct observation of 9μs lifetime phosphorescence, λ max ~ 830 nm, and by quenching experiments. The triplet yield is ~0.95 and the triplets may be quenched either by energy transfer (anthrocene; O_2) or by electron transfer.

Oxidative quenching yields a transient with λ max ≃ 440 nm. An identical transient has been observed upon flash photolysis of $[Rh_2(bridge)_4]_2^{6+}$, Fig. 3. Either in protic or aprotic solution, the latter route yields a transient which decays by clean second order kinetics, and an ionic strength dependence study, Fig. 4, indicates that decay involves reaction between two particles of charge +3. Oxidative scavenging studies showed that the $[Rh_2(bridge)_4]^{3+}$ fragment could be readily oxidized to $[Rh_2(bridge)_4]^{4+}$, and detailed kinetic and quantum yield studies provided further confirmation[5,6] of the proposed mechanism.

Flash photolysis studies in the presence of halide ions evidence more complicated behavior. The 440 nm transient is still present, with similar quantum yield ($\phi \simeq 10^{-2}$) and clean second-order decay. However, a second, independent set of transients is also observed, notably with strong absorption at 700 nm. Decay of this transient(s) eventually results in net disproportion to $[Rh_2(bridge)_4]^{4+}$ and $[Rh_2(bridge)_4]_3^{8+}$, Fig. 5. These metastable products eventually decay back to starting material on a timescale of seconds to hours, depending on temperature and medium.

Some insight into the mechanism of formation of these intermediates was provided by flash photolysis of solutions similar to those of Fig. 3, but containing the nonthermal reductant Fe^{2+}. As shown by Fig. 6, production (and decay) of the 440 nm transient is unaffected. However, a new transient absorbing at 700 nm is also observed, the intensity being proportional to $[Fe^{2+}]$. Like the 440 nm transient, the rise time is less than 2 ns, and reductive quenching of the tetranuclear excited state of $[Rh_2(bridge)_4]_2^{6+}$ is suggested. Decay of the 700 nm transient yields, cleanly, $[Rh_2(bridge)_4]_3^{8+}$, Fig. 7, with further decay back to starting material (presumably by back reaction with Fe^{3+}) again occurring on a very long time scale.

The 700 nm transient is presumably $[Rh_2(bridge)_4]_2^{5+}$. Dimerization of this complex would yield the previously characterized $[Rh_2(bridge)_4]_4^{10+}$, and further reaction with starting material would yield $[Rh_2(bridge)_4]_3^{8+}$. Not surprisingly, the kinetics of formation of the latter are indeed observed to be complex, and we have not yet unraveled the details of the mechanism.

The kinetics for photolysis in the presence of halide ion are even more complex. We can at best guess from the similar 700 nm-absorbing transient that heterolytic photochemical cleavage is occurring in addition to the well-characterized homolytic cleavage. It is known, from spectral changes, that $[Rh_2(bridge)_4]_2^{6+}$ binds halide ion. This could either result in formation of halogen radicals upon excitation, Eq. (3), or simply perturb the molecule towards unsymmetrical cleavage, Eq. (4).

$$[X^-\text{-}Rh_2\text{-}Rh_2]^{5+} \xrightarrow{h\nu} X\cdot + [Rh_2\text{-}Rh_2]^{5+} \quad (3)$$

$$[X^-\text{-}Rh_2\text{-}Rh_2]^{5+} \xrightarrow{h\nu} [XRh_2]^{3+} + Rh_2^{2+} \quad (4)$$

Some evidence for (3) is provided by our studies of $[X_2Rh_2(bridge)_4]^{2+}$ photolysis, where X· formation does occur. In either case, reduced complexes would be formed, consistent with our observations. It is tempting to relate the formation of such reduced species with the photochemical production of hydrogen. Finally, we have begun to study the reactions of the long-lived $[Rh_2(bridge)_4]^{2+}$ excited state with reductive quenchers, e.g., tertiary amines. A new transient is indeed observed in visible wavelength flash-photolysis experiments, back-reaction regenerating starting material, and we are hopeful that this presumed $[Rh_2(bridge)_4]^+$ species, which should be a very powerful reductant, may yield interesting chemistry with reagents such as the proton.

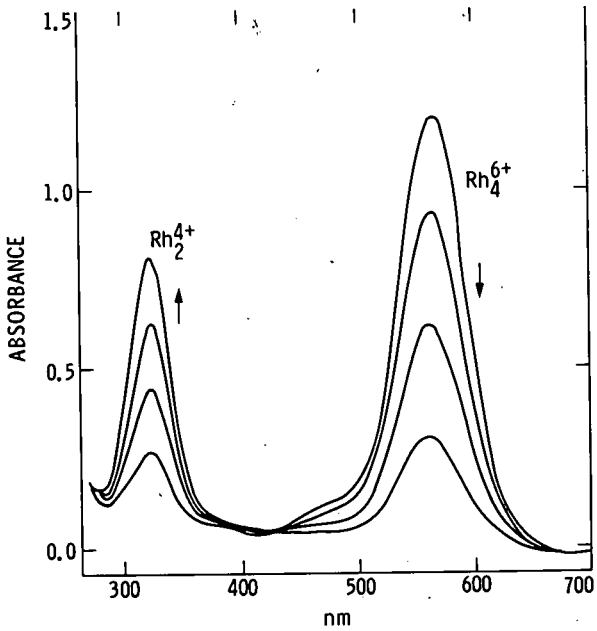

Fig. 1 Titration of Rh_4^{6+} (λmax = 558 nm) to Rh_2^{4+} (λmax = 311 nm) with Ce^{4+} in 1 N H_2SO_4(aq). Each aliquot of Ce^{4+} contains 0.5 equivalents/initial equivalent of Rh_4^{6+}.

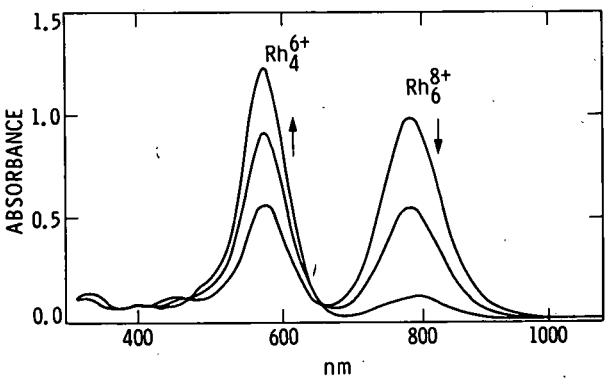

Fig. 2 Titration of Rh_6^{8+} (λmax = 780 nm) to Rh_4^{6+} (λmax = 572 nm) with Ce^{4+} in 10 M H_2SO_4(aq). Each aliquot of Ce^{4+} yields 1.5 equivalents of Rh_4^{6+}.

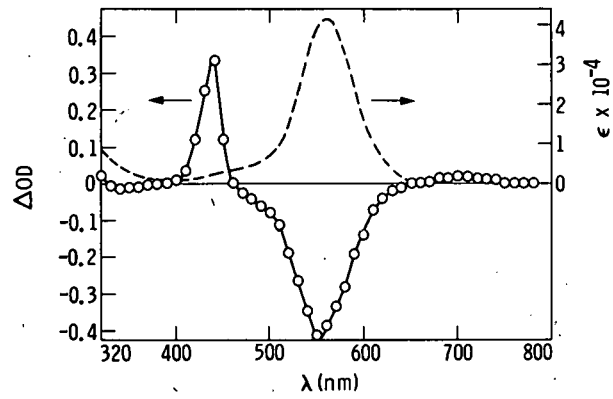

Fig. 3 Absorption spectrum (---) and transient difference spectrum (——) for Rh_4^{6+} in 1 N H_2SO_4(aq), 25C.

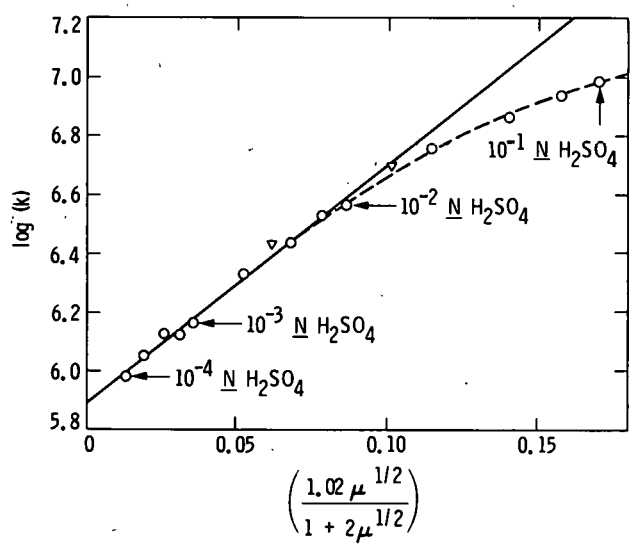

Fig. 4 Plot of log (recombination rate constant) vs. Wellers ionic strength (μ) function. For the points (⊖), μ was adjusted only with H_2SO_4. For the points (▽), H_2SO_4 was 10^{-3} N, and μ was further adjusted with $Li_2SO_4H_2O$.

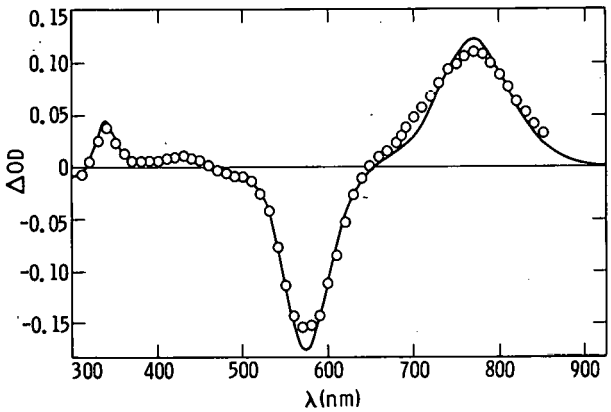

Fig. 5 Transient difference spectrum 100 ms after flash for $[Rh_2(bridge)_4]_2^{6+}$ in 0.1 M HCl(aq): ⊙; the line (——) is a thermal disproportionation spectrum synthesized from experimental difference spectra for oxidation to $[Rh_2(bridge)_4Cl_2]^{2+}$ and reduction to $[Rh_2(bridge)_4]_3^{2+}$ in the same solvent.

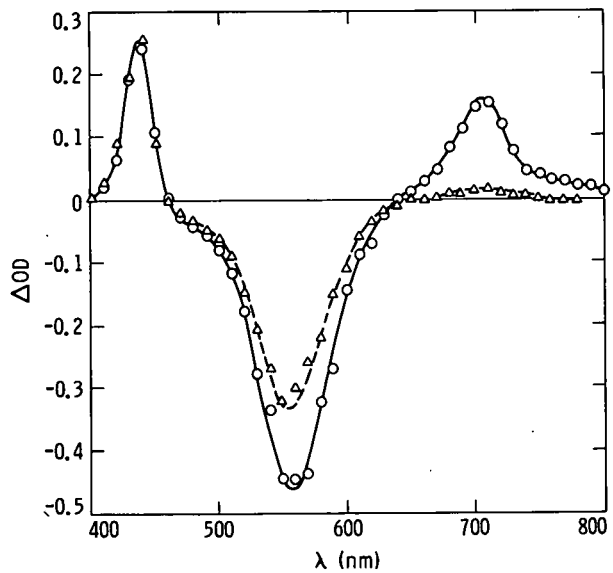

Fig. 6 Comparison of difference spectra 1 ms after flash for Rh_4^{6+} in 1 N H_2SO_4(aq) with: (⊙), $[Fe^{2+}]$ = 0.2 M; (▽), $[Fe^{2+}]$=0.

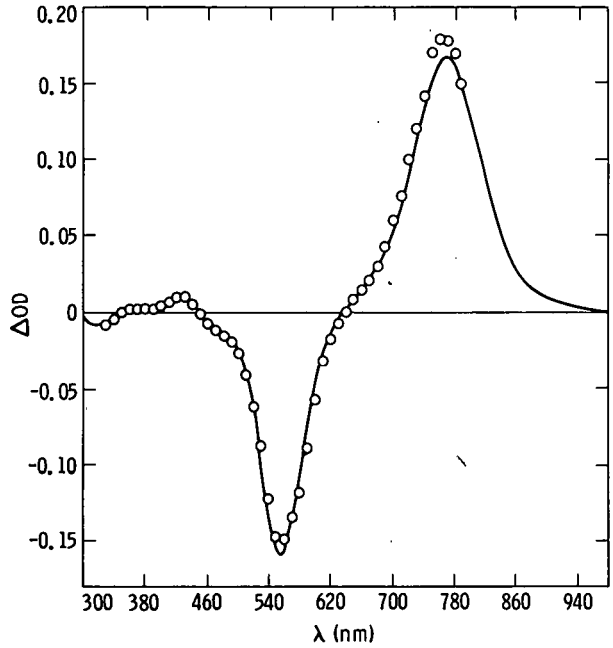

Fig. 7 Transient difference spectrum 200 ms after flash for Rh_4^{6+} in 1 N H_2SO_4(aq) containing 0.2 M Fe^{2+}: (⊙); difference spectrum for thermal H_2 reduction in 1 N H_2SO_4(aq): (—).

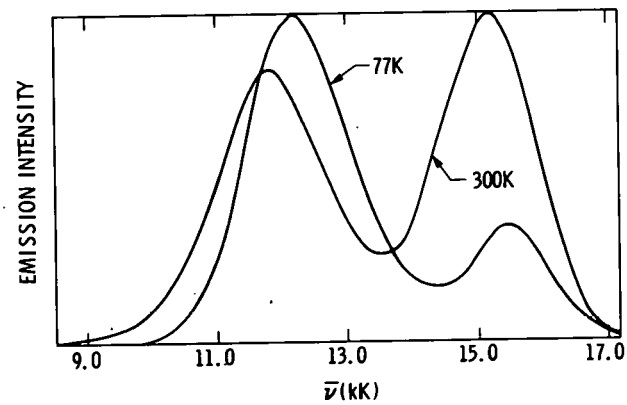

Fig. 8 Total corrected emission spectrum of $[Rh_2(bridge)_4]^{2+}$ in 2:1-methyl-THF: proprionitrile at R.T. and 77K. The phosphorescence is considerably more temperature-sensitive than the fluorescence, and the vertical scales for the two spectra are not the same.

References

1. Mann, K.R., Lewis, N.S., Miskowski, V.M., Erwin, D.K., Hammond, G.S., Gray, H.B., J. Am. Chem. Soc. (1977) 99, 5525-5526.

2. Epstein, A.J., Miller, J.S., Sci. Am. (1979) 241, 52-61.

3. Mann, K.R., Gray, H.B., Advan. Chem. Series (1979) 173, 225-235.

4. Miskowski, V.M., Nobinger, G.L., Kliger, D.S., Hammond, G.S., Lewis, N.S., Mann, K.R., Gray, H.B., J. Am. Chem. Soc. (1978) 100, 485-488.

5. Miskowski, V.M., Sigal, I.S., Mann, K.R., Gray, H.B., Milder, S.J., Hammond, G.S., Ryason, P.R., J. Am. Chem. Soc. (1979) 101, 4383-4385.

6. Gray, H.B., Miskowski, V.M., Milder, S.J., Smith, T.P., Maverick, A.W., Buhr, J.D., Gladfelter, W.L., Sigal, I.S., Mann, K.R., Proceedings of the 1st International Symposium on Homogeneous Catalysis, M. Tsutsui, ed., Plenum, in press.

7. Unfortunately, a very strong absorption band of $Cl_2Rh_2(bridge)_4^{2+}$ is coincident with the ~340 nm UV absorption of Cl_2^- severely limiting our ability to directly detect halogen radicals.

PRELIMINARY EVALUATION OF PROCESSES FOR RECOVERING HYDROGEN FROM HYDROGEN SULFIDE

R. W. Bartlett, D. Cubicciotti, D. L. Hildenbrand, D. D. Macdonald, K. Semrau
SRI International, Menlo Park, California 94025
and M.E.D. Raymont
Scitech Enterprises, Ltd.

Abstract

A theoretical study was made of the concept of recovering hydrogen as well as sulfur from hydrogen sulfide. Hydrogen sulfide is a by product from the desulfurization of fossil fuels. In current practice the sulfur values are recovered but the hydrogen is not. Recovery of the hydrogen, if economically feasible, would help conserve fossil fuels.

Introduction

Background

Hydrogen is a valuable commodity which is currently produced from fossil fuels. The increasing amount of hydrogen sulfide, H_2S, being generated from desulfurization of fossil fuels represents another potential source of hydrogen, so that the incentive exists for developing efficient processes to recover H_2 from H_2S. Any process to achieve that goal would have to be economically attractive to be accepted commercially. The present study was a technoeconomic assessment of the feasibility of such processes.

The sharp increase in costs coupled with the restricted supply of hydrocarbon fuels since 1972 has encouraged the search for new sources. As a result, it has become economically attractive to drill into very deep formations (for example, down to 25,000 feet) for natural gas. Many of these deep wells and numerous shallow ones contain large amounts of hydrogen sulfide; H_2S content as high as 35% is common, and wells containing as much as 90% have been found. Because of pollution problems from SO_2 and the toxicity of H_2S itself, H_2S must be removed from the gas before distribution to the consumer. However, at normal temperature and pressure, H_2S is a gas, and although it is easily liquefied, storage presents considerable economic and technical problems. Therefore, the H_2S needs to be converted into a form that can be easily stored and handled and that is marketable in its own right.

Significant amounts of hydrogen sulfide are also produced during the refining of many crude oils and the potential supply anticipated from coal gasification, coal desulfurization, and synthetic fuel production is enormous. Accurate estimates of the volumes expected from these sources do not appear to be available. It is likely, however, that these sources will add substantial quantities of H_2S to the already large amounts produced by the natural gas industry.

At present, H_2S recovered from natural gas is converted to elemental sulfur by the Claus process. In this process, one-third of the H_2S stream is oxidized to SO_2, which then reacts with the remaining two-thirds via a gas-phase redox reaction to produce elemental sulfur:

$$H_2S + 3/2\ O_2 = SO_2 + H_2O$$

$$2H_2S + SO_2 = 3S + 2H_2O$$

Although the Claus process is highly efficient, it has the disadvantage that the potential hydrogen values are lost in the form of water.

Study Performed

This paper is a condensation of a more extensive report that presents the results of a theoretical study of processes for recovering hydrogen from hydrogen sulfide and whether such processes should be developed for commercial implementation. (The complete 175 page report, with the same title as this paper, is available from the authors.)

An assessment was made of the potential amounts of H_2S available in the future. It is conservatively estimated that the amount of hydrogen potentially available from H_2S is equivalent to 0.1 quad of fuel energy annually by the year 2000. The value of this fuel would be about one billion dollars (1978 prices). The potential supply of hydrogen from sulfide is expected to be geographically well matched to and only a fraction of the demand for industrial hydrogen. It was concluded that new plants will need to be constructed between 1980 and 2000 to process 75% of the H_2S.

A literature survey for potential processes was made and combined with SRI concepts for processing. The types of processes were classified as follows: direct thermal decomposition, thermochemical splitting, liquid metal processes, and electrolysis. Specific cases of these classes of process were considered in sufficient detail to generate a potential process flow sheet and to identify possible technical difficulties. A preliminary partial assessment of the economics of processes was made to provide an indication of the probable relative costs. None of the processes is sufficiently advanced at present to permit a well-based choice for development to commercial scale. Since there are potential advantages (and disadvantages) for each process, bench scale research on all four classes should be carried out to provide information to select a process for larger scale development.

Market Assessment

Potential Hydrogen Supply from Hydrogen Sulfide in North America - For the United States, the picture from 1980-2000 reflects three trends in recovered sulfur production from hydrogen sulfide. First, as U.S. refinery crude feedstocks become more sour and the demand for low sulfur products increases, hydrogen sulfide processing at U.S. refineries will continue to increase significantly. Second, hydrogen sulfide processing in sour gas operations

will also increase. Finally, starting in about 1985, coal gasification and liquefaction should begin to add to sulfur recovery from hydrogen sulfide.

Thus strong growth in hydrogen sulfide processing is anticipated through the year 2000 because of both hydrocarbon desulphurization and later, coal conversion and its accompanying desulfurization. Major processing will occur in the Gulf Coast and southwestern states area with some on the west coast, while the mid-continent and mountain states will become significant processors late this century.

By the year 2000 some 20 million tons of sulfur will be recovered from hydrogen sulfide streams in North America, with almost 70% of this production in the United States. If instead of processing via the Claus process, hydrogen sulfide is decomposed to yield hydrogen, these hydrogen sulfide streams could represent a potential source of some 14 billion cubic meters of hydrogen annually by 2000. At least 75% of the hydrogen sulfide processed in North America will be converted in new plants constructed between 1980 and 2000 and thus should be available for processing via new technology without effecting current facilities and their associated capital investment. At today's prices, the value of this potential hydrogen supply would exceed $1 billion per year in the United States alone.

With respect to the geographic distribution of potential hydrogen supply from hydrogen sulfide and hydrogen demand, there is a good correlation between regions with potential supply and areas with demand. Analysis of available data for 1977 shows that the regions with the greatest potential for hydrogen supply from hydrogen sulfide are also the regions with significant demand for hydrogen and that distribution is expected to continue at least over the near future. In most regions hydrogen from hydrogen sulfide could usefully supply 5-15% of the demand, thus saving like amounts of hydrocarbon fuel that would otherwise have to serve as a hydrogen source.

Description and Qualitative Economic Comparison of Potential Processes for Recovering Hydrogen From Hydrogen Sulfide

Method

To do economic assessments on a limited budget we attempted to screen the processes by determining for each process in sequence (1) materials and energy balances, (2) net raw materials and utilities requirements, and (3) the cost of raw materials and utilities at current prices. Finally, credits for hydrogen or other useful products are taken. The analyses consider a plant treating enough H_2S to produce 500 tons/day of sulfur as either elemental sulfur or other useful sulfur compounds. The utilities include fuel, electric power, steam, and water. Labor and capital dependent operating costs are not being estimated for the present analysis because a great amount of detailed plant design information is needed to estimate capital costs with enough reliability. Nevertheless, H_2S processes that are not energy efficient in providing hydrogen or that otherwise excessively consume utilities or raw materials can be eliminated from further consideration by this approach. The most useful part of this study is probably the identification of critical steps or technical constraints on each process that need to be solved for economic viability, and therefore stimulates a search for solutions to these problems. For most processes only a very few steps are dominant in their effect on technical viability and production cost.

The processes selected for economic assessment are discussed below.

Direct Thermal Decomposition

In this process, H_2S is heated to high enough temperatures that it begins to decompose by the reaction

$$H_2S(g) \rightarrow H_2(g) + 1/2\ S_2(g)$$

The temperatures required are moderate for partial decomposition, for example, 14% occurs at 927°C. Analysis of the thermal decomposition of hydrogen sulfide indicates that difficulties arise with product yield and separation of both hydrogen and sulfur vapor from an H_2S stream without excessive recycling and cooling/heating transformation to the gas stream. In principle, H_2 can be separated by a permeation membrane or porous filter, but the sulfur product back pressure limits yields unless a method of removing sulfur from H_2S at dissociation temperatures can be found. Also we are very skeptical about long-term reliability of a high temperature hydrogen permeable membrane. SRI proposed a counter system involving high temperature extraction of dissociated sulfur and room temperature separation of H_2 from H_2S.

Our preliminary analysis showed that thermal decomposition of H_2S can be justified if the price of natural gas and coal are higher than the price of electric power generated from nuclear, fusion, or other power sources. Energy cost parity would exist when the cost of the required electrical energy is equal to the price of the hydrogen produced. As with R and D investments for thermal decomposition of water, the estimate of when electric power from plentiful sources will be cheap in relation to the price of hydrogen determines one's optimism about the economic future of direct thermal decomposition of H_2S.

Thermochemical Decomposition

Because of the relatively low thermodynamic stability of H_2S, there appear to be several two-step, closed-cycle processes that are feasible at moderate temperatures from a Gibbs energy viewpoint. One of several open-cycle processes also appear feasible. A typical closed-cycle process selected for further economic evaluation is the following:

$$FeS(s) + H_2S(g) \rightarrow FeS_2(s) + H_2(g) \qquad (\sim 227°C)$$

$$FeS_2(s) \rightarrow FeS(s) + 1/2\ S_2(g) \qquad (\sim 727°C)$$

Both steps are thermodynamically favorable at the indicated temperatures, but there may be serious kinetic limitations to the low temperature step. This aspect of process chemistry requires further evaluation.

In the above process, the product gases (H_2 and S_2) are formed in different reaction vessels so that their separation is not a problem; however, H_2 and

H_2S can intermix. Therefore, the process conditions and reactor design must be devised so that the product is pure H_2 and a separation step for gaseous H_2 and H_2S is not required.

In our energy economic calculations we assumed that electric power would be used because of the availability of nuclear fission or fusion power plants producing relatively low cost electric power. For all cases of interest, the fossil fuel equivalent energy required to generate electric power is greater than the energy required to produce H_2 by reforming of natural gas. However, for nearly every case, the actual net energy input is less than the energy required to produce H_2 from natural gas if equivalent fossil fuel heat were used directly instead of generated electric power. Hence, the iron sulfide thermochemical cycle is fairly attractive from an energy economy standpoint. The most interesting case for the long-term situation would be the use of nuclear process heat or electric heating based on an assumed plentiful and inexpensive supply of nuclear fission power in an environment of fossil fuel scarcity.

Liquid Metal Process

An alternative thermochemical cycle that produces hydrogen and SO_2 from H_2S was also examined. The process takes place in two steps:

(1) Sulfidation of a liquid metal, such as copper, to produce hydrogen and molten matte (metal sulfide),

$$2Cu(\ell) + H_2S(g) \rightarrow Cu_2S(\ell) + H_2(g)$$

(2) Oxidation of metal sulfide to SO_2 and reduced metal,

$$Cu_2S(\ell) + O_2(g) \rightarrow 2Cu(\ell) + SO_2(g)$$

The SO_2 can be liquefied or converted to sulfuric acid.

The liquid metal processing differs substantially from the classical thermochemical cycle for dissociating H_2S in that the products are hydrogen and sulfuric acid rather than hydrogen and sulfur. Clearly any other marketable form of oxidized sulfur, such as SO_2 or sulfate chemicals, is an alternative to sulfuric acid. Because sulfur is oxidized during the liquid-metal process, the net energy requirements are substantially lower than those needed in the direct thermal dissociation or thermochemical cycles that produce hydrogen and sulfur. Net energy requirements for the Cu/Cu_2S system are essentially those needed for electric power to drive fans and blowers.

The process appears to be economic when a market for SO_2 or sulfuric acid is available. However, when such a market is available it is also possible to burn H_2S with air to produce H_2S and SO_2 which is used to make liquid SO_2 or acid. Hence, it is uncertain whether the additional capital and operating costs of the proposed Cu/Cu_2S process are worth the hydrogen obtained in contrast to the much lower capital and operating costs involved with burning H_2S.

In the final analysis, justification of the liquid metal process must be borne on the basis of sales of hydrogen in the event that either no market for sulfuric acid is available or that an acid market could be sustained by simply burning H_2S. Consequently, the economic justification of the liquid metal processes was assessed by considering the hydrogen price in relationship to the additional operating costs that would be incurred from the Cu/Cu_2S process as compared with the process of burning H_2S to produce sulfuric acid. In both the H_2S-burning case and in the Cu/Cu_2S case, all of the energy and other operating costs associated with an acid plant are required. Therefore, in comparing the added value of hydrogen, we need only consider the Cu/Cu_2S reactor process exclusive of the acid plant.

Consideration of total plant operating costs indicated that hydrogen prices only somewhat above 1978 values would be required. Consequently, the liquid metal processes that produce both hydrogen and sulfuric acid merit further investigation. The critical factor in the Cu/Cu_2S system is the extent to which H_2S is completely converted to hydrogen during its short residence time in the liquid copper converter.

Electrochemical Methods

Electrolysis of H_2S dissolved in aqueous electrolytes is a process that has been investigated on a bench scale and has been patented. From a thermodynamic viewpoint, the electrolysis of aqueous H_2S systems for the production of hydrogen looks very promising, particularly in comparison with the electrolysis of water. Thus, the equilibrium potential at 25°C for the reaction $H_2S(g) \rightarrow S(s) + H_2(g)$ is ~ 0.18 V compared with ~ 1.23 V for the electrolytic decomposition of water. The electrode reactions are

$$\text{Cathode:} \quad HS^- + e^- \rightarrow 1/2\ H_2(g) + S^{=}\ (\text{solution})$$

$$\text{Anode:} \quad 1/2\ S^{=}\ (\text{solution}) \rightarrow e^- + S\ (\text{solid}).$$

The production of solid sulfur at the anode presents a problem because the sulfur coats the anode and must be removed periodically. We believe that the major technical problem in the electrolysis of aqueous H_2S systems will be the development of a sufficiently active surface for the oxidation of H_2S to elemental sulfur. (This problem is similar to that of the oxygen electrode in water electrolysis.)

No specific system was found in the literature or developed conceptually to the extent that energy requirements or other economic results could be estimated.

Conclusions

The following conclusions about the technical and economic aspects of hydrogen recovery from hydrogen sulfide could be drawn,

(1) Market assessment

- Strong growth in H_2S processing is projected from the present to beyond the year 2000 because of both hydrocarbon desulfurization and coal conversion.
- Major new hydrogen sulfide processing

facilities will be required in North America before the year 2000 to treat the burgeoning amounts of H_2S produced from natural gas and desulfurization of fossil fuels. At least 75% of the H_2S processed in North America will be converted in new plants constructed between 1980 and 2000.

- From a very conservative estimate the annual potential amount of hydrogen available from H_2S by the year 2000, if a suitable process is developed, is about 14 x 10^9 cubic meters (5 x 10^{11} standard cubic feet). This amount is equivalent to about 0.1 quad of fuel energy, worth approximately one billion dollars, per year, at current prices.

- The regional potential supply of H_2S would be well distributed in each of the five Petroleum Administration for Defense (PAD) districts, and would provide in the range of 5% to 15% of any district's demand for hydrogen for industries such as petroleum refining or ammonia and methanol production.

(2) Technical Feasibility of Process for Recovering H_2 from H_2S

The decomposition of H_2S into its elements H_2 and S is thermodynamically more favorable than the corresponding water splitting process, and can be accomplished by direct thermal means as well as less direct chemical or electrochemical means. However, the recovery of the hydrogen produced, that is its separation from the sulfur, may be difficult and the overall process is complex. Several potential processes are attractive but none has been sufficiently tested to provide the basis for commercial development.

(3) Economic Evaluation of H_2 Recovery

The hydrogen potentially recoverable from H_2S has a greater economic value than the sulfur; therefore there is a strong economic incentive for H_2 recovery processes. These conclusions are based on preliminary process evaluations and require further study. As with water-splitting methods for H_2 recovery, most of the H_2S-splitting processes require considerable energy and the economics will be strongly influenced by the economics of energy.

Dup

STUDY OF THE BEHAVIOR OF GAS DISTRIBUTION EQUIPMENT IN HYDROGEN SERVICE — PHASE II

Walter J. Jasionowski and H. Ding Huang

Institute of Gas Technology
Chicago, Illinois 60616

Abstract

IGT has completed the assembly and checkout of experimental facilities to determine the hydrogen permeability characteristics of contemporary plastic natural gas pipes and to ascertain if there is preferential leakage of hydrogen from small leaks in a system operating with mixtures of hydrogen and natural gas. The goal of this program is to assess the impact of permeability and preferential leakage on the operation of a distribution loop when converted to service of hydrogen and mixtures of hydrogen and natural gas.

Information on permeability cells was collected and reviewed. A cell utilizing aluminum construction was designed, eight cells were fabricated, and a permeability test setup was assembled and leak tested. Plastic gas distribution pipe manufacturers were contacted and samples of different types of commercially available polyethylene pipe were received from seven companies. Permeability determinations are now under way.

Existing gas distribution test facilities were modified for hydrogen-natural gas leakage experiments. Four different-sized simulated leaks (capillaries and sintered discs) were incorporated into three different pressurized branches of the residential/commercial test loop, and the compressor used to develop the pressure and flow for recycle of test gases was overhauled.

Introduction

This program is part of a multi-year effort to supply needed information about hydrogen delivery in natural gas distribution equipment. The overall program will identify operating, safety, and materials problems associated with the use of hydrogen in conventional distribution systems. One of the major incentives behind nonfossil-based hydrogen as a future supplement and eventual replacement for natural gas is the expectation that the existing gas delivery system can be used without major modifications.

Under DOE Contract No. EY-76-C-02-2907 (Phase I), IGT conducted an experimental study with contemporary gas distribution equipment in hydrogen service. [1] The observations and results of two test loops initially operated on natural gas (baseline) and then on cylinder-grade hydrogen for 6 months indicate no major incompatibilities in performance. Existing in-place components and piping (with the possible exception of meters) should be adequate for hydrogen delivery. The observed overall hydrogen-to-natural gas volumetric leak ratio ranged between 3.00 and 3.35 and the overall energy loss ratio ranged between 1.00 and 1.04. In isolated situations, the difference in pipe flow characteristics of hydrogen may necessitate a small increase in delivery pressure to provide equivalent energy delivery. Experiments in a third test loop demonstrated that the Joule-Thomson hydrogen effect of heating upon expansion is minute, not affecting distribution operations. Hydrogen leaks to the atmosphere will not ignite spontaneously without an ignition source; hydrogen escaping from a leak expands somewhat adiabatically and cools. Short-term (6 months) exposure to hydrogen did not significantly affect the properties of the metallic materials of system components. Some plastic products, lubricants, and adhesives were noticeably affected by the exposure. Plastic (polyethylene) pipe was "softened" by exposure to hydrogen, and ring-tensile tests showed more deformation in exposed plastic pipe.

In general, the results and observations indicate that, for short-term exposure, contemporary distribution equipment is suitable for hydrogen service (except for certain lubricants and adhesives and for meter capacity to deliver an equivalent amount of energy). However, before hydrogen can be utilized as a universal fuel, or as supplemental fuel, a number of problems must be addressed. Most important is long-term verification testing to demonstrate that the gas distribution equipment remains compatible with hydrogen and that certain observed material degradation does not reach critical levels. Among the many problems still to be addressed, this program will a) determine experimentally the absolute and relative permeabilities of commercially-available plastic gas distribution piping for hydrogen and methane, b) experimentally characterize leakage of hydrogen-methane blends through orifices (simulated leaks), and c) assess the impact of selective leakage via permeation and/or orifice flow on the distribution of hydrogen and blends of hydrogen and methane.

Permeability Investigations

Mass Transfer Mechanism

The transmission of gas through a plastic material has been studied and described by many investigators. Gas flow is visualized as a complex transport process caused by a partial pressure differential between the two sides of the material. It requires a) adsorption and solution of a component on the high-pressure side, b) diffusion through the material under a concentration gradient, and c) desorption and evaporation on the low-pressure side. Diffusion is the rate-determining process and under steady-state it obeys Fick's law. The flow through a polymeric material is expressed as —

$$q = \frac{DSA\ (p' - p'')t}{\ell} = \frac{PA\ (p' - p'')t}{\ell}$$

where —

q = amount of gas diffusing

D = diffusion constant

S = solubility constant

A = area

p' = high pressure

p" = low pressure

t = time

ℓ = thickness

P = DS = permeability constant

Thickness

Normally, gas transmission rate is inversely proportional to thickness. This relationship is shown graphically in Figure 1.

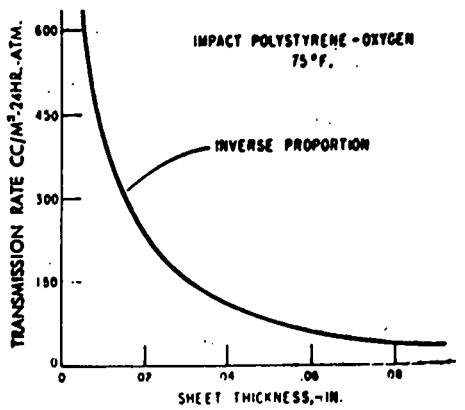

Fig. 1 Transmission rate versus thickness [2]

Effect of Temperature

The effect of temperature on diffusivity, D, is the same as for any rate process; the diffusion coefficient increases rapidly with a rise in temperature. Solubility coefficients alternatively are much less affected by temperature variation so that permeability, P, as a product of diffusivity and solubility coefficients, as a function of temperature is more closely related to the diffusion coefficient than to the solubility coefficient.

Most polymeric substances show an increase in permeability with increasing temperature. Graphs of logarithms of permeability constant versus the reciprocal of absolute temperature give good linear plots (Figure 2).

However, there are instances of negative temperature coefficients and nonuniformity in behavior. It is recommended that enough permeability values be determined to cover the temperature range involved.

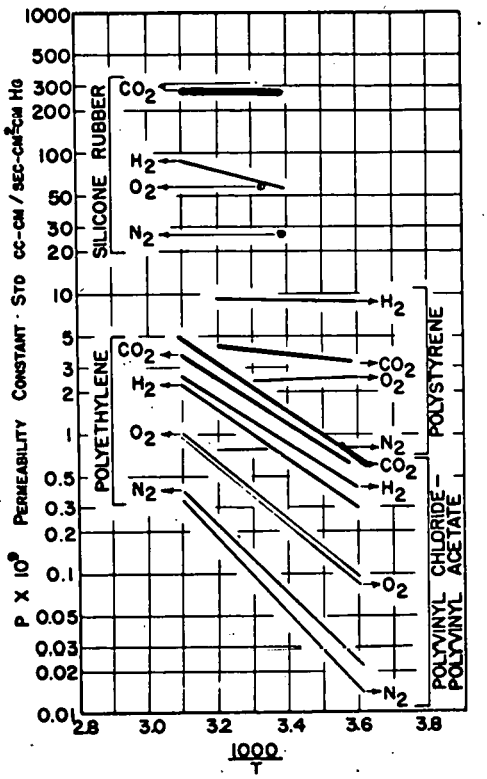

Fig. 2 Gas permeabilities through polymeric materials [3]

Effect of Pressure

Ordinary pressure differentials (up to several atmospheres) have little effect on permeability, diffusion, or solubility coefficients. The universal practice of reducing transport data to units of pressure differential (1 atmosphere, 1 centimeter mercury, or 1 millimeter mercury) is usually valid and consistent with theory. Some polymeric materials deviate from ideal behavior when there are strong interactions between the gas and the polymeric material by virtue of swelling or plasticizing, which varies with partial pressure.

Transport increases with an increase in pressure differential across the polymeric substance. The limit to which the pressure differential may be raised is determined by the physical strength of the material.

Materials Permeabilities

Table 1 presents permeability data of various plastic pipe materials reported in the A.G.A. Plastic Pipe Manual for Gas Service. [4] The permeability constants are converted to (std ft^3)(mil thickness)/(ft^2 area)(day)(atm Δp) for the purpose of comparison.

Acrylonitrile-Butadiene-Styrene (ABS), Cellulose-Acetate-Butyrate (CAB), Polyethylene (PE), and Polyvinyl Chloride (PVC) are the only significant piping materials used for gas distribution. CAB pipe was introduced in 1942 when steel pipe was in short supply. PE pipe was developed in 1948 and in

Table 1 Permeability properties of plastic piping compounds

Material	Material Type and Grade	Pipe Designation	Gas Permeability, $\frac{ft^3\text{-mil}}{ft^2\text{-day-atm}}$ Methane	Gas Permeability, $\frac{ft^3\text{-mil}}{ft^2\text{-day-atm}}$ Hydrogen	Selective Flow Ratio H_2/CH_4
Acrylonitrile-butadiene-styrene	ABS-1-2	ABS-1210	0.59×10^{-3}	51.71×10^{-3}	87.6
Cellulose acetate-butyrate	CAB-MH	CAB-MH08	11.8×10^{-3}	517.0×10^{-3}	43.8
	CAB-MS	CAB-S004	56.7×10^{-3}	N.A.	N.A.
Polyamide (Nylon)	PA VII-2	Nylon 6:6/6	N.A.	N.A.	N.A.
Polybutylene	PB-II-I	PB-2110	3.3×10^{-3}	61.0×10^{-3}	18.5
Polyethylene	PE-II-3	PE-2306	4.2×10^{-3}	21.0×10^{-3}	5.0
	PE-III-3	PE-3306	2.4×10^{-3}	15.7×10^{-3}	6.5
	PE-III-4	PE-3406	N.A.	N.A.	N.A.
		PE-3408	N.A.	N.A.	N.A.
Polyvinyl chloride	PVC-1-1	PVC-1120	N.A.	N.A.	N.A.
	PVC-1-2	PVC-1220	N.A.	N.A.	N.A.
	PVC-II-1	PVC-2110	0.2×10^{-3}	13.7×10^{-3}	68.5
	PVC-II-1	PVC-2116	--	--	N.A.
Reinforced epoxy thermoset	RTRP-150	--	nil*	N.A.	N.A.

N.A. — Not available.

* No measurable amount after 1200 hours of test; test discontinued.

1949 it became the fastest growing plastic pipe material. ABS pipe appeared in about 1954 and it offered higher tensile strength and heat distortion temperatures than CAB. ABS pipe soon forced CAB pipe off the market, except for some very special applications, among them gas service relining.

PVC pipe appeared in about 1955 in Europe and began to compete with ABS. Test data showed that PVC could be assigned a 2000-psi design stress rating, while ABS earned only 1000 psi. This eliminated ABS as a pressure pipe contender, except where its unique properties were required.

PVC pipe was not accepted readily. Factors that deterred its use were —

a) Requirements to achieve sound solvent joints

b) Ductility was suspect

c) It was not available in coiled lengths.

Currently, PE is the only plastic pipe material of interest in North America for gas distribution. DuPont, Phillips, and Gulf (under Phillips' license) are the primary polyethylene pipe resin manufacturers. DuPont extrudes pipe from its own resins but does not sell resins to other pipe manufacturers. Phillips produces pipe from its own resins and sells them to other pipe extruders, whereas Gulf only sells resins. Plastic pipe designated as PE-2306, PE-3406, and PE-3408 is currently available for gas distribution applications. PE-3306 is now primarily used as irrigation piping.

Manufacturers of PE gas distribution pipe were contacted and samples of their 2-inch iron pipe size (ips) standard dimension ratio (SDR) 11 pipe were requested. DuPont, Phillips, Plexco, Continental Industries, Tex-Tube Division of Cyclops Corp., Nipak, and Oil Creek Plastics furnished samples of their PE pipe materials for permeability testing.

Permeability Apparatus

Information on permeability cell designs was reviewed from previous work at A.G.A.-Battelle, Phillips Products Co., Lone Star Gas Co., and DuPont. The A.G.A.-Battelle permeability cell design uses two o-rings at each end and epoxy potting of the o-rings to seal the annular space between the plastic piping and the enclosing metallic cylinder. [5] The Phillips Products Co. cell design features a brass plug fitted with an o-ring inserted into the inner diameter of the plastic pipe and a stainless steel band drawn around the OD over the brass plug. [6] The brass plugs are joined to bushings with pipe fittings and to an enclosing length of pipe to define the annular space for the collection of permeated gas. The Lone Star Gas Co. cell design uses o-rings to seal the annular space between the OD of the plastic pipe and the enclosing metal housing. [7] The DuPont cell design resembles the A.G.A.-Battelle design and uses a single o-ring seal at each end, but does not use any epoxy potting. [8]

On the basis of the review, a cell design was prepared that utilizes ethylene-propylene rubber (EPR) o-rings to seal the inner diameter to plugs and another set of EPR o-rings to seal the annular space between an enclosing metal cylinder and the outer diameter of the plastic pipe specimen. The cell was designed to accommodate a 2-inch ips SDR-11 plastic pipe; OD averages 2.375 inches, and the

minimum wall thickness is specified at 0.216 inches.

Figure 3 shows various subassemblies of the permeability cell. The cell is constructed from 6061-T6 aluminum pipe, bar stock, and tubing; joining was accomplished by dip brazing. A plastic pipe specimen (item D) is inserted into the housing (item C). Preinstalled EPR o-rings (item B), in the two collars of the housing, seal the annular space between the housing and the pipe OD. Two identical plugs with EPR o-rings (items A and E) are inserted into the pipe specimen and then fastened to collars of the housing with lock washers and cap screws. One-quarter-inch pipe taps in the plugs facilitate flushing and pressurization of the specimen with the test gases, whereas 1/4-inch tubes on the housing facilitate flushing of the annular space, collection/sampling of permeated gas, and measurement of annulus pressure.

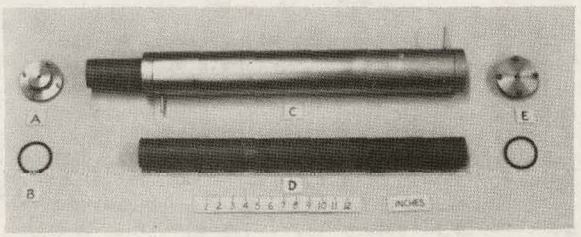

Fig. 3 Permeability cell subassemblies

Figure 4 shows the permeability test setup. Six cells are being utilized for hydrogen and two cells for methane. Common manifolds supply hydrogen, methane, and nitrogen from gas cylinders. Each cell has its own sample collection bottle, pressure gauge, and mercury manometer.

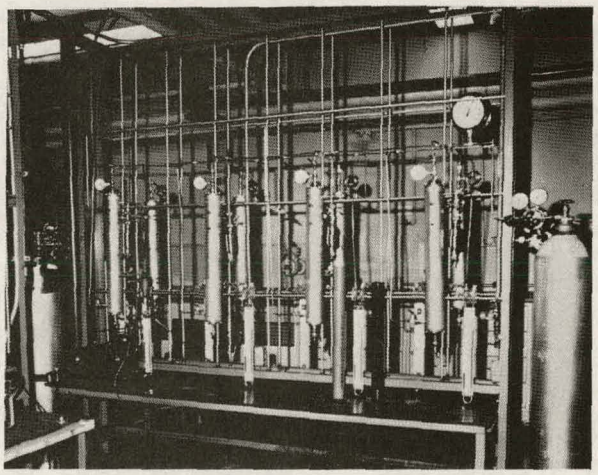

Fig. 4 Permeability test setup

Test Procedure

Samples of regular production PE gas pipe were cut to an appropriate length and the OD and wall thickness were measured. The samples were assembled into the apparatus and leak tested. Then, the volume of the annular space was determined using the gas law relationship $P_1V_1 = P_2V_2$.

The permeation cells were connected to a single pressure-regulated source of hydrogen or methane and flushed. At the same time nitrogen was used to purge the annular space of air. The pressure of the annular space was reduced to atmospheric and the pipe sample pressurized to 60 psig with hydrogen or methane. The pressure in the pipe samples is maintained at 60 ± 0.5 psig throughout the duration of the test period.

The permeation is measured in two ways. One, by the pressure build-up in the annular space; and two, by periodically withdrawing gas samples from the annular space in collection bottles and analyzing the gas samples with a mass spectrometer.

Preliminary Permeability Results

Table 2 presents the permeability constants of various PE pipe specimens as determined by the gas law relationships, annular volume, and the pressure build-up in the annular space. This is the first permeation run over a period of 18 days at 70° ± 2°F. The data correlate with values reported in the A.G.A. Plastic Pipe Manual for Gas Service for PE-2306.

Table 2 Preliminary permeability constants of pipe samples

Test Cell	Test Gas	PE Pipe Sample	Gas Permeability Constant, $\frac{ft^3\text{-mil}}{ft^2\text{-atm-day}}$
1	H_2	DuPont 2306	26.0×10^{-3}
2	H_2	Oil Creek Plastics 2306	20.2×10^{-3}
3	H_2	DuPont 3406	16.5×10^{-3}
4	CH_4	DuPont 3406	3.5×10^{-3}
5	H_2	Continential Industries 2306	20.0×10^{-3}
6	H_2	Plexco 3406	15.6×10^{-3}
7	H_2	Phillips 3408	20.9×10^{-3}
8	CH_4	Phillips 3408	6.8×10^{-3}

Hydrogen/Natural Gas Leakage Investigations

Mass Transfer Mechanism

If there is a pressure difference across a microporous solid, mass transport can proceed by several mechanisms: a) molecular effusion, b) molecular streaming or Knudsen flow, c) streamline or Poiseuille flow, d) turbulent flow, and e) orifice flow. Poiseuille, turbulent, and orifice flow are the most common types, being a function of micropore geometry, gas density, gas viscosity, and mean pressure; they are classified as nonseparative.

Knudsen flow and/or molecular flow are separative flows. The difference in flow rates of the

various gaseous species depends upon the relative frequency with which the molecules of the various components strike the surface; that is, the more frequently they strike the surface the greater the probability of their entering a micropore. Because each component of a gaseous mixture has the same average kinetic energy, this frequency is directly proportional to their molecular weights. Hence, in a mixture of gaseous molecules, the lighter component will permeate more rapidly than the heavier component. The lighter and heavier molecules will both pass through the microporous media, but in a given time interval more lighter molecules will permeate and the abundance of lighter molecules will be greater on one side of the microporous media than the other.

Microporous Structure

Separative flows depend upon the relation between the capillary diameter of the microporous media and the mean free path (λ) of gas molecules. The pores must be of such size and relation to the mean free paths of the gaseous components that intermolecular collisions are avoided as much as possible. The pore diameters must therefore be appreciably less than λ. At standard conditions of temperature and pressure the λ of CH_4 is about 165 angstroms, and the λ of H_2 is about 3000 angstroms. The microporous media must have pore sizes considerably smaller to produce molecular flow and the separation phenomenon.

If the pore diameters are small in comparison with λ, flow takes place by molecular effusion following Knudsen's law. A λ/d ratio of 2.5 is often the practical limit; however, reasonably good separations have been achieved at a ratio of 1. In a microporous solid with capillaries of various diameters both Knudsen and Poiseuille flow may occur.

Adsorptive Flow

Microporous solids are capillary systems, and, therefore, exhibit varying degrees of adsorptive activity. This gives rise to adsorbed or surface flow from concentration gradients due to excessive adsorption of, usually, the heavier molecules within the porous matrix. The process produces flow rates that are greater than those predicted on the basis of molecular weight, thus partially nullifying the Knudsen effect. Investigators have shown by experiments that vapor mixtures and gas-vapor mixtures cannot be expected to separate in the direction predicted by the square root of the inverse ratio of component molecular weights.

Leakage Test Setup

The existing residential commercial test loop (RCL), developed under DOE Contract EY-76-C-02-2907, was modified. As shown in Figure 5, a schematic of the modified RCL, a single-stage compressor circulates gas through the closed loop system at a rate of about 900 SCF/hr with an intake pressure of 5-inches water column and a discharge pressure of 60 psig. Surge tanks are provided on either side of the compressor to dampen pressure pulsations.

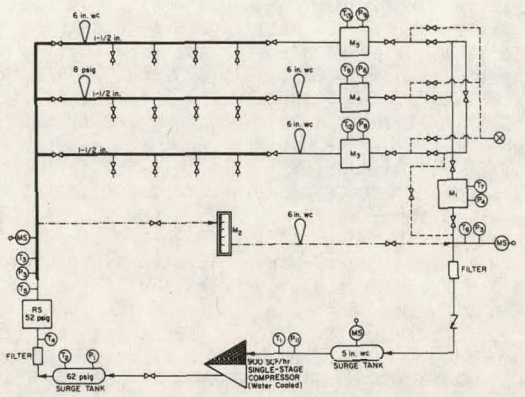

Fig. 5 Modified design of RCL for leakage test

Following the loop clockwise, flow from the compressor is regulated from 62 psig at a regulator station to 52 psig and then flow into a 1-1/2-inch steel manifold with four parallel branches. One of the four branches is the primary bypass. The flow through the primary bypass is controlled by valves and is metered using a glass tube flowmeter at 52 psig. Pressure is dropped to 6-inches water column through a regulator prior to joining up with the compressor intake piping.

Two of the four branches feed into two different service regulators that reduce the pressure to 6-inches water column and 8 psig prior to being routed through two diaphragm meters. Flow is controlled by adjusting spring tension on the service regulator. Three capillary tubes with diameters of 0.003 inch, 0.010 inch, and 0.030 inch, and 15 micron-sized sintered stainless steel discs were potted in four different swagelok male connectors as shown in Figure 6 and were attached to the branches at three different pressures: 50 to 60 psig to simulate high-pressure distribution, 5 to 25 psig to simulate medium-pressure distribution, and 6 to 10 inches water column to simulate low-pressure distribution.

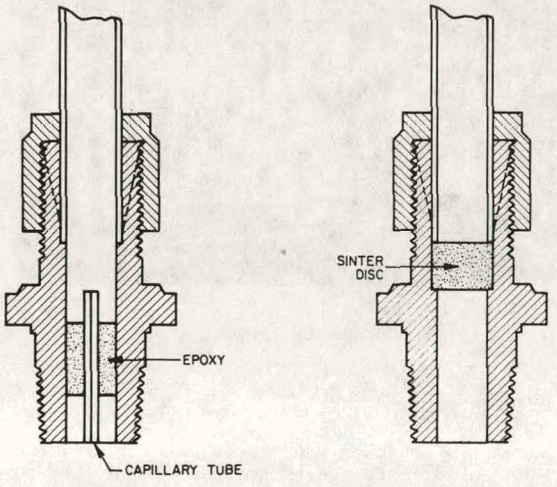

Fig. 6 Potted capillary test fitting

After check-out testing, the KCL will be purged, filled, and operated with mixtures of hydrogen and natural gas, containing approximately 10%, 20%, and 40% hydrogen. The leakage from the simulated leaks, the capillary tubes of 0.003-inch and 0.01-inch diameter, will be determined by the bubble piston technique. The leakage from the capillary tube of 0.030-inch diameter and sintered discs will be measured by wet test meters. Samples of the gas circulating in the test loop and samples of the gas leaking from the simulated leaks will be analyzed by a mass spectrograph.

References

1. Johnson, D.G. and Jasionowski, W.J., "Study of the Behavior of Gas Distribution Equipment in Hydrogen Service," DOE Report COO-2907-30, Chicago: Institute of Gas Technology, April 1979.

2. Brown, W. and Sauber, W., "Gas Transmission by Plastic Films," Modern Plastics 36, 107 (1959).

3. Kammermeyer, K., "Gas Diffusion Through Microporous and Adsorbant Membranes," Chemical Engineering Progress Symposium, Series No. 24, 55, 115 (1959)

4. American Gas Association, "Plastic Pipe Manual for Gas Service," Catalogue No. XR0877, Arlington, Va., November 1977.

5. Kuhlmann, H.W., Wolter, F., Sowell, S., Beatty, G., Leininger, R.I., and McClure, G.M., "The Development of Improved Plastic Pipe for Gas Distribution Purposes," Catalogue No. M40515, Columbus, Ohio: American Gas Association-Battelle Memorial Institute, 1968.

6. Ayers, R.L., "What's Needed to Test Polyolefin Pressure Pipe," SPE Journal 26 No. 5, 48-52 (1970) May.

7. Lindsay, R.F. and Grenier, G., "Permeability of Polyethylene Pipe," A.G.A. 4th Plastic Pipe Symposium, 1973.

8. Timmer, R.C., Private Communications, June 1979.

THE HYDROGEN COMPATIBILITY OF STRUCTURAL MATERIALS FOR ENERGY STORAGE AND TRANSMISSION

William R. Hoover
J. J. Iannucci
J. R. Spingarn
S. L. Robinson
R. E. Stoltz
Sandia Laboratories
Livermore, CA 94550

1. Introduction

The primary objective of this program is to assess the feasibility of transporting large quantities of gaseous hydrogen through the existing natural gas pipeline network. The hydrogen compatibility of these pipeline steels and their weldments is being assessed by conducting experiments in three major areas. (1) In our experimental pipeline loop, we are evaluating the performance of flawed pipeline segments in flowing 1000 psig hydrogen gas. (2) The degradation of pipeline steel fracture toughness is being studied in high pressure hydrogen using J-integral techniques and (3) the hydrogen compatibility of pipeline weldments is being investigated to determine if any of the metallurgical microstructures produced by welding are particularly susceptible to hydrogen embrittlement. In addition to the main activities on this program, we have been requested to conduct two systems studies evaluating the optimum storage techniques and locations for fixed-site storage of hydrogen fuel.

This report summarizes our contributions and accomplishments during FY79. For a detailed discussion of these results, the reader is directed to the annual report for this contract which will be available in January, 1980 and to the systems studies reports which are currently available upon request (the specific references are included in the text).

2. Experimental Pipeline Operation and Burst Testing

S. L. Robinson

The experimental pipeline continues operation with test cycle III in place. As a result of failures occurring in cycle II, a pipeline fatigue facility has been designed. The pipeline phase of testing is complemented by burst testing of pipe segments.

2.1 Experimental Pipeline

The purpose of testing in the experimental hydrogen pipeline is a) to expose actual flawed pipe segments to simulated hydrogen pipeline service including high pressure, high purity hydrogen gas, and b) to gather data and determine if sustained load cracking occurs in low-strength, mild steels and in pipeline steels.

The experimental procedure has been to place increasingly severely flawed A106-B steel pipes into the hydrogen pipeline for six month cycles of exposure. To date, longitudinal flaws on both internal and external surfaces have been tested in cycles I thru III. In order to determine if slow crack growth (SCG) occurred during pipeline exposure, severely flawed pipes removed from the pipeline have been both burst tested and examined fractographically for evidence of SCG. To date, no evidence of SCG has been found in the A106-B steel.

Test cycle III included severe internal flaws up to 10 inches length and 85-90% penetration. Two failures occurred on pressurization. The remaining unbroken test sections have stress intensities up to 75 ksi $\sqrt{in}$ (calculated from the generalized Irwin "thumbnail" crack model but without back surface and plasticity corrections) which is extremely high and should be 90% of $K_{critical}$. We believe that if slow crack growth occurs, it will be in these most severely flawed modules.

2.2 Fatigue Testing

Although no evidence of slow crack growth has been found, accelerated fatigue crack growth is a serious reality. At the beginning of test cycle II, two pipes carried over from cycle I failed upon pressurization at ~ 500 psi, after sustaining 1000 psi for 6 months with no indication of incipient failure. Subsequent fractographic analysis showed the presence of four large amplitude fatigue striations corresponding exactly to the number of pressure cycles prior to failure. It was possible to calculate the stress intensity (ΔK) per cycle and to measure the crack growth per cycle. The growth per cycle agreed to within 50%, with the published data on laboratory specimens (double cantlever beam) at a given ΔK. Failure occurred by hydrogen assisted fatigue crack growth, the ΔK increasing with each cycle until a critical length was obtained, and failure occurred.

Analysis of these fractures pointed out the need to study fatigue crack propagation in pressure cycled pipes. Two specific questions need to be addressed. They are, 1) what is the threshold stress intensity for crack propagation in mild steels in hydrogen? and 2) what is the effect of high-cycle, high mean-load, small fluctuation loading on flaws in hydrogen carrying pipelines?

A dedicated pipeline fatigue facility has been designed to allow addressing these questions. Because of the time consuming nature of these tests, the lack of availability of testing machines, and geometrical considerations relevant to curved shells, a dedicated facility was deemed most effective. The facility will test 10 pipes, in pairs, by pressure cycling them through set limits. Microprocessor control will facilitate this operation, and data gathering. A limited number of flaw geometries will be tested at first. Fractographic and metallographic examination will allow determination of crack growth rates, fracture mode changes, and ultimately the extent of the operational hazard resulting from pipeline maintenance shutdowns, and daily operations involving many small pressure changes about a high mean pressure.

2.3 Burst Testing Program

Both of the previous efforts are, and will continue to be, supported by a program of burst testing of flawed pipes. From burst testing we learn a) the quantitative extent of degradation of burst pressure, b) the apparent fracture toughness and toughness loss in air and hydrogen, c) the effects of flaw geometry, location, and pre-exposure upon burst pressures and toughness, and d) changes in fracture mode as dictated by items in (c) and by preparation of the flaw. We are also better able to design tests for the hydrogen pipeline using the data obtained.

Burst testing with hydrogen is performed by pressurizing to a specific pressure, i.e. 1000 psi, with hydrogen. Pressurization with nitrogen is continued until failure occurs. External flaws are subjected to a 16 hour, 100°C, 150 psi soak in hydrogen prior to the burst test. This soaking (or thermal charging) procedure will be used in the future on selected internally flawed pipes.

Internally flawed pipes, flawed by cutting a longitudinal scratch with a lathe tool, were degraded by about 15% in burst pressure at 1000 psi. Extensive fracture mode changes occurred near the crack tips, changing from ductile rupture to a mixed or quasi cleavage mode of fracture, with mostly ductile rupture with some quasi cleavage occurring away from the crack tip. This loss of burst strength implies a loss in factor of safety; to retain an equivalent factor of safety to the inert gas case, a 15% reduction in operating pressure may be dictated. Test on unflawed pipes are planned to complete the data.

Testing of externally flawed pipes has only begun recently. Preliminary results indicate a loss in burst pressure of about 10%, somewhat less than the (uncharged) internally flawed case. The stress states of the internal flaw and the external flaw are different and this may contribute to the variation in effects. In addition, less hydrogen is present at the crack tip which should reduce the observed degradation. No fracture mode change has been observed; instead, an increase in dimple size occurs, which implies an acceleration of the normal ductile rupture processes. This class of flaw is therefore much less severe than the internal, uncharged flaws.

Apparent fracture toughness values have been calculated from the burst values; the values obtained are not K_{IC} or "valid" data. However, these numbers have value for comparative purposes. For internally flawed specimens, the K values (obtained as explained above using the Irwin Analysis) are calculated as 105 ksi $\sqrt{in}$ in N_2, and 77 ksi $\sqrt{in}$ in 1000 psi H_2/N_2 to burst mixtures. This 27% decrease agrees well with the values obtained by J-integral procedures, and enables prediction of failures in pipes of similar thickness.

3. Fracture Toughness Testing

R. E. Stoltz

Activities in FY1979 have centered on measuring the fracture toughness of A516 steel in hydrogen pressures greater than 1 atm. This task is intended to provide laboratory measurements that can be effectively integrated into an analysis of the burst test data presented in the previous section.

3.1 Facility development

An existing 2 inch diameter pressure vessel was modified for J tests of double edge notch tensile (DENT) samples. A four wire electrical feed through was adapted to the vessel in order to measure the output from an extensometer in the vessel itself. The simultaneous measurement of sample load-line displacement and applied load made accurate J determination possible. A low-profile extensometer was found to perform in hydrogen with no drift at pressures up to 10,000 psi.

Double edge notch tensile specimens were employed in all tests. Only one notch had an active fatigue precrack; the other notch was machine cut to prevent crack initiation (crack initiation did occur in some tests as described below). Due to loading constraints, a 0.250 in sample thickness was used. Loads were determined to 100 lbs and sample extensions to 0.002 in. were routinely measured. Hydrogen gas purity was assured by using pure input gas with an in-line filter for water and oxygen. Levels of oxygen and water were below 2 ppm.

3.2 Experimental observations

Tests for determining J_{IC} in air using the double edge notch configuration were first performed in order to provide a baseline for further tests in high pressure hydrogen. Using the same R-curve technique described in the FY 1978 Annual Report, a J_{IC} of ~ 900 in-lb/in^2 was measured. This is significantly higher than the 650 in-lb/in^2 measured using the compact tension geometry and a 0.750 in. thick sample. The difference is attributed to the 0.250 in thickness of the double edge notch sample in the present investigation. While J has been determined to be a proper fracture criterion for thin section, the value may not be extrapolated to thicker section sizes. For these reasons, the J_{IC} value for the DENT samples in air should be used as a base-line to compare to the results in hydrogen.

The second series of test involved measurements of J_{IC} in 1000 and 3000 psi hydrogen, and 1000 psi helium. A number of observations can be made:

1) A J_{IC} ~ 350 in-lb/in^2 was measured in both 1000 and 3000 psi hydrogen. This is significantly lower than the 900 in-lb/in^2 measured in air and confirms the trend observed in 1 atm hydrogen. The value 350 in-lb/in^2

is approximately equal to that observed in 1 atm hydrogen; however due to the different sample geometries this may be coincidental. Interestingly there is no difference in J_{IC} between 1000 and 3000 psi so that a saturation pressure less than 1000 psi must exist.

2) The slope of the J vs a curve is equivalent for 1000 and 3000 psi hydrogen, indicating that the resistance to stable crack growth has also saturated. The dJ/da slope is a factor three lower than that in air, again following the trend in 1 atm hydrogen.

3) Hydrogen assisted crack initiation occurs at flaws much less sharp than the fatigue precrack. Crack initiation was observed at a machined slot with a root radius of 0.001 in., i.e. ten-fold greater than the precrack opening radius. This indicates that hydrogen is effective in initiating fracture at flaws similar to those observed in service, such as weld strikes or machining grooves.

4) Fracture surface morphology was quasi-cleavage in all cases of hydrogen fracture. Little or no true cleavage was observed.

5) Limited test in 1000 psi helium were comparable in J vs a values to those in ambient air. However, due to slight differences in loading response with the pressurized system, all base-line tests will be performed in the future in helium at the equivalent hydrogen pressure.

4. Pipeline Weldment Studies

J. R. Spingarn

During the past year, tensile tests have been used to screen pipeline steels, both base metals and weldments, for possible 6.9 MPa (1000 psi) H_2 gas service. We had previously established that for A516-70 steel both base metal microstructure and weld practice seem to have little effect on H_2 compatibility. Further testing has demonstrated three important points: (1) On the basis of tensile stress-strain data the various steels and microstructures appear to perform equally well in H_2, regardless of differences in air behavior. Specifically, no reductions in strength were observed during gaseous H_2 testing, and the reduction in area (RA) values showed relatively little variation from material to material, 35% ± 5% RA in H_2 for smooth bars and 9% ± 2% for notched bars. In no case was the measured RA value sufficiently low to suggest potentially catastrophic brittle fracture. On this basis, one may conclude that weld fusion zones and heat affected zones need not be singled out for special concern regarding H_2 embrittlement. (2) A close examination of the notched stress-strain curves reveals notable differences among the line pipe steels. By defining a parameter based on the extension necessary to induce substantial H_2 crack growth in a rising load test, we found that A106-Grade B was fairly tolerant of plastic extension, while the high toughness Arctic-grade steel failed almost immediately upon yielding. Other steels fell between these two extremes. This type of observation could prove important when designing against plastic strain due to ground subsidence. (3) The extent of hydrogen-assisted surface crack penetration in tensile fracture surfaces varied significantly from material to material and weldment to weldment. Interestingly, this finding does not necessarily correlate with the differences in tolerance to notched plastic strain. The physical interpretation of these results is still unclear and efforts will be made to attempt to understand these experimental observations.

Differences were also noted between the very compatible A106 and A516 steels and the newer higher toughness line pipe. We plan to explore these differences further by performing J-integral fracture toughness tests using seam welded, high toughness pipe steel recently purchased. We propose to compare the toughness of various locations within the weldment as well as compare the H_2 toughness losses for different pipeline steels.

5. Systems Studied of Fixed-Site Hydrogen Storage

J. J. Iannucci and S. L. Robinson

5.1 National Scale

Understanding of hydrogen storage is a critical link in the development of large-scale hydrogen usage. Production, transport and end use are important, but storage is, in general, necessary to smooth mismatches between supply and demand. In a scenario of wide-spread use and availability, however, one still must attempt to minimize or optimize storage of any fuel due to the expense involved. This is particularly true of a gaseous fuel such as hydrogen. Therefore this work focused upon the necessity, viability and economics of bulk hydrogen storage.

To determine the needs and characteristics of hydrogen storage, the hydrogen energy cycle was broken into three sections: production, distribution and end use. In each of these sectors storage of hydrogen may be beneficial towards smooth and economical operation.

Hydrogen storage at constant production rate sites will not be needed (as there is no advantage to storing at all). Variable production rate locations (such as solar powered conversion plants) present a slightly different picture. Here a tradeoff exists between the cost of storage (to smooth transmission rates and hence lessen pipeline sizes and costs) versus the cost of the transmission line. For the solar hydrogen production case, storage is a more expensive option than simply oversizing the transmission lines to handle the maximum production rate. This result, of course, depends on the cost of storage and the cost and length of the transmission line, but nonetheless is quite broadly applicable. Unless extremely inexpensive storage is available (less than 100$/MBTU, 1972 dollars) or the length of the line is extremely

long (say, more than 100 miles), storage is not the preferred option. The case of using off peak electricity for electrolysis is very similar to the solar case and for similar reasons storage is not attractive here either.

Hydrogen storage is most important and beneficial at distribution sites. This storage will be seasonal in nature (as natural gas storage is used currently). Even accounting for hydrogen's lower heating value (with respect to natural gas) the current underground natural gas storage facilities would provide almost all of the seasonal storage requirements envisioned. (Further, the amount of underground natural gas storage in the U. S. continues to increase while the consumption of gaseous fuels is decreasing.) Should this or similar storage not be acceptable for hydrogen service, the next best alternative may be above ground constructed vessels in the 1000 $/MBTU range. Since currently $7x10^9$ MBTU of natural gas storage is used, a rough estimate of the cost of above ground hydrogen storage would be $7x10^{12}$ (seven trillion) dollars. This would probably be unacceptable to both hydrogen utilities and their customers. Hence effort should be put into assuring the viability of inexpensive storage, such as conversion of current natural gas storage facilities to hydrogen service.

Storage at the end use point is not really an issue. In a postulated scenario of widespread hydrogen usage, hydrogen will be available on demand from distribution and delivery networks as natural gas now is. Residential users will almost never be interrupted and industrial and commercial users will prefer oil as a back-up heat source rather than expensive hydrogen storage. Thus storage at the end-use point will rarely be required.

In summary then, the most pressing need for hydrogen storage is not at the production point (even for intermittent production) or the end use point, but rather at distribution locations. This is consistent with current natural gas practice. Conversion of natural gas storage to hydrogen service may well provide for storage at the distribution point.

5.2 Small Scale

Small users may desire to store hydrogen, provided compatible, affordable modes are available. In this study, presently available and some possible future technologies are studied with the intent of identifying the minimum cost storage technique for various combinations of quantity, cycling frequency and parasitic energy costs. Peg points of 10 MwHr electric equivalent (34 MBTU), and a least-cost size scale are identified for each technology.

Three basic storage forms are considered: pressurized gas, cryogenic liquid and hydride; a fourth form, microballoon storage is also estimated. For each form it is necessary to develop (1) installed capital cost, (2) filling and emptying equipment costs, and (3) parasitic energy consumption costs.

For storage of pressurized gas, a variety of conventional pressure vessel forms are available. Those considered are, standardized API spherical and spheroidal vessels, steel pipes, and steel pressure vessels. Commercial estimates were used where possible. The question of an optimum pressure is considered; in fact the capital cost minimum is very broad. At high pressure, hydrogen embrittlement phenomena dictate rapidly increasing thicknesses with increasing pressures, to ensure safety. Economically, low and moderate pressure storage looks most attractive with installed costs below $1500/million BTU.

Nonconventional pressure vessel technologies include (1) prestressed cast iron (PCIV) with integral liner, (2) prestressed concrete, (PCCV), (3) filament wound metal bladder, and (4) underground using overburden pressure to lessen structural requirements from the gas containing bladder. The PCCV is competitive with low pressure storage in conventional vessels and at large sizes and high pressures PCIV is computational. Burial of pressure vessels is uneconomical due to the costs of underground construction; great depths are required for significant structural contributions from the overburden.

The installed capital costs of cryogenic nydrogen storage are developed, and seen to be attractive (<$75/MBTU) for large scale storage; at small sizes the cost in $/MBTU is near that for gas storage, about $1400/MBTU. Hydride storage capital costs approach $3400/MBTU, because of the high price of hydride and the necessity of a pressure vessel. Microballoon storage has the lowest vessel capital costs, current estimates being in the $18-32/MBTU range.

Single cycle parasitic energy costs are determined: pressurization costs, liquefaction costs, combined heat and pressure for the microballoon system all were developed and applied to the appropriate system. Cycling requirements (daily, weekly and seasonal) were added to the above costing data. Using two scales, the 34 MBTU and optimum size, the total cost (installed capital plus parasitic energy (present valued) plus cycling requirements) was calculated using electric rates as a parameter.

For either the 34 MBTU or the optimum scale, energy intensive systems such as liquefaction or microballoons, fared poorly for daily cycling. Low pressure storage was the most economical technique, with costs ranging from 1200 $/MBTU (present value) depending upon energy costs. For weekly cycling, a complex mix developed dependent upon energy costs. For seasonal cycling, the energy intensive, low capital cost systems, were superior in large sizes; for small (34 MBTU) quantities microballoon storage appeared to be superior (less than $100/MBTU) with low pressure and liquefaction storage costing $1100-1500/MBTU. The costs obtained are estimates, and indicated clear choices for large seasonal, and both large and small daily cycling. Several choices are viable for the other duty cycles. While

microballoon storage estimates are rough, this technology does look promising.

Detailed reports on these systems studies are available upon request. The reports are:

Applications Analysis of Fixed-site Hydrogen Storage
J. J. Iannucci & S. L. Robinson
SAND78-8272
May 1979

Fixed-site Hydrogen Storage: A Comparison of Technologies and Economics
S. L. Robinson & J. J. Iannucci
SAND79-8646
Oct. 1979

Summary of Accomplishments

1. Hydrogen induced slow crack growth does not appear to be a major concern in typical pipeline steels. Gaseous hydrogen does, however, degrade the burst strengths of flawed pipeline segments and significantly accelerates fatigue crack growth rates.

2. Techniques have been developed to measure the fracture toughness, J_{IC}, of pipeline steels in high pressure hydrogen. Preliminary results indicate that the J_{IC} of these steels is reduced by ~ 60% in 1000 psig hydrogen.

3. Tensile tests of both laboratory simulations of pipeline weldments and actual pipeline weldments indicate that neither the fusion zone nor the heat affected zone are more susceptible to hydrogen embrittlement than the parent metals.

4. Two rather extensive systems studies considering the fixed-site storage of hydrogen gas have been completed. For large scale storage, it was concluded that underground storage is the most economical option and is available in sufficient quantity. For smaller scale storage, the optimal storage technique is a function of the quantity stored, the cycle rate, and the cost of electrical power.

THE INFLUENCE OF FERROUS MICROSTRUCTURE ON THE FATIGUE CRACK GROWTH RATE IN AIR AND IN HYDROGEN

Harry F. Wachob

Failure Analysis Associates at
NASA-Ames Research Center
Materials Science and Applications Office
Mail Stop: STO:230-4
Moffett Field, CA 94035

Abstract

An improvement in the fatigue crack growth resistance of a commercial low strength steel in air and high pressure hydrogen may be possible by the proper selection of microstructure. Various ferrous microstructures--tempered martensite, austempered bainite, and normalized pearlite--were produced by standard heat treatments of an A516-G70 carbon steel. The near-threshold, fatigue crack growth rate was measured as a function of microstructure, environment, R ratio (P_{min}/P_{max}), and alternating stress intensity. Results are presented which indicate that increased amounts of free ferrite and pearlite increase the crack growth rates and decrease the fatigue threshold stress intensity. Additionally, these observations are supported by fractographic and metallographic correlations.

Introduction

Hydrogen is a viable supplement to the present natural gas supply system. Independent of the production, storage, or transmission method used, the interaction of hydrogen with various containment materials plays an integral role in the success of a hydrogen technology program. In order to implement a hydrogen energy system at a reasonable cost, low-cost materials must be developed that are compatible with high pressure hydrogen.

Previously, low strength ferrous alloys were believed to be immune to degradation in a hydrogen environment. However, the results of Chandler and Walter,[1] Clark,[2] and Nelson,[3-4] indicated potential problems with hydrogen-iron interactions under cyclic loading conditions. Under the containment materials element of the HEST Project, studies were initiated to fully understand the interaction of high pressure hydrogen with low strength structural steels under static and cyclic loading conditions. Their results suggest that hydrogen produces dramatic changes in the fatigue and fatigue crack growth behavior of steel.

Evidence[5-9] suggests that the metallurgical microstructure plays a major role in determining the material's resistance to hydrogen degradation. However, these results are for high strength steel alloys. One cannot directly apply the high strength microstructural correlations to the low strength alloys without supporting experimental evidence. Thus, the goal of this program is to determine the influence of microstructure on the crack growth resistance of low strength ferrous alloys exposed to high pressure gas-phase hydrogen.

Experimental Procedure

An ASTM steel plate alloy A516-G70 was chosen as a representative steel to perform the experimental phase of the program. The chemical composition (.22 w/o C, 1.1 w/o Mn, and .21 w/o Si) is similar to the ferritic-pearlitic steels frequently used in pressure vessels and natural gas pipelines.

Tensile and compact tension (CT) specimen blanks were cut from the 1.25 cm thick plate. The tensile specimens were cut with the testing axis in the long transverse (L-T) direction. The compact tension specimens were cut in the L-T direction (crack growth in the short transverse-rolling direction plane). The blanks were heat-treated according to one of the following schedules:

1. Normalized microstructure - 870°C as received condition.
2. Bainite -
   a. Austenitize at 1200°C for 3/4 hr.
   b. Isothermally quenched to 450°C and held for 1-1/2 hours.
3. Quench and tempered martensite -
   a. Austenitize at 1200°C for 3/4 hr.
   b. Agitated ice water quench.
   c. Temper at 450°C for 1-1/2 hr.

The normalized microstructure is a dual-phase microstructure; 30% pearlite and 70% α-ferrite. The ferrite grain size is ∿35μm. Numerous manganese sulfide (MnS) stringers or inclusions have been elongated in the rolling direction. A typical metallographic section of the normalized material is shown in Figure 1.

The bainitic microstructure is a combination of a continuous ferrite network surrounding the 200μm bainite-pearlite grains. Packets of bainitic and pearlitic carbides make up the interior portion of the grains.

The martensitic microstructure is similar to the bainitic material. However, in this case, no free-ferrite is observed. Inside the 200μm grain boundaries, packets of tempered martensite and bainite are the dominant metallographic feature.

A summary of the metallurgical and mechanical properties of the various microstructures is given in Table 1. The tensile properties listed were measured in an ambient air environment. Tests were performed at the plastic strain rates of

$2 \times 10^{-2} s^{-1}$ and $2 \times 10^{-3} s^{-1}$. No large strain rate sensitivity was observed. This is in agreement with results of Banerjee.[10]

Standard 1/2T-CT specimens were used to measure fatigue crack growth rates. Specimens were machined and loaded according to ASTM E399-74. However, an improved equation for stress intensity, proposed by Newman,[11] which accounts for the influence of the pin-loaded holes and applies over a wider range of a/w was used instead of the ASTM E399-74 proposed equation.

Fatigue tests were performed under constant crack opening displacement. Under this condition, the alternating load increment (P_{max}-P_{min}), and thus ΔK, decreased as the crack front extends. This load decay and associated compliance change, as a function of cycles, was recorded and subsequently used in the data reduction program. The fatigue tests were performed at R ratios (P_{min}/P_{max}) between 0.1 and 0.15. Tests were performed either in an ambient air environment or in a 6.9 MPa gaseous hydrogen environment.

Fractographic and metallographic analyses were performed on the specimens after testing was completed. If etching of the fracture surface or metallographic sections was required, a 4 mg Picric acid in 100 ml of methanol solution was used.

Results and Discussion

Fatigue Tests

The cyclic properties of this ferritic-pearlitic grade of steel were influenced greatly by the high pressure hydrogen environment. For all microstructures investigated (pearlitic, martensitic, and bainitic), the fatigue crack growth rates (FCGR) were faster in hydrogen than in air. In addition, for a given microstructure the fatigue threshold stress intensity was slightly lower in hydrogen than in air.

The crack growth velocities at $\Delta K \geq 15$ MPa$\cdot$m$^{\frac{1}{2}}$, in an air environment (see Figure 2) appeared to be independent of microstructure. However, at this value of ΔK, the bainitic and martensitic specimens appear to have had a common fatigue threshold. On the other hand, the normalized microstructure specimens continued to crack and approached a threshold value of 8-9 MPa$\cdot$m$^{\frac{1}{2}}$. Work by Masounave and Bailon,[12] Aita and Weertman,[13] and Nelson[3] on pearlitic-ferrites is in good agreement with the present normalized microstructure results. These researchers used a wide variety of irons and steels which indicates that the FCGR is relatively independent of base metal chemistry and minor microstructural variations.

The fatigue threshold values for the martensitic and bainitic microstructures were somewhat higher than anticipated. In general, one would anticipate higher strength steels to have lower fatigue thresholds. One possible explanation for the higher thresholds is that microstructures having larger prior austenitic grain sizes have higher threshold values. This trend has been observed by Ritchie[14] and Masounave.[12] Experiments are presently underway to determine the effect of prior austenite grain size. A second explanation is that the martensitic network exerts a strong constraint upon the degree of plastic deformation that can occur at the crack tip. This could explain the results of Suzuki and McEvily[15] in a duplex ferritic-martensitic microstructure. In their experiment a continuous martensitic network resulted in an increase in strength and fatigue threshold level as compared to a continuous ferrite network. Whether these arguments are valid for the tests performed in air and can be extended to the results in hydrogen is yet to be determined.

The effect of hydrogen on the FCGR and threshold has not been fully investigated. The results on the normalized material in a 6.9 MPa hydrogen environment are essentially a linear extrapolation from the higher ΔK values of Nelson's results[3] on a 1020 steel.

In a hydrogen environment, the bainitic and martensitic microstructures exhibit a similar behavior to the normalized microstructures above $\Delta K \approx 13$ MPa$\cdot$m$^{\frac{1}{2}}$. The hydrogen FCGR's are shown in Figure 3. Below this value, the martensitic material has an apparent fatigue threshold of $\approx$12.5 MPa$\cdot$m$^{\frac{1}{2}}$; the bainitic material has a threshold of $\approx$11.5 MPa$\cdot$m$^{\frac{1}{2}}$; and lastly, the normalized pearlitic material has a threshold of $\approx$8 MPa$\cdot$m$^{\frac{1}{2}}$. Similar arguments could be used to explain this threshold ordering as were used for those observed in the air environment, particularly with respect to the restraint of plastic deformation at the crack tip.

Fractographic Analysis

A change in fatigue fracture topography occurred upon going from air to a 6.9 MPa hydrogen environment. The most drastic changes occurred for the normalized microstructure. The primary fractographic features for the normalized microstructure after fatigue in air ($R \sim 0.15$; $\nu = 1$ Hz) are: (1) ductile tearing of α-ferrite and fatigue striations (see Figure 4) which may be the result of plastic blunting and resharpening of the crack tip; (2) strong influence of the rolling inclusions of MnS, which appeared as sharp elongated secondary cracks on the fracture surface; and (3) a large amount of secondary cracking along pearlite-α-ferrite interfaces, as shown in Figure 5. These features were seen over the entire range of alternating stress intensity. However, as ΔK decreased, there were indications of less overall gross plasticity associated with the fracture process.

When the normalized specimens were fatigued in 6.9 MPa hydrogen, the fracture mode changed from transgranular at $\Delta K \approx 24$ MPa$\cdot$m$^{\frac{1}{2}}$ to intergranular near the threshold, $\Delta K \approx$8-10 MPa m$^{\frac{1}{2}}$. The majority of intergranular failures occurred at ferrite-pearlite boundaries, with the remainder occurring at ferrite-ferrite interfaces. After the fracture surface was etched, the intergranular nature of the failure can easily be seen (see Figure 6). In addition, evidence of secondary cracking and MnS inclusion effects were absent. A summary of these fractographic features is given in Table 2.

The failure mode in the bainitic and martensitic specimens was primarily transgranular in both hydrogen and air environments. Summaries of

the actual fractographic features are listed in Tables 3 and 4, respectively. Scanning micrographs of the bainitic specimens (Figures 7 and 8) and the martensitic specimens (Figures 9 and 10) show the general features observed in the air and hydrogen environments. In the bainitic microstructure intergranular failures occur at pearlite-ferrite interfaces. Of the 10% intergranular failures observed in the martensitic specimens, no evidence was found that these areas can be correlated to free ferrite or pearlitic type regions. The general indication seems to be that increased amounts of free ferrite and/or free ferrite-pearlite interfaces appear to decrease the fatigue threshold value and/or increase the FCGR at comparable ΔK levels. This is consistent with the idea of decreased deformation at crack tips producing the same effect. One would expect to see increased plastic deformation with increased amounts of free ferrite. Clarification of the role of ferrite and/or deformation mechanisms will be of high priority in future experiments.

Summary

1. At ΔK's $\simeq$15 MPa$\cdot$m (ν = Const., R = Const.) crack growth rates (CGR) for all three microstructures are the same in air; CGR's are accelerated in H_2 but are again approximately equal.

2. Bainite and Q+T martensite have a higher fatigue threshold value at 10^{-8} mHz than the normalized microstructure in both H_2 (6.9 MPa) and air.

3. The hydrogen fatigue thresholds are decreased from those observed in air.

4. For A516, higher strength levels do not necessarily reduce the fatigue threshold values or increase da/dN as might be inferred from the literature. An increase in ΔK_0 may be the result of a reduced plastic zone size. This is supported by the fact that increased amounts of α-ferrite appear to cause a decrease in the fatigue threshold value and subsequently higher CGR's at comparable ΔK levels.

References

1. W. T. Chandler and R. J. Walter, "Hydrogen Environment Embrittlement of Metals and Its Control," in Hydrogen Energy (T. N. Vezirogłu, ed.), p. 1057, Plenum Press, NY, 1975.
2. W. G. Clark, "The Effect of Hydrogen Gas on the Fatigue Crack Growth Rate Behavior of HY80 and HY130 Steels," in Hydrogen in Metals (I. M. Bernstein and A. W. Thompson, eds.), p. 149, ASM, Metals Park, OH, 1974.
3. H. G. Nelson, "Hydrogen-Induced Slow Crack Growth of a Plain Carbon Pipeline Steel under Conditions of Cyclic Loading," in Effect of Hydrogen on Behavior of Materials, p. 602, AIME, NY, 1975.
4. H. G. Nelson, "On the Mechanism of Hydrogen-Enhanced Crack Growth in Ferritic Steels," in Proceedings of the Second International Conference on Mechanical Behavior of Materials, p. 690, ASM, Metals Park, OH, 1976.
5. R. T. Ault, K. O. McDowell, P. L. Hendricks, and T. M. F. Ronald, "Increased Reliability of a High Strength Steel through Thermal-Mechanical Treatments," Trans. Quarterly ASM, Vol. 60, p. 79, 1967.
6. C. N. Ahlquist, "Influence of Ausforming on Stress Corrosion Susceptibility of Some High-Strength Steels," Metals Engineering Quarterly, Vol. 8, p. 52, 1968.
7. E. Snape, "Roles of Composition and Microstructure in Sulfide Cracking of Steel," Corrosion, Vol. 24, p. 261, 1968.
8. J. D. Hobson and C. Sykes, "Effect of Hydrogen on Properties of Low-Alloy Steels," JISI, Vol. 169, p. 209, 1951.
9. M. Henthorne and R. N. Parkins, "Some Aspects of the Influence of Structure Upon Stress Corrosion Cracking in Grain Boundary Corrosion in Mild Steels," British Corrosion Journal, Vol. 2, p. 186, 1967.
10. S. Banerjee, "Influence of Specimen Size and Configuration on the Plastic Zone Size, Toughness, and Crack Growth," to be published.
11. J. C. Newman, Jr., "Stress Analysis of the Compact Specimen Including the Effect of Pin Loading," Fracture Analysis, ASTM STP 560, ASTM, 1974, p. 120.
12. J. Masounave and J. P. Bailon, "Effect of Grain Size on the Threshold Stress Intensity Factor in Fatigue of a Ferritic Steel," Scripta Met., Vol. 10, p. 165, 1976.
13. C. R. Aita and J. Weertman, "The Effect of Microstructure on Fatigue Crack Propagation in Iron-Carbon Alloys," Metallurgical Transactions, Vol. 10, p. 535, 1979.
14. R. O. Ritchie and M.F. Carlson, "On the Effect of Prior Austenite Grain Size on Near-Threshold Fatigue Crack Growth," Scripta Met., Vol. II, p. 113, 1977.
15. H. Suzuki and A. J. McEvily, "Microstructural Effects on Fatigue Crack Growth in a Low Carbon Steel," Metallurgical Transactions, Vol. 10, p. 475, 1979.

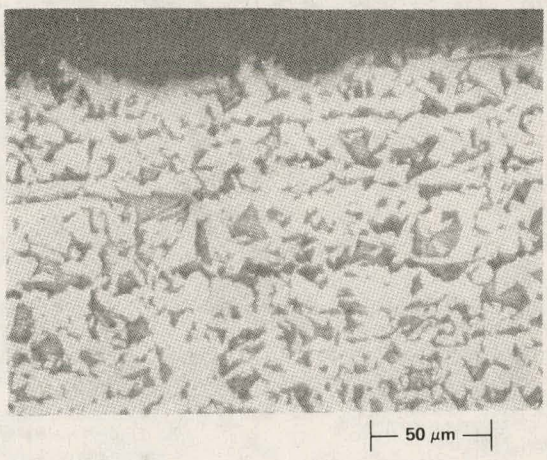

Figure 1. Microstructure of a Normalized A516-G70

CONDITION	YS MPa	UTS MPa	ϵ_f %	HARDNESS	MICROSTRUCTURE
NORMALIZED 1600°F	330	565	25	81_B	30% PEARLITE 70% FERRITE (35 μm)
BAINITIC γ - 2200°F ISQ 850°F	415	650	15	85_B	CONTINUOUS NETWORK OF α-FERRITE AT GRAIN BOUNDARIES (10% VOL) BAINITE + PEARLITE (200 μm)
MARTENSITIC γ - 2200°F IWQ 850°F	820	920	5	24_C	TEMPERED MARTENSITE AND BAINITE (200 μm)

Table 1. Heat Treated Properties of A516.

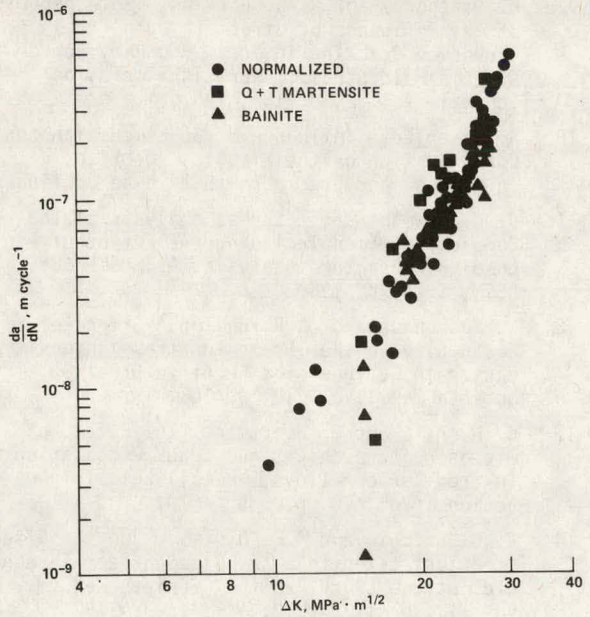

Figure 2. Fatigue Crack Growth Rate of A516 Air at R ∿ 0.15

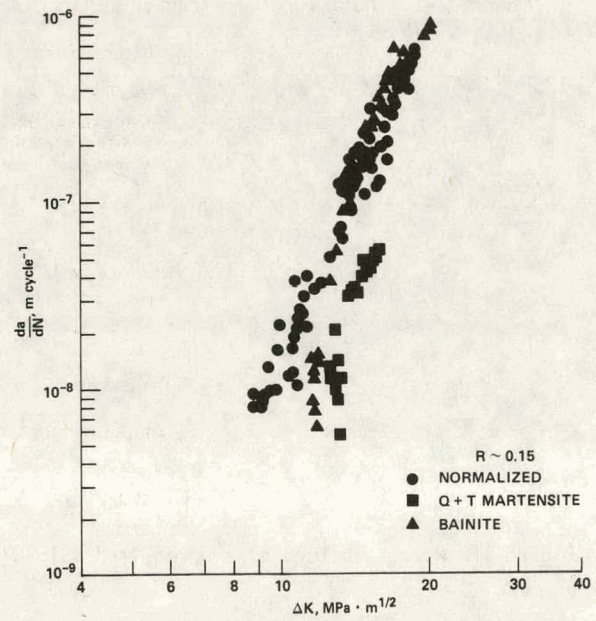

Figure 3. Fatigue Crack Growth Rate of A516 in 6.9 MPa Hydrogen

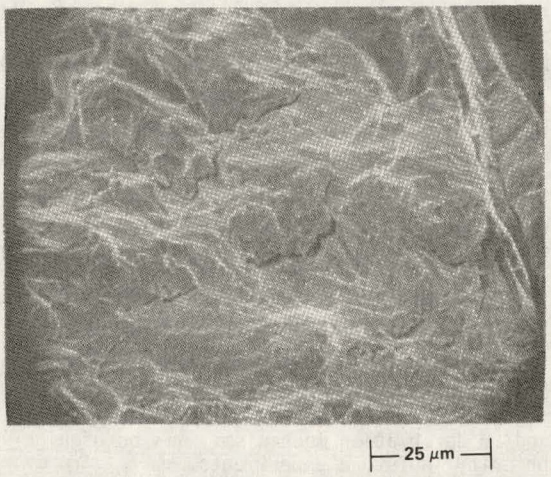

Figure 4. Typical Air Fatigue Fracture Surface

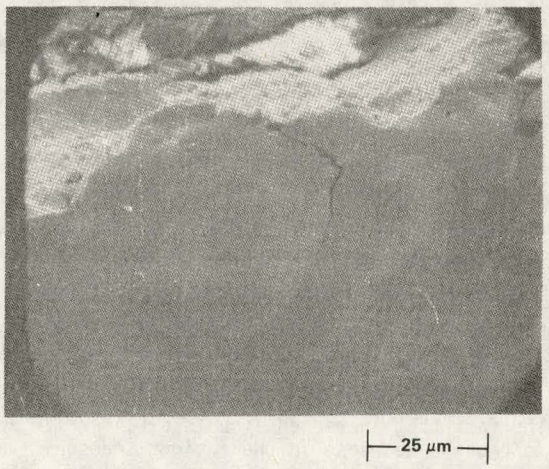

Figure 5. Secondary Fatigue Cracks Produced in Air

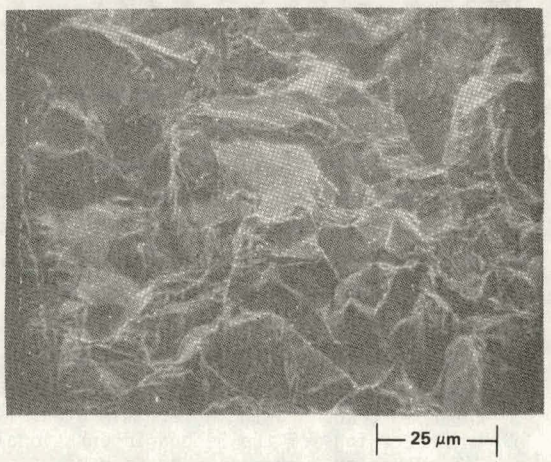

Figure 6. Intergranular Failure of A516 in 7 MPa H_2 $\Delta K \simeq 12$ MPa·m$^{\frac{1}{2}}$

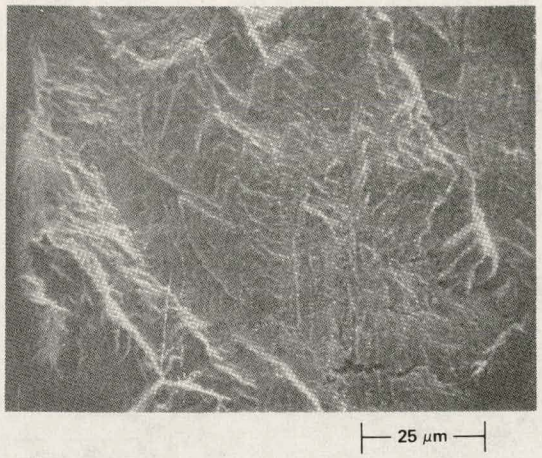

Figure 7. Herringbone Transgranular Failure of Bainitic Specimen After Air Fatigue.

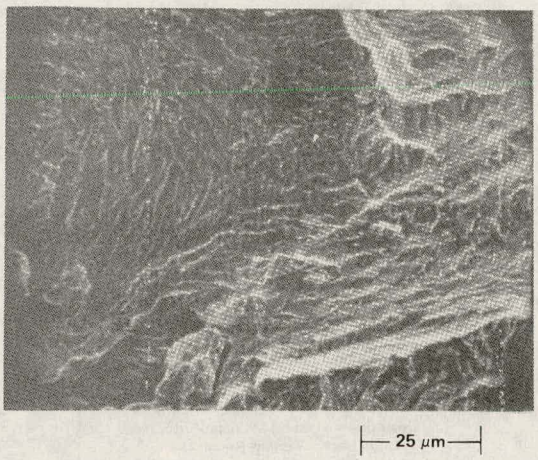

Figure 8. Transgranular Failure in a Bainitic Specimen After Fatigue in 6.9 MPa H_2.

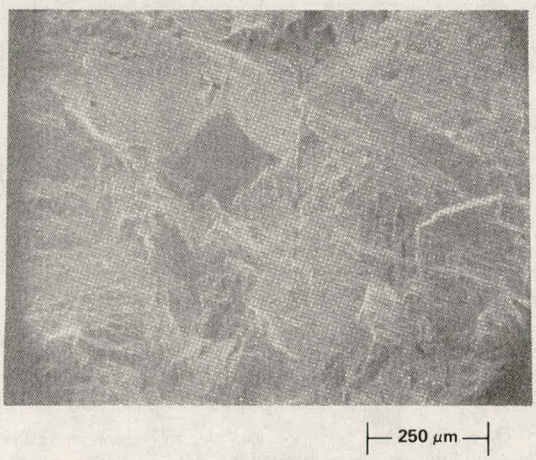

Figure 9. Typical Fracture Surface of a Martensitic Specimen After Fatigue in Air.

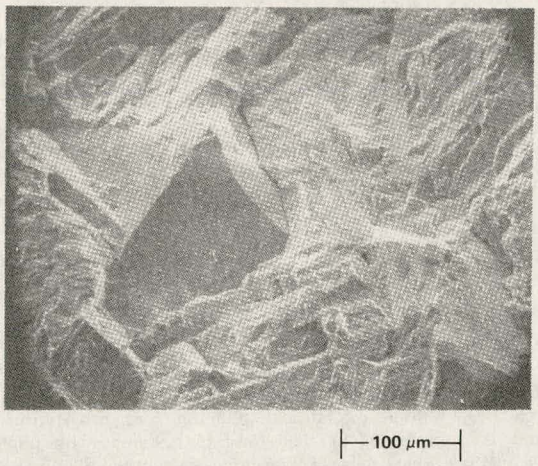

Figure 10. Fracture Surface of a Martensitic Specimen Fatigued in 6.9 MPa H_2.

ENVIRONMENT	ΔK, MPa · $m^{1/2}$ RANGE	FEATURES
AIR	10-30	–DUCTILE TEARING, FATIGUE STRIATIONS –STRONG INFLUENCE OF MnS –LARGE AMOUNT OF SECONDARY CRACKING AT PEARLITE-FERRITE
H_2	~24	–TRANSGRANULAR –REDUCED MnS EFFECT –DECREASED FREQUENCY OF SECONDARY CRACKS
	~17	–TRANSGRANULAR THRU α - FERRITE –SMALL AMOUNT INTERGRANULAR –EVIDENCE OF PLASTIC DEFORMATION
	~12	–INTERGRANULAR AT BOTH α - α AND α - PEARLITE BOUNDARIES –SMALL AMOUNT TRANSGRANULAR

Table 2. Fractography of Normalized A516

ENVIRONMENT	ΔK, MPa · $m^{1/2}$ RANGE	FEATURES
AIR	15-30	– HERRINGBONE TRANSGRANULAR FAILURE – REDUCED MnS EFFECT – SOME INTERGRANULAR FAILURE AT PEARLITE-α-FERRITE BOUNDARIES – STEPPED CRACK FRONT
H_2 (6.9 MPa)	11-20	– TRANSGRANULAR FAILURE – INTERGRANULAR AT PEARLITE- α-FERRITE – QUASI- CLEAVAGE IN G.B. FERRITE

Table 3. Fractography of Bainitic A516.

ENVIRONMENT	ΔK, MPa · $m^{1/2}$ RANGE	FEATURES
AIR	15-30	– TRANSGRANULAR FATIGUE STRIATIONS – SMALL AMOUNTS OF INTERGRANULAR FAILURE
H_2 (6.9 MPa)	13-20	– TRANSGRANULAR CLEAVAGE – REDUCED PLASTICITY – 10% INTERGRANULAR FAILURE

Table 4. Fractography of Quench and Tempered A516.

EVALUATION OF LASER WELDING TECHNIQUES FOR HYDROGEN TRANSMISSION

J. Mucci and J. A. Harris
Pratt & Whitney Aircraft Group
Government Products Division
West Palm Beach, Florida 33402

ABSTRACT

This program was established to determine the feasibility of laser beam welding as a fabrication method for hydrogen transmission and is a precursor in the effort to systematically provide the technological base necessary for large-scale, economic pipeline transmission of fuel for a hydrogen energy system. The study contributes to the technology base by establishing the sensitivity of two classes of steels to gaseous hydrogen environment effects and determining the effect of conventional weld processes and laser beam welding on properties. Screening evaluation of the tensile, low-cycle fatigue and fracture toughness properties and metallurgical analyses provide the basis for concluding that laser beam welding of AISI 304L stainless steel and ASTM A106B carbon steel can produce weldments of comparable quality to those produced by gas-tungsten arc and electron beam welding and is at least equally compatible with 13.8 MPa (2000 psig) gaseous hydrogen environment.

INTRODUCTION

The evolution of a hydrogen energy system requires major technology development programs. Regardless of the means of production, transmission and storage of hydrogen will be required. Current gas transmission pipeline technology forms the base from which hydrogen transmission will grow. However, unlike natural or hydrocarbon gases, hydrogen has a unique effect upon many metals in that it embrittles or degrades properties. This effect upon material properties has been studied most extensively in the development of hydrogen-fueled rocket engines. For space applications, use of expensive, highly alloyed materials and very stringent processing is justified. The economics of gas transmission systems, however, require the use of lower cost, more plentiful structural materials.

Mild and low alloy steels are being considered because of the economic factor. A problem exists, however, in that most ferritic steels are susceptible to degradation of structural properties resulting from hydrogen exposure over a wide range of conditions. Since numerous welded joints are required in the fabrication of transmission pipelines and storage systems, an additional problem exists — weldments appear more susceptible to hydrogen degradation (embrittlement) than the parent alloys. Moreover, various welding processes may yield different degrees of susceptibility. In general, welding processes that minimize fusion and heat-affected zones tend to produce high integrity welds that are less susceptible to hydrogen degradation and also produce joints that maintain many of the characteristics of the parent material. Preliminary research by United Technologies Research Center indicated that laser weldments possess these desired qualities.

This program was established to determine the feasibility of laser welding as a fabrication method for hydrogen transmission and is a precursor in the effort to systematically provide the technological base necessary for large-scale, economic pipeline transmission of fuel for a hydrogen energy system. The study contributes to the technology base by establishing the sensitivity of two classes of steels to gaseous hydrogen environment effects and determining the effect of gas tungsten arc welding (GTAW), electron beam welding (EBW), and laser beam welding (LBW) on properties. Screening evaluation of the important mechanical and metallurgical properties of the materials provided the basis for conclusions concerning the feasibility of LBW.

The logic upon which this program was structured is diagramed in Figure 1.

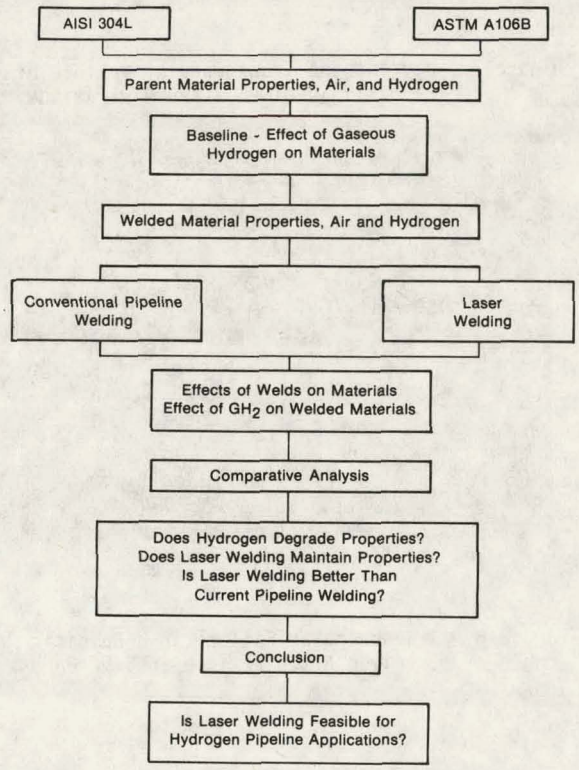

Figure 1. Process for Obtaining Program Results and Conclusions from the Laser Welded Hydrogen Transmission Pipeline Evaluation

Experimental efforts in this program included 154 mechanical properties tests of AISI 304L stainless steel and A106B carbon steel in ambient pressure air and gaseous hydrogen. The hydrogen environment tests were conducted at a pressure of 13.8 MPa (2000 psig), the pressure projected for economical transmission of hydrogen (Reference 1). Testing involved going directly to the anticipated operating pressure and establishing the sensitivity of the materials and weldments to hydrogen environment. The effects of potential hydrogen pickup during welding or evaluation of thermally charged specimens were not investigated since they were not within the scope of work included in this program.

The primary goal of these tests was to document, rather than define, the hydrogen phenomenon and provide preliminary data for use in designing a hydrogen energy system. The overall test program is diagramed in Figure 2 and outlined in Table I (Appendix). The specific mechanical properties tests and metallurgical analyses are:

1. Tensile Properties — Smooth and notched tensile properties were determined using ASTM E-8 procedures.

2. Low-Cycle Fatigue — Low-cycle fatigue life was established using constant total strain testing techniques.

3. Fracture Toughness — Fracture toughness parameters were established using ASTM E-399 procedures, where applicable, and J-Integral techniques.

4. Metallography — Metallurgical evaluation was conducted to characterize the parent and welded materials. Also, fractographic evaluation was conducted on representative samples of failed test specimens to aid in explaining test result abnormalities.

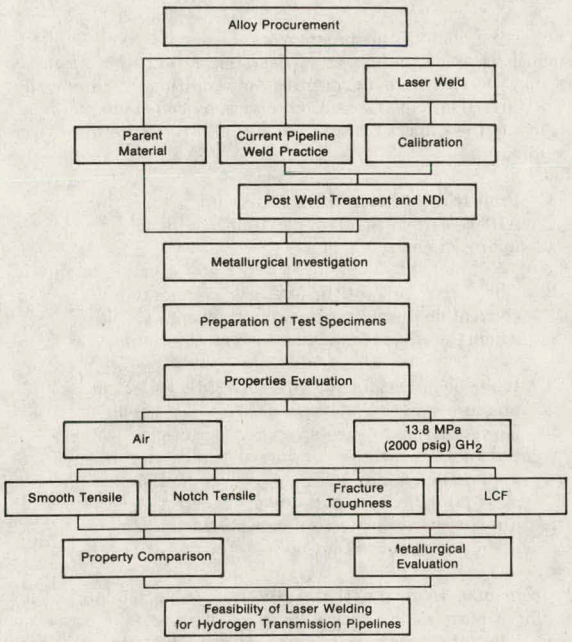

Figure 2. Program Outline for the Evaluation of Laser Welded Hydrogen Transmission Pipelines

This program, DOE Contract EC-77-C-02-4355, was sponsored by Dr. James H. Swisher, assistant director, Physical Storage Systems, Department of Energy, Washington D.C., under the technical cognizance of Dr. H. F. Walchob, NASA-Ames Research Center, Moffett Field, California. Mr. Joseph Mucci was the Pratt & Whitney Aircraft Group Government Products Division Program Manager.

This program as initially designed has been completed, the results and conclusions of which are contained herein. At the time of writing this paper, a contract modification had been received. The scope of work has been increased to complete the test matrix as shown in Table I. The testing of an additional seventeen welded low-cycle fatigue specimens will enable an assessment as to the effect of hydrogen environment on the welded materials. This assessment will permit the selection of the welding technique which results in a weld least susceptible to hydrogen degradation. Publicaton of the final report will be deferred until completion of the work covered in the contract modification and its inclusion therein.

John A. Harris Jr. and J. Mucci are project materials engineer and assistant project materials engineer, respectively, in the Materials and Mechanics Technology Laboratory of the Pratt & Whitney Aircraft Group Government Products Division of the United Technologies Corporation, P.O. Box 2691, West Palm Beach, Florida, 33402.

CONCLUSIONS

General

The test efforts in this program consisted of conducting parent and welded material mechanical properties tests of two classes of pipeline steels, AISI 304L stainless steel and A106B carbon steel, proposed for use in a hydrogen energy system. Properties determined in the hydrogen environment were compared to properties determined in air at the same conditions to establish environment degradation. The effect of gas tungsten arc, electron beam and laser beam welding on the mechanical and metallurgical properties of the two steels was also determined.

The following rating system was established to determine the degree of degradation due to 13.8 MPa (2000 psig) gaseous hydrogen environment and served as an aid in making alloy comparisons:

1. Extremely Degraded (ED) — Hydrogen environment reduced the property or life (in air) greater than 50%.

2. Severely Degraded (SD) — Hydrogen environment reduced the property or life (in air) greater than 25%, but less than 50%.

3. Degraded (D) — Hydrogen environment reduced the property or life (in air) greater than 10%, but less than 25%.

4. Negligible Degradation (ND) — Hydrogen environment reduced the property or life (in air) less than 10%, or had no detrimental effect.

This is the same rating system used in previous P&WA Group hydrogen environmental degradation investigations, several of which are indicated in References 2, 3, and 4. Using this rating system, the Table shown below displays the degree of degradation based on test result averages, for the AISI 304L and A106B materials in the parent and welded conditions tested, where a comparable test in air was conducted. In the case of the smooth tensile tests, if any property (yield strength, ultimate strength, elongation or reduction of area) was degraded, the degradation rating is that of the most severely degraded property.

Use of these degradation conclusions must be tempered by the fact that very limited numbers of tests were conducted for each condition and normal data scatter could influence or change the degradation rating.

Degree of Degradation of AISI 304L and A106B in 13.8 MPa (2000 psig) Gaseous Hydrogen at 24°C (75°F)

Material	*Weld Type*	*Smooth Tensile*	*Notch Tensile*	*Low-Cycle Fatigue*
AISI 304L	Parent Material	ND	ND	ED
	GTAW	ND	ND	ED
	GTAW (HAZ)		ND	
	EBW	D	ND	
	EBW (HAZ)		ND	
	LBW	ND	ND	
	LBW (HAZ)		ND	
A106B	Parent Material	SD	D	ED
	GTAW	D	D	
	GTAW (HAZ)		D	
	EBW	SD	D	
	EBW (HAZ)		D	
	LBW	D	D	
	LBW (HAZ)		D	

Effect of Hydrogen

The most prominent effect of hydrogen environment on the mechanical properties evaluated in this program occurred in the low-cycle fatigue (LCF) tests. The LCF life was *extremely* degraded for both materials in the parent material condition, due to 13.8 MPa (2000 psig) gaseous hydrogen. Reduction in mean lives of approximately 60 and 88% was indicated for the AISI 304L and A106B materials, respectively.

The AISI 304L material tensile properties were the least degraded of all properties evaluated. In fact, with the exception of electron beam welded (EBW) material, negligible degradation if any, was exhibited in the AISI 304L parent and welded material conditions. For the A106B material degradation from the *degraded* to *severe* degree was exhibited for all conditions evaluated.

The prime effect of hydrogen on the tensile properties of the A106B material was the degradation of ductility. The degradation ratings, for the most part, are therefore based primarily upon ductility effects. The relative extent of hydrogen degradation is summarized in Table II (Appendix).

The effect of hydrogen environment on the fracture toughness properties was not established in this program since all tests were conducted in air.

Effect of Welding

The most prominent effects of welding also occurred in the LCF tests. For both materials, conventional welding [gas tungsten arc welding (GTAW) and electron beam welding (EBW)] resulted in substantial reductions in mean LCF life. Approximately 60% reduction in mean LCF lives (compared to parent material) occurred as a result of both GTAW and EBW of the AISI 304L material. The GTAW and EBW of the A106B material resulted in approximately 50 and 27% reductions in mean lives, respectively.

The most beneficial effect of laser beam welding (LBW) was seen in the LCF tests. The LBW reduced the mean LCF life from that of the AISI 304L parent material only 23%. For the A106B material, no detrimental effect on LCF life was indicated, clearly demonstrating the potential of this means of joining materials. The relative effects of welding on mean LCF lives are summarized in Table III (Appendix).

The GTAW, EBW, and LBW of the AISI 304L and A106B materials resulted in reduced tensile ductility. No significant differences between any of the welding processes could be establshed in terms of tensile strength properties. The effects of welding on tensile properties are summarized in Table IV (Appendix).

As was anticipated for AISI 304L and A106B steels in the specimen configuration tested (½-in. thick, 1W compact tension), valid K_{IC} parameters per ASTM E399 could not be met. The alternate method of this procedure covers the determination of the specimen strength ratio, R_{SC}, a function of the total stress (Mc/I and P/A stresses) at the crack tip, resulting from the maximum load the specimen can sustain and the yield strength of the material. The specimen strength ratios, established for the fracture toughness tests in this program, can be significant as a measure of material toughness when results are compared for specimens of the same form and size. This method allows a quantitative comparison to determine the effect of the various welded conditions on the subject materials.

The R_{SC} analysis for both the AISI 304L and A106B materials indicates that for the GTAW, EBW, and LBW conditions, R_{SC} values are all comparable to that of the parent materials. On a statistical basis, no significant differences in R_{SC} could be established due to the various weldments. Moreover, firm conclusions as to the effect of the various weldments on R_{SC} could not be made due to the small sample sizes evaluated and the data scatter experienced. The effects of welding on R_{SC} are summarized in Table V (Appendix).

In accordance with ASTM E399-74, specimen size requirements must be met to assure linear elastic behavior. Thickness must be ample such that the crack tip plastic zone is constrained by sufficient elastically loaded material to assure failure without significant plastic deformation. Testing of the subject materials, in the 1W configuration, indicated considerably insufficient thickness to obtain plane-strain conditions. Therefore, the J-Integral approach was used in an attempt to obtain K_{IC} values (References 5 and 6). This approach to fracture behavior yields linear elastic fracture toughness values from thinner plastically loaded specimens.

The J-Integral analysis of the A106B parent material indicated a $K_{IC}(J)$ fracture toughness value of 195.1 $MPa\sqrt{m}$ (177.5 ksi $\sqrt{in.}$). For the AISI 304L parent material no K_{IC} (J) value could be obtained, as such large amounts of plastic deformation occurred that only a reduction in specimen thickness resulted. No crack growth whatsoever occurred as anticipated for the small specimens of AISI 304L material. It was hoped that "embrittlement" due to the welding processes would result in typical fracture toughness specimen behavior; however, this did not happen.

The testing done in this program was of necessity very limited, and conclusions as to the degree of degradation and the effects of welding may be shown to be incorrect by additional, statistically significant, investigations. General observations can be made, however, to classify the subject materials and establish the merits of laser beam welding:

1. Properties of both AISI 304L stainless steel and A106B carbon steel are extremely affected by hydrogen environment.

2. The LBW process is at least comparable to conventional weld processes in terms of LCF life, where the effects of welding were most prominent.

3. Laser beam welding of pipe to ASME boiler and pressure vessel code specifications is possible. However, due to excessive variation in pipe wall thickness, which is considered typical for this application, additional weld process development is required. Over and under penetration was directly attributable to pipe wall thickness variation and the resultant porosity.

We conclude, therefore, that LBW is feasible for fabricating systems for transmission and storage of high-pressure gaseous hydrogen. It has the potential to improve weldment integrity and performance, and subsequently, the safety of those systems.

Materials and Welding

Test Materials

The test materials, AISI 304L stainless steel and ASTM A106B carbon steel, were evaluated in the form of No. 5 Schedule 160 seamless pipe [141.3-mm (5.562-in.) outside diameter, 15.9-mm (0.625-in.) wall thickness].

Chemical analysis and tensile evaluation of the test materials established them as meeting basic contract requirements.

Weld Procedures

Weld joints were produced in the pipe materials by the gas tungsten arc welding (GTAW), electron beam welding (EBW), and laser beam welding (LBW) processes by joining two 50.8-mm (2.0-in.) lengths of pipe as illustrated in Figure 3.

Weld schedules were established for each material prior to joining of the pipe segments. Weldments were produced using current process specifications or, in the absence of specifications, state-of-the-art procedures. No post-weld heat treatment was performed.

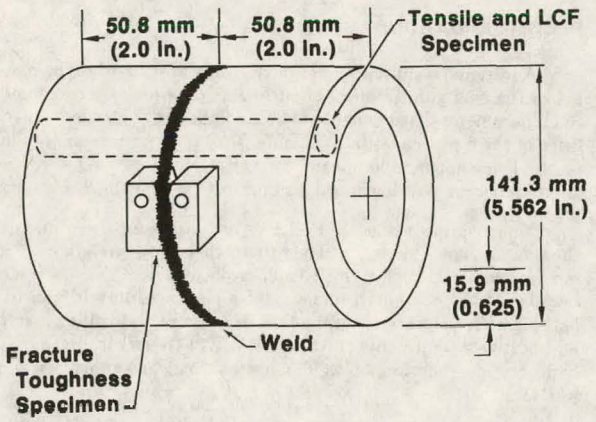

Figure 3. Pipe Weldment Showing Specimen Orientation

Weld Characterization

Gas Tungsten Arc Welds

Weld metal in the AISI 304L material welded by the GTAW process consisted entirely of γ (austenite) grains and metal carbides. Varying grain sizes were observed corresponding to the multipass nature of the weld. For the A106B material, the weld metal consisted of a layered structure caused by the multipass nature of the weld. Subsequent weld passes transformed initially deposited material back to austenite and refined the grain size. The lower weld passes contained fully tempered martensite, whereas the upper passes contained untempered martensite. The last weld pass consisted of coarse grains of untempered martensite. Typical AISI 304L and A106B GTAW joints are presented in Figure 4.

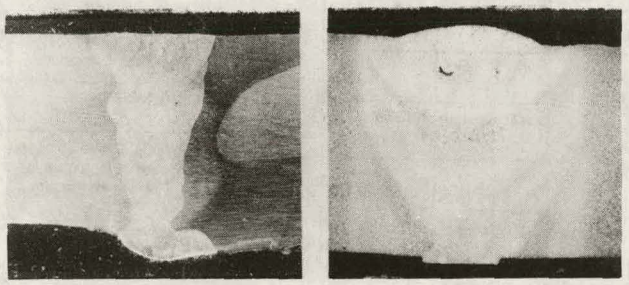

Figure 4. Typical AISI 304L (Left) and A106B (Right) Gas Tungsten Arc Welded Joints

Electron Beam Welds

Weld metal in the AISI 304L material welded by the EBW process also consisted entirely of austenite grains and metal carbides. An austenite dendritic structure was more pronounced near the face of the weld. For the A106B EBW material, weld metal consisted of ferrite at prior austenite grain boundaries and within grains in a plate-like morphology, all in a matrix of pearlite. Metal carbide dispersions were also observed. Typical AISI 304L and A106B EBW joints are presented in Figure 5.

Laser Beam Welds

Nonuniform penetration was generally evident in the sample welds, especially in A106B material, and incomplete penetration was evident in some cases. The weld nonuniformity was attributed to the variation in the pipe wall thickness. Not only did the thickness variation lead to variation in penetration requirements, but it also resulted in an out-of-roundness condition which caused change in beam focus at the surface as the pipe was rotated. Since penetration is strongly dependent on beam focus, the change in weld surface location was felt to be a principal cause for penetration variation. Selected welding parameters represented a compromise between higher power, which resulted in local drop-through, formation of bottom bead globules and top bead underfill in these regions and lower power which provided inadequate penetration in thicker sections.

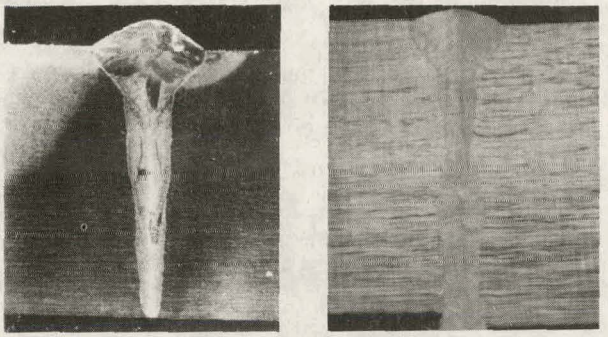

Figure 5. Typical AISI 304L (Left) and A106B (Right) Electron Beam Welded Joints

Visual examination of welds indicated smooth positive reinforcements of both face and root beads in sections in which wall thickness was within parameter limits. A macrograph cross section through a typical stainless steel weld shown in Figure 6, illustrates the narrowsided, deep penetration weld obtained by the high-power laser process. This weld exhibits a relatively small crown approximately 3.8 mm (0.15 in.) wide at the surface which rapidly narrows to a parallel-sided fusion zone approximately 1.6 mm (0.063 in.) wide. Evidence of scattered fine [<0.5-mm (0.020-in.) dia] and medium [<0.8-mm (0.031-in.) dia] porosity can also be observed in the cross section. Existence of scattered porosity in the welds was evident in radiographs taken both normal to the workpiece surface and at a 30-deg angle to the surface normal. In weld regions which were visually acceptable, the porosity levels were, in general, within the acceptable limits of the ASME Boiler and Pressure Vessel Code. However, in regions in which over penetration or under penetration occurred, weld porosity levels and other weld bead characteristics did not meet code requirements. These areas of weld code nonconformance were not used for specimen fabrication.

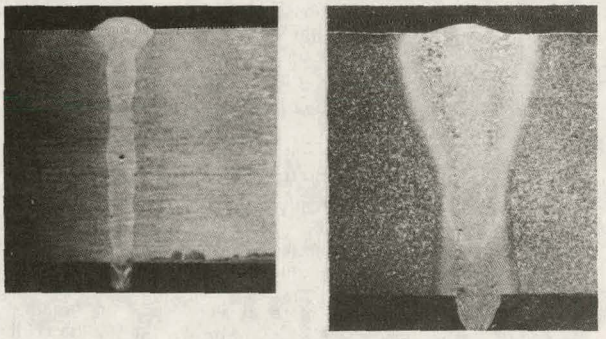

Figure 6. Typical AISI 304L (Left) and A106B (Right) Laser Beam Welded Joints

An A106B carbon steel weld cross section is shown in Figure 6 and illustrates the positive face and root bead reinforcements produced in this material. The weld exhibits a 4.8-mm (0.19-in.) wide crown at the surface and 1.9-mm (0.075-in.) wide crown at the bottom

of the weld. The depth of the final pass, approximately 10.2 mm (0.4 in.), is clearly visible in the macrograph, as is the gradual widening toward the top of the weld and the smooth contour at the weld face. These latter characteristics were the result of the slower weld speed as well as the fact that the final pass was a partial penetration weld. As evident in Figure 6, the pass does not appear to have caused additional weld defects. However, the depth of penetration of the pass may be excessive and could probably be substantially reduced. These results also indicate the potential of this procedure for repair welding.

The weld metal of the LBW AISI 304L material consisted solely of austenite grains and metal carbides. As in the EBW AISI 304L material, the austenite appears more dendritic in nature near the top of the weld.

Nearly all of the weld metal of the LBW A106B material consisted of ferrite (light phase) both at prior austenite grain boundaries and as totally transformed austenite grains. There is a grain refined ring consisting of fine ferrite and pearlite colonies near the top of the weld. This area corresponds to the heat-affected zone of the final pass.

Weld metal porosity was evident in all weldments of both materials. Small, egg-shaped pores were observed on the fracture surfaces of most EBW and GTAW, and to a lesser extent, LBW specimens. Similar voids are commonly found in carbon and stainless weldments and may be associated with a high, preweld oxygen level (Reference 7). Chromatographic analysis indicated that both steels used in this program would be classified as being susceptible to weld pore formation.

DISCUSSION

The mechanical properties evaluation of LBW materials was encouraging and additional development is indicated. We feel that LBW is certainly feasible for pipeline fabrication. Much of the optimism is based on the performance of the LBW material in the LCF tests. We have observed that tests which involve relatively long-term exposure to hydrogen environments at high strain/stress levels, such as LCF or creep-rupture, are the most severe tests of a material for hydrogen degradation. Short-term tensile tests will not always indicate a material's long-term susceptibility to hydrogen degradation. Creep-rupture is not a consideration for a pipeline since the operating temperatures are ambient and nowhere near the creep regime for these materials. Low-cycle fatigue could become an increasing concern for hydrogen pipelines because of their long expected life and the potential consequences of failure. Fortunately, however, most pipelines are designed for operating stresses below the level where LCF is a concern.

Pipeline sizes projected for economical transmission of gaseous hydrogen approach a 1.23m (4-ft) diameter with operating pressures of 13.8 MPa (2000 psig). This would imply wall thicknesses of 178 mm (7 in.) using the materials studied in this program. The use of more expensive, but considerably stronger materials, may become economically attractive due to the reduced amount of material involved and the resultant lighter weight. The lighter weight would also result in less expensive handling and construction costs. It is in the joining of these high-strength alloys that LBW should excel.

Regardless of the material employed, the quality of the weldments must be considerably improved. Aerospace welding standards, significantly more rigid than current pipeline standards, may be required. Experience with high-pressure hydrogen aerospace systems indicates weld defects of the type encountered during this program could lead to pipeline or vessel failure. Ultimately, only actual pipeline testing of representative size materials and pressures will establish final weldment quality and design criteria.

RECOMMENDATIONS

Additional weld parameter development for LBW of the materials in the configuration evaluated in this program is recommended. Such parameter development should include provisions for centerless drive of the pipe to maintain the outer surface at a fixed point relative to the beam focus, and means for variation of welding speed with circumferential position in proportion to pipe wall thickness.

Upon optimization of the LBW technique for these materials, the process should be transitioned to another alloy, preferably a high-strength material such as A-286 and/or one of the HY-series of steels, because of their strength and weight advantage. In addition to the optimization of process parameters, the use of weld filler materials and postweld treatments (LASERGLAZE™) (Reference 8) to prevent hydrogen degradation of weldments are logical extensions of this program.

These and other areas of recommended activity to develop LBW as a viable fabrication method for hydrogen transmission and storage systems are outlined in Figure 7. These activities are outlined in a step-by-step sequence with allowances after each step for decisions regarding the merit of continued development. The end goal is to have a reliable and safe means for fabrication of systems ready, when the widespread use of hydrogen fuel becomes economically possible.

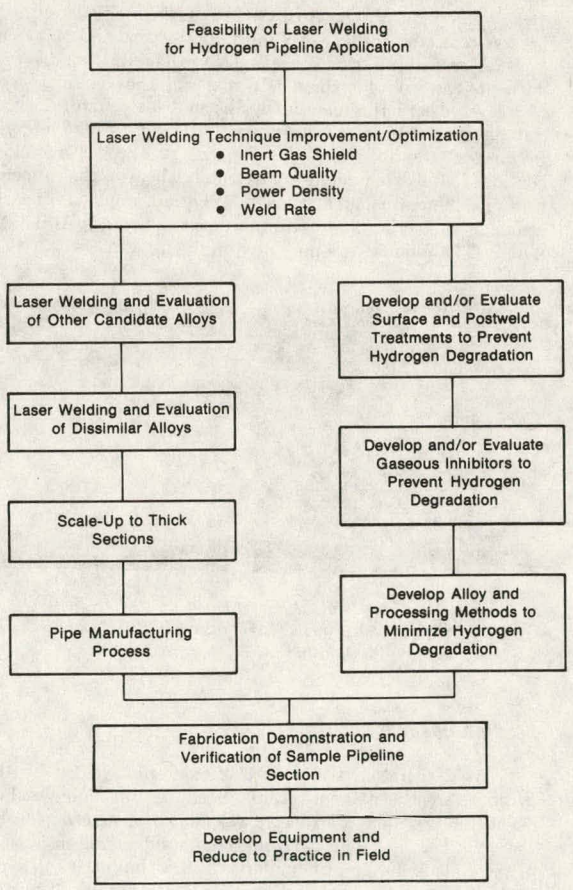

Figure 7. Recommended Areas of Activity to Enhance This Program for Developing Laser Beam Welding as a Viable Fabrication Method for Hydrogen Transmission/Storage Systems

APPENDIX

Table I. Experimental Test Outline to Determine the Effects of Welding and Susceptibility of Welded Pipeline Materials to Hydrogen Degradation

Material	Weld Type	Environment[1]	Mechanical Properties Tests: Smooth Tensile	Notch Tensile[2]	Low-Cycle Fatigue	Fracture Toughness
AISI 304L	Parent Material	Air	2	2	3	2
		Hydrogen	2	2	2	
	GTAW	Air	2	2	1[3]	2
		Hydrogen	2	2	3	
	GTAW (HAZ)	Air		2		2
		Hydrogen		2		
	EBW	Air	2	2	[4]	2
		Hydrogen	2	2	6	
	EBW (HAZ)	Air		2		2
		Hydrogen		2		
	LBW	Air	2	2	[4]	2
		Hydrogen	2	2	3	
	LBW (HAZ)	Air		2		2
		Hydrogen		2		
ASTM A106B	Parent Material	Air	2	2	3	2
		Hydrogen	2	2	4	
	GTAW	Air	2	2	[4]	2
		Hydrogen	2	2	4	
	GTAW (HAZ)	Air		2		2
		Hydrogen		2		
	EBW	Air	2	2	[4]	2
		Hydrogen	2	3	4	
	EBW (HAZ)	Air		2		2
		Hydrogen		2		
	LBW	Air	2	2	[4]	2
		Hydrogen	2	2	4	
	LBW (HAZ)	Air		2		2
		Hydrogen		2		
Total Specimen Tests — 154			32	57	37	28

[1]Air Tests at 24°C (75°F), 1 atmosphere; hydrogen tests at 24°C (75°F), 13.8 MPa (2000 psig)
[2]Stress Concentration Factor, K_T = 8.0
[3]Two tests added per contract modification
[4]Three tests added per contract modification

Table II. Degradation of Tensile Properties of AISI 304L and A106B in 13.8 MPa (2000 psig) Gaseous Hydrogen at 24°C (75°F)

Material	Weld Type	Notch Factor	Degradation* Decrease from Air (%): Strength 0.2% Yield	Strength Ultimate	Ductility El	Ductility RA	Ratio of Ultimate Strength H_s/Air	Ratio of Notch/Smooth Ultimate Strength: Air	Ratio of Notch/Smooth Ultimate Strength: H_s
AISI 304L	Parent Material	Smooth	**		**	2.5	1.05	1.36	1.23
		8.0		5.0			0.95		
	GTAW	Smooth	**	**	**	**	1.09	1.43	1.28
		8.0		2.5			0.97		
	GTAW (HAZ)	8.0		2.3			0.98	1.51	1.36
	EBW	Smooth	**	**	1.7	13.0	1.04	1.44	1.34
		8.0		3.3			0.97		
	EBW (HAZ)	8.0		4.1			0.96	1.44	1.33
	LBW	Smooth	**	**	**	2.1	1.02	1.42	1.30
		8.0		6.6			0.93		
	LBW (HAZ)	8.0		5.0			0.95	1.43	1.33
A106B	Parent Material	Smooth	**	**	12.9	29.2	1.05	1.64	1.35
		8.0		13.3			0.87		
	GTAW	Smooth	**	1.0	17.6	7.5	0.99	2.01	1.81
		8.0		11.0			0.89		
	GTAW (HAZ)	8.0		22.8			0.77	1.68	1.30
	EBW	Smooth	**	1.1	18.8	30.2	0.99	1.63	1.45
		8.0		11.9			0.88		
	EBW (HAZ)	8.0		21.2			0.79	1.62	1.29
	LBW	Smooth	**	**	13.3	22.2	1.01	1.76	1.49
		8.0		15.0			0.85		
	LBW (HAZ)	8.0		20.3			0.80	1.85	1.47

*Degradation calculated using average values of air and hydrogen tests.
**Average value in hydrogen approximately equal to, or greater than, that in air.

Table III. Effect of Welding on the Mean LCF Life of AISI 304L and A106B Steels in 13.8 MPa (2000 psig) Hydrogen

Material	Weld Type	Mean LCF Life	Ratio of Welded/Parent Material Mean LCF Life
AISI 304L	Parent Material	2,074	
	GTAW	842	0.41
	EBW	864	0.42
	LBW	1,588	0.77
A106B	Parent Material	489	
	GTAW	244	0.50
	EBW	358	0.73
	LBW	599	1.22

Table IV. Effect of Welding on the Tensile Properties of AISI 304L an A106B Steels

				Ratio of Weld/Parent Material			
				Strength		Ductility	
Material	Weld Type	Notch Factor	Environment*	0.2% Yield	Ultimate	El	RA
AISI 304L	GTAW	Smooth	Air	1.36	0.99	0.48	0.35
		Smooth	Hydrogen	1.24	1.03	0.84	0.91
		8.0	Air		1.05		
		8.0	Hydrogen		1.07		
	GTAW (HAZ)	8.0	Air		1.10		
		8.0	Hydrogen		1.14		
	EBW	Smooth	Air	1.24	0.98	0.66	0.97
		Smooth	Hydrogen	1.19	0.97	0.60	0.87
		8.0	Air		1.04		
		8.0	Hydrogen		1.06		
	EBW (HAZ)	8.0	Air		1.04		
		8.0	Hydrogen		1.05		
	LBW	Smooth	Air	1.21	0.99	0.69	0.93
		Smooth	Hydrogen	1.12	0.96	0.65	0.94
		8.0	Air		1.04		
		8.0	Hydrogen		1.02		
	LBW (HAZ)	8.0	Air		1.04		
		8.0	Hydrogen		1.04		
A106B	GTAW	Smooth	Air	0.95	1.04	0.75	0.99
		Smooth	Hydrogen	0.91	0.98	0.71	1.22
		8.0	Air		1.28		
		8.0	Hydrogen		1.32		
	GTAW (HAZ)	8.0	Air		1.06		
		8.0	Hydrogen		0.95		
	EBW	Smooth	Air	0.96	1.03	0.86	0.98
		Smooth	Hydrogen	0.92	0.97	0.80	0.97
		8.0	Air		1.03		
		8.0	Hydrogen		1.04		
	EBW (HAZ)	8.0	Air		1.02		
		8.0	Hydrogen		0.92		
	LBW	Smooth	Air	1.10	1.05	0.81	0.96
		Smooth	Hydrogen	1.07	1.00	0.80	1.06
		8.0	Air		1.13		
		8.0	Hydrogen		1.11		
	LBW (HAZ)	8.0	Air		1.19		
		8.0	Hydrogen		1.09		

*Air tests at 1 atmosphere, hydrogen tests at 13.8 MPa (2000 psig).

Table V. Effect of Welding on the Strength Ratio (R_{SC}) of AISI 304L and A106B Steels

Material	Weld Type	Ratio of Welded/Parent Material Average R_{SC}
AISI 304L	GTAW	0.88
	GTAW (HAZ)	0.97
	EBW	0.97
	EBW (HAZ)	1.00
	LBW	1.02
	LBW (HAZ)	1.06
A106B	GTAW	1.11
	GTAW (HAZ)	1.08
	EBW	0.96
	EBW (HAZ)	1.00
	LBW	0.90
	LBW (HAZ)	1.20

REFERENCES

1. Gray, H. R. and H. G. Nelson et al., "Potential Structural Materials Problems in a Hydrogen Energy System," NASA TM X-71752 NASA Lewis Research Center, Cleveland, Ohio, June 1975.

2. Harris, J. A., Jr. and M. C. VanWanderham, "Properties of Materials in High-Pressure Hydrogen at Cryogenic, Room, and Elevated Temperatures," FR-5768, Contract NAS8-26191, Marshall Space Flight Center, Alabama, July 1973.

3. Mucci, Joseph, "Influence of Gaseous Hydrogen on the Mechanical Properties of AISI 304 Stainless Steel," Final Report, Contract NAS8-29883.

4. Harris, J. A., Jr. and M. C. VanWanderham, "Influence of Gaseous Hydrogen on the Mechanical Properties of Incoloy 903," FR-7175, Contract NAS8-30744, Marshall Space Flight Center, Alabama, September 1975.

5. Begley, J. A. and J. D. Landes, "The J-Integral as a Fracture Criterion," ASTM STP 514, 1972.

6. Bucci, R. J. and P. C. Parris, et al., "J-Integral Estimation Procedures," ASTM STP 514, 1972.

7. Nagao, T., S. Kosuge and S. Kobayashi. A Study of Electron Beam Welding — Porosity in Electron Beam Welds of Carbon Steels, Advanced Welding Technology, 1975, pp. 75-80.

8. Breinan, E. M. and C. M. Banas, et al., "Physics Today," November 1976.

INFLUENCES OF STRESS STATE ON HYDROGEN EMBRITTLEMENT

M. R. Louthan, Jr., R. P. McNitt, T. A. Adler, J. Murali and P. E. Smith
Virginia Polytechnic Institute and State University
Blacksburg, VA 24061

Abstract

Experimental hydrogen embrittlement studies of A-106 and 4340 steels have shown that hydrogen increases the ease of crack propagation in both alloys. Delayed failure tests with 4340 steel samples have demonstrated that the onset of hydrogen embrittlement is quite sensitive to macroscopic stress state and specimen thickness. The thickness effect is rationalized in terms of the need for a critical stress existing to a microstructurally significant depth in the loaded sample. No delayed failure was observed in A-106 steel samples; however, crack initiation and growth studies have shown that the crack path is primarily macroscopically perpendicular to the maximum normal stress, primarily transgranular although not planar within each ferrite grain. No strong dependence on triaxial stresses is required and crack initiation sites are typically surface flaws or internal defects such as inclusions and stringers. Plastic deformation is an apparent precursor to hydrogen induced crack growth in these steels. These observations imply that the susceptibility of steels to hydrogen embrittlement can be minimized by proper design criteria.

Introduction

Qualification of materials for hydrogen service is a difficult, time consuming task. Short time tensile tests in gaseous hydrogen may show large scale surface cracking and severe losses of ductility in metals and alloys which are apparently unaffected by exposure to similar hydrogen environments under sustained static loading. Cyclic testing may indicate hydrogen induced losses in fatigue life and monotonically increasing the load on compact tension samples may show hydrogen enhances crack growth in materials which have been successfully used in hydrogen service for several decades. Because of the apparent difference between laboratory testing and in-service experience, industrial and laboratory workers may disagree as to meaning of "a qualified material." The researcher, in recommending a material for a new hydrogen application may suggest a high priced material of limited availability instead of a low cost common steel, even though the steel has shown years of successful use in an application similar to the new process. The researcher may be concerned about the higher hydrogen pressure and possible cyclic loads in the new application and therefore feels that the old material is unqualified. Similarily, the industrial worker is concerned with the lack of experience with the new "unqualified" material. Clearly, any safe, efficient hydrogen storage and/or transfer system must be constructed from "qualified" materials; however, a standard for material qualification has not yet been established. Furthermore, establishment of such a standard is unlikely until test programs include a wide variety of tests and until the results of such tests can be correlated, almost directly, with in service experience. Such correlations are often difficult because of the lack of data which demonstrate the effect of stress state on hydrogen embrittlement processes. Stress state data is necessary because laboratory testing is often done with samples experiencing uniaxially applied loads while in-service components generally experience very complex stress states. Because of the lack of stress state data, Virginia Tech is conducting an experimental test program to assess the influence of stress state on hydrogen embrittlement processes. This report describes results of that test program.

Materials and Procedures

The steels tested in this investigation were ASTM type A-106 grade B steel pipe, AISI-1015 and AISI-4340 steel plate. The composition ranges for these steels are shown in Table 1. Previous reports to this conference, [1,2,3] describe test results from the VPI studies of tubular, disk rupture, and smooth bar tensile samples have concluded that delayed failure hydrogen embrittlement of ferritic-pearlitic steels is unlikely and the major concern is hydrogen effects on crack growth. Because of these past results, recent efforts have concentrated on tests of compact tension and preflawed disk rupture samples. These samples were prepared from ferritic-pearlitic steels. However, because of the portent of delayed failure in any hydrogen system, static load tests were also continued with the 4340 and A-106 steels. No delayed failures of A-106 steel specimens were obtained although several important features of the delayed failure process were found in 4340 specimens loaded in bending so that the surface stresses were either biaxial or uniaxial. All tests were made at room temperature in test equipment described in Reference [4].

Compact Tension Samples

The amount of crack growth which accompanied a given crack opening displacement in a compact tension sample machined from A-106 pipe stock was much greater when tests were conducted in 14 MPa hydrogen than when tests were conducted in air or oxygen environments (Figure 1). Estimates of J_c from these crack opening vs. crack growth data showed that the critical J for crack growth was less in 14 MPa hydrogen than in the other environment (Figure 2). For specimens tested in oxygen the critical J value was sensitive to specimen and hence inclusion orientation. No such orientation dependence on the initiation of crack growth was observed for specimens tested in hydrogen. However, as is apparent from (Figure 1) crack growth in samples tested in both hydrogen and oxygen is sensitive to inclusion orientation and was easiest when the crack was propagating parallel to the long axis of the inclusions.

Measurements of the size of the Luders bands associated with a given crack opening (Figure 3) showed that hydrogen had little or no effect on macroscopic flow characteristics of the metal prior to crack growth. However, hydrogen did effect crack growth. The path of hydrogen affected fractures was

primarily transgranular, not planar within each ferrite grain and macroscopically perpendicular to the maximum normal stress, even in the area of plane stress. Significant local plastic deformation accompanied crack growth although no large scale crack blunting or stretch zone formation preceeded the initiation of crack growth. These observations show that the often proposed dependence of hydrogen embrittlement on triaxial stresses is not apparent in these tests. In fact, these observations are not consistant with any single theory for hydrogen embrittlement. However, the large observed effects of hydrogen on crack growth processes in A-106 steel demonstrate that similar ferritic-pearlitic steels should not be used for hydrogen service unless design criteria are developed which insure that the structure will experience little or no plastic deformation during its service lifetime.

Disk Rupture Tests

The disk rupture tests of AISI 1015 steel samples support the results from the compact tension samples. Tests with preflawed samples showed that gaseous hydrogen significantly increased flaw growth and lowered the rupture pressure of the 0.4 mm thick samples. In spite of the microscopically localized adverse effects in the near flaw tip region, pressure deflection and curvature-pressure measurements (Figure 4) showed that the macroscopic deformation characteristics, under biaxial loadings, were not affected by hydrogen.

The hydrogen enhanced flaw growth caused the samples tested in hydrogen to leak by the development of a through thickness elliptical shaped crack (Figure 5) while the typical sample tested by oxygen pressurization failed by rupture. Scanning electron microscopy showed that the flaws began to grow in the latter stages of the deformation and that the hydrogen enhanced growth was by faceted fracture processes. Microvoid coalesence was the typical failure mechanism in the oxygen tested samples. Clearly, hydrogen enhanced flaw growth is an undesirable effect; however, because of the tendency for stable crack growth it is possible that a leak-before-break criteria for hydrogen storage system could be achieved by choosing ferrite-pearlitic steels as materials of construction. Significant prior plastic deformation has been necessary for each hydrogen induced failure produced in this series of tests. Furthermore, the earlier tests, described in previous reports to this conference, have shown that internally pressurized cylinders stressed to 95% of their rupture pressure will not fail during 5000 hours exposure even when the stress state in the cylinder wall is cycled from cylindrical to spherical by the application of an external load. These severely stressed tubular samples were subsequently overpressurized to failure after the long term exposures and no losses in rupture pressure were observed. Perhaps the most significant conclusion that can be reached from these studies is that smooth surfaces do not indicate the adverse hydrogen effects always found in flawed samples. Because engineering structures will almost certainly have some flaws (sharp corners, weld defects, etc.) extrapolation of test results from smooth samples is not conservative and can lead to the assumption that materials degradation is unlikely when, in fact, severe degradation will occur because of microscopic, plastic deformation in a near flaw region. Delayed failure tests with AISI 4340 samples elucidate this "flawed region concept" and indicate that for a flaw to be of concern it must be of a microstructurally significant size.

Delayed Failure Tests

Delayed failure tests of four point loaded strip samples of oil quenched, martensitic steel samples showed that the minimum surface stress required to cause failure decreased from approximately 1170 MPa the thinnest samples tested (0.13 cm) to about 830 MPa for samples about 0.25 cm thick (Figure 6). Considerable data scatter was observed in the delayed failure tests; however, the results of over 50 tests summarized in Figure 6 clearly indicate an definite trend. Fractographic studies of the failed "uniaxial" samples showed that failure initiated in the near surface region by intergranular cracking. The size of the hydrogen affected area (or volume) apparently increased until some critical crack was obtained and the remainder of the sample failed by unstable crack propagation. This rapid crack growth occurred by microvoid coalesence and was accompanied by extensive plastic deformation which caused surface roughening (or minute cracking) and an associated shear lip. The region of intergranular fracture was located in the region of maximum stress in all failed samples. The center and edges of the samples both served as crack initiation regions with about 40$ of cracks starting at the edges.

Failure of the clamped and unclamped plate samples (biaxial surface loadings) differed from failure of the four point loaded samples in several respects. No thickness effect was observed in the "biaxial" samples for the range of thicknesses examined. Samples stressed to principal stresses in excess of 830 MPa generally failed during the 120 hour exposure while samples stressed below that level were not apparently affected. Intergranular cracking was observed throughout the fracture surface as were limited regions of microvoid coalesence. Typical crack pattern for the "biaxial" samples (Figure 7) was for multiple cracks with at least two cracks meeting a right angle. No macroscopically multiple cracking was observed in the "uniaxial" samples. Rationalization and understanding of the differences in hydrogen induced delayed failure in the two classes of samples shows that macroscopic stress state plays a major role in the embrittlement process. A detailed interpretation of the thickness effect is incomplete; however, the thickness effect can be rationalized through a critical stress - critical zone model similar to that developed to explain the temperature dependence of K_{IC}[5]. This model predicts that a failure will occur when a critical failure stress, σ^*, exists over a microstructurally significant depth a into the sample. This characteristic microstructural parameter is postulated to be greater than a grain diameter and has been estimated at 50 grain diameters [6].

The stress through the cross section of an elastically loaded four point bend sample increases linearly with distance from the neutral axis. Thus the ratio of the surface stress, σ_m, to the stress at any depth, σ, must equal the ratio of the specimen half thickness, t, to t - a where a is the depth of which σ is measured. If σ is equated to some critical stress below which hydrogen embrittlement might not occur, σ^* the following is obtained:

$$\frac{\sigma_m}{\sigma^*} = \frac{t}{t-a} \quad (1)$$

In this equation σ_m is the minimum surface stress required to provide a zone of depth a which has stresses above the critical stress for hydrogen embrittlement. If a is related to microstructural features and is a constant for a given material and loading then σ_m is clearly a function of specimen thickness. Empirical fitting of the data in Figure 6 to Equation 1 gives values of several hundred grain diameters. Although such values are larger than the 50 grain diameters estimated for overload fracture obtained by considering the probability of favorable orientation for slip, they may be reasonable if one considers that in this case the probability is not for slip but for grain boundary fracture because of hydrogen accumulation. If this rationalization is correct, the critical zone must decrease when biaxial stresses are applied. Such a decrease is to be expected because the probability of favorable grain orientations should increase as the stress state goes from uniaxial to biaxial. Based on this critical size rationale other biaxial samples should show a thickness effect if the same thickness is reduced sufficiently. Such an investigation is under current study.

Closure

That specimen configuration, stress state and static vs. dynamic loading are important in the material qualification process for use in hydrogen service can be seen in the following observations regarding particular tests.

Compact tension - A-106 steel - when pulled in H_2 as compared to O_2 it was observed that

a) crack growth initiated at lower loads
b) crack growth rate was higher
c) for a given load Luders Band zone was unaffected
d) no crack front stretch zone seen in "H_2 samples"
e) H assisted fracture was transgranular as contrasted to microvoid coalesence in O_2.

Disk rupture - AISI 1015 steel - pressurized by either H_2 or O_2

a) H_2 pressurization in preflawed samples lead to elliptical front crack growth in sample
b) crack growth in H_2 was by faceted fracture
c) crack growth caused leak before burst in H_2
d) O_2 pressurization led to specimen bursting with accompanying microvoid coalesence.

Delayed failure - 4340 steel uniaxially and biaxially statically stressed in a H_2 environment

a) uniaxial loading failures started from a site of intergranular cracking then failed by unstable crack propagation
b) thickness effect noted wherein the thicker samples required a lower max surface stress.
c) biaxial tests showed no thickness effects.

In view of the numerous effects observed that depend on the particular loading it seems clear that proper certification of a material for hydrogen service include testing of that material in its probable operation mode.

Reference

1. M. R. Louthan, Jr. and R. P. McNitt p. 161-166 CONF-761134 Brookhaven National Laboratory (1977).
2. M. R. Louthan, Jr. and R. P. McNitt p. 158-163 JPL Publication 78-1, Jet Propulsion Laboratory (1978).
3. M. R. Louthan, Jr., R. P. McNitt, T. S. Sudarshan, J. Murali and T. A. Adler, p. 351-366 CONF-781142, Brookhaven National Laboratory (1979).
4. M. R. Louthan, Jr., R. P. McNitt and N. Sridhar, p. 745-756 Environmental Degradation of Engineering Materials, Virginia Polytechnic Institute, Blacksburg, VA (1977).
5. J. R. Rice, Journal of the Mechanics and Physics of Solids, Vol. 21, p. 395 (1973).
6. B. L. Auerbach, Fracture, Vol. 1, Chapter 7, Edited by H. Liebowitz Academic Press, New York (1969).

Table I. Compositions of steels tested in this investigation, wt. %.

	C	M_n	P Max	S Max	Si	Ni	Cr	Mo	Fe
ASTM A-106 grade B	0.25 max	0.27-0.93			0.10 min				balance
AISI 1015	0.13-0.18		0.040	0.050					balance
AISI 4340	0.38-0.43	0.60-0.80	0.040	0.040	0.20-0.35	1.65-2.00	0.70-0.90	0.20-0.30	balance

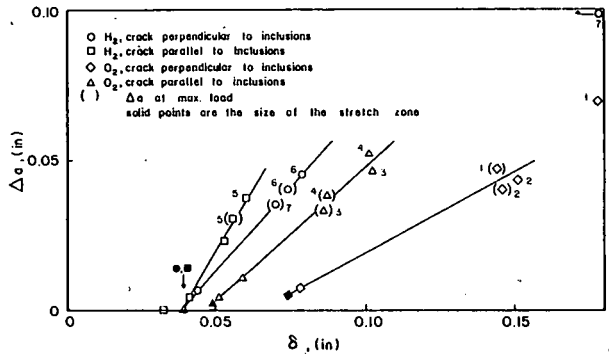

Figure 1

Crack growth, Δa, as a function of crack opening displacement, δ, for compact tension samples of ASTM A-106 steel. The samples were loaded in 14 MPa (2000 psi) H_2 or O_2. Crack growth at maximum load was estimated by drawing straight lines through the data.

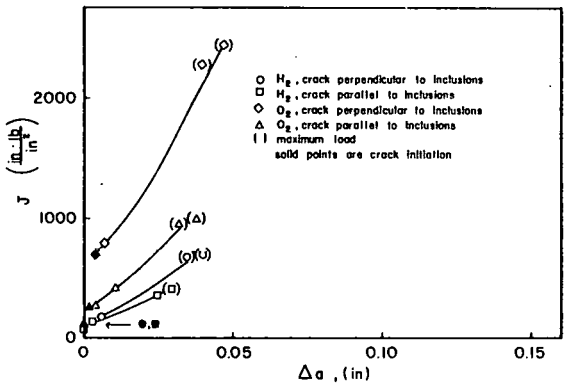

Figure 2

J integral as a function of crack growth, Δa, for compact tension samples of ASTM A-106 steel. The samples were loaded in 14 MPa (2000 psi) H_2 or O_2.

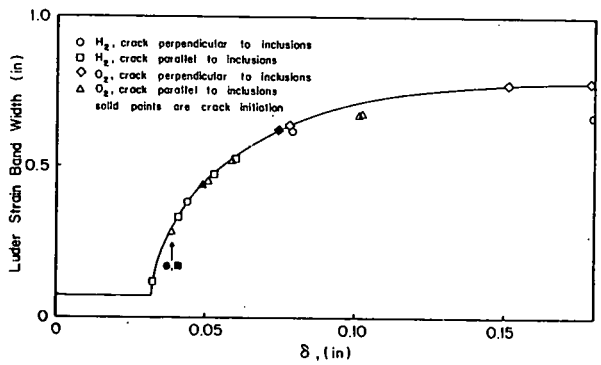

Figure 3

Under strain band width as a function of crack opening displacement, δ, for compact tension samples of ASTM A-106 steel. The samples were loaded in 14 MPa (2000 psi) H_2 or O_2.

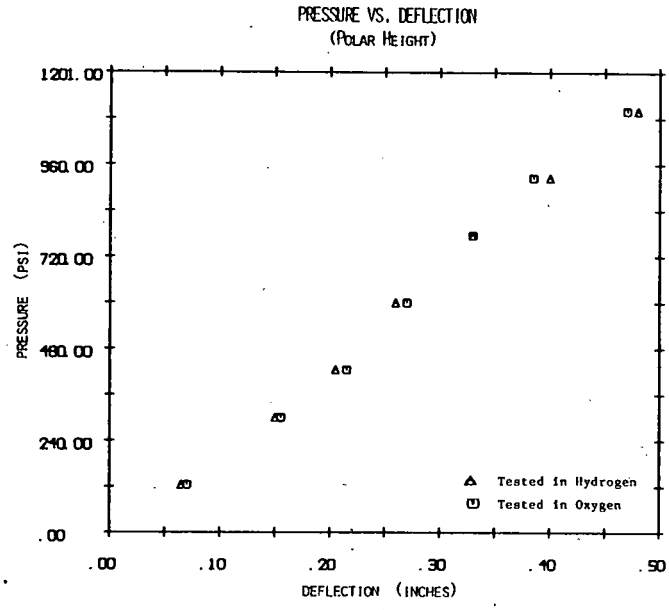

Figure 4a

Pressure-deflection curves for flawed samples of AISI 1015 steel tested in hydrogen and oxygen.

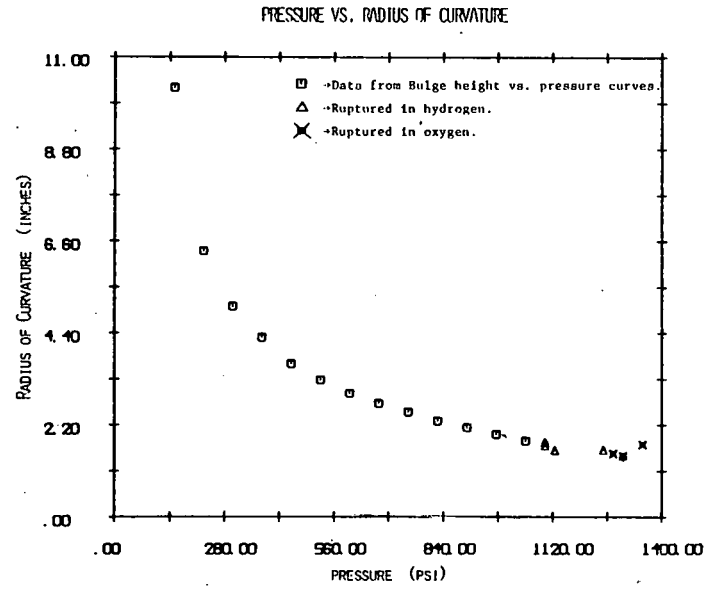

Figure 4b

Curvature pressure measurements for flawed samples of AISI 1015 steel tested in hydrogen and oxygen.

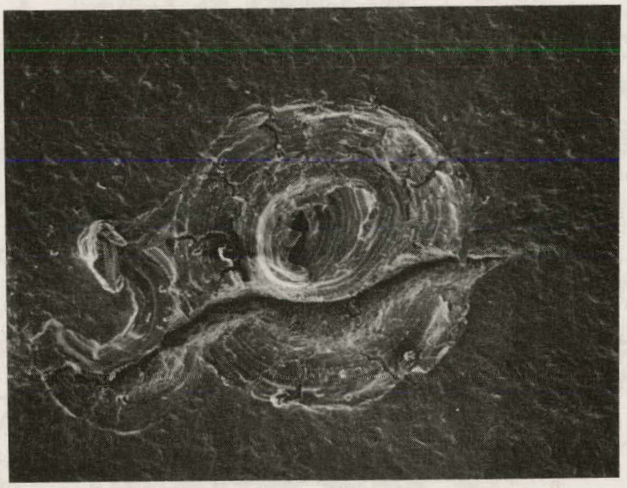

Figure 5

Scanning electron fractograph of flawed sample tested in hydrogen which failed by the development of through thickness crack. (50x)

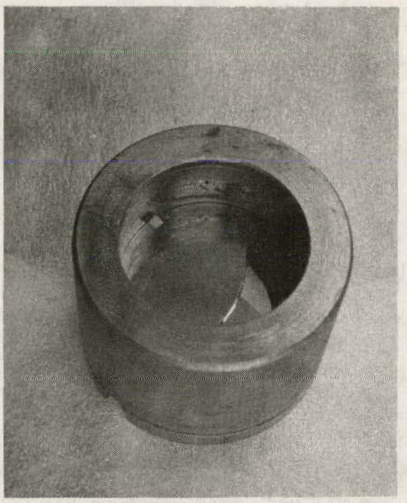

Figure 7

Fractured biaxial sample showing typical crack pattern for clamped samples.

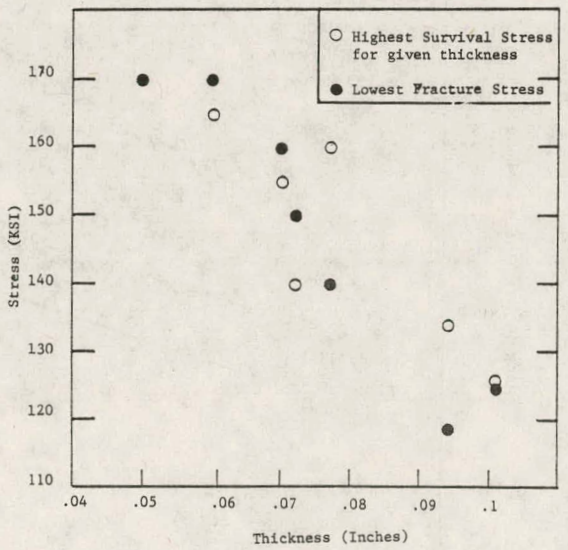

Figure 6

Minimum failure stress and maximum survival stress versus thickness.

NEAR-THRESHOLD FATIGUE CRACK PROPAGATION IN PIPELINE STEELS IN HIGH PRESSURE ENVIRONMENTS

By
M. R. Mitchell[1] N. E. Paton[2] R. O. Ritchie[3] and N. Q Nguyen[4]

ABSTRACT

The use of hydrogen for energy storage and transport holds particular promise as a significant option for energy transportation in the not too far distant future. To meet this need, large-scale gas pipeline systems will be required to transport hydrogen and combinations of hydrogen and other gases, such as natural gas, under high pressure conditions.

Since such pipeline systems must contain in-line compressors, possible sub-critical crack growth of incipient flaws under cyclic loading conditions offers a potential problem. Existing information on fatigue crack growth in pipeline steels under representative environmental conditions is scarce and limited to intermediate and high growth rate ($\sim 10^{-5}$ mm/cycle) data. It is the purpose of this research to generate fatigue crack propagation data in a typical pipeline steel under anticipated high pressure environments over a wide range of growth rates including low crack growth rates (10^{-5} mm/cycle) which approach the threshold for fatigue crack growth (ΔK_{th}).

INTRODUCTION

Growing concern over dwindling supplies of natural gas as one of this country's major energy sources has prompted consideration of hydrogen as an alternative both for energy storage and as a transport medium. To meet the requirement of hydrogen transport and distribution, large-scale pipeline systems will need to be developed to convey hydrogen gas and other gases, such as natural gas, under high pressure conditions 7×10^6 - 1.4×10^7 MPa (1000-2000 psi). Such pipeline systems will require large diameter pipe, and must contain in-line compressors which will impose additional cyclic loading on the structures. Possible degradation in material properties due to this potentially agressive environment, particularly with imposed fatigue loading, will thus be of special concern to assure long service life.[1]

From a fracture mechanics viewpoint, new and existing pipelines may be assumed to contain microdiscontinuities that are potential initiation sites for the sub-critical growth of cracks. Accordingly, any estimate of the life of such a structure will require detailed information on rates of fatigue crack propagation in candidate steels over a wide range of growth rates under appropriate environmental conditions. Such data, however, are extremely scarce in the literature. One study, due to Nelson,[1] has shown that, at intermediate and high growth rates ($\sim 10^{-5}$ mm/cycle), atmospheric pressure hydrogen leads to a significant increase in crack propagation rates (~1 order of magnitude) above those in air for an AISI 1020 low strength steel. However, there is a total lack of data at low stress intensities where growth rates approach the threshold for fatigue crack growth, ΔK_{th} (i.e., between 10^{-5} and 10^{-8} mm/cycle). This is unfortunate, in view of the defect sizes and stresses likely to be present in a pipeline, since the majority of the lifetime of the structure will be spent in this region. Extrapolation of Nelson's results for 1020 steel (Fig. 1) gives the impression that growth rates for different environments (i.e., H_2, air and vacuum) could converge at near-threshold levels, yet several studies on higher strength steels[2] have suggested that in this regime the maximum effort of hydrogen-assisted cracking occurs. It is thus apparent that an extensive characterization of the influence of gaseous hydrogen on near-threshold fatigue crack propagation in low strength steels is required, both to generate reliable engineering data for applications such as hydrogen pipeline structures, and to provide a mechanistic basis for the effects observed. This is considered to be of paramount importance if the transport of hydrogen or hydrogen-natural gas mixtures through existing pipelines is to be made feasible.

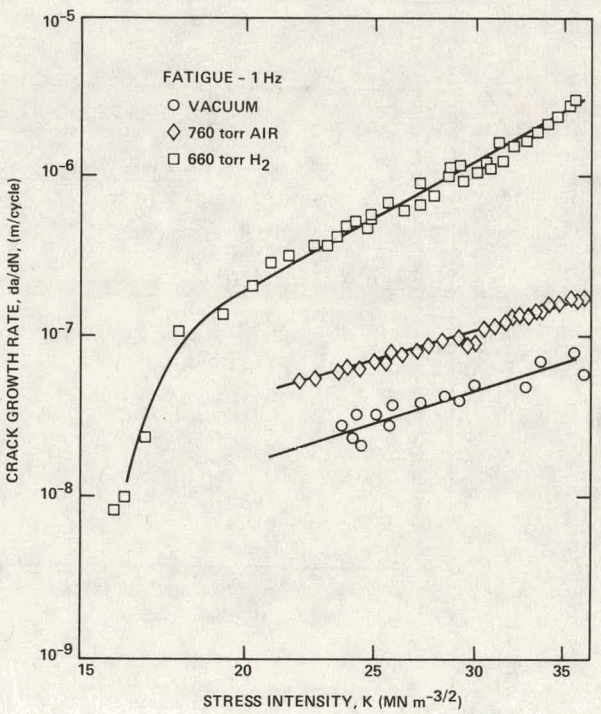

Fig. 1 Cyclic crack growth of SAE 1020 steel in vacuum, air and hydrogen environment.

To investigate the environmental influence of hydrogen-containing environments on near-threshold growth in candidate pipeline steels, fatigue crack

(1) Manager, Physical Metallurgy
(2) Director, Material Synthesis and Processing Rockwell International Science Center
(3) Prof., Mass. Inst. Tech.
(4) Senior Staff Associate, Physical Metallurgy

propagation data will be gathered in the range of alternating stress intensity (ΔK) between 4.55 - 22.75 MPa $m^{1/2}$ (5 and 25 ksi $\sqrt{in}$) for the following environments: (a) vacuum (~10^{-6} torr) as a baseline reference, (b) dry air at one atmosphere for comparison to existing data on pipeline steels,[1,3] (c) gaseous hydrogen at one atmosphere, (d) hydrogen at $7x10^6$ Pa (1000 psi) approximating actual pipeline pressures, (e) methane at $7x10^6$ Pa (1000 psi) and (f) gaseous methane and hydrogen mixtures at $7x10^6$ Pa (1000 psi).

Thus, it is the objective of this research to fully characterize fatigue crack propagation behavior at near-threshold levels for a pipeline steel in vacuum and air in addition to pressurized hydrogen, natural gas and hydrogen/natural gas mixtures. With this understanding, predictions of limiting defect sizes, inspection intervals, remaining lifetime, as well as cost efficient new designs may be ascertained.

APPROACH

An HSLA pipeline steel, API 5Lx60, has been selected for the investigation. A similar X-65 material has been well-characterized previously in terms of fatigue behavior at intermediate and high growth rates,[3] but as yet, no near-threshold behavior has been documented. Uniaxial tensile properties and metallographic examination will be performed for the long transverse (TL) direction in the material. Fatigue crack propagation studies will be conducted using 1/2-T compact test pieces (CT), also of the TL orientation. Growth rates will be determined at three load ratios or R = 0.1, 0.5 and 0.8, at ΔK levels between 4.55-22.75 MPa $m^{1/2}$ (~5 and 25 ksi $\sqrt{in}$) in the environments detailed above. A test matrix is shown in Table 1.

Near threshold crack growth rate testing will be performed under load control on servo-hydraulic test equipment, where the crack length is continuously monitored using an electrical potential system described by Ritchie.[4] This system is capable of measuring absolute crack length to within 0.1 mm and to detect changes of the order of 0.01 mm. Growth rates will be computed by numerical differentiation of crack length vs number of cycles data, curve-fitted using finite difference and incremental-step polynominal procedures.[4,5] The threshold, ΔK_{th}, will be calculated in terms of the stress intensity at which no measureable growth occurs within 10^7 cycles. Since the crack monitoring technique is at least accurate to 0.1 mm, this corresponds to a maximum growth rate of 10^{-8} mm/cycle ($4x10^{-10}$ in/cycle). Thresholds will be approached using a procedure of successive load shedding (of no greater than approximately 10-15 percent reduction in K_{max} at every step) followed by crack growth to minimize residual stress effects. Measurements will be taken, at each load level, over increments of crack growth of 1-1.5 mm, representing a distance of no less than four times the maximum plastic zone size at the previous load. Following threshold ΔK_{th} measurements, the load will be increased in steps and the same procedure followed for higher growth rate data.

The crack propagation testing at low pressures (i.e., vacuum and atmospheric) will be accomplished at Rockwell International's Science Center. Values of ΔK_{th} plus complete metallographic examination and interpretation of fracture surfaces will be supplied. Simultaneously, the high pressure tests on similar fracture mechanics samples of the pipeline steel will be accomplished at Rockwell's Rocketdyne Division. This vessel has the capability of pressurization of hydrogen and combined hydrogen and other gases to $4.2x10^7$ Pa (6,000 psi) with temperature capabilities of -185 to +760°C (-300 to +1,400°F).

TABLE 1

Load Ratio ($R = K_{min}/K_{max}$)	Environment	Pressure (Pa)	Samples Required
0.1	Vacuum	10^4 (10^{-6} torr)	6
	Air	10^5 (1 atm)	
	H_2	10^5 (1 atm)	
	H_2	$7x10^6$ (1000 psi)	
	CH_4	$7x10^6$ (1000 psi)	
	CH_4+10% H_2	$7x10^6$ (1000 psi)	
0.5	as above		6
0.8	as above		6

Progress to Date

During the first two months of this project, a 1m x 1m x 2cm (3 ft x 3 ft x 0.75) inch thick plate of API 5LX60 high strength low alloy steel (HSLA) was procured. The composition of the plate is given in Table 2 and is within the limit of the API specification. A portion of the plate was forwarded to NASA. Fatigue crack growth specimens of the design shown in Fig. 2 have been machined (approximately 60 total) as have tensile and low cycle fatigue specimens of the design shown in Fig. 3. Metallography of the samples revealed a fine, equiaxed grain structure (approximately 10 μm in diameter) with "banded" ferrite. Note that the crack growth specimens are machined in order that propagation during testing will progress along the direction of the banded ferrite structure (i.e., TL direction).

Installation of D.C. potential drop equipment necessary for monitoring crack growth characteristics in this HSLA steel was accomplished. Because this is a newly designed system, several modifications were found necessary,

TABLE 2
COMPOSITION OF PLATE, WEIGHT PERCENT

C = 0.147	Va = 0.006
Mn = 1.40	Cu = 0.049
P = 0.008	Nb = 0.047
S = 0.012	Al = 0.029
Si = 0.255	Co = 0.014
Cr = 0.008	Mg = 0.003
Mo = 0.24	Ca = 0.010
	Fe = Bal

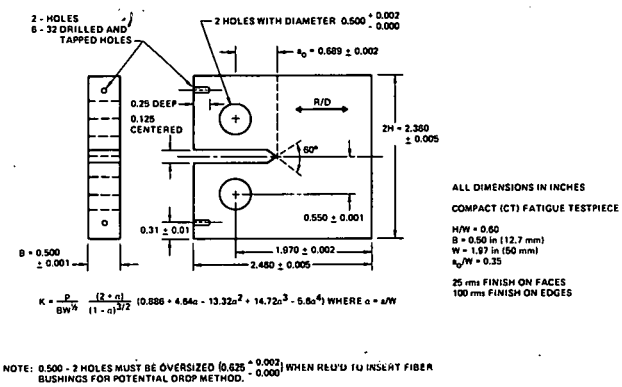

Fig. 2 Compact (CT) fatigue test specimen design.

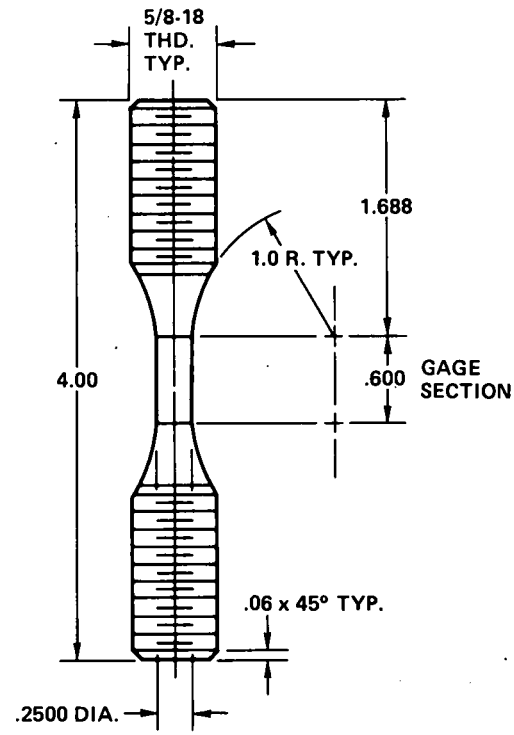

Fig.3 Monotonic and cyclic test specimen design.

including the installation of digital filtering via a PDP 11/04 computer and isolation grounding of the power supply and closed loop test system to eliminate "background noise." It was also deemed desirable to implement amplification of the voltage signal in three stages with individual gains of ten. Thus, a total amplification of differential voltage changes (at constant current) of 1000. A subsequent further amplification to 5000 was accomplished to achieve the accuracy we desire in computer control.

An initial "trial test" was performed on one of the fatigue crack growth specimens. Monitoring of crack growth rates was accomplished, using both a bench microscope with Filar eyepiece and via the D.C. potential drop equipment while subjecting the sample to constant stress intensity levels. The crack path in this sample was exceptionally straight and flat. Discrepancies in the growth rates measured microscopically and with the D.C.P.D. equipment revealed that a 3rd order holynomial fit of Δv vs. Δa curve originally intended for use would not be adequate at a/w values >0.70[6]. If a/w values <0.70 are of interest either curve would suffice.

A second specimen was subsequently mounted in a milling machine and the D.C.P.D. equipment attached. After a 24-hour equilibration period, machine cuts were made in the sample in 0.254 mm (0.010 inch) increments, while the voltage change from an initial potential of 2 mV was recorded at constant current of approximately 32 amps. A comparison of these results and the third order polynominal fit curve is shown in Fig. 4. Note that the curves are essentially linear and do not deviate significantly to a/w values of approximately 0.70. However, at values greater than 0.70, the third order polynomial fit curve approaches a finite voltage even when complete separation of the sample (i.e., a/w = 1) is imminent. This is a physical impossibility, since the differential voltage should approach infinity, as is shown by the newly generated curve. Because the Δv vs. Δa curve for the machined specimen closely matches the third order polynomial fit curve for a/w values up to 0.70 the new curve will be employed in subsequent tests as a standard. Further, we have developed a physical model using parallel and series resistors that accurately describes the crack growth behavior of the X-60 pipeline steel for a/w valves from 0 to 1.0.

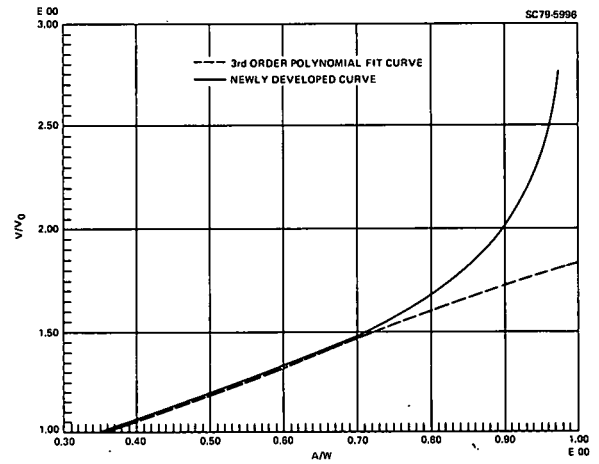

Fig. 4 Comparison of proposed master curve and newly generated curve.

Finally, a computer program has been developed which accurately controls (real time) the load range, ΔP, and thus a small increment in the range of stress intensity, ΔK, for a given crack growth increment, Δa (which depends on the reverse plastic zone size at that stress intensity level). Once the increment in crack growth is achieved, ΔP, is further decreased for a subsequent crack growth increment. Threshold levels of stress intensity factor are being approached in at least five levels of ΔK (i.e., load shedding technique). Subsequent data at higher stress intensity levels is then obtained by the increasing ΔK method[7] for crack growth rate measurements at approximately 10^{-5} mm/cycle and greater in accordance with the program proposal.

Preparations are presently being made at Rockwell's Rocketdyne Division to conduct the high pressure, 7×10^6 Pa (1000 psi), test part of this program.

REFERENCES

1. H. G. Nelson in "Effect of Hydrogen on Behavior of Materials," eds. A.W. Thompson and I.M. Bernstein, TMS-AIME, 1975.

2. R.O. Ritchie, Metal Science, Vol 11, 1977, p. 368.

3. O. Vosikovsky, J. Eng. Matls. and Tech., Trans. ASME Series H, Vol 97, 1975, p. 298.

4. R.O. Ritchie, "Crack Growth Monitoring - Some Considerations of the Electrical Potential Method," Dept. of Metallurgy and Materials Science Internal Report, Jan. 1972, University of Cambridge.

5. R.O. Ritchie, J. Eng. Matls. and Tech., Trans. ASME Series H. Vol. 99, 1977, p.195.

6. G.H. Aronson and R.O. Ritchie, "Optimization of the Electrical Potential Technique for Crack Growth Monitoring in Compact Test Pieces Using Finite Element Analyses," Jol. of Testing and Evaluation, JTEVA Vol. 7, No. 4, July 1979, pp 208-215.

7. "Proposed Method of Test for Measurement of Fatigue Crack Growth Rates, ASTM E 647-78T, Tentative Test Method for Constant-Load-Amplitude Fatigue Crack Growth Rates Above 10^{-8} m/cycle," American Society for Testing and Materials, 1978 Annual Book of ASTM Standards, Vol. 10.

HYDROGEN AND FATIGUE PROPERTIES OF STEEL

Herbert H. Johnson

Cornell University
Ithaca, New York 14853

Abstract

A major area of uncertainty in the application of carbon and low alloy steel in hydrogen containing gas environments is cyclic loading and consequent fatigue damage. The present program, just underway, is intended to greatly strengthen the knowledge base for the influence of hydrogen upon fatigue properties, with emphasis upon the factors controlling the initiation of fatigue cracks in hydrogen gas environments.

Technical Background

Walter and Chandler[1] studied cyclic crack growth rate behavior of ASME SA-105 Grade II steel, with a yield strength of 39 ksi, in hydrogen at pressures from 100 psi to 15,000 psi. A considerable increase of fatigue crack growth rates in hydrogen was observed, although the influence of hydrogen pressure over the 1,000 to 15,000 psi range was not large. Fatigue crack growth rates in hydrogen were not affected by pre-loading in air, but were decreased by pre-loading in helium.

Nelson[2] studied the compatibility between a plain carbon steel and various hydrogen-containing environments, including pure hydrogen, at much lower pressures, near 1 atm. No evidence of hydrogen-induced crack growth was observed for static loading; but under cyclic loading a substantial enhancement in crack growth was observed, along with a change in fracture mode from dictile to brittel transgranular separation. Small additions of oxygen to the hydrogen decreased the crack growth rate to the air value, while H_2S additions enhanced crack growth. Other additives such as CH_4, natural gas, CO_2, etc., had little or no effect upon the hydrogen controlled fatigue crack growth rate.

Clark[3] determined the fatigue crack growth rate properties of HY-80 and HY-130 steels in a low pressure and high purity hydrogen gas environment. Both steels exhibited a substantial increase in fatigue crack growth rate when tested in hydrogen, by factors of three to thirty depending on the range of stress intensity employed. Both steels showed similar crack growth behavior when tested in air; however, in a reversal of the usual trend with strength level, hydrogen increased fatigue crack growth rates significantly more for HY-80 than HY-130.

Several investigators (e.g.,[4-6]) have explored the effect of hydrogen upon the mechanical behavior, including fatigue, of the higher strength steels. For applied stress intensities above the static threshold, cyclic loading variables can be correlated reasonably well[6] by a superposition model which uses as base data crack growth rate measured under static loading. This suggests a close connection between the mechanisms for stress corrosion and corrosion fatigue. However, this is not applicable to a description of hydrogen-accelerated fatigue crack growth in lower strength steels, since they rarely exhibit static load cracking.

The influence of oxygen upon hydrogen-accelerated fatigue crack growth has been assessed[4] for high strength steels. Oxygen additions of as little as 0.4% by volume eliminated the accelerating influence of hydrogen except at the highest strength level studied, 215 ksi yeidl strength.

There is scattered but sufficient evidence to show that hydrogen-accelerated fatigue is a serious problem with the medium and low strength steels that are natural candidates for hydrogen storage and transport systems. Smooth section specimens of low and medium strength steels show only minor effects of hydrogen under sustained loading, but the cyclic load response has received little attention. Nor have studies of notched specimens been reported; virtually all fatigue studies of low and medium strength steels in hydrogen have been carried out with pre-cracked specimens. Thus, a complete and balanced understanding of the effect of hydrogen upon fatigue in low and medium strength steels is not available.

Research Program

The fatigue properties of representative low and medium strength steels in hydrogen gas environments will be evaluated. Steels will be selected for study that are compatible with other elements of the program; candidate steels at present are A106-B, A516-70, X-60, X-65, etc. Hydrogen gas environments at pressures up to approximately 1000 psi will be employed.

Primary attention will be directed to initiation of fatigue cracks under varying conditions of microstructure, stress and strain concentration, and hydrogen environment. This should complement the projects under other tasks in the overall program. Fatigue studies will be carried out on both

smooth section and notched specimens. To permit the maximum information to be extracted from each test, notch designs will be employed for which elastic-plastic solutions are available. Tests will be carried out under controlled plastic strain amplitudes, using a plastic strain computer which is compatible with the mechanical testing equipment. This should allow a detailed correlation to be established between fatigue crack initiation characteristics and local stress and strain states.

Past experiments of this nature have suffered from ambiguity of interpretation arising from uncertainty over the roles of impurities, especially oxygen, in the hydrogen gas and of films, usually thought to be oxides, on the steel surface. With pre-cracked specimens, these concerns are less prominent because it is reasonable to suppose that the local strain concentration at the crack tip is sufficient to rupture any protective films present, and allow hydrogen access to the underlying metal. However, sufficient mechanical film rupture is not thought to occur with smooth section and notched specimens.

It is proposed to eliminate this concern by a novel technique developed in this laboratory in which palladium is electroplated or otherwise deposited on the metal surface. Extensive tests have established that a thin palladium layer eliminates the influence of oxide films and allows hydrogen unimpeded access to the underlying base metal. This characteristic is no doubt associated with the well known and often exploited ability of palladium to act as a strong catalyst for the decomposition of the hydrogen molecule. In the present context palladium would function as a highly efficient injection medium, allowing atomic hydrogen rapid entry into the steel. This should permit an assessment of the maximum embrittlement potential of any gas environment containing hydrogen. The information to be obtained could serve as base-line data for possible future programs to evaluate the effect of gas phase impurities and surface treatments on hydrogen-enhanced fatigue.

Experiments will be carried out with uniform hydrogen concentrations, obtained by sufficient hydrogen exposure of this pallodium coated steel prior to cyclic loading; and with hydrogen gradients, obtained by near simultaneous exposure to hydrogen and stress. This procedure should allow definitive experiments to establish the site of crack initiation with different hydrogen distributions and notches of varying sharpness, with contours such that the elastic/plastic stress and strain states are well characterized.

References

1. R. J. Walter and W. T. Chandler, Effect of Hydrogen on Behavior of Materials, TMS-AIME, New York (1976), edited by A. W. Thompson and I. M. Bernstein, p. 273.
2. H. G. Nelson, reference 1, p. 602.
3. W. G. Clark, Jr., Hydrogen in Metals, ASM (1974), edited by I. M. Bernstein and A. W. Thompson, p. 149.
4. H. H. Johnson, Stress Corrosion Cracking and Hydrogen Embrittlement of Iron Base Alloys, NACE (1977), edited by R. W. Staeble et al., p. 382.
5. H. G. Nelson and D. P. Williams, reference 5, p. 390.
6. R. P. Wei and G. W. Simmons, reference 5, p. 751.

PROJECT SUMMARY

Project Title: Hydrogen Energy Storage Technology (HEST) Project

Principal Investigator: James H. Kelley

Organization: Jet Propulsion Laboratory
4800 Oak Grove Drive M/S 507-228
Pasadena, CA 91103
(213) 577-9279

Project Goals: The broad objectives of the HEST project are as follows:

To explore and develop thermochemical hydrogen production cycles.

To monitor and maintain the pace of technological developments in gaseous pure hydrogen and hydrogen blends transmission, distribution and storage to the end that these technologies maintain a level of maturity consistent with the development of hydrogen production and end-use technologies.

To stimulate, monitor and manage the proposal, evaluation and development of advanced hydrogen production and storage concepts.

To develop a scientific and engineering foundation of knowledge and practice which will allow the use of low-cost, plentiful containment materials in hydrogen production, storage, transport and use.

To develop and maintain coherent and valid projections of hydrogen market penetration in the near, mid-and-long-range future.

To develop hydrogen production-to-use systems concepts which will support the earliest possible implementation of non-petroleum or natural gas-based hydrogen production/energy storage technologies.

Project Status: Under STOR's Hydrogen Energy Storage Technology program JPL is managing this project and the following elements of the program: Thermochemical Cycles; Advanced Production Concepts; Transmission, Distribution and Gaseous Storage; and System Studies. The NASA Ames Research Laboratory is managing the Containment Materials Element under this project.

Contract Number: IA ET-78-I-01-3112

Contract Period: FY'79

Funding Level: $1,100K

Funding Source: Department of Energy - STOR

PROJECT SUMMARY

Project Title: Solar/Hydrogen System Assessment

Principal Investigator: W.J.D. Escher

Organization: Escher: Foster Technology Associates, Inc.

Project Goals: The objectives of this task is to develop system conceptual designs wherein hydrogen energy storage and related technology can be employed to advance the implementation of solar energy.

Project Status: After considerable in-house progress, the remainder of the work was contracted with the contract beginning June 6, 1979. To date, the study is 80% complete. The Executive Summary draft of Volume II of the final repott has been submitted to JPL by the contractor. The due date for submittal of the draft of Volume II has been slipped by the contractor from August 15, 1979 to September 1. Due date for Volume 1 remains September 30.

Contract No.: 955492

Contract Period: 11/06/78 to 09/06/79

Funding Level: 53K

Funding Source: JPL

PROJECT SUMMARY

Project Title: Sulfur/Iodine Thermochemical Cycle

Principal Investigator: G. Besenbruch

Organization: General Atomic Company
P.O. Box 81608
San Diego, California 92138
(714) 455-2090

Project Goals: This program involves experimental research and development of the Sulfur/Iodine thermochemical water splitting cycle. Specific objectives include development of a bench-scale unit which demonstrates the major aspects of the cycle, and development of engineering flowsheets for estimation of process costs and efficiency. Funding of closely related work on cycle chemistry is provided by the Gas Research Institute.

Project Status: A closed cycle laboratory apparatus was operated in January to demonstrate the major chemical steps of the process. This was the first continuous demonstration of a pure thermochemical cycle, i.e., a cycle without a major electrochemical step. New engineering flowsheets were developed which incorporated improvements in the energy-intensive steps of sulfuric acid concentration and decomposition of hydrogen iodide. Intensive investigation of the chemistry of hydrogen iodide resulted in the substitution of a catalytic decomposition of this acid to produce hydrogen at 120 C for a homogeneous decomposition at 600 C. This results in dual benefits of lower energy and capital. Process efficiency in the revised engineering flowsheets is approximately 47%, up from the 42% reported previously. Project work centers on development of the DOE-STOR bench-scale demonstration which will incorporate both chemical and separation steps to aid further process development.

Contract Number: EY-76-C-03-0167, P.A. 63

Contract Period: October, 1978 - September, 1979

Funding Level: $300K (DOE, FY1979)
$250K (GRI, CY1979)
$100K (GA, CY1979)

Funding Source: Department of Energy - STOR
Gas Research Institute
General Atomic Company

PROJECT SUMMARY

Project Title: A Study of Industrial Hydrogen and Syngas Supply Systems

Principal Investigator: William J. Amos

Organization: Air Products and Chemicals, Inc.
Allentown, PA

Project Goals: One of the conclusions reached at the Houston Workshop on Hydrogen as Chemical Feedstock in December, 1977 was that the production and distribution of syngas ($CO + H_2$) by coal gasification is an option worth considering for industrial users. This study was designed to assess the economics of coal gasification vs. competing technologies based on natural gas and petroleum in three geographical areas--Texas Gulf Coast, Mid-Atlantic and the Ohio Valley. The focus is on future markets for hydrogen and syngas as feedstocks for the chemical industry.

Project Status: Study completion (anticipated) by October, 1979.

Contract Number: 955421

Contract Period: April, 1979 to October, 1979

Funding Level: $72K

Funding Source: DOE/STOR

PROJECT SUMMARY

Project Title: Workshop on Cost of Hydrogen from Coal

Principal Investigator: Roger E. Billings

Organization: Billings Energy Corp.
P. O. Box 555
Provo, Utah 84601

Project Goals: The objectives of this task are to develop an authoritative preliminary assessment of the most attractive processes for producing hydrogen from coal, to estimate the expected prices of such hydrogen, and to assess the economic, socio-political, environmental, and institutional barriers and incentives associated with the hydrogen-from-coal option.

Project Status: The workshop has been planned and conducted. Preliminary results were provided in the July 79 monthly progress report from the contractor to JPL. The final report is in preparation: draft due to JPL for review, September 15.

Contract No.: 955261

Contract Period: 11/06/78 to 09/06/79

Funding Level: 54K

Funding Source: JPL

PROJECT SUMMARY

Project Title: Sulfur Cycle Hydrogen Production Process

Principal Investigator: G. H. Porter

Organization: Westinghouse Electric Corporation
Advanced Energy Systems Division
Post Office Box 10684
Pittsburgh, Pennsylvania 15236
(FTS)

Project Goals: The purpose of this program is to develop an efficient, low-cost electrochemical cell for conversion of sulfur dioxide and water to hydrogen and sulfuric acid. Work under DOE/Solar sponsorship related to decomposition of this acid to regenerate the sulfur dioxide and release oxygen. Work on the cell includes efforts to lower the cost of electrodes by reducing or eliminating platinum as a catalyst, and work on cell design to lower the electrical energy requirements for the cell.

Project Status: Basic eletrochemical studies were conducted on the oxidation of sulfur dioxide to determine fundamental limitations to voltage-current relationships. Studies showed that early results of 0.6 volts at 2000 A/M^2 on platinum electrodes were optinum results for electrolysis of dilute sulfurous acid. Developmental work has centered on palladium oxide catalysts which promise better and less expensive electrodes. Much of the technology has centered on preparing dispersed electrocatalysts on stable carbon electrodes. Goals were set for electrodes capable of 0.8 volts at 2000 A/M^2 for this year. Results so far have been excellent in that this goal now appears achievable with the new electrodes. Additional work is being conducted on mixed oxide electrodes to further reduce the costs of electrocatalysts.

Contract Number: JPL 955380

Contract Period: February 1, 1979 - January 31, 1980

Funding Level: $251K

Funding Source: Department of Energy - STOR

PROJECT SUMMARY

Project Title: Copper Sulfate Thermochemical Cycle

Principal Investigator: S. Foh

Organization: Institute of Gas Technology
3424 S. State Street
Chicago, IL 60616
(312) 567-3942

Project Goals: This study investigates the technology of a thermochemical cycle based on the high-temperature decomposition of copper sulfate. The resulting sulfur dioxide is electrochemically oxidized to produce hydrogen and sulfuric acid or copper sulfate. The purpose of this work is to examine the electrolysis of sulfurous acid in low concentrations of sulfuric acid and in the presence of oxides of copper. High-temperature decomposition of copper sulfate is also studied as it can be accomplished with solar heat.

Project Status: Initial results showed that electrolysis in 30% sulfuric acid could be accomplished at 0.6 volts and at current densities greater than 200 ma/cm. This result promises to reduce the electrical energy requirements over the Westinghouse Sulfur Cycle which requires, from process considerations, electrolysis in 50% acid.

Contract Number: JPL 955494

Contract Period: July 1, 1979 - March 31, 1980

Funding Level: $75K

Funding Source: Department of Energy-STOR

PROJECT SUMMARY

Project Title: Thermochemical Process for Hydrogen Production

Principal Investigator: Melvin G. Bowman

Organization: University of California, Los Alamos Scientific Laboratory
P.O. Box 1663
Los Alamos, New Mexico 87545
FTS 843-5101

Project Goal: This project encompasses work on bismuth sulfate chemistry as part of a thermochemical cycle, design studies on thermochemical cycles for fusion sources, support work for the DOE-STOR thermochemical program, and coordination of the IEA-Annex I (Thermochemical Cycles) work for DOE.

Project Status: Accurate thermodynamic measurements have been made for the first step in the thermal decomposition of bismuth trisulfate (to form bismuth monoxy-disulfate). Initial studies of decomposition rates for this step have also been made. The experimental data support the concept that incorporating bismuth sulfate into sulfuric acid cycles could lead to enhanced efficiencies.

A first case design study has been completed in a program to access the potential for hydrogen production via thermochemical water splitting using fusion reactors. This first study was directed toward a hybrid bismuth sulfate cycle involving the formation and complete decomposition of bismuth trisulfate. Thermochemical data from experiments described above plus some estimated parameters were utilized in the rather detailed design analysis. In the continuing program, designs based on the formation and decomposition of the lower sulfates (oxysulfates) will be studied. In principle, even higher process efficiencies can result.

Preliminary evaluation has been made of the magnesium-iodine cycle being developed in Japan. Insufficient experimental data are available, but an initial assessment suggests the cycle will exhibit relatively low efficiency.

As a continuing activity, reports and papers from U.S. programs, relevant to Annex I of the I.E.A. Agreement on Hydrogen Production, are collected and sent to the Operating Agent for Annex I for distribution to participating countries. Reports are also received from the foreign participants and duplicated and distributed to appropriate U.S. Laboratories.

Arrangements are being made for the second Annex I Workshop to be held September 24-27, 1979 at the Los Alamos Scientific Laboratory.

Contract Number: C8-01-01-02-3

Contract Period: October, 1978 - September, 1979

Funding Level: $250K

Funding Source: Department of Energy - STOR

PROJECT SUMMARY

Project Title: Materials Development for Thermochemical Cycles

Principal Investigator: O.H. Krikorian

Organization: Lawrence Laboratories, Livermore
P.O. Box 808
Livermore, California 94550
(415) 422-8076

Project Goals: This study investigates material performance in service for vaporizing sulfuric acid. The work supports the engineering of thermochemical cycles which utilize the high-temperature decomposition of sulfuric acid vapor as the oxygen-producing step. Specific objectives include testing of commercial acid-resistant materials and development of new materials more suitable for large-scale facilities.

Project Status: Tests of silicon-rich materials are continuing in both static and circulating test setups. Commercial samples of Durachlor 51 and Duriron showed good resistance in both setups. These should be considered suitable for pilot-scale or small commercial plants. Several attempts were made over the last year to prepare high alloys coated with chromium silicide. The packed cementation method used was not satisfactory. Samples were subsequently obtained from Lockheed (Sunnyvale). Upon test, they proved resistant to vaporizing sulfuric acid in the static tests. It is believed that silicon-rich coatings on high alloys will be acceptable for large thermochemical hydrogen plants if the integrity of the coating can be assured. Testing is continuing in the continuous vaporizing/condensing test setup developed this year.

Contract No.: W-7405-ENG-48

Contract Period: October, 1978 - September, 1979

Funding Level: $100,000

Funding Source: Department of Energy - STOR

PROJECT SUMMARY

Project Title: Hydrogen Production by Photoelectrolytic Solar Energy Conversion

Principal Investigator: R. David Rauh

Organization: EIC Corporation
55 Chapel Street
Newton, MA 02158
(617) 965-2710

Project Goals:

The hydrogen photoelectrolytic conversion effort will investigate and determine the practicability of semiconductor-electrolytic devices (Honda-Fujishima concept) that use solar energy to decompose water into hydrogen and oxygen in an apparent single-step process. The overall aim of the program is the achievement of practical device for water photoelectrolysis.

Project Status:

During the second year effort, over 100 photoanodes and photocathodes were synthesized and evaluated. Exploratory efforts have been conducted on basic photocurrent-limiting mechanisms of photocathodes. Water decomposition has been demonstrated using small partially platinized semiconductor particles (~5 microns) in a fluidized liquid electrolite suspension.

Contract Number: JPL Contract #955271

Contract Period: FY79

Funding Level: $93K

Funding Source: Department of Energy - STOR
Jet Propulsion Laboratory

PROJECT SUMMARY

Project Title: Hydrogen Produced by Solar Radiation Task

Principal Investigator: H.B. Gray, A. Gupta

Organization: California Institute of Technology
Pasadena, CA 91125
FTS 792-5783

Project Goals:

The photocatalytic decomposition of water subtask will prepare and study organic rhodium-bridged complexes and determine the feasibility of the use of these complexes for the catalytic photo-decomposition of water, hydrobromic acid and hydroiodic acid. This photocatalytic system will utilize visible light (~500 nm) to accomplish the process of reduction.

Project Status:

The mechanism of photocatalyzed hydrogen production from concentrated HBr and HI has been investigated using the bridged rhodium photocatalyst. A closed cyclic system has been achieved by using Fe^{2+} as a reducing agent for the oxidized form of the photocatalyst. Flash photolysis and preliminary electrochemical studies indicate that the cycle closure may also be achieved in absence of Fe^{2+}.

Contract Number: IA-ET-78-I-01-3112

Contract Period: FY79

Funding Level: $40K

Funding Source: Department of Energy - STOR
Jet Propulsion Laboratory

PROJECT SUMMARY

Project Title: Hydrogen Sulfide Decomposition

Project Investigator: D. Cubicciotti

Organization: SRI International
333 Ravenswood Avenue
Menlo Park, Ca 94025

Project Goals: To investigate the feasibility of recovering hydrogen from large scale hydrogen sulfide waste process streams.

Project Status: A study was conducted on the feasibility of recovering H_2 from H_2S process stream. Some of the major conclusions are:

1. Strong growth in H_2S processing is projected from the present to beyond the year 2000.
2. Major new H_2S processing facilities will be required before the year 2000.
3. Before the year 2000, about 0.1 quad/year of hydrogen could be produced.
4. Direct thermal decomposition of H_2S is the recommended process.

The report will be distributed in the first quarter FY80.

Contract Number: JPL Contract #955272

Contract Period: FY79

Funding Level: $25K

Funding Source: Department of Energy - STOR
Jet Propulsion Laboratory

PROJECT SUMMARY

Project Title: Study of the Behavior of Gas Distribution Equipment in Hydrogen Service; Phase II

Principal Investigator(s): Walter J. Jasionowski
Dale G. Johnson

Organization: Institute of Gas Technology
3424 S. State Street
Chicago, IL 60616
(312) 567-3938

Project Goals: This project will empirically determine the suitability of existing natural gas distribution equipment for distribution of gaseous hydrogen. During Phase I of the study, natural gas components, joined by typical natural gas distribution manifolding techiques, were exposed to pure hydrogen during a six-month period of operation under conditions which simulated residential and commercial distribution loops.

During Phase II of the study, the hydrogen permeability of polyethylene plastic pipe used for natural gas distribution will be measured for 10 samples of pipe. Preferential leakage of hydrogen from mixtures of hydrogen and natural gas will be investigated. Effects of hydrogen exposure on the physical properties of polyethylene plastic pipe will be determined. IGT will assess the impact of Phase II results.

Project Status: Phase I of the test program has been completed. Results, which indicate that natural gas component designs will be adequate for hydrogen distribution with only the necessary modifications to accommodate the increased volumetric flow required for energy equivalence, were published in a final report in April 1979.

Phase II is progressing normally with sample procurement and setup fabrication. Pipe samples are being obtained from 10 vendors. The permeability cell has been designed and eight cells are being fabricated.

Contract Number: JPL 955447

Contract Period: May 1979 to July 1980

Funding Level: 95K (FY'79)

Funding Source: Jet Propulsion Laboratory

PROJECT SUMMARY

Project Title:	Hydrogen Compatibility of Structural Materials for Energy Storage and Transmission
Principal Investigator:	W. R. Hoover and S. L. Robinson
Organization:	Sandia Laboratories - Livermore P.O. Box 969 Livermore, California 94550 (415) 422-2391
Project Goals:	Assess feasbility of using the existing natural gas pipeline network to transport hydrogen on a national scale.
Project Status:	Preliminary results from tests in our Experimental Hydrogen Pipeline Loop indicate that transport of hydrogen through natural gas pipelines may be feasible although reductions in working pressures may be necessary.
Contract Number:	CB-01-01-02-03
Contract Period:	FY79
Funding Level:	$293K
Funding Source:	Department of Energy-STOR

PROJECT SUMMARY

Project Title:	Thermal Processing Task
Principal Investigator:	Dr. Harry F. Wachob
Organization:	NASA-Ames Research Center Materials Science & Applications Office, 230-4 Moffett Field, CA 94035 FTS 448-5407
Project Goals:	The goal of this project is to establish which of the ferrous microstructures that can be easily obtained via normal thermal processing procedures is least susceptible to hydrogen degradation.
Project Status:	Tensil tests have been performed using three different ferrous microstructures which indicate a reduction in mechanical properties occurs in the presence of high pressure hydrogen. Preliminary fatigue data has been obtained at a frequency of 1 Hz and a load R ratio of .15 for these microstructures in air and in hydrogen. Refinement of the test technique, variation in test frequency and higher values of R will be used in experiments during the next quarter.
Contract Number:	778-61-03-12-33-21
Contract Period:	FY79
Funding Level:	$60K
Funding Source:	Department of Energy-STOR

PROJECT SUMMARY

Project Title:	Evaluation of Laser Beam Welding Techniques
Principal Investigator:	J. Mucci and J.A. Harris
Organization:	Pratt & Whitney Aircraft Group Government Products Division P.O. Box 2691 West Palm Beach, Florida 33402 (305) 840-3280
Project Goals:	The objectives of this project is to determine the feasibility of laser beam welding as a fabrication method for a hydrogen transmission network. The study extends to the technology base by establishing the sensitivity of two classes of steels to gaseous hydrogen environment effects. The effects of conventional weld processes and laser beam welding on properties of the materials will be established.
Project Status:	Screening evaluation of the tensil, low-cycle fatigue. and fracture toughness properties and metallurgical analyses provide the basis for the conclusionsthat laser beam welding of AISI 304L stainless steel and ASTM A106B carbon steel can produce weldments of comparable quality to those produced by gas tungstun arc and electron beam welding and is least equally compatible with a 13.8 MPa gaseous hydrogen environment. Additional low-cycle fatigue tests will provide a qualitative ranking of the individual welding techniques which is not possible with the present data base.
Contract Number:	EC-77-C-02-4365
Contract Period:	FY79
Funding Level:	$8K (modification funding level of an original $73.7K program)
Funding Source:	Department of Energy-STOR

PROJECT SUMMARY

Project Title:	Effect of Stress State of Hydrogen Embrittlement
Principal Investigator:	M.R. Louthan, Jr., and R. P. McNitt
Organization:	Virginia Polytechnic Institute Department of Materials Engineering Blacksburg, Virginia 24061
Project Goals:	The goals are to determine effect of stress state on the susceptibility of pipeline steels to hydrogen embrittlement and develop effective design criteria to permit safe, efficient materials utilization.
Project Status:	Tensile, notched tensile, disc rupture, and fracture mechanics tests of samples machined from the perlitic-ferritic pipeline steel A-106 grade B, have shown that this alloy is susceptible to hydrogen embrittlement. Tests in 7 to 14 MPa hydrogen gas and tests in air after prolonged storage in 14 MPa hydrogen gas have shown that hydrogen exposure reduces the strength and ductility of the steel, increases the probability of fracture by cleavage or quasi-cleavage mechanisms, lowers the stress intensity or J_c for crack propagation and reduces the cycles to failure in "low cycle fatigue" or "ratcheted tensile" type tests. These adverse hydrogen affects are promoted by sharp notches and triaxial loadings or large degrees of constraint. Surfaces finish, hydrogen purity and test strain rates also play important roles in determining the susceptibility to hydrogen damage. However, in spite of these clear indications of hydrogen embrittlement susceptibility, no delayed failures have been produced in any samples, even when the samples were held for thousands of hours under cyclic biaxial stresses after being loaded to within 55% of the ultimate rupture pressure. These results are rationalized by considering the effect of stress on hydrogen embrittlement mechanisms.
Contract Number:	E(40-1)-5255
Contract Period:	FY79
Funding Level:	$45K
Funding Source:	Department of Energy-STOR Virginia Polytechnic Institute

PROJECT SUMMARY

Project Title:	Near Threshold Fatigue Crack Propagation in Pipeline Steels in High-Pressure Environments
Principal Investigator:	Dr. Neil Paton
Organization:	Rockwell International Science Center 1049 Camino Dos Rios, P.O. Box 1085 Thousand Oaks, CA 91360 (805) 498-4545
Project Goals:	The goal of this program is to fully characterize fatigue crack propagation behavior at near-threshold levels in an X-65 pipeline steel in vacuum, air, high-pressure hydrogen, hydrogen/natural gas mixtures and natural gas. With this understanding, predictions of limiting defect sizes, inspection intervals, remaining lifetime, as well as cost-efficient new designs may be ascertained.
Project Status:	Experimental work on this program will begin in mid-August. The fatique crack growth rate as a function of alternating stress intensity range ΔK, and threshold stress intensity will be determined for an X-65 pipeline steel in a variety of environments as a low-load ratio of 0.1 during the first quarter.
Contract Number:	778-61-03-12-33-21
Contract Period:	August 1, 1979-July 31, 1980
Funding Level:	$75K
Funding Source:	Department of Energy-STOR

PROJECT SUMMARY

Project Title: Hydrogen and Fatigue Properties of Steel

Principal Investigator: Professor Herbert H. Johnson

Organization: Cornell Unviersity
Materials Science & Engineering, Bard Hall
Ithaca, NY 14853

Project Goals: The goal of this program is to evaluate the fatigue properties of representative low and medium strength steels in high pressure hydrogen gas environments. Primary attention in this project will be directed to the initiation of fatigue cracks under varying conditions of microstructure, stress and strain concentration, and hydrogen environment.

Project Status: Material acquisition, specimen design and preparation, test technique development, and environmental chamber design will begin in August. Fatigue tests and baseline data will be obtained on the parent base metal during the first quarter of the program.

Contract Number: 778-61-03-12-33-21

Contract Period: August 15, 1979-August 14, 1980

Funding Level: $45K

Funding Source: Department of Energy- STOR

PROJECT SUMMARY

Project Title: An Assessment of Hydrogen Compressor Technology for Energy Storage and Transmission Systems.

Principal Investigator(s): Dr. T. N. Veziroglu

Organization: University of Miami
School of Engineering and Architecture
Coral Gables, Florida 33124
(305) 284-2404

Project Goals: This project will survey the compressor industry and assess the capability of existing compressor technology to provide long-term service for the storage and transmission of gaseous hydrogen. Inherent deficiencies in present compressor technology will be identified and recommendations for the time-phased correction of these deficiencies will be made.

Project Status: This project has been completed and the results which show that present compressor technology is adequate for near-term requirements were published in a final report in January 1978.

Contract Number: EC-77-S-05-5598

Contract Period: September 1977 to January 1979

Funding Level: $30K

Funding Source: Department of Energy-STOR

PROJECT SUMMARY

Project Title: Direct Thermal Water Splitting

Principal Investigator: P. Genequand

Organization: Battelle - Geneva Research Center
Geneva, Switzerland
(022) 439831

Project Goals:

This effort is to investigate the feasibility of high temperature thermal decomposition of water as a hydrogen production process. The concept involves the high temperature thermal dissociation of water vapor and the separation of the hydrogen and oxygen gases by differential molecular diffusion thru a porous refractory metal oxide membrane.

Project Status:

In the proof of concept experiments conducted at temperatures of 1900°K to 2900°K, hydrogen was observed. The report on this work will be available in the first quarter of FY80.

Contract Number: JPL Contract #955277

Contract Period: FY79

Funding Level: $44K

Funding Source: Department of Energy - STOR
Jet Propulsion Laboratory

PROJECT SUMMARY

Project Title: Assessment of Thermochemical Cycles

Principal Investigator: James E. Funk

Organization: University of Kentucky
College of Engineering
Lexington, Kentucky 40506
(606) 257-1688

Project Goals: This program provides a broad-based panel for the evaluation of the leading thermochemical processes for the production of hydrogen from water. The processes are examined to determine their efficiency, cost, and overall technical feasibility.

Project Status: The panel completed its evaluation of the Sulfur Cycle process of Westinghouse Electric Corporation. The cost and efficiency was highly dependent on the electrolytic cell which produces hydrogen and sulfuric acid from sulfur dioxide and water. The panel considered the projected voltage and costs of this cell were low. With revised costs, the cycle still appears competitive with electrolysis as a method to produce hydrogen. Work began on evaluation of the Sulfur/Iodine cycle of General Atomic Company. The flowsheets for this process are still in a state of change, and agreements between the panel and General Atomic are needed on the state of the technology. Recent technical improvements are now being incorporated.

Revised flowsheets are being examined on the basis of technical feasibility and efficiency. This work will be completed in December, 1979.

Contract Number: EC-77-S-05-5522

Contract Period: October, 1978 - September, 1979

Funding Level: $60K

Funding Source: Department of Energy-STOR

PROJECT SUMMARY

Project Title: Solid Polymer Electrolyte Water Electrolyzer Technology Development

Principal Investigator: J. H. Russell

Organization: General Electric Company
Direct Energy Conversion Programs
50 Fordham Road
Wilmington, MA 01887
(617) 657-5277

Project Goals: The main objective of this program is to develop low cost (<$100/kw) hydrogen generation plants (100kw - 5MW) for electric utility/industrial chemical applications using the solid polymer electrolyte technology. For the purpose of minimizing capital and operating costs, it is necessary to generate hydrogen under pressure (about 40 atmos) at high current densities ($\geq$ 1 amp cm^{-2}) and cell voltages close to the thermo-neutral potential (1.48 volts).

Project Status: The tasks in this program include analytical design, materials evaluation, dynamic evaluations, mechanical scale up and manufacturing process development necessary to fabricate and operationally test large-sized cells. Accomplishments to date include assembly and test of 2.5 ft^2 cells and 50kw module (12-cell stack); Design and fabrication of 200kw module; design and analysis of 10 ft^2 cell components. Optimization studies on catalysts, electrode design and manufacturing processes have brought the technology to within 20% of the projected cost goals.

The tasks for FY 80 will be: 1) completion of fabrication of 200kw system and its performance; 2) design and fabrication of 10 ft^2 cell; 3) design of a 5MW system.

Contract Number: ET-78-C-02-4689

Contract Period: October 1979 - September 1980

Funding Level: $1,500,000

Funding Source: Department of Energy

PROJECT SUMMARY

Project Title: Selection and Evaluation of Materials for Advances Alkaline Water Electrolyzers

Principal Investigators: G. Kissel, J. McBreen and S. Srinivasan

Organization: Brookhaven National Laboratory
Upton, NY 11973

Project Goals: The main objectives of this program along with that at the University of Virginia are to find stable materials required for electrodes, separators and other cell components for advanced alkaline water electrolyzers operating at 120-150°C.

Project Status: In FY 79, various conventional components and materials were tested for advanced alkaline water electrolyzers operating at 120-100°C. Components/materials tested included beryllium-nickel, beryllium-copper, Ni whisker and high surface area Ni electrodes, treated asbestos, Mallory barrier material and PBI.

Tasks in FY 80 are:

1. Elucidation of role of hydrogen permeation in metals on mechanism of time variation of overpotential.

2. Improvement of electrode configuration to lower over-potential losses

3. Develop and test composite barrier materials as separators

Contract Number: EY-76-C-02-0016

Contract Period: October 1979 - September 1980

Funding Level: $100,000

Funding Source: Department of Energy

PROJECT SUMMARY

Project Title: Advanced Alkaline Water Electrolyzer Development

Principal Investigator: J. N. Murray

Organization: Teledyne Energy Systems
110 West Timonium Road
Timonium, MD 21093
(301) 252-8220

Project Goals: The project is directed toward the design, fabrication and testing of advanced alkaline water electrolyzers, operating at 100-150°C., at nearly 100% energy efficiency and at current densities of approximately 500 $mAcm^{-2}$.

Project Status: In FY 1979, the construction and testing (with standard materials) of the five cell Applied Research Industrial Electrolysis System (ARIES) was completed. Some promising materials were tested as components (anode, cathode, separator) in the ARIES test rig in the temperature range of 100-125°C. These included DAUG-Ni_2B cathode, TES-110-C (with and without Pt) cathode, $NiCo_2O_4$ anode (suppled by Prof. Tseung, England) and TES-A-010 anode. Tasks in FY 80 are:

1. Computerized Assisted Hydrogen Production Cost, Analysis and Optimization in Advanced Electrolyzers.

2. ARIES testing of seven additional modules with emphasis on lower ohmic resistance and anode screening.

Contract Number: BNL 480421-S

Contract Period: April 1979 - January 1980

Funding Level: $79,727

Funding Source: Brookhaven National Laboratory

PROJECT SUMMARY

Project Title: Selection and Evaluation of Materials for Advanced Alkaline Water Electrolyzers

Principal Investigator: Glenn E. Stoner

Organization: Applied Electrochemistry Laboratory
Department of Materials Science
University of Virginia
Thorton Hall
Charlottesville, Virginia 22901
(804) 924-3277

Project Goals: The aim of the work at UVA is to assist in the selection of stable materials for cell components in advanced alkaline water electrolyzers operating at 100-150°C.

Project Status: In 1979 the University of Virginia focused its efforts on the preparation of polycrystalline Ni whisker electrode and evaluation of the electrocatalytic activites for the hydrogen and oxygen electrode reactions. Preliminary investigation on the correlation of hydride (such as NiH_2) formation with time variation of cathode overpotential was made. The major task in FY 80 is the completion of the investigations on the mechanism of the time variation of overpotential at the hydrogen cathode and methods for its inhibition.

Contract Number: BNL 451320-S

Contract Period: July 1978 - July 1980

Funding Level: $44,000

Funding Source: Brookhaven National Laboratory

PROJECT SUMMARY

Project Title: Optical and Electrocatalytic Investigations of Oxides of Ruthenium and Iridium

Principal Investigator: Fred Pollak

Organization: Brooklyn College, CUNY
Physics Department
Bedford Avenue and Avenue H
Brooklyn, NY 11210
(212) 780-5818

Project Goals: The objectives of this study are to (1) correlate optical measurements of oxide film characteristics with electrocatalytic activity and (2) determine the dependence of electrocatalytic activity on crystal orentation.

Project Status: (1a) Three crystallographic orientations of RuO_2 have been grown using the vapor phase oxygen transport technique. The (111), (100) and (110) RuO_2 surfaces have been examined using cyclic voltammetry and standard potentiostatic methods. The cyclic voltammograms reveal that the surface characteristics are quite different for the three orientations. The oxygen evolution electrocatalysis was also found to depend on crystal orientation. These findings will thus have important ramifications for the preparation of anode electrocatalysis for G.E. solid polymer electrolyte water electrolyzers.

(1b) Tasks for FY 1980

1. Growth of larger crystals of RuO_2 and IrO_2.
2. Detailed kinetic and mechanistic studies of oxygen evolution on these single crystal surfaces using rotating disc techniques.
3. Combined electrochemical optical studies on these single crystals and on oxidized metals to determine the intrinsic source of the catalytic activity of these materials.

Contract Number: EC-77-5-02-4590

Contract Period: October 1979 - September 1980

Funding Level: $20,000

Funding Source: Brookhaven National Laboratory

PROJECT SUMMARY

Project Title: Selection and Evaluation of Materials for Solid Polymer Electrolyte Water Electrolyzers

Principal Investigators: R. S. Yeo and S. Srinivasan

Organization: Brookhaven National Laboratory
Upton, N.Y. 11973

Project Goals: The main objectives of the project are to find highly active anode electrocatalysts and coatings for current collector materials, which are stable, for the solid polymer electrolyte water electrolyzer.

Project Status: Mixed oxides of ruthenium with Ta, Zr, Hf, W, La, Ir, Mn, Pb and Sr were prepared by the thermal decomposition method on a titanium substrate and were examined as oxygen evolution electrocatalysts. Anode catalysts, E-50 and WE-3, prepared by General Electric were also evaluated. Electrochemical-ellipsometric studies on ruthenium-based alloys to draw correlations between the optical and electrocatalytic properties of their oxides have been initiated.

Tasks for FY 80 included:

- investigation of alternative membranes for SPE cells, a collaborative effort with RAI Corp.
- complete the study on ruthenium-based mixed oxides.
- continue the combined electrochemical-ellipsometric studies on ruthenium-based alloys.
- LEED-Auger-ESCA studies on oxygen electrodes for SPE cells.

Contract Number: EY-76-C-02-0016

Contract Period: October 1979 - September 1980

Funding Level: $100,000

Funding Source: Department of Energy

PROJECT SUMMARY

Project Title: Hydrogen/Halogen Energy Storage System

Principal Investigator: James McBreen and Supramaniam Srinivasan

Organization: Brookhaven National Laboratory
Building 801
Upton, NY 11973
(516) 345-4513 and (516) 345-4494

Project Goals: Application of hydrogen/halogen reversible electrochemical systems to large scale energy storage requires: (1) an assessment of the safety considerations associated with handling bulk quantities of hydrogen, hydrochloric acid and halogens (chlorine) consistent with environmental and industrial procedures and regulations; (2) an assessment of costs associated with large scale electric storage for various siting alternatives; and, (3) systems performance analyses (energy cost and efficiency).

Project Status: Oronzio De Nora Co. of Milano, Italy conducted a safety and cost assessment of hypothetical 20 MW/200 H_2/Cl_2 and H_2/Br_2 storage systems considered for dispersed, utility and remote sites. It was concluded that current technology and equipment are applicable to systems designs and operations but safety considerations will preclude storage in dispersed urban sites. BNL activities and cell testing at General Electric have shown that round-trip electric efficiencies approaching 74% are achievable. System performance and cost is very dependent on operating pressure and temperature. System costs and efficiencies have been estimated based on presently available hardware. The cost figures are \$457/kW and \$73/kWh for the H_2/Cl_2 system and \$431/kW and \$67/kWh for the H_2/Br_2system. The respective overall efficiencies for the H_2/Cl_2 and H_2/Br_2 systems are 67% and 20%.

Contract Number: EY-76-C-02-0016

Contract Period: October 1977 - September 1978

Funding Level: \$140,000 (including Battery Branch funding)

Funding Source: Brookhaven National Laboratory

PROJECT SUMMARY

Project Title: Hydrogen-Technology Advanced Component Test System (HYTACTS)

Principal Investigator: G. Strickland and M. Rosso

Organization: Brookhaven National Laboratory
Building 835
Upton, New York 11973
(516) 345-4091 and (516) 345-4506

Project Goals: To utilize the HYTACTS and its associated data acquisition system for testing of the Hydrogen Storage Devices. (VPTU-2)
To evaluate requirements and costs for upgrading HYTACTS for high pressure operation. (6000 psi)

Project Status: The HYTACTS has been under construction for the past two years. Completion of the system is scheduled for September, 1979. The HYTACTS first application will be in tests of Variable Parameter Test Unit-2 (constructed by Foster-Wheeler). The test program on VPTU-2 will consist of determinimg basic performance characteristics; time of sustained hydrogen flow rates, heat-transfer rates for U-tube heat exchanger, and bed loosening by brief fluidization. It is expected that this work will be completed early in FY '80 (Oct.-Nov. 1979); thus the program on large size beds will essentially be terminated because of higher priority activities.

A design and cost analysis effort will be initiated in FY '80 for upgrading the HYTACTS capability for high-pressure operation. (Approximately 6000 psi). This capability would be useful in chemical-compressor work and in microsphere filling and test operations. The work in FY '80 would be limited to determining the modifications/additions needed and associated costs, but no actual construction would be undertaken.

Contract Number: EY-76-C-02-0016

Contract Period: October 1977 to September 1979

Funding Level: $350,000 FY 78 and FY 79
$100,000 FY 80

Funding Source: Brookhaven National Laboratory

PROJECT SUMMARY

Project Title: Hydride-Bed Heat-Transfer Modeling Study

Principal Investigator: J. S. Watson

Organization: Oak Ridge National Laboratory
Chemical Technology Division
P.O. Box X
Oak Ridge, Tennessee 37830
(615) 483-8611, ext. 36966

Project Goals: To develop an analytical model that accurately describes the heat-transfer characteristics of beds of hydride particles. The model will correlate the data taken at BNL on a 6" diameter and a 2" diameter bed.

Project Status: Work was initiated in late FY 78 at ORNL to scope the modeling effort and to establish the parameters, boundary conditions, and data base to be used.

Tasks for 1979 are: 1) Develop models for heat-transfer controlled systems. Review literature for available models or modify or provide new models as needed to produce results which agree with BNL data. The results should be in forms suitable for design purposes. 2) Generate solutions for the simplest cases (such as the small-scale BNL tests) at a number of different hydrogen flow-rates. 3) Generate solutions for the more complex geometries and organize the results into generalized forms convenient for design engineers.

The model, after some corrections, has been verified for low hydrogen charging rate for a given bed configuration and a single water cooling tube. Results from sensitivity studies which are almost complete indicate that the specific metal hydride isotherm is the most critical parameter in determining bed heat transfer rates. The next phase of the work extending into FY 80 will investigate higher hydrogen charging rates, the effects of multiple cooling tubes and external heating/cooling on the heat transfer rates.

Contract Number: BNL 456367-S

Contract Period: August 1978 - December 1979

Funding Level: $50,000

Funding Source: Brookhaven National Laboratory

PROJECT SUMMARY

Project Title: Modification and Operation of the Hydrogen Homestead Hydride Vessel Energy Storage System.

Project Investigator: R. Woolley

Organization: Billings Energy Corporation
P.O. Box 555
Provo, Utah 84601
(801) 375-0000

Project Goals: To provide operational experience with the hydrogen storage section of the Hydrogen Homestead project, including an evaluation of the safety aspects of the system.

Project Status: The initial phase of the Hydrogen Homestead project addressed testing of the 4000 lb. metal hydride reservoir used to store and supply the hydrogen fuel needs of the Homestead for heating, cooking, and vehicular traction purposes. One complete charge/discharge cycle has been evaluated.

FY 79 activities were planned to characterize supply/demand aspects of the Homestead consonant with safety considerations. Tasks include: 1) determine the ability of the reservoir to sustain various rates of fuel delivery consistent with demand profiles for hydrogen-fueled systems and the reservoir design and operating constraints; 2) perform a thorough and detailed safety evaluation of the Hydrogen Homestead, identifying monitoring and control actions of systems in place or as required.

A new contract was written to cover this phase of the work resulting in a delay in starting the FY '79 activities. As of mid-July 1979 a program plan had been submitted by Billings and approved by BNL and the test work was just being initiated.

Contract Number: BNL 481417-S
Previous Contract No. 420501-S

Contract Period: August 1977 - January 1979 (Previous contract)
June 1979 - April 1980 (Current contract)

Funding Level: $123,000 FY 77-78
$ 60,000 FY 78-79

Funding Source: Brookhaven National Laboratory

PROJECT SUMMARY

Project Title: Conversion of Hybrid MERADCOM Fork Lift Truck from Gaseous Hydrogen Fuel Storage to a Hydride Hydrogen Storage System

Principal Investigator: Roger Billings

Organization: Billings Energy Corp.
2000 East Billings Ave.
Provo, UT 84601
(801) 375-0000

Project Goals: To identify design/performance considerations of storage systems for hydrogen fueled traction systems to be used in conjunction with fuel cells.

Project Status: This is a joint activity involving the Billings Energy Corporation, the U.S. Army Mobility Equipment Research and Development Command (MERADCOM) located at Ft. Belvoir, and BNL. Billings will design, fabricate and install a metal hydride hydrogen storage system for fuel storage and supply in a fuel cell/battery hybrid fork lift truck provided by MERADCOM. Billings will perform a "shakedown" test prior to delivery of the vehicle to MERADCOM and will then provide a report on the design and test activities. MERADCOM will monitor the operating performance of the vehicle for an undefined period of time and will keep BNL informed on the project.

The project has been fully approved and is scheduled to begin in September 1979. Vehicle delivery to Ft. Belvoir (MERADCOM) is scheduled for three months later, or around January 1, 1980.

Contract Number: To be determined.

Contract Period: September 1979 - January 1980

Funding Level: $16,900

Funding Source: Brookhaven National Laboratory

PROJECT SUMMARY

Project Title: Hydrogen Storage Using Glass Microspheres for Automotive Applications

Principal Investigator: R.J. Teitel

Organization: Robert J. Teitel Associates
P.O. Box 81921
San Diego, CA 92138
(714) 565-6441

Project Goals: The goals of the program in FY '79 were to obtain experimental verification of the characteristics of microspheres for the automotive hydrogen application.

Project Status: The work performed by Teitel Associates in FY '78 indicated that microsphere storage has potential advantages over metal hydride storage particulary for the automotive application. Key assumptions made in the analysis concerned permeability, microsphere production, pressure fill and usage characteristics. The main areas of work in FY '79 were the experimental verification of the above parameters and a more detailed engineering evaluation of the filling operation and hydrogen distribution system.

During FY '79 the experimental apparatus was assembled and testing conducted on small samples (10 ml) of commercially available microspheres. The preliminary results indicate that hydrogen can be enclosed in microspheres at pressures up to 400 ATM. stored for a couple of weeks, recovered at rates and at temperatures compatible with the automotive hydogen storage application. Performance of the microspheres during testing indicate that assumptions made in the analysis were too pessimistic and that lower cost could be expected for production and filling.

The FY '79 program was accelerated somewhat based on the promising results and will be completed by October 1, 1979. Plans for FY '80 include testing of larger size samples and an expanded engineering development program.

Contract Number: BNL 436153-S

Contract Period: January 1978- January 1980

Funding Level: FY '78 65,000
FY '79 90,000

Funding Source: Brookhaven National Laboratory

PROJECT SUMMARY

Project Title: FeTi Storage System for Bulk Hydrogen Storage

Principal Investigator: H.N. Franklin

Organization: Foster Wheeler Energy Corporation
110 South Orange Ave.
Livingston, NJ 07039
(201) 533-3609

Project Goals: To design and fabricate an advanced 50-kw, 500-kwh FeTi-based hydride reservoir, reflecting improvements to override hydride expansion consistent with safe and cost-effective performance considerations.

To develop a realistic cost basis for reservoir designs applicable to stationary storage systems.

Project Status: A 26-in. diameter x 10-ft. long reservoir has been designed capable of storing 35 lb. of hydrogen in $TiFe_{0.9}Mn_{0.1}H_x$. This unit is identified as the Variable Parameter Test Unit-2 and will permit the test and evaluation of heat and mass transfer data associated with alternative internal assembly configurations that include: (1) bed-loosening by high-pressure pulsing of charging gas, compatible with U-tube heat-exchanger configuration; (2) limited bed depth configuration using a tube array; (3) limited bed depth configuration using trays.

The test vessel UPTU-2 was delivered to BNL in February, 1979. A second test unit (one tube, water-on-shell-side design) for hydride expansion studies had delivered earlier in FY '79. The design report was completed and submitted to BNL for review in March, 1979. The report contains extensive design analysis on vessel size, weight, design approach, heat-transfer and flow data and the relative merits of three design concepts addressing heat transfer and hydride expansion. The report concluded that the water-on-shell-side approach is the most cost-effective design compared to a water-on-tube side design and one involving conical trays.

This completed Foster-Wheeler's activities under the current contract. Foster-Wheeler has expressed interest in following the test program and keeping abreast of the technology.

Contract Number: BNL 418210-S

Contract Period: July 1977 - July 1979

Funding Level: Total Funding $144,000

Funding Source: Brookhaven National Laboratory

PROJECT SUMMARY

Project Title: Energy Storage Systems for Automobile Propulsion

Principal Investigator: Hugh Forsberg, LLL and Gerald Strickland, BNL

Organization: Lawrence Livermore Laboratory
Transportation Systems, L-387
P. O. Box 808
Livermore, California 94550
(415) 422-6423

Brookhaven National Laboratory
Building 120
Upton, New York 11973
(516) 345-4091

Project Goals: To identify storage systems that exhibit energy density and power density characteristics suited to automotive propulsion use in the remaining years of the century and to analyze comparative cost-performance tradeoffs among candidate systems that include Electrochemical, Mechanical, Chemical, and Thermal Storage Systems.

This project is under the direction of Lawrence Livermore Laboratory with a number of the National Laboratories participating supported by industrial contractors. The main product is a comprehensive study report on energy storage devices and power systems for automobiles.

Project Status: The BNL activities involve characterization of hydrogen storage reservoirs including liquid hydrogen stored in cryogenic containers, metal hydrides, and glass microballoons. In each case, the hydrogen is delivered to a modified internal combustion engine. Findings indicate that liquid hydrogen is the most favorable alternative, being comparable in weight to conventional automotive systems at higher capital and operating cost. The main disadvantage of liquid hydrogen concerns consumer handling problems. The hydride storage systems compare favorably with battery systems and exhibit three to four-fold improvement in energy density (by weight) and order of magnitude improvement in power density over Nickel-Zinc batteries, while offering a rapid refueling capability. Safety and cost factors require further evaluation.

The tasks in FY 79 included developing the performance characteristics of alkaline-fuel-cell battery vehicles (hydrogen from metal hydrides), updating the metal-hydride storage information, and providing cost and engineering data for microballoon storage systems. A draft report will be completed by October 1979 with the entire project expected to be completed in early FY 1980 after the publication of the final report.

Contract Number: SANL 622-001

Contract Period: October 1977 - September 1979

Funding Level: $30,000 FY 78
$30,000 FY 79

Funding Source: Lawrence Livermore Laboratory

PROJECT SUMMARY

Project Title: The Development of Metal Hydride Systems for Hydrogen Compressor Applications

Principal Investigator: Mr. Frank Lynch - (DRI)

Organization(s): Ergenics--Denver Research Institute (DRI)

Project Goals: The goal of this project is to evaluate the performance of a bench-scale hydrogen chemical compressor based on decomposable metal hydrides. This information will be the basis of the decision to develop a commercial size unit.

Project Status: This work was initiated at DRI in 1978 under funding from Ergenics Division of MPD Technology Corp. which is a subsidiary of INCO. Funding from Ergenics was exhausted, and the current work is the result of an unsolicited proposal from EDRI to DOE STOR. The present work consists of completing the design and fabrication of the small-scale chemical compressor and obtaining basic performance and life-cycle test data on the unit. The first phase is scheduled to begin on or about August 1, 1979 and require about six months. Information will be obtained on materials, heating technique, safety aspects, hydride expansion, particle attrition, heat transfer, and compressor performance.

Assuming the test results are favorable, a second phase of the program will be authorized for the development of a larger size compressor. This second phase is expected to last about a year and would be funded at $130,000 with Ergenics cost sharing about 25%.

Contract Number:

Contract Period: Phase I--August 1979 - January 1980
Phase II--January 1980 - January 1981 (if authorized)

Funding Level:	FY '79	FY '80	(if authorized)
	$41K	$98K	

Funding Source: BNL

PROJECT SUMMARY

Project Title: Underground Storage of Hydrogen

Principal Investigator: Philip L. Randolph

Organization: Institute of Gas Technology
IIT Center
3424 South State Street
Chicago, IL 60616
(312) 567-3766

Project Goals: The purpose of this program is to make a technical and economic assessment of underground storage of hydrogen. Specific objectives are to 1) establish the engineering feasibility of using geologic or engineered underground sites for hydrogen storage, 2) identify the Research and Development (R&D) needs related to both cost reduction and safety problems, 3) identify possible sites where hydrogen may be stored, and 4) develop realistic cost estimates for underground hydrogen storage facilities.

Project Status: Dames & Moore is characterizing the 4 types of underground storage facilities. Their complete report is expected by the end of the calendar year. IGT, with the cooperation of Transco, Texas Gas Transmission Corp., and Northern Illinois Gas, is performing preliminary technical and economic assessments of hydrogen storage. Preliminary assessments will be followed by in-depth, site-specific analyses of the Hanson, Media and Eminence storage facilities. Analysis of depleted well storage systems suggests technical feasibility if appropriate engineering and procedural controls are introduced. Cost-of-service will be greatly influenced by charges associated with the requirement for "non-deliverable" cushion gas (or base-gas) inventories.

Contract Number: BNL 453439-S

Contract Period: August 1978 - September 1979

Funding Level: $144,000

Funding Source: Brookhaven National Laboratory

PROJECT SUMMARY

Project Title: Hydrogen Storage Materials Developement

Principal Investigator: John R. Johnson

Organization: Brookhaven National Laboratory
Building 815 DEE
Upton, NY 11973
(516) 345-4510

Project Goals: The development of new applications for metal hydride materials involving the safe storage and separation of hydrogen which would be utilized as an energy carrier in both mobile and stationary systems.

Project Status: The hydrogen storage materials development program has identified and characterized several new alloy hydrogen systems suitable for a variety of near-term end use applications. Emphasis in this project during FY 79 has been redirected. Areas of research which have actively been pursued involve the identification of hydrides for hydrogen separation from industrial gas streams and the characterization/development of low cost, high capacity hydrides. A lower level of effort than in past years was expended in the latter area.

Several hydrides have been found to be suitable for hydrogen recovery from methane-10 volume percent hydrogen mixtures and these are: $TiFe_{0.85}Mn_{0.15}$, $LaCuNi_4$, $LaNi_5$ and TiFe. In the area of high hydrogen capacity, low cost hydrides, systems based on Mn substituted $TiCr_2$ have been identified as promising for nonmechanical compression applications.

This project will not continue in FY 80 as the hydride development program at BNL will come to an end as of September 30, 1979.

Contract Number: EY-76-C-02-0016

Contract Period: October 1978 - September 1979

Funding Level: $60,000

Funding Source: Brookhaven National Laboratory

PROJECT SUMMARY

Project Title: Advanced Hydrides Technical Support

Principal Investigator: John R. Johnson

Organization: Brookhaven National Laboratory (BNL)
Building 815 DEE
Upton, NY 11973
(516) 345-4510

Project Goals: The prime objectives of this activity will be to provide technical support, of a laboratory nature, for both in-house BNL activities and subcontract work leading to near-term application for hydrides and to provide management coordination for materials subcontract research.

Project Status: This has been a continuting effort with work performed in the areas of materials characterization, poisoning and safety studies and technical/economic evaluations for proposed storage materials.

Tasks for FY 79 are:

1. sample testing on an as-needed basis for both BNL in-house engineering activities and subcontractor research; and

2. provide technological direction and coordination of contractor activities.

This project will not continue in FY 80 as there will be no in-house hydride work at BNL after FY 79.

Contract Number: EY-76-C-02-0016

Contract Period: October 1978 - September 1979

Funding Level: $30,000

Funding Source: Brookhaven National Laboratory

PROJECT SUMMARY

Project Title: Development of New Hydrogen Storage Systems for Automotive Hydrogen Fuel Storage

Principal Investigator: John J. Sheridan III

Organization: Air Products and Chemicals, Inc. (APCI)
P.O. Box 538
Allentown, PA 18105
(215) 398-6508

Project Goals: The principal goal of this program is the development and characterization of metal-hydrogen systems with >3 wt% hydrogen storage capacity and dissociation pressures of at least 1 atm. at 175°C. The objective in FY 79 is the completion of characterization studies on binary, ternary and quaternary alloys of Mg.

Project Status: Facilities and equipment were assembled to investigate specifically both the chemical and structural/geometric factors in the hydriding of magnesium-based, light weight alloys. Studies of the effects of geometrical and chemical factors on the hydriding properties of these alloy types were completed and materials from the binary Mg-Al system were found to be most promising. Work was initiated to define the kinetics and reaction paths of the Mg-Al alloys with hydrogen and to investigate the use of catalysts in such systems.

Tasks for 1979 are:

1. completion of the evaluation of binary, ternary and quaternary alloys of Mg with respect to their hydriding properties (storage capacity and thermodynamic characteristics);

2. studies of the kinetics of hydrogen absorption-desorption in the most promising Mg-based alloys which were identified as Mg-Al intermetallics;

3. investigations of the reaction pathways for the Mg-Al compounds upon hydriding; and

4. studies of the effects of catalysts on the kinetics and reaction paths for the Mg-Al alloys.

Contract Number: BNL 435582-S

Contract Period: February 1978 - September 1979 (expect continuation proposal for FY 80 in September 1979)

Funding Level: $160,000 (FY 78 and FY 79)

Funding Source: Brookhaven National Laboratory

PROJECT SUMMARY

Project Title: Development of Hydrogen Storage Materials for Application to Energy Needs

Principal Investigator: Charles E. Lundin

Organization: Denver Research Institute (DRI)
2450 South Gaylord Street
Denver, CO 80208
(303) 753-2621

Project Goals: The primary goal of DRI's research effort is to develop improved hydrides for energy storage and conversion applications The specific objective is to define the properties of alloy-hydrogen systems with ≥3 wt% storage capacity, resonable thermal properties, decreased materials cost, contamination resistance, good kinetics, etc. using the DRI developed predictive technique.

Project Status: Based on the DRI developed predictive technique which relates interstitial alloy hole size to the thermodyanmic stability of the resulting alloy-hydride several different alloys were chosen for investigation (hydriding properties were investigated). Of all the alloys investigated, none was found, to date, to have better general properties than the classic AB alloy hydride $TiFeH_2$ for energy storage applications.

Tasks for FY 79 are:

1. completion of studies on AB_2 type Laves phases and Ti and V-based solid solutions;
2. screening investigations of selected AB, AB_3 and AB_9 intermetallics completed by 9/30/79; and
3. screening studies of complex alloys of the form A_xB_y completed by 9/30/79.

As a result of the FY 79 research it was expected that a series of fully characterized hydrides with ≥ 3 wt% hydrogen storage capacities and good thermal properties would be made available for a variety of storage applications. Since this goal is no where near being realizable as of 8/1/79m the program at the Denver Reasearch Institute will not be continued in FY 80.

Contract Number: EY-78-5-02-5104-A000

Contract Period: September 1978 - September 1979

Funding Level: $100,000

Funding Source: Department of Energy, SRSA

PROJECT SUMMARY

Project Title: Metallurgical Studies of Hydrogen Storage Alloys

Principal Investigator: Gary D. Sandrock

Organization: The International Nickel Co., Inc. (INCO)
INCO Research and Development Center
Sterling Forest
Suffern, NY 10901
(914) 753-2761

Project Goals: Experimental studies will be performed and data collected and analyzed to determine mechanisms of poisoning of TiFe, $TiFe_{0.85}Mn_{0.15}$ and $LaNi_5$ compounds by common contaminants such as O_2, $H_2O_{(v)}$ and CO. Also, an assessment of the overall probability of developing poison resistant hydrides by alloy modification, utilizing the results of the mechanistic studies, will be carried out.

Project Status: Poisoning studies for all three alloys with the different contaminants are nearly complete. All experimental work will be finished for FY 79 on 9/1/79. Data analysis (interpretation) will be finished as of 9/30/79 and the contract final report will be submitted no later than 10/31/79.

Tasks for FY 79 are:

1. completion of poisoning studies for TiFe, $TiFe_{0.85}Mn_{0.15}$ and $LaNi_5$ alloys including the developemnt of models for the mechanisms of poisoning by the different contaminants;

2. metallographic examination of BNL experimental alloys; and

3. preparation of test alloys for BNL on an as-needed basis.

Tasks (2) and (3) are simply low level metallurgical support for BNL. It is likely that INCO's participation in this proprogram will continue in FY 80. As of 8/1/79 it is uncertain, however, as to whether their program will be a continuation of work on understanding mechanisms of alloy hydride poisoning leading to the development of poison resistant hydrides or a new program concerned with near-term commericalization of devices utilizing metal hydrogen storage systems.

Contract Number: BNL 451117-S

Contract Period: July 1978 - September 1979

Funding Level: $90,000

Funding Source: Brookhaven National Laboratory

PROJECT SUMMARY

Project Title: Hydrogen Production from Small Hydropower Systems

Principal Investigator: E.L. Wilkinson

Organization: Air Products & Chemicals Inc.
Box 538
Allentown, PA 18105
(215) 398-8146

Project Goals: To conduct analytical, design and engineering investigations leading to a funding decision regarding the field demonstration of the commercial viability of hydrogen production from small hydropower sites. The following tasks will be undertaken:
Phase I - Program Analysis and Economic Evaluation (specific program plan, systems analysis, sensitivity analysis);
Phase II - Site Selection (criteria selection, site recommendations);
Phase III - Site Engineering, Definitive Facility Cost Estimate (hydropower site restoration/development design, hydrogen production/storage disposition, hydrogen production cost estimates).

Project Status: APCI has submitted its program plan and current efforts concentrate on site selection. Criteria for site selection has been broadened to extend beyond "over-the-fence" applications to merchant hydrogen markets. Cost tradeoffs are being conducted dealing with piping vs. trucking of hydrogen from a hydropower site to the use or distribution site.

Contract Number: BNL 478647-S

Contract Period: July 1979 to March 1980

Funding Level: $168,087

Funding Source: Brookhaven National Laboratory

PROJECT SUMMARY

Project Title: Hydrogen Production from Small Hydropower Sites

Principal Investigator: Dr. Rudolph Wiley

Organization: New York State Energy Research and Development Authority (NYSERDA)
Empire State Plaza
Albany, NY 12223
(518) 465-6251

Project Goals: To verify the commercial prospects for merchant hydrogen production from a hydropower site in Potsdam, New York, leading to field demonstration. The following tasks will be undertaken: Phase I - Planning and Analysis (program plan, systems analysis, cost sensitivity analysis); Phase II - Site Selection (criteria development, site recommendation); Phase III - Site Engineering (hydropower site restoration/development design, hydrogen production/storage/disposition, hydrogen production cost estimate).

Project Status: Final negotiations with NYSERDA have been virtually completed and project start-up target date has been set as 9-1-79. The project will be cost shared by:

- DOE/STOR - DOE/HRD
  (Division of Energy Storage Systems and
  Division of Hydroelectric Resource Development)
- NYSERDA
- City of Potsdam

Contract Number: BNL 479955-S

Contract Period: September 1979 - May 1980 (anticipated)

Funding Level: $174,900 (anticipated)

Funding Source: Brookhaven National Laboratory

PROJECT SUMMARY

Project Title: Methanol-Based Heat Pump for Storage of Solar Thermal Energy

Principal Investigator: Dr. Peter Offenhartz

Organization: EIC Corporation
55 Chapel Street
Newton, MA 02158
(617) 965-2710

Project Goals: The purpose of this program is to test a 100,000 BTU thermal storage capacity $CaCl_2$ - CH_3OH system and evaluate the data obtained. Under the previous phase of this contract, the system was constructed. Specified program objectives are to: 1) initiate unit testing, 2) complete a stage of hardware debugging, 3) complete a first series of thermal storage test cycles and initiate any needed redesign, 4) complete any needed redesign, 5) initiate and complete off-design cycle tests including simulated process upsets and control failure, 6) initiate and complete long-term (> 1000 cycles) testing, 7) evaluate salt bed heat exchanger performance, 8) complete preliminary heat and mass balance, 9) evaluate thermal loss terms, 10) calculate the system COP, including all parasitics, 11) evaluate cycle performance and issue performance claims and specifications, and 12) issue a final report including a revised development plan.

Project Status: EIC Corporation has completed construction of the 10^5 BTU thermal storage capacity $CaCl_2$ - CH OH unit. This followed the laboratory screening of twenty candidate inorganic salts before choosing $CaCl_2$ - CH_3OH system kinetics, and other chemical behavior has been carried out. A 1000 BTU bench-top unit was then built to provide data for the continuation into the present phase of work.

Contract Number: BNL 490105-S

Contract Period: August 1979 - September 1980

Funding Level: $193,398

Funding Source: Brookhaven National Laboratory

PROJECT SUMMARY

Project Title: Sulfuric Acid/Water Chemical Heat Pump

Principal Investigator: Mr. E.C. Clark

Organization: Rocket Research Company
Redmond, WA
(206) 885-5000

Project Goals: The project is structured to verify the capability of the sulfuric acid-water system and to enhance near-term commercialization. The primary objective is to design, construct and test a sulfuric acid CHP/CES verification test unit which incorporates as many commercial, mass producible design features as necessary to demonstrate system economic and technical feasibility. The unit shall, as a minimum, be designed with low cost chemical storage tanks, and shall be capable of operation in the COP > 1 mode as well as provide space cooling with simultaneous charge and discharge capability (absorption cycle refrigeration mode). For purposes of gaining scaling criteria, the nominal storage design capacity shall be $\sim 10^6$ Btu with a nominal delivered heat rate of $\sim$ 150,000 Btu/hour.

Project Status: The initial Phase I effort with sulfuric acid-water was a 9-month conceptual design and laboratory demonstration of the primary components, which proved the feasibility of the thermal storage concept and demonstrated the separation and recombination of the chemicals. During the Phase II program, the chemical heat pump concept was identified; and an engineering model was designed, constructed, and demonstrated. The Phase II-A program extended the system analysis to study economics. Also completed during Phase II-A was component optimization testing with the Phase II engineering system and an assessment of the institutional barriers to commercialization of the sulfuric acid/solar/CHP/CES. Final reports on all phases have been completed. The proposed follow-on program is under review by BNL.

Contract Number: TBD

Contract Period: 24 months (total proposed program)

Funding Level:*

Phase I, Requirements Analysis	$ 94,470
Phase II, Verification Test Unit Design	285,439
Phase III, " Fabrication & Assembly	182,792
Phase IV, " Performance Testing	142,460
TOTAL PROPOSED PROGRAM	$705,159

Funding Source: Brookhaven National Laboratory

* As requested in RRC proposal to BNL dated July 23, 1979

PROJECT SUMMARY

Project Title: HYCSOS: A Two Metal Hydride System for Energy Storage and Conversion

Principal Investigators: J. G. Asbury, C. A. Blomquist, and D. M. Gruen

Organization: Argonne National Laboratory
9700 South Cass Avenue
Argonne, IL 60439
(312) 972-3513

Project Goals: To develop and characterize an engineering test unit of a chemical heat pump utilizing metal hydrides and exhibiting rapid cycling times. Such a system would be directed towards applications utilizing low grade waste heat or solar.

Project Status: Proof of concept has been demonstrated. Several hydride systems have been characterized with regard to their application to chemical heat pumps. Pairs of hydrides with kinetics favorable to rapid cycling have been identified, and $CaNi_5$ hydrides have been identified as being unsuitable due to disproportionation under a hydrogen atmosphere. System studies are in the process of defining the least expensive and most efficient system configurations. Extensive heat exchanger design and analysis is being carried out to facilitate removal of sensible heat from the hydride beds in times consistent with minimal cycle times.

Contract Number: C8-03-02-01-3 (DOE); 49405 (ANL)

Contract Period: October 1978 - September 1979

Funding Level: $240,000

Funding Source: United States Department of Energy

Meeting of the Review Committee

Thursday, November 15, 1979

REVIEW COMMITTEE

Dr. James Funk	University of Kentucky
Mr. William Hoagland	Solar Energy Research Institute
Dr. Ben Mehta	Electric Power Research Institute
Mr. Edwin Read	Exxon Enterprises, Inc.
Dr. I. O. Salyer	University of Dayton
Dr. F. Dee Stevenson	U. S. Department of Energy
Mr. C. J. Swet	Consultant
Dr. M. Rasin Tek	University of Michigan

OTHERS

Mr. Michael Bonner	Brookhaven National Laboratory
Dr. Christopher England	Jet Propulsion Laboratory
Mr. John Gahimer	U. S. Department of Energy
Mr. James H. Kelley	Jet Propulsion Laboratory
Dr. D. David Lawson	Jet Propulsion Laboratory
Mr. Alessio Mezzina	Brookhaven National Laboratory
Mr. Robert Reeves	U. S. Department of Energy
Dr. James Swisher	U. S. Department of Energy
Mr. Laurence Williams	Aerospace Corporation

U. S. DEPARTMENT OF ENERGY

DIVISION OF ENERGY STORAGE SYSTEMS

CHEMICAL ENERGY STORAGE & HYDROGEN ENERGY SYSTEMS CONTRACTS REVIEW

November 13 & 14, 1979
Sheraton International Conference Center
Reston, Virginia

LIST OF PARTICIPANTS

ALDRIDGE, Frederick T.
Lawrence Livermore Laboratory
L-372
Livermore, California 94550
(415) 422-7004

BESENBRUCH, G. E.
General Atomic Company
P. O. Box 81608, TO-307
San Diego, California 92138
(714) 455-2915

BILGEN, Ertugrul
Ecole Polytechnique de Montreal
2500 Marie-Guyard
Montreal, Quebec H3P 1T8
CANADA
(514) 344-4892

BILLINGS, Roger E.
Billings Energy Corporation
2000 East Billings Avenue
Provo, Utah 84601
(801) 375-0000

BONNER, Michael F.
Brookhaven National Laboratory
Building 120
Upton, New York 11973
(516) 345-2207

BOTTS, Thomas
Brookhaven National Laboratory
Building 129
Department of Nuclear Energy
Upton, New York 11973
(516) 345-2421

BUXBAUM, Robert S.
Teledyne Energy Systems
110 West Timonium Road
Timonium, Maryland 21093
(301) 252-8220 x267

CHAPMAN, Lloyd E.
General Electric Company
50 Fordham Road
Wilmington, Massachusetts 01887
(617) 657-5256

CLARK, E. C.
Rocket Research Company
York Center
Redmond, Washington 98052
(206) 885-5000

COX, Kenneth E.
Los Alamos Scientific Laboratory
P. O. Box 1663
Los Alamos, New Mexico 87545
(505) 667-7059/6074
FTS 843-7059

CUBICCIOTTI, Daniel
SRI International
333 Ravenswood
Menlo Park, California 94025
(415) 326-6210 x3940

DELMONACO, John L.
Public Service Electric & Gas Company
80 Park Place
Newark, New Jersey 07101
(201) 430-6551

ECKLUND, E. E.
U. S. Department of Energy
CS/TP
Washington, D.C. 20585
(202) 376-4892

ENGLAND, Christopher
Jet Propulsion Laboratory
4800 Oak Grove Drive
Pasadena, California 91103
(213) 577-9060
FTS 792-9060

FISHER, Paul W.
Oak Ridge National Laboratory
P. O. Box X
Building 4505
Oak Ridge, Tennessee 37830
(615) 574-6817

FOH, Stephen E.
Institute of Gas Technology
3424 South State Street
Chicago, Illinois 60616
(312) 567-3942

FRANKLIN, Howard N.
Foster Wheeler Energy Corporation
110 South Orange Avenue
Livingston, New Jersey 07039
(201) 533-3609

FUNK, James E.
University of Kentucky
206 Administration Building
Lexington, Kentucky 40506
(606) 258-8636

GAHIMER, John
U. S. Department of Energy
Energy Storage Systems
Room 416
600 E Street, N.W.
Washington, D.C. 20545
(202) 376-9296

GOODELL, Paul Douglas
INCO Research & Development Center
Sterling Forest
Suffern, New York 10901
(914) 753-2761

GRANT, C. Stephen
Aerospace Corporation
20030 Century Boulevard
Germantown, Maryland 20767
(301) 428-2727

* GRASSLEY, Charles E.
U. S. House of Representatives
1227 Longworth House Office Building
Washington, D.C. 20515
(202) 225-3301

GUPTA, Amitava
Jet Propulsion Laboratory
Energy & Materials Research Section
MS 67-201
4800 Oak Grove Drive
Pasadena, California 91103
(213) 354-5783
FTS 792-3549

HANSON, Joe A.
Jet Propulsion Laboratory
4800 Oak Grove Drive
Pasadena, California 91103
(213) 577-9282
FTS 792-9282

HOAGLAND, William
Solar Energy Research Institute
1536 Cole Boulevard
Building 4, First Floor
Golden, Colorado 80401
(303) 231-1368
FTS 327-1368

HOLDING, Virginia
California Institute of Technology
c/o A. Gupta, Jet Propulsion Laboratory
Energy & Materials Research Section
MS 67-201
4800 Oak Grove Drive
Pasadena, California 91103
(213) 354-5783
FTS 792-3549

HOOVER, W. R.
Sandia Laboratories
Division 8314, P. O. Box 969
Livermore, California 94550
(415) 422-2391

* Guest Speaker

HOROWITZ, J. S.
Argonne National Laboratory
9700 South Cass Avenue
Argonne, Illinois 60439
(312) 972-7696

HURWITCH, Jonathan W.
Battelle, Washington Operations
2030 M Street, N.W.
Washington, D.C. 20036
(202) 785-8400

JACKSON, A. W.
Brookhaven National Laboratory
400 North Capitol Street
Room 185
Washington, D.C. 20001
(202) 376-4042

JAEGER, F. A.
Martin Marietta Aerospace
P. O. Box 179
MS SO482
Denver, Colorado 80201
(303) 973-4804

JASIONOWSKI, Walter J.
Institute of Gas Technology
3424 South State Street
Chicago, Illinois 60616
(312) 567-3938

JOHNSON, Herbert H.
Cornell University
Materials Science Center
627 Clark Hall
Ithaca, New York 14853
(607) 256-4272

JOHNSON, John R.
Brookhaven National Laboratory
Department of Energy & Environment
Building 815
Upton, New York 11973
(516) 345-4510

KELLEY, James H.
Jet Propulsion Laboratory
MS 507-207
4800 Oak Grove Drive
Pasadena, California 91103
(213) 577-9279

KINCAIDE, William C.
Teledyne Energy Systems
110 West Timonium Road
Timonium, Maryland 21093
(301) 252-8220

KRIKORIAN, Oscar H.
Lawrence Livermore Laboratory
P. O. Box 808, L-369
Livermore, California 94550
(415) 422-8076

KUHN, JR., Ira F.
B-K Dynamics, Inc.
15825 Shady Grove Road
Rockville, Maryland 20850
(301) 948-0650

KUSH, Edward A.
Brookhaven National Laboratory
Solar Technology Group
Building 701
Upton, New York 11973
(516) 345-3567

LAKNER, John F.
Lawrence Livermore Laboratory
P. O. Box 808
Livermore, California 94550
(415) 422-7977

LAWSON, Daniel D.
Jet Propulsion Laboratory
4800 Oak Grove Drive
Pasadena, California 91103
(213) 354-3615
FTS 792-3615

LIBOWITZ, George G.
Allied Chemical Corporation
P. O. Box 1021R
Morristown, New Jersey 07960
(201) 455-3583

LIU, James
Denver Research Institute
Metallurgy and Materials Science Division
University of Denver
2450 South Gaylord
Denver, Colorado 80208
(303) 753-2621

LIVESAY, B. R.
Georgia Institute of Technology
225 North Avenue, N.W.
Atlanta, Georgia 30332
(404) 894-3489

LIVINGSTONE, Philip N.
Battelle, Washington Operations
2030 M Street, N.W.
Washington, D.C. 20036
(202) 785-8400

LOUTHAN, JR., M. R.
Virginia Polytechnic Institute
Blacksburg, Virginia 24061
(703) 961-6825

LUDWICZAK, Robert
Office of Charles E. Grassley
U. S. House of Representatives
1227 Longworth House Office Building
Washington, D.C. 20515
(202) 225-3301

MACHIDA, Y.
c/o Graydon Associates
P. O. Box 566
Redbank, New Jersey 07701
(201) 741-2690

MATHUSA, Parker D.
New York State ERDA
Energy Technologies
Agency Building #2
Rockefeller Plaza
Albany, New York 12223
(518) 465-6251

MAVROIDES, John
Massachusetts Institute of Technology
244 Wood Street, Lincoln Laboratory
Lexington, Massachusetts 02173
(617) 862-5500 x5474

MEHTA, Ben
Electric Power Research Institute
3412 Hillview Avenue
Palo Alto, California 94303
(415) 855-2546

MEZZINA, Alessio
Brookhaven National Laboratory
Building 120
Upton, New York 11973
(516) 345-3920
FTS 666-3920

MICHAELS, Allan I.
Argonne National Laboratory
Solar Energy Group
Building 362
9700 South Cass Avenue
Argonne, Illinois 60439
(312) 972-7785

MITCHELL, M. R.
Rockwell International Science Center
1049 Camino Dos Rios
Thousand Oaks, California 91360
(805) 498-4545 x173

MORAN, Patrick J.
Applied Electrochemistry Laboratory
University of Virginia
Charlottesville, Virginia 22901
(804) 924-3277

MORGAN, Olwen M.
Rocket Research Corporation
11441 Willows Road
Redmond, Washington 98052
(206) 885-5000

MOTE, Jim D.
Denver Research Institute
Metallurgy & Materials Science Division
University of Denver
2450 South Gaylord
Denver, Colorado 80208
(303) 753-2621

MURRAY, John N.
Teledyne Energy Systems
110 West Timonium Road
Timonium, Maryland 21093
(301) 252-8220

NELSON, Howard G.
NASA Ames Research Center
MS 230-4
Moffett Field, California 94035
(415) 965-6137

NEWMAN, Franklin H.
Aerospace Corporation
20030 Century Boulevard
Germantown, Maryland 20767
(301) 428-2774

OFFENHARTZ, Peter O'D.
EIC Corporation
55 Chapel Street
Newton, Massachusetts 02158
(617) 965-2710

PARKER, Gerald H.
Westinghouse Advanced Energy Systems
P. O. Box 10864
Pittsburgh, Pennsylvania 15236
(412) 892-5600 x6264

PATON, N. E.
Rockwell International Science Center
1049 Camino Dos Rios
Thousand Oaks, California 91360
(805) 498-4545 x343

PEZDIRTZ, George F.
U. S. Department of Energy
600 E Street, N.W.
MS 404
Washington, D.C. 20545
(202) 376-9287

RAMUNDO, Kevin J.
Air Products and Chemicals Inc.
P. O. Box 538
Allentown, Pennsylvania 18105
(215) 398-5549

RAUH, R. David
EIC Corporation
55 Chapel Street
Newton, Massachusetts 02158
(617) 965-2710

READ, Edwin C.
Exxon Enterprises Inc.
P. O. Box 45
Linden, New Jersey 07036
(201) 474-2182

REEVES, Robert
U. S. Department of Energy
Division of Energy Storage Systems
600 E Street, N.W.
Room 416, MS 600E
Washington, D.C. 20545
(202) 376-4013

REMICK, Robert J.
Institute of Gas Technology
3424 South State Street
Chicago, Illinois 60616
(312) 567-5731

ROBINSON, S. L.
Sandia Laboratories
Division 8314
P. O. Box 969
Livermore, California 94550
(415) 422-2209

ROCKAR, Evelyn M.
Institute of Gas Technology
3424 South State Street
Chicago, Illinois 60616
(312) 567-5825

ROHY, David A.
Solar Turbines International
2200 Pacific Highway
San Diego, California 92138
(714) 238-5604

ROSSO, JR., Matthew J.
Brookhaven National Laboratory
Building 835
Upton, New York 11973
(516) 345-4506

RUSSELL, John H.
General Electric Company
50 Fordham Road
Wilmington, Massachusetts 01887
(617) 657-5277

SALYER, I. O.
University of Dayton Research Institute
Kettering Laboratory #503
300 College Park
Dayton, Ohio 45469
(513) 229-4235

SALZANO, F. J.
Brookhaven National Laboratory
Building 120
Upton, New York 11973
(516) 345-4458

SANDROCK, Gary
INCO Research & Development Center
Sterling Forest
Suffern, New York 10901
(914) 753-2761 x330

SCHROEDER, Robert
Allis-Chalmers
P. O. Box 512
Milwaukee, Wisconsin 53201
(414) 475-3046

SCHUSTER, John R.
General Atomic Company
P. O. Box 81608, TO-307
San Diego, California 92138
(714) 455-2915

SCHWERZEL, Robert E.
Battelle, Columbus Laboratories
505 King Avenue
Columbus, Ohio 43201
(614) 424-5637

SHEFT, Irving
Argonne National Laboratory
9700 South Cass Avenue
Argonne, Illinois 60439
(312) 972-3522

SMITH, Anthony J.
Tennessee Valley Authofity
T287-NFDC
Muscle Shoals, Alabama 35660
(205) 383-4631 x2371

SNAPE, Ed
MPD Technology Corporation
Ergenics Division
681 Lawlins Road
Wyckoff, New Jersey 07481
(201) 891-9103

SOLOMON, James
Air Products & Chemicals, Inc.
P. O. Box 538
Allentown, Pennsylvania 18105
(215) 398-7417

SRINIVASAN, Supramaniam
Brookhaven National Laboratory
Department of Energy & Environment
Building 801
Upton, New York 11973
(516) 345-4494

STEVENSON, F. Dee
U. S. Department of Energy
Office of Basic Energy Sciences
MS J-309
Germantown, Maryland 20767
(301) 353-5802

STONER, Glenn E.
Applied Electrochemistry Laboratory
University of Virginia
Charlottesville, Virginia 22901
(804) 924-3277

STRICKLAND, Gerald
Brookhaven National Laboratory
Building 120
Upton, New York 11973
(516) 345-4091
FTS 666-4091

SWET, C. J.
Consultant
P. O. Box 258
Route 4, Woodville Road
Mount Airy, Maryland 21771
(301) 831-7446

SWISHER, James H.
U. S. Department of Energy
Physical Storage Systems
600 E Street, N.W.
Room 416
Washington, D.C. 20545
(202) 376-4919

TAYLOR, Arthur
Aerospace Corporation
20030 Century Boulevard
Germantown, Maryland 20767
(301) 428-2733

TAYLOR, Earl Jennings
University of Virginia
10-7 Copeley Hill
Charlottesville, Virginia 22903
(804) 293-8309

TEITEL, Robert J.
Robert J. Teitel Associates
9145 Chesapeake Drive
San Diego, California 92123
(714) 565-6441

TEK, M. R.
University of Michigan
60 Underdown
Ann Arbor, Michigan 48109
(313) 764-3386

THOMAS, W. R. L.
Exxon Research & Development Company
Building 28, Room B 129
Linden Avenue
Linden, New Jersey 07036
(201) 474-2180

THORN, William F.
Rocket Research Company
11441 Willows Road
Redmond, Washington 98052
(206) 885-5000

WACHOB, Harry F.
Failure Analysis Associates
NASA Ames Research Center
STO: 230-4
Moffett Field, California 94035
(415) 965-5407/5410
FTS 448-5407

WALLACE, Terry C.
Los Alamos Scientific Laboratory
CMB-3/348
P. O. Box 1663
Los Alamos, New Mexico 87545
(505) 667-6074
FTS 843-6074

WATSON, J. S.
Oak Ridge National Laboratory
P. O. Box X
Building 4501
Oak Ridge, Tennessee 37830
(615) 574-6795

WETHERINGTON, Joseph B.
Air Products and Chemicals, Inc.
P. O. Box 538
Allentown, Pennsylvania 18105
(215) 398-7366

WILEY, Rudolf A.
New York State ERDA
Agency Building #2
Rockefeller Plaza
Albany, New York 12223
(518) 465-6251

WILKINSON, E. L.
Air Products and Chemicals Inc.
P. O. Box 538
Allentown, Pennsylvania 18105
(215) 398-8146

WILLIAMS, Laurence O.
Aerospace Corporation
20030 Century Boulevard
Germantown, Maryland 20767
(301) 428-2733

WYMAN, Charles
Solar Energy Research Institute
1536 Cole Boulevard
Building 4, First Floor
Golden, Colorado 80401
(303) 231-1368
FTS 327-1368

WYNN, C. S.
Airco, Inc.
100 Mountain Avenue
Murray Hill, New Jersey 07974
(201) 464-2400

YAFFE, Max R.
Teledyne Energy Systems
110 West Timonium Road
Timonium, Maryland 21093
(301) 252-8220

ZAGNOLI, David A.
Air Products & Chemicals, Inc.
P. O. Box 538
Allentown, Pennsylvania 18105
(215) 398-6708

*U.S. GOVERNMENT PRINTING OFFICE : 1980 0-620-309/2541